

Some pages of this thesis may have been removed for copyright restrictions.

If you have discovered material in AURA which is unlawful e.g. breaches copyright, (either yours or that of a third party) or any other law, including but not limited to those relating to patent, trademark, confidentiality, data protection, obscenity, defamation, libel, then please read our [Takedown Policy](#) and [contact the service](#) immediately

THE GEOCHEMISTRY AND PETROGENESIS OF THE MINOR
INTRUSIVE SUITE ASSOCIATED WITH THE LATE CALEDONIAN
CRIFFELL-DALBEATTIE PLUTON, SW SCOTLAND

PAUL JAMES HENNEY

Doctor of Philosophy

THE UNIVERSITY OF ASTON IN BIRMINGHAM

February 1991

This copy of the thesis has been supplied on condition that anyone who consults it is understood to recognise that its copyright rests with the author and that no quotation from the thesis and no information derived from it may be published without the author's prior, written consent.

The University of Aston in Birmingham

The Geochemistry and Petrogenesis of the Minor Intrusive Suite Associated With the Late Caledonian Criffell–Dalbeattie Pluton, SW Scotland

Paul James Henney

Doctor of Philosophy

1991

The Criffell–Dalbeattie pluton from SW Scotland is one of a suite of late Caledonian granitoids which are associated with extensive, contemporaneous and compositionally diverse suites of minor intrusions. The minor intrusive suite associated with the Criffell–Dalbeattie pluton is dominantly composed of a series of porphyritic microdiorites, microgranodiorites and microgranites known collectively as the porphyrite–porphyry series. This series can be divided into two groups, the porphyrites and the quartz porphyries, on the basis of petrography and geochemistry although there is some compositional overlap between the two. Compositionally, the porphyrites and quartz porphyries appear to correspond to the granodiorites and granites, respectively, which comprise the Criffell–Dalbeattie pluton, suggesting that the porphyrite–porphyry series of dykes represent magmas which were tapped from the evolving granitic magma chamber.

The most mafic component of the minor intrusive suite is represented by calc–alkaline hornblende– and mica–bearing lamprophyres. Geochemical studies, including fractional crystallisation, combined assimilation–fractional crystallisation (AFC) show that these are mafic, LILE and LREE enriched melts derived by low degrees of partial melting of a subduction-modified mantle source. It is suggested that the source of the lamprophyres is “Lake District” lithosphere, metasomatised by Lower Palaeozoic subduction, and thrust under the southern part of the Southern Uplands. AFC modelling using chemical and isotopic data further suggest that there is a close genetic link between the lamprophyres and the Criffell–Dalbeattie granitoids and that lamprophyres represent the mantle derived precursors of the Criffell–Dalbeattie granitoids.

Keywords: Lamprophyre, porphyrite–porphyry series, petrogenesis, subduction, partial melting, granitoid

Acknowledgements

I would like to thank my supervisors, Dr J W Gaskarth and Dr N.M.S. Rock, for their assistance and support during the period of research and writing up of this thesis. I would like to thank Jane Evans for her assistance with the production of the isotope data and Dr Nick Rogers for carrying out the neutron activation analysis. I would also like to thank all the technical staff in the Dept. of Geological Sciences for their invaluable assistance during my research.

I would particularly like to thank many of my fellow research student for the numerous discussions and debates about the thesis, especially David Adamson, John Naden, David Rae and Ken Ratcliffe. My special thanks to Brian Drabble for “saving the day” on many occasions with his computing skills, and to Paul Shand for his constructive criticism of the models and ideas.

Finally my thanks to my wife, Sandra, who provided inspiration throughout as well as invaluable assistance with the manuscript.

Chapter 3 Geohemical and isotopic characteristics of SW Scotland
calk-alkaline lamprophyres's (CALs)

3.1)	Geochemical characteristics	40
3.1.1)	Alteration in lamprophyres	40
3.1.2)	Hornblende lamprophyres	43
3.1.3)	Mica lamprophyres	46
3.1.4)	Comparative geochemistry of hornblende and mica lamprophyres	52
3.1.5)	Mineral chemistry of Criffell lamprophyres	54
3.1.5.1)	Micas	54
3.1.5.2)	Clinopyroxenes	58
3.1.5.3)	Amphiboles	67
3.2)	Comparisons between the Criffell lamprophyres and other late Caledonian basic magmas.	68
3.2.1)	Comparisons with other late Caledonian lamprophyres	70
3.2.2)	Comparison with calc-alkaline lamprophyres from other areas.	75
3.3)	Isotope Characteristics	77
3.3.1)	Rb-Sr and Sm-Nd isotope variations	81
3.4)	Comparison with late Caledonian basic magmas and late Palaeozoic mantle xenoliths	83
3.5)	Comparison with other CALs	88
3.6)	Summary	92

Chapter 4 Modelling of lamprophyre geochemistry:
The petrogenesis of the Criffell CAL

4.1)	Petrogenesis of CAL: Inferences from geochemistry and published models	94
4.2)	Fractional crystallisation	97
4.2.1)	Constraints from major elements	98
4.2.2)	Hornblende-lamprophyres	102
4.2.3)	Mica-lamprophyres	112
4.3)	Crustal contamination	117
4.3.1)	Patchett (1980) & Huppert & Sparks (1985) models	121
4.3.2)	Assimilation-fractional crystallisation modelling (AFC)	127
4.3.2.1)	Compatible and incompatible element variations	128
4.3.2.2)	Isotopic variation	131

4.4)	The Criffell CAL: Window on the mantle?	134
4.4.1)	Isotopic composition of the mantle source	138
4.4.2)	LILE and LREE composition of Criffell CAL: Source heterogeneity, partial melting or both?	140
4.4.3)	Differences between Hornblende- and phlogopite-bearing lamprophyres	142
4.5)	The tectonic setting and significance of lamprophyric magmatism in the Southern Uplands	143
4.6)	Summary	144

Chapter 5 Lamprophyre-granitoid associations:
A case study of the Criffell-Dalbeattie pluton.

5.1)	Introduction	146
5.2)	The nature of the lamprophyre-granitoid association	146
5.2.1)	Petrogenesis of late Caledonian granites	148
5.2.2)	Petrogenesis of Criffell-Dalbeattie granitoid complex: Existing models	149
5.2.3)	The composition of the parental magmas	150
5.3)	Evidence for lamprophyre involvement in the petrogenesis of the Criffell-Dalbeattie granitoid	151
5.4)	Petrogenetic modelling of the Criffell-Dalbeattie granitoid-lamprophyre association	154
5.4.1)	Fractional crystallisation	154
5.4.2)	Crustal contamination-binary mixing and AFC	155
5.4.3)	CAL contribution to granitoid petrogenesis: Thermal triggers and/or magmatic component?	163
5.5)	Petrogenetic model for the Criffell-Dalbeattie granitoid	165
5.6)	Summary	167

Chapter 6 The Porphyrite-Porphyry series: Intermediate and acid dykes
associated with the Criffell-Dalbeattie pluton

6.1)	Introduction	168
6.2)	Field relations and petrography	168
6.2.1)	Porphyrites	169
6.2.2)	Porphyries	171
6.3.1)	Alteration of the porphyrite-porphyry series	172

6.3.2)	Chemistry of the porphyrite–porphyry series	176
6.4)	Comparative chemistry of the Criffell pluton and porphyrite–porphyry series	178
6.4.1)	Liquid-crystal separation & crystal mushes: Differences in composition between dykes & plutons.	185
6.5)	Petrogenesis of the porphyrite–porphyry series	190
6.6)	Summary	193

Chapter 7 Conclusions and recommendations for future work

7.1)	Conclusions	196
7.2)	Recommendations for future work	198
	References	200
	Appendix A	216
	Appendix B	237
	Appendix C	247
	Appendix D	268
	Appendix E	270
	Appendix F	281

List of Figures, Tables and Plates

	Page
Fig. 1.1	16
Map of Criffell-Dalbettie area	
Fig. 3.1(a)	42
Nb-TiO ₂ in lamprophyres	
Fig. 3.1(b)	42
Nb-Zr in lamprophyres	
Fig. 3.1(c)	44
Rb-Ba in lamprophyres	
Fig. 3.1(d)	44
Rb-K ₂ O in lamprophyres	
Fig. 3.1(e)	45
Ba-LOI in lamprophyres	
Fig. 3.1(f)	45
U-Th in lamprophyres	
Fig. 3.2(a)	47
MgO-SiO ₂ in lamprophyres	
Fig. 3.2(b)	47
CaO-SiO ₂ in lamprophyres	
Fig. 3.2(c)	48
TiO ₂ -SiO ₂ in lamprophyres	
Fig. 3.2(d)	48
P ₂ O ₅ -SiO ₂ in lamprophyres	
Fig. 3.2(e)	49
Sr-SiO ₂ in lamprophyres	
Fig. 3.2(f)	49
Ba-SiO ₂ in lamprophyres	
Fig. 3.2(g)	50
Rb-SiO ₂ in lamprophyres	
Fig. 3.2(h)	50
Ni-SiO ₂ in lamprophyres	
Fig. 3.2(i)	51
La-SiO ₂ in lamprophyres	
Fig. 3.2(j)	51
Zr-SiO ₂ in lamprophyres	
Fig. 3.3	53
Chondrite diagram of Criffell CAL REE	
Fig. 3.4	53
Primordial mantle diagram of Criffell CAL	
Fig. 3.5(a)	55
K ₂ O-MgO in lamprophyres	
Fig. 3.5(b)	55
K ₂ O/Na ₂ O-MgO in lamprophyres	
Fig. 3.5(c)	56
Ba/Nb-MgO in lamprophyres	
Fig. 3.5(d)	56
Rb/Sr-MgO in lamprophyres	
Fig. 3.6	57
Mica compositions in Criffell CAL	
Fig. 3.7(a)	59
Mg# variation across micas	
Fig. 3.7(b)	59
K ₂ O variation across micas	

Fig 3.7(c)	MnO variation across micas	60
Fig 3.7(d)	TiO ₂ variation across micas	60
Fig. 3.8(a)	Ni-Mg# in micas	61
Fig. 3.8(b)	Cr-Mg# in micas	61
Fig. 3.9	Clinopyroxene compositions in Criffell CAL	62
Fig. 3.10(a)	Cr-Mg# in clinopyroxenes	63
Fig. 3.10(b)	MnO-Mg# in clinopyroxenes	63
Fig. 3.10(c)	Al ₂ O ₃ -Mg# in clinopyroxenes	64
Fig. 3.10(c)	TiO ₂ -Mg# in clinopyroxenes	64
Fig. 3.11(a)	Al ₂ O ₃ -Mg# in amphiboles	65
Fig. 3.11(b)	TiO ₂ -Mg# in amphiboles	65
Fig. 3.11(c)	MnO-Mg# in amphiboles	66
Fig. 3.11(d)	Na ₂ O-Mg# in amphiboles	66
Fig. 3.12(a)	PM diagram comparing CAL & SWH lavas	69
Fig. 3.12(b)	PM diagram comparing CAL & MV lavas	69
Fig. 3.13	Chondrite diagram comparing CAL & lavas REE	71
Fig. 3.14(a)	PM diagram comparing CAL & Lakes	72
Fig. 3.14(b)	Chondrite diagram comparing CAL & Lakes REE	72
Fig. 3.15(a)	PM diagram comparing CAL & Colima	76
Fig. 3.15(b)	Chondrite diagram comparing CAL & Colima REE	76
Fig.3.15(c)	PM diagram comparing CAL & SW England	78
Fig. 3.15(d)	Chondrite diagram comparing CAL & SW England	78
Fig. 3.16(a)	E Sr-Rb/Sr in lamprophyres	82
Fig. 3.16(b)	E Nd-Sm/Nd in lamprophyres	82
Fig. 3.17	E Nd-E Sr in lamprophyres & lavas	84
Fig. 3.18	Sm/Nd-Rb/Sr in lamprophyres	85
Fig. 3.19	E Nd-E Sr in lamprophyres & xenoliths	87
Fig. 3.20(a)	E Nd-Sm/Nd in lamprophyres & xenoliths	89
Fig. 3.20(b)	E Sr-Rb/Sr in lamprophyres & xenoliths	89

Fig. 3.21	E Nd-E Sr in Criffell , Colorado & Hercynian CAL	90
Fig. 3.22(a)	E Nd-Sm/Nd in Criffell, Colorado & Hercynian CAL	91
Fig. 3.22(b)	E Sr-Rb/Sr in Criffell , Colorado & Hercynian CAL	91
Fig. 4.1(a)	MgO-SiO ₂ model in hornblende lamprophyres	100
Fig. 4.1(b)	Fe ₂ O ₃ -SiO ₂ model in hornblende lamprophyres	100
Fig. 4.1(c)	CaO-SiO ₂ model in hornblende lamprophyres	101
Fig. 4.2(a)	K/Rb-MgO in hornblende lamprophyres	106
Fig. 4.2(b)	Ce/Th-MgO in hornblende lamprophyres	106
Fig. 4.2(c)	Ni/V-MgO in hornblende lamprophyres	107
Fig. 4.2(d)	Rb/Sr in hornblende lamprophyres	107
Fig. 4.3(a)	Ba-V RFC model in hornblende lamprophyres	108
Fig. 4.3(b)	Y-V RFC model in hornblende lamprophyres	108
Fig. 4.3(c)	K/Rb-Ni/V model in hornblende lamprophyres	109
Fig. 4.4(a)	Nb-Zr model in hornblende lamprophyres	110
Fig. 4.4(b)	Y-Zr model in hornblende lamprophyres	110
Fig. 4.5(a)	Rb-Ce model in hornblende lamprophyres	111
Fig. 4.5(b)	Ba-Sr model in hornblende lamprophyres	111
Fig. 4.6(a)	K/Rb-MgO in mica lamprophyres	115
Fig. 4.6(b)	K ₂ O/Na ₂ O in mica lamprophyres	115
Fig. 4.6(c)	Ba/Rb-MgO in mica lamprophyres	116
Fig. 4.6(d)	Rb/Sr-MgO in mica lamprophyres	116
Fig. 4.7(a)	Ni-Cr RFC model in mica lamprophyres	118
Fig. 4.7(b)	Rb-Ni RFC model in mica lamprophyres	118
Fig. 4.7(c)	Rb-Ba RFC model in mica lamprophyres	119
Fig. 4.7(d)	Rb-Ce RFC model in mica lamprophyres	119
Fig. 4.7(e)	Nb-Zr RFC model in mica lamprophyres	120
Fig. 4.8(a)	E Sr-SiO ₂ in lamprophyres	123
Fig. 4.8(b)	E Sr-MgO in lamprophyres	123

Fig. 4.8(c)	E Sr-Ni in lamprophyres	124
Fig.4.9(a)	E Nd-SiO ₂ in lamprophyres	125
Fig. 4.9(b)	E Nd-MgO in lamprophyres	125
Fig. 4.9(c)	E Nd-Ni in lamprophyres	126
Fig. 4.10(a)	Ni-Sr AFC model in hornblende lamprophyres	129
Fig. 4.10(b)	Ba-Sr AFC model in hornblende lamprophyres	129
Fig. 4.10(c)	Ba-K AFC model in hornblende lamprophyres	130
Fig.4.10(d)	Y-Zr AFC model in hornblende lamprophyres	130
Fig. 4.11(a)	Ni-K AFC model in mica lamprophyres	132
Fig. 4.11(b)	Rb-Ba AFC model in mica lamprophyres	132
Fig. 4.11(c)	Ce-Ba AFC model in mica lamprophyres	133
Fig. 4.11(d)	Y-Zr AFC model in mica lamprophyres	133
Fig. 4.12(a)	Sr(i)-K AFC model in lamprophyres	135
Fig.4.12(b)	Sr(i)-Ce AFC model in lamprophyres	135
Fig. 4.13(a)	E Nd-K AFC model in lamprophyres	136
Fig. 4.13(b)	E Nd-Ce AFC model in lamprophyres	136
Fig. 5.1	Map of granitoid-CAL associations in Scotland	147
Fig. 5.2	PM diagram with Criffell CAL & Enclaves	153
Fig. 5.3	E Nd-E Sr diagram with CAL, Enclaves, granitoids	153
Fig.5.4(a)	Y-Ce AFC model for CAL & granitoids	157
Fig. 5.4(b)	Sr-Ba AFC model for CAL & granitoids	157
Fig. 5.4(c)	Ba-K AFC model for CAL & granitoids	158
Fig. 5.4(d)	Rb-Sr AFC model for CAL & granitoids	158
Fig. 5.5	E Nd-E Sr diagram with sediments, CAL,granitoids	160
Fig. 5.6(a)	Sr(i)-Ce AFC model for CAL & granitoids	161
Fig. 5.6(b)	Sr(i)-Y AFC model for CAL & granitoids	161
Fig. 5.6(c)	Sr(i)-Sr AFC model for CAL & granitoids	162
Fig. 5.6(d)	Sr(i)-Ba AFC model for CAL & granitoids	162

Fig. 6.1(a)	Ba-TiO ₂ alteration plot with BSM samples	173
Fig. 6.1(b)	Rb-TiO ₂ alteration plot with BSM samples	173
Fig. 6.2(a)	Y-TiO ₂ alteration plot	174
Fig. 6.2(b)	Rb-K ₂ O alteration plot	174
Fig. 6.3(a)	Ba-TiO ₂ alteration plot	175
Fig. 6.3(b)	Rb-TiO ₂ alteration plot	175
Fig. 6.4(a)	MgO-SiO ₂ in porphyrite-porphyry series	179
Fig. 6.4(b)	CaO-SiO ₂ in porphyrite-porphyry series	179
Fig. 6.4(c)	TiO ₂ -SiO ₂ in porphyrite-porphyry series	180
Fig. 6.4(d)	P ₂ O ₅ -SiO ₂ in porphyrite-porphyry series	180
Fig. 6.4(e)	La-SiO ₂ in porphyrite-porphyry series	181
Fig. 6.4 (f)	Ba-SiO ₂ in porphyrite-porphyry series	181
Fig. 6.4(g)	Rb/Sr-SiO ₂ in porphyrite-porphyry series	182
Fig. 6.4(h)	K/Rb-SiO ₂ in porphyrite-porphyry series	182
Fig. 6.5	PM diagram of porphyrite-porphyry series	183
Fig. 6.6(a)	PM diagram of porphyrites & Criffell granodiorites	184
Fig. 6.6(b)	PM diagram of Qtz porphyries with Criffell granites	184
Fig. 6.7(a)	MgO-SiO ₂ porphyrite-porphyry series & granitoids	186
Fig. 6.7 (b)	CaO-SiO ₂ porphyrite-porphyry series & granitoids	186
Fig. 6.7(c)	TiO ₂ -SiO ₂ porphyrite-porphyry series & granitoids	187
Fig. 6.7(d)	P ₂ O ₅ -SiO ₂ porphyrite-porphyry series & granitoids	187
Fig. 6.7(e)	La-SiO ₂ porphyrite-porphyry series & granitoids	188
Fig. 6.7(f)	Ba-SiO ₂ porphyrite-porphyry series & granitoids	188
Fig. 6.7(g)	Rb/Sr-SiO ₂ porphyrite-porphyry series & granitoids	189
Fig. 6.7(h)	K/Rb-SiO ₂ porphyrite-porphyry series & granitoids	189
Fig. 6.8(a)	Rb-K AFC model for porphyrite-porphyry series	192
Fig. 6.8(b)	Rb-Sr AFC model for porphyrite-porphyry series	192
Fig. 6.8(c)	Y-Cr AFC model for porphyrite-porphyry series	194

Fig. 6.8(d)	Zr-Sr AFC model for porphyrite-porphyry series	194
Fig. A.1a	Cr XRF comparison	223
Fig. A.1b	V XRF comparison	223
Fig. A.1c	Zr XRF comparison	224
Fig. A.1d	Ni XRF comparison	224
Fig. A.1e	Nb XRF comparison	225
Fig. A.1f	Y XRF comparison	225
Fig. A.1g	Rb XRF comparison	226
Fig. A.1h	Sr XRF comparison	226
Fig. A.1i	Pb XRF comparison	227
Fig. A.1j	Ba XRF comparison	227
Fig. A.1k	Cu XRF comparison	228
Fig. A.1l	Zn XRF comparison	228
Fig. A.1m	Th XRF comparison	229
Fig. A.2a	Rb XRF comparison	230
Fig. A.2b	Sr XRF comparison	230
Fig. A.3a	La INAA-XRF comparison	231
Fig. A.3b	Ce INAA-XRF comparison	231
Fig. A.3c	Nd INAA-XRF comparison	232
Fig. A.3d	Nd ID-XRF comparison	233
Fig. A.3e	Nd INAA-ID comparison	233
Fig. A.3f	Sm INAA-ID comparison	234
Table 3.1	Mean of Criffell CAL, LORS lavas & CAL	73
Table 3.2	Sr-Nd isotopes of Criffell CAL	79

Table 4.1	Bulk distribution coefficients for HL RFC models	105
Table 4.2	Bulk distribution coefficients for ML RFC models	114
Table 6.1	Representative compositions from the porphyrite-porphyry series	177
Table A.1	XRF analytical conditions	218
Table A.2	XRF reproducibility data	219
Table A.3	XRF accuracy data	220
Plate 2.1(a)	Detail of hornblende lamprophyres	33
Plate 2.1(b)	Detail of hornblende lamprophyres	33
Plate 2.2(a)	Detail of mica lamprophyres	36
Plate 2.2(b)	Detail of mica lamprophyres	36

Chapter 1

Introduction

1.1) Aim of research

The principal aim of this thesis is to investigate and characterise the chemistry of the compositionally diverse suite of minor intrusions associated with the late Caledonian Criffell–Dalbeattie granitoid pluton in SW Scotland (Fig 1.1). The chemical data are used to develop a model for the petrogenesis of the minor intrusions and to determine both their relationship to the Criffell–Dalbeattie pluton and their significance in the tectonic and magmatic evolution of the Southern Uplands during the late Caledonian.

1.2) The Criffell–Dalbeattie pluton and associated minor intrusions

The late Caledonian Criffell–Dalbeattie granitoid, dated at 397 ± 2 Ma (Halliday *et al.* 1980), is one of a number of similar intrusions emplaced into the lower Palaeozoic sediments of the Southern Uplands during the final stages of the Caledonian orogeny (Phillips, 1956a; Stephens & Halliday 1979; Halliday *et al.* 1980). It is compositionally zoned with a marginal ring of clinopyroxene–hornblende granodiorites surrounding an inner core of biotite and biotite–muscovite granites. Chemical studies show that there is a discontinuous chemical and isotopic zonation corresponding approximately with the lithological variations (Stephens & Halliday, 1980). The outer granodiorites are generally less evolved than the inner granites, with higher MgO, CaO, FeO, Ni and Cr, lower $^{87}\text{Sr}/^{86}\text{Sr}$ ratios and more radiogenic ϵNd values.

The zonation in the pluton is not thought to have occurred simply by fractionation of a mafic precursor or by the progressive assimilation of country rock, as these processes should produce continuous isotopic and chemical trends (Stephens & Halliday, 1979; Halliday *et al.* 1980). The granodiorites and granites may represent separate pulses of magma, with the outer granodiorites derived from a mantle or lower crustal source and the granites produced by partial melting of middle and upper crustal rocks, composed of lower Palaeozoic sediments (Halliday, 1983). A model for the



Aston University

Illustration removed for copyright restrictions

evolution of the pluton has been presented (Stephens *et al.* 1985) in which the isotopic and chemical zonation is explained by the operation of an AFC style process involving combined contamination and fractionation of a mafic precursor, using lower Palaeozoic country rocks as the contaminant.

The extensive suite of minor intrusions associated with the Criffell–Dalbeattie pluton is dominated by members of the “porphyrite–porphyry” series, a term introduced by the Geological Survey to describe a varied group of generally porphyritic microdiorites, microgranodiorites and microgranites (Greig, 1971). Less abundant are representatives of the calc–alkaline lamprophyres, hornblende–bearing spessartites and mica–bearing minettes and kersantites (Rock, 1984), the petrography and field relations of the minor intrusions having been described in some detail by King (1927), Macgregor (1937) and Phillips (1956b). The recent study of the Black Stockarton Moor complex (Leake & Cooper, 1983) provides perhaps the best synthesis of the evolution and age relations of the minor intrusions. It is located at the western margin of the Criffell–Dalbeattie pluton and is thought to represent a late Caledonian sub–volcanic complex (Leake & Brown, 1979; Brown *et al.* 1979). Both lamprophyres and members of the porphyrite–porphyry series of dykes occur associated with sheets and stocks of granodiorite, breccia pipes and volcanic vents. Three main phases of activity have been identified based on the orientation of the minor intrusions. The earliest phase of activity predates the intrusion of Criffell–Dalbeattie granitoids and has been correlated with the development of a volcanic vent at the Shoulder O’ Craig in Kirkcudbright Bay (Fig 1.1) from which lamprophyres give dates ranging from 418–400Ma (± 10) (Rock *et al.* 1986a, 1986b). The second and third phases of activity overlap with the emplacement of the Criffell–Dalbeattie pluton, with dykes of the porphyrite–porphyry series being intruded into both the outer granodiorites and inner granites.

1.3) Significance of the Criffell–Dalbeattie dyke swarm.

Although numerous studies have been done on many of the late Caledonian granitoid intrusions in Scotland, they have largely ignored the large numbers of minor intrusions

associated with many of these plutons (Harmon et al. 1984). Where studies have been made of the minor intrusions, they are based mainly upon field and petrographical data with little or no chemical information. A common conclusion is that the dykes were derived from the same magmas as those of the plutons (Richey, 1939). Recent studies of the regional dyke swarm in the Southern Uplands, particularly those carried out in the Wigtown Peninsula, have highlighted the compositional diversity of these minor intrusions and their potential importance in studies of the tectonic evolution of the Southern Uplands (Barnes et al. 1986; Rock et al. 1986a, 1986b; Stone et al. 1987).

1.3.1) The porphyrite–porphyry series

Previous workers on dykes from the vicinity of the Criffell–Dalbeattie pluton concluded that the porphyrites and porphyries are derived from the same or similar magmas to those which form the pluton itself (Phillips, 1956b; Leeder, 1971). If this is correct, and the dykes represent magmas periodically tapped from the same magma chamber as the pluton, then a study of the mineralogy and chemistry of the dykes may provide an insight into the processes operating within a granitic magma chamber, information that may not be obtainable from a study of the pluton itself (Phillips et al. 1981). The textural and mineralogical diversity, previously described from the porphyrite–porphyry series, indicates that the dyke swarms may contain magma compositions not represented in the pluton. These include mafic compositions that may be possible precursors to the more evolved magmas and examples of late stage differentiates not preserved within the main body of the pluton. Multiphase, episodic dyke emplacement occurs (Leake & Cooper, 1983) and this provides information about the mode of emplacement of the pluton, the relative timing of the plutonic phases and the longevity of the magmatism. Thus part of the study has focussed on characterising the chemistry of the porphyrite–porphyry series of dykes and comparing these data with the compositions reported from the pluton. They are also used in modelling the petrogenesis of the porphyrite–porphyry series.

1.3.2) The calc–alkaline lamprophyres

Lamprophyres are the most mafic component of the suite of minor intrusions associated with the Criffell–Dalbeattie pluton and recent studies of similar lamprophyres from SW Scotland and Northern England have demonstrated that they represent primitive, mantle–derived magmas, enriched in LILE and LREE (Macdonald et al. 1985; Barnes et al. 1986; Rock et al. 1986, Macdonald et al. 1986). The occurrence of lamprophyres within the Southern Uplands has been used, in conjunction with recent structural and sedimentological studies of the Lower Palaeozoic sediments, in a reappraisal of tectonic models for the Lower Palaeozoic evolution of the region. The most widely accepted model in recent years has been that the Lower Palaeozoic sediments of the Southern Uplands are the remnants of a Lower Palaeozoic accretionary prism which formed at the NW continental margin of the Iapetus Ocean in response to the subduction of oceanic lithosphere (Leggett et al. 1979, 1982, 1983).

Recent remapping of the SW Southern Uplands by the British Geological Survey has raised doubts about the validity of the accretionary prism model for this area (Stone et al. 1987). These authors suggest that the Lower Palaeozoic sediments of the Southern Uplands were deposited during the Ordovician behind a volcanic arc, which shed detritus northwards into a developing back–arc sedimentary basin. These sediments were subsequently deformed, uplifted and thrust southwards on a series of low angle thrust faults. This thrust pile is thought to have supplied sediment during the Silurian to a series of foreland basins developing further south. During the final stages of the orogeny a transpressional regime may have controlled the tectonics of the Southern Uplands, with extensive strike–slip faulting, and during which mantle–derived lamprophyres were intruded (Stone et al. 1987). The presence of potassic, mantle–derived lamprophyres so close to the postulated suture is used as evidence (Rock et al. 1986) against the presence of an active lower Palaeozoic subduction zone under the Southern Uplands. The authors argue that similar potassic magmas found in areas of active subduction occur several hundred kilometres from the trench and not in a “forearc” setting as they are in the Southern Uplands.

Chemical studies of the Silurian–early Devonian volcanic rocks in Scotland reveal that the Caledonian mantle under Scotland appears to have been chemically heterogeneous, with magmas from the SW Highlands being enriched in LILE and LREE compared to contemporaneous ones erupted in the Midland Valley. These compositional variations may have been produced by the differing degrees of metasomatism of the mantle wedge, during Lower Palaeozoic subduction, as a function of the differing distances between the trench and the site of magma generation and depth to the subducting plate, under the Midland Valley and SW Highlands respectively (Thirlwall, 1981; 1982; 1983; 1986). Recent studies of mantle xenoliths and xenocrysts, recovered from late Palaeozoic and Tertiary mantle–derived intrusions, further indicate that metasomatic effects associated with Lower Palaeozoic subduction were superimposed on pre–existing, long–lived heterogeneities within the lithospheric mantle under Scotland (Halliday *et al.* 1985; Menzies *et al.* 1987; Menzies & Halliday, 1988).

Part of the current study has been to compare the chemical and isotopic compositions of the lamprophyres with data for the late Silurian volcanic rocks and the mantle xenoliths to help constrain the nature and composition of the lamprophyre source and to investigate how the lamprophyres relate to models for petrogenesis of other late Caledonian, mantle–derived magmas and the evolution of the sub–Caledonian mantle. The chemistry of the Criffell–Dalbeattie lamprophyres is also compared with data for calc–alkaline lamprophyres from a number of localities from around the world and of different ages to constrain petrogenetic and tectonic models. The study also addresses the significance of lamprophyres for constraining a recent model, based on Rb–Sr isotope dates, suggesting that late Caledonian magmatism south of the Southern Upland fault is younger than magmatism north of the fault and thus cannot be related to the same subduction event (Thirlwall, 1988). Using Pb–, Sr– and Nd–isotope data, Thirlwall *et al.* (1989) further proposed that late Caledonian magmas emplaced in the southern part of the Southern Uplands include a component derived from an ancient, enriched source. This component has been identified as enriched “Lake District”

lithosphere thrust beneath the southern part of the Southern Uplands during the final stages of late Caledonian continental collision.

The lamprophyres are the most mafic component of the dyke swarm associated with the Criffell–Dalbeattie pluton and this has led to speculation about their possible role in the genesis of the granitoid magmas (Macdonald *et al.* 1986; Henney *et al.* 1989). Many petrogenetic models for the late Caledonian “Newer Granites” postulate the involvement of a component derived from the mantle, but the nature and composition of this component is not described in any detail. Shoshonitic mantle-derived magmas, typified by the calc–alkaline lamprophyres, may have been involved in the genesis of several of the late Caledonian granitoids from the Highlands of Scotland as well as several of the earlier syenite complexes (Thompson & Fowler, 1986; Rock & Hunter, 1987; Fowler, 1988). This study also investigates the relationship between calc–alkaline lamprophyres and the parental magmas for Criffell–Dalbeattie pluton, and models possible petrogenetic links using new chemical and isotopic data.

1.4) Summary

The main aims of the thesis are to characterise the chemistry and investigate the petrogenesis of the late Caledonian dyke swarm associated with the Criffell–Dalbeattie pluton. This includes a geochemical study of the porphyrite–porphyry series of intermediate–acid dykes to test the hypothesis that dykes represent the same or similar magmas to those that form the Criffell–Dalbeattie pluton. This may provide information about the evolution and genesis of the granitoids which may not be obtainable from a study of the pluton itself. A geochemical study of the lamprophyres has several aims, (a) to model their petrogenesis within the context of pre-existing models for the genesis of contemporaneous basic magmas and the evolution of the sub–Caledonian mantle under Scotland; (b) to investigate the role and significance of lamprophyres in the controversy surrounding the Caledonian evolution of the Southern Uplands, and in particular, models involving the underthrusting of “Lake District” basement beneath the

Southern Uplands; (c) to investigate the relationship between the lamprophyres and the Criffell–Dalbeattie granitoid within the context of petrogenetic models for the granitoids involving the interaction of mantle derived magmas with the crust.

Chapter 2

Characteristics of lamprophyric magmatism and petrography and field relations of the Criffell lamprophyres

2.1) Introduction

Lamprophyres (from the Greek meaning 'glistening porphyry') are a widespread but volumetrically trivial group of igneous rocks that occur throughout geological history and in a variety of geological settings (Rock, 1977, 1987). Many workers have commented on their distinctive mineralogy, textures and chemistry, but no systematic work was carried out on this rock type until the first attempt at a synthesis was made by Rock (1977), which refined the classification of lamprophyres and divided the lamprophyre "clan" into four main sub-groups or "branches". The groups are the calc-alkaline (CAL), alkaline (AL), ultramafic (UML), lamproitic and kimberlitic groups (LL) of which the first three are the most widespread and widely recognised. Several authors (Dawson, 1987, Bergman, 1987) feel that the LL group should not be counted amongst the lamprophyres as they are petrologically distinctive and only distantly related to the lamprophyres. Full descriptions of these sub-groups are given by Rock (1987).

2.2) Field relations and associations

Lamprophyres most commonly form dykes, stocks and sills though diatremes and vents also occur associated with ultramafic, lamproitic and kimberlitic varieties. Igneous breccias are commonly associated with all lamprophyre types but particularly with the more alkaline varieties (Roden, 1981). Large plutonic bodies of lamprophyre are not known although some related plutonic rocks with lamprophyric affinities do occur; eg: the ultramafic pipe complexes of Alaska (Taylor, 1967; Murray, 1972; Irvine, 1974). Emplacement of lamprophyric magma is commonly structurally controlled on both the local scale (Currie & Ferguson, 1970; Delaney & Pollard, 1981)

and on the regional scale (Rock et al 1986), and their associations and tectonic settings are summarised in Rock (1987).

The most important and simplest association of lamprophyres is with continental crust, with the exception of some alkaline and ultramafic ones which occur in oceanic regions (Furnes & Stillman, 1987–Cape Verde Islands; Nixon et al. 1980–Malaita, Solomon Islands), and this has been taken to imply a genetic link (Rock, 1984). As might be expected, the different lamprophyre types have different rock associations. Calc-alkaline lamprophyres most commonly occur both in association with post-orogenic granitoids (the Caledonian of the UK) and with shoshonitic volcanic suites (Devon, SW England) as well as in regional dyke swarms unrelated to central magmatism (Navajo province, USA). They occur most commonly in orogenic belts (Europe–Caledonian & Hercynian) as well as in island arcs (Japan, NW Mexico) and intracratonic environments (USA–Navajo province). Alkaline lamprophyres are associated with plutonic rocks, in this case alkaline syenite-gabbro complexes (the Montereian province, Canada) regional dyke swarms (the Upper Palaeozoic of Scotland) and, more rarely, carbonatite complexes (Oka, Canada and Fen, Norway).

Tectonic settings range from zones of crustal tension, such as rift valleys and transcurrent fault zones (New Zealand and Rhine Graben), to "hot spot" style settings such as oceanic islands. Ultramafic lamprophyres are almost totally restricted to carbonatite type intrusions (Fen, Norway and Alno, Sweden) in intracratonic and rift valley environment. The lamproitic and kimberlitic associations (Dawson, 1980; Bergman, 1987, Mitchell, 1986) are restricted to isolated pipe or diatreme complexes unrelated to other magma types. They occur in intracratonic and craton margin settings with the notable exception of the Mesozoic lamproites of southern Spain which occur in an orogenic collision setting (Venturelli et al. 1984)

2.3) Petrography and mineralogy

The mineralogical diversity of lamprophyric rocks is one of the main reasons for the complications encountered in relating lamprophyres to other 'normal' igneous rocks. They are mineralogically distinctive, characteristically with euhedral phenocrysts of mica and/or amphibole set in a matrix of amphibole and/or mica together with feldspar or feldspathoids. Other volatile-rich phases, including carbonates, are also common. Phlogopites and Ti-rich amphiboles are the most abundant phenocrysts but diopsidic clinopyroxene and forsteritic olivine are common in the UML and LL groups. Orthopyroxene is restricted to the LL group rocks. Feldspars are, by definition, restricted to the groundmass and in the CAL and AL groups are represented by plagioclase (usually andesine-oligoclase but occasionally albite) and K-feldspar. In the more alkaline UML and LL groups feldspars are absent and feldspathoids, including nepheline and analcime are found. The LL group commonly contain exotic Nb-Zr-REE-Ti-Ba bearing silicate accessory phases, including priderite and wadeite, along with perovskite (Bergman, 1987). Distinctive features of all lamprophyres are the absence of feldspar (or feldspathoid) and quartz phenocrysts (Rock, 1984; 1987), though they do occur as xenocrysts, and the common occurrence of globular structures and felsic segregations (Rock, 1977, 1987; Cooper, 1979; Eby, 1980; Foley, 1984). The chemistry of the mineral phases in lamprophyres is distinctive, with high Ba, Ti, Mn and LREE abundances in phases such as mica and amphibole, commonly far in excess of those found in equivalent phases in other igneous rocks; eg: BaO contents in K-feldspars >1.5% and TiO₂ in phlogopites > 8% (Rock, 1987, 1991).

Although not a distinctive characteristic of lamprophyres as such, there is a wide diversity and range of both mantle and crust derived xenoliths as well as xenocrysts in lamprophyric rocks. These inclusions are important for attempts to model the source regions for lamprophyric magmatism and provide information on the composition of the upper mantle as a whole (Ehrenberg, 1979, 1982; Menzies & Hawkesworth, 1987 and references therein, Menzies & Halliday, 1988). Mantle-derived xenoliths, including lherzolites and garnet peridotites, are more common in the

AL, UML and LL groups and crustal xenoliths are more common in the CAL group (Rock, 1984, 1987, 1991). Xenocryst populations are dominated by volatile-rich phases including mica, amphibole and apatite. The compositions of these minerals are commonly similar to those found in MARID nodules (Waters, 1987) and are thought to have crystallised from volatile-rich basic magmas (Menzies et al., 1987).

2.4) Geochemistry

The essential geochemical characteristics of lamprophyric rocks are extreme LILE and LREE enrichments combined with 'primitive' levels of MgO, Ni and Cr (Barnes et al. 1986; Macdonald et al. 1985) over a range of SiO₂ contents. Abundances of Sr, P, Th, Ba, K, Cl and F are commonly the highest of any silicate igneous rocks (Rock, 1987, 1991). K generally dominates over Na, giving the lamprophyres a potassic character with $K/Na \geq 1$. High volatile contents (H₂O, CO₂, F, Cl, SO₄) are distinctive and are considered to be a primary feature of the magmas (Rock, 1984, 1987). Chondrite normalised REE profiles are generally steep and show the LREE enriched nature of the lamprophyres with La and Ce abundances up to 1000x chondritic and with Ce_n/Yb_n ratios as great as 112 (LL group).

In almost all groups, apart from some LL and AL, contents of Sc, Y, Ti and HREE are close to typical MORB in value (Rock, 1987). Isotope data for lamprophyres are sparse but reported $^{143}Nd/^{144}Nd$ values are commonly extremely unradiogenic and $^{87}Sr/^{86}Sr$ ratios extremely radiogenic. This is particularly true for some LL group rocks implying the source areas for these particular rocks must have been LREE and LILE enriched for a considerable period of time (Bergman, 1987). The essential features of lamprophyric rocks are their geochemical diversity and range in compositions. The majority are not as extreme in their elemental abundances as those of the LL group but at equivalent SiO₂ contents they are nevertheless enriched relative to 'normal' basaltic or andesitic rocks from contemporaneous tectonic settings and show distinct isotope characteristics (Alibert et al. 1986)

2.5) Calc-alkaline lamprophyres

This group forms the most abundant and widespread of the lamprophyres (Rock, 1984), including those associated with the Criffell–Dalbeattie pluton examined in this thesis. As with all lamprophyres their mineralogy is most commonly characterised by phenocrysts of either Ti-rich hornblende or phlogopitic mica, with plagioclase and K-feldspar restricted to the groundmass. They are divided into two groups, the mica lamprophyres (minettes and kersantites) and the 'hornblende' lamprophyres (spessartites and vogesites) based on phenocryst type and feldspar composition (Rock, 1984, 1987). Minor quantities of clinopyroxene are present in both groups and olivine is restricted to the mica lamprophyres where it occurs as sparse, heavily corroded, phenocrysts.

The CAL are generally less-enriched in LREE and LIL elements, and contain more SiO₂ than rocks from other lamprophyre groups which has led to comparisons with the shoshonitic group of volcanic rocks (Thompson & Fowler, 1986). They are more shoshonitic than calc-alkaline in terms of their K content and it has been suggested that they be called the "shoshonitic" lamprophyres (Rock, 1984). However there are sufficient significant differences in terms of volatile content, phase relations and geochemistry to maintain the CAL as a distinct suite of magmas not directly equated with basaltic rocks (Alibert et al. 1986; Roden & Smith, 1979; Roden, 1981; Turpin et al. 1988).

CAL occur in several tectonic environments, the most common of which is the orogenic setting (Rock, 1984, 1987) where they are commonly emplaced as one of the last episodes of magmatic activity of the orogenic cycle. This appears to be the case in the Caledonian (Rock & Rundle, 1986), the Hercynian (Turpin et al. 1988; Leat et al. 1987) and the Alpine (Dal Piaz et al. 1979, Venturelli et al. 1984). In some of these cases the CAL are associated with late stage granite plutons and minor shoshonitic basalts. Other CAL occurrences appear to be related less directly to orogenic activity; eg: the Colorado Plateau, but there is evidence that these rocks are also associated with a palaeo-subduction regime (Alibert et al. 1986; Rogers et al. 1982). A common feature

of CAL magmatism is an association with intermediate-acid dyke swarms, some of which have mineralogical, textural and chemical features in between those of 'normal' dioritic magmas and lamprophyres (Rock, 1984; Wimmenauer & Muller, 1985; Rock & Hunter, 1987).

In the UK CAL are the most widespread and abundant variety of lamprophyre, occurring from the Channel Islands (Lees, 1974) up to the Shetlands (Mykura, 1976) and were emplaced during both the Caledonian and Hercynian orogenies (Rock, 1984). Hercynian CALs are restricted to SW England and are represented by a suite of minettes associated with the potassic Exeter "traps" and the Dartmoor granite (Leat *et al.* 1987; Thorpe *et al.* 1986). In the north of England and Scotland they are widespread and abundant, forming both regional dyke swarms and dyke suites around granitoid plutons, and were intruded during the final stages of the Caledonian orogeny (Rock *et al.* 1988). The latter include members of the appinite suite, a group of miscellaneous basic rocks associated with many of the late Caledonian granitoids in the Highlands (Read, 1961; Wright & Bowes, 1979).

2.5.1) Distribution of late Caledonian calc-alkaline lamprophyres in Scotland

Regional and pluton associations of these rocks in the Caledonian of Scotland are mainly concentrated in the Highlands and Southern Uplands (Rock *et al.* 1988; Rock & Hunter, 1987; Smith, 1979). Also see figure 5.1, this volume.

In the Northern Highlands these lamprophyres are associated with the Assynt alkaline suite (Loch Ailsh-Borroilan) together with a suite of more alkaline minor intrusions (Sabine, 1953; Rock, 1984). From the sparse geochemical data available they appear to be more alkaline, being more LREE and LILE enriched than other Caledonian lamprophyres (Rock *et al.* 1988), with minettes and vogesites (K-feldspar > plagioclase) as the main rock varieties. The CAL are also associated with the Migdale and Ratagan granitoid plutons, the latter of which has a pronounced shoshonitic character (Thompson *et al.* 1984). It has been suggested that there was a petrogenetic link between syenitic magmatism and minette lamprophyres in the Glen Dessary

complex (Thompson and Fowler, 1986) but as there is a considerable age difference between the two magmatic episodes (syenites—457Ma, minettes—415-400Ma, Thompson & Fowler, 1986; Smith, 1979) the nature of this relationship is unclear.

In the Western and Grampian Highlands the CAL are associated with many of the late Caledonian granitoids (Rock et al. 1988, Rock & Hunter, 1987) and form part of extensive and compositionally variable dyke swarms (Rock, 1984). The CAL variants appinites and kentallanites have type localities in this area (Bailey, 1960) both of which are coarse-grained and may possibly represent cumulates from lamprophyric magmas (Rock, 1984).

In the Southern Uplands, the CAL have only recently been studied in detail (Barnes et al. 1986; Rock et al. 1986a, b; Macdonald et al. 1986; Rock et al. 1988). Rock et al. (1986a, b) recognised a narrow linear zone in the south of the Southern Uplands, stretching from the Ards Peninsula to Berwick, in which mica lamprophyres are abundant. In addition to this regional lamprophyre swarm, there are other local swarms, dominated by hornblende lamprophyres, closely associated with the Loch Doon and Criffell–Dalbeattie plutons (Philips, 1956b; Henney et al. 1989).

2.6) Calc-alkaline lamprophyres associated with the Criffell–Dalbeattie pluton

Lamprophyres and large numbers of less mafic dykes (the porphyrite-porphyrity series) are emplaced as part of the same dyke swarms. This association is typified by the multi-phase Black Stockarton Moor complex where lamprophyres form an essential, but minor, component of the D1 and D2 phases of activity (Leake & Cooper, 1983). All the lamprophyre dykes are narrow bodies (< 3m) and are distinguished, in porphyritic and coarse-grained varieties, by their abundant large euhedral crystals of hornblende or mica set in a variably coloured groundmass. The matrix of the hornblende lamprophyres is most commonly of pale pink-orange feldspar but in the mica lamprophyres it tends to be a dull grey or brown. Mica lamprophyres have a lustrous glint on fresh fracture surfaces. The fine-grained types are massive, grey-green in colour and are difficult to identify unambiguously in the field and may be

misidentified as dolerites. Both types contain felsic globular structures and, more diffuse, segregations set in a darker matrix (Rock, 1984). In some places these structures are abundant, comprising up to 10% of an exposed surface, and are up to 5 centimetres across. They are commonly pale pink to white and are composed of varying proportions of carbonates, feldspar, quartz, epidote and chlorite. A few have “cores” of sulphides, most commonly pyrite.

Contacts with the country rocks (turbidite sediments) are sharp with some showing a chilled margin. There is little evidence of hornfelsing in the sediments or fluid exchange (veining, etc) with the wall rocks (the exception to this is the Newmains lamprophyre; Macdonald et al. 1986). Some lamprophyres are associated with igneous breccias (Bombie Glen, Gribdae; Rock et al. 1986a), and in one occurrence are associated with volcanic vent activity (Shoulder o' Craig, Kirkcudbright; Rock et al. 1986b). In the Wigtown area some lamprophyres are folded by the late stages of deformation of the local country rocks (Barnes et al. 1986), however no deformed dykes occur around Criffell area. Some thin lamprophyre dykes, from the Sandyhills Bay area, are foliated and thermally metamorphosed: however it is thought that the foliation is due to the forceful emplacement of the Criffell-Dalbeattie pluton and not to any regional deformation event.

2.6.1) Petrography

Full reviews of lamprophyre petrography in general are given by Rock (1977, 1984, 1987) together with descriptions given in many of the standard petrological texts. The petrology of CALs from the Wigtown peninsula and Kirkcudbright Bay are given in Barnes et al. (1986) and Rock et al. (1986a) respectively. Petrological descriptions of the Criffell lamprophyres are given by King (1927) and Phillips (1956b). The following section provides a general summary of the petrography of the lamprophyres from the Criffell swarm analysed during this study.

2.6.1.1) Hornblende lamprophyres

These rocks are dominantly composed of hornblende and feldspar with minor (<10%) clinopyroxene. The typical texture displayed is that of randomly orientated, subhedral–euhedral needles and prisms of brown-green amphibole set in a panidiomorphic groundmass of interlocking plagioclase laths with minor amounts of interstitial K-feldspar and quartz (Plate 2.1a). Spessartites are the most abundant variety around the Criffell pluton with vogesites occurring only as a minor facies of the Newmains dyke (Macdonald et al. 1986). Accessory phases include apatite, chlorite, carbonates, epidote, sericite and minor opaques disseminated through the groundmass and in minor patches of alteration associated with the breakdown of the major phases.

By definition, hornblende should form more than 20% of the mode (Rock, 1984). The habit of hornblende is generally dependent on the grainsize of the rock. Coarse-grained varieties have subhedral–euhedral prisms and laths of brown-green amphibole (Plate 2.1b) whereas a needle-like, acicular habit is usual for fine-grained rocks (Plate 2.1a). Colour zoning is uncommon and occurs only in the more coarsely grained varieties where it is generally discontinuous with clearly defined dark-brown cores and light-green margins. In fine-grained rocks, hornblendes are unzoned except for a few, very narrow, actinolitic rims and either totally green or brown. Twinning is common, particularly in hornblendes from the fine-grained rocks. These variations in colour are believed to be controlled by the oxidation state of the iron and the titanium content of the amphibole (Deer et al. 1963). In many of the more coarsely grained rocks (Plate 2.1b) the hornblendes appear to have been strained and disrupted, with fracturing along and across cleavage directions. In several hornblende lamprophyres, in which there is a distinctly brown hornblende, a pale green–colourless diopsidic clinopyroxene occurs as fresh anhedral phenocrysts (Macdonald et al. 1986). In some rocks these pyroxenes have coronas of brown-green hornblende in a reaction relationship but in most both hornblende and clinopyroxene co-exist as discrete crystals without any reaction relationship between the two phases.

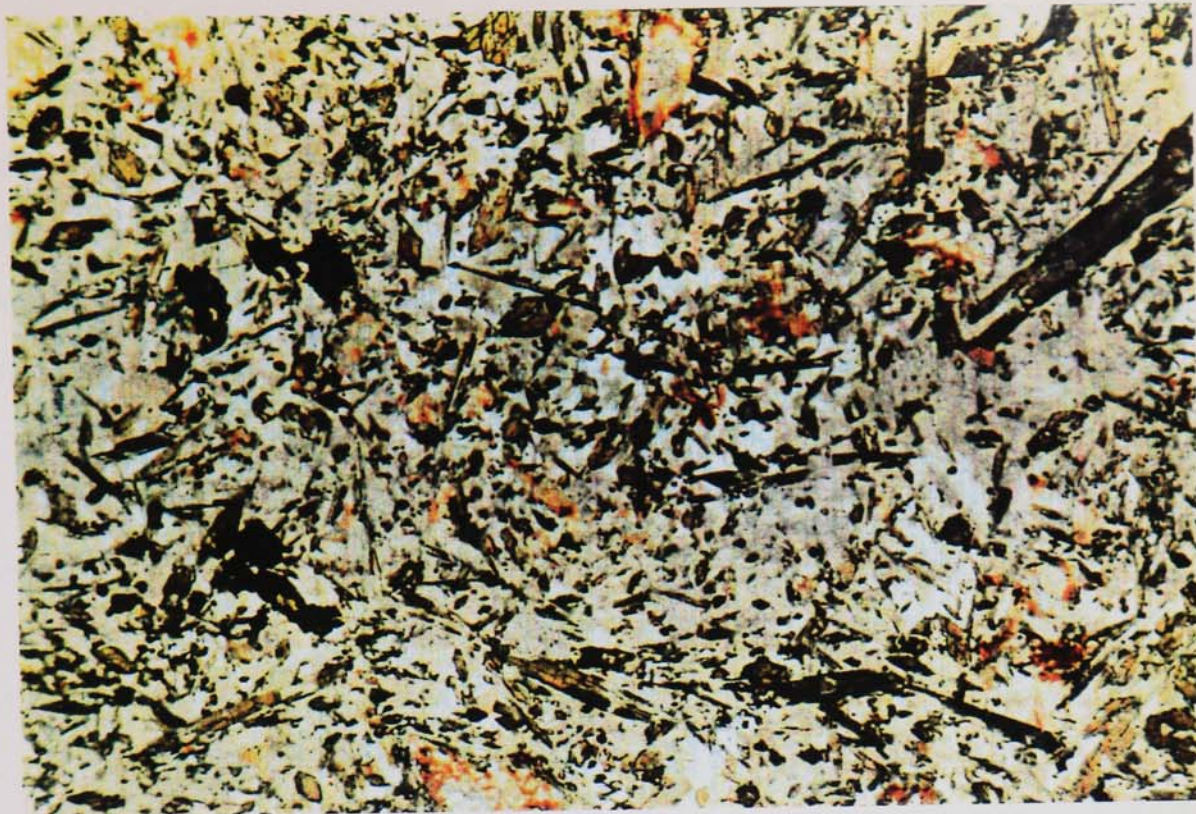
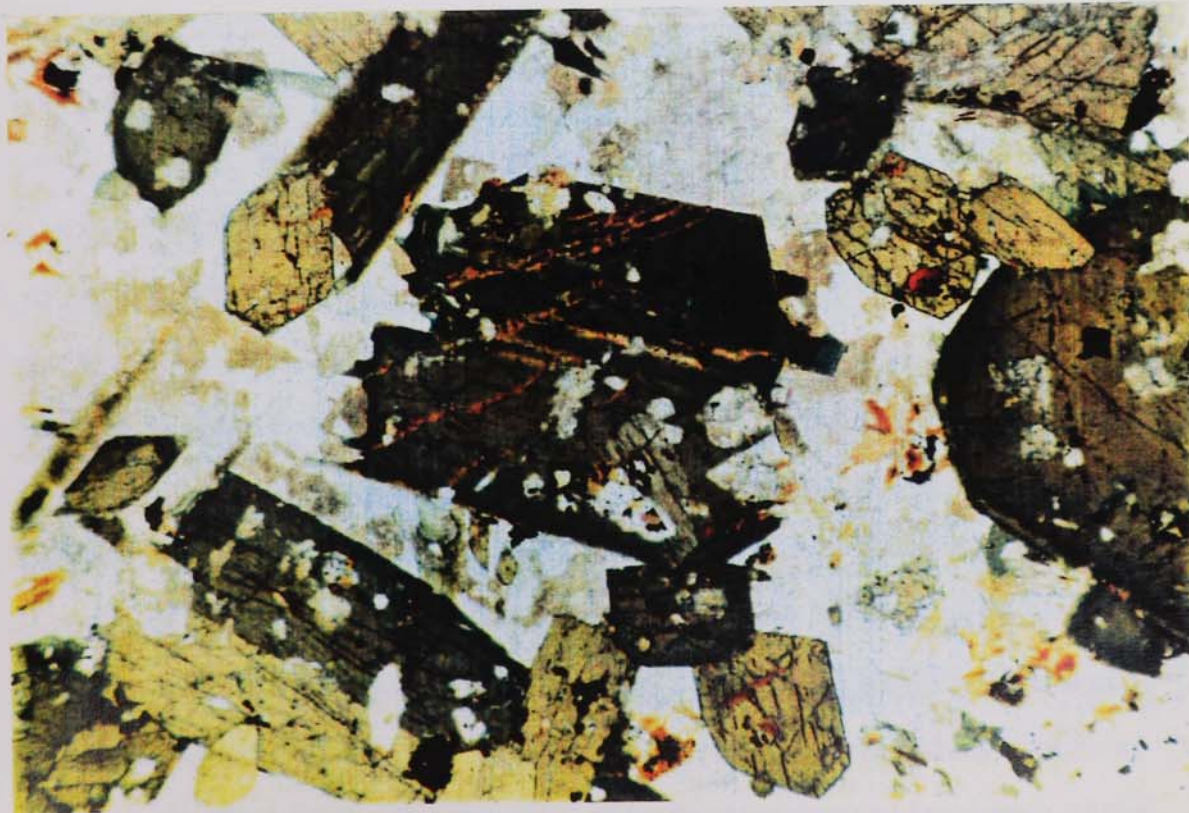


Plate 2.1(a) Typical fine-grained hornblende lamprophyre with acicular and prismatic hornblende set in an altered feldspathic groundmass.

Plate 2.1(b) Coarse grained hornblende lamprophyre with euhedral hornblende set in an altered feldspathic groundmass with interstitial quartz and alkali feldspar.



Feldspars are restricted to the groundmass of hornblende lamprophyres and as the proportion of plagioclase > alkali feldspar these are therefore classified as spessartites. Plagioclase occurs as interlocking laths and forms a distinctive panidiomorphic decussate groundmass. Alteration makes accurate optical determinations of plagioclase compositions difficult but, where determined, compositions are between An₁₀-An₄₀. In most hornblende lamprophyres the plagioclases show albite twinning and some have clear albite rims, particularly in the more coarsely grained samples. Some plagioclase cores have inclusions of acicular pale brown amphibole which supports the suggestion that hornblende is an early crystallising phase.

Alkali-feldspar most commonly occurs as anhedral crystals, intimately associated with quartz in interstitial "pools" between the plagioclase and amphibole and is best developed in the more coarsely grained rocks. Apatite is the most distinctive accessory and most commonly occurs as acicular needles dispersed throughout the groundmass. In more coarsely grained samples it occurs both as discrete euhedral microphenocrysts in the feldspathic matrix and as subhedral inclusions within the amphibole phenocrysts. Chlorite occurs mainly as an alteration product of amphibole and as the filling to sub-spherical "globular structures". It is associated with quartz, epidote and minor carbonate. The two most common opaque phases are Fe-Ti oxides and pyrite. The Fe-Ti oxides occur closely associated with alteration patches and zones in the mafic phases, and as disseminated grains throughout the rock. Pyrite occurs with felsic segregations, veinlets and "globular structures", as minor veinlets and disseminated grains in combination with carbonate, alkali-feldspar, chlorite and quartz. It appears that at least some of this pyrite is late magmatic because it forms cores or veinlets with early felsic materials and appears unrelated to post intrusion hydrothermal alteration and mineralisation processes. In some specimens however, pyrite together with chalcopyrite is accompanied by alteration of the host rock and quartz-carbonate veining and is clearly the result of a post-magmatic phase of mineralisation. Carbonate and epidote are most commonly associated with the alteration and breakdown of the

mafic phases and are intimately associated with chlorite. Xenoliths and inclusions are uncommon. They are restricted to a few small quartzitic bodies (<1cm) of unknown affinity and xenoliths of the sedimentary country rock occurring at the dyke margins. The pelitic xenoliths commonly have well developed reaction rims, marked by the development of a fine-grained mixture of chlorite, sericite and epidote at their contact with the lamprophyric magma. Rare igneous xenoliths (<5cm) are porphyritic, with sparse quartz and feldspar phenocrysts, set in a fine-grained reddish groundmass.

Felsic segregations are more common and are found in both fine- and coarse-grained rocks. The segregations are either diffuse, irregular patches of quartz, carbonate, epidote, chlorite, pyrite and feldspar or sub-spherical "globular structures", essentially containing the same minerals sharply defined by grain size and colour from the surrounding rock. Irregular, cross cutting veinlets of felsic material also occur but are less common and are similar to those described from the Newmains dyke (Macdonald *et al.*, 1986). The felsic structures are restricted to the dyke and do not cut the contact or invade the country rocks. They are present in both fresh and altered dykes suggesting that they are related to a late stage magmatic differentiation or fluid separation processes rather than some post magmatic alteration event.

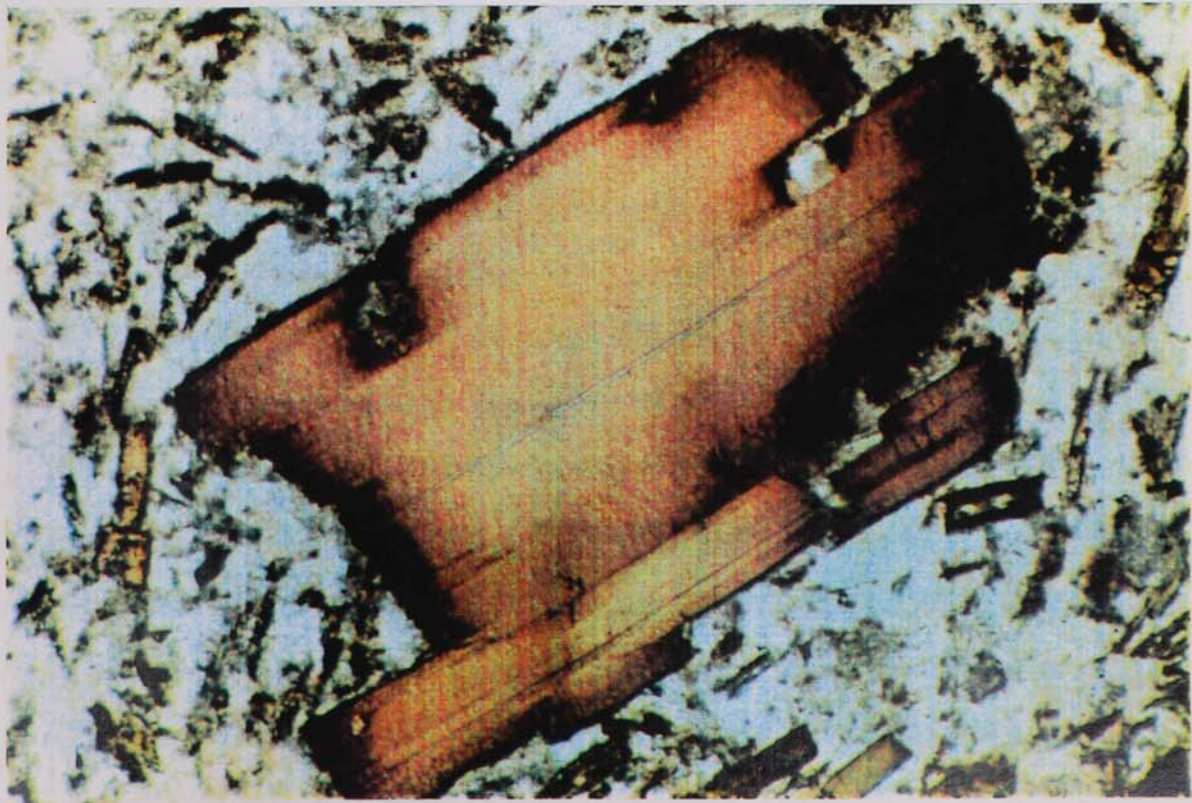
2.6.1.2) Mica lamprophyres

These are not common around the Criffell pluton and comprise <20% of the lamprophyres collected. They are most commonly porphyritic with large (5-10mm) flakes of light to dark brown mica set in a variably coloured (grey-reddish brown), essentially feldspathic, matrix (Plate 2.2a). This groundmass is typically more finely grained than that of the hornblende lamprophyres and a strong flow alignment of the phenocrysts is common. Both minettes and kersantites are present with the latter the most abundant, though alteration of the groundmass feldspar makes unequivocal identification difficult in many instances. Clinopyroxene is present in some mica lamprophyres as colourless to pale green, anhedral phenocrysts (<10%) and some also have a few pseudomorphs after olivine composed of carbonate, opaques and



Plate 2.2(a) Typical porphyritic mica lamprophyre with phenocrysts of phlogopite set in altered feldspathic groundmass including small flakes of brown mica.

Plate 2.2(b) Detail of typical phlogopite phenocryst showing pale core, dark rim and "castellated" outline.



"clays". Apatite is a common accessory along with chlorite, epidote and opaques. Carbonate is more abundant than in hornblende lamprophyres.

Mica occurs both as phenocrysts and as small flakes in the groundmass with typical CAL features such as undulose extinction, castellated sections, pale cores with darker rims and cores crowded with inclusions, particularly of apatite (Plate 2.2b) (Rock, 1984; 1987). The occurrence of undulose extinction together with evidence of deformed cleavage is thought to indicate that the micas crystallised early and were deformed during the ascent and final emplacement of the magma. The light to reddish brown colour is thought to indicate a high Ti content and the pale to dark zoning in basal sections may result from increased substitution of Fe for Mg (Deer *et al.* 1963).

Feldspars are restricted to the groundmass, most commonly as subhedral, interlocking laths. Both plagioclase and alkali-feldspar are present but accurate determination of their composition and relative proportions is difficult as the groundmass is commonly heavily altered. Apatite is the most abundant accessory, occurring as acicular needles in the micas, parallel to the cleavage. It also occurs disseminated throughout the groundmass and as stubby prisms in the cores of the mica phenocrysts. Fe-Ti oxides, chlorite and epidote are commonly associated with the alteration and breakdown of mica and groundmass feldspar. Secondary carbonate is associated with the breakdown of feldspar and olivine and also occurs as discrete patches both disseminated throughout the rock and within felsic "globular structures".

Xenoliths and inclusions are more common in the mica lamprophyres and include fragments of local sedimentary country rocks and porphyritic felsic igneous material. The most distinctive inclusions are milky-white to colourless, sub-spherical, quartzitic xenoliths, of unknown origin, which are commonly poly-granular and display strain related undulose extinction. Felsic segregations and "globular structures" are abundant in mica lamprophyres and are very similar to those described from the hornblende lamprophyres. One type of "globular structure" is unique to mica lamprophyres and consists of sub-spherical "vugs" filled with a varied combination of carbonate, alkali feldspar, chlorite, epidote and quartz. These "vugs" are frequently

concentrically zoned with quartz + alkali–feldspar cores speckled with granules of epidote and surrounded by a rim of chlorite with the whole “globular structure” rimmed by tangentially orientated flakes of mica. Mauger (1988) modelled the evolution of similar “globular structures” in the Concorde minette (USA) and suggested that feldspar+chlorite+quartz rich structures were formed by the separation of a aqueous vapour phase during the rapid ascent of the lamprophyric melt whereas carbonate rich segregations formed by the separation of an immiscible CO₂ liquid.

2.7) Summary

Lamprophyres represent a compositionally diverse suite of mantle–derived igneous rocks, with high MgO, Ni, Cr and V contents together with elevated LREE and LIL element abundances. They are further characterised by their mafic, hydrous mineralogy which is dominated by high modal abundances of amphibole and phlogopite, and many act as hosts for crustal and mantle–derived xenoliths. Four main subgroups are identified on the basis of composition, igneous association and tectonic setting of which the calc–alkaline lamprophyres (CAL) are perhaps the most abundant and widespread. The CAL are found in several tectonic settings, the most common of which is an association with the final stages of orogenic activity, in which they are most commonly found as regional dyke swarms and as plugs, stocks and dykes associated with granitoid plutons. In such settings, typified by the Caledonian orogenic belt of the UK, the CAL are often one of the final phases of magmatic activity and associated with the uplift and extension of the fold–belt. CAL from the suite of minor intrusions associated with the late Caledonian Criffell–Dalbeattie granitoid show many of the petrographic and mineralogical characteristics typical of the CAL group and are found as thin dykes cutting lower Palaeozoic sedimentary country rocks. Hornblende lamprophyres (spessartites) are characterised by abundant amphibole set in a commonly altered feldspathic matrix, while mica lamprophyres (minettes & kersantites) are characterised by phlogopite set in an altered feldspathic matrix. Clinopyroxene occurs in both groups but pseudomorphs after olivine phenocrysts are only found in the mica lamprophyres.

Both groups contain examples of “globular structures” and felsic segregations, though these are best developed in the mica lamprophyres. The hornblende lamprophyres are closely associated with the granitoid pluton while the mica ones are part of a regional dyke swarm which traverses the southern part of the Southern Uplands.

Chapter 3

Geochemical and isotopic characteristics of SW Scotland Calc-alkaline lamprophyres (CALs)

3.1) Geochemical characteristics

The first coherent chemical classification of the calc-alkaline lamprophyres group (Rock 1984, 1987) presented a set of chemical screens which, when used in conjunction with mineralogical and textural features, helped discriminate the calc-alkaline lamprophyres from other rock types. The main source of scatter in the Criffell CAL is in SiO₂ and some exceed the recommended upper limit of 60% (Rock, 1984). Despite this, however, these are still classified as lamprophyres on the basis of other chemical and textural criteria (Rock 1984, 1987). Most lamprophyres have bulk compositions similar to those reported for high-K andesites and other shoshonitic basalts (Gill, 1981).

3.1.1) Alteration in lamprophyres

One of the most difficult questions in studies of lamprophyres is the recognition, characterisation and, if possible, the quantification of the effects of post-magmatic alteration and weathering, particularly when using the accepted criteria of alteration, such as scatter on mobile and immobile element plots, high LOI, presence of secondary hydrous phases and the occurrence of secondary carbonate (Rock, 1991). It is widely recognised that lamprophyres, including CAL, appear to show petrographic evidence for post-magmatic fluid-rock interaction, with variable alteration of either the groundmass or phenocrysts phases, the presence of “secondary” carbonates and hydrous phases and high LOI values (Rock, 1984, 1987, 1991). However, there appears to be considerable ambiguity over the significance of these criteria in discriminating the effects of true post-magmatic alteration and late-magmatic “autometasomatism”, considering that all lamprophyres show relatively high LOI values (CAL mean 4.5%; Rock, 1991). Also experimental studies demonstrate that lamprophyric magmas are characterised by relatively high magmatic volatile contents

(>5 wt% in minette, Esperanca & Holloway, 1987) thus many of the textural peculiarities of lamprophyres may be due, in part, to the rapid emplacement of volatile rich melts to high levels in the crust and their rapid cooling (Esperanca & Holloway, 1987). Rock (1984, 1987, 1991) also noted the sporadic and unsystematic nature of “alteration” in lamprophyres, even within single intrusions, with either the phenocrysts or the groundmass altered but very rarely both at the same time and also the presence of hydrous “secondary” phases together with unaltered olivine, clinopyroxene, phlogopite and/or amphibole in the same sample.

Rock (1991), using a database over 5,000 lamprophyre analyses and information obtained from over 1,500 references, concluded that lamprophyres as a group are characterised by the effects of late-stage autometasomatism due to their high magmatic volatile content, leading to erroneous conclusions about the extent of post-magmatic alteration. This author also concluded that many of the petrographic features traditionally ascribed to secondary alteration in lamprophyres were in fact due to late-stage magmatic fluid activity, unrelated to post-magmatic interaction with fluids from the surrounding country rocks.

Brief details of observed petrographic alteration for the Criffell CAL are given in Appendix E, although as mentioned earlier, all samples which showed clear petrographic evidence for alteration were not analysed or were screened out of the data set. However, in order to further constrain the possible effects of alteration, efforts have been made to characterise the possible effects of alteration upon the whole rock chemistry of the Criffell CAL, based on the comments of Thirlwall (1979) and Thirlwall (pers.comm). Figures 3.1 (a-b) illustrate the interrelationship between several high field strength elements (HFSE–Nb, Ti, Y, Zr), which are considered to be immobile under most conditions of post-magmatic alteration (Pearce & Norry, 1979 and references therein). In unaltered rocks these should give linear correlations on bivariate plots and this is exactly what is observed in the Criffell CAL. However, of more significance is the relative “immobility” of the LILE elements which are considered the most susceptible to remobilisation during alteration (Thirlwall, 1979).

Fig. 3.1a

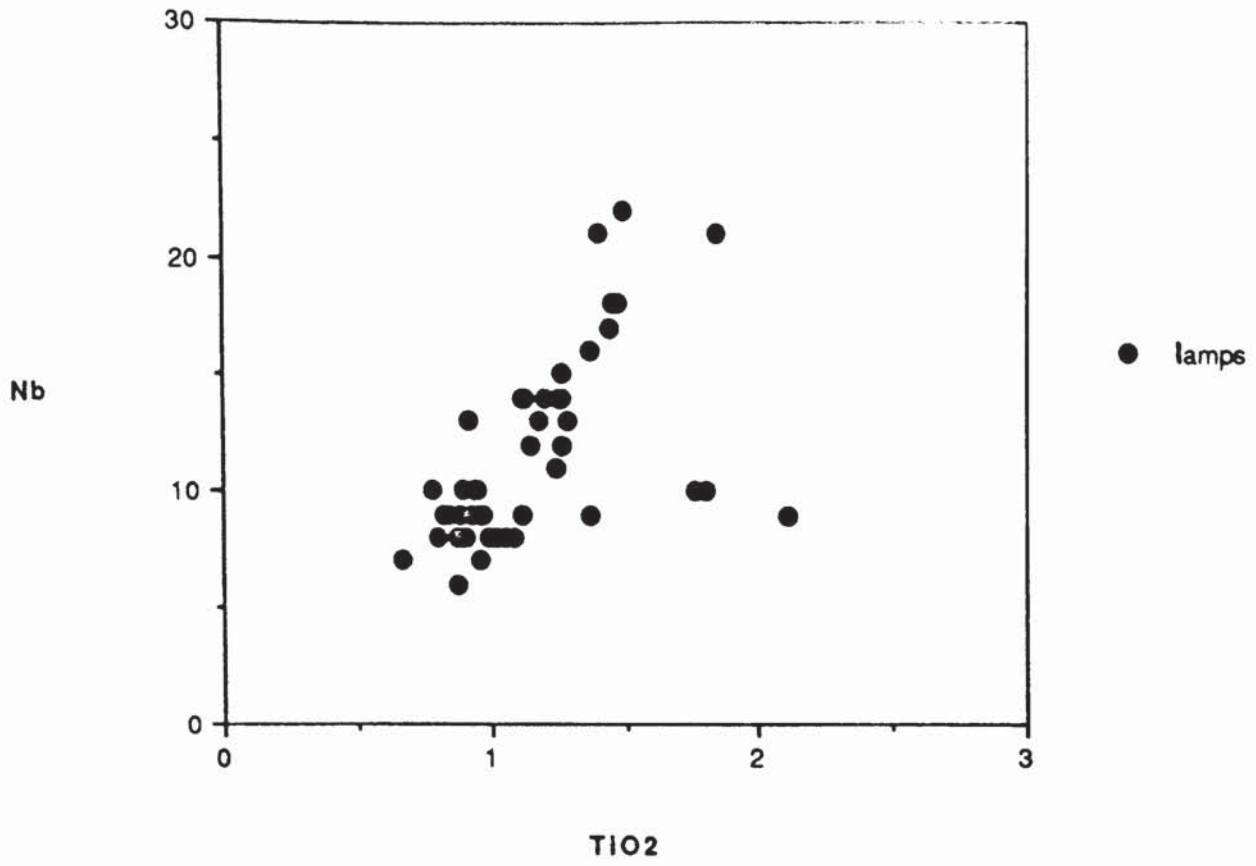
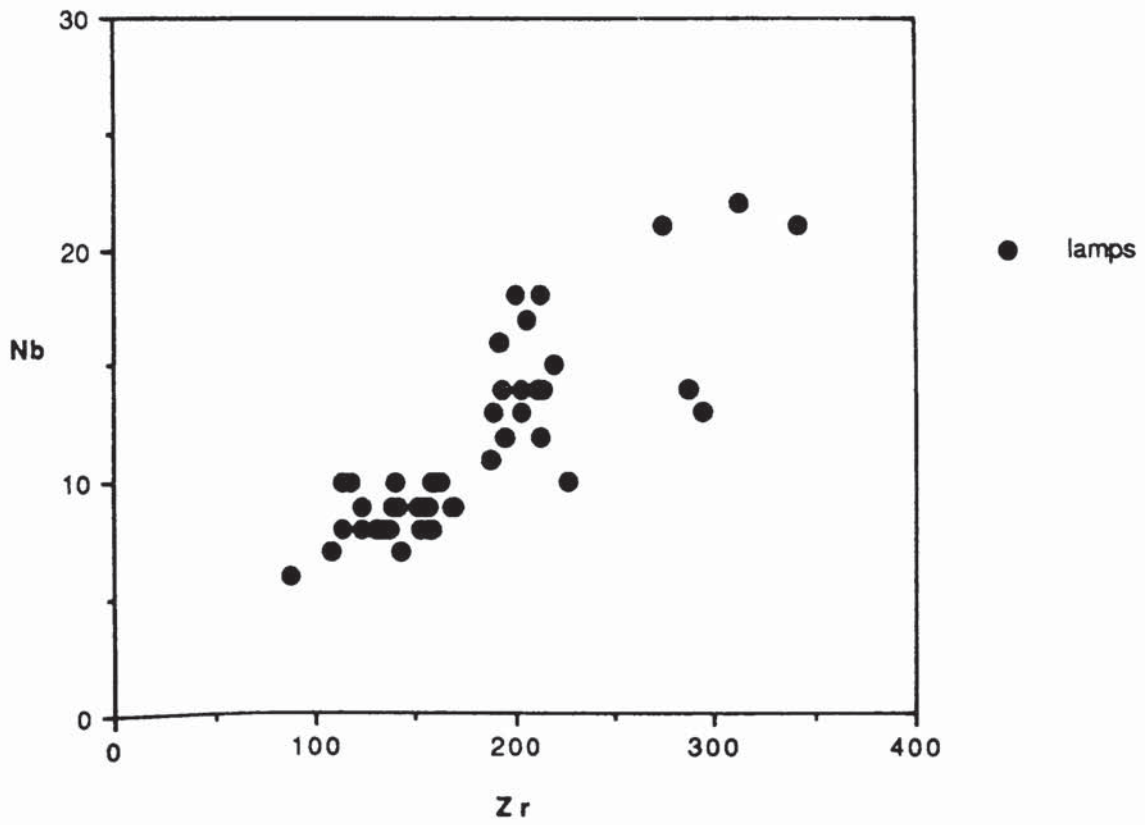


Fig. 3.1b



Where these elements have been remobilised during alteration, scatter will be introduced into bivariate plots including these elements. In figures 3.1 (c-d), the relationships between several large ion lithophile elements (LILE) in the Criffell CAL are illustrated and it is clear that, to a large degree, significant positive correlations are maintained between these elements. The degree of scatter is greater in the Rb-Ba plot, particularly for the data from mica lamprophyres, and it is possible that this may reflect minor remobilisation of Ba in some of the mica lamprophyres due to alteration. However, as suggested by Thirlwall (1979), if samples with high LOI do represent, chemically, the most altered compositions then there should be some evidence of a correlation between LILE and LOI values. However, in figure 3.1(e), Ba abundances show no correlation with LOI values suggesting, if LOI is indeed an index of alteration, that Ba abundances have not been significantly modified by alteration in the Criffell CAL. Thirlwall (1986) argued that the linear correlation between U, one of the most mobile of the LILE and Th, considered to be relatively immobile, he observed in the LORS lavas in Scotland suggested that these elements had not been significantly affected by hydrothermal alteration. The U-Th data derived from the Criffell CAL by INAA methods is illustrated in figure 3.1(f) and shows a significant linear correlation between the two elements suggesting that the Criffell CALs have also experienced little U remobilisation due to post-magmatic alteration.

Therefore it is concluded on the basis of HFSE-HFSE, LILE-LILE, LILE-LOI and LILE-HFSE plots that the Criffell CAL analysed for this study have suffered little significant change in composition due to post-magmatic alteration and weathering and that LILE (and by implication LREE) abundances of the samples largely reflect their original magmatic values.

3.1.2) Hornblende Lamprophyres

Hornblende lamprophyres range from basic to intermediate in composition with silica contents from 47.17 – 61.55 % and Al_2O_3 from 12.29 – 17.87%. Silica shows negative correlations with MgO (13.43–4.72%), Fe_2O_3 (10.37–5.26), CaO (10.33–

Fig. 3.1c

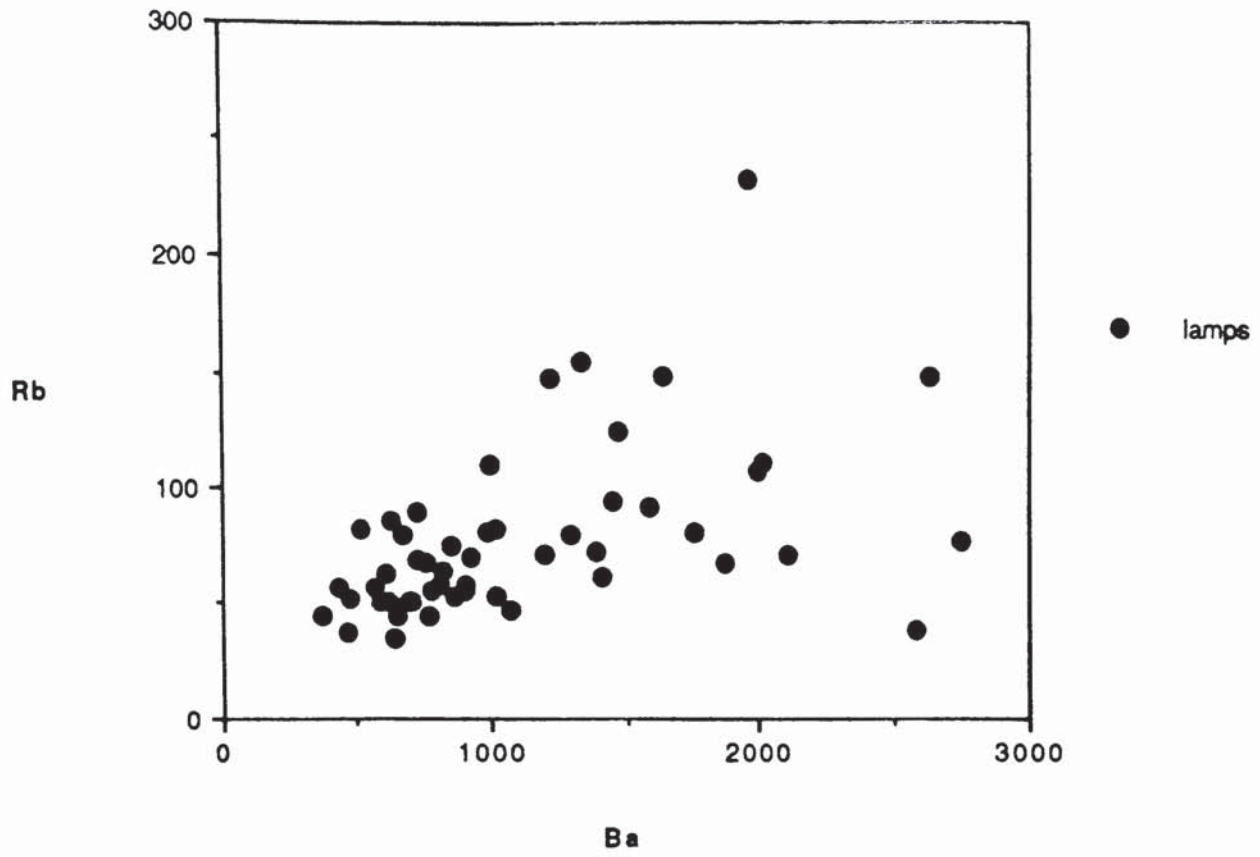


Fig. 3.1d

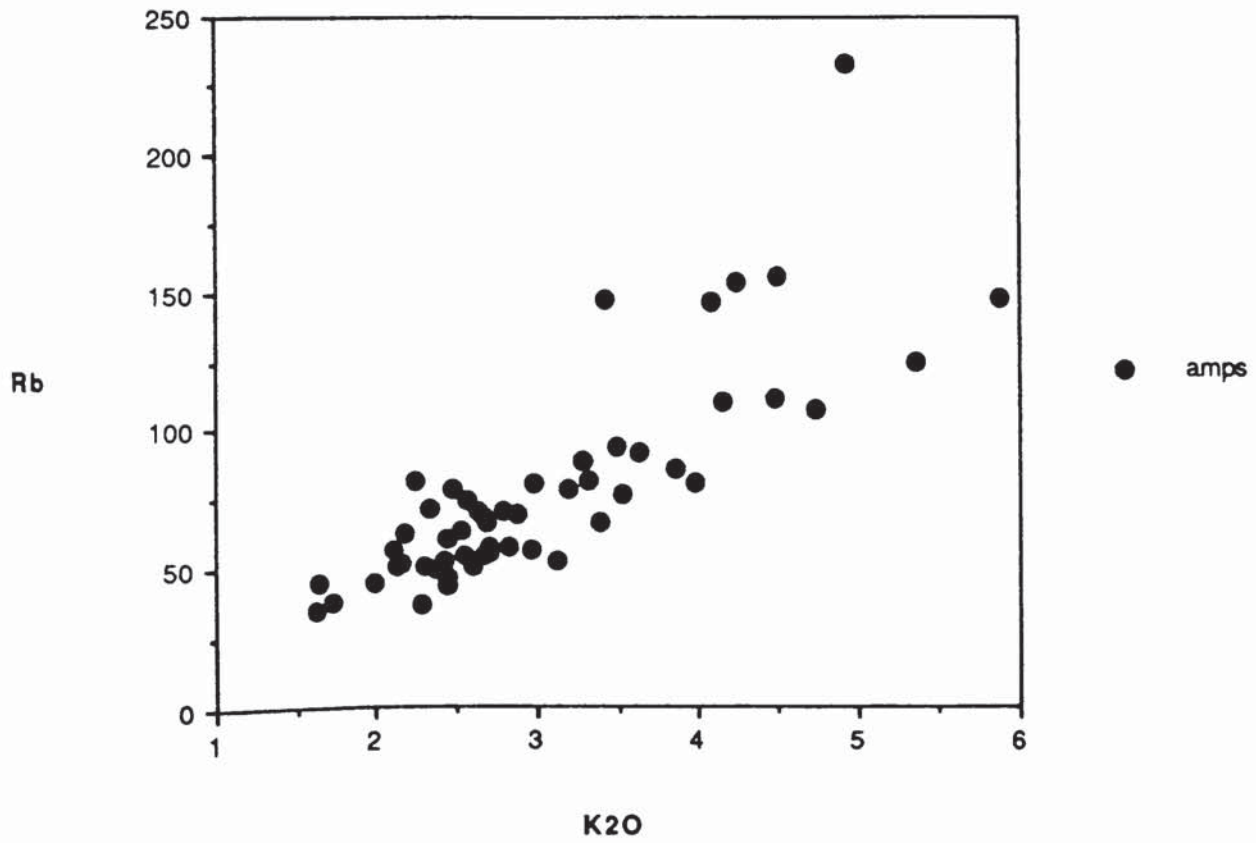


Fig. 3.1e

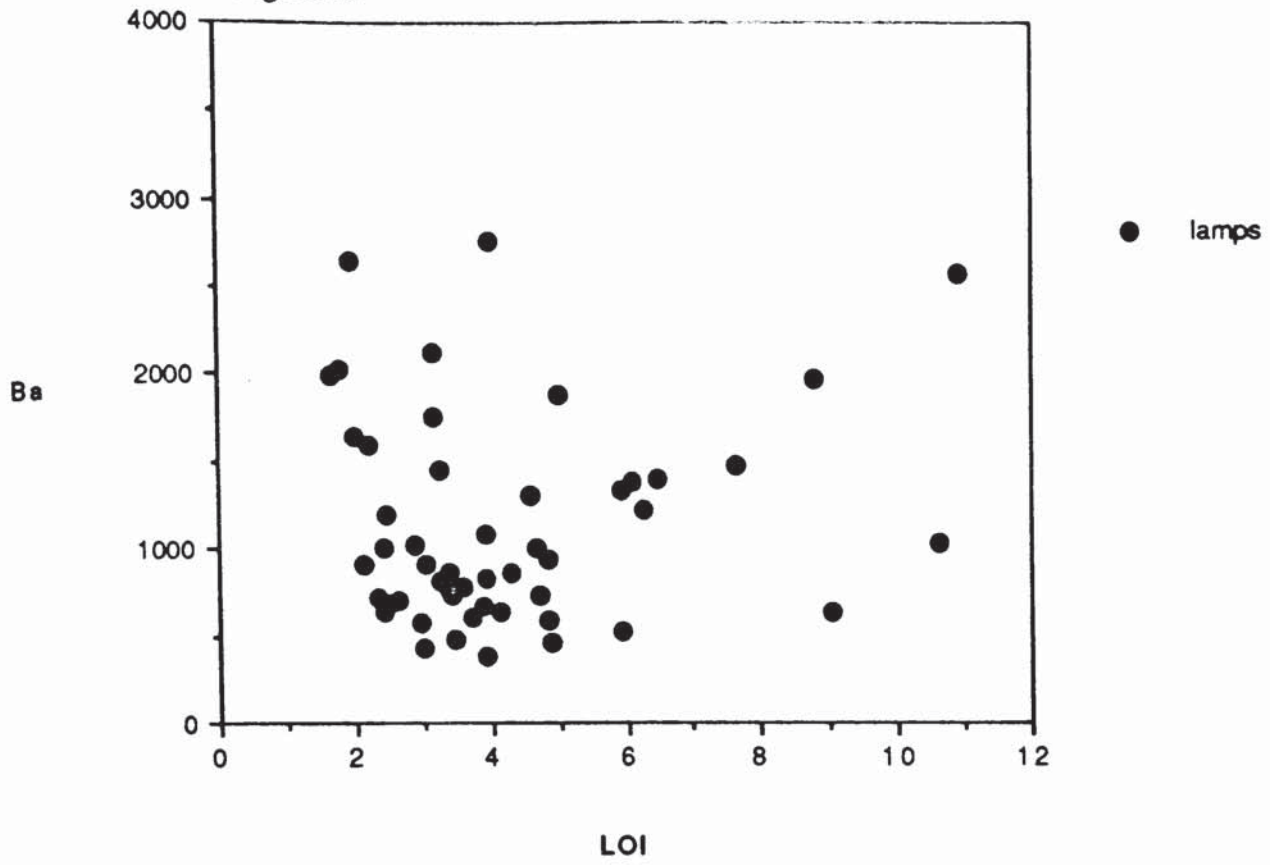
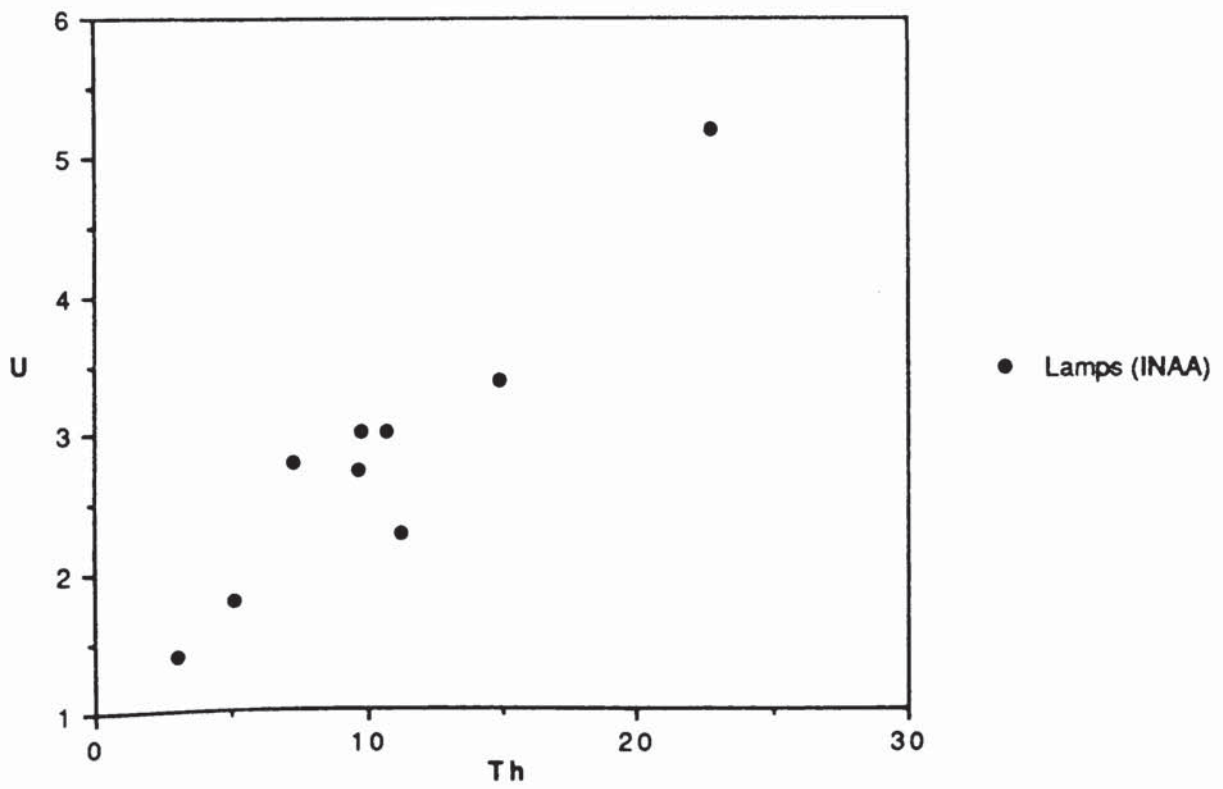


Fig. 3.1f



2.43), P₂O₅ (1.73–0.23), TiO₂ (2.11–0.78%) and K₂O/Na₂O (2.17–0.45) (Figs. 3.2a–c) and positive correlations with Al₂O₃, DX, Na₂O (6.28–1.57%) and Na₂O+K₂O. K₂O (4.74–1.62%) shows no significant correlation with silica or most major elements but has a poor negative correlation with Na₂O. Several of the hornblende lamprophyres are quartz normative (< 9.86) and a few are also corundum normative (<5.29) but the majority have normative compositions reflecting their generally primitive nature with high normative diopside (<20.08) and olivine (<21.87). One sample has a small amount of nepheline in the norm (<0.28) and all samples have high normative apatite (<4.04).

There is a wide range in trace element content characterised by high transition (Ni <328ppm, Cr <593ppm, V <292ppm) and LILE (Ba <2114 ppm, Rb <143ppm, Sr <1738ppm) abundances compared to most other basic calc–alkaline magmas (Rock, 1984, 1987, 1991). High field strength (HFS) element abundances (Nb <22ppm, Zr <312ppm, Y <29ppm) are more typical of primitive arc magmas, though U (5ppm) and Th (27ppm) are higher (Gill, 1981). Zn, Cu and Pb abundances are variable but generally < 150ppm. Significantly, many of the trace elements show only poor or scattered correlations with silica (Figs. 3.2d–j) which suggests that the distribution of the trace elements is not strongly controlled by fractionation processes. The hornblende lamprophyres are LREE enriched with high La (104ppm), Ce (205ppm) and Nd (86.7ppm) abundances which are also reflected in steep chondrite–normalised (Nakamura, 1974) REE profiles (Fig. 3.3) with high Ce_N/Yb_N (25.6) and low Sm/Nd (0.150) ratios.

3.1.3) Mica lamprophyres

The mica lamprophyres have major element compositions similar to those of the hornblende lamprophyres but with less variation. Silica (50.06–55.78%) has rough negative correlations with MgO (14.01–6.99%), CaO (9.16–3.46%), Fe₂O₃ (9.94–6.44%) and scattered positive correlations with K₂O (5.88–1.74%), Na₂O (3.70–0.82%), Na₂O+K₂O and DX. TiO₂ (1.87–0.87%), Al₂O₃ (16.02–12.33%) and P₂O₅

Fig. 3.2a

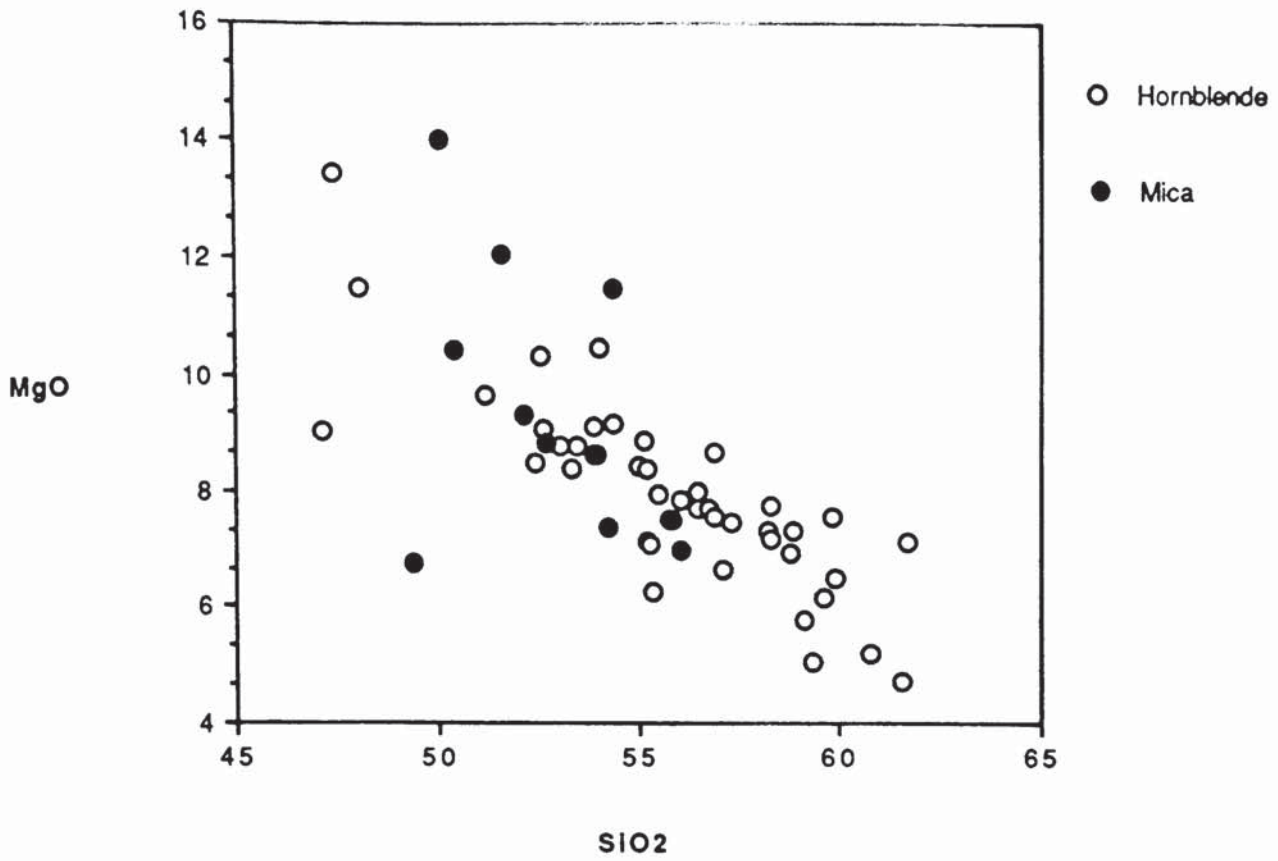


Fig. 3.2b

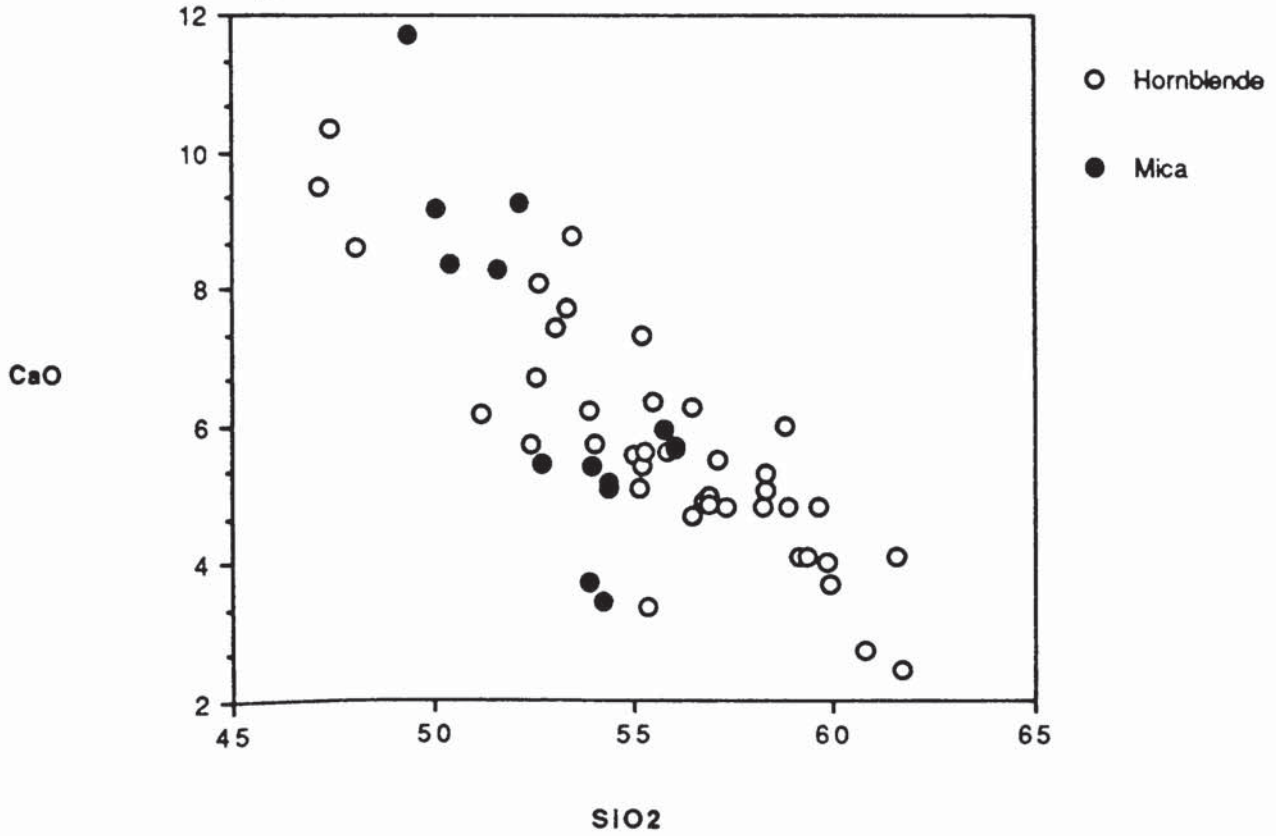


Fig. 3.2c

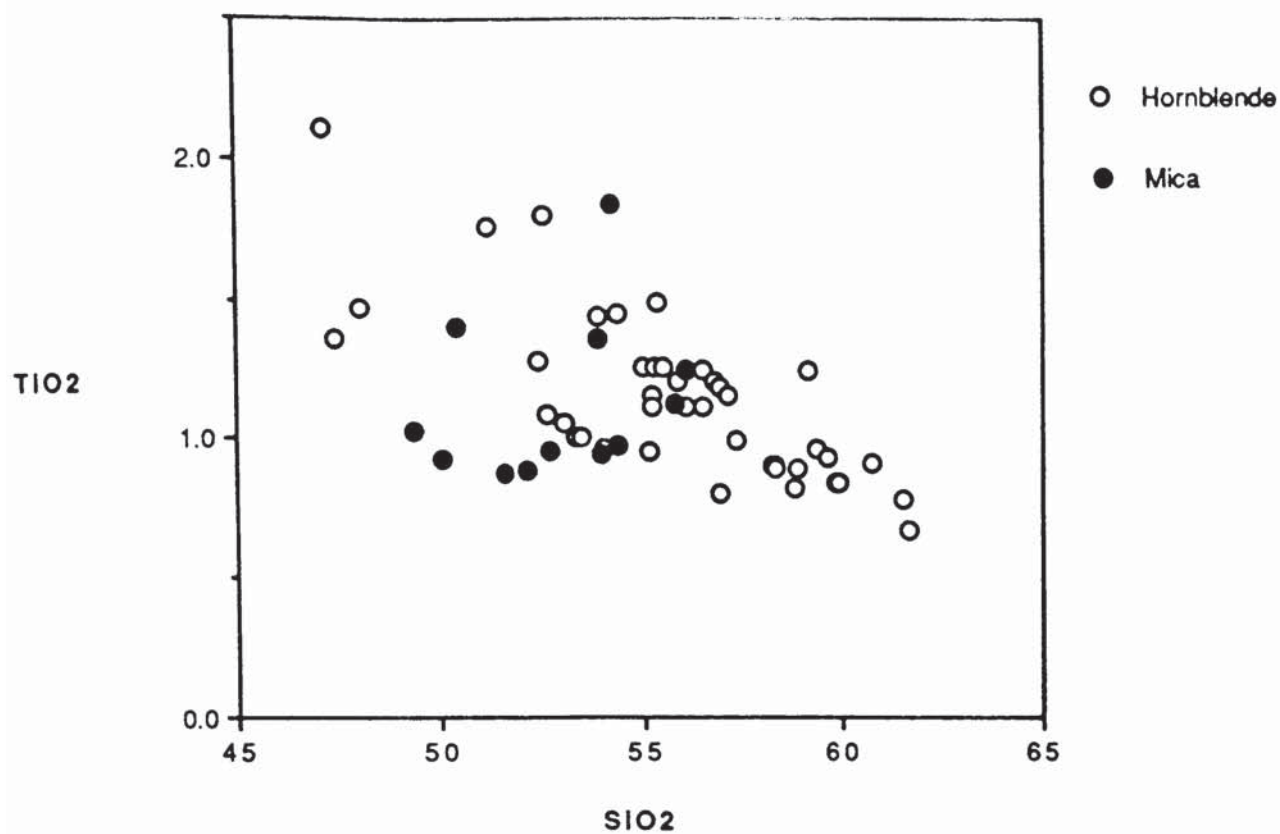


Fig. 3.2d

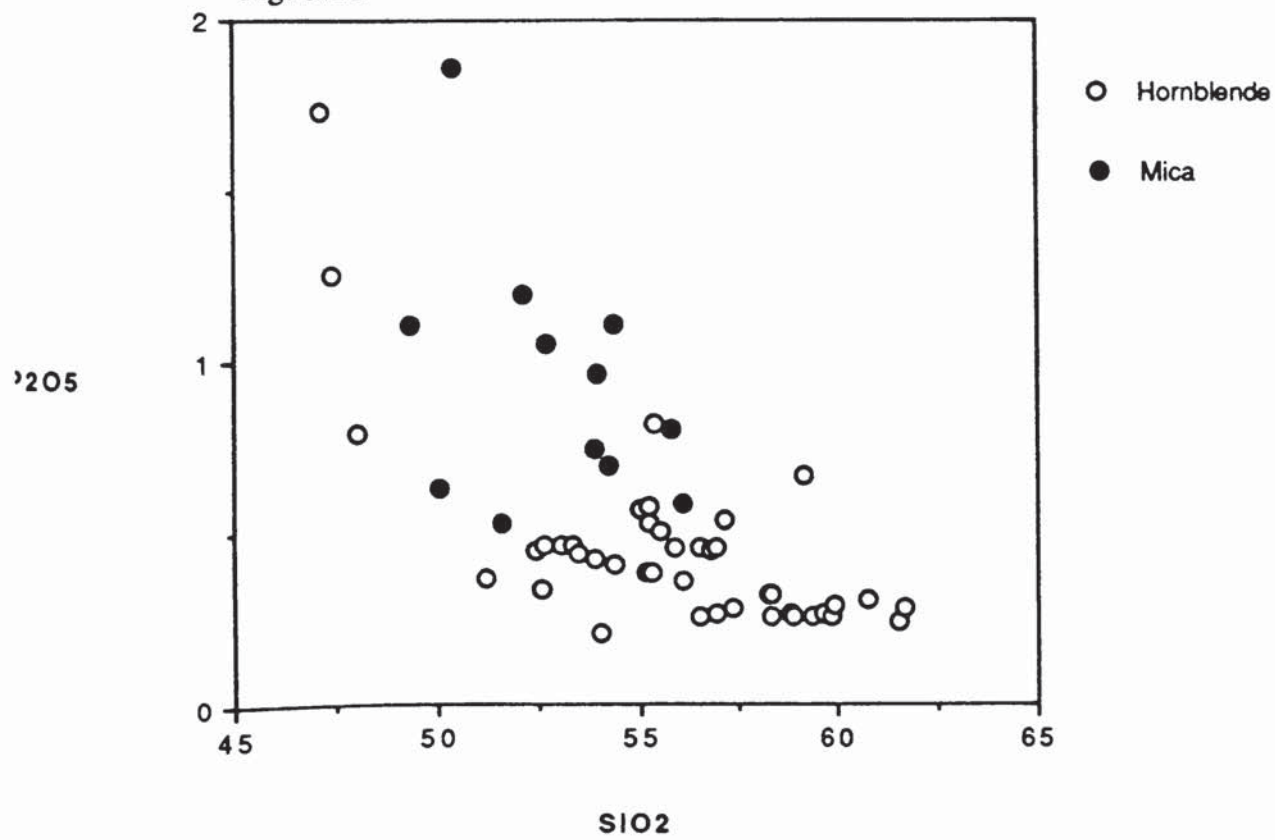


Fig. 3.2e

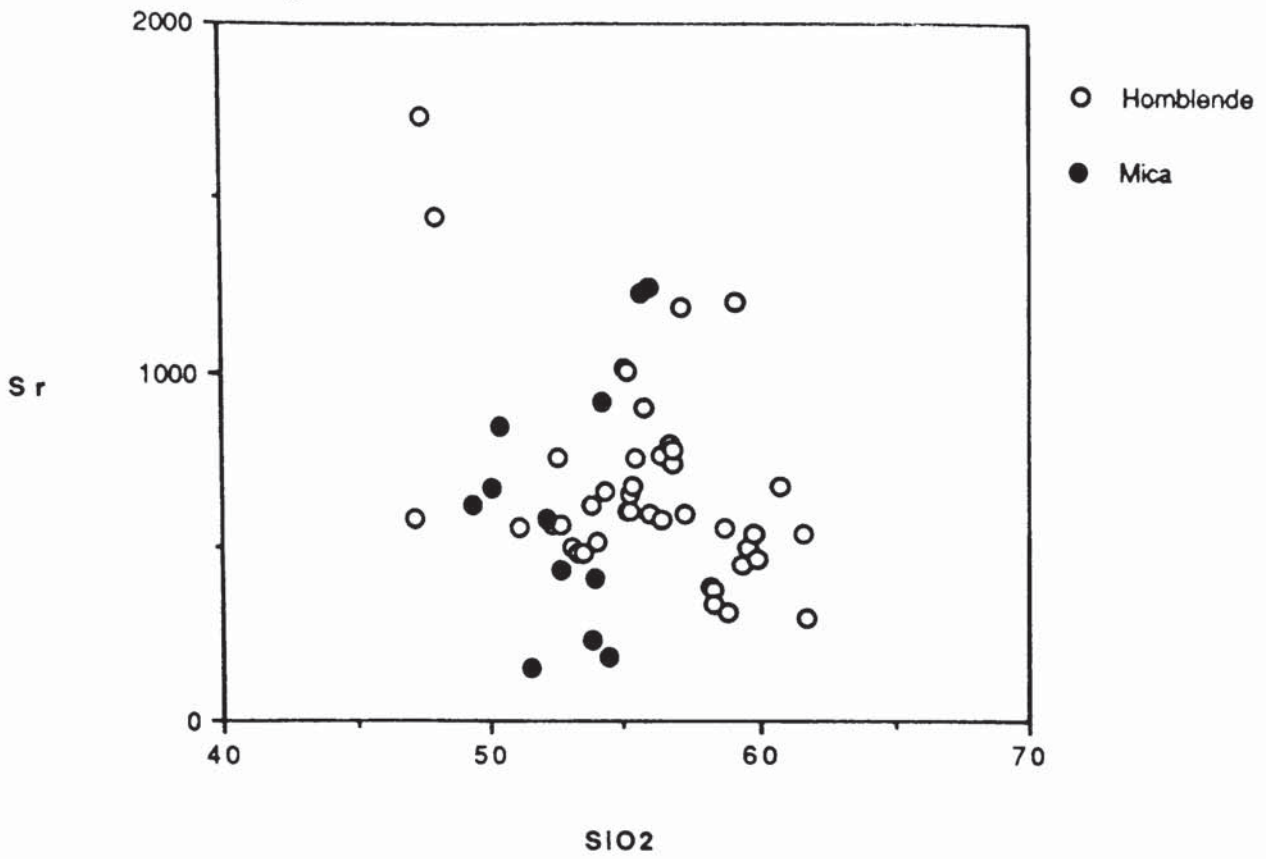
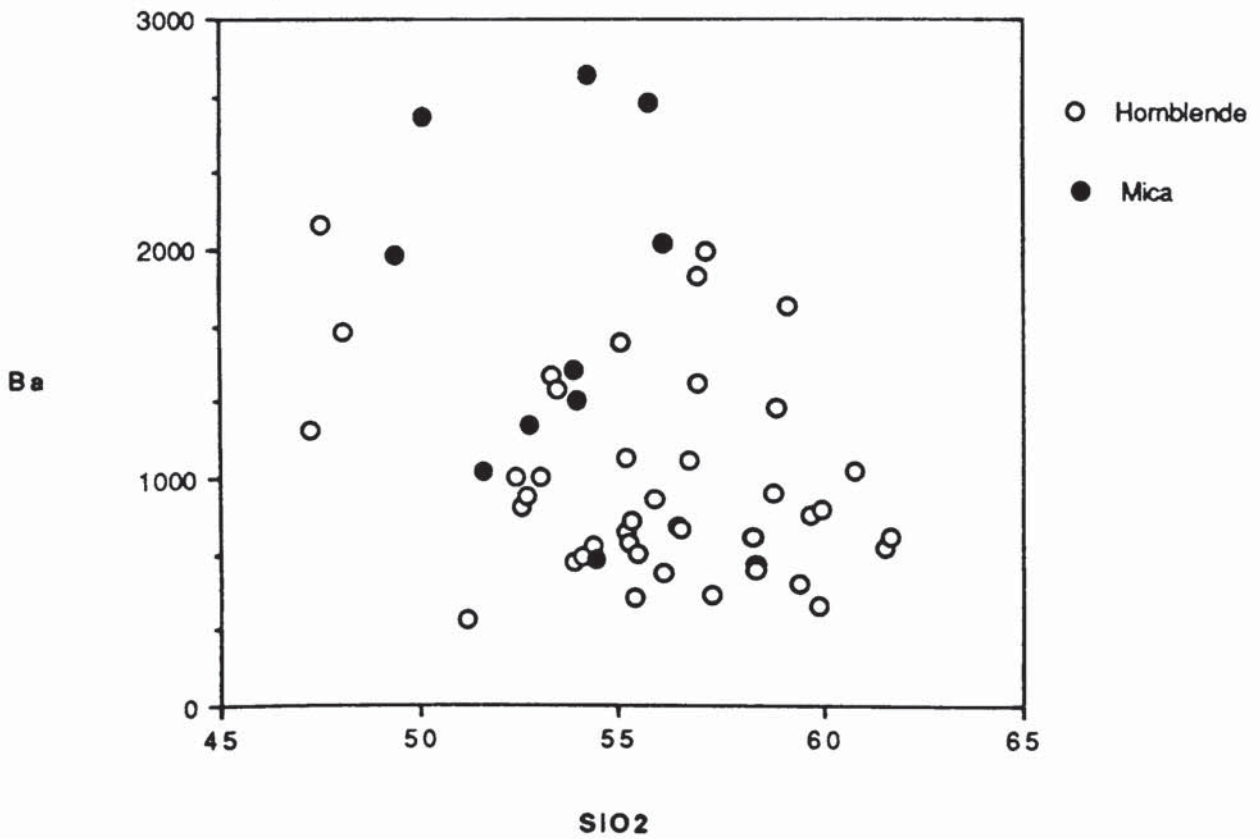


Fig. 3.2f



(0.81–0.53%) have less significant positive correlations with silica. Some of these correlations are shown in Figs 3.2(a–c) in which the mica lamprophyres show greater scatter for these oxides than the hornblende lamprophyres. Several mica lamprophyres are quartz normative (<3.00) and have normative corundum (<7.66). The majority are either olivine (<10.45) or diopside normative (<16.33) and none have any normative nepheline.

Abundances of transition (Ni <381ppm, Cr <886ppm, V <230ppm) and LIL (Ba <2745ppm, Rb <148ppm, Sr <1254ppm) elements in the mica lamprophyres are high but variable. The HFS element values (Zr <294 ppm, Nb <21ppm, Y <25ppm) are similar to those of the hornblende lamprophyres as are Th (21ppm) and U (7ppm). Zn, Cu and Pb values are also low (<150ppm). As with the hornblende lamprophyres, many of the trace elements show poor or scattered correlations against silica (Figs 3.2d–i). LREE contents are generally high (La <111ppm, Ce <231ppm, Nd <95ppm) but again variable and chondrite normalised REE profiles are steep with high Ce_n/Yb_n (47.0) and low Sm/Nd (0.154) ratios (Fig 3.3).

3.1.4) Comparative geochemistry of hornblende and mica lamprophyres

These rocks have very similar major element and normative compositions although the hornblende lamprophyres have a wider range of abundances for many major elements (Figs.3.2a–c). On a primordial mantle normalised spider diagram (Wood *et al.* 1979) hornblende and mica lamprophyres from the Criffell dyke swarm show very similar patterns, with a general increase in element abundance from right to left with increasing element incompatibility, except for Nb and Sr (Fig. 3.4). Both groups have very similar Nb, Ti, Zr, P and Y contents (Table 3.1) but the mica lamprophyres have higher maxima at Nd, U, Ba and Rb. Chondrite normalised REE plots (Nakamura, 1974) show that both mica and hornblende lamprophyres are strongly enriched in LREE (Fig 3.3). Neither group has a Eu anomaly but high volatile contents, particularly H₂O, recorded in lamprophyric magmas (Esperanca & Holloway, 1987) suggest oxidising

Fig. 3.3

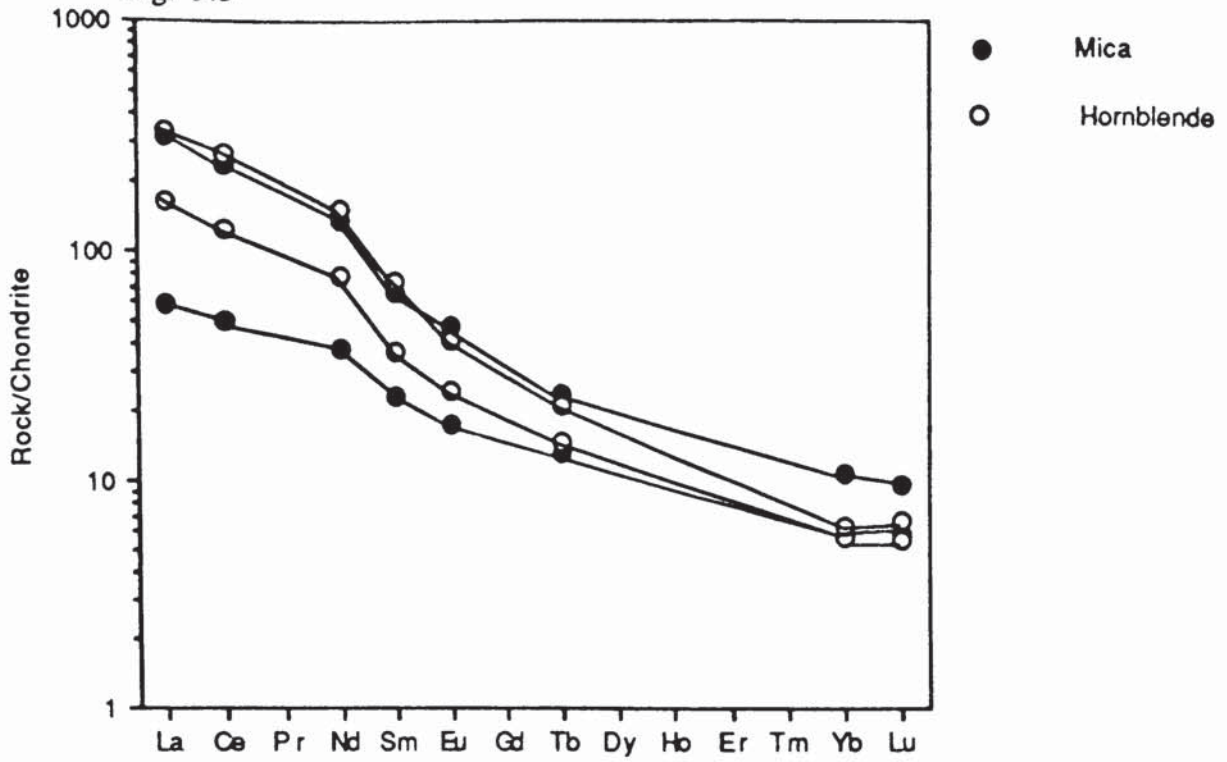
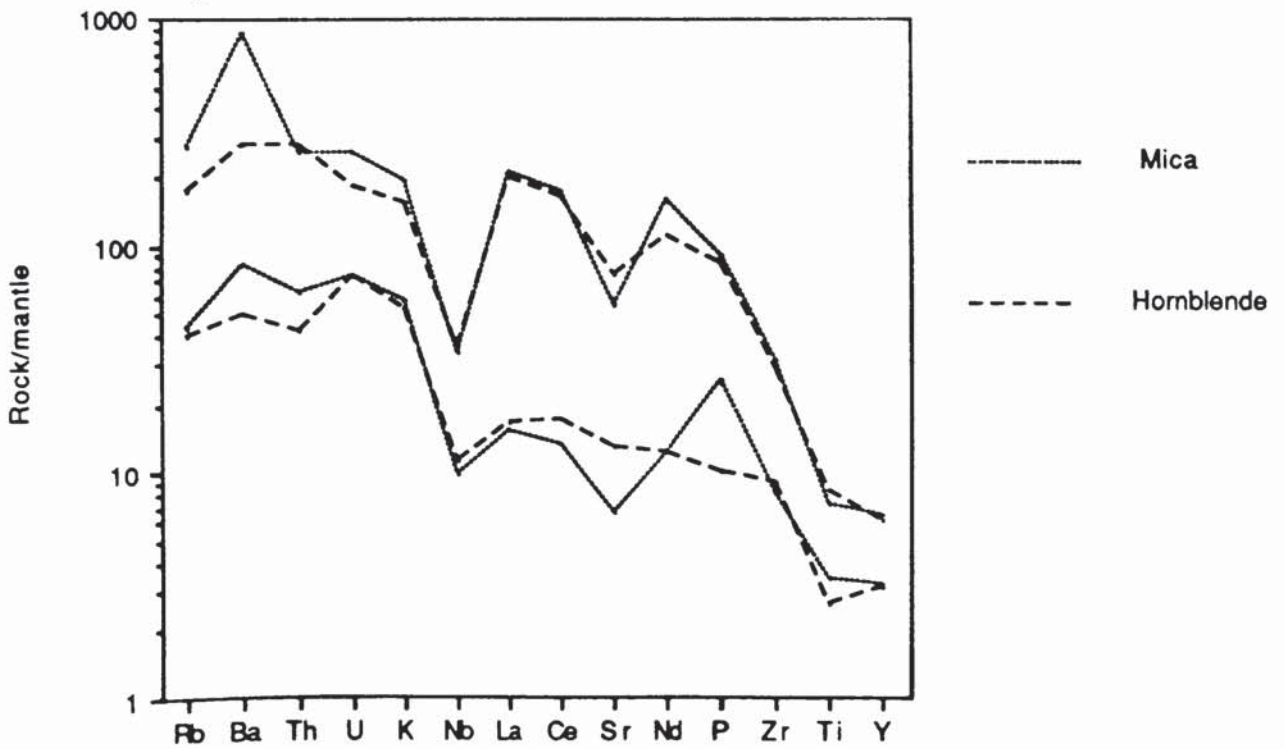


Fig. 3.4



conditions which may restrict the development of Eu^{2+} in such magmas (Fowler, 1988).

Figs 3.5(a–d) illustrate some of the differences between mica and hornblende lamprophyres in more detail. The mica lamprophyres are generally more potassic, with higher K_2O and $\text{K}_2\text{O}/\text{Na}_2\text{O}$, and are more enriched in LILE, with higher Ba/Nb and Rb/Sr, than the hornblende lamprophyres. The high LILE/Nb and LREE/Nb ratios, low Ti abundance and prominent Nb anomaly displayed by both groups are characteristic of magmas associated with active or recently terminated subduction (Pearce, 1983).

3.1.5) Mineral chemistry of Criffell lamprophyres

Polished slides were prepared for electron microprobe analysis of the mafic minerals (micas, amphiboles and clinopyroxenes) from several hornblende and mica lamprophyres. These were analysed for their major element content as well as several minor elements (Ni and Cr) using a wave-length dispersive (WD) CAMECA microprobe at the University of Edinburgh. Analytical data are listed in appendix with analytical methods described in appendix A.

3.1.5.1) Micas

The core and rim points of several mica phenocrysts were analysed from sample 1370, together with two core–rim profiles across suitably orientated basal sections. These micas are all phlogopites, based upon the criteria of Deer et al. (1963) with Mg/Fe ratios >2 , with the exception of the outermost (ie: closest to the outer rim) analyses of the two traverses which have Mg/Fe ratios of 1.9 (Appendix F). In figure 3.6, the data for the micas from the Criffell lamprophyres falls within the phlogopite field, in agreement with that defined by the data for other CAL micas in Rock (1984). In addition, total Si+Al+Ti is always > 8.0 and the mean TiO_2 content is 3.68%, indicating that they can be classed as normal titanphlogopites (Rock, 1982) and fall within the range of 62 minette micas listed by Bachinski & Simpson (1984).

Fig. 3.5a

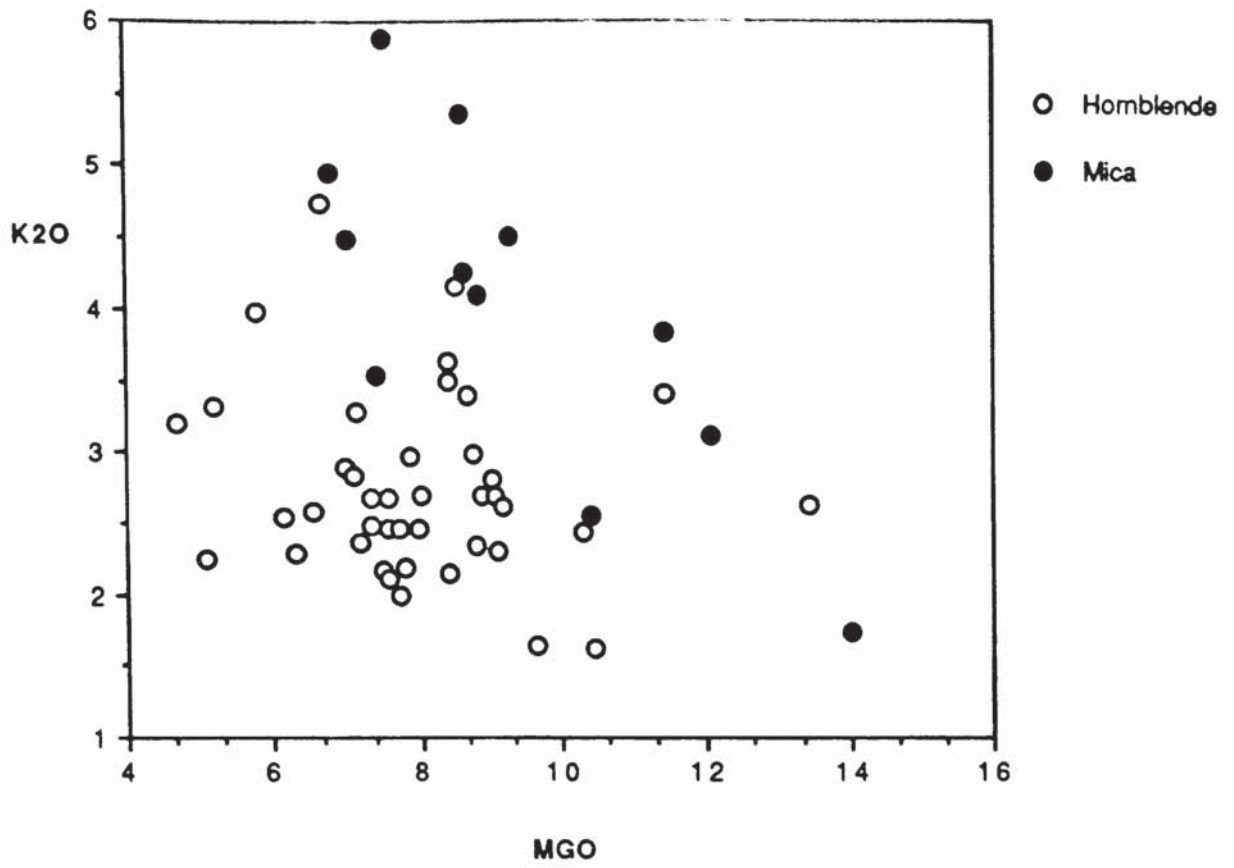


Fig. 3.5b

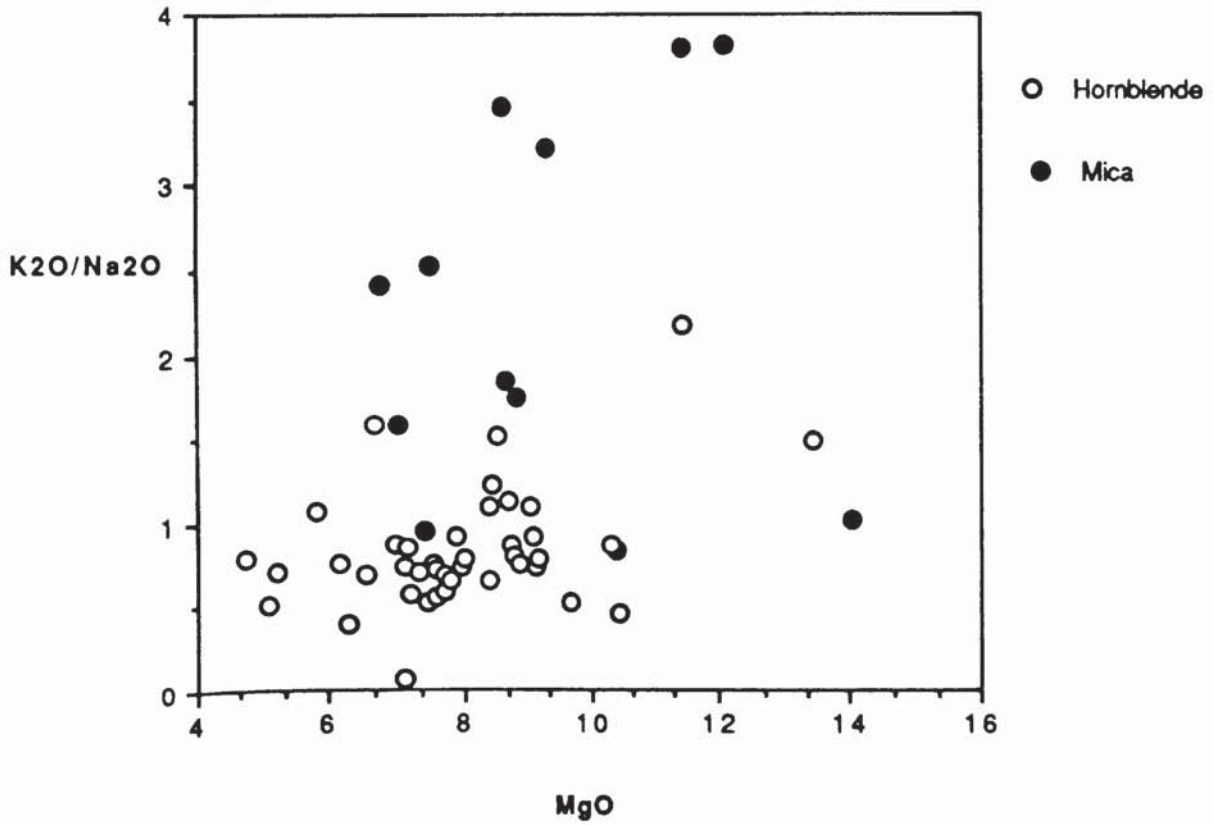


Fig. 3.5c

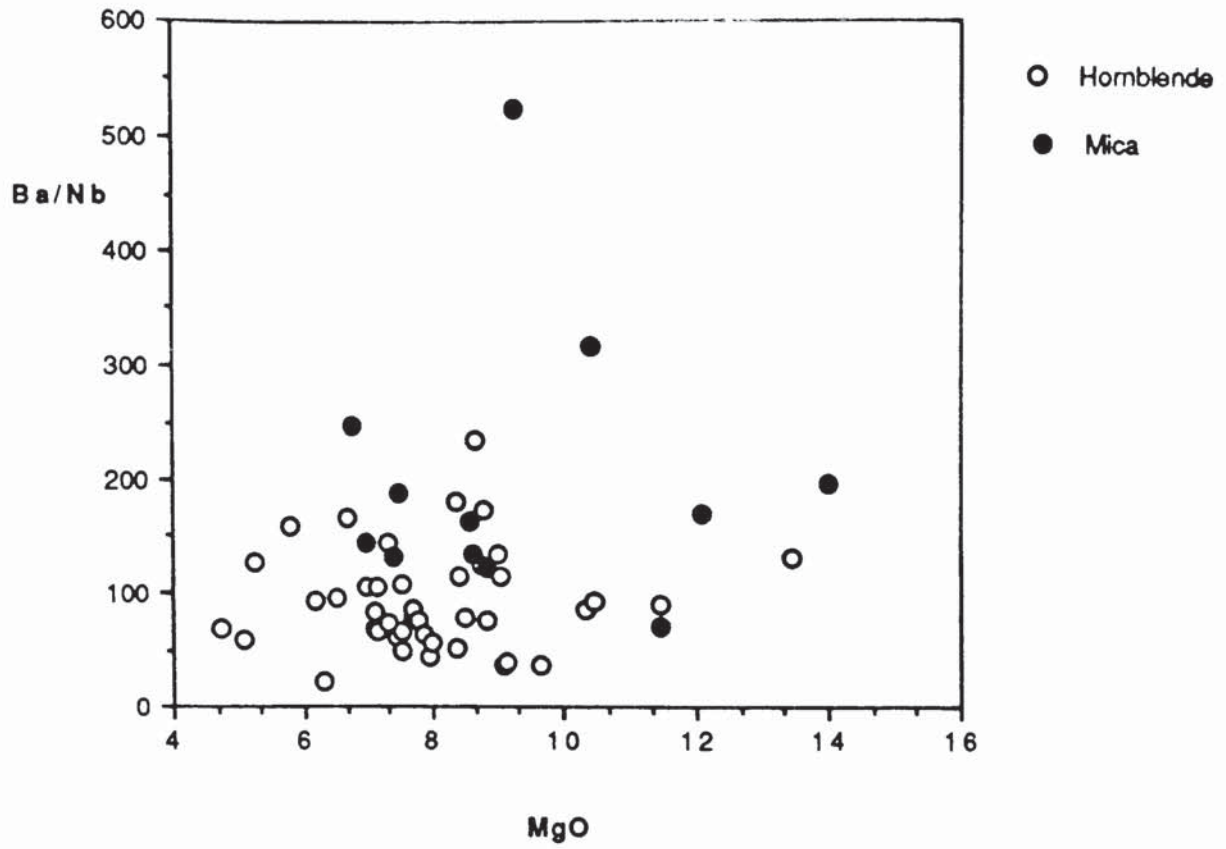
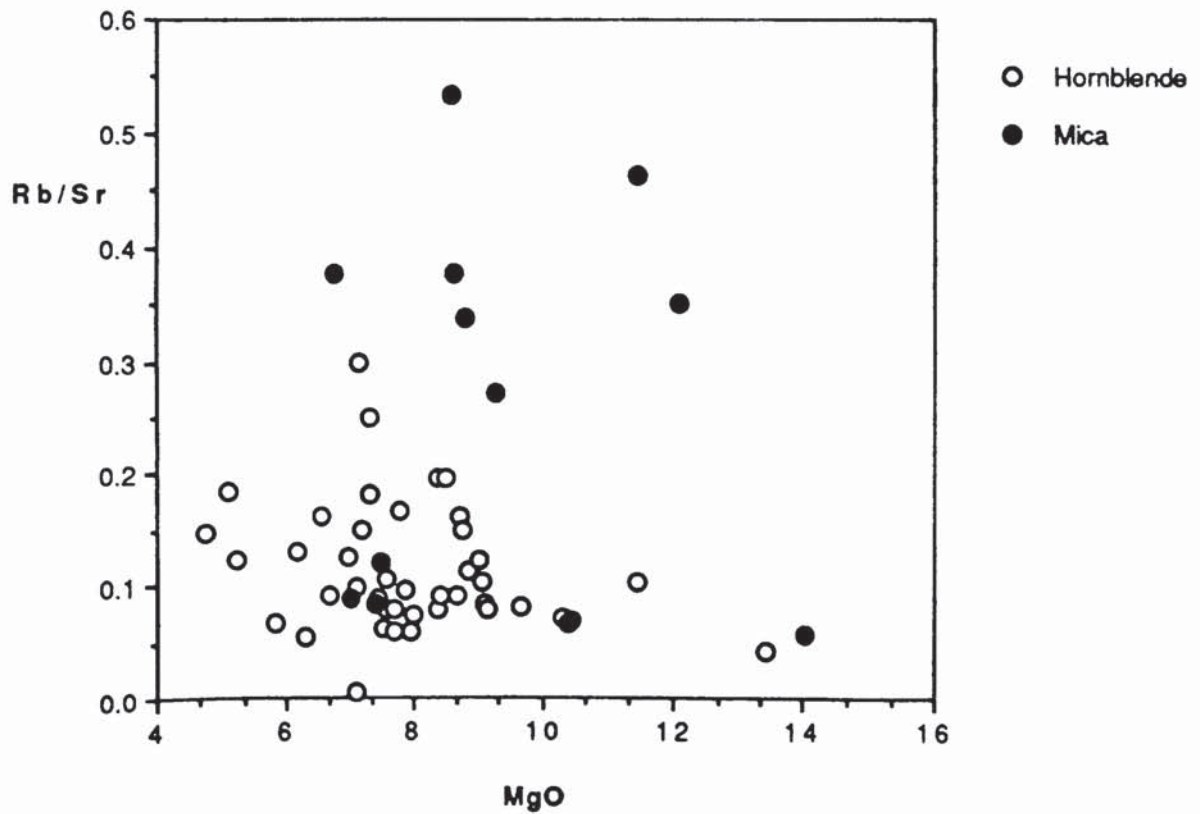


Fig. 3.5d



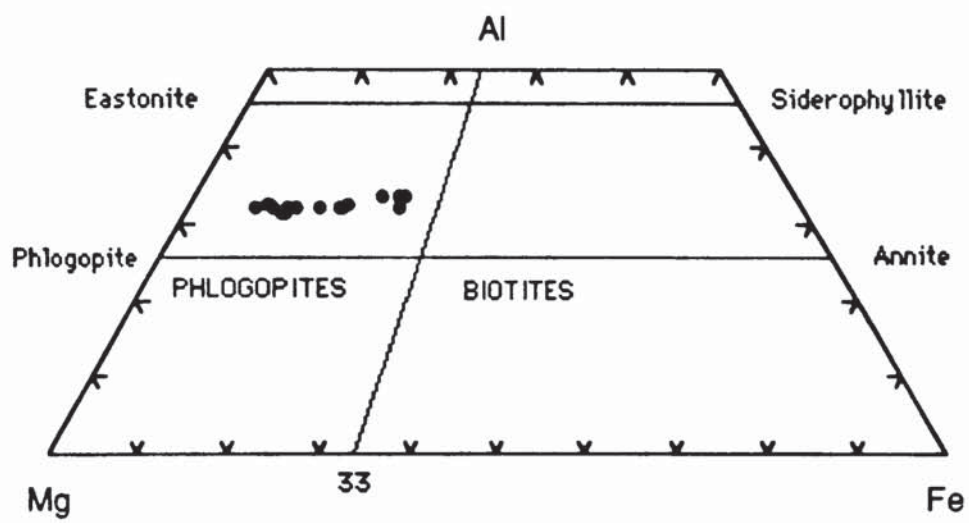


Fig. 3.6

The data from two traverses across selected basal sections are plotted in figures 3.7(a-d), with data from selected core and rim points plotted in figures 3.8(a-d). From core to rim the micas show a simple, normal, zoning pattern (Bachinski & Simpson, 1984) with MnO and TiO₂ contents increasing while Mg[#] and K₂O abundances decrease, as do NiO and Cr₂O₃ contents. These compositional variations are similar to those reported from other CAL micas by Bachinski & Simpson (1984), although phlogopites described from the CALs of the Mexican Volcanic Belt (MVB) (Wallace & Carmichael, 1989) show a decrease in TiO₂ towards the rim, highlighting the compositional variation observed in some CAL micas (Rock 1984, 1991). The Cr₂O₃ contents of the Criffell lamprophyres (0.01–1.0%) overlap with the values reported by Wallace & Carmichael, (1989) and Luhr & Carmichael (1981) for phlogopites from primitive, mantle derived, minettes in the MVB (0.8% & 0.6-1.6% respectively).

Full descriptions of CAL mica chemistry and comparisons with other potassic rocks are given by Bachinski & Simpson (1984), Schulze *et al.* (1985) and Rock (1984, 1987, 1991) and thus will not be repeated here.

3.1.5.2) Clinopyroxenes

Core and rim points of several clinopyroxene phenocrysts and microphenocrysts from several samples were analysed for the major elements and for Ni and Cr. In figure 3.9, the analyses mainly fall across the diopside-endiopside-salite-augite field boundaries within the pyroxene quadrilateral, again in a similar position to the field described for CAL clinopyroxenes in Rock (1984) although the Criffell lamprophyre clinopyroxenes appear to be slightly more magnesian. Core to rim variations in Cr₂O₃, MnO, Al₂O₃ and TiO₂ in the Criffell lamprophyre clinopyroxenes are illustrated in figures 3.10(a-d) and it is clear that there is considerable compositional overlap between core and rim in these clinopyroxenes. Compositionally the Criffell lamprophyre clinopyroxenes are similar to those described from the Newmains hornblende lamprophyre (Macdonald *et al.* 1986) and from phlogopite and hornblende lamprophyres from the Colima Graben in the MVB (Allen & Carmichael, 1984; Luhr & Carmichael, 1981). Of particular note

Fig. 3.7a

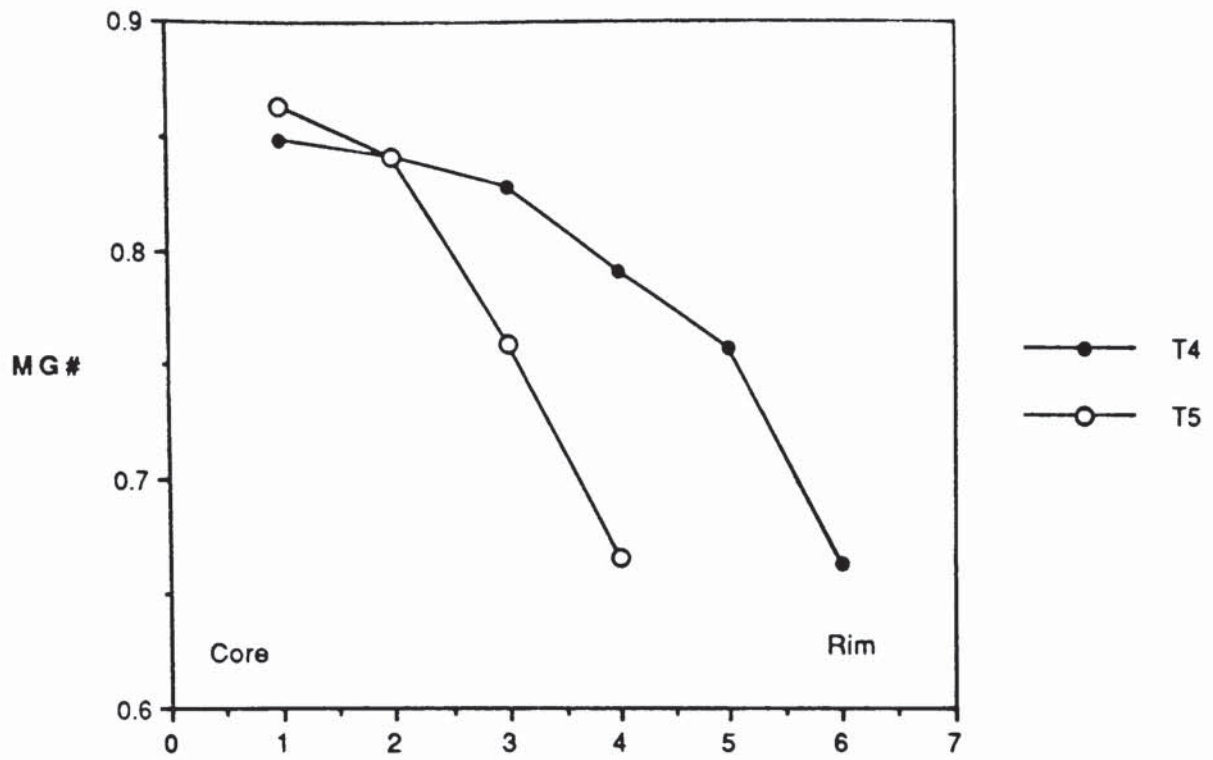


Fig. 3.7b

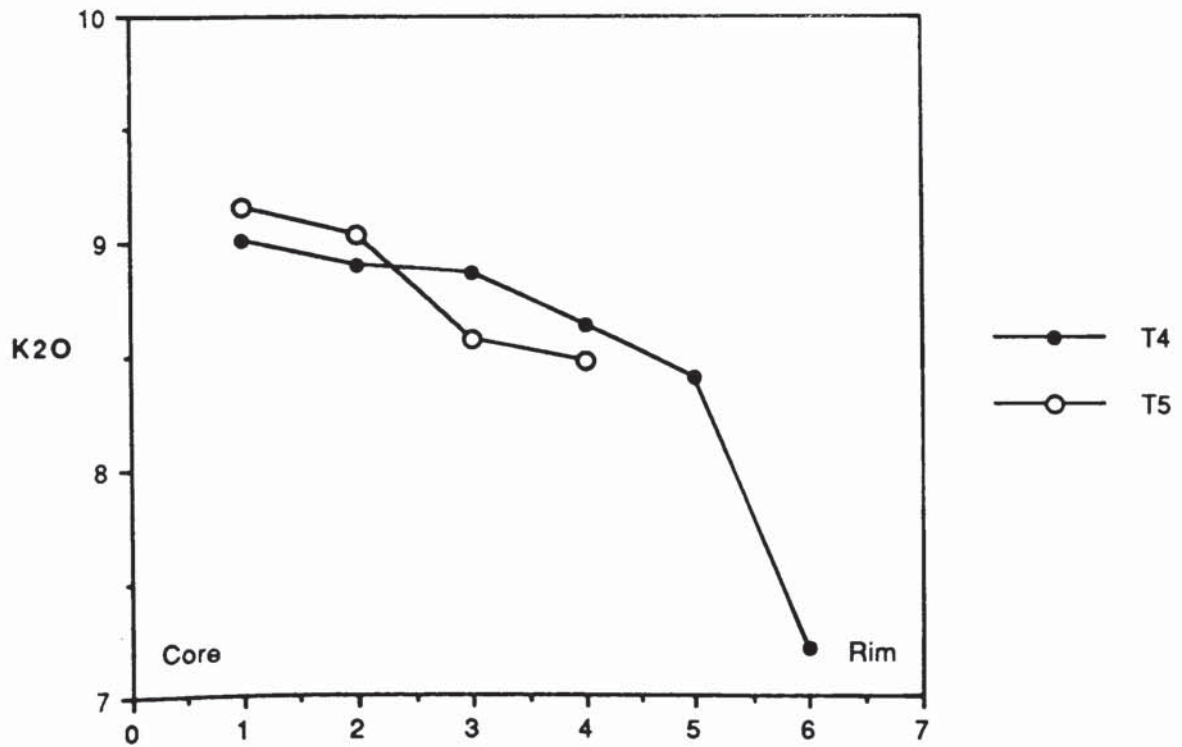


Fig. 3.7c

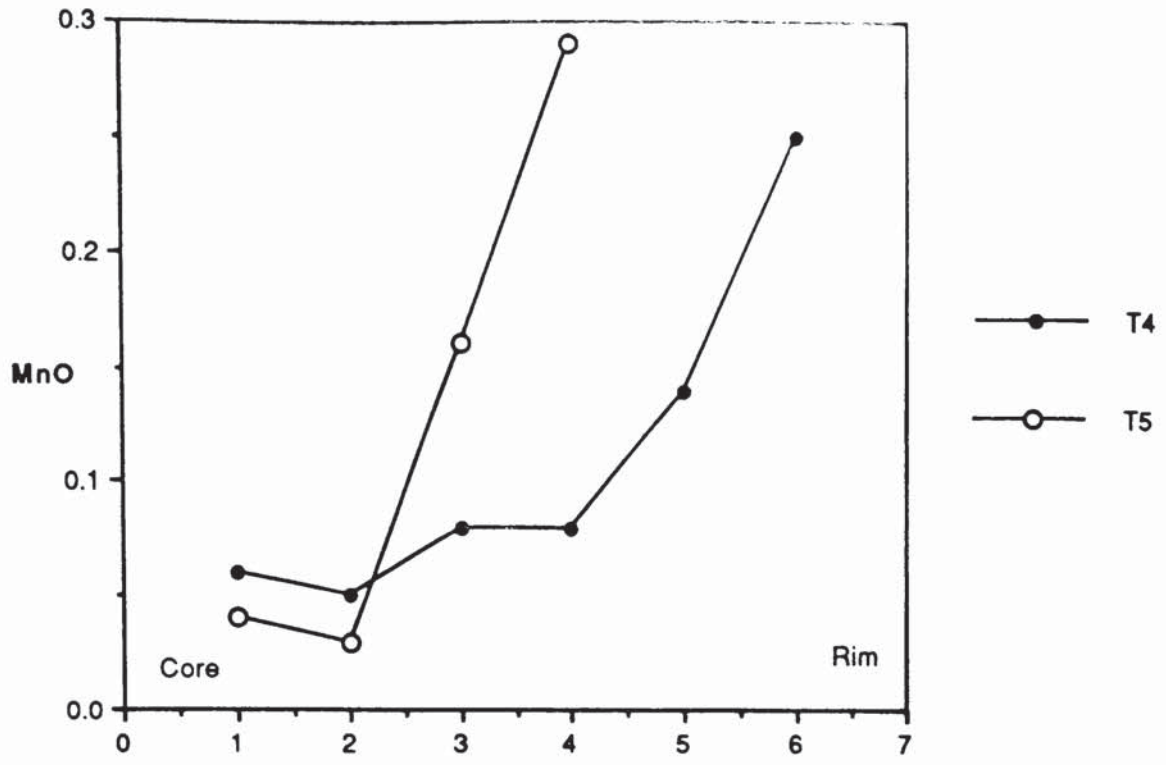


Fig 3.7d

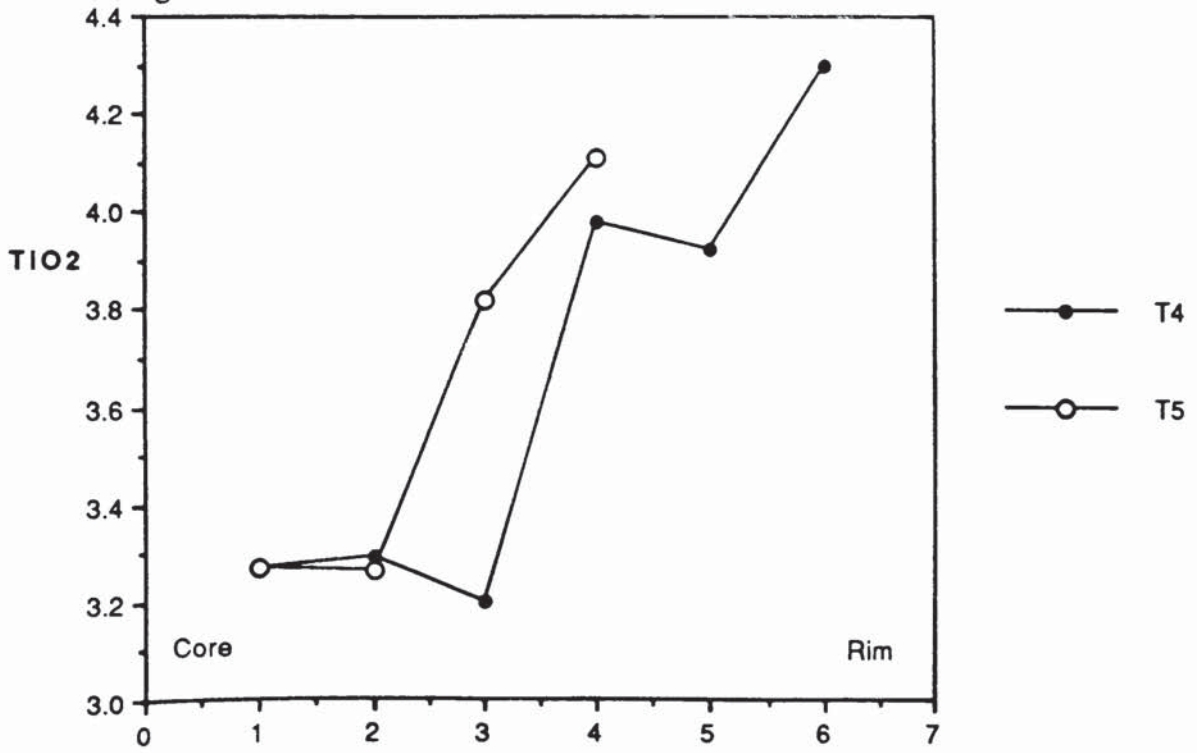


Fig. 3.8a

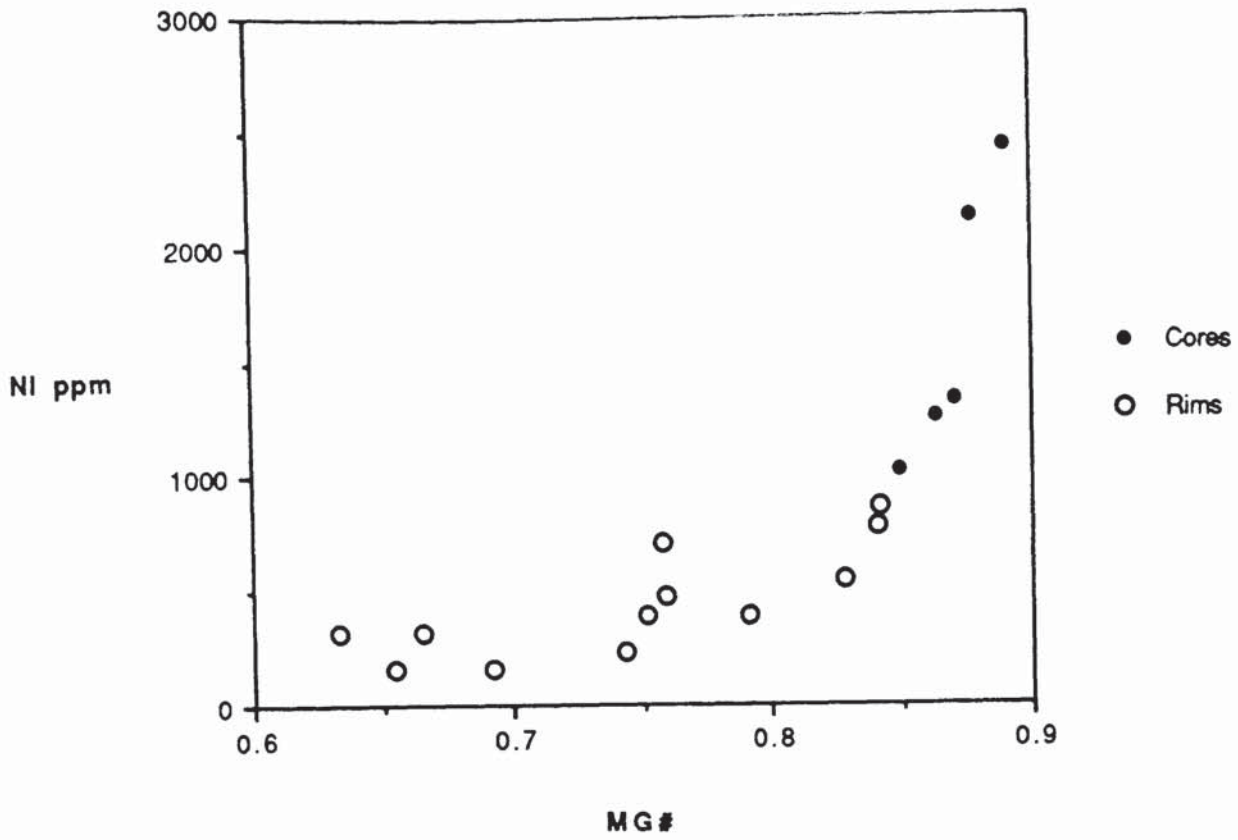
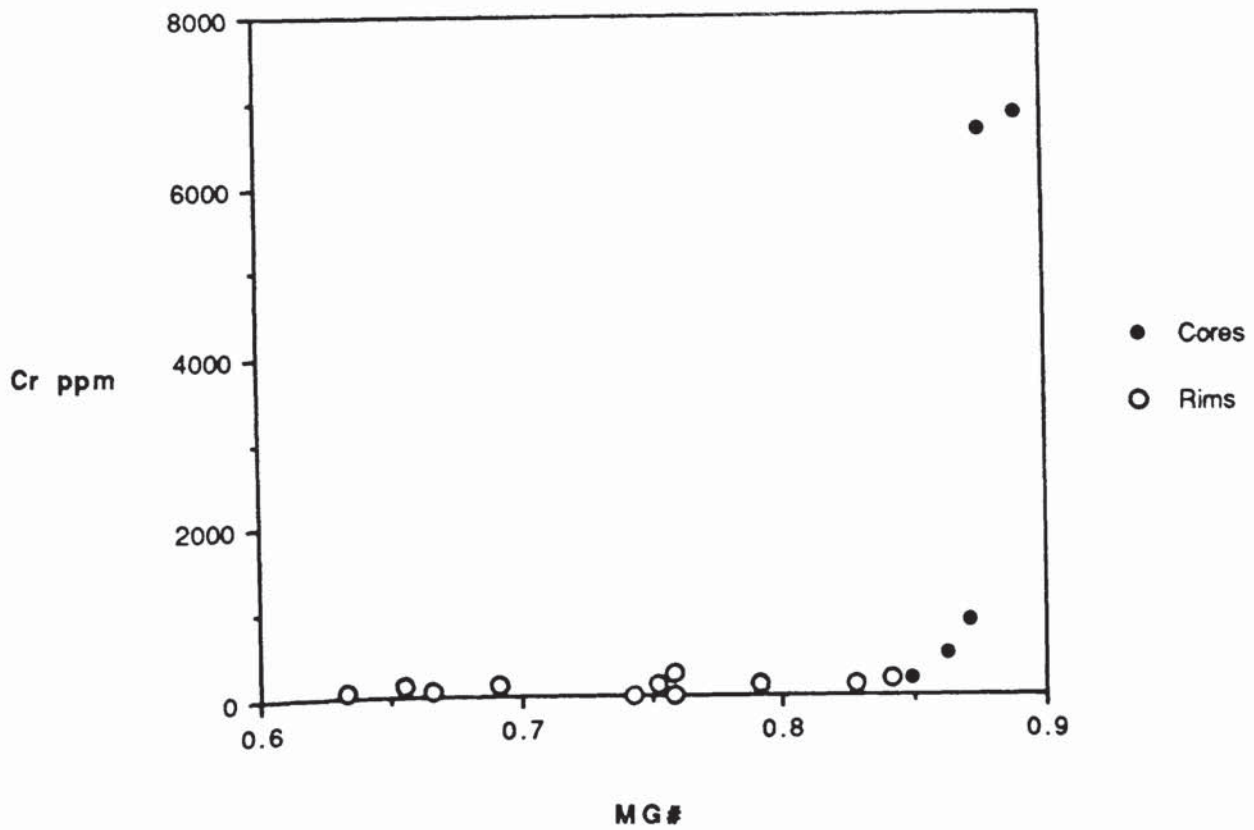


Fig. 3.8b



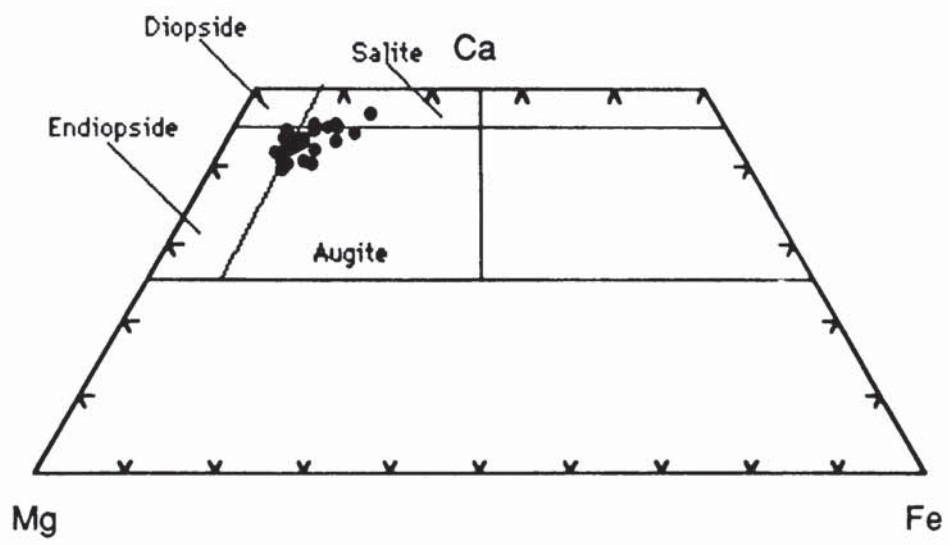


Fig. 3.9

Fig. 3.10a

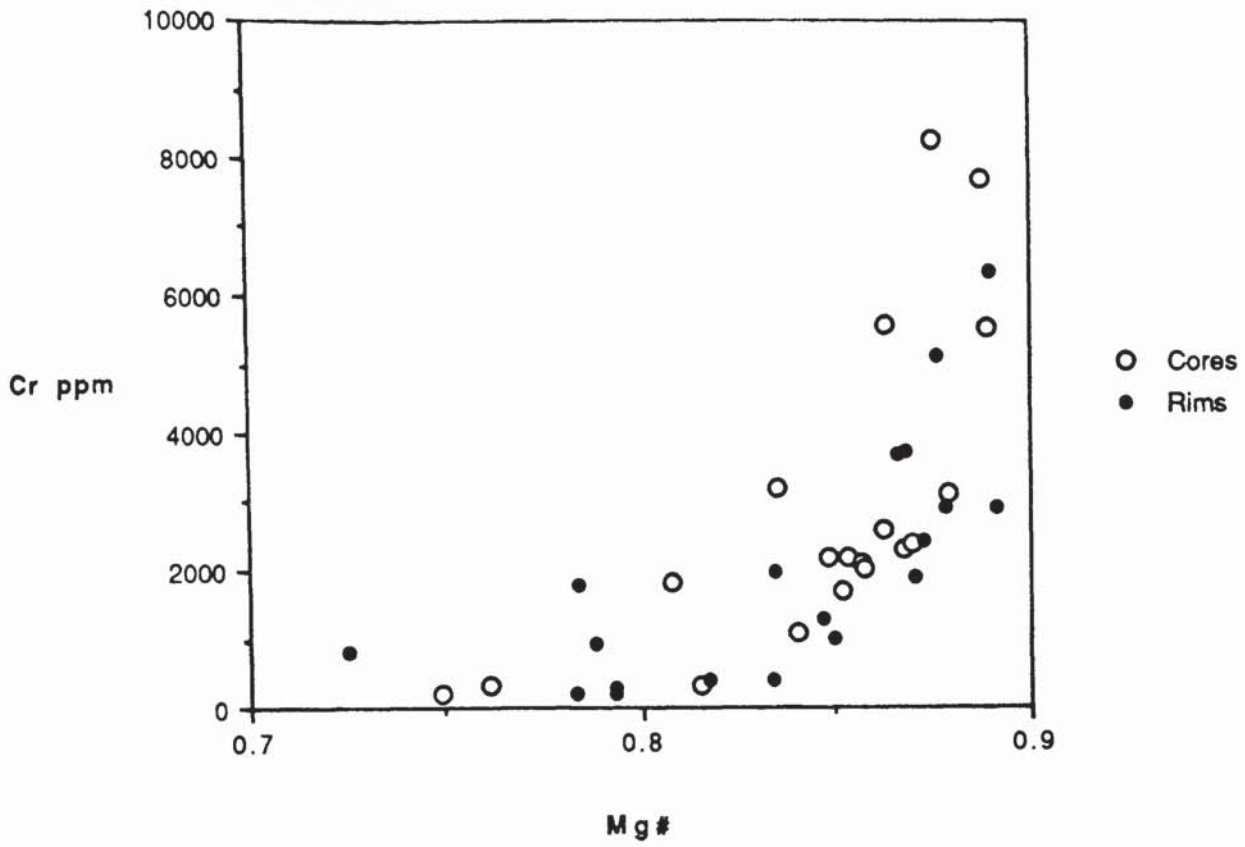


Fig. 3.10b

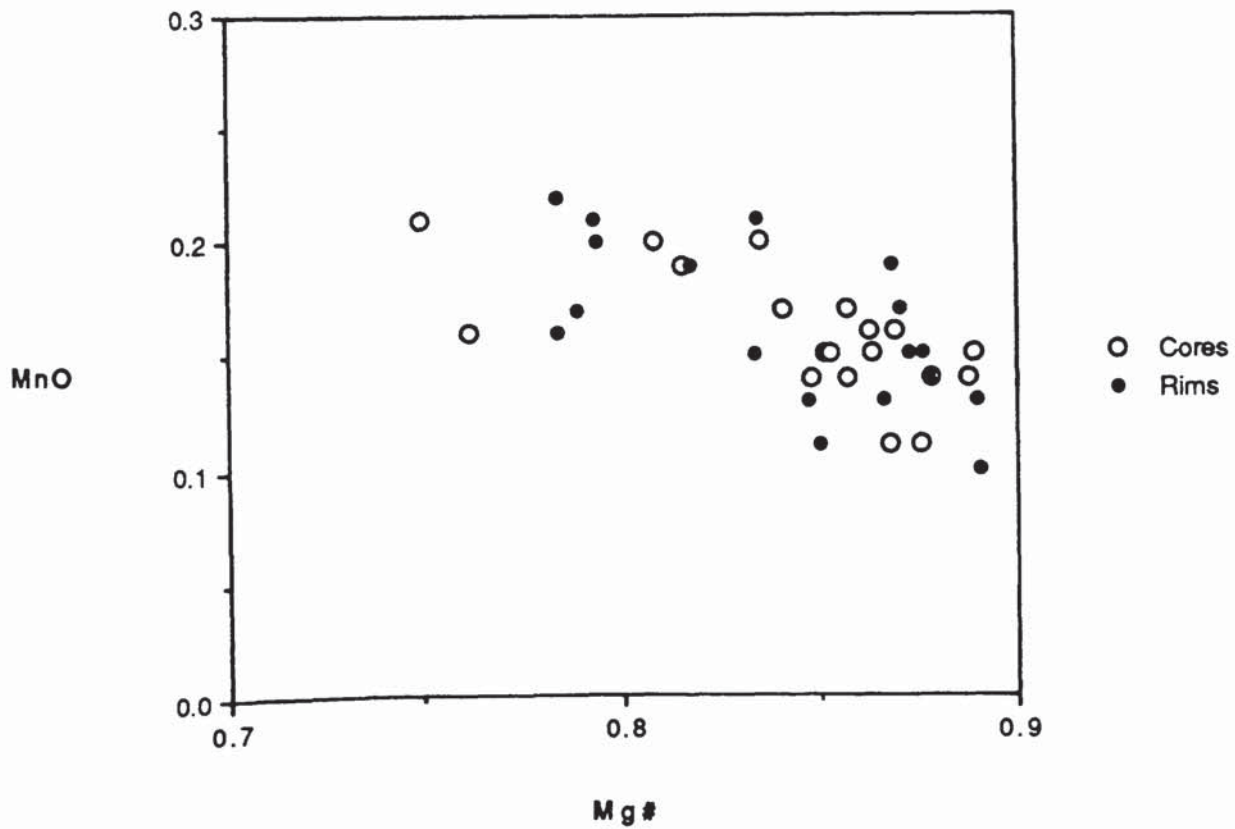


Fig. 3.11a

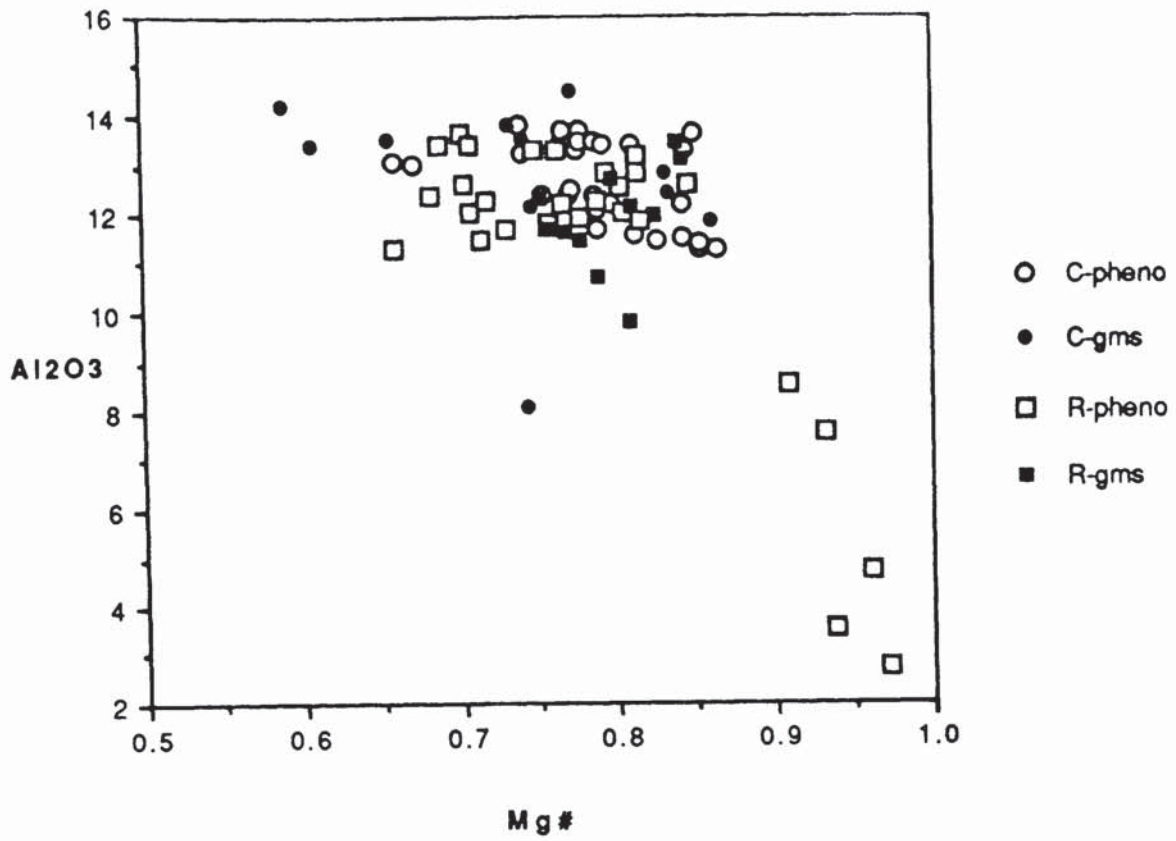


Fig. 3.11b

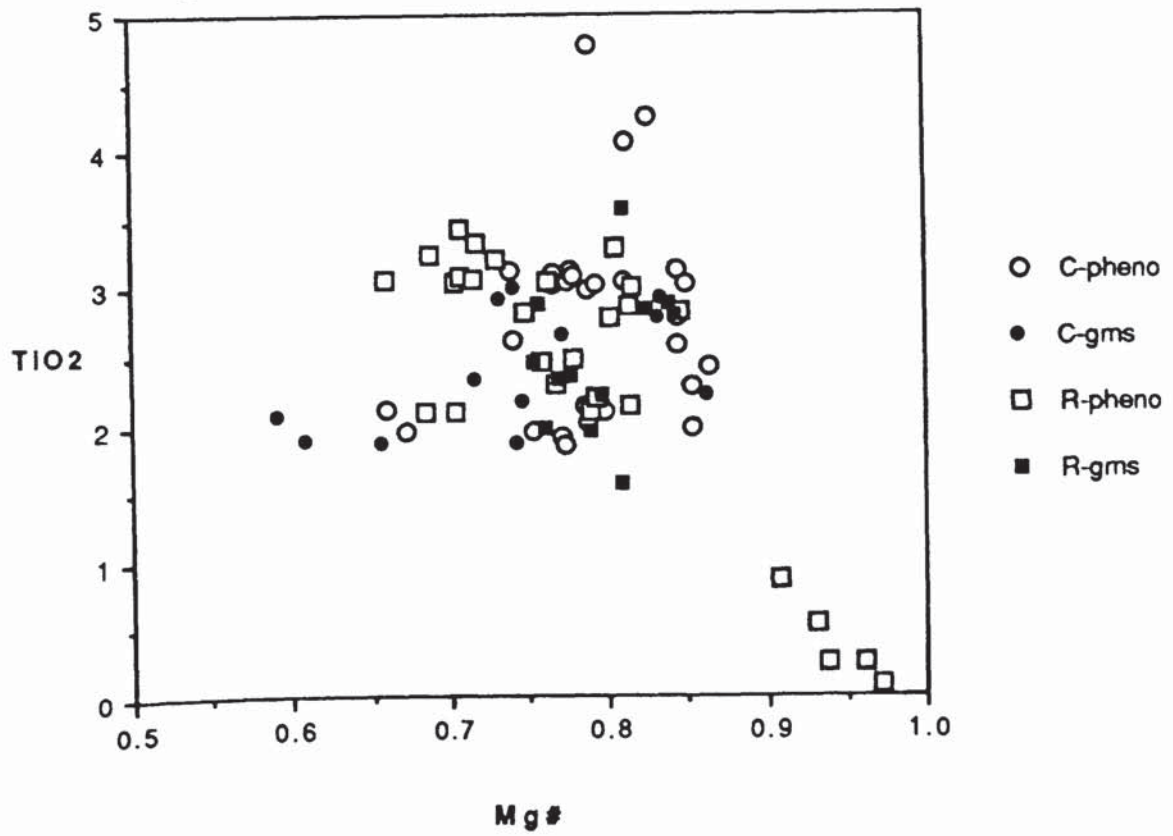


Fig. 3.11c

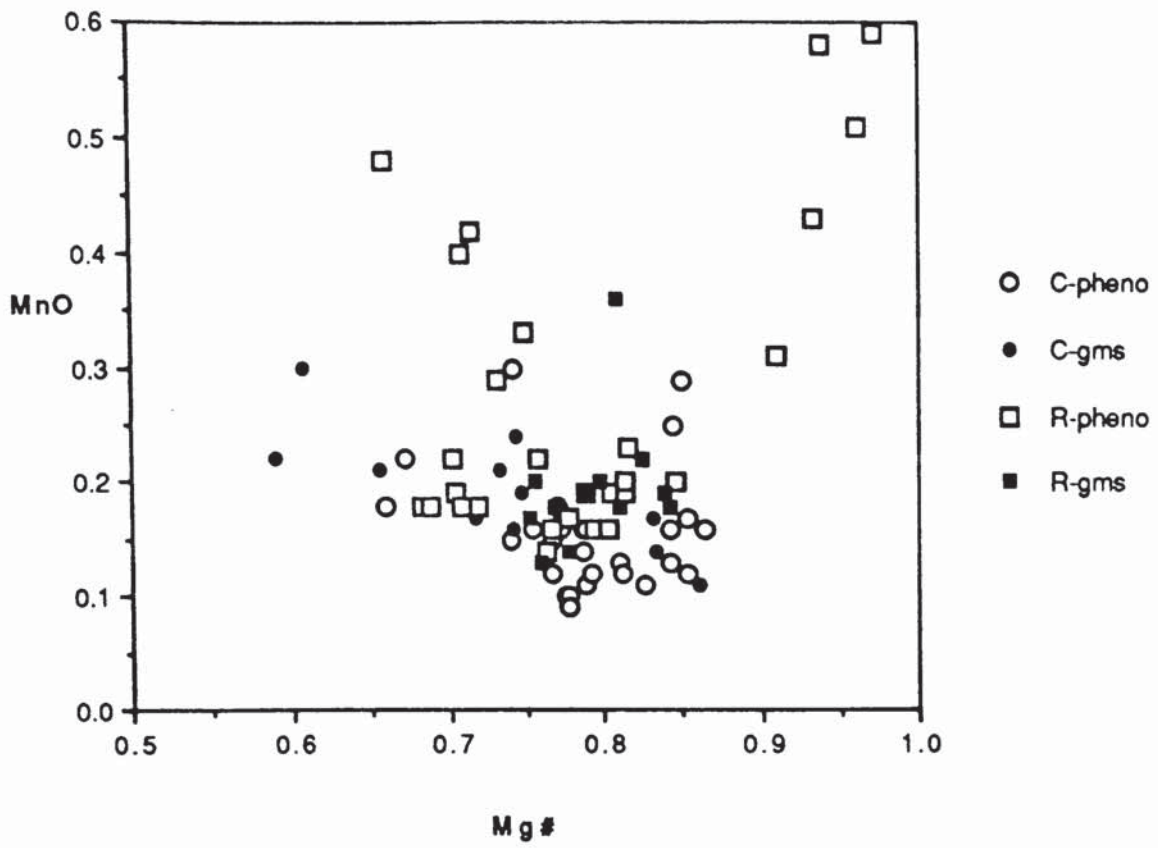
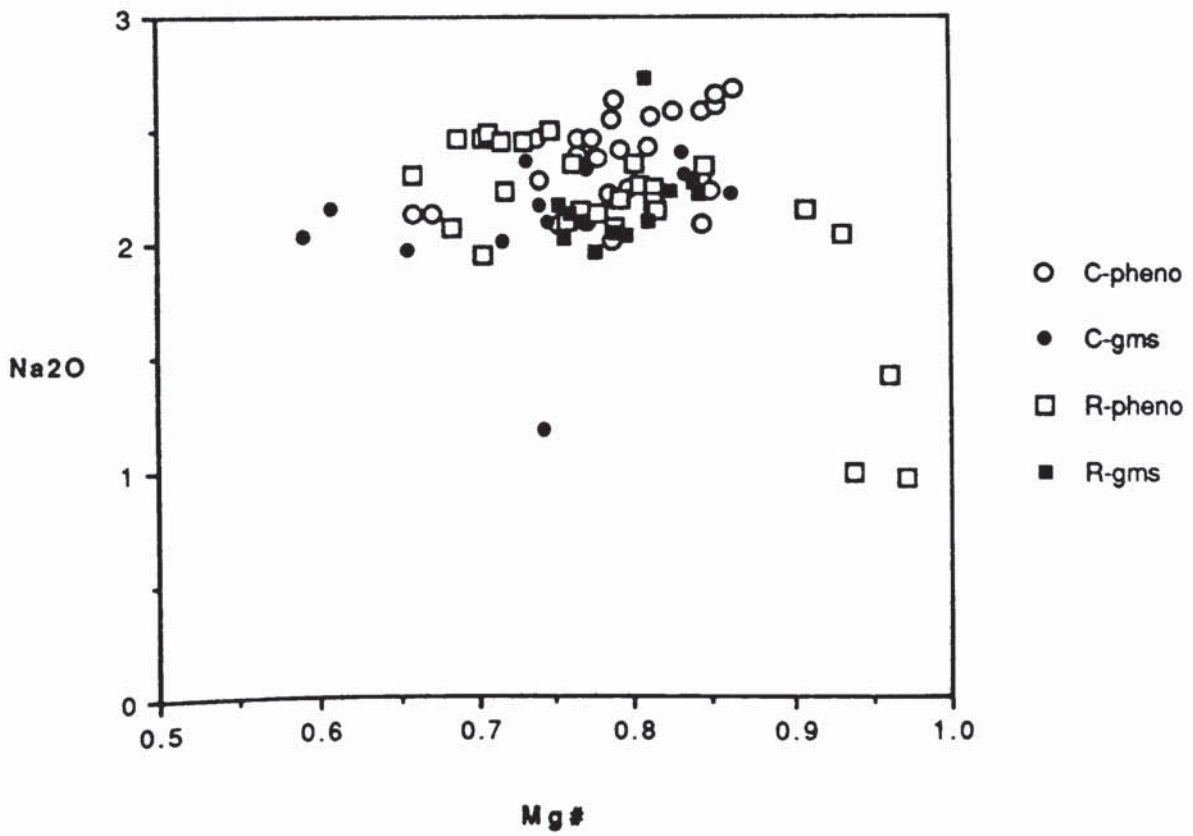


Fig. 3.11d



are the Cr₂O₃ contents of the Criffell lamprophyre clinopyroxenes (mean 0.36%, maximum of 1.21%) which overlap with values reported from the Colima lamprophyres (maximum of 0.87%, Allen & Carmichael, 1984). Such values are comparable to those observed in clinopyroxenes in garnet peridotite xenoliths described from minettes in Colorado (Ehrenberg, 1979). Full descriptions of CAL clinopyroxene chemistry are given by Rock (1984, 1987, 1991).

3.1.5.3) Amphiboles

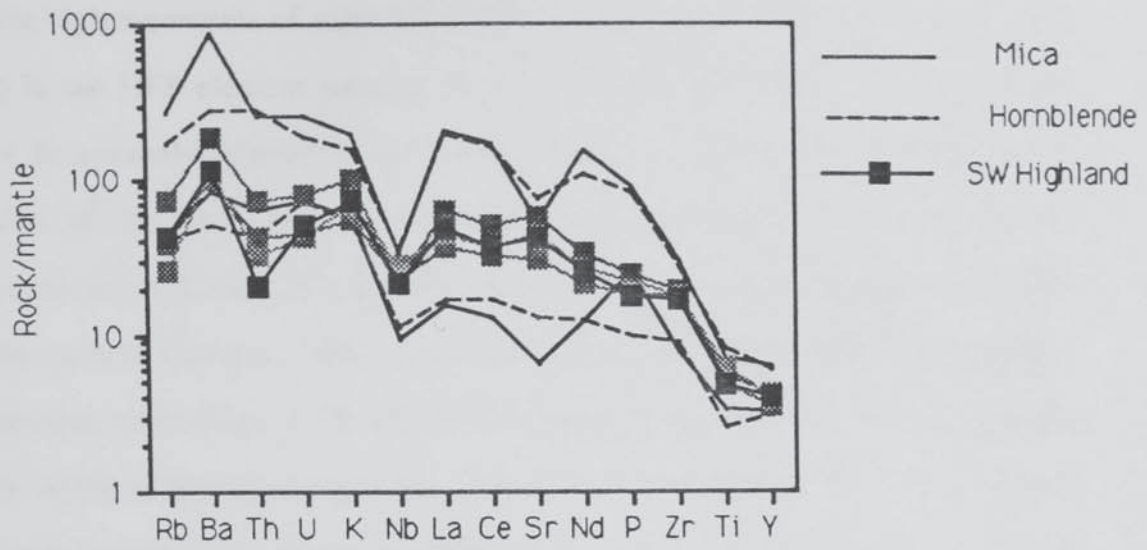
Core and rim points of amphiboles phenocrysts and groundmass crystals were analysed from several hornblende lamprophyres. The analyses were processed using the Amphcalc recalculation programme kindly provided by Dr N. M. S. Rock, described by Rock & Leake (1984) and classified according to the IMA recommendations (Leake, 1978). The majority of the analyses can be classed as members of the hornblende and hastingsite sub-groups of the calcic amphiboles, with the majority of the cores being potassian-titanian and/or magnesio hastingsites. Rims are more varied but are mainly titanian magnesio-hastingsites, magnesio-hornblendes or, in some instances (e.g. 1326), tremolitic hornblendes. Hastingsitic and hornblendic compositions are amongst the most common types of amphiboles described from CAL (Rock, 1984, 1987, 1991). Core to rim variations of Al₂O₃, TiO₂, MnO and Na₂O versus Mg# for the Criffell lamprophyre phenocryst and groundmass amphiboles are illustrated in figures 3.11(a-d) In general core and rim compositions, both within each group and also between each group, show a large degree of overlap, except for some rims which show a trend towards low Mg# with high in MnO (figure 3.11a-d) However, the rims of amphibole phenocrysts in sample 1326 show a distinctly different trend to the other core and rim compositions. In detail these examples show higher Mg# coupled with high MnO but low Na₂O, Al₂O₃ and TiO₂ and analyses are classed as ferri-magnesio-hornblendes and ferri- or ferrian-tremolitic hornblendes. These variations may be due to reaction of the rims of the amphibole phenocrysts with late stage magmatic fluids or to variations in the composition and/or fO₂ of this fluid (Deer *et al.* 1963). The

compositions of the Criffell lamprophyre amphiboles are comparable to those reported from the Newmains hornblende lamprophyre (Macdonald *et al.* 1986) and to hornblendes described from lamprophyres in the Colima Graben by Allen & Carmichael (1984). A full description of CAL amphibole chemistry is given by Rock (1984, 1987, 1991).

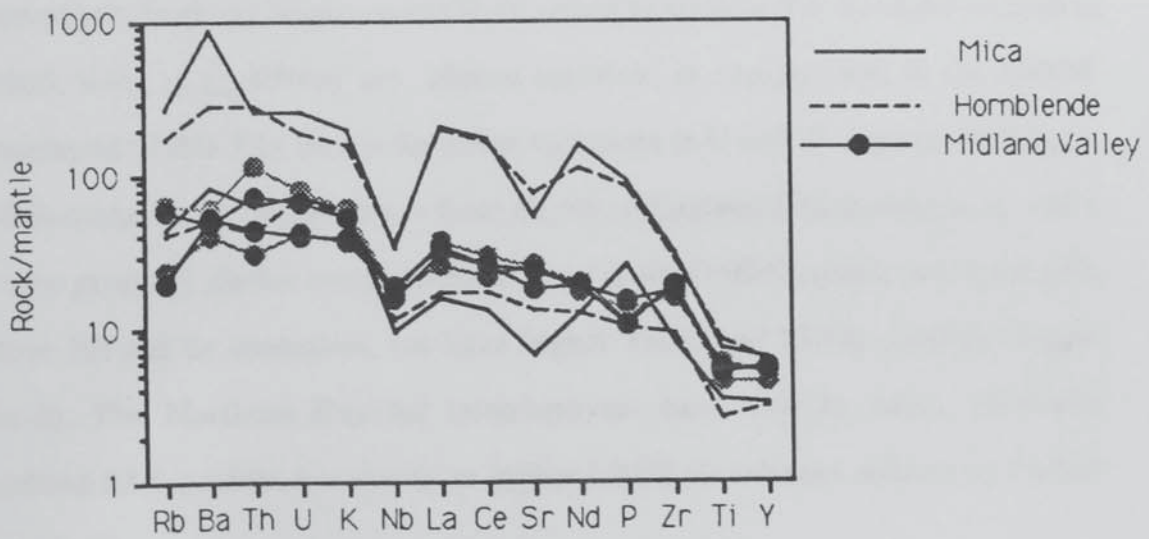
3.2) Comparisons between the Criffell lamprophyres and other late Caledonian basic magmas.

Large volumes of primitive basaltic and andesitic magmas were extruded during the late Caledonian in Scotland, particularly in the Midland Valley and SW Highlands. These Siluro–Devonian magmas were probably produced in a volcanic arc, related to the NW directed subduction of Iapetus ocean lithosphere under Scotland, during the lower Palaeozoic (Thirlwall, 1981, 1982, 1983, 1986). Thirlwall (*op. cit.*) reported that basalts and andesites exhibit a trace element and isotopic zonation normal to the trace of the subduction zone with the magmas from the SW Highlands enriched in LILE and LREE elements compared to samples from the Midland Valley. He argued that the high Ni, Cr and MgO contents of the basalts indicated their primitive nature, thus minimising the role of crustal contamination in producing variations in isotopic signatures and trace element abundances. He further suggested that the chemical and isotopic variations in the basaltic rocks reflected geochemical heterogeneities in the late Caledonian mantle under Scotland.

The lavas have similar major element compositions to the lamprophyres but are generally less magnesian and less potassic (Rock *et al.* 1986a). These lavas and the lamprophyres have very similar, broadly overlapping "spidergram" patterns with prominent Nb anomalies, variable but high LILE and LREE abundances and similar Ti and Y values (Figs 3.12a-b). However the lamprophyres have a much wider compositional spread than the lavas which, by contrast, have a relatively restricted range. The mica lamprophyres extend to higher LILE and LREE contents than the lavas, including the enriched lavas from the SW Highlands, although there is also



3.12a



3.12b

considerable overlap. Abundances of the HFS element are very similar for both groups with complete overlap of the patterns at Nb, Ti and Y. The hornblende lamprophyres also have higher contents of some LILE (Th, U) and the LREE, and show the same overlap in the HFS element patterns. The SW Highland lavas have a pronounced positive Sr anomaly relative to the LREE, which contrasts with the negative Sr anomalies of the lamprophyres, and have been related to the presence of old, metasomatically enriched, lithospheric mantle under the SW Highlands (Thirlwall, 1983; Menzies & Halliday, 1988). The lamprophyres have high REE content relative to the basaltic rocks (Figs. 3.13). The SW Highland lavas have higher LREE contents than the Midland Valley samples but lower HREE abundances. Both the mica and hornblende lamprophyres extend to higher LREE abundances than the lavas but have overlapping HREE abundances.

3.2.1) Comparisons with other late Caledonian lamprophyres

The Criffell lamprophyres are part of a phase of late Caledonian lamprophyric magmatism which occurs in the Southern Uplands of Scotland and Northern England. Lamprophyres from the Wigtown and Kirkcudbright areas of SW Scotland (Barnes *et al.* 1986; Rock *et al.* 1986a) are almost identical in composition to the Criffell lamprophyres (Table 3.1), except for minor variations in U and Th contents. Similarly, late Caledonian mica lamprophyres from Northern England (Macdonald *et al.* 1985) also have generally similar compositions to those of the Criffell swarm, with prominent negative Nb and Sr anomalies, but have higher Th, U and LREE contents (Figure 3.14a–b). The Northern England lamprophyres have similar, steep, chondrite normalised REE profiles but extend to higher LREE abundances relative to Criffell lamprophyres.

The Criffell lamprophyres have many geochemical characteristics in common with other late Caledonian basic rocks in Scotland and Northern England, the most prominent of which are high LILE/Nb and LREE/Nb ratios characteristic of subduction related magmas (Pearce, 1983; Macdonald *et al.* 1985). The implications are that

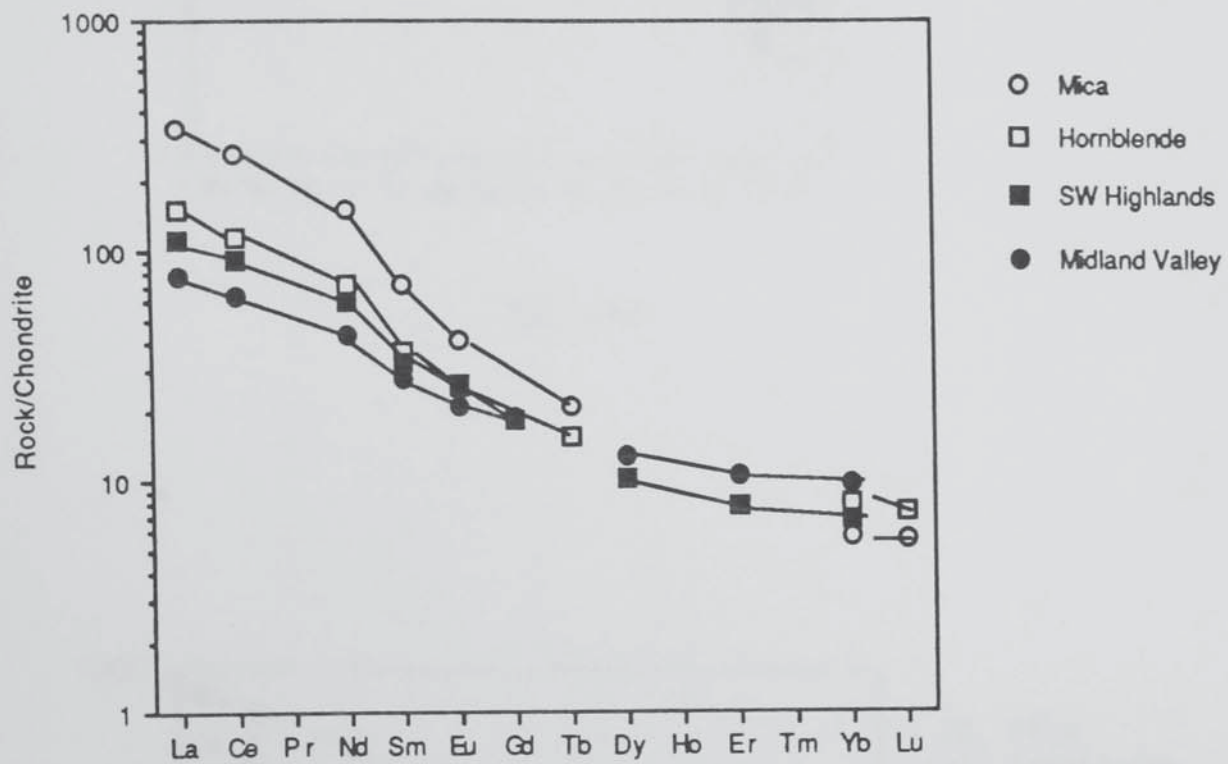


Fig. 3.13

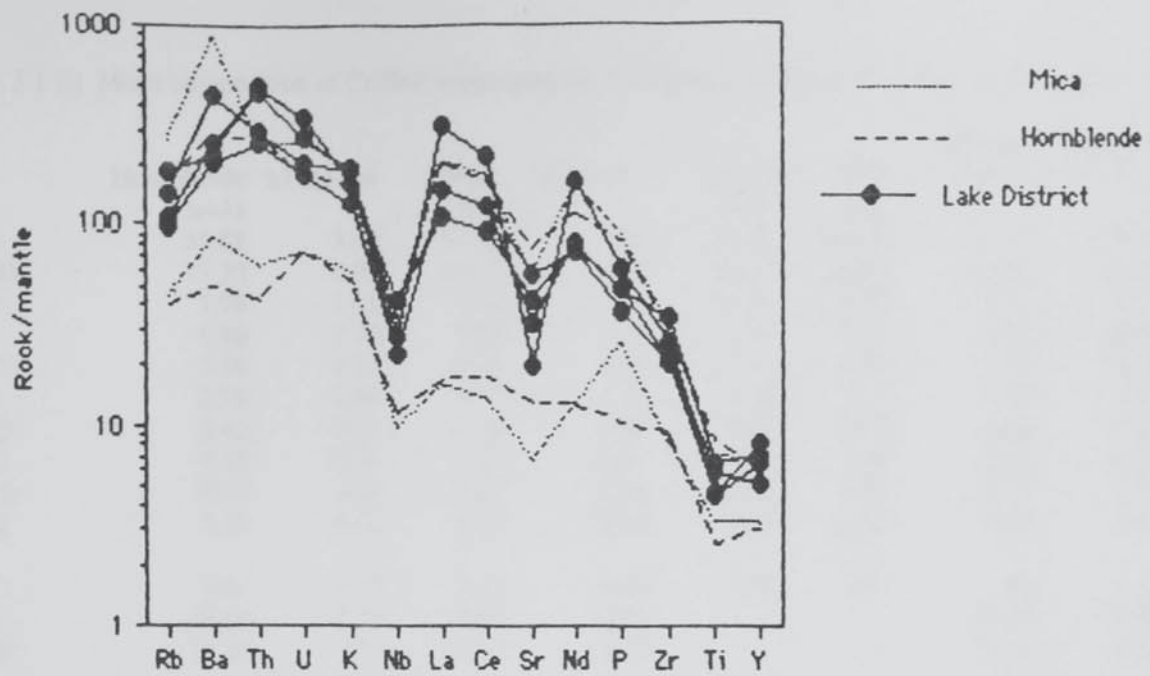


Fig. 3.14a

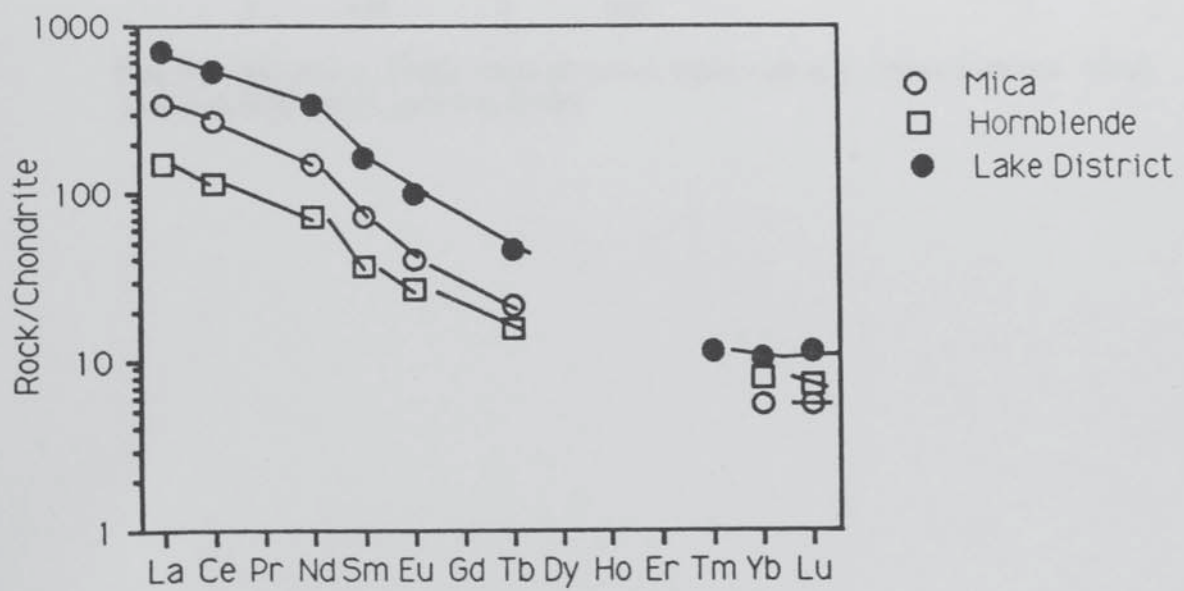


Fig. 3.14b

Table 3.1 [i] Mean composition of Criffell lamprophyres, Caledonian basalts & Wigtown lamprophyres.

	Homblende n=41	±1 std dev	Mica n=6	±1 std dev	SWH lava	MV lava	Wigtown Hnbde	Wigtown Mica
SiO ₂	55.85	3.51	53.61	2.36	54.95	54.66	54.30	50.40
Al ₂ O ₃	15.22	0.99	14.37	1.56	16.46	16.86	14.90	12.70
MgO	7.98	1.66	9.42	2.91	5.37	5.09	7.20	8.30
CaO	5.68	1.72	6.05	2.32	6.91	8.36	5.80	6.60
Fe ₂ O ₃	7.39	1.24	8.34	1.43	7.95	8.10	7.20	7.60
K ₂ O	2.74	0.64	4.02	1.53	2.34	1.43	2.20	3.00
Na ₂ O	3.42	0.71	2.15	1.02	3.82	3.72	3.60	2.20
TiO ₂	1.13	0.30	1.22	0.35	1.32	1.28	0.90	0.92
P ₂ O ₅	0.45	0.28	0.67	0.10	0.45	0.27	0.33	0.71
MnO	0.11	0.02	0.12	0.03	0.10	0.10	0.12	0.12
LOI	3.61	1.13	6.15	4.14	3.32	4.47	3.40	7.30
DX	48.56	8.14	43.07	13.77			47.70	43.30
MG#	75.12	2.33	75.57	3.77			72.30	74.70
Ni	181	68.15	224	128	158	143	109	166
Cr	346	113.32	420	320	308	302	389	520
V	175	74.26	178	65.23	168	175	170	200
Rb	68	21.83	91	42.8	40	34	46	86
Sr	665	293	739	476	1103	515	818	401
Ba	971	446	2082	705.6	1045	437	1296	2141
Y	20	3.36	20	3.76	20	25	23	23
Nb	11	3.53	13	5.11	14	9	8	9
Zr	174	38.17	221	82	200	197	143	150
La	32	26.06	40	25.32	37	22		
Ce	77	56.16	84	54.07	81	49		
Nd	38	24.77	49	25.2	38	25		
Th	9	4.95	11.5	5.22			6	9
U	3	0.89	4	0.93			4	5

Data from Barnes et al. (1986); Thirlwall (1981); Macdonald et al. (1985); Luhr et al. (1989); Leat et al. (1987) and Turpin et al.(1988)

Representative compositions of calc-alkaline lamprophyres.

Table 3.1 [ii]

	Mica Lakes BiD	Mica SW England 7997	Mica Colima SAY-8H	Mica Hercynian K19
SiO ₂	46.8	49.89	48.24	51.75
Al ₂ O ₃	11.2	12.1	12.43	15.03
MgO	9.55	10.75	11.54	7.27
CaO	7.2	7.29	8.83	6.95
Fe ₂ O ₃	7.82	7.43	7.5	7.6
K ₂ O	5.12	7.13	4.38	2.51
Na ₂ O	0.63	1.63	2.55	2.7
TiO ₂	1.03	1.08	1.36	0.96
P ₂ O ₅	0.89	2.04	1.13	0.48
MnO	0.29	0.17	0.15	0.1
LOI	8.79	6.24		5.37
DX				
MG#				
Ni	340	264	282	370
Cr	427	396	600	365
V	144		235	
Rb	126	299	35	87.6
Sr	738	1173	2189	650
Ba	3446	6425	2060	850
Y	31	40	21	
Nb	14	27	14	
Zr	227	624	359	
La	105	123	40.1	40
Ce	220	237	91	87
Nd	105	106	46	45
Th	29	51	3.23	18
U	9.4	12.9	1.13	4.15

Some LOI values and trace element not available

processes related to subduction, including fluid transfer of elements and the stabilisation of new phases in the mantle wedge, have played a significant role in creating the trace element characteristics of these magmas. The Criffell lamprophyres are however enriched in several LILE and LREE elements compared to most late Caledonian basaltic lavas and are geochemically similar to other late Caledonian lamprophyres.

3.2.2) Comparison with calc-alkaline lamprophyres from other areas.

A significant body of geochemical data has been accumulated in recent years for calc-alkaline lamprophyres of various ages from a number of orogenic belts and related settings around the world. These compilations include data for lamprophyres from the Canadian Archaean (Wyman & Kerrich, 1989); the Tertiary of the Colorado Plateau (Alibert *et al.* 1986); the Hercynian of central Europe (Turpin *et al.* 1988) and the Caledonian of northern Britain (Rock *et al.* 1988). The calc-alkaline lamprophyres from the Colima graben of Northern Mexico (Luhr & Carmichael, 1981; Luhr *et al.*, 1989) and the Hercynian fold belt of SW England (Thorpe *et al.* 1986; Leat *et al.* 1987) are of particular interest as they were emplaced in a tectonic environment similar to that of the late Caledonian in Scotland.

The first of these is an area of late Tertiary crustal extension in the western part of the Mexican Volcanic belt associated with subduction of the Cocos and Riviera plates beneath the southern margin of North America. In this area Pliocene and late Pleistocene hornblende and mica lamprophyres occur associated with minor alkali basalts and larger volumes of calc-alkaline basalts and andesites. The second is a post-orogenic setting characterised by regional uplift and mild extension (Thorpe, 1987) where mica lamprophyres occur spatially associated with transitional calc-alkaline to alkaline basaltic volcanics and large volumes of granitic magma (Cornubian batholiths). Figs (3.15a-d) compare the geochemistry of the Colima and SW England rocks with the Criffell lamprophyres.

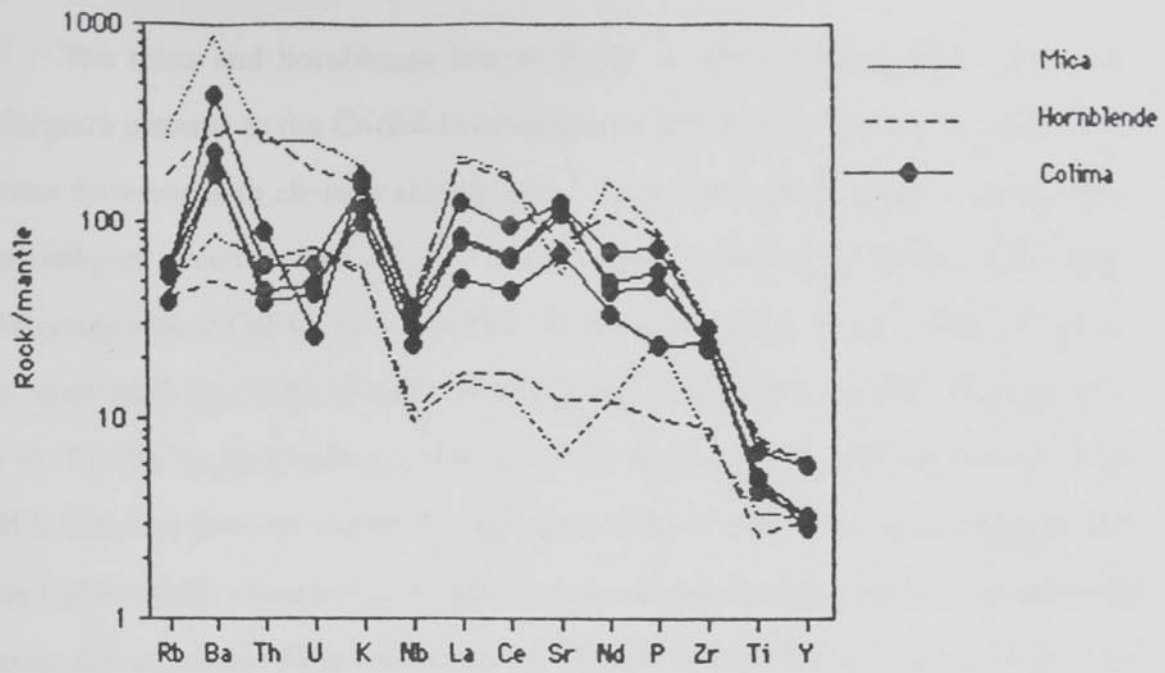


Fig. 3.15a

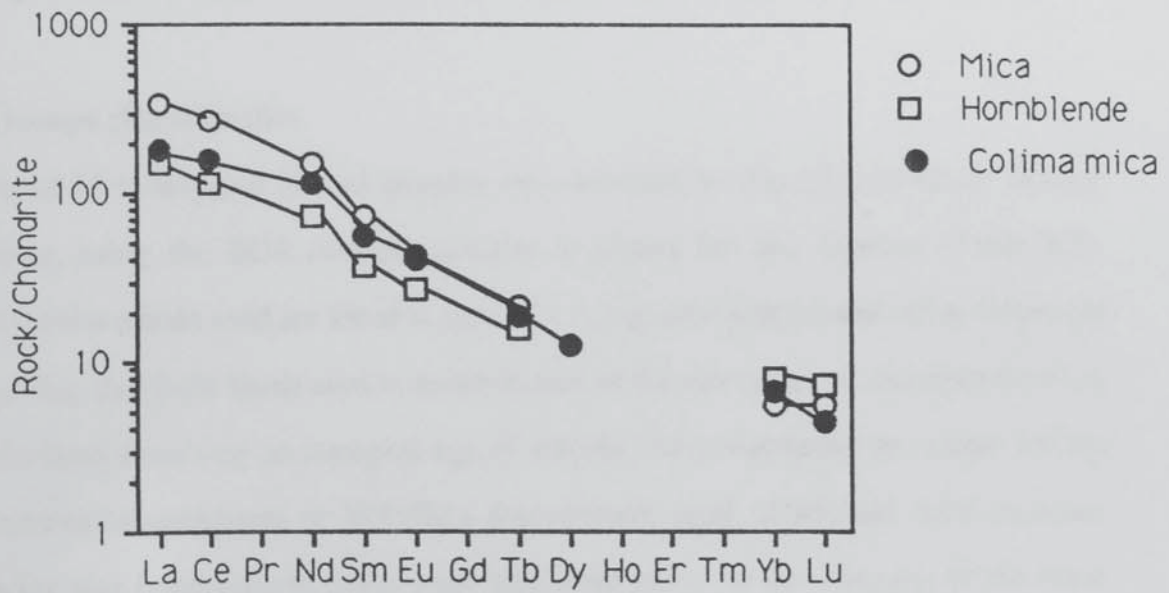


Fig. 3.15b

The mica and hornblende lamprophyres of Colima have almost identical spidergram patterns to the Criffell lamprophyres (Fig. 3.15a) though they have some distinct differences in element abundances. This is particularly apparent in the mica lamprophyres which are low in Th, U and Rb relative to those of Criffell. Both types of lamprophyres at Colima have a positive Sr anomaly relative to the LREE, similar to that observed in the lavas from the SW Highland. Chondrite normalised REE patterns for the Colima lamprophyres are very similar to those of the Criffell dykes with steep LREE enriched profiles and no Eu anomalies (Figs 3.15b). The mica lamprophyres have higher LREE abundances compared to the hornblende lamprophyres, though both groups fall within the field defined by the Criffell dykes. The mica lamprophyres of SW England (Fig. 3.15c) also have very similar “spidergram” patterns to the Criffell lamprophyres, with prominent negative Nb and Sr anomalies. However they generally have higher trace element abundances, particularly of U, Th, Rb and Zr. Chondrite normalised plots for REE are very steep with high Ce_n/Yb_n ratios (95.2–15.05) and have generally elevated REE abundances compared to the lamprophyres of Criffell.

3.3) Isotope characteristics

A set of 15 of the least altered samples were selected for Sm–Nd and Rb–Sr isotope analysis, using the BGS isotope facilities at Grays Inn Rd, London (Table 3.2). Analytical methods used are listed in appendix A together with normalisation values for T_{chur} , T_{dm} and Bulk Earth used in recalculation of the raw data. All initial ratios were recalculated assuming an intrusion age of 400Ma. This was based on a date for the Newmains lamprophyre at 395 ± 7 Ma (Macdonald *et al.* 1986) and field evidence showing that lamprophyre dykes were emplaced prior to the intrusion of the main Criffell pluton (Rock *et al.* 1988) dated at 396 ± 2 Ma (Halliday *et al.* 1980). The Rb/Sr ratios of the samples are all < 0.159 which precludes significant change in the $^{87}Sr/^{86}Sr$ ratio through growth of radiogenic Sr if the 400Ma age assumed was in error even by as much as 10Ma (Thirlwall, 1983).

Fig. 3.15c

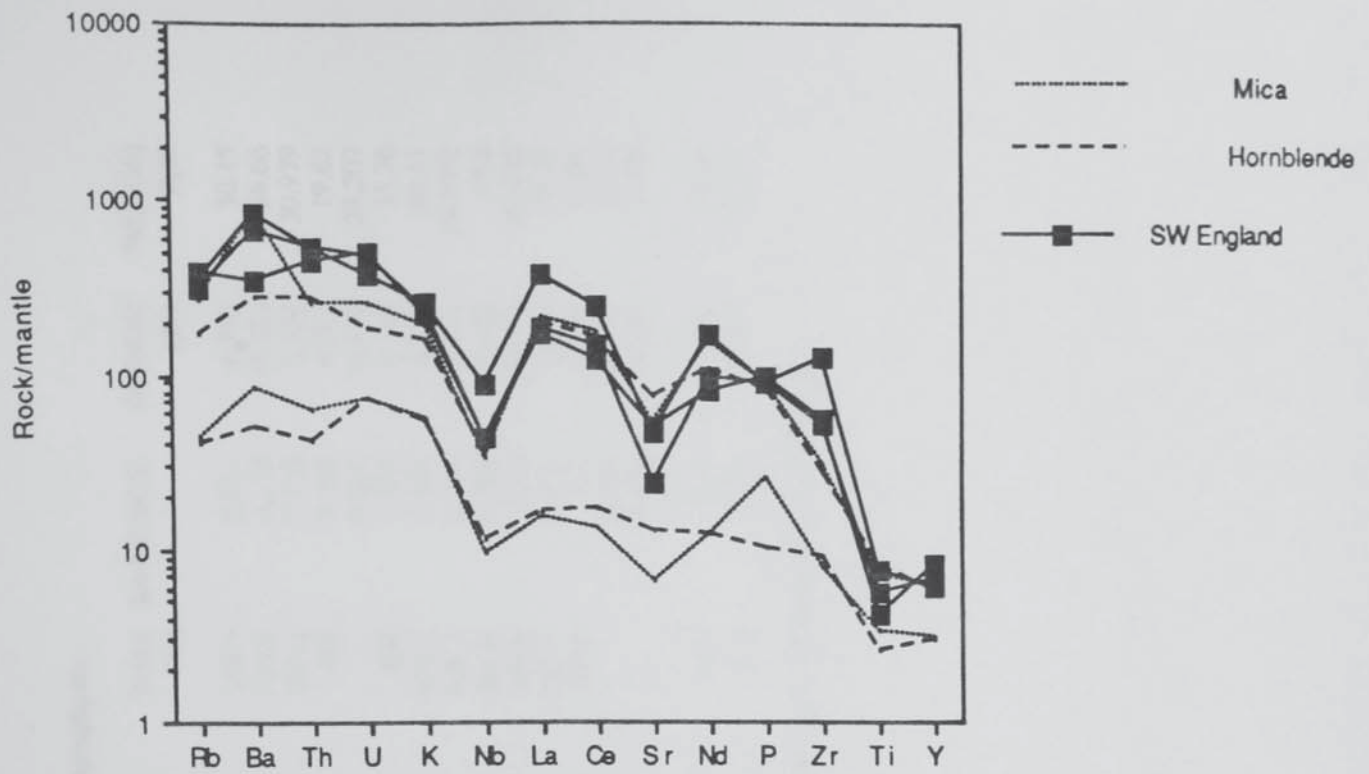


Fig. 3.15d

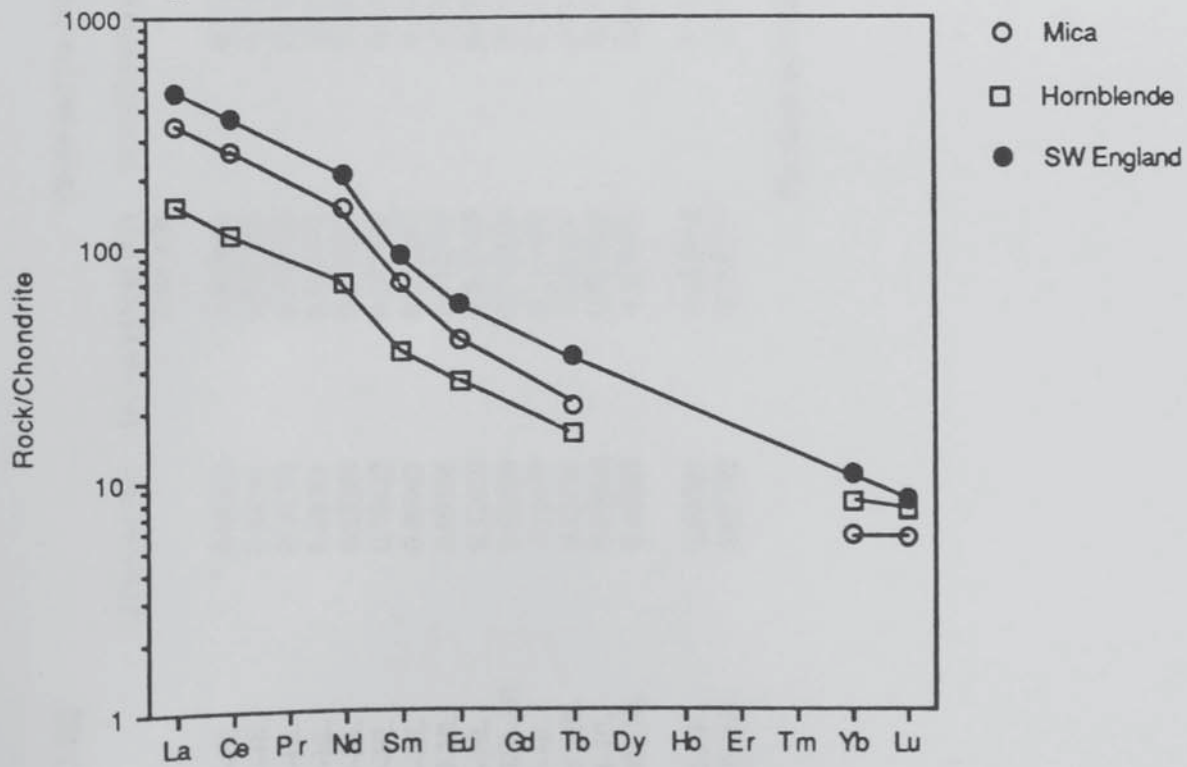


Table 3.2[i]

Rb–Sr and Sm–Nd isotope data for the Criffell Lamprophyres

	$^{147}\text{Sm}/^{144}\text{Nd}$	$^{143}\text{Nd}/^{144}\text{Nd}(\text{PD})$ 2 σ to ± 38	$^{143}\text{Nd}/^{144}\text{Nd} (400)$	ENd	Tdm ± 100	Tchur ± 60	Sm/Nd(BGS)	Sm(BGS) ppm	Nd(BGS) ppm
1367-HL	0.12750	0.512492	0.512158	0.6	950.5	326.7	0.211	6.357	30.15
BP21-HL	0.10745	0.512338	0.512057	-1.3	988	516.5	0.178	10.071	56.66
1381-HL	0.10783	0.512403	0.512121	-0.1	906.9	407.2	0.178	5.526	30.979
1314-HL	0.01261	0.512449	0.512119	-0.1	1003	413	0.209	4.092	19.62
1380-HL	0.13368	0.512661	0.512311	3.73			0.221	6.237	28.207
1360-HL	0.10422	0.512409	0.512091	-0.7	992	464	0.172	6.164	35.76
1305-HL	0.09967	0.512369	0.512108	-0.3	889.2	426.5	0.165	10.24	62.11
BP19-HL	0.09586	0.512330	0.512079	-0.9	909	469.3	0.159	8.896	56.1002
1366-HL	0.12600	0.512405	0.512075	-1	1069.7	507.4	0.208	5.961	28.6
PFT02B-HL	0.08469	0.512310	0.512088	-0.7	858.5	449.8	0.14	20.662	147.486
1365-HL	0.10420	0.512409	0.512136	0.2	872.2	381.4	0.172	6.164	35.76
1296C-HL	0.12120	0.512521	0.512204	1.5	850.5	240.8	0.2	4.974	24.81
BP11-HL	0.09000	0.512330	0.512090	-0.6			0.149	22.59	151.2
BSM01-HL	0.10100	0.512390	0.512130	0			0.168	13.08	77.98
BP22-ML	0.09092	0.512312	0.512074	-1	896	473	0.15	8.354	55.54
PFT03-ML	0.08372	0.512259	0.512040	-1.7	907	515	0.138	14.307	103.32

Standards on VG354 at time of analysis: LaJolla: 0.511833 \pm 19; NBS 987: 0.710233 \pm 28

Table 3.2[ü]

	Rb(BGS) ppm	Sr(BGS) ppm	Rb/Sr(BGS)	87Rb/86Sr ±0.5%	87Sr/86Sr(PD) 2 rno ±20	87SR/86Sr(400)	ESr	Tbulk ±43
1367-HL	44.03	564.08	0.078	0.202	0.70621	0.70506	14.8	1014.1
BP21-HL	91.46	1005.52	0.091	0.263	0.70692	0.70542	19.8	943.2
1381-HL	69.52	624.16	0.111	0.322	0.70721	0.70538	19.3	797.6
1314-HL	60.89	386.92	0.157	0.478	0.70966	0.70694	41.5	917.5
1380-HL	44.03	564.08	0.078	0.226	0.70590	0.70462	8.48	
1360-HL	77.38	522.53	0.148	0.429	0.70834	0.70590	26.6	779.8
1305-HL	53.28	784.47	0.068	0.206	0.70627	0.70510	15.3	1017.2
BP19-HL	104.58	1174.69	0.089	0.258	0.70695	0.70548	20.7	985
1366-HL	56.17	522.24	0.108	0.311	0.70673	0.70496	13.2	686.6
PFT02B-HL	146.46	1449.22	0.101	0.292	0.70692	0.70525	17.5	812.3
1365-HL	56.09	597.65	0.094	0.272	0.70704	0.70549	20.9	946
1296C-HL	50.39	587.63	0.086	0.248	0.70695	0.70554	21.5	1042.2
BP11-HL	67.8	1948	0.348	0.1	0.70605	0.70549	20.8	
BSM01-HL	52.7	996.6	0.528	0.152	0.70598	0.70511	21	
BP22-ML	107.91	1259.69	0.086	0.248	0.70682	0.70540	19.6	988.1
PFT03-ML	146.52	1235.8	0.119	0.343	0.70789	0.70593	27.1	913.9

$^{87}\text{Sr}/^{86}\text{Sr}$ initial ratios of hornblende lamprophyres at 400Ma show a wide variation ranging from 0.70461 to 0.70694 ($\epsilon\text{Sr} +8.48$ to $+41.8$). Model ages relative to bulk earth range from 1042.1 to 686.6Ma. Data for two mica lamprophyres have a $^{87}\text{Sr}/^{86}\text{Sr}$ initial ratios of 0.70540 and 0.70593 ($\epsilon\text{Sr} +19.0$, $+27.1$). These overlaps with the field for hornblende lamprophyres as do their bulk earth model ages (988.1, 913.9).

$^{143}\text{Nd}/^{144}\text{Nd}$ initial ratios for hornblende lamprophyres vary from 0.512131 to 0.51205 ($\epsilon\text{Nd} +3.73$ to -1.3) with the majority close to the bulk earth value at 400Ma. Model ages relative to depleted mantle and to CHUR range from 1069.1 to 850Ma and from 516.5 to 240.2Ma respectively. $^{143}\text{Nd}/^{144}\text{Nd}$ initial ratios for the two mica lamprophyres of 0.512074 to 0.512040 ($\epsilon\text{Nd} -1.0$ and -1.7) are slightly more unradiogenic than the hornblende lamprophyres, and the mica lamprophyres also have slightly lower Sm/Nd. Depleted mantle and CHUR model ages range from 896 to 907.1Ma and 515 to 473Ma respectively overlapping with the values for hornblende lamprophyres.

3.3.1) Rb–Sr and Sm–Nd isotope variations

In lamprophyres it appears that the Sr isotope ratios are at least partially decoupled from the Rb and Sr trace element abundances in that there is no significant correlation between high Rb/Sr values and high ϵSr initial ratios (Fig. 3.16a). There are several possible reasons for the lack of correlation between Rb/Sr and ϵSr , including variable contamination of a primitive lamprophyric magma, derivation of lamprophyres from sources with different Rb/Sr ratios (which may be combined with the effects of contamination) or the scattering of primary magmatic Rb/Sr ratios by late stage hydrothermal fluids or weathering. In order to minimise the possible effects of alteration only petrographically fresh samples were selected for isotope analysis (see section 3.1).

Variation in Nd isotopic composition of the lamprophyres should be relatively unaffected by weathering or hydrothermal processes (Faure, 1987; DePaolo, 1988).

Fig. 3.16a

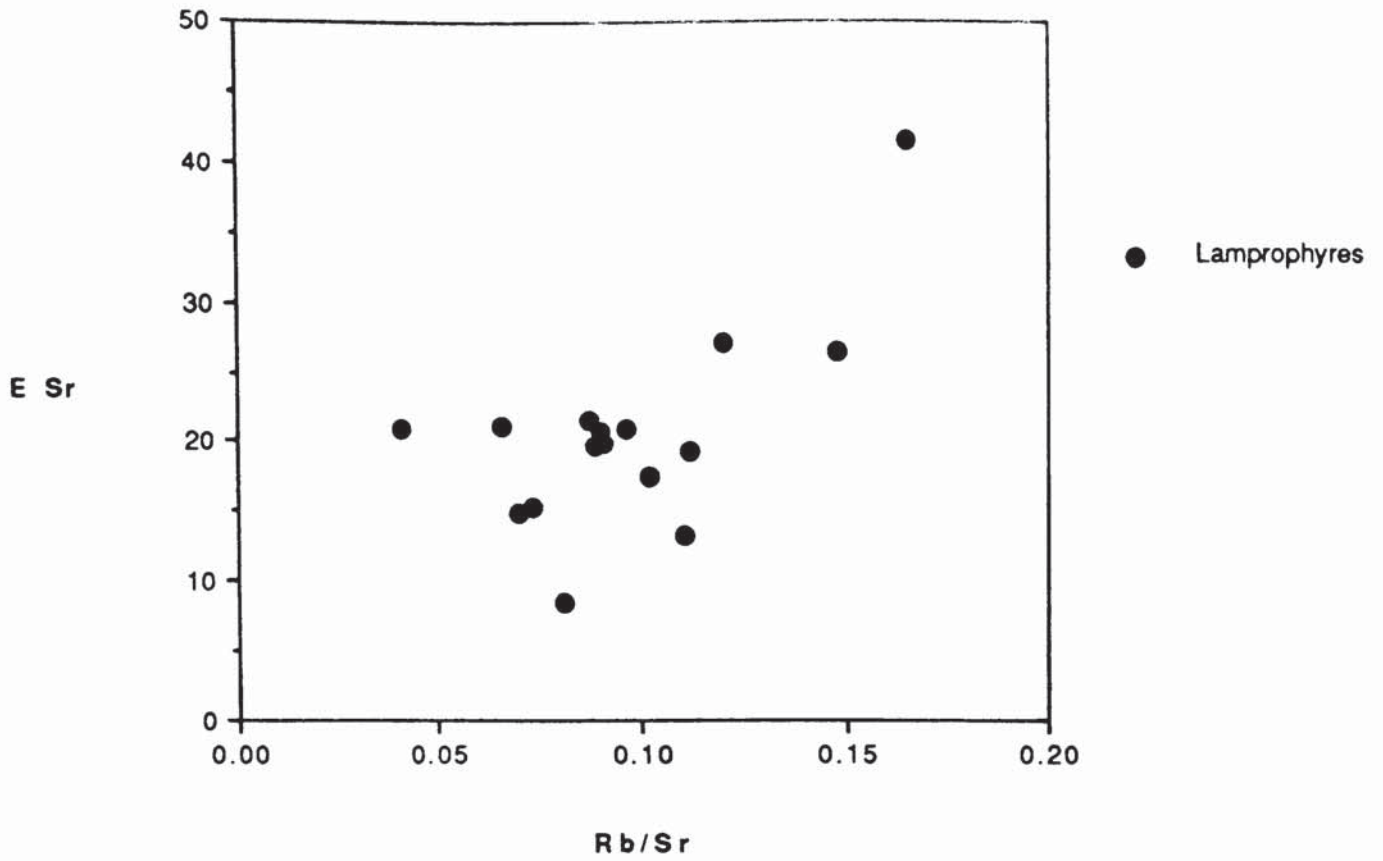
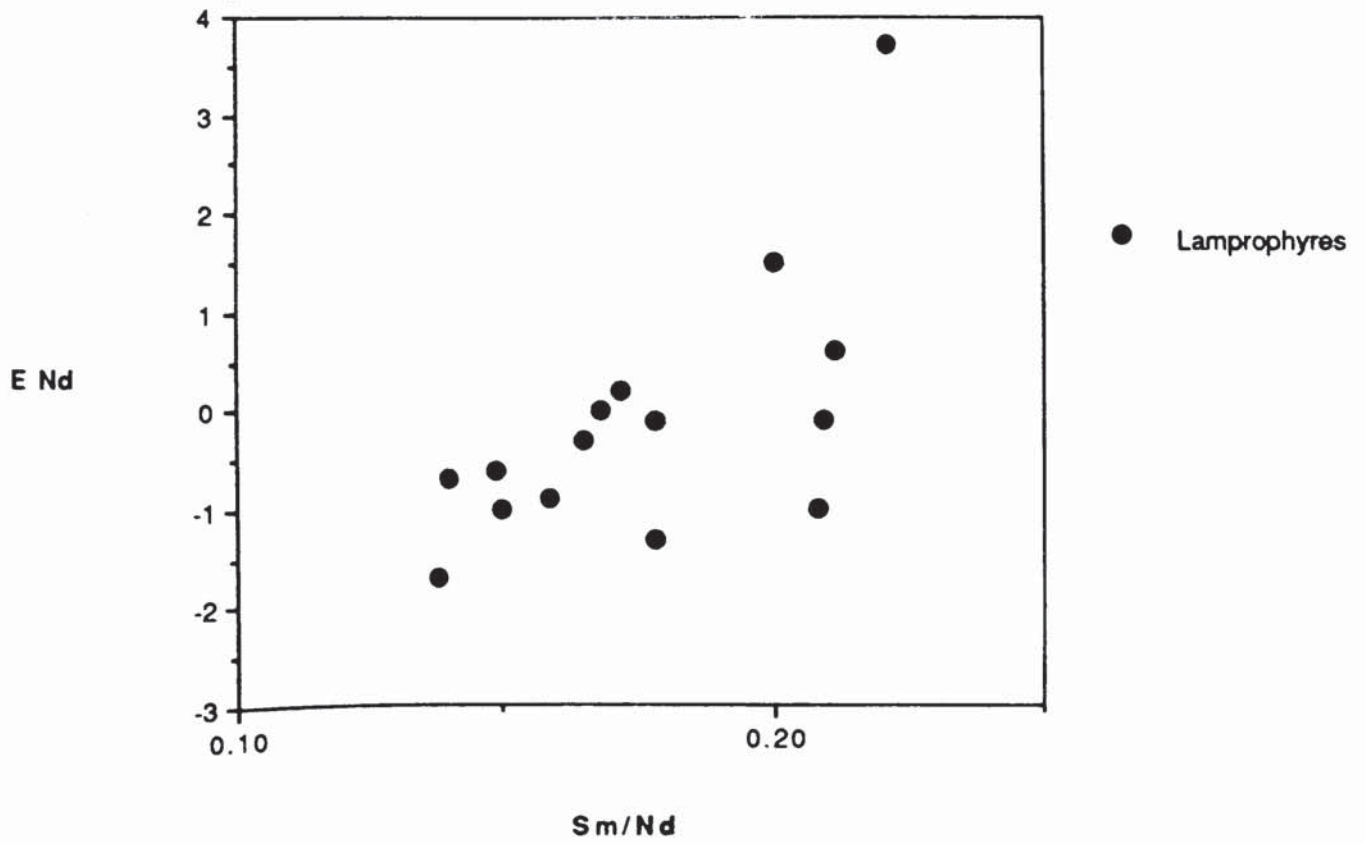


Fig. 3.16b



The majority of the lamprophyres cluster around the ϵ_{Nd} bulk earth value and although there is a weak positive correlation between ϵ_{Nd} and Sm/Nd the source of the lamprophyres does not appear to have had their low observed Sm/Nd (Fig. 3.16b) ratio for any significant period of time prior to the melting responsible for the lamprophyres. The ϵ_{Nd} and ϵ_{Sr} compositions of the lamprophyres are shown, together with those of the late Caledonian basaltic lavas from the Midland Valley and the SW Highlands, in Fig 3.17. The Criffell lamprophyres form a scattered field clustering around the bulk earth ($\epsilon_{Nd}=0$) line and are displaced to the right of the fields for the Midland Valley and SW Highland lavas, reflecting their more radiogenic ϵ_{Sr} compositions. There is no significant correlation between ϵ_{Nd} and ϵ_{Sr} values in the lamprophyres which suggests that their Nd and Sr isotope composition has not been influenced by systematic crustal contamination or mixing as this should lead to the development of trends on a plot of $\epsilon_{Nd}-\epsilon_{Sr}$. The scattered trends on plots of $\epsilon_{Sr}-Rb/Sr$ and $\epsilon_{Nd}-Sm/Nd$ suggest that there have been changes in the Rb/Sr and Sm/Nd of the mantle prior to melting which have not had time to be reflected in the isotopic composition of the melts. A plot of Rb/Sr–Sm/Nd (Fig 3.18) shows the Rb/Sr and Sm/Nd of the lamprophyres relative to values for a bulk earth composition. The lamprophyres have significantly lower Sm/Nd ratios and higher Rb/Sr than bulk earth as expected from their high LILE and LREE contents. The high Rb/Sr ratio of the lamprophyres is reflected in their relatively radiogenic Sr isotope values but their Nd isotope compositions do not reflect their low Sm/Nd (Fig. 3.18), suggesting that the Nd isotope system is decoupled from the Sm and Nd abundances in the lamprophyres.

3.4) Comparison with late Caledonian basic magmas and late Palaeozoic mantle xenoliths

The most voluminous basic magmas are represented by the late Silurian basaltic lavas which were erupted across Scotland, from the Western Highlands down to the Cheviot Hills, during the latter part of the Caledonian orogeny. The majority these rocks were derived from melting of a variably enriched mantle modified by processes associated

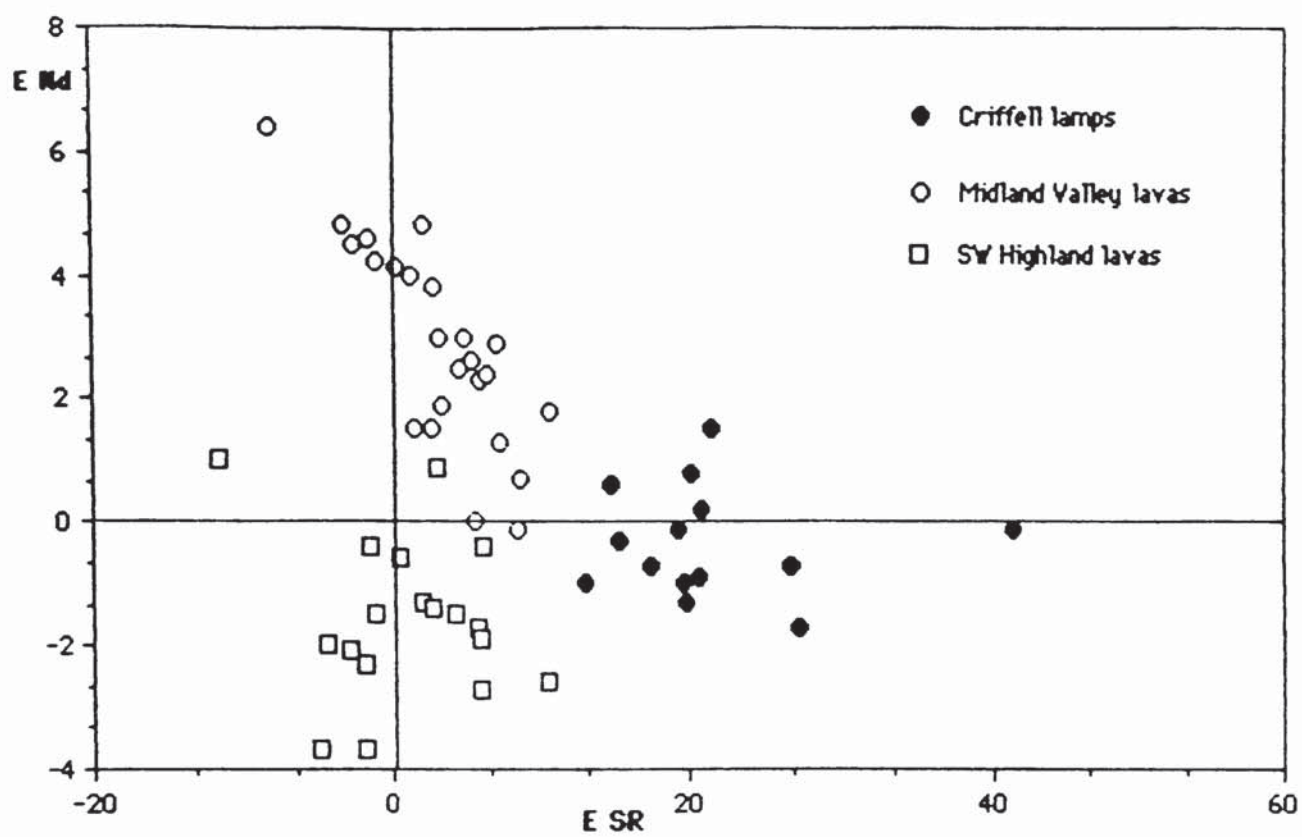


Fig. 3.17

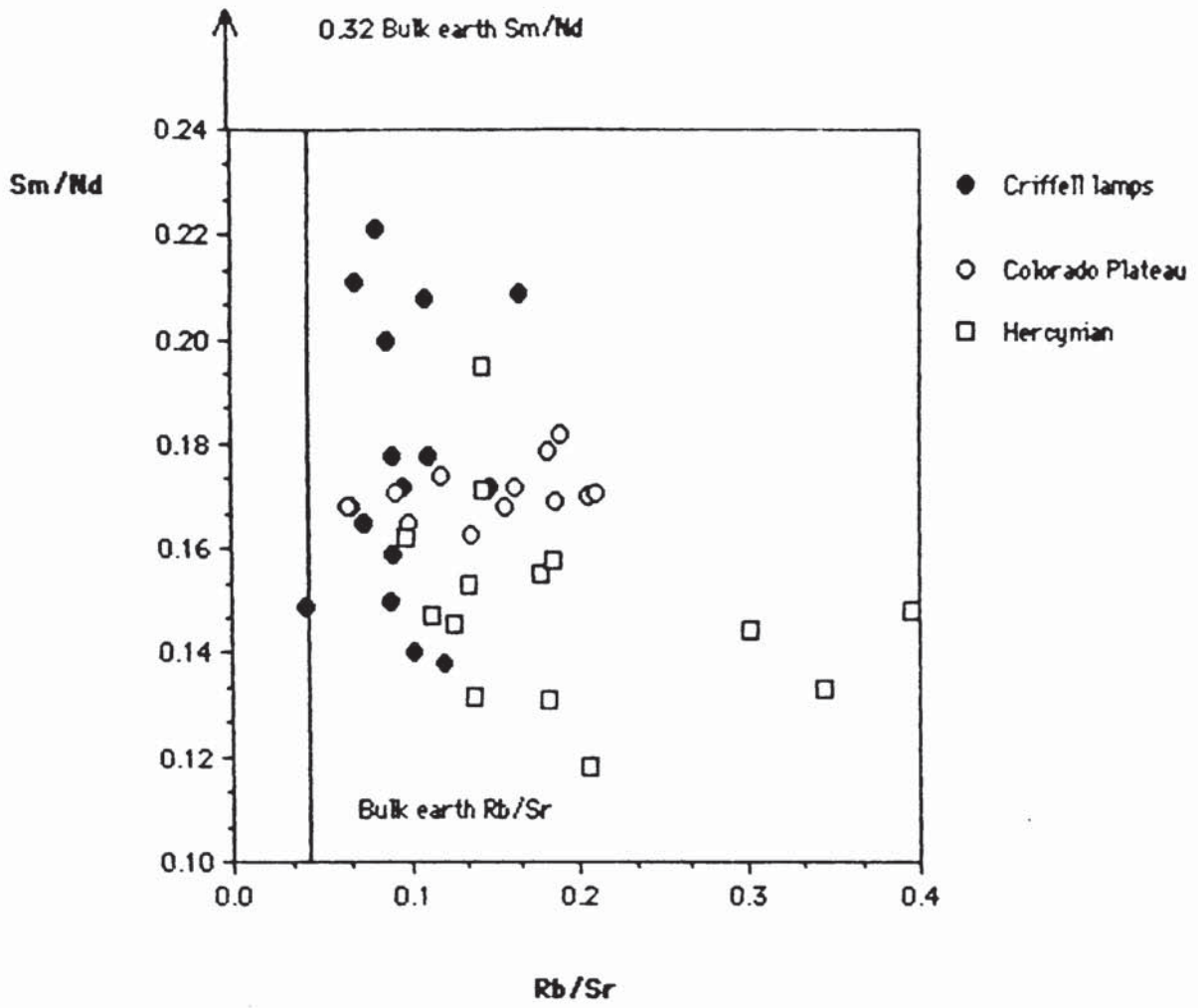


Fig. 3.18

with the NW directed subduction of oceanic lithosphere at the northern margin of the Iapetus Ocean (Thirlwall, 1981, 1983, 1986, 1988). Thirlwall (op.cit) argued that the isotopic composition of these more primitive lavas reflected the isotopic composition of their mantle source.

The lamprophyres are isotopically distinct from the lavas in having significantly more radiogenic Sr compositions than either the SW Highland (SWH) or Midland Valley (MV) rocks (Fig. 3.17). Although the Nd isotope composition of the lavas and lamprophyres overlap, the lamprophyres have a more restricted range of ϵ Nd values. The MV lavas are characterised by radiogenic Nd and slightly radiogenic Sr values, whereas the SWH lavas have more unradiogenic Nd compositions than the MV lavas but similar ϵ Sr values. Therefore, although the SWH and MV lavas have similarities in major and trace element composition to the Criffell lamprophyres (Figs 3.12a-b; 3.13), the lamprophyres appear to have been derived from an isotopically distinct source. Unfortunately no systematic isotope data is yet available for late Caledonian lavas from south of the Southern Uplands fault (SUF) so that lateral variations in the composition of the source of the lavas to the south of the fault cannot be ruled out (Thirlwall, 1988).

Mantle and lower crustal xenoliths occur in Late Palaeozoic and Tertiary lamprophyre dykes in a variety of locations in Scotland (Halliday *et al.* 1985, Menzies *et al.* 1987, Menzies and Halliday, 1988). The most important of these are at Loch Roag (Lewis), Streap Chomlaidh (NW Highlands), Kilchatten (Colonsay) and Black Rocks (Midland Valley). It has been suggested (Menzies and Halliday, 1988) that many of the xenoliths represent fragments of the Scottish lithospheric mantle and that they preserve, in their isotopic and trace element compositions, evidence of the complex evolutionary history of that mantle. Therefore Sr and Nd isotope data for the lamprophyres and xenoliths are compared to see if the lithospheric mantle contains material similar isotopically to the Criffell lamprophyres (Fig. 3.19).

The lamprophyres have very similar ϵ Nd values to both the Streap Comlaidh and Kilchatten xenoliths but have more radiogenic ϵ Sr compositions than those from Kilchatten although both the lamprophyres and Kilchatten xenoliths fall within the field

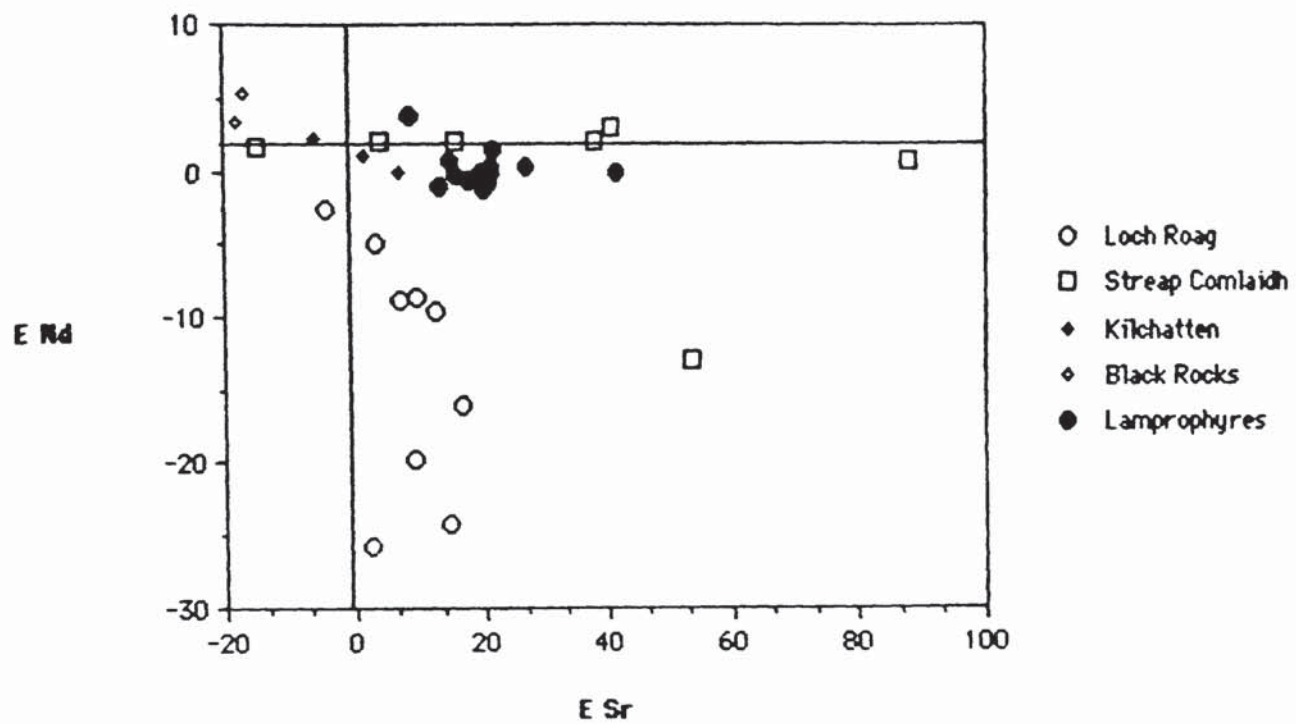


Fig. 3.19

of ϵ_{Sr} values for the Streap Comlaidh xenoliths. The Criffell lamprophyres also overlap with the Kilchatten and Streap Comlaidh xenoliths on a plot of $\epsilon_{\text{Nd}}\text{--Sm/Nd}$ (Fig. 3.20a) and define a flat-lying trend similar to those for the xenoliths with a restricted range of ϵ_{Nd} values and wide range of Sm/Nd. On a plot of $\epsilon_{\text{Sr}}\text{--Rb/Sr}$ (Fig. 3.20b) the lamprophyres also define a flat-lying trend, with a restricted range of ϵ_{Sr} but wide range of Rb/Sr. This contrasts with the sub-vertical trend defined by the the Streap Comlaidh xenoliths which have a much wider range of ϵ_{Sr} values together with a restricted range of Rb/Sr.

The lamprophyres have very similar ϵ_{Sr} and ϵ_{Nd} composition to xenoliths from Streap Comlaidh and Kilchatten suggesting that isotopic compositions similar to those of the lamprophyres are present in the lithospheric mantle under Scotland. Both the xenoliths and lamprophyres have “decoupled” Nd isotope and LREE values, evidence for recent enrichment in or modification of LREE abundances and ratios, but have markedly different trends on a plot of $\epsilon_{\text{Sr}}\text{--Rb/Sr}$. This suggests that the Rb–Sr isotope system in the xenoliths and lamprophyres have evolved differently, possibly due to differences in the timing and mechanisms responsible for the LREE and LILE modification (Menzies & Halliday, 1988).

3.5) Comparison with other CALs

Isotopic data for CAL from the Hercynian of Europe (Turpin *et al.* 1988) and the Tertiary of the western USA (Alibert *et al.* 1986) are compared with those from the Criffell area (Fig. 3.21). The Criffell, Tertiary and Hercynian lamprophyres have largely overlapping ϵ_{Sr} and ϵ_{Nd} composition, although the Hercynian rocks extend to more radiogenic ϵ_{Sr} and unradiogenic ϵ_{Nd} values than both the Criffell and Tertiary lamprophyres. On a plot of $\epsilon_{\text{Nd}}\text{--Sm/Nd}$ (Fig. 3.22a) the Tertiary lamprophyres (TCP's) define a steep, slightly negative trend with a wide range in ϵ_{Nd} combined with a very restricted range of Sm/Nd, while the field for the Hercynian rocks forms a scatter which overlaps with the the data for the Tertiary and Criffell lamprophyres. The Hercynian lamprophyres have a wide range in Rb/Sr which shows no correlation with

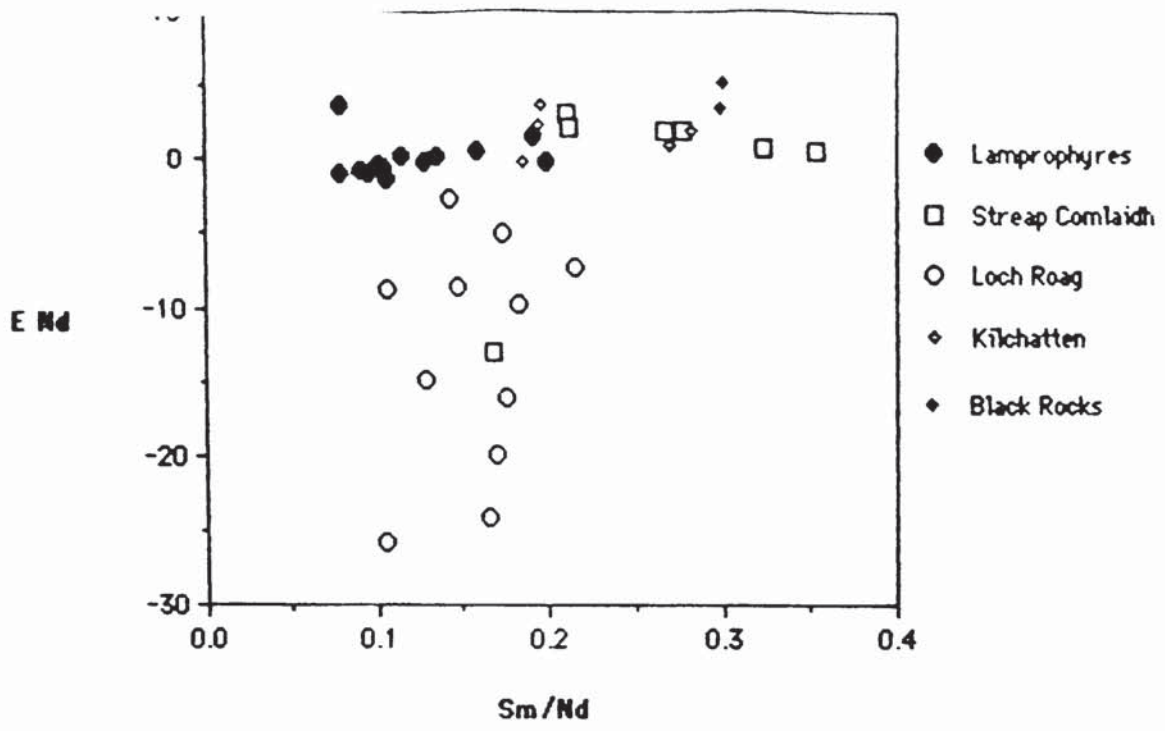


Fig. 3.20a

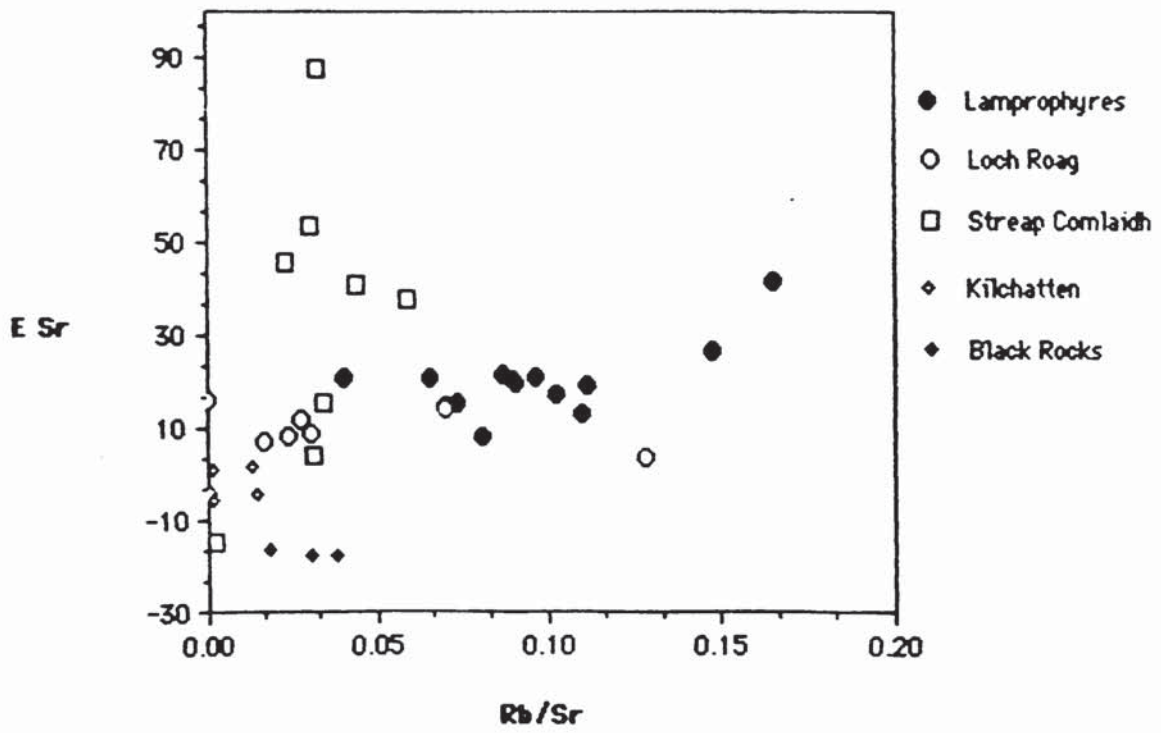


Fig. 3.20b

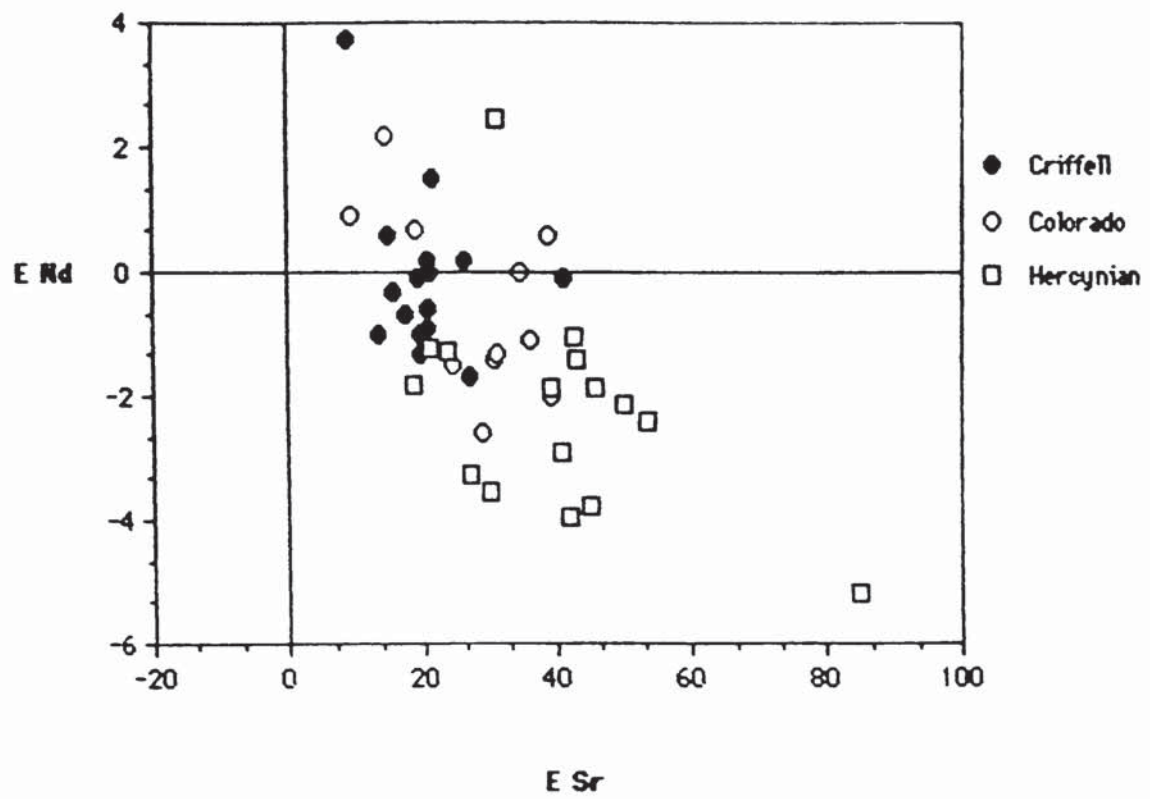


Fig. 3.21

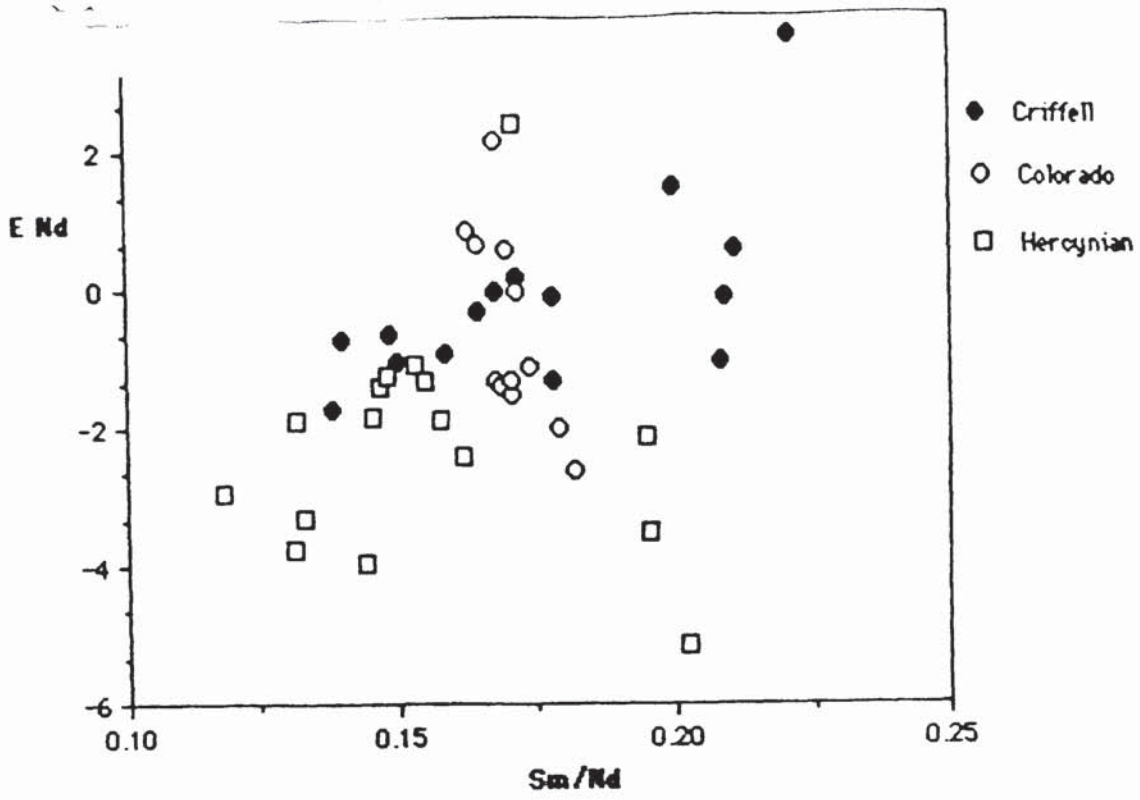


Fig. 3.22a

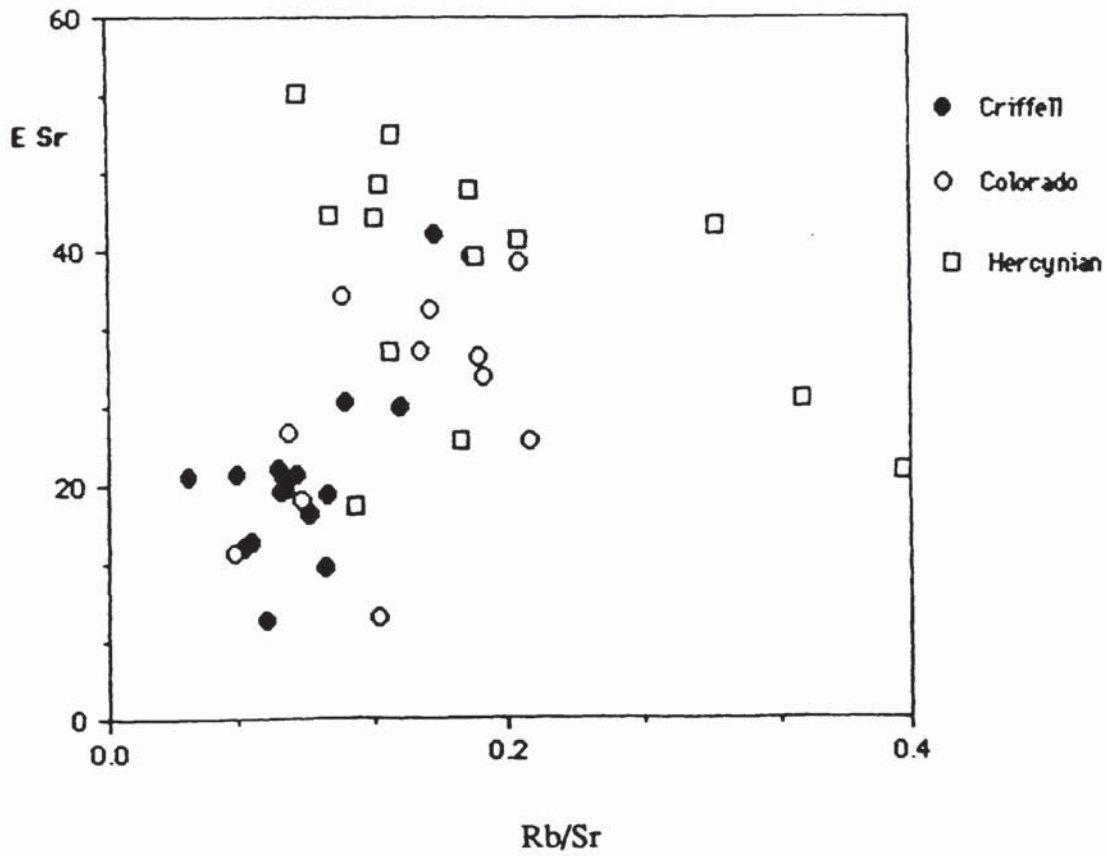


Fig. 3.22b

ϵ Sr (Fig. 3.22b) suggesting that the Sr isotope composition is decoupled from the Rb and Sr abundances (Turpin *et al.* 1988). The fields for the Criffell and Tertiary lamprophyres overlap extensively although the Tertiary rocks extend to higher Rb/Sr. Both Turpin *et al.* (1988) and Alibert *et al.* (1986) argued that the isotopic characteristics of the Hercynian and Tertiary lamprophyres, respectively, reflected the isotopic characteristics of the mantle source and were not modified by crustal contamination during emplacement. In both cases it was argued that the Sr and Nd isotope composition of the lamprophyres reflected their derivation from an isotopically heterogeneous lithospheric mantle which had been variably enriched in LILE and LREE immediately prior to melting. The isotopic similarity of the Hercynian and Tertiary lamprophyres with those from Criffell suggests that similar processes may influence the isotopic composition of these lamprophyres.

3.6) Summary

Late Caledonian lamprophyres from the dyke swarm around Criffell form two mineralogically distinct groups of mafic, mantle-derived magmas. These both have elevated LILE and LREE abundances. The mica lamprophyres are, in general, more enriched in these elements than the hornblende lamprophyres and slightly more potassic with higher K_2O and K_2O/Na_2O ratios >1 . The lamprophyres are enriched in LILE and LREE compared to contemporaneous basaltic lavas and also have higher Ni, Cr and MgO contents. The Criffell lamprophyres are petrographically and chemically very similar to other late Caledonian lamprophyres from SW Scotland and Northern England and are thus thought to be related to them. Both the lamprophyres and basaltic lavas are characterised by high LILE/HFS and LREE/HFS element ratios, prominent negative Nb anomalies on “spidergrams” and low Nb and Ti abundances. These are all features normally associated with magmas produced in subduction related volcanic arcs. The lamprophyres are comparable with calc-alkaline lamprophyres from analogous tectonic settings in other orogenic belts of different ages, in particular, the late Tertiary of Northern Mexico and the Hercynian of SW England. Petrogenetic studies of these

latter lamprophyres suggest that they originated as low degree partial melts of a mantle modified by cryptic and modal metasomatism related to fluids produced by dehydration reactions in a subduction zone. Late Caledonian lamprophyres from SW Scotland, in common with lamprophyres from other areas, have Sr and Nd isotopic characteristics which may reflect their mantle sources.

In the case of the Criffell lamprophyres, this source is distinct from that of the late Caledonian basaltic lavas magmas but has some similarities with xenoliths of Scottish lithospheric mantle recovered from intrusions at Streap Comlaidh and Kilchatten. The lamprophyres have ϵ_{Nd} values which cluster close to bulk earth and markedly radiogenic ϵ_{Sr} values displaced to the right of bulk earth values. Poor correlations between ϵ_{Nd} and Sm/Nd values suggest that the majority of the lamprophyres are derived from a source in which the Nd isotopes are “decoupled” from their LREE abundances. Sm/Nd–Rb/Sr variations suggest that the mantle source of the lamprophyres has a lower Sm/Nd and higher Rb/Sr than bulk earth and that there was some addition of LREE to the mantle prior to melting or possibly during melting. The Criffell lamprophyres have similar Sr and Nd isotope compositions to Hercynian and Tertiary lamprophyres from Europe and the USA. The isotopic composition of these lamprophyres is thought to reflect their derivation from an isotopically heterogeneous mantle, enriched in LREE and LILE, derived from fluids and sediments incorporated into the mantle during subduction, and it is suggested that the Criffell lamprophyres may be derived from a similar source. Some these hypothesis and models are tested in Chapter 4.

Chapter 4

Modelling of lamprophyre geochemistry: The petrogenesis of the Criffell CAL

4.1) Petrogenesis of CAL: Inferences from geochemistry and published models

As in the Caledonian, lamprophyres from both Colima and SW England are enriched in LILE and LREE compared to contemporaneous basaltic magmatism. Subduction related processes, including dehydration of the subducting slab and the geochemical and mineralogical effects of metasomatism brought about by the resultant fluids (Tatsumi *et al.*, 1983) are thought to have played a significant part in the petrogenesis of the Colima and SW England lamprophyres (Luhr *et al.* 1989, Leat *et al.* 1987, Thorpe, 1987). It has been suggested (Luhr *et al.* 1989) that subduction related metasomatism produced phlogopite–garnet rich veins in the asthenosphere enriched in LILE and LREE. Low degrees (<0.5%) of partial melting of such veins would produce primitive, LILE and LREE enriched, lamprophyric magmas and leave residual phlogopite and garnet. Larger degrees of melting (10%) would produce larger volumes of less–enriched basaltic magmas. It has been argued that lamprophyres from both Colima and SW England have a range of LILE and LREE abundances (Table 3.1) that cannot be explained by fractionation or contamination due to their high compatible element abundances (Luhr *et al.* 1989, Thorpe *et al.* 1986).

Furthermore, these high LILE and LREE abundances have been ascribed to geochemical heterogeneities in the source for the lamprophyres, possibly due to minor variations in the mineralogy of the mantle or varying degrees of metasomatic enrichment (Luhr *et al.* 1989, Leat *et al.* 1987). In the case of the Hercynian and Tertiary lamprophyres, Turpin *et al.* (1988) and Alibert *et al.* (1986) proposed that the isotopic heterogeneities in the lithospheric mantle resulted from the incorporation of subducted sediment into the mantle and from the addition of radiogenic Sr by metasomatic fluids derived from the subduction zone. Luhr *et al.* (1989), in their study of the Colima lamprophyres, suggested that these metasomatic fluids, as well as

transporting LILE and LREE, would promote the growth of hydrous phases, including amphibole and phlogopite, in the mantle wedge above the subduction zone. Phlogopite is characterised by high Rb/Sr ratios, which, over time, will lead to the development of radiogenic $^{87}\text{Sr}/^{86}\text{Sr}$ compositions and also act as a reservoir for LILE and possibly some LREE. Subsequent partial melting of the phlogopite and/or amphibole bearing mantle would produce potassic liquids with variable LILE and LREE abundances and radiogenic Sr compositions.

The similar spidergram patterns, characterised by negative Nb anomalies and low Ti and Y abundances, of the Criffell lamprophyres and the subduction-related late Caledonian basaltic lavas from the SW Highlands and Midland Valley, suggest that the lamprophyres have been derived from a mantle source which has also been modified by subduction-related processes. It is thought that fluids released from the subducting plate may transfer LILE and LREE elements into the overlying mantle wedge enriching it in these elements, as well as modifying the mineralogy of the mantle by promoting the development of new phases such as amphibole and phlogopite (Wyllie & Sekine, 1982; Gill, 1981). These processes are also thought to stabilise numerous accessory phases, including ilmenite, which have high distribution coefficients for Nb and Ti. These may be residual phases during later partial melting events (Gill, 1981; Thompson *et al.* 1984; Wilson, 1989) although recent experimental work on the solubility of TiO_2 (Green & Pearson, 1986; Ryerson & Watson, 1987) suggests that the arc mantle may actually be depleted in Ti group elements.

The high MgO, Ni, Cr and V contents of both mica- and hornblende-bearing Criffell CAL suggest that they represent primitive, mantle-derived, melts which have suffered only minor fractionation during intrusion. Therefore the high LILE and LREE element abundances in the lamprophyres may be a characteristic inherited from their mantle source (Macdonald *et al.* 1985; Leat *et al.* 1987; Thorpe, 1987). However before we can use the data from the composition of mantle-derived magmas to draw conclusions about the composition of the mantle, it is important to try and constrain the effects of processes which may alter the composition of these magmas during

emplacement. Fractional crystallisation and crustal contamination processes are the most likely to influence the geochemical evolution of basic magmas during their ascent from the mantle through the crust. It is possible to simulate the gross effects of many these processes using simplified numerical models. In this section the results of modelling Rayleigh fractionation and combined assimilation–fractional crystallisation (AFC) processes together with an examination of the models of Patchett (1980) and Huppert & Sparks (1985) are presented in an attempt to constrain fractionation and contamination effects. Using the results of this modelling a petrogenetic model is suggested for the Criffell CAL including an assessment of the role of source heterogeneity and partial melting processes (McKenzie, 1985).

The use of simplified theoretical models to explain the chemical variations observed in igneous rocks is made difficult by to the number of assumptions that must be made about natural systems, e.g., the choice of endmembers, contaminants, fractionating assemblages etc. For this thesis the endmember magmas (PFT02b; 1371) were selected on the basis of their fine–grained, non– or sparsely– porphyritic nature which together with their high MgO, Ni and Cr contents supports the assumption that they represent, as far as possible, unfractionated, non–cumulate, mantle–derived magmas. The fractionating mineral assemblages were selected on the basis of petrographical observation and data from reported experimental studies of mineral stabilities in high–K magmas. In the more complex AFC models additional assumptions were made about the nature of the contaminant and the rate of assimilation relative to crystallisation (r). A representative melt of Lower Palaeozoic sediments was used as the crustal contaminant because these rocks are the most abundant crustal lithology in the area. However the vertical extent of these rocks is unknown and other lithologies more typical of the middle and lower crust, such as granulites, may be present at depth. It is significant in regard to this question that no granulites or similar lithologies have been recorded as xenoliths in the late Caledonian lamprophyres whereas late Palaeozoic lamprophyres from the Midland Valley and the northern part of the Southern Uplands do contain numerous such xenoliths (Upton *et al.* 1983). Thus a

lower Palaeozoic crustal contaminant is thought to be the most realistic and appropriate for use in an AFC model in these circumstances.

4.2) Fractional crystallisation

It has been argued that the high compatible element (Ni, Cr, V, MgO) abundances of most calc-alkaline lamprophyres argue against any significant amount of crystal fractionation involving olivine and pyroxene (Macdonald et al. 1985; Turpin et al. 1988). To test the applicability of this hypothesis, simple quantitative modelling of the variation of several key compatible and incompatible elements in mica and hornblende-lamprophyres has been carried out using the Rayleigh equations for perfect fractional crystallisation as listed in Henderson (1982) and Cox et al. (1979). A Rayleigh fractionation model was used in preference to the equilibrium crystallisation model because it was considered more appropriate for fractional crystallisation of a hot basic magma in which relatively rapid crystal-liquid separation should occur in low viscosity, lower silica liquids (Cox et al. 1979). The general similarity in major element composition of lamprophyres and the basalt-andesite series suggests that distribution coefficient data for minerals in the latter (Gill, 1981; Henderson, 1982; Pearce and Norry, 1979) may be applicable to lamprophyres for which no data have yet been published (Leat et al. 1988). To check on the validity of this approach, approximate Kd values were calculated for Ni and Cr in clinopyroxene and amphibole in CAL using data gathered by EMPA studies these phases in the Criffell (Appendix F) and Colima graben (MVB) lamprophyres (Luhr & Carmichael, 1984). Values for the Kd (mineral/whole rock) of Ni and Cr in the Criffell CAL are circa 6.5_{Ni} and 22_{Cr} for clinopyroxene and 7.7_{Ni} (1.5-3.0 excluding sample 1313) and 9.1_{Cr} (1-2.5 excluding sample 1313) in amphibole while data from Allen & Carmichael (1984) give values of circa 30_{Cr} in clinopyroxene and 2.3_{Ni} in amphibole. Apart from the Cr-amphibole values in the Criffell CAL and the Ni-amphibole value in the Colima lamprophyres, the values are within the ranges quoted by Gill (1981; Table 6.3) for orogenic andesites. Unfortunately no data is available for V values. While it would be unrealistic to expect

that the mineral/whole rock determined values to give as reliable or as accurate as Kd values determined by experimental methods, the fact that the values do approach the those reported by Gill (1981) gives some confidence in the use of this authors compilation of experimentally derived values in modelling the Criffell CAL.

Fine-grained, non- or sparsely- porphyritic samples (PFT02b, 1371) with high contents of MgO, Ni, Cr and V were used as endmembers because they are considered to be the closest approximation to actual lamprophyric liquids. It would of course have been possible to select a number of endmembers for modelling, including 'convenient' average or theoretical compositions but the use of real whole rock values has been preferred in this study. Other candidate endmembers from the dataset are of course possible, particularly when chosen using chemical criteria alone; e.g. 1325. However, although this sample has high Ni, Cr and MgO coupled with low LILE and LREE abundances, it is also significantly more siliceous than PFT02b and has significantly lower CaO and TiO₂.

4.2.1) Constraints from major elements

Correlations between major elements in the mica lamprophyres are scattered and thus it is not believed that the distribution of major element data for the mica lamprophyres can be explained by phenocryst mineral fractionation. However, the hornblende lamprophyres show definite linear trends for several major element oxides on Harker diagrams, in particular CaO, MgO and Fe₂O₃. Therefore some attempt has been made to constrain the likely effects of crystal fractionation upon the distribution of these major element oxides in the hornblende lamprophyres using analyses for the dominant phenocryst mineral phases (amphibole & clinopyroxene) derived by electron microprobe methods. Although complex computer based linear programming solutions are available for calculating best fit lines and residual errors for major elements (Wright & Doherty, 1970) these usually deal with multiple oxides, often significantly more than the number of likely crystallising phases, and are thus often considered to be geologically over-constrained (Cox *et al.* 1979; Maaloe, 1985; Wilson, 1989). As this

study is dealing with only three oxides plotted on Harker diagrams, a simple graphical test has been applied using the Lever Rule (Cox *et al.* 1979). This method should be effective at indicating the proportions of minerals in the fractionating assemblages as well giving an indication of the degree of crystal fractionation (Wilson, 1989). The Harker diagrams for the three oxides are illustrated in Figures 4.1(a-c) together with the best fit regression lines through the data points and correlation coefficients. Also marked are the points representing the mineral compositions together with relevant 'tie-lines' linking the extract, parental and daughter magmas. Significantly, PFT02b, the parental magma selected as a likely parental magma sits on or very close to the regression line in all three diagrams. The results of the modelling are also listed in the figures.

In all cases, the composition of the fractionating assemblage (cpx+amph) is dominated by amphibole with the proportion of clinopyroxene being <21% in all cases although the results of this modelling suggest no clinopyroxene is present in the fractionating assemblage for CaO. This agrees well with the greater proportion of amphibole relative to clinopyroxene, where both are present, in hornblende lamprophyres (Chapter 2). However, the percentage of fractional crystallisation required of the cpx-amph assemblage to explain the range of compositions between PFT02b and the most siliceous hornblende lamprophyres ranges from 68.5% in the case of CaO up to 81.3% for Fe₂O₃. These values are very difficult to reconcile with the high Ni, Cr and V and of the lamprophyres. Lower degrees of fractionation could be achieved if a more siliceous parent composition was used but this leads to difficulties in explaining the less siliceous samples with high CaO, MgO and Fe₂O₃, many of which are relatively fine grained, thus precluding crystal accumulation. It could also be argued that not all the fractionating minerals have been accounted for in this model, i.e. Fe-Ti oxides. However, although opaque minerals are found in the lamprophyres and could possibly explain some of the Fe₂O₃ variation, it is unlikely that it would significantly contribute to MgO or CaO variations.

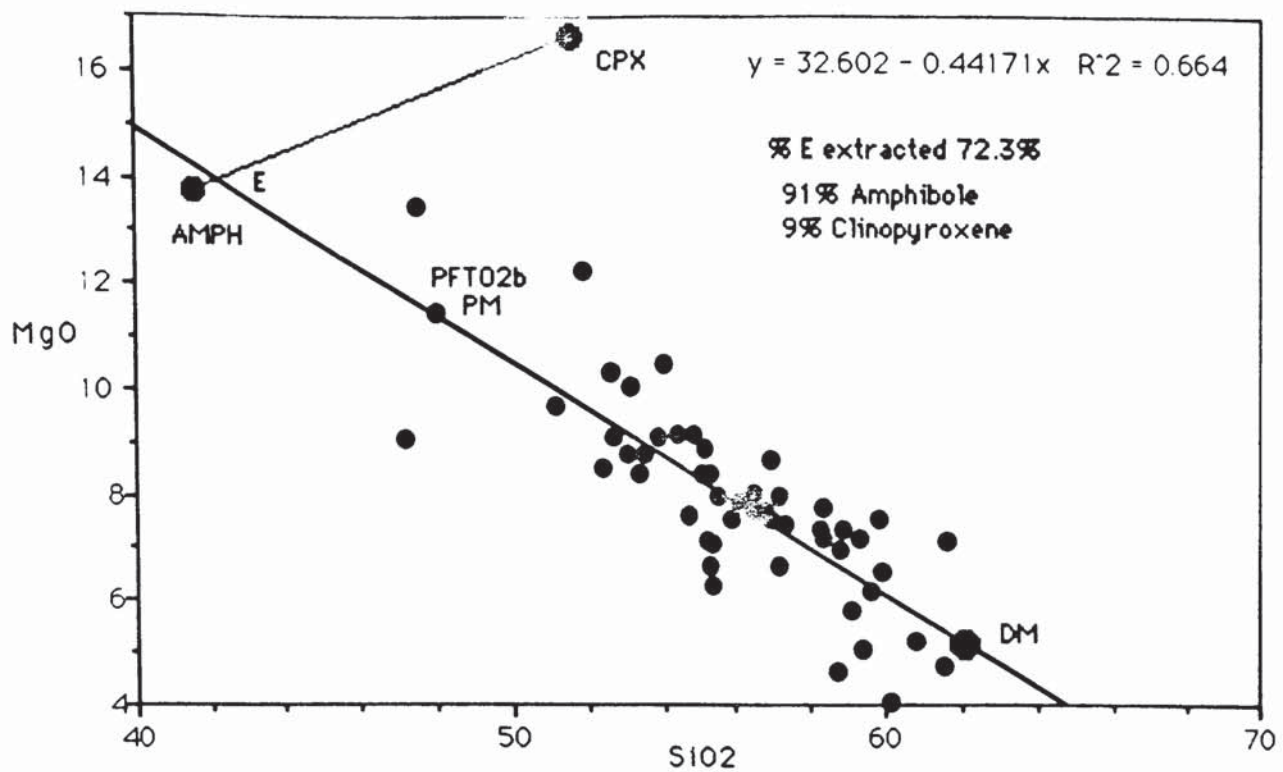


Fig. 4.1a

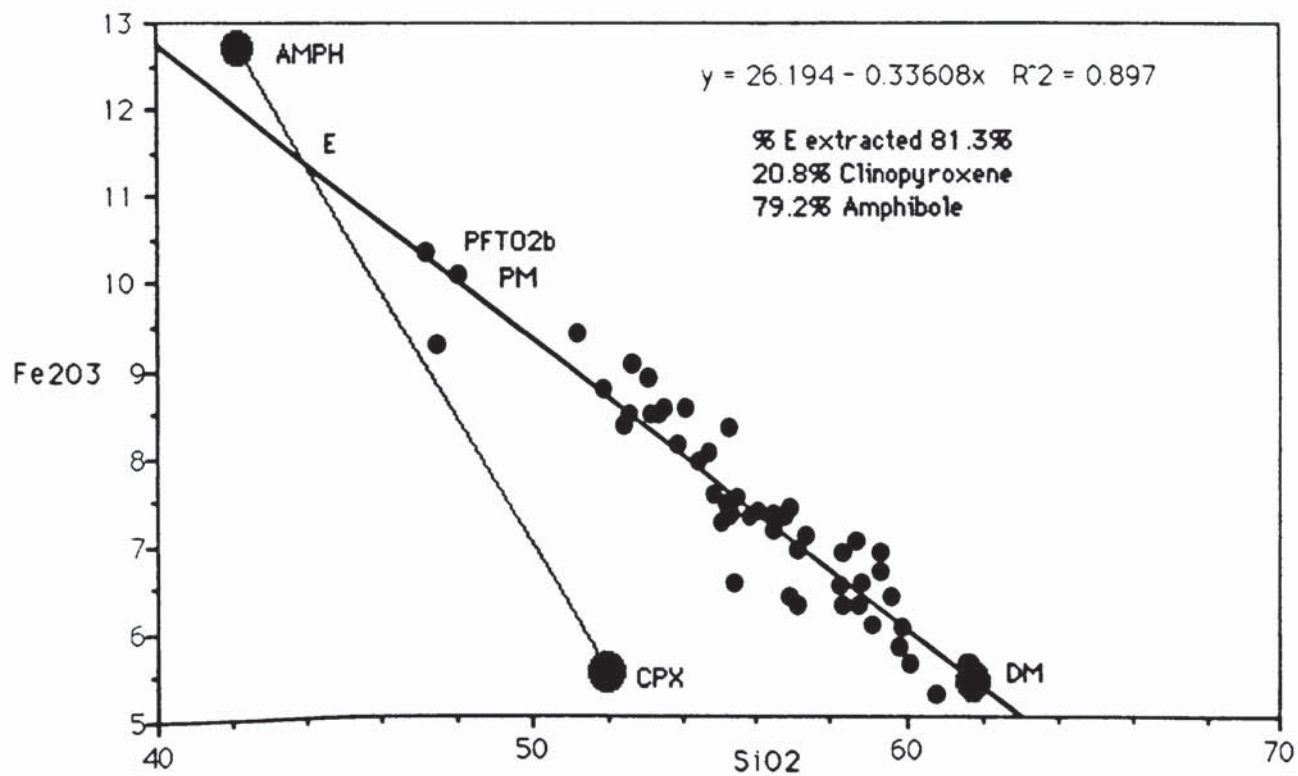


Fig. 4.1b

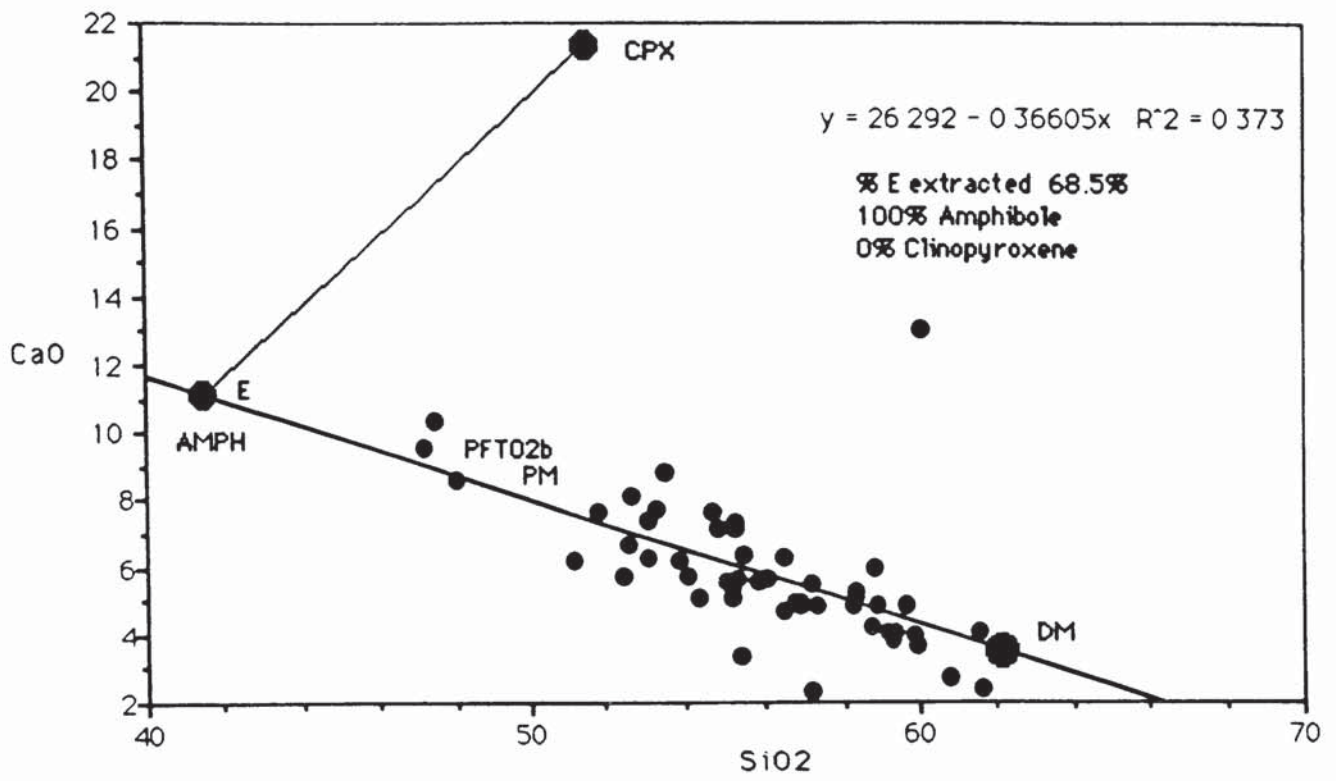


Fig. 4.1c

It is concluded upon the basis of simple Lever Rule modelling of CaO, MgO and Fe₂O₃ vs SiO₂ that the high degrees of crystal fractionation required to explain the distribution of these oxides are unrealistic given the high relatively high Ni, Cr and V contents of these rocks.

What then is the origin of the c.47%–c.60% SiO₂ range in the hornblende lamprophyres? A number of factors may be contributing including the presence of discrete pulses of lamprophyric magma, each varying in SiO₂ content and/or pulses experiencing minor degrees of fractionation both of which are very difficult to constrain. However, as Bergman (1987) summarised, it is possible to produce siliceous, magnesian and potassic lamproitic magmas (up to 60% SiO₂) in the mantle, particularly under hydrous melting conditions. Peccerillo & Manetti (1985) proposed a similar origin for primitive but siliceous lamprophyric magmas in the central Italian volcanic province.

4.2.2) Hornblende–lamprophyres

Petrographic examination of hornblende–lamprophyres shows the fractionating assemblages to be dominated by amphibole, the most abundant phenocryst, together with minor amounts of clinopyroxene. The role of amphibole fractionation in the evolution of calc-alkaline magmas has been investigated by a number of workers, including Cawthorn and O'Hara, 1976; Gill 1981 and Yagi and Takeshita, 1987. The latter authors have suggested that amphibole+plagioclase dominated fractionation of a hydrous high-alumina basalt at 1000°C and 7-10 kb pressure may generate calc-alkaline andesites. Gill (1981) investigated the role of amphibole fractionation in the genesis of andesites and observed that the presence of amphibole as a liquidus phase required H₂O contents greater than those reported for most natural andesites. The stability field for amphibole in calc-alkaline melts is restricted by its resorption when the magma H₂O content is lowered and temperature is increased. Gill (1981) stated that the amphibole could only be stable on the liquidus of andesitic melts at pressures > 8 kb and H₂O contents of 5-10% . Such high H₂O contents would severely restrict the

stability field of plagioclase and thus may explain the lack of feldspar phenocrysts in lamprophyres. Gill (1981) concluded that amphibole fractionation was of minor importance in the genesis of the majority of andesitic magmas, with the exception of some medium- to high- K andesites and rare high-MgO rocks with abundant amphibole phenocrysts. This has implications for the genesis of calc-alkaline hornblende-lamprophyres which have high volatile contents and amphibole as a stable liquidus phase (Rock, 1984, 1987). These studies suggest that for amphibole to be stable in lamprophyric magmas, it must have begun to crystallise at depth, under high volatile pressures, with the magmas undergoing rapid emplacement to prevent reaction and resorption of the amphibole.

Most amphiboles are Ne normative (Gill, 1981; Deer *et al.*, 1963), thus removal of amphibole (or assemblages dominated by amphibole) from a melt would increase the SiO₂ content of the residual liquid (Bowen, 1928) and produce some Fe enrichment, though this is commonly masked by the crystallisation of oxides such as magnetite (Gill, 1981). Amphibole has high distribution coefficients for many trace elements, particularly V, Ti, Nb (in basic-intermediate magmas) and the HREE, and its fractionation will rapidly deplete the melt in these elements. The distribution coefficient for V in amphibole is reported as being greater than that for Ni (Gill, 1981) therefore fractionation of amphibole should produce distinctive increases in Ni/V. However, as a word of caution, although published K_d values for V in amphibole are high (Gill, 1982) there is some question as to whether K_d values for V would be as high in H₂O-rich magmas such as lamprophyres (M.Thirlwall, *pers.com*) presumably due to higher fO₂ values altering its oxidation state. Unfortunately no data is available to confirm this although it is still likely that V will still have appreciably high K_d values in amphibole in high fO₂ lamprophyric magmas, although perhaps not as high as values quoted by Gill (1981). However, magnetite is also likely to act as a sink for V in high fO₂ melts so that fractionating assemblages may still have high bulk distribution coefficients for V (Gill, 1981). Amphibole also has a high K/Rb and its fractionation would lower the K/Rb ratio in the residual magma (Beswick, 1976; Gill, 1981). Bulk

distribution coefficients (D) were calculated for different assemblages composed of varying proportions of amphibole, clinopyroxene and plagioclase based on petrographic observations and published data (Rock, 1984, 1987). Olivine was not included because it is not present in any of the hornblende–lamprophyres from the area. Fractionation curves were calculated for differing assemblages and a number of elements, ranging from the compatible (Ni, Cr, V) to the highly incompatible (Rb, Ba, Th) (Table 4.1).

Ni, Cr and V have D's ≥ 1 for all the assemblages while Ba, Th, Ce, Rb, K, Zr, and Y have Ds ≤ 1 for all assemblages. Ba, Th, Ce, Rb and Zr are the most incompatible elements and concentrations of these elements in the residual liquids should increase significantly during fractionation. Rb is considerably more incompatible than Sr with regard to these assemblages and the Rb/Sr of the residual liquids should increase with fractionation. Zr/Y and Zr/Nb should increase but K/Rb and Ce/Th ratios decrease during fractionation involving amphibole. However, K/Rb and Ce/Th have a wide scatter (Figs. 4.2a-b) as do Ni/V and Rb/Sr (Figs. 4.2c-d) and many of the most evolved (lowest MgO) samples have the lowest Ni/V ratios, contrary to what might be expected during amphibole dominated fractionation. The variation of V and Ni/V with several incompatible elements for hornblende–lamprophyres, together with curves representing the compositional range and evolutionary paths of the model fractionated liquids, are shown in Figures 4.3(a–c).

It is clear that the range of compositions represented by model fractionation curves for both incompatible and compatible elements cannot fully explain the distribution of the data for the hornblende lamprophyres in any of these plots using the initial melt composition represented by PFT–02b (Figures 4.3a-c; 4.4a-b and 4.5a-b) or sample 1325 (Figures 4.3a-b). Moreover, the portions of the model curves illustrated in figures 4.3a & 4.3b represent less than 10% fractionation of an initial magma, as V is rapidly depleted in the liquid using the high Kd value given by Gill (1981) for amphibole. This shows that, even if an initial melt composition with slightly lower Ba and Y abundances were used in the model, the spread of data for the hornblende lamprophyres restricts the

Table 4.1 Bulk distribution coefficients

Phases	A1	A2	A3	A4	A5	A6	A7
Amphibole	0.5	0.4	0.3	0.35	0.4	0.5	1
Clinopyroxene			0.1	0.15	0.1	0.5	
Plagioclase	0.5	0.6	0.6	0.5	0.5		
Ba	0.125	0.132	0.125	0.114	0.118	0.05	0.09
Sr	1.015	1.172	1.157	0.992	1	0.15	0.23
Th	0.08	0.066	0.052	0.059	0.066	0.08	0.15
Ce	0.225	0.22	0.22	0.225	0.225	0.25	0.25
Rb	0.06	0.062	0.059	0.055	0.057	0.035	0.05
K	0.22	0.198	0.167	0.173	0.189	0.175	0.33
Nb	0.663	0.535	0.435	0.5125	0.562	0.8	1.3
Zr	0.205	0.166	0.151	0.1825	0.19	0.325	0.4
Y	0.515	0.418	0.368	0.44	0.465	0.75	1
Ni	5.05	4.006	3.606	4.405	4.6	8	10
Cr	15.05	12.006	12.006	15.005	15.005	30	30
V	16.05	12.806	9.716	11.37	12.915	16.5	32

Fig. 4.2a

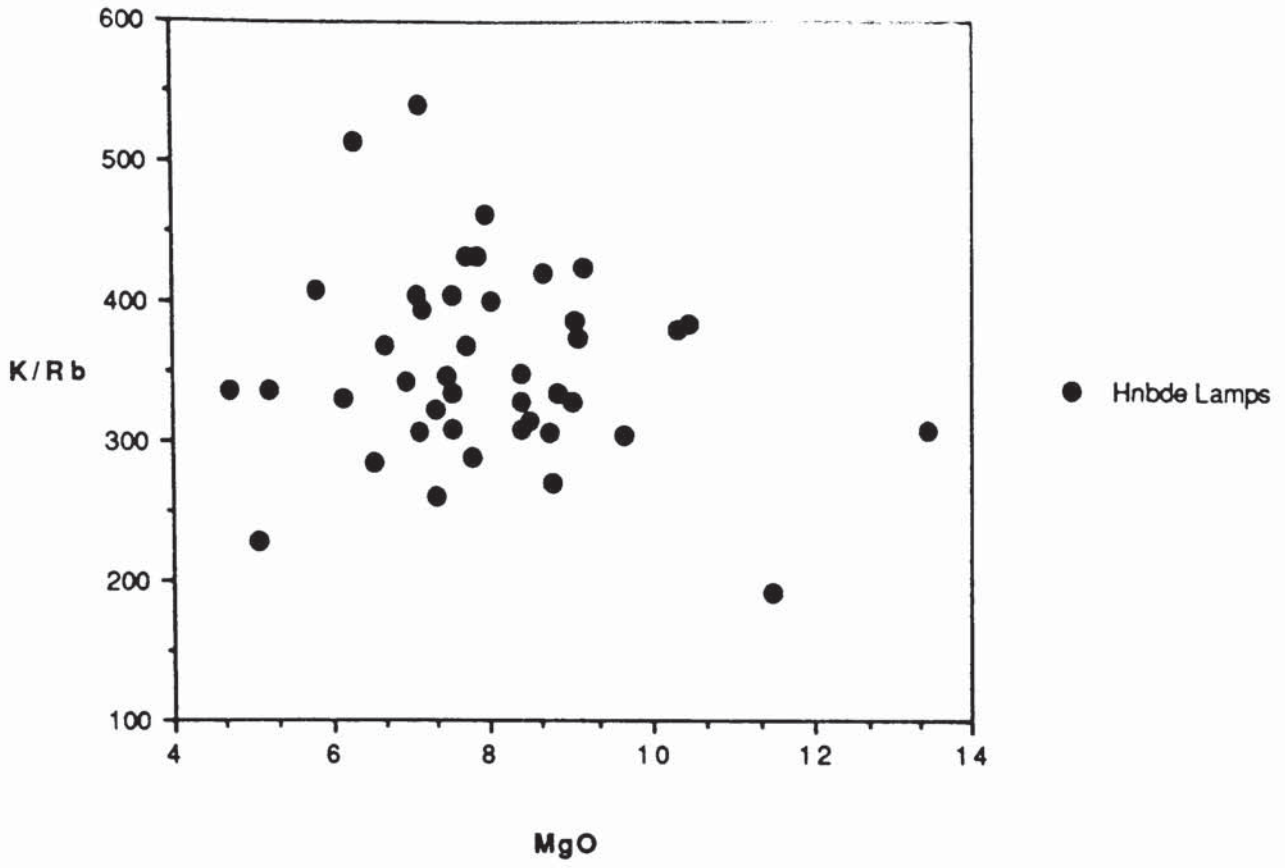


Fig. 4.2b

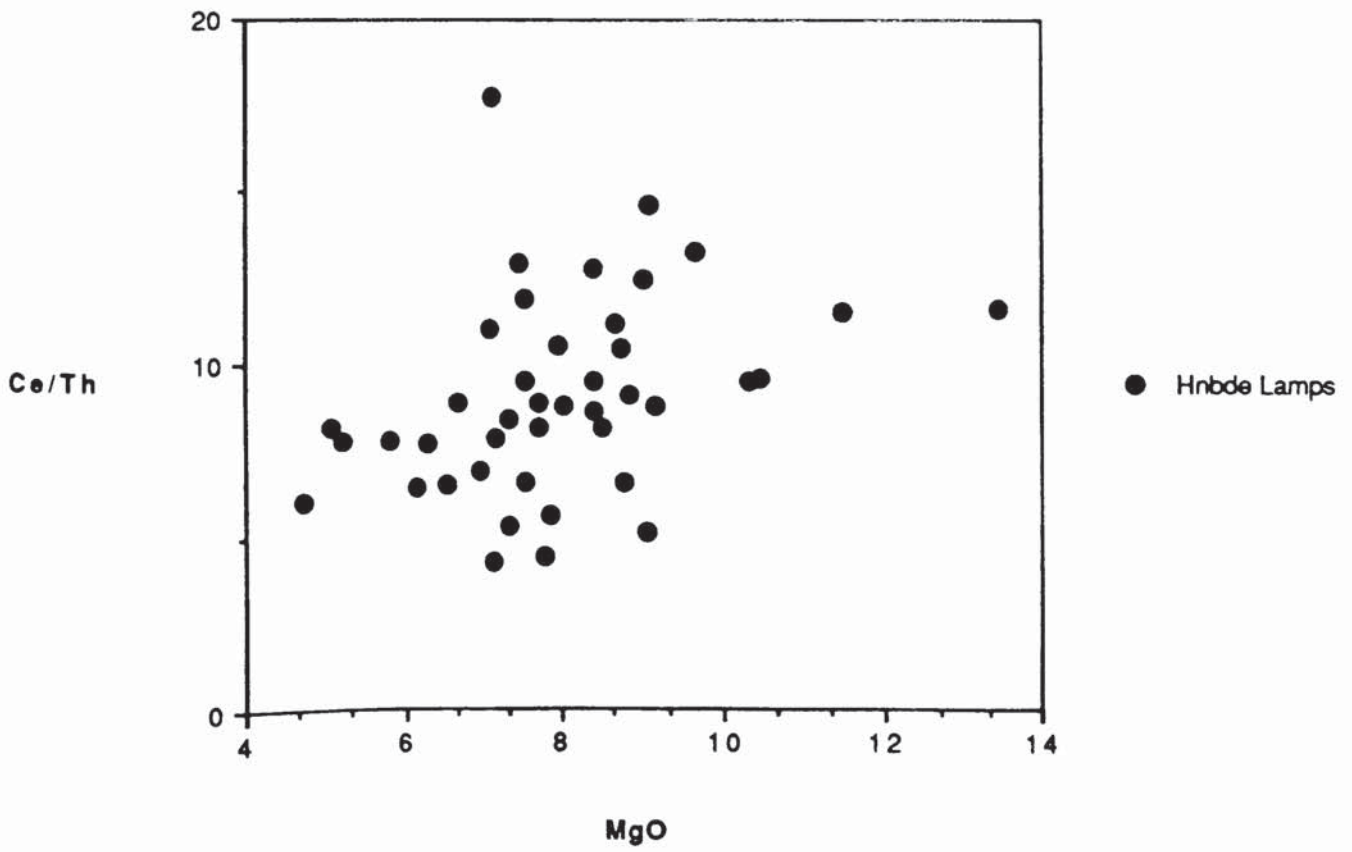


Fig. 4.2c

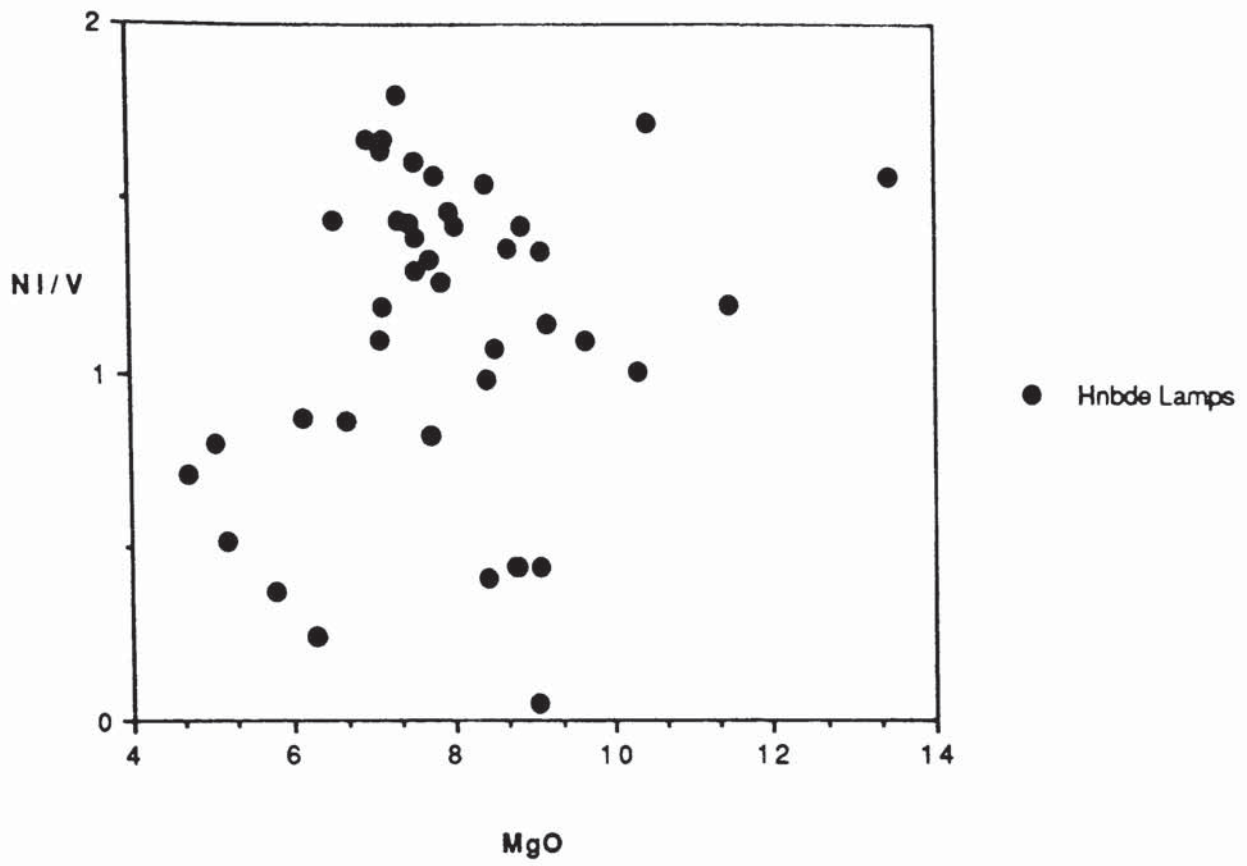


Fig. 4.2d

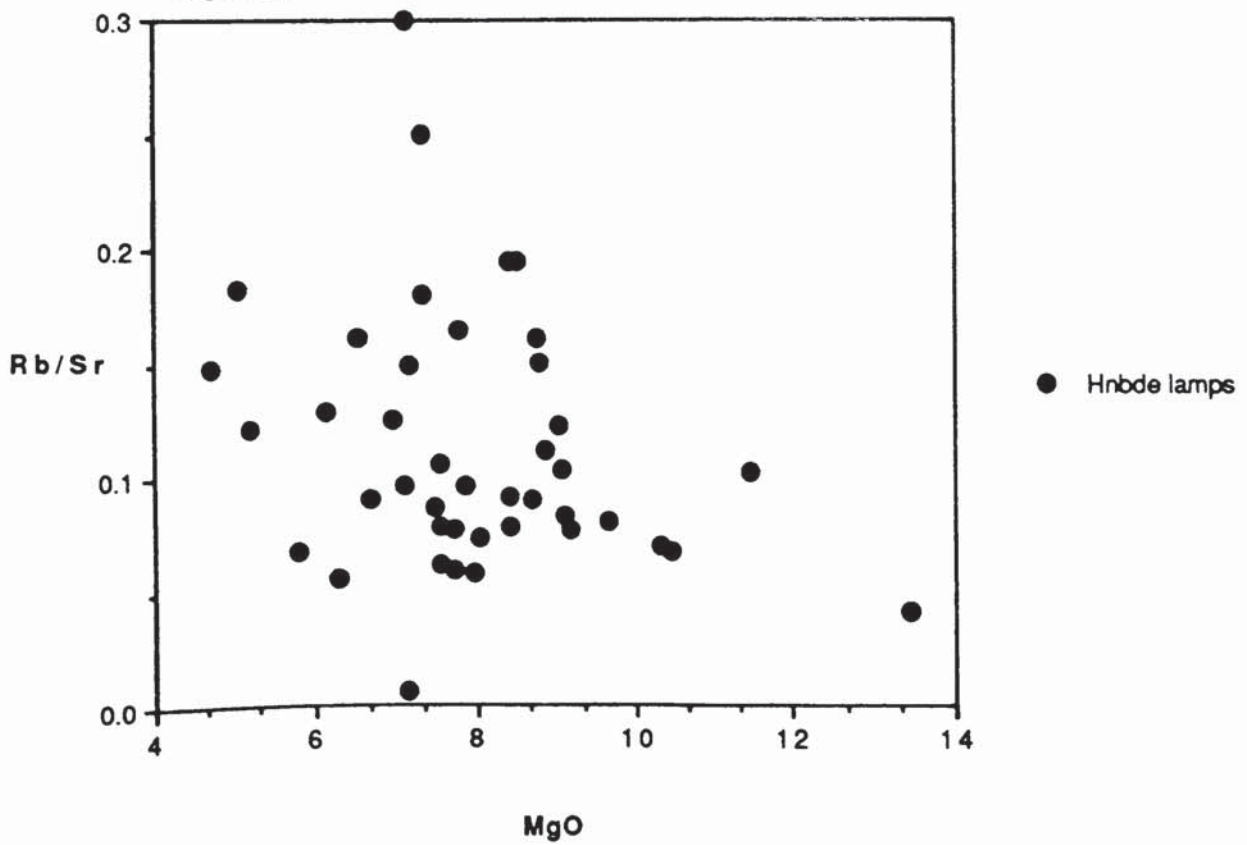


Fig. 4.3a
Open symbols represent % crystallised

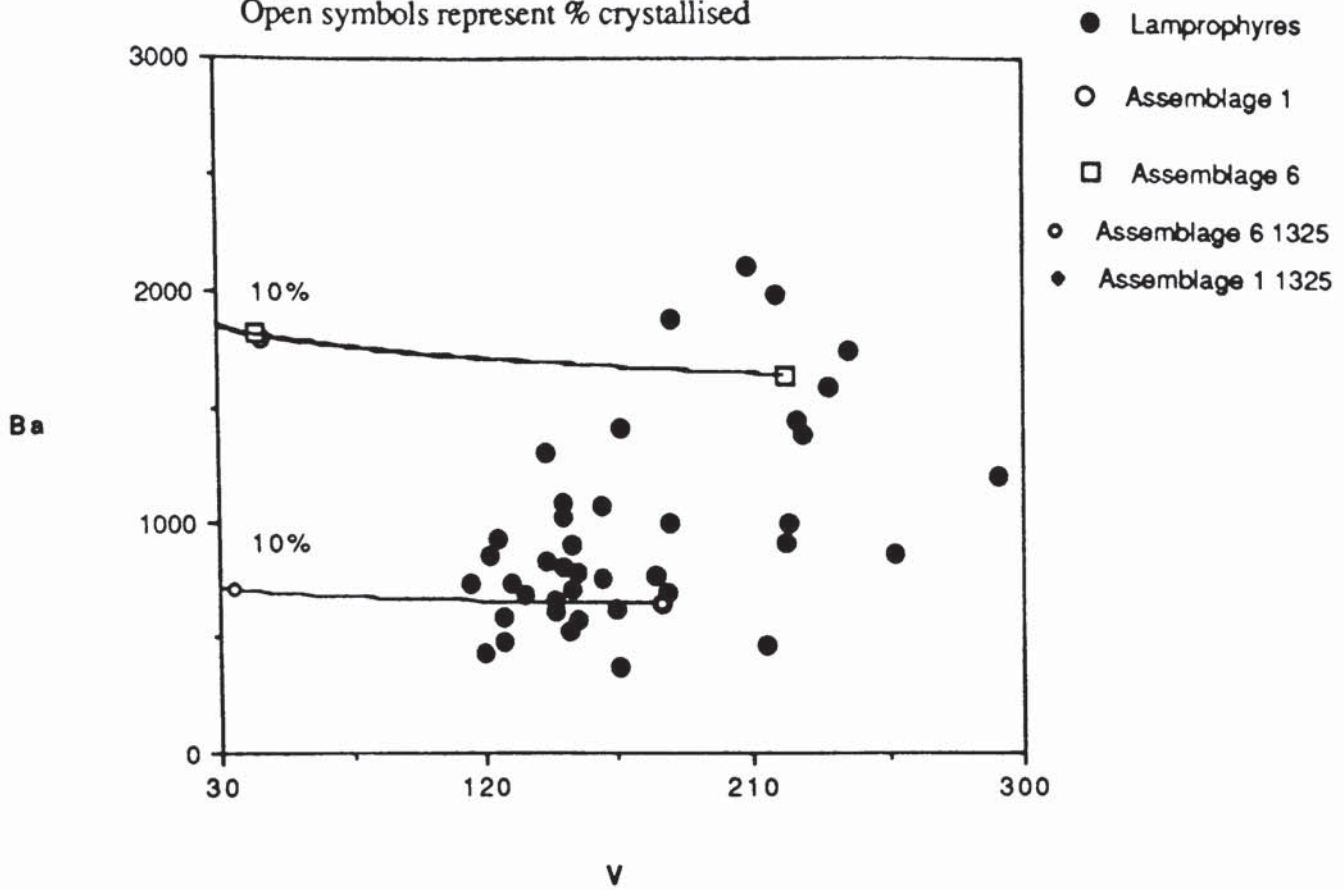


Fig. 4.3b

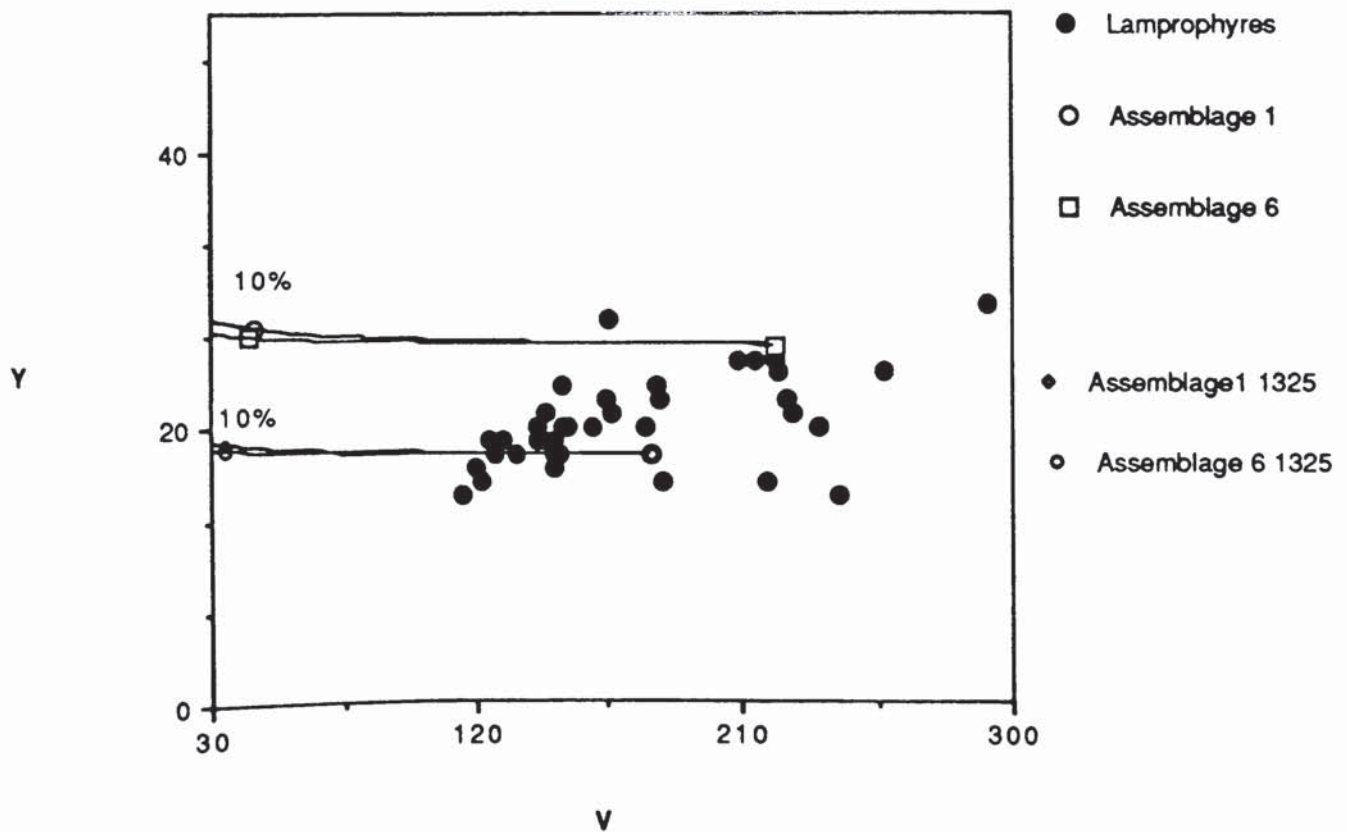


Fig. 4.3c

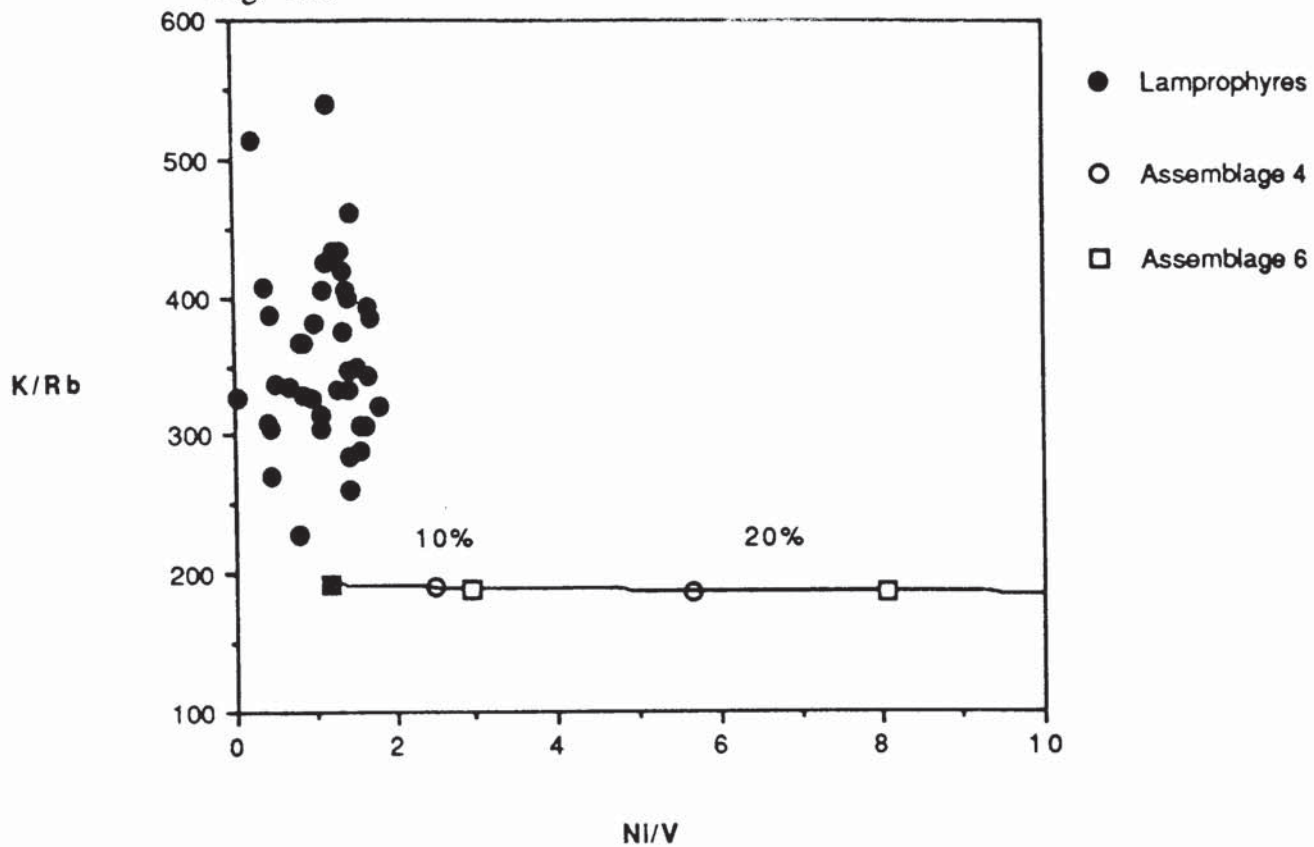


Fig. 4.4a

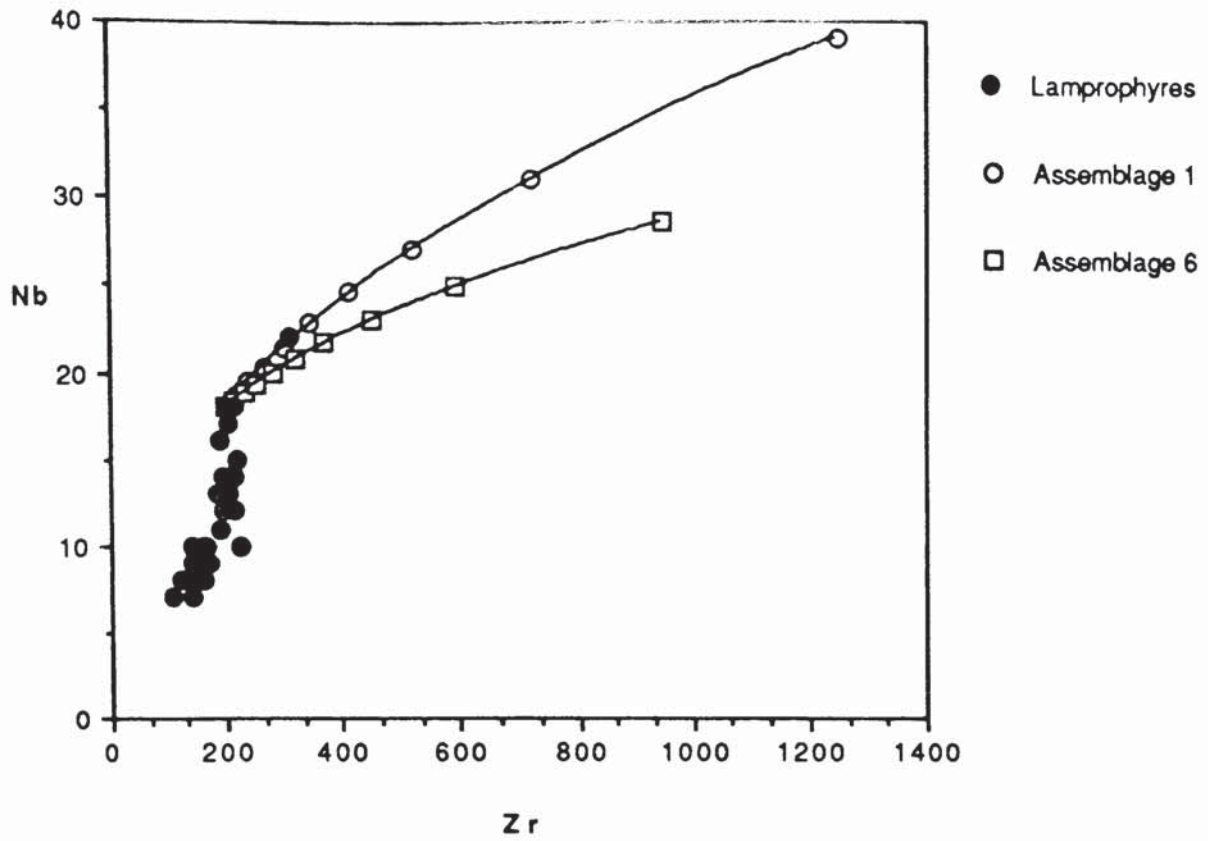


Fig. 4.4b

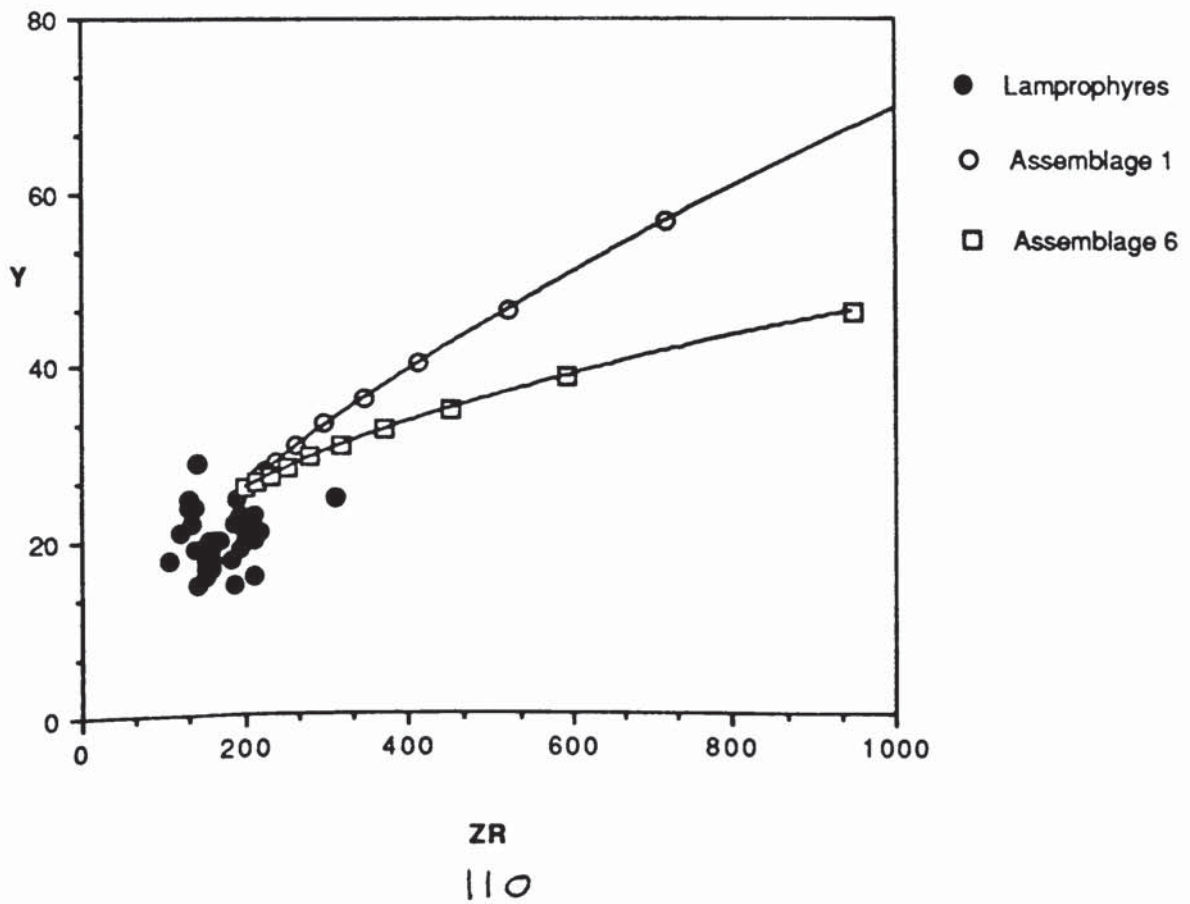


Fig. 4.5a

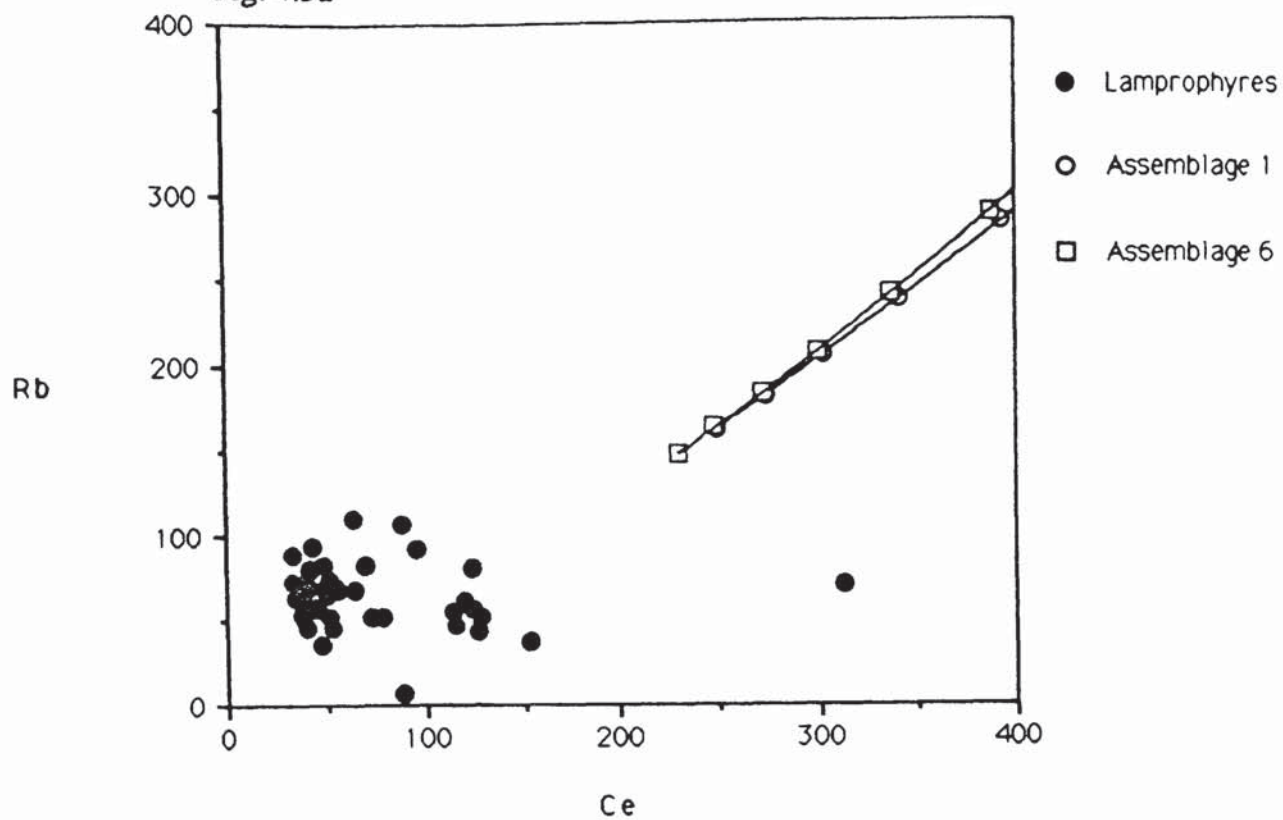
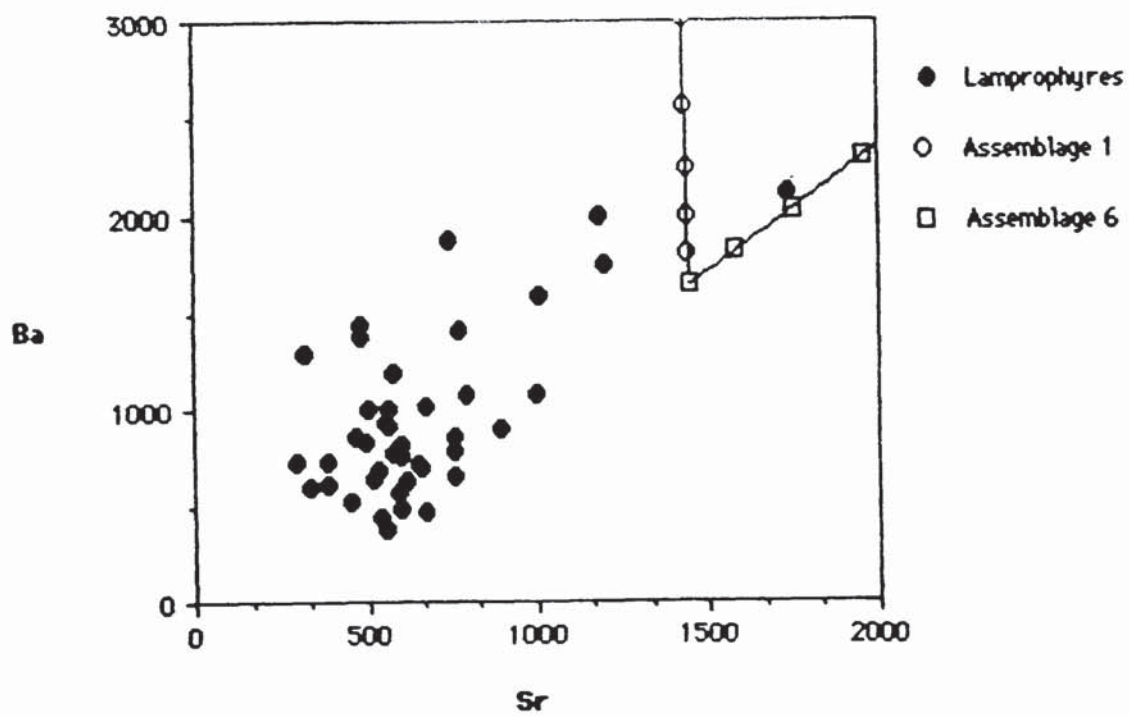


Fig. 4.5b



amount of crystal fractionation to < 10% in order to maintain the high compatible element abundances of the lamprophyric magmas. Even using a lower K_d value for V would not change the direction of these curve, just the rate of V removal from the liquid and would imply greater degrees of fractionation, a conclusion not supported by data for the other compatible elements (Table 4.1). These results also conflict with the very high degrees of crystal fractionation required by CaO, MgO and Fe₂O₃ distributions. Also, selection of another parental magma cannot explain the data distribution (Figures 4.3a-b). Modelling of Rayleigh fractional crystallisation processes, using petrographically constrained endmembers and mineral assemblages, cannot satisfactorily explain all the LILE, HFSE and LREE variations in hornblende lamprophyres from the Criffell dyke swarm. This suggests that the compositional range of the hornblende lamprophyres cannot be explained by the progressive fractionation of a single parental lamprophyre melt and suggests that fractional crystallisation has played only a minor role during the evolution of these magmas.

4.2.3) Mica–lamprophyres

Experimental studies have demonstrated that phlogopite, co-existing with clinopyroxene and olivine, is an early forming phase during the crystallisation of a calc–alkaline lamprophyres and other compositionally similar melts (Barton & Hamilton, 1979; Esperanca & Holloway, 1987). Arima and Edgar (1983) suggested, on the basis of experimental studies of a katungite, that phlogopite and clinopyroxene crystallised under high pressures, whereas at lower pressures olivine and melilite formed, through the reaction clinopyroxene + phlogopite – olivine + melilite. Other experimental data suggests that phlogopite crystallises under a wide range of pressures and temperatures and has a broader stability field than amphibole under upper mantle conditions but that its crystallisation requires a liquid with high contents of both K₂O and H₂O (Kushiro *et al.* 1967; Yoder & Kushiro, 1969; Beswick, 1976; Edgar & Arima, 1983).

Phlogopite is the most abundant phenocryst in the mica–lamprophyres from SW Scotland and is commonly associated with minor amounts of clinopyroxene. There is no petrographic evidence for reaction relations between the two phases (Chapter 2) and it is therefore likely that phlogopite and clinopyroxene are the dominant liquidus phase in these rocks (Esperanca & Holloway, 1987). Phlogopites generally have high values for both K_2O/Na_2O , Rb/Sr and low K/Rb thus fractional crystallisation involving phlogopite or assemblages dominated by phlogopite should lower the K_2O/Na_2O and Rb/Sr values of the residual liquids while raising the K/Rb (Beswick, 1976). Six assemblages, composed of varying proportions of phlogopite, clinopyroxene, olivine and plagioclase were chosen for modelling purposes using several compatible and incompatible elements (Table 4.2). As with the hornblende lamprophyres, plagioclase was included in some assemblages to investigate its effect on, and extend the range of, modelled compositions.

For all model assemblages, Cr is the most compatible element, followed by Ni and V, and values of D for Cr are generally 2–3 times those for Ni. Ni/Cr values therefore should increase during phlogopite–dominated fractionation and Ni/V and Cr/V should decrease. In contrast to the hornblende–lamprophyres, both K and Rb are compatible in the modelled assemblages with Rb having marginally higher D values than K (Henderson, 1982). Perhaps the most surprising bulk distribution coefficient values is for Ba which, according to Henderson (1982), has a K_d in phlogopite of 1.1. This seemingly low value is confirmed by calculated (mineral/whole rock) K_d values of only 1.04–1.53 for Ba in phlogopites from the Los Volcanoes CAL in the Mexican Volcanic Belt (Wallace & Carmichael, 1989) The differing behaviour of Rb, Ba and Sr should lead to a decrease in Rb/Sr in the residual liquids and a slight increase in Ba/Rb. Ce/Th should remain relatively constant because of the similar D values for Ce and Th in the majority of the assemblages. The patterns for all these ratios show either a complete scatter or poorly defined trends (K/Rb–MgO) which conflict with those expected to be produced by the fractionation of phlogopite or phlogopite bearing assemblages (Figures 4.6a-d).

Table 4.2

Phases	Bulk distribution coefficients					
	A1	A2	A3	A4	A5	A6
Phlogopite	0.5	0.5	0.5	0.4	0.5	0.7
Clinopyroxene	0.5	0.4	0.3	0.2	0.1	0.3
Plagioclase			0.2	0.4	0.4	
Olivine		0.1				
Ba	0.56	0.56	0.59	0.51	0.62	0.78
Sr	0.08	0.073	0.42	0.77	0.77	0.08
Th	0.16	0.16	0.16	0.13	0.16	0.22
Ce	0.14	0.12	0.13	0.14	0.12	0.1
Rb	1.56	1.56	1.57	1.27	1.58	2.176
K	1.36	1.36	1.38	1.13	1.4	1.896
Nb	0.65	0.62	0.6	0.47	0.54	0.79
Zr	0.425	0.4	0.38	0.29	0.33	0.5
Y	0.265	0.22	0.17	0.12	0.08	0.17
Ni	4.75	9.95	3.55	2.6	2.35	4.25
Cr	18.5	18.9	12.5	8.8	6.5	13.9
V	1.55	1.45	1.33	1.02	1.11	1.73

Fig. 4.6a

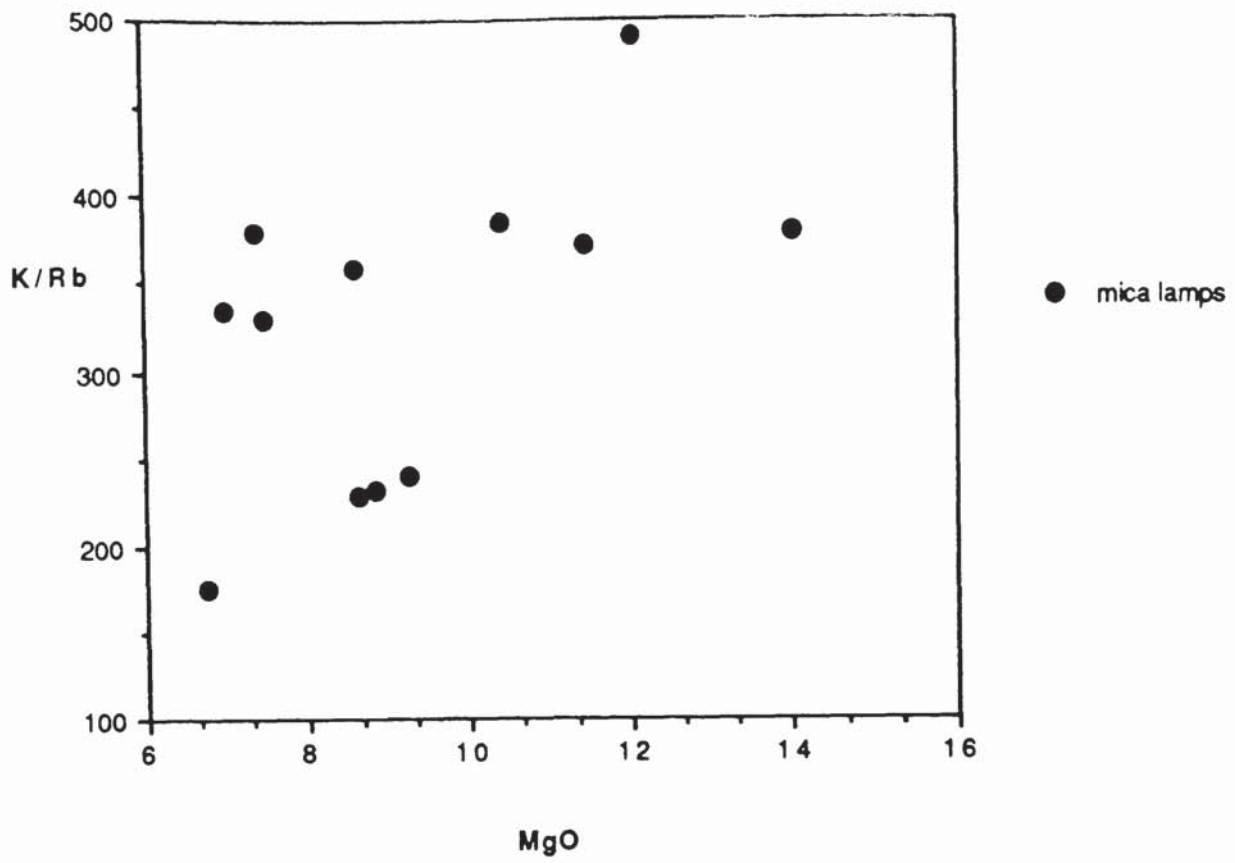
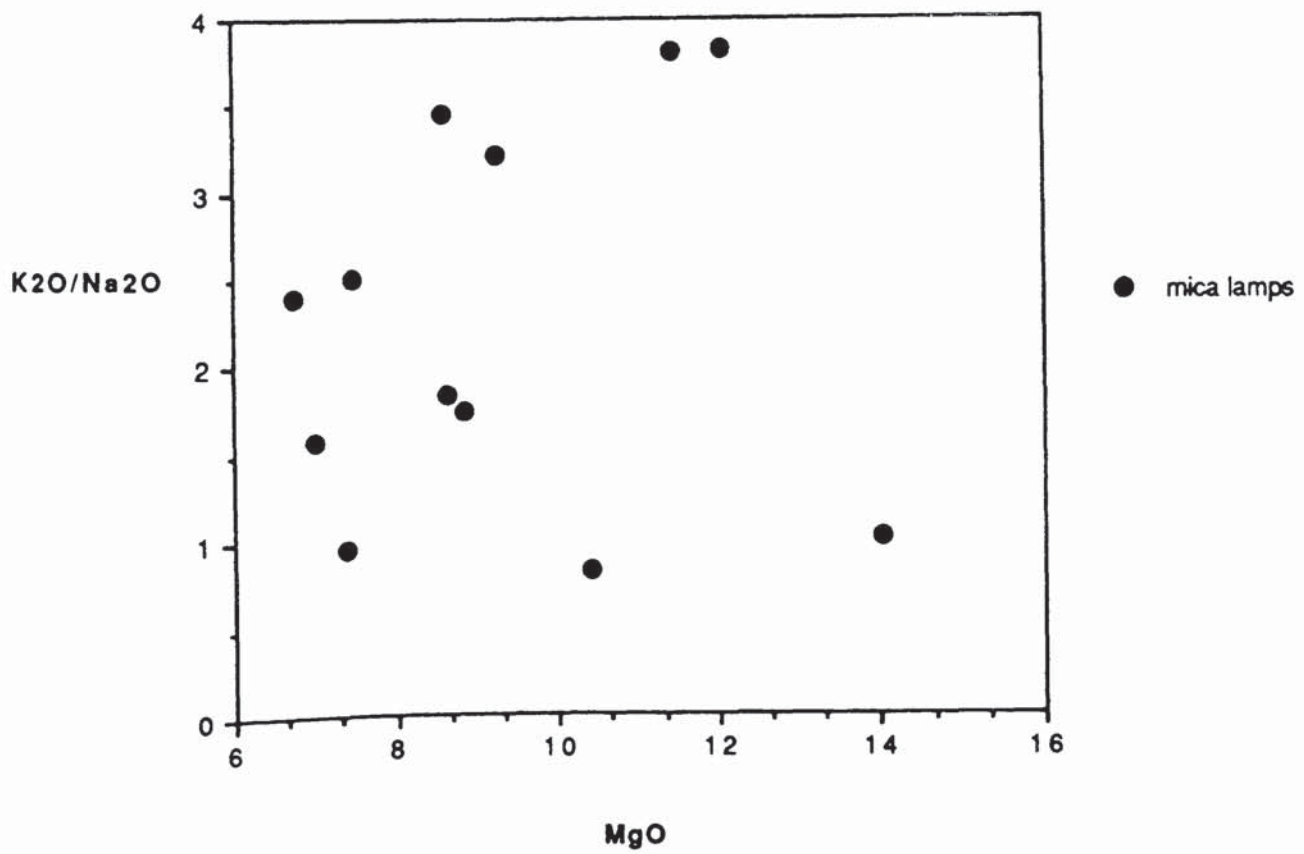


Fig. 4.6b



MgO

Fig. 4.6c

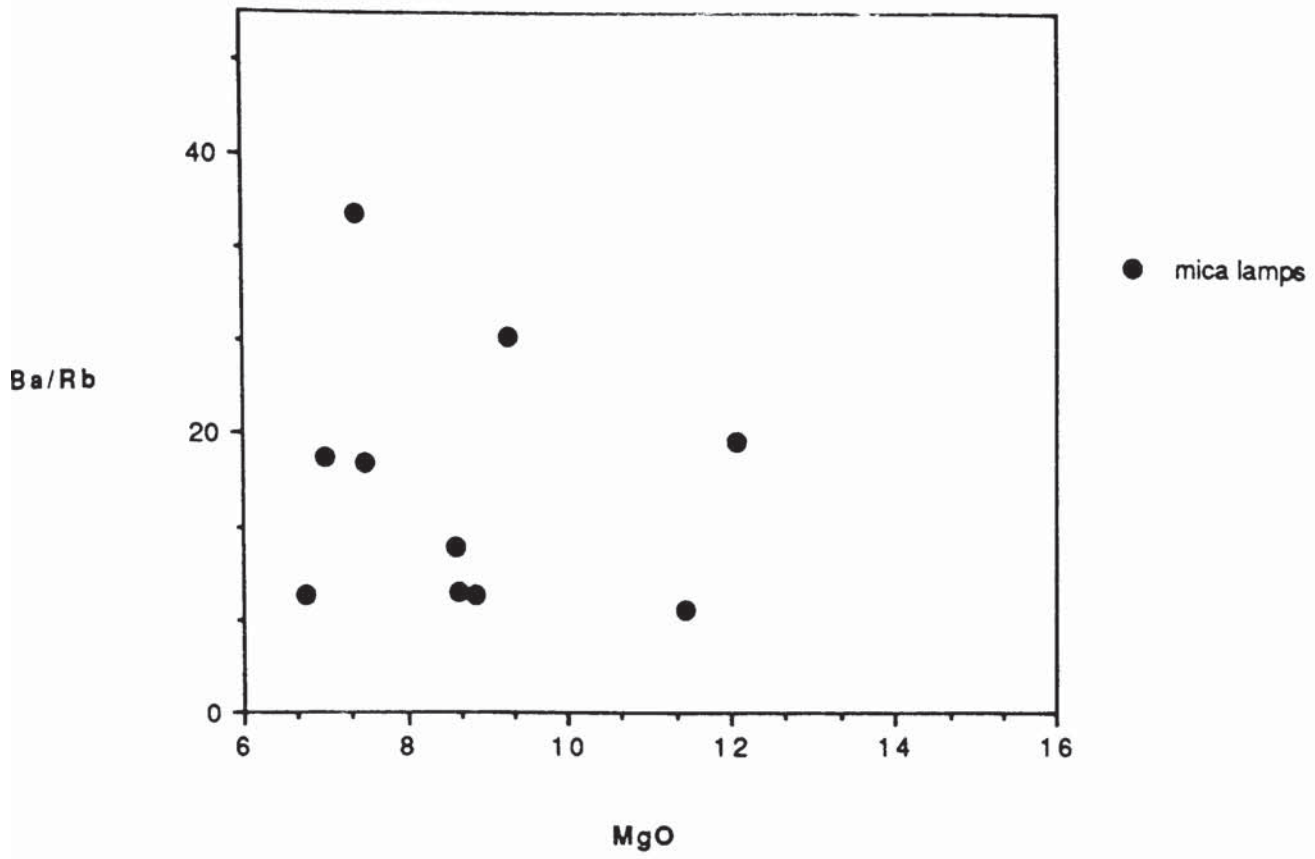
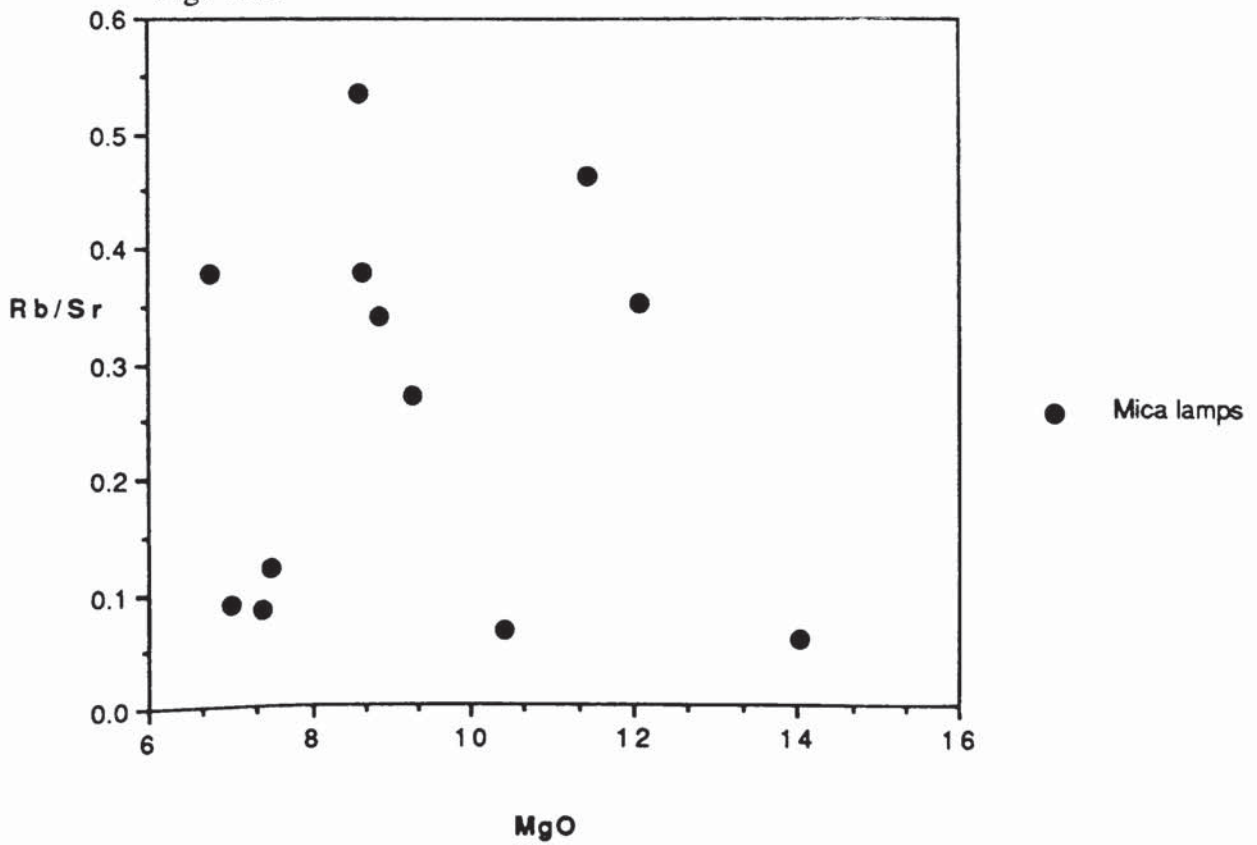


Fig. 4.6d



MgO

116

A fine grained, high-MgO, mica lamprophyre (1371, appendix D) from the Criffell dyke swarm was used as the end-member melt in Rayleigh fractionation modelling and the results of this modelling are shown in figures 4.6(a-e). Ni-Cr variation in the mica-lamprophyres shows a scattered positive trend below any of the model curves (Fig. 4.7a). The curve which fits most closely to the actual data is that for assemblage 2, containing 10% olivine, 40% clinopyroxene and 50% phlogopite. However fractionation of an assemblage with a greater proportion of olivine could not explain the high values of Ni and Cr in samples which have lower Ni/Cr values and there is no petrographical evidence in the most mafic lamprophyres for the 25-30% olivine required in such assemblages. The weakness of a crystal fractionation model are further demonstrated by consideration of the LREE and LILE. The mica-lamprophyres from the Criffell swarm show a scattered negative trend with low Ni samples (thus theoretically the most fractionated) having the highest Rb contents (Fig. 4.7b). Similar results are obtained from plots of Rb-Ba and Rb-Ce (Figs. 4.7c-d). It is clear that the Rb and Ba abundances in the Criffell mica-lamprophyres cannot have been controlled by fractionation of a low Rb, Ba parent using the model fractionating assemblages. Similarly, the model curves show that Nb, and particularly Zr abundances, in the residual liquids increase during fractionation, to much higher levels than found in the Criffell mica-lamprophyres.

4.3) Crustal contamination

The possible effects of crustal contamination on the composition of basic, mantle derived rocks have been summarised by Wilson (1989) who highlighted the two main environments in which melts could undergo crustal contamination. The first of these is in crustal magma chambers in which heat from the cooling and crystallising magma would promote assimilation of the country rocks forming the walls of the magma chamber (DePaulo, 1981). The other is during transport of melts in dykes from the mantle up into the crust during which the hotter, more primitive melts would undergo the greatest degree of contamination, mainly through partial melting of the fusible

Fig. 4.7a

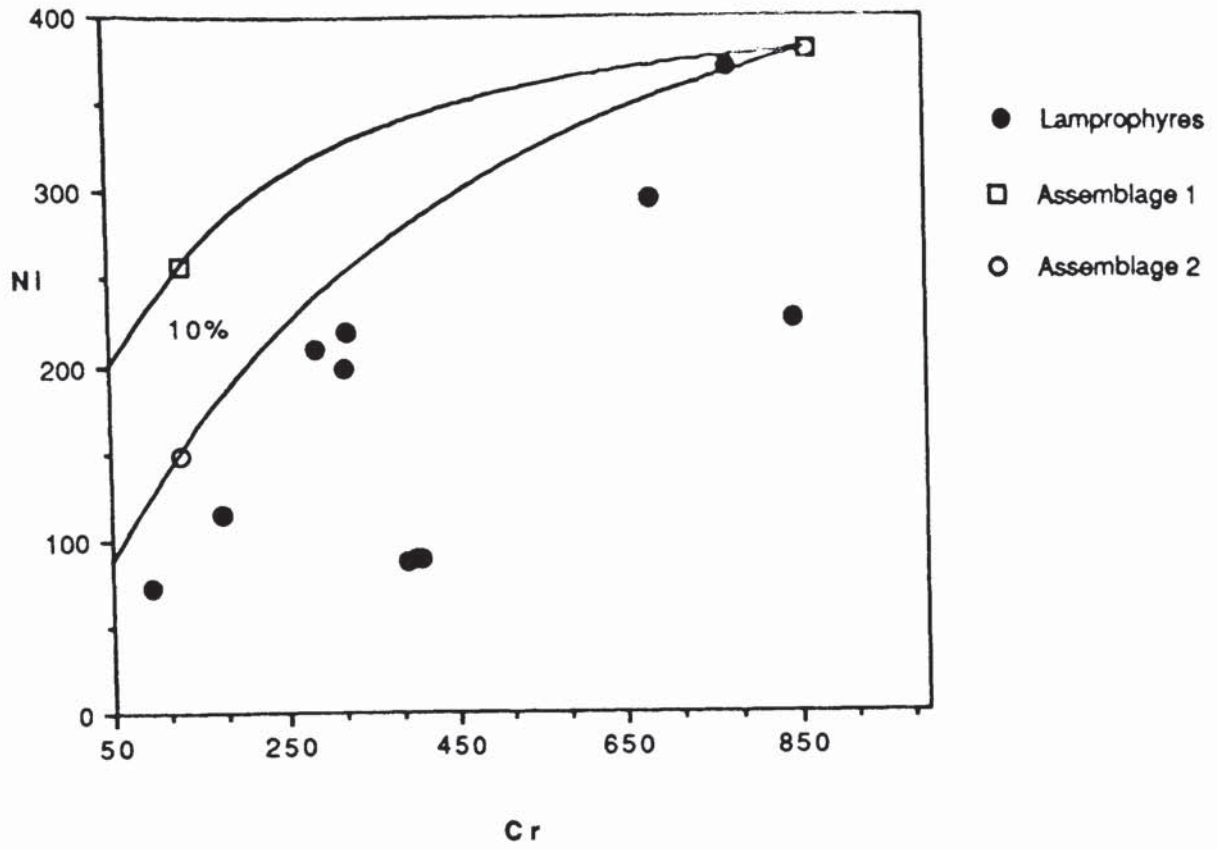


Fig. 4.7b

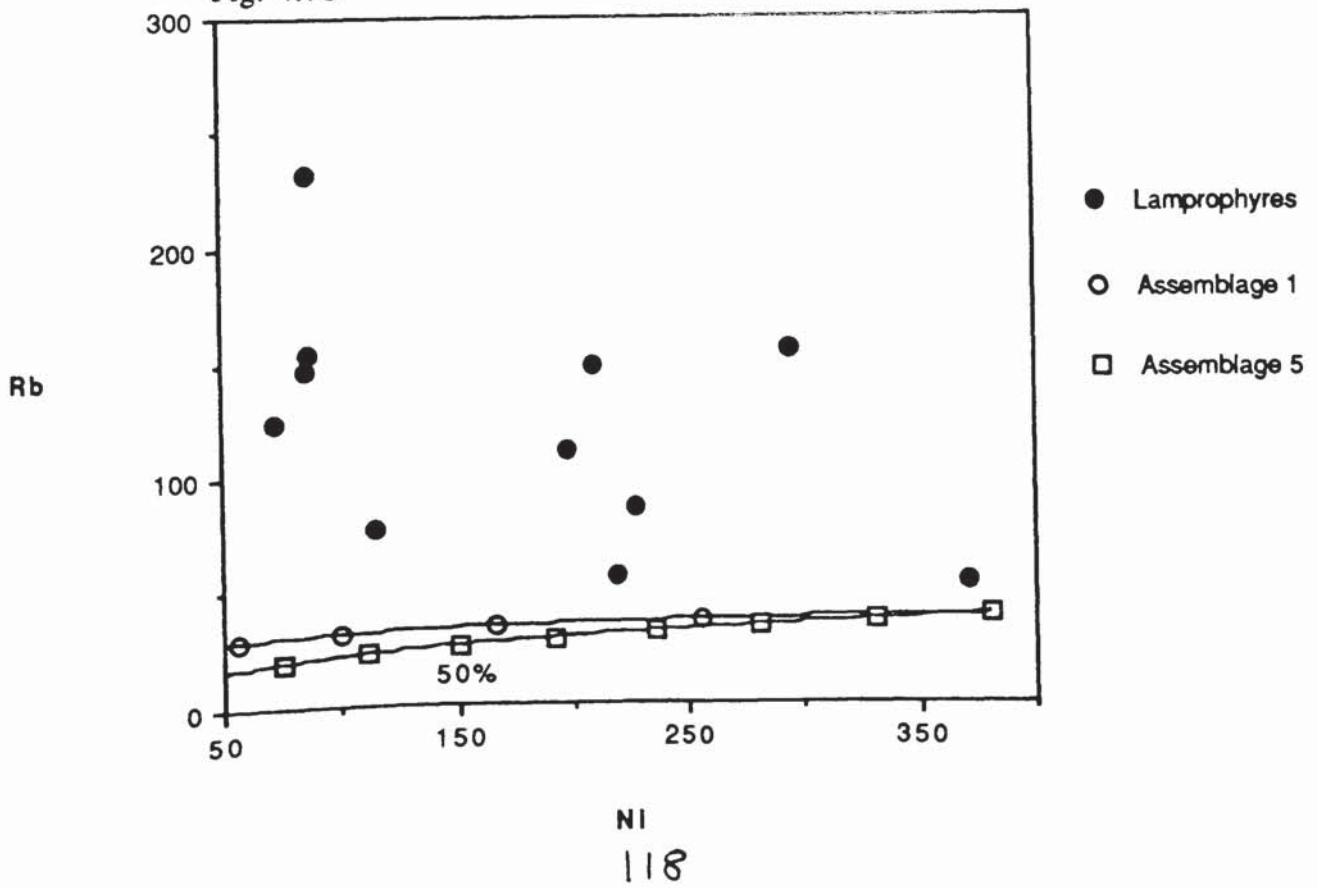


Fig. 4.7c

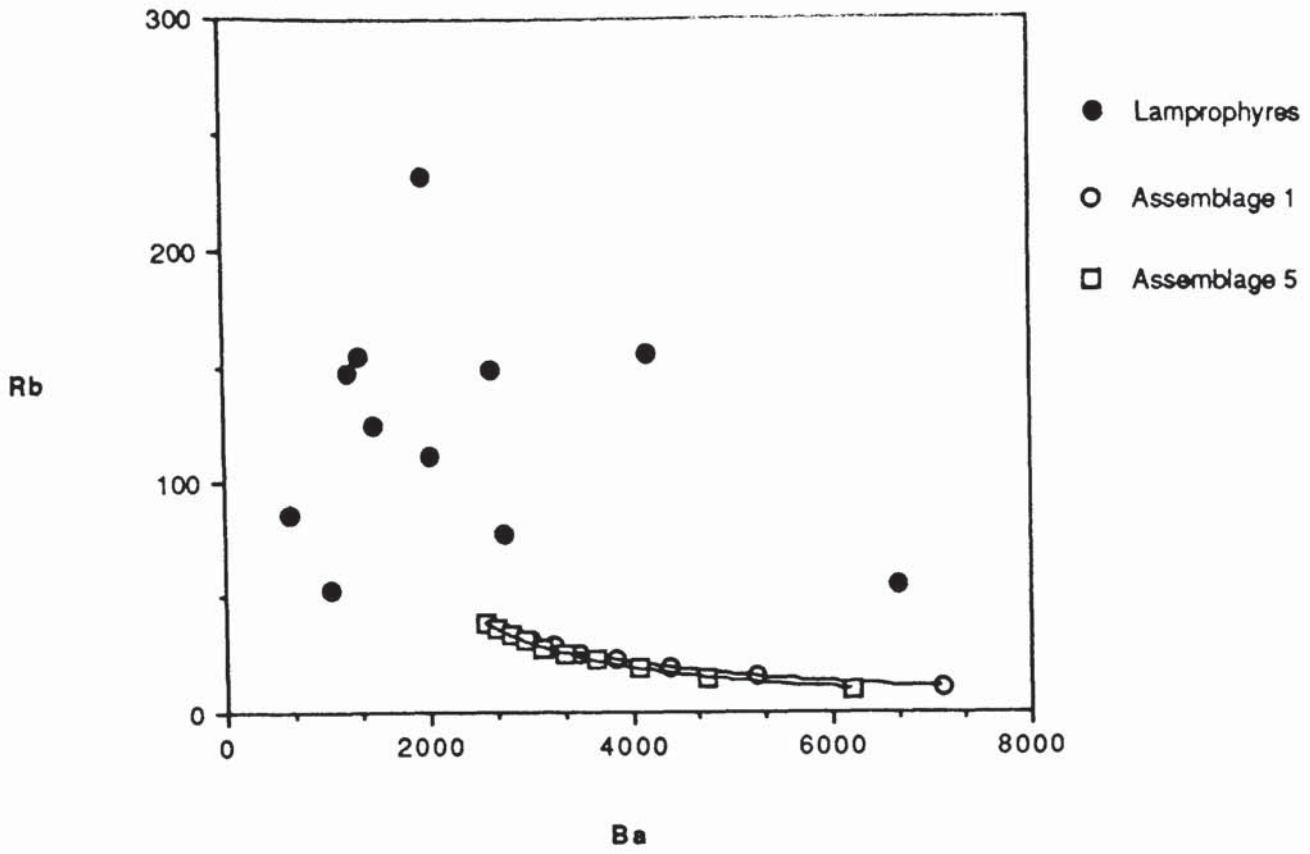
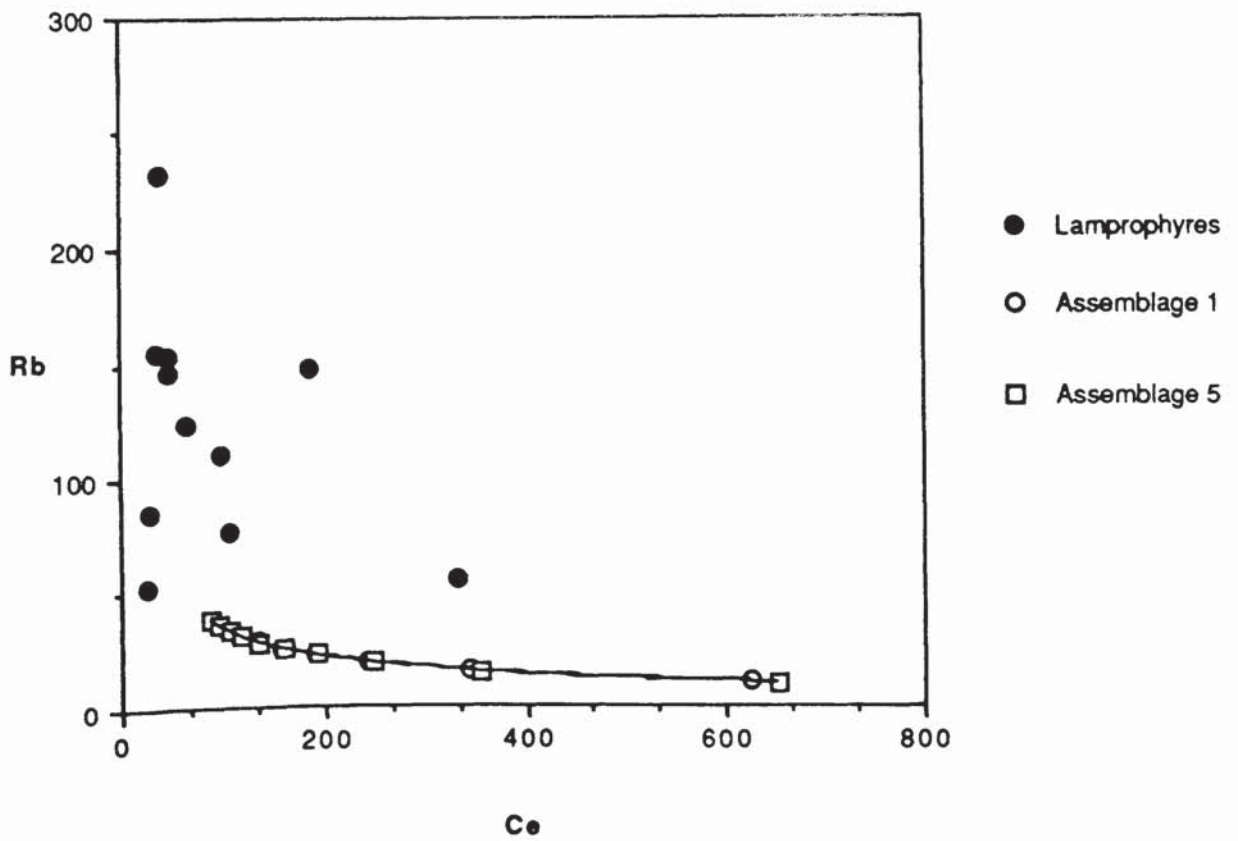
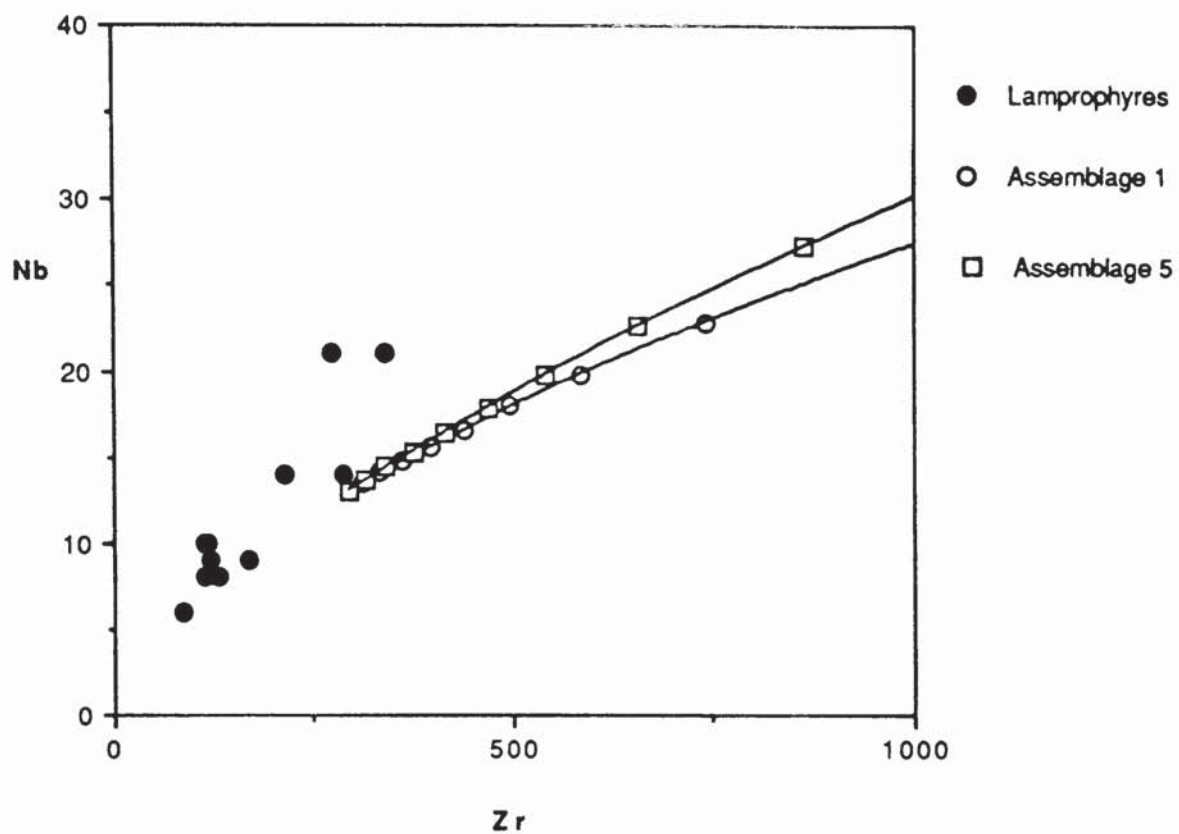


Fig. 4.7d



Co

Fig. 4.7e



components of the surrounding wall rocks (Huppert & Sparks, 1985; Patchett, 1980). In both cases the contaminated magmas may well be enriched in LILE and LREE elements derived from the crustal contaminant as well as undergo shifts in their isotopic composition, usually, in the case of Rb-Sr and Sm-Nd, to more evolved compositions. The possible effects of both these mechanisms on the composition of the Criffell CAL is investigated.

4.3.1) Patchett (1980) & Huppert & Sparks (1985) models

The details of these models are fully explained in the relevant references and will not be repeated here. The key element of such models is that the more primitive, i.e. the hotter a melt is, the more likely it is to be contaminated with partial melts derived from the more fusible components of the surrounding rocks. The efficacy of this mechanism is thought to be at its greatest if the melts are intruded as dykes, with large melt-wall rock contact areas (Patchett, 1980). In addition, the width of the dykes is also thought to influence the efficiency of contamination as melts being transported in wider dykes (> 3m, according to Huppert & Sparks (1985), though Patchett (1980) quotes 10m as the minimum width) are thought to undergo turbulent flow, facilitating erosion and incorporation of the crustal rocks. Melts in narrow dykes are believed to undergo less abrasive laminar flow, with the formation of chilled margins which inhibit contamination with crustal material. The results of this contamination mechanism should be to produce negative correlations between contamination indices and indicators of fractionation (Huppert & Sparks, 1985). Thirlwall & Jones (1983) demonstrated that the Tertiary lavas on Skye had undergone contamination by this mechanism with correlations between ϵNd and indices of silica saturation.

Therefore, is it possible that a similar process has affected the Criffell CAL. At first examination they would seem the ideal candidates as they are intruded as dykes, have high liquidus temperatures (circa 1100°C, Esperanca & Holloway, 1987) and high LILE abundances, combined with high MgO, Ni and Cr values. However, there are several factors which mitigate against such a process operating on the Criffell CAL.

Firstly, as a general point, both Patchett (1980) and Huppert & Sparks (1985) described their models upon the basis of feeder dykes in a complex basaltic volcanic system (e.g. Continental Flood Basalt provinces, CFB, such as the Deccan). These are likely to involve significant volumes of magma erupted through, presumably, relatively long-lived dyke systems. In fact this is a prerequisite, as melt must flow through the dyke in sufficiently large volumes, at relatively high flow rates, to experience significant contamination (Huppert & Sparks, 1985). This results in large volumes of magma being produced, either in volumetrically significant dyke swarms (with dykes > 3m, and where dykes are likely to be wider in the brittle regime at high crustal levels than at depth) or large volumes of lava flows. It is questionable whether such an environment is applicable to the low volumes of lamprophyric magma observed at the present day surface around Criffell, where most dyke widths are < 3m (Chapter 2) and no late Caledonian age lavas flows are preserved. Further, as most lamprophyre dykes around Criffell are < 3m wide, and this can be considered as a maximum if the arguments about brittle behaviour in the upper crust are accepted, then it is likely that the lamprophyres experienced laminar flow during intrusion and thus little contamination by this mechanism (Huppert & Sparks, 1985).

However, evidence from combined isotope and chemical variations is possibly more compelling. The lack of correlations, either negative or positive, between ϵSr and fractionation indices, such as SiO_2 , MgO and Ni tend to argue against contamination (Figs 4.8a-c) as one might expect negative correlations between differentiation indices and isotopic parameters. Similarly, the lack of correlation between ϵNd values and similar differentiation indices lend themselves to a similar conclusion (Figs 4.9a-c). However, Huppert & Sparks (1985) advised that although such correlations could be expected in simple systems, complexities involving variations in magma flow rate, temperature and variations in the composition of the initial magma could scatter these correlations. These authors, however, also suggested that, because phenocryst composition in the magma reflected the composition of the pre-contamination melt, comparison of the Sr isotopic composition of the phenocrysts and the groundmass in

Fig. 4.8a

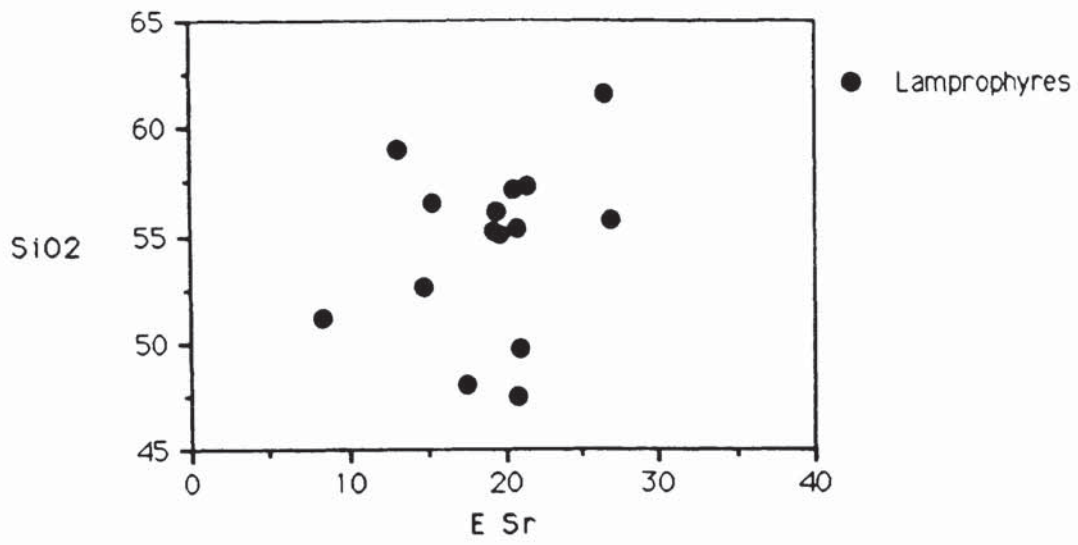


Fig. 4.8b

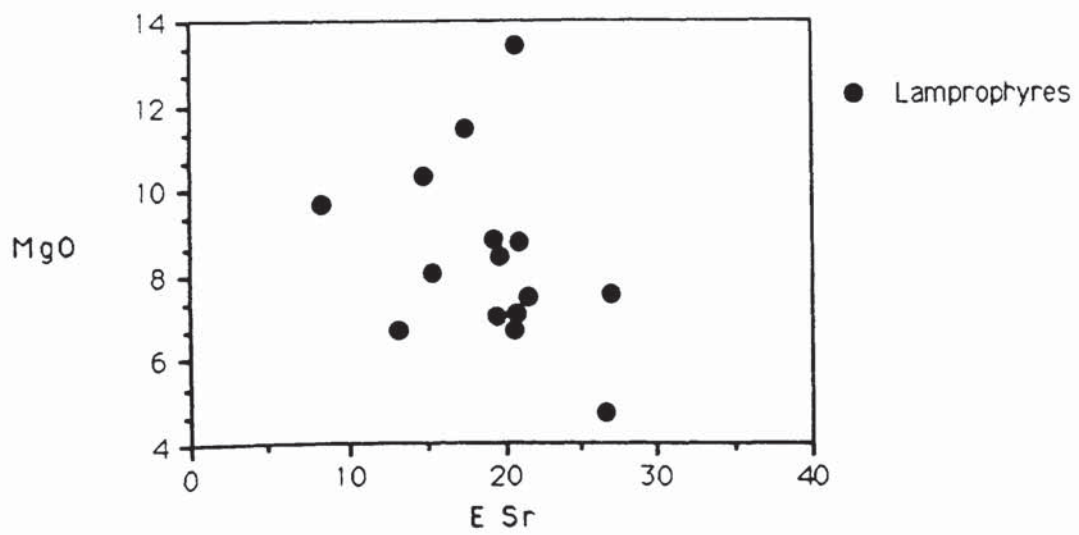


Fig. 4.8c

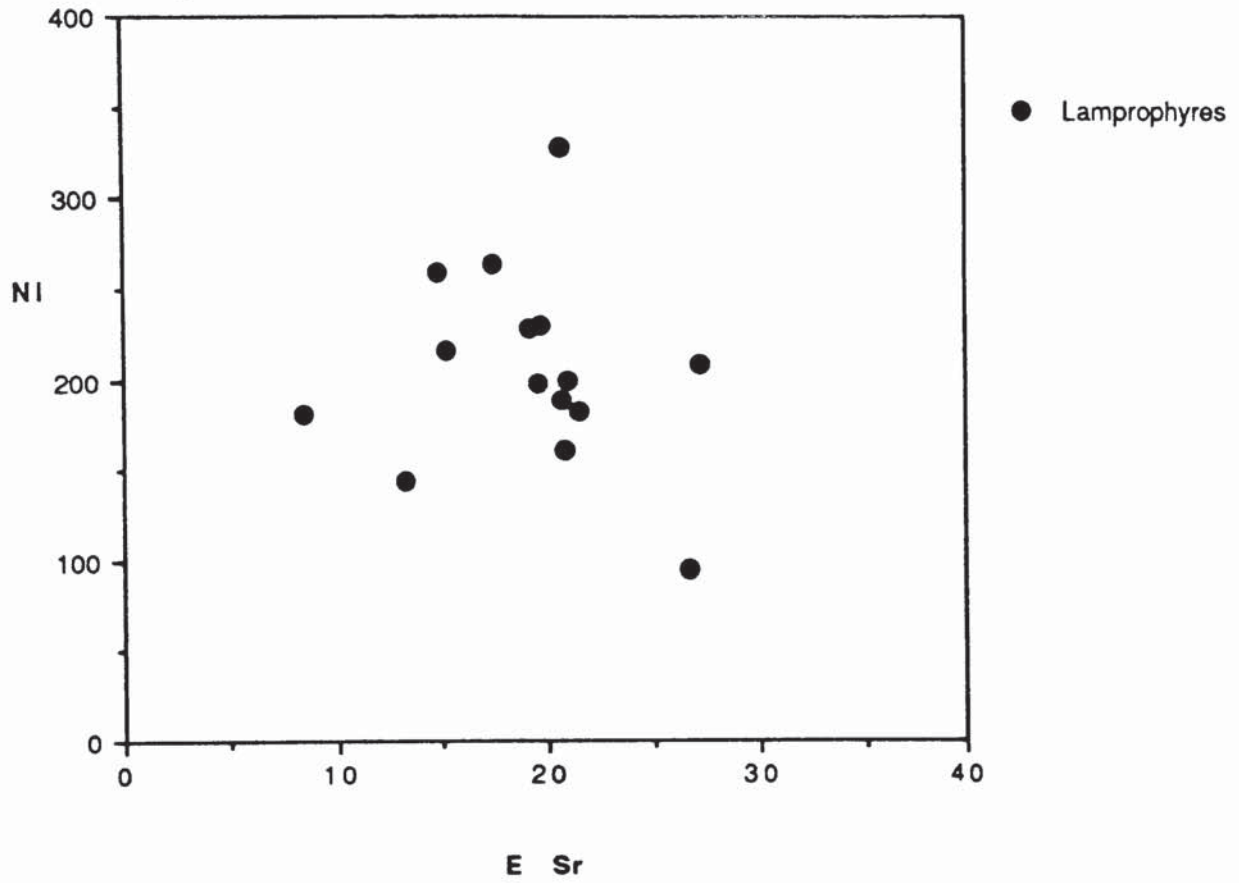


Fig. 4.9a

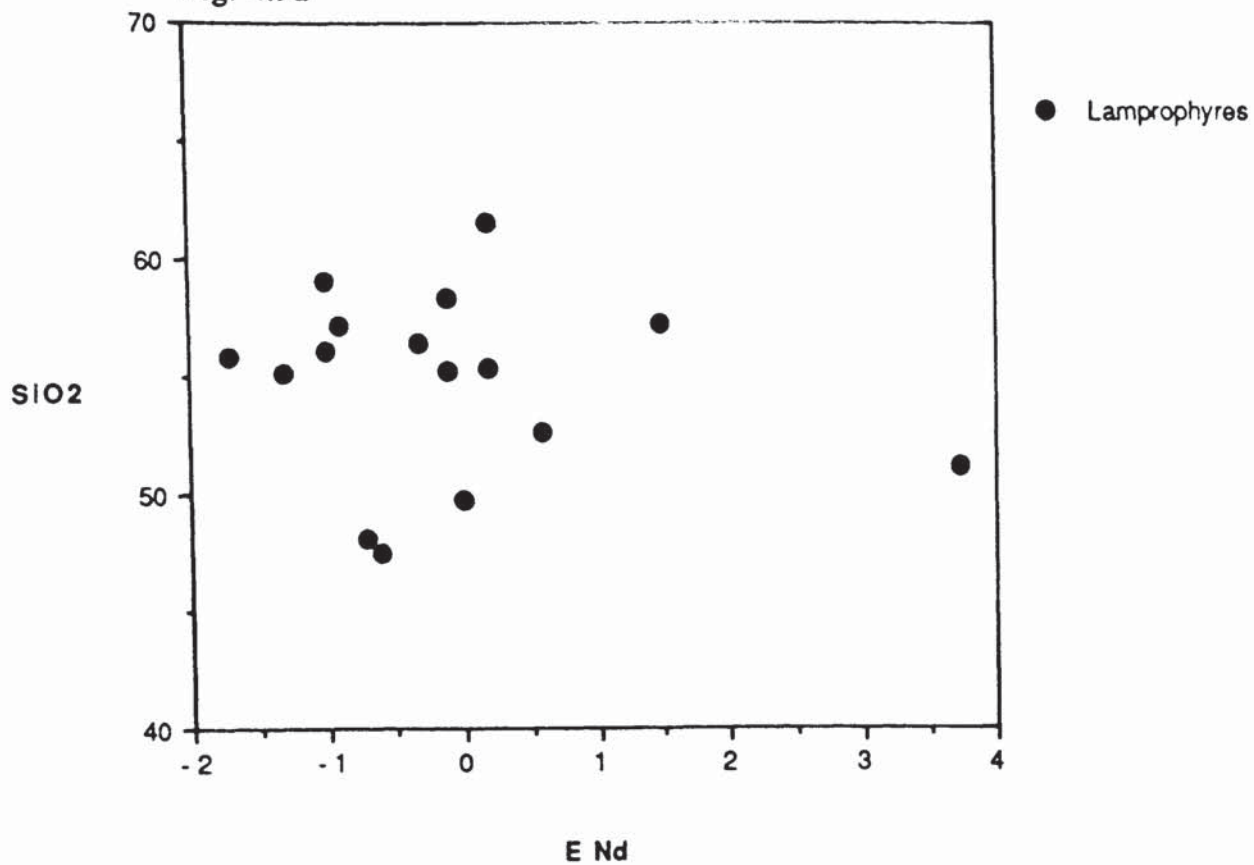


Fig. 4.9b

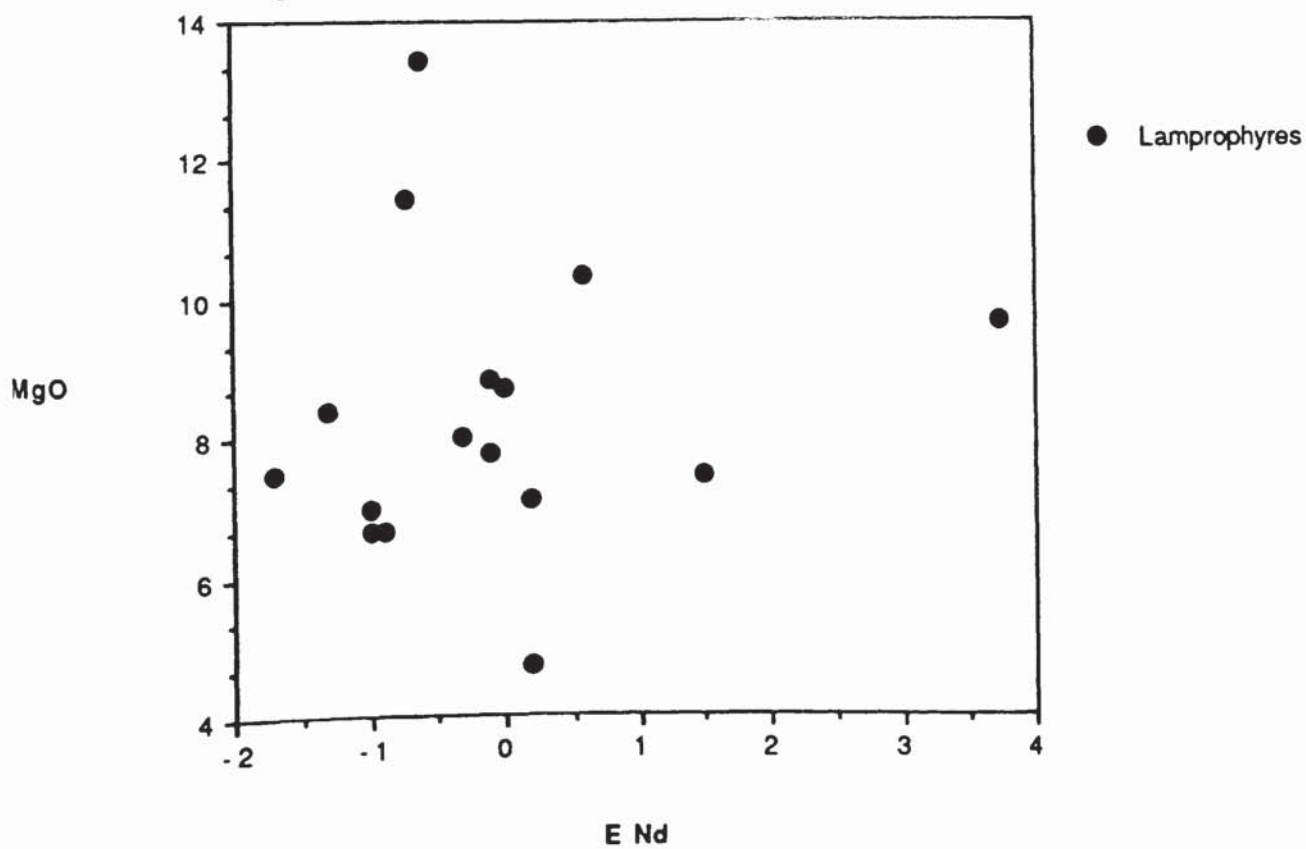
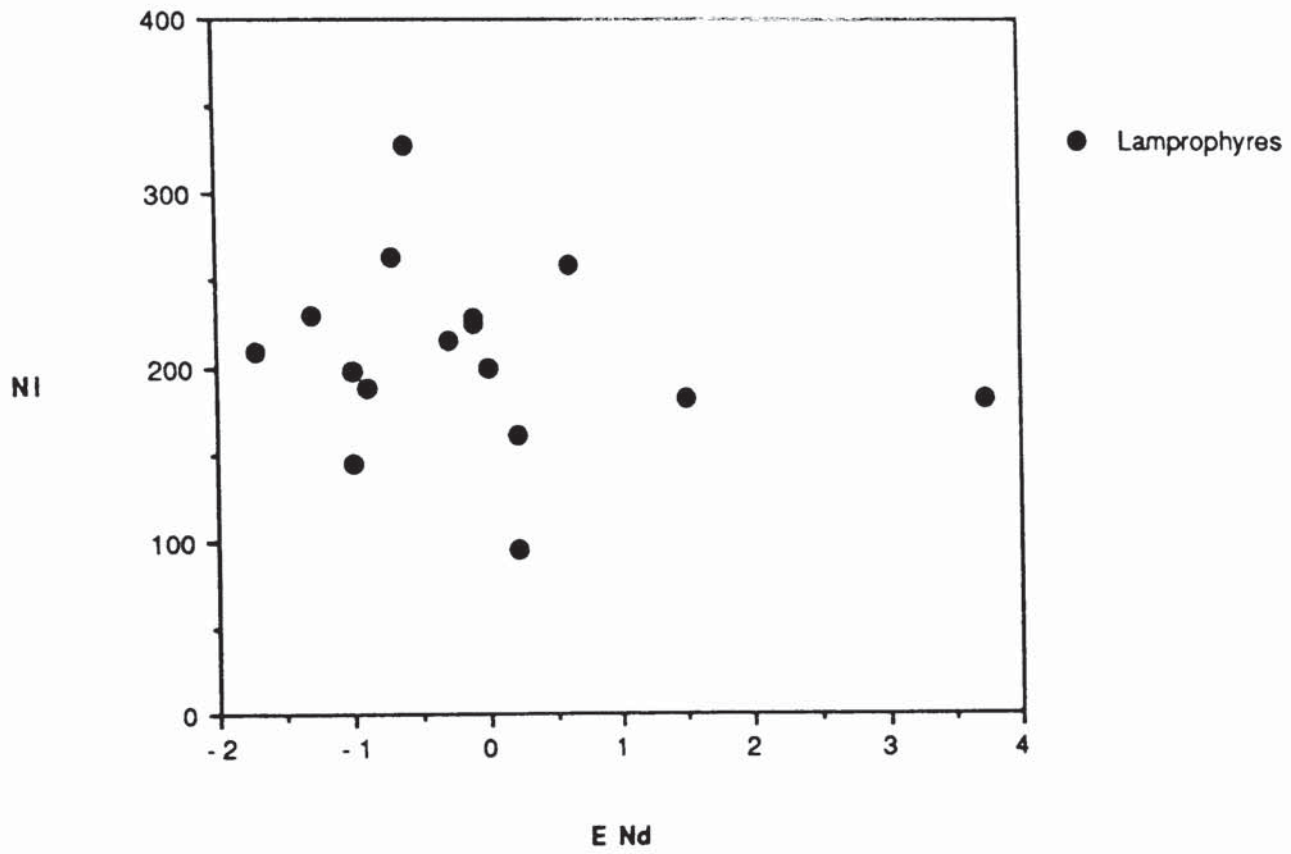


Fig. 4.9c



contaminated rocks should reveal differences in Sr isotope composition if the magma had experienced this style of contamination. Using this argument it should also be possible to use the chemical composition of the phenocryst and groundmass phases in the CAL to check whether this style of contamination has taken place.

In contaminated rocks, the phenocrysts should show signs of the magma interacting with a siliceous, evolved crustal contaminant, with the development of compositional zoning, possibly even reaction and resorption rims. At the least, significant differences between phenocryst and groundmass phases should be observed. As noted in Chapter 3 and Appendix F, there is no evidence for this type of contamination in the relatively restricted compositional variation observed in the core-rim variations in clinopyroxenes, phlogopites and amphiboles of the Criffell CAL. Most importantly, there is no apparent significant difference between 'groundmass' and phenocryst amphibole compositions in the Criffell CAL, bar one example (1326) which is most likely due to late-stage fluid-rock interaction. It could be argued that the phenocrysts have re-equilibrated with the contaminated magma but this is highly unlikely given the lack of petrographic evidence for reaction and the high Cr content of some of the clinopyroxenes which are similar to values reported from mantle xenoliths (Chapter 3).

Therefore, it is concluded that Patchett (1980) and Huppert & Sparks (1985) models involving greatest contamination of the most mafic rocks have not played a significant role in the petrogenesis of the Criffell CAL.

4.3.2) Assimilation–fractional crystallisation modelling (AFC)

If the composition of the Criffell CAL is not significantly affected by crustal contamination during ascent of the magma into the crust, then it is possible for crustal contamination to modify the composition of the melts within the upper crust. It is likely that a hot, basic magma intruded into a cool crust will undergo crystal fractionation as the magma is cooled by conduction of heat into the surrounding country rocks. However heat from the cooling magma would also promote partial melting of the

country rocks and the assimilation of crustal xenoliths into the magma. Thus the composition of the evolving magma would not only be influenced by the composition of the fractionating mineral phases but also by the composition of the surrounding country rocks and the amount of this material assimilated into the magma. A model to describe the likely trace element and isotopic effects of combined fractional crystallisation and crustal contamination (AFC) was introduced by DePaolo (1981).

The lamprophyres of the Criffell dyke swarm exhibit a range in isotopic, major and trace element composition as well as petrographical evidence for the incorporation of crustal materials into the magmas in the form of xenoliths of the local Lower Palaeozoic sediments (Chapter 2). It is therefore possible that at least part of the compositional variation observed in the lamprophyres, in particular the elevated LILE and LREE abundances, result from the assimilation of crustal material during emplacement. Incorporation of crustal material into a hot, basic lamprophyric melt would be accompanied by crystal fractionation thus an AFC model is probably more appropriate for modelling the compositional variation than simple mixing. AFC-style modification of the lamprophyres, involving local country rocks, is most likely to result in enrichments in the “incompatible elements” including the LREE and LILE as well as the development of more radiogenic Sr and unradiogenic Nd isotope signatures.

4.3.2.1) Compatible and incompatible element variations

The same hornblende–lamprophyre endmember (PFT–02b), as used in the Rayleigh fractionation model, was used for the AFC model with the crustal endmember represented by the composition of a model partial melt of the Lower Palaeozoic country rocks, derived from data published by Halliday *et al.* (1980) and Thirlwall (1983). A set of theoretical distribution coefficients and mineral assemblages, covering the range of values thought to be realistic on the basis of petrography and the earlier Rayleigh modelling (Gill, 1981; Henderson, 1982, Pearce & Norry, 1979), were used in the in the AFC model (Table 4.1) and the equations have been calculated using a value for r (rate of assimilation/rate of crystallisation) of 0.4. Curves were produced representing

Fig. 4.10a
Open symbols represent % liquid remaining

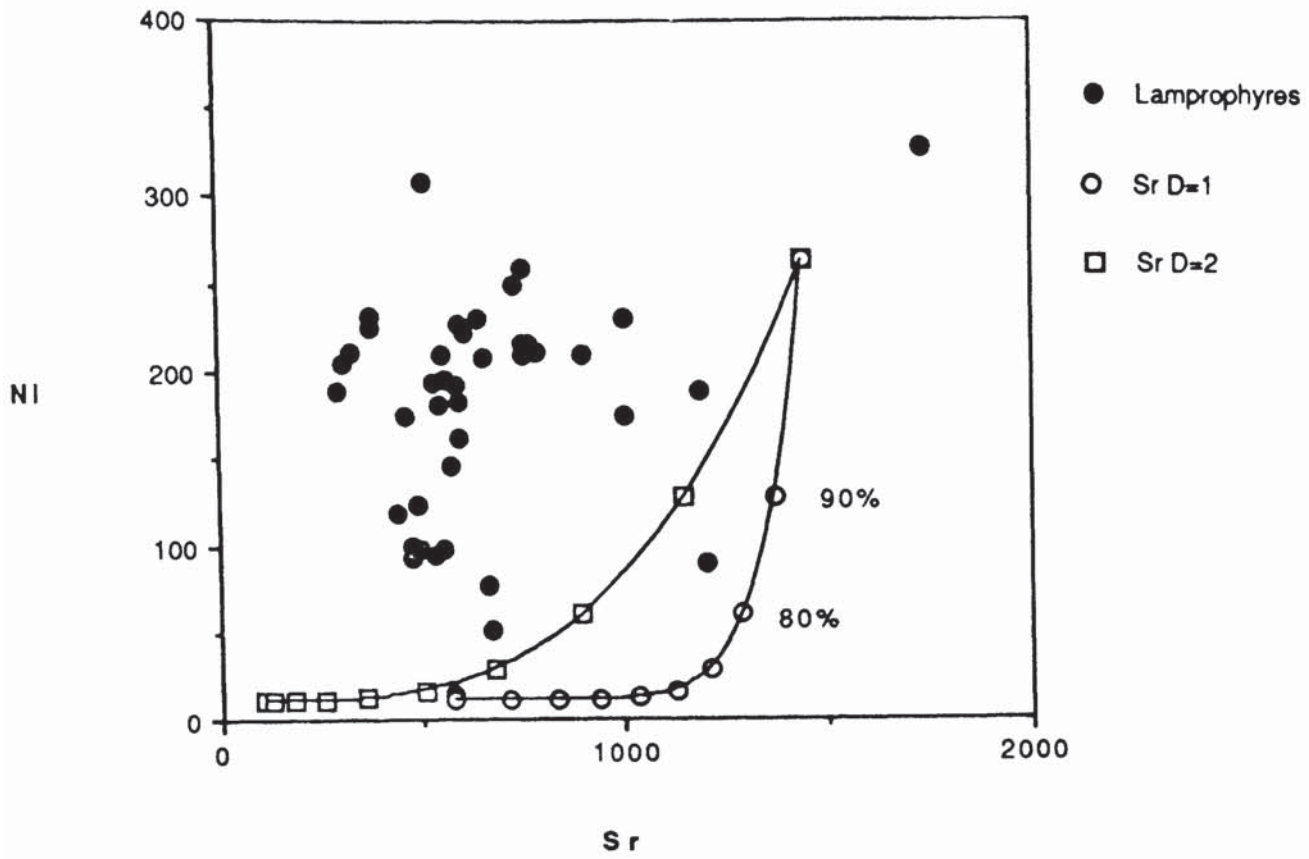


Fig. 4.10b

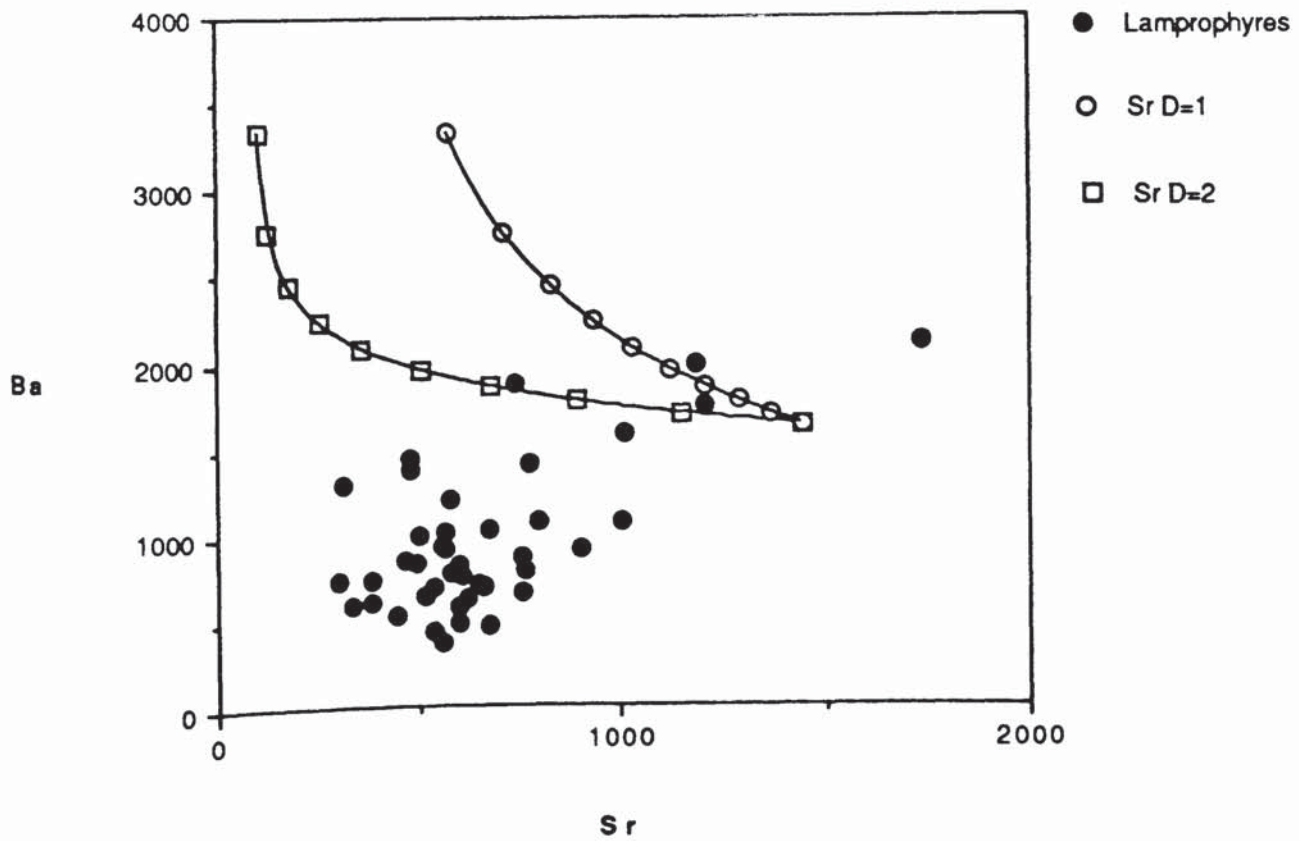


Fig. 4.10c

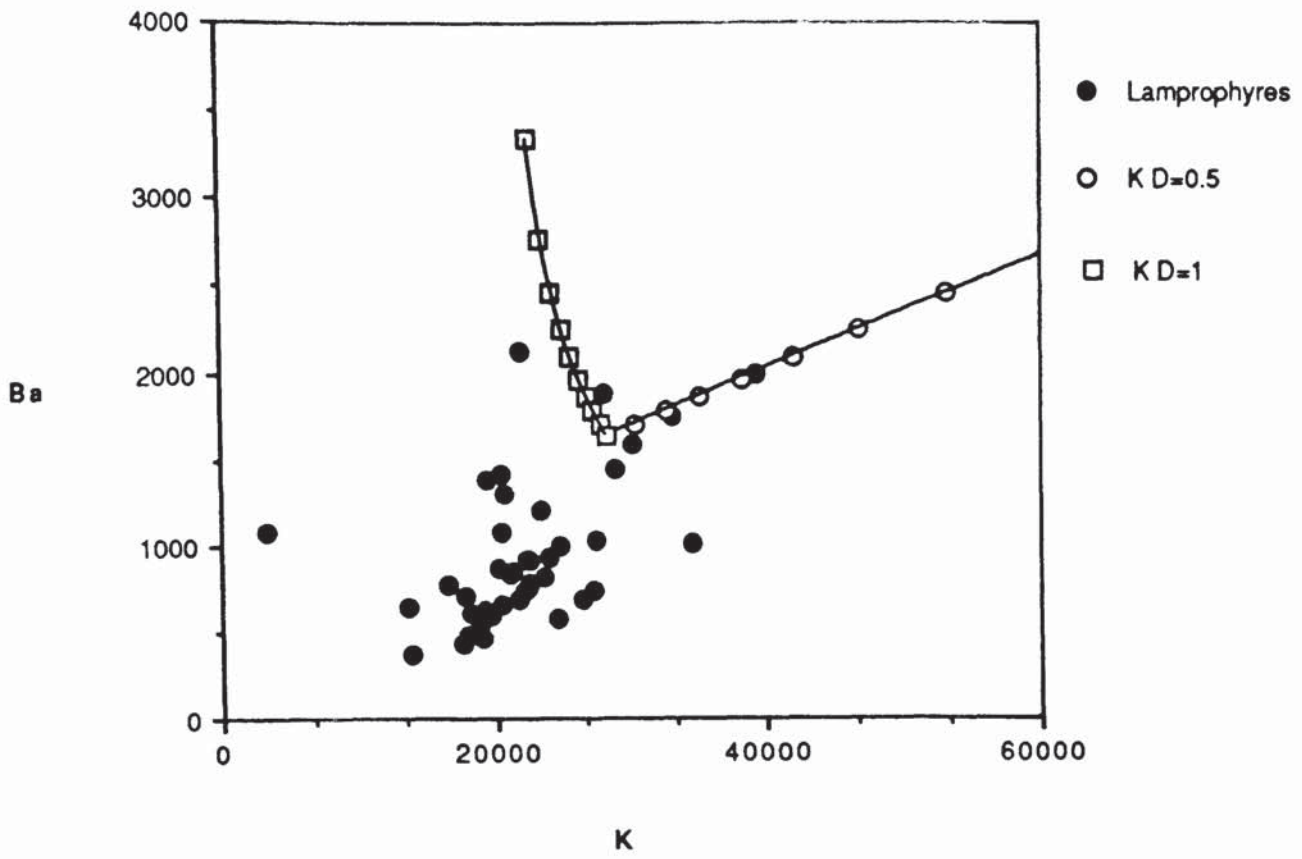
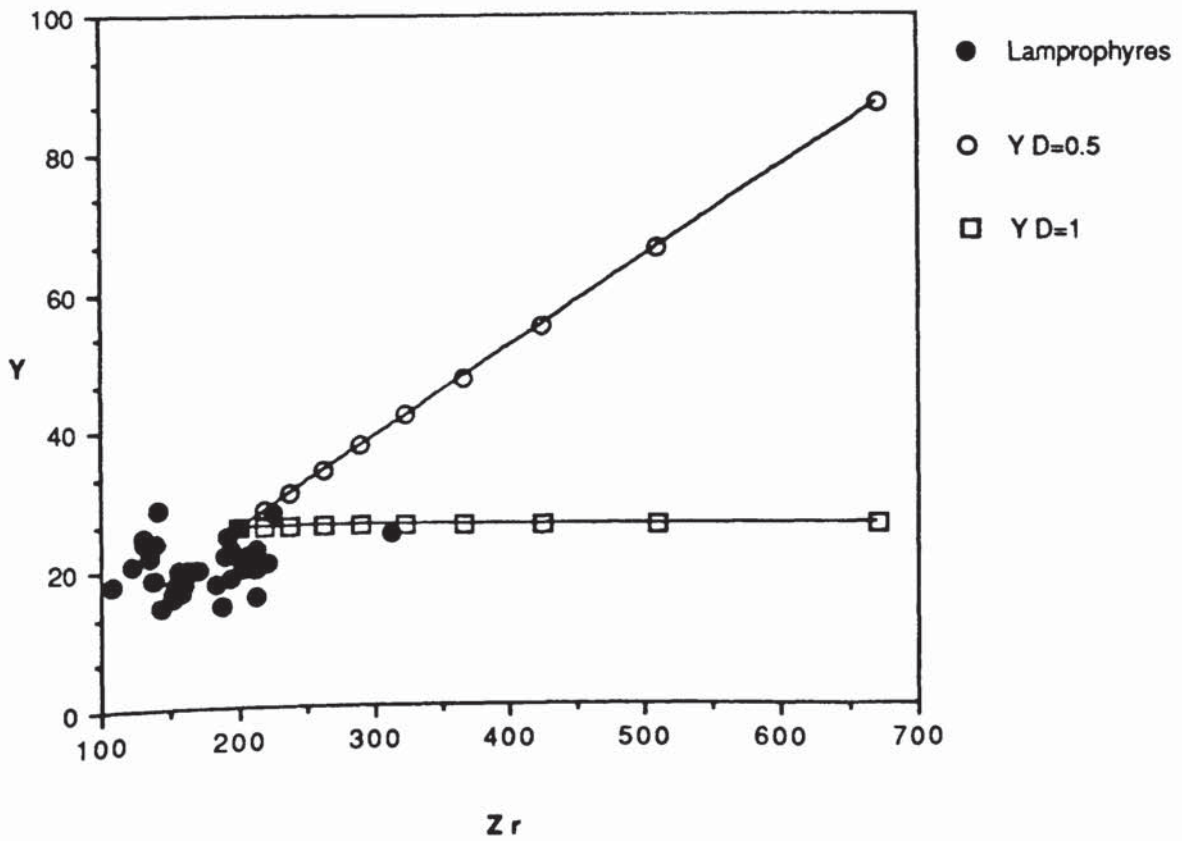


Fig. 4.10d



the evolutionary path of the magma undergoing AFC using these data and endmembers. Several of these model curves are illustrated in figures 4.10(a–d) for a range of compatible and incompatible elements in hornblende–lamprophyres. The model AFC curves (fig 4.10a) show that abundances of both Ni and Sr decrease rapidly in the residual liquids. The area between the two curves covers the range of Sr distribution coefficients for the model assemblages listed in Table 4.1. Both the curves trend below the field for the Criffell hornblende–lamprophyres towards low–Sr, low–Ni liquids. Plagioclase free assemblages will have bulk distribution coefficients for Sr <1 and will show an increase in Sr with fractionation. The divergences between the model trends and the data for hornblende–lamprophyres in plots of Ba–Sr, Ba–K and Y–Zr (Figs 4.10b–d) show the model curves to commonly have a trend opposite to that required to explain the range of the Criffell hornblende lamprophyre data.

Figures 4.11(a–d) reveal a similar story for the mica–lamprophyres. The fine–grained, mafic mica–lamprophyre (1371) was again used as the lamprophyric endmember in the AFC model, together with the crustal endmember described above (Appendix D). The range of distribution coefficients used for the model curves is based on those of Table 4.2. The model curves show that the residual liquids should be depleted in Ni and K if AFC was operating (Fig 4.11a) whereas the Criffell data show that samples with lower Ni still have high K contents. Rb–Ba, Ce–Ba and Zr–Y plots (Figs 4.11b–d) similarly show that the AFC model does not fit the LILE or LREE patterns observed in the mica–lamprophyres.

4.3.2.2) Isotopic variation

AFC curves were calculated for Sr and Nd isotopic parameters using the same data used for the earlier models. These have only been calculated for the hornblende lamprophyres as there are insufficient Sr and Nd isotope data available for the mica–lamprophyres. The Sr isotope system should be the most sensitive to any crustal contamination because there is a significant isotopic contrast between the initial magma and the country rocks (Appendix D). Also the mineral hosts for radiogenic Sr and Rb

Fig. 4.11a

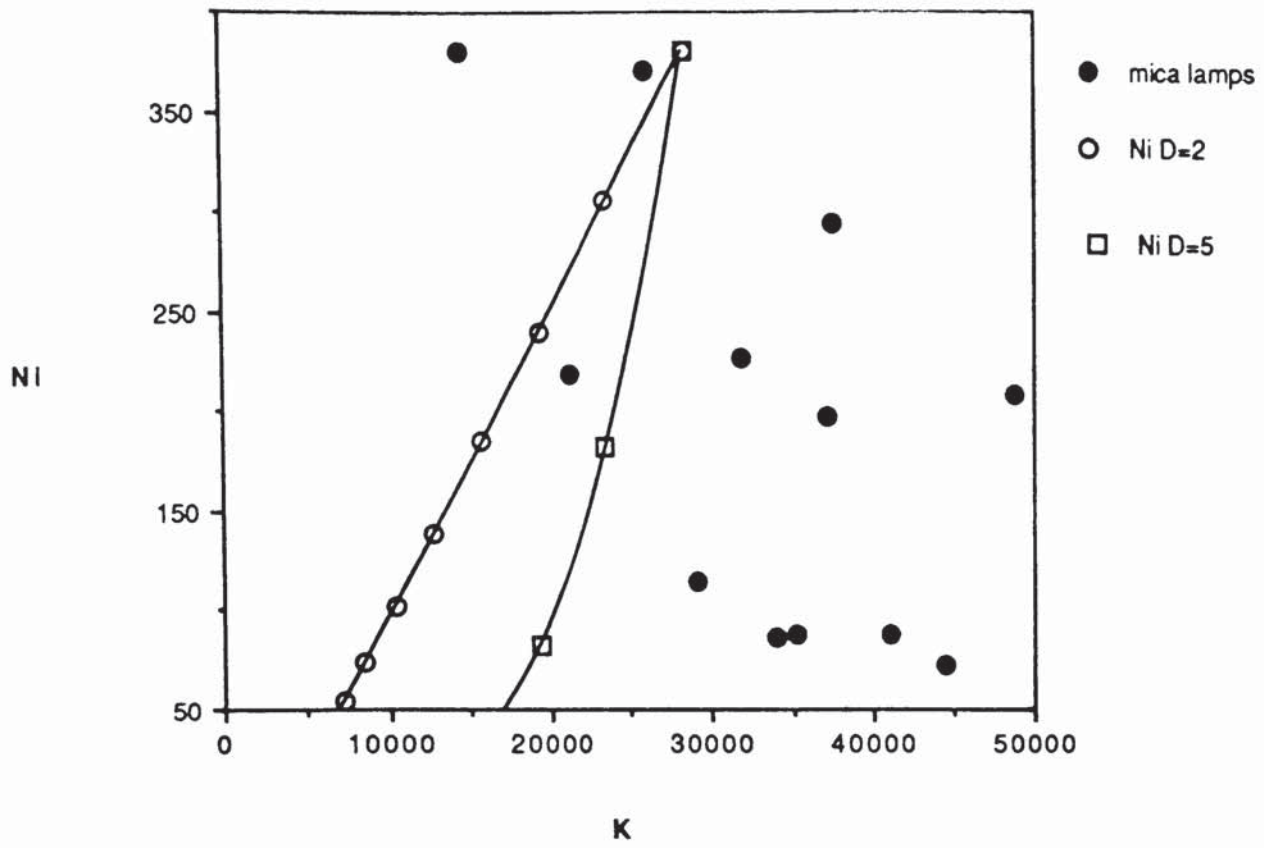


Fig. 4.11b

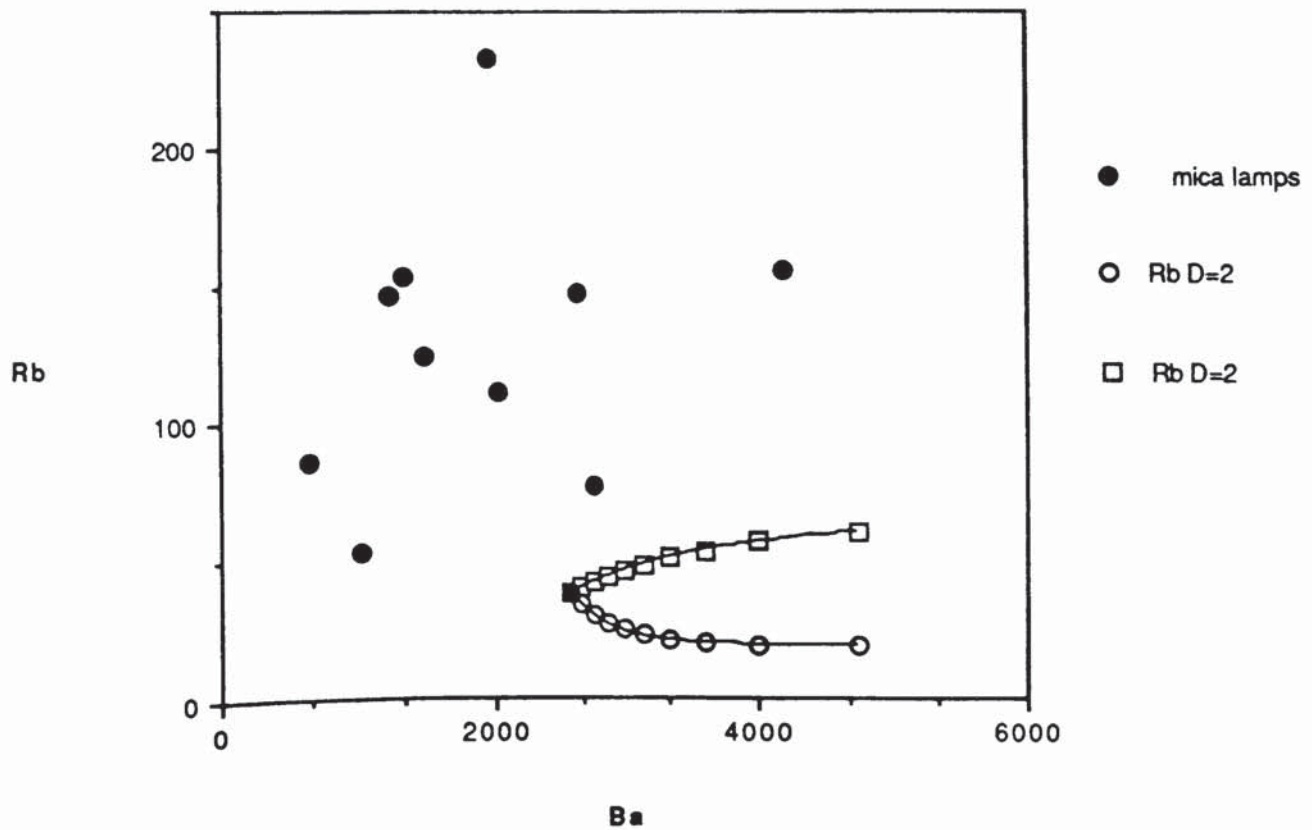


Fig. 4.11c

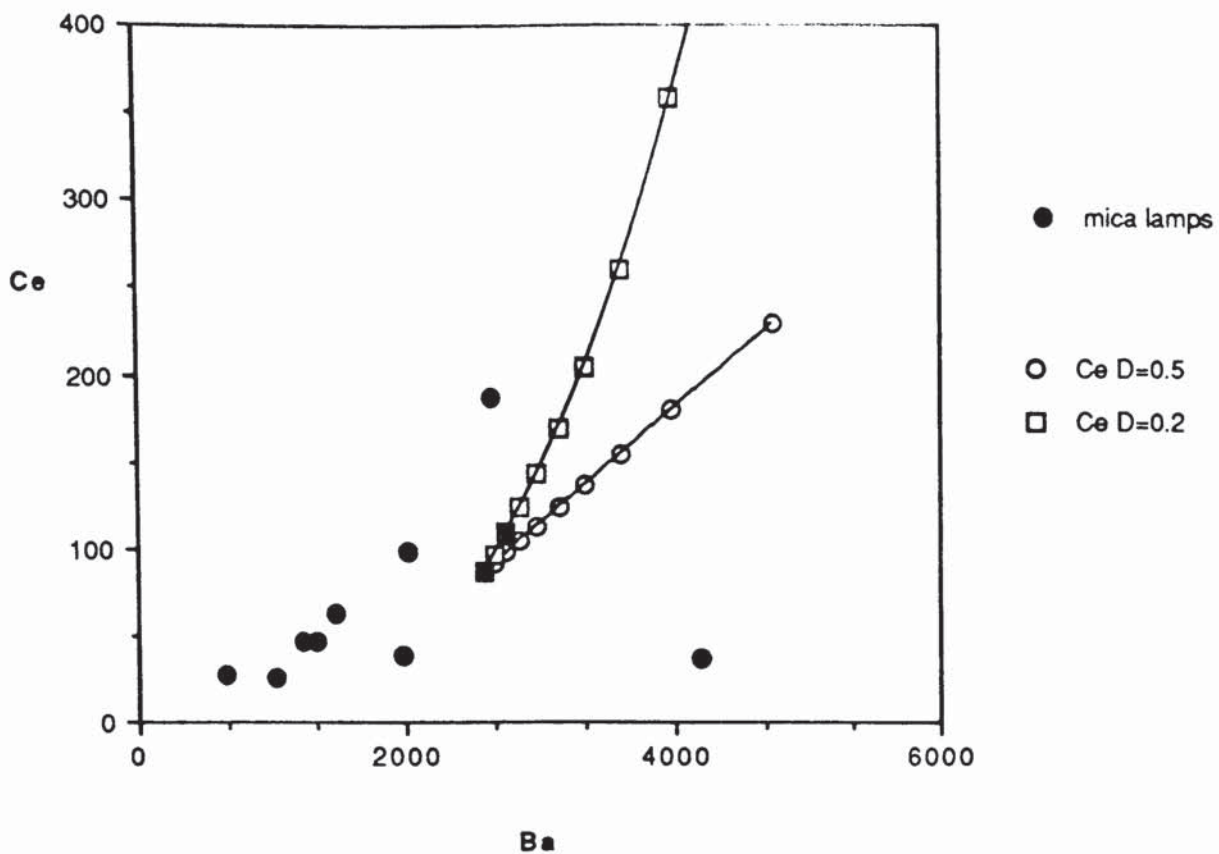
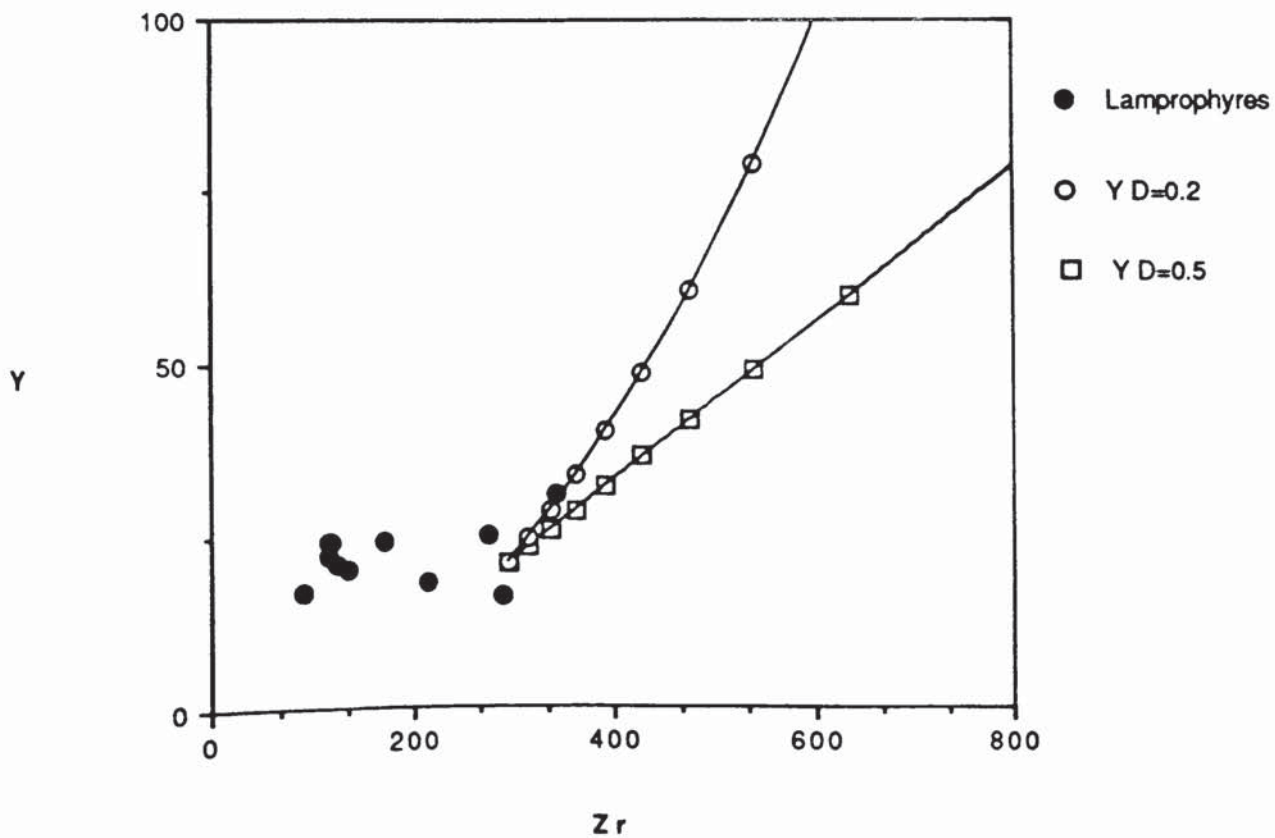


Fig. 4.11d



(mica, feldspar) are generally more susceptible to breakdown (via assimilation and partial melting) than those that host the REE (accessory phases). The co-variation between $^{87}\text{Sr}/^{86}\text{Sr}$ initial ratio and LILE and LREE abundances is illustrated in figures 4.12(a–b). The curves bracket the range of realistic bulk distribution coefficients for the elements in hornblende–lamprophyres and the isotopic composition of a sample lying between these curves may have been influenced by AFC.

In figure 4.12(a) a few samples do lie between the two model AFC curves but the majority of the lamprophyres have K abundances and $^{87}\text{Sr}/^{86}\text{Sr}$ initial ratios which cannot be explained by the operation of the modelled AFC process. Similarly, figure 4.12(b) shows that an AFC type process has not controlled the Ce abundance of the lamprophyres. In both cases, if AFC has operated, it should have produced good correlations between LILE, LREE and Sr isotope initial ratios. Similarly, figures 4.13(a–b) show that the AFC model cannot explain the ϵNd –K and ϵNd –Ce variations observed in the Criffell lamprophyres. Also AFC modification of lamprophyric magma in a crustal magma chamber should result in good positive correlations between isotopic parameters and differentiation indices (DePaulo, 1981; Huppert & Sparks, 1985). However, this is clearly not the case for (Figures 4.8 a-c; 4.9 a-c) data from the Criffell CAL. Also, if AFC processes had affected a phenocryst bearing magma, then the influx of K_2O , SiO_2 , Na_2O and other “fusible” components from the crustal contaminate would almost certainly result in compositional zoning or rimming of these phenocrysts. Similarly, groundmass and phenocryst compositions might be expected to be different given the increased K_2O , SiO_2 and Na_2O contents of the contaminated magma. In addition, if contamination was with a bulk, solid, assimilate, then the cooling effect of this materials incorporation into the melt would promote crystallisation, presumably of phases of different composition to existing phenocrysts due to the change in the melts composition. However, as described in Chapter 3, available mineralogical data for Criffell CAL does not support this hypothesis.

4.4) The Criffell CAL: Window on the mantle?

Fig.4.12a

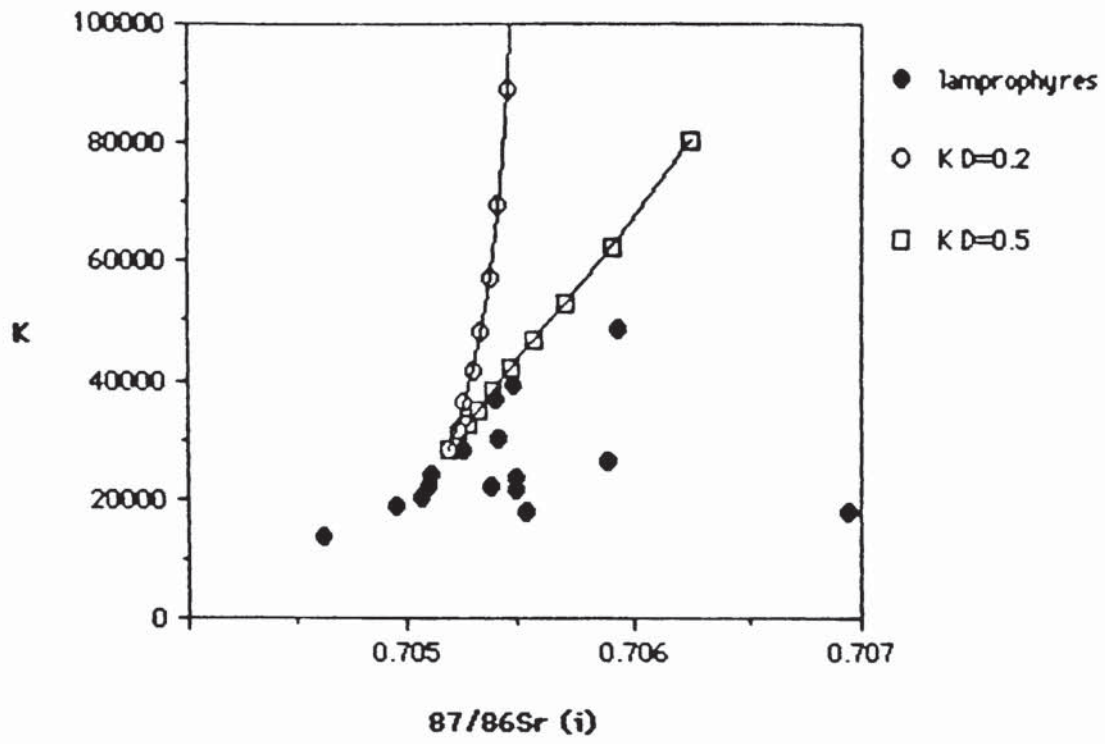


Fig. 4.12b

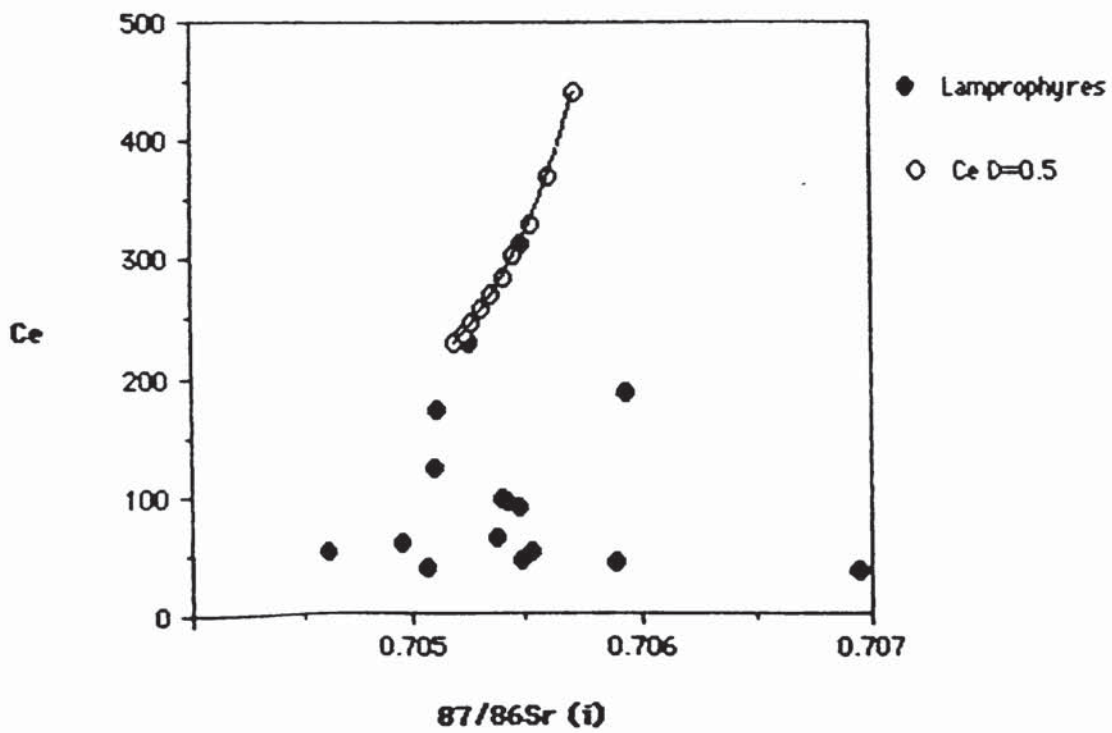


Fig.4.13a

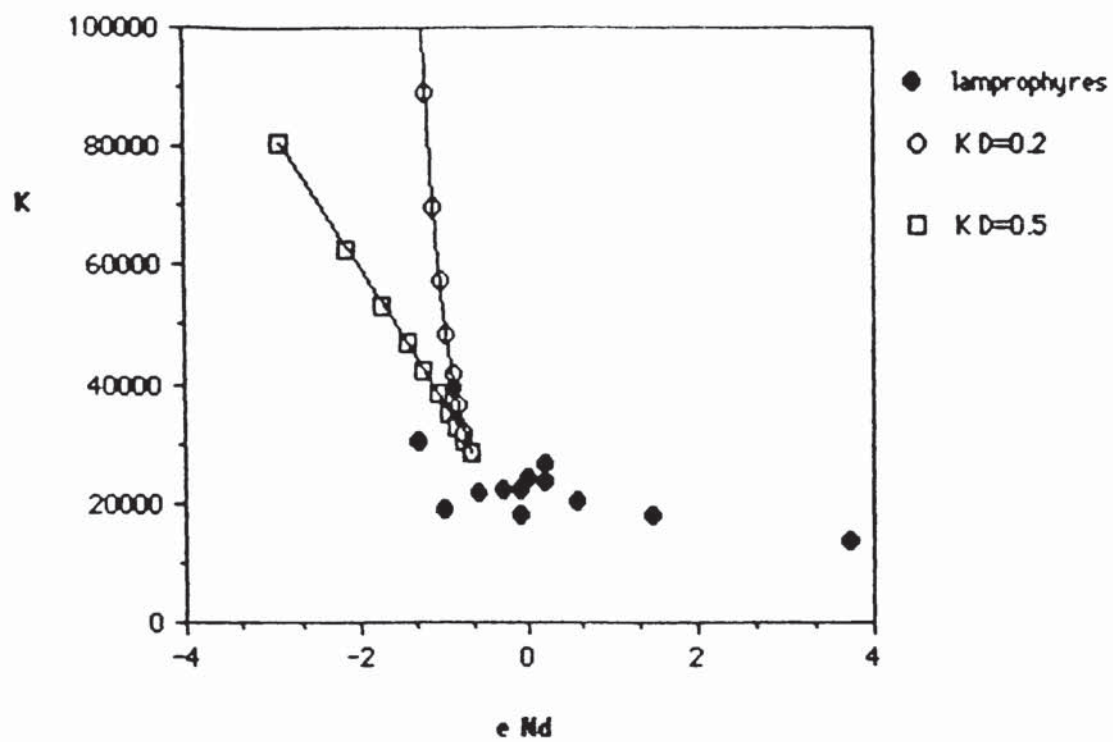
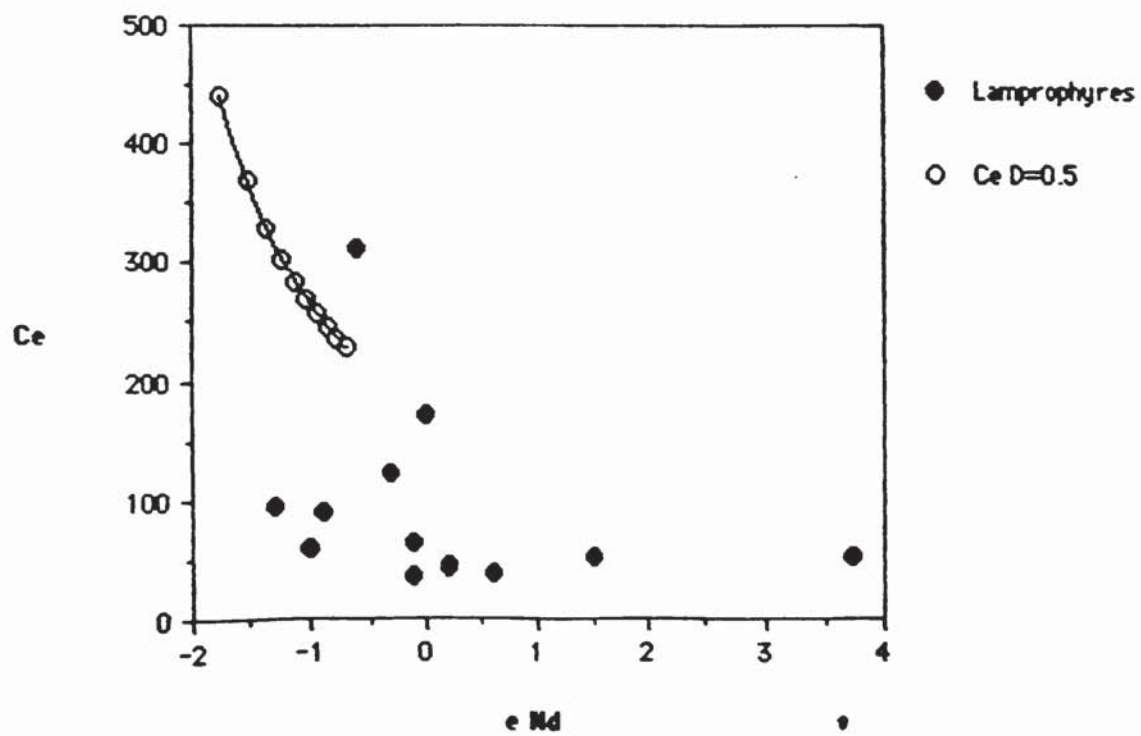


Fig. 4.13b



If the conclusions of the fractionation and contamination modelling are correct, this suggests that the origin of the LILE, LREE and isotopic variation observed in the Criffell CAL results either from variations within their source area and/or the nature of the partial melting processes responsible for lamprophyric magmatism. The arc-like chemistry of the lamprophyres, characterised by high LILE/HFS and depletions in Ta, Nb and Ti, indicates that their mantle source was modified by processes related to subduction (c.f Chapter 3). This is supported by the chemical and isotopic similarity between the Criffell lamprophyres and calc-alkaline lamprophyres from other areas which are clearly associated with active or recently terminated subduction (Luhr *et al.* 1989; Peccerillo *et al.* 1988; Leat *et al.* 1987; Peccerillo & Manetti, 1985). During subduction a number of processes are thought to occur which can modify the composition of the mantle wedge overlying the subducting oceanic plate and produce the distinctive geochemical characteristics of arc magmatism (Pearce, 1982).

These include the release of fluids from dehydration reactions in the subducted slab and the incorporation of subducted sediments into the mantle. Fluids from the breakdown of hydrous phases in the subducted oceanic plate are capable of scavenging and transporting LILE and LREE from the subducted plate into the overlying mantle wedge where these elements may be fixed in hydrous phases, typified by phlogopite and amphibole, formed during the metasomatic reactions that occur in the mantle under these conditions (Tatsumi, 1989; Tatsumi *et al.* 1986; Tatsumi *et al.* 1983). These fluids may also promote melting of both the subducted sediments and the mantle wedge immediately above the subducting slab, producing siliceous LILE- and LREE-rich melts which may migrate upwards into the overlying mantle peridotite, again promoting the development of metasomatic phases within the mantle, such as phlogopite and amphibole, as well as enriching it in LILE and LREE (Wyllie & Sekine, 1982). The introduction of these components into the mantle wedge is thought to create heterogeneities within the mantle wedge depending upon the extent and degree of fluid and/or melt migration. The situation is complicated by the fact that these heterogeneities may be superimposed on existing compositional variation within the pre-subduction

mantle (Wilson, 1989). Thus the mantle source of arc-derived rocks can be highly variable both in its mineralogy and LILE, LREE and isotopic composition. However, does the compositional variation described from the Criffell CAL reflect their source or has its characteristics been obscured by the partial melting processes responsible for the Criffell CAL?

4.4.1) Isotopic composition of the mantle source

If the mantle has a heterogeneous trace element distribution, with variations in LILE and LREE abundances (and therefore variable Rb/Sr and Sm/Nd), then these trace element variations will produce isotopic heterogeneities within the mantle if left undisturbed for a sufficient period of time eg; if they are present in the non-convecting lithospheric mantle. Subsequent partial melting of this mantle would result in liquids with both variable incompatible element abundances and a range of isotopic values. In such cases, the isotope and trace element abundances are coupled, with magmas characterised by low Sm/Nd and high Rb/Sr having the most evolved isotope signatures. The Criffell lamprophyres have low Rb/Sr and Sm/Nd but have variable $^{87}\text{Sr}/^{86}\text{Sr}$ and $^{143}\text{Nd}/^{144}\text{Nd}$ initial ratios which indicates that the trace element and isotopic systems have been at least partially decoupled in the mantle (Figure 3.18). Thus it would appear that at least the Sm/Nd ratio of the Criffell CAL has been significantly lowered either just prior to or during the melting event responsible for the lamprophyric magmatism. However, the Nd isotope data for the lamprophyres suggests (Table 3.2) that their mantle source must still have had a relatively mild LREE enriched character, with a Sm/Nd close to bulk earth values, in order to produce a suite of magmas with a mean ϵNd value of c. -1. Such compositions have already been described from mantle xenoliths thought to represent fragments of the Scottish lithospheric mantle (Menzies & Halliday, 1988), in particular those from Streap Comlaidh (which also have very similar ϵSr values). However, the Criffell CAL have significantly higher Rb/Sr and lower Sm/Nd than the Streap Comlaidh xenoliths, although these values may be controlled by partial melting processes (M. Thirlwall,

pers.comm) or by real LILE and LREE heterogeneities within the mantle. Thus it is possible that the Criffell CAL represent low degree partial melts of a lithospheric mantle, possibly with heterogeneous LILE and LREE element distributions, of similar isotopic composition to that thought to be represented by the Streat Comlaidh xenoliths. However, alternative explanations are possible. Thirlwall & Burnard (1990) also observed that the mantle source of the Loch Borrallan syenites was characterised by ϵNd values c. -1 and demonstrated that this required the mantle source of the syenites to have been stabilised at c. 1100my BP (assuming a Sm/Nd of 0.15), clearly at odds with the much older ages suggested for stabilisation of the sub-lewisian lithospheric mantle (Menzies & Halliday, 1988). They suggested that the source of the Borrallan parental magmas may well have been produced by mixing between a mantle source with low ϵNd values, unlike 'normal' asthenosphere, and subducted Lower Palaeozoic sediments (SLPS).

The presence of two samples with relatively radiogenic (ϵNd c. +3 & +1.5) values suggests that isotopically less evolved mantle was also present in the source region of the Criffell CAL. Thirlwall (1983) argued that the isotopic diversity observed in many of the LORS lavas in Scotland could be explained by mixing between a relatively depleted mantle source and SLPS within the mantle. Thus, is it possible that the source of the Criffell CAL was produced in a similar manner? Poor correlations between Sm/Nd and ϵNd and Rb/Sr and ϵSr (3.16a-b) suggest otherwise as mixing, in its simplest form between two endmembers, might be expected to give rise to mixing trends on these diagrams. This would be particularly true if mixing was taking place between a depleted, radiogenic c. +3 (possibly asthenospheric) component, and material derived from SLPS (ϵNd c. -3, $^{87}\text{Sr}/^{86}\text{Sr}$ c.0.706; Thirlwall & Burnard, 1990). However mixing trends on such diagrams may be obscured by the effects of variable degrees of partial melting or the addition of a LILE and/or LREE enriched component immediately prior to melting. Nevertheless, mixing of depleted mantle and SLPS would also be expected to produce trends on isotope-isotope diagrams, such as a plot of ϵNd – ϵSr (figure 3.17), and these are not observed. Using the arguments of

Thirlwall & Burnard (1990), however, it is possible that the source of the Criffell CAL could have been produced by mixing between a relatively unradiogenic mantle (ϵNd c. 0) and SLPS. The low isotopic contrast between the two endmembers would allow the incorporation of a sizable component of subducted sediment as well as obscuring any mixing trends, particularly if both endmembers had slightly variable isotopic compositions. Thus it is quite feasible for the mantle source of the Criffell CAL to have been produced by mixing between SLPS and a mantle source with ϵNd close to 0. However, what then is the significance of the lamprophyre samples with ϵNd c. +3 & +1.5, as these demonstrate that radiogenic compositions are also present within the mantle source of the Criffell CAL? One possible explanation is that the pre-mixing mantle was also isotopically heterogeneous prior to incorporation of the SLPS endmember, similar, in fact, to local isotopic variations described by Menzies & Halliday (1988) from samples of the lithospheric mantle recovered from several localities across Scotland.

These relatively radiogenic compositions may also provide evidence about the composition of the pre-subduction mantle, was it within the lithosphere or asthenosphere? The sample with the most radiogenic ϵNd also has the most unradiogenic ϵSr value (c.+8), suggesting that at least parts of the pre-subduction mantle were relatively depleted. However, the next most radiogenic sample, with ϵNd c. +1.5, has an ϵSr value c.+21 and it may be that mixing with SLPS has obscured most of the original pre-subduction ϵSr values. However, the requirement for a pre-subduction mantle source with gross ϵNd close to 0 (Thirlwall & Burnard, 1990) suggests that a source for the pre-subduction mantle in convecting and characteristically depleted asthenosphere appears unlikely. Some constraints may be placed upon the depth of the mantle source by the phlogopite and amphibole stability fields (c. 20 kbars; Peccerillo & Manetti, 1985; Esperanca & Holloway, 1987).

4.4.2) LILE and LREE composition of the Criffell CAL: Source heterogeneity, partial melting or both?

Studies of CAL from the Mexican Volcanic Belt (Allen & Carmichael, 1984; Wallace & Carmichael, 1989, Luhr *et al.* 1989), Colorado (Alibert *et al.* 1986), the Hercynian (Turpin *et al.* 1988; Thorpe *et al.* 1986, Thorpe, 1987) suggested that CAL represent low degrees of partial melting of subduction modified lithospheric mantle which had been variously enriched in LILE and LREE derived by fluids from the subducting slab. Therefore it is likely, on the basis of the isotopic and chemical similarity between the Criffell CAL and many of those described above (Chapter 3) that the Criffell CAL originated in a similar manner. However, is it possible to distinguish between the effects of variations in the degree of partial melting and real variations in the composition of the source on the LILE and LREE abundances in the Criffell CAL?

McKenzie (1985) suggested that volatile-rich melts would be expected to separate from their source areas relatively efficiently and at extremely low melt fractions (<0.1%). Furthermore, he suggested that volatile rich melts may undergo further enrichment in incompatible elements as they ascend by scavenging these elements from the surrounding matrix. Therefore, LILE and LREE abundances in volatile-rich melts, such as CAL, observed at the surface may well bear no relation to the actual abundances of these in their source regions. This may explain the discrepancy between the observed Sm/Nd and Rb/Sr ratios in the lamprophyres (figure 3.18) and their observed ϵ_{Nd} and ϵ_{Sr} values.

If, as is suggested, the isotopic composition of the mantle source of the lamprophyres is the product of incorporation of a component of SLPS then it is also feasible that much of the LILE and LREE variation observed within the Criffell CAL may reflect variable degrees of mixing with this component, i.e. is related to source heterogeneity. The SLPS component is likely to be enriched in LILE and LREE elements relative to the pre-subduction mantle as well as displaying evolved isotopic characteristics (Thirlwall, 1983). Therefore it might be expected that LILE and LREE abundances show good correlations, both with isotopic values and with each other, if they reflect varying degrees of mixing between a SLPS component and a mantle with a gross ϵ_{Nd} c. -1 and with a relatively flat REE pattern. Indeed, in figures 4.14(a-b)

linear correlations are observed between high LILE abundances and isotopic values (Ba/Nb- ϵ Nd and K/Ti- ϵ Sr, barring one sample). However, given the uncertainty over the original LILE and LREE abundances in the pre-subduction mantle, the proportion and nature of possible SLPS components and the complications arising from the efficiency with which hydrous, low degree, partial melts can increase their LILE and LREE abundances, it is not possible to adequately constrain the relative contributions of these various factors to the observed chemistry of the Criffell CAL.

4.4.3) Differences between hornblende- and phlogopite-bearing lamprophyres.

Peccerillo & Manetti (1985) argued that the diverse group of high-K magmas, including minettes, of the Roman volcanic province could be explained by the partial melting of a phlogopite bearing mantle under different pressures. Melting at relatively low pressures ≤ 14 kb would result in qz-normative, silica oversaturated liquids represented by the minettes, while melting at higher pressures, up to 50kb will produce silica undersaturated liquids, such as the highly potassic kamafugitic rocks of the province. Luhr et al. (1989) also suggested that minettes in the MVB had equilibrated within the phlogopite stability field resulting in the saturation of the melts with phenocryst phlogopite.

It is suggested that a similar mechanism is responsible for differences between the phlogopite-bearing and hornblende-bearing lamprophyres of the Criffell dyke swarm, with the less siliceous mica-lamprophyres produced by partial melting at slightly greater depths and the hornblende-lamprophyres resulting from melting at shallower depths. This may also explain the difference in mineralogy between the two groups with the mica-lamprophyres being generated at depths below the stability field of amphibole while the hornblende-lamprophyres originated at shallower depths, within the amphibole stability field. Variations in the depth of magma generation may be coupled with changes in the H₂O/CO₂ ratio of the fluid present during melting with higher H₂O/H₂O+CO₂ ratios producing more silicic melts while lower ratios promote the production of silica undersaturated melts (Bachinski & Scott, 1979, Rock *et al.*

1988). A similar mechanism was proposed for the genesis of silica saturated members of the lamproite suite (Bergman, 1987) and orendites from the Leucite Hills, USA (Barton & Hamilton, 1982).

4.5) The tectonic setting and significance of lamprophyric magmatism in the Southern Uplands

The Criffell lamprophyres are thought to be part of a widespread phase of lamprophyre intrusion in southern Scotland, Northern Ireland and Northern England during the final stages of the Caledonian orogeny (Chapter 3). Recent structural mapping and radiometric age dating of lamprophyres from southern Scotland suggests that intrusion occurred between 420Ma and 395Ma (Rock et al. 1986; Macdonald et al. 1986), broadly contemporaneous with the collision associated with final closure of Iapetus (Leggett et al. 1979). Structural and geochemical studies by Barnes et al. (1986) and Rock et al. (1986) indicated that the lamprophyres cannot readily be reconciled with models which propose that the Southern Uplands represent the remnants of a lower Palaeozoic accretionary prism. It has been proposed (Stone et al. 1987) that the lamprophyres were emplaced in a post-tectonic “transpressional, strike-slip, regime”, and intruded into the uplifted remnants of a back-arc thrust duplex structure and not a fossil accretionary prism. However, the debate about the origins and nature of the Southern Uplands is far from resolved and it is difficult to place the lamprophyre magmatism within any single palaeotectonic model.

It is clear that intrusion of the lamprophyres was one of the final magmatic events in the late Caledonian evolution of the Southern Uplands and that many of their geochemical characteristics are the result of petrogenetic processes associated with subduction. However, it seems unlikely that they could be related to the same NW directed subduction zone thought to be responsible for the late Silurian lavas because the lamprophyres are found only 20-30 km from the trace of the Iapetus suture, the so-called “Solway Line”. At such distances, even allowing for crustal shortening and steep subduction angles, several factors would preclude the production of lamprophyric magmas in a forearc environment. For example, the geotherms in the mantle wedge

would not be at a high enough temperature to support partial melting and the subducted plate would not yet be deep enough to allow dehydration reactions to take place and promote the development of the characteristic LILE and LREE enrichments in the mantle wedge.

New Rb–Sr data (Thirlwall, 1988) indicate that the majority of the late Caledonian magmatism in the southern part of the Southern Uplands occurred at around 395 Ma. This implies that these magmas represent the final phase of late Caledonian magmatism in Scotland and are unrelated to any subduction event which may have been responsible for the earlier magmatism found north of the Southern Uplands fault and in the northern part of the Southern Uplands. These differences in timing of magmatism are mirrored by variations in the composition of the magmas with the southern part of the Southern Uplands characterised by high LILE and LREE abundances together with radiogenic $^{207}\text{Pb}/^{204}\text{Pb}$ isotope ratios compared to magmas from further north (Thirlwall et al. 1989). The 395Ma granitoid magmas from the southern part of the Southern Uplands are considered by Thirlwall (1988) and Thirlwall et al. (1989) to be derived from old, enriched “Lake District” lithosphere thrust under the southern margin of the Southern Uplands during the final stages of collision. Lithosphere such as this would be an ideal source for the Criffell lamprophyres, particularly if it had recently been metasomatised by a lower Palaeozoic subduction event, such as that postulated for the Ordovician Borrowdale and Eycott volcanics of the Lake District (Fitton & Hughes, 1970).

4.6) Summary

The LILE and LREE enrichments which characterise lamprophyres from the Criffell dyke swarm may indicate derivation from an enriched mantle source, low degrees of partial melting or they may be the result of variable degrees of fractionation and contamination of mantle–derived melts during their ascent through the crust. Quantitative modelling indicates that variations in LILE, LREE in both mica– and hornblende–lamprophyres cannot be explained by progressive fractional crystallisation

of a “parental” lamprophyre melt. Consideration of Patchett (1980) and Huppert & Sparks (1985) models for contamination during melt transport in dykes were examined but are not thought to have played a significant role in the Criffell CAL. Similarly, AFC models, involving contamination with local crustal rocks combined with the effects of crystal fractionation in the upper crust, also fail to explain satisfactorily the observed incompatible element and isotope variations. The elevated LILE, LREE abundances and isotopic composition of lamprophyres are thus thought to have been little modified by fractionation or contamination during intrusion and the lamprophyres are thought represent relatively unmodified mantle-derived magmas. The Criffell CAL are believed to have been generated by low degrees of partial melting from a mantle source modified by subduction processes. It is thought that the Nd and Sr isotopic composition of the lamprophyres reflects a source produced by the incorporation of subducted Lower Palaeozoic sediments into a mantle source which was characterised by ϵ_{Nd} values close to bulk earth. However it is not possible to resolve the relative contribution of source heterogeneity and low degrees of partial melting upon the observed LILE and LREE abundances of the Criffell CAL. Differences in mineralogy and composition between the phlogopite and hornblende lamprophyres is thought to reflect variations in the depth of melting as well as possible variation in CO_2/H_2O . The source of the subduction-derived enrichment in the lamprophyres is not thought to be the subduction zone responsible for the late Silurian lavas in the Midland Valley and SW Highlands. This is because of the reported spatial variations in the geochemistry of late Caledonian igneous rocks and the difficulties in dehydrating a subducted slab, at such shallow depths, so close to the trench. It is thought that the lamprophyres represent low degrees of partial melting of subduction-modified “Lake District” lithospheric mantle thrust under the southern margin of the Southern Uplands during the final stages of collision, as has been suggested for the contemporaneous granitoid plutons in southern part of the Southern Uplands.

Chapter 5

Lamprophyre–granitoid associations: A case study of the Criffell– Dalbeattie granitoid complex.

5.1) Introduction

Many of the late Caledonian granitoid plutons in Scotland are spatially and temporally associated with large suites of dykes which are mainly intermediate–acid microdiorites, microgranodiorites and microgranites (Richey, 1939). The dykes are commonly porphyritic and are commonly labelled as porphyrites or the porphyrite–porphyry series on published geological maps (Sheets 5W, 5E). Associated with these voluminous intermediate–acid minor intrusions are less numerous lamprophyre dykes with a few stocks and plugs of the compositionally similar “appinite suite” (Read, 1961; Wright & Bowes, 1979). These basic minor intrusions are widespread and occur associated with granitoids from the northern Highlands, the Western and Grampian Highlands and the Southern Uplands (Fig. 5.1). Similar associations occur in Donegal (Pitcher & Berger, 1972) and SW England (Leat *et al.* 1987). These lamprophyric bodies occur around the margins of the granitoids and either predate or are synchronous with the earliest phases of the pluton. In many cases, they are the only basic rocks intimately associated with many of the granitoids though they have been largely ignored in the numerous petrogenetic studies of the larger intrusions.

5.2) The nature of the lamprophyre–granitoid association

The occurrence of mafic, mantle derived lamprophyres in association with compositionally zoned granitoids, components of which are thought to be at least partially derived from the mantle (Harmon *et al.* 1984; Halliday, 1983), raises the possibility that the lamprophyres represent this mantle component and are parental in some way to the granitoids. Hot, mantle–derived melts (eg: lamprophyres) injected into the crust could act as melting triggers, initiating partial melting of this crust and producing granitic magmas (Huppert & Sparks, 1988a; 1988b). In the simplest case,



Illustration removed for copyright restrictions

the basic magmas would just supply heat to promote melting of the crust with no further interaction and here the granites will reflect the isotopic and chemical composition of the crustal source rocks. These models may be applicable to granitoid plutons where there is little evidence for the direct involvement of mantle-derived material in the composition of the granite magmas but where a heat source is required to initiate melting, eg: the "S-type" granites of the Lachlan fold belt of Australia (White & Chappell, 1988). However in situations where some of the granitoids appear to have a mantle component, eg: the Scottish Caledonides, then the basic magmas responsible for crustal melting must impart some of their own chemical and isotopic characteristics to the granitoid magmas (Harmon *et al.* 1984).

5.2.1) Petrogenesis of late Caledonian granites

The general ideas on and outstanding controversies surrounding the genesis of late Caledonian granitoids in Northern Britain are summarised in Harmon *et al.* (1984). On the basis of geochemical and isotopic data it is thought that many of these plutons arise from interactions between mantle-derived magmas and various crustal components. Recent studies, particularly those utilising Pb isotope data, have raised questions about the relative contributions of different endmembers to the granitic magmas and the true composition of many of these endmembers. It has been argued that the granites of the SW Highlands contain a significant contribution from the mantle as typified by the composition of the late Silurian SW Highland lavas (Thirlwall, 1986). However, it has also been suggested that the granites of the SW Highlands and Central Highlands respectively are dominated by recycled crustal material with little or no input of juvenile, mantle-derived material (Frost & O'Nions, 1985; Clayburn, 1988).

The arguments over the significance of crustal recycling and crustal addition processes are further complicated by the ambiguity surrounding the composition of the mantle and crustal endmembers. It has been recognised that some mantle-derived rocks have "crustal" isotopic characteristics, eg: unradiogenic ϵ_{Nd} and radiogenic ϵ_{Sr} values (Fraser *et al.* 1986), while some crustal rocks, such as Rb depleted Lewisian gneisses,

have depleted ϵSr isotope compositions more typical of mantle rocks. Because of this some authors may assign a crustal source to a particular geochemical characteristic of a granitoid pluton while others may consider the same characteristic to have a mantle source. The majority of published petrogenetic models for late Caledonian granitoids assume that the mantle component is represented by the composition of the late Silurian lavas (Thirlwall, 1983, 1986) or by depleted mantle compositions similar to MORB (Harmon *et al.*, 1984). Such assumptions may well be correct where such lavas are associated with granitoids but may not be realistic in situations where lavas are absent. Models invoking the presence of a depleted MORB-type mantle are also unrealistic where contemporaneous mantle derived rocks show no evidence for the existence of such mantle compositions, eg: in the northern and western Highlands.

The significance of the lamprophyres to the petrogenesis of the late Caledonian granitoids has not been fully investigated though it has been suggested that lamprophyric and associated shoshonitic magmas may be involved in the genesis of several late Caledonian granitoids in the Highlands (Rock & Hunter, 1987; Fowler, 1988). The present study investigates the nature and significance of the close spatial and temporal relationship between the lamprophyres of the Criffell minor intrusive suite and the Criffell–Dalbeattie pluton.

5.2.2) Petrogenesis of Criffell–Dalbeattie granitoid complex: existing models

Halliday *et al.* (1980) and Stephens *et al.* (1985) presented isotopic and chemical data which suggested that the Criffell–Dalbeattie granitoid is a composite intrusion the main body of which has an outer zone of “I-type” hornblende–clinopyroxene granodiorites and a core of “S-type” biotite–muscovite granites. The junction between the granodiorites and granites correlates with both a marked change in the composition of the intrusions and a significant change in Sr and Nd isotope values. From this it was concluded that the granodiorites and granites represent discrete but sequential magma pulses. A further petrogenetic model for the Criffell–Dalbeattie pluton (Halliday, 1983) proposes that mantle- and/or lower crust derived intermediate magmas, represented by

the granodiorites, were intruded into a middle and upper crust composed of lower Palaeozoic sediments. These magmas started to crystallise, producing felsic differentiates, and promoted partial melts of the surrounding country rocks, producing melts which contaminated the evolving granodioritic magmas. The resultant felsic magmas separated from this zone of crustal melting, due to their lower density, and ascended to intrude the core of the still plastic granodiorite, forming the inner granites. An elaboration of this model (Stephens *et al.* 1985) explains the REE and isotopic compositions of the individual magma pulses by an AFC-style process, involving the fractionation of an amphibole + clinopyroxene + plagioclase assemblage combined with the assimilation of sedimentary country rocks.

5.2.3) The composition of the parental magmas

Halliday (1983) did not specify any particular parental magma for the granodiorites, saying only that they were derived from the mantle or lower crust, while Stephens *et al.* (1985) used one of the less evolved granodiorite samples as the primitive endmember in their AFC model. Halliday *et al.* (1980) argued, on the basis of simple binary mixing calculations, that the parental melt of the Criffell–Dalbeattie granitoid magmas must have contained up to 2000ppm Sr and had a $^{87}\text{Sr}/^{86}\text{Sr}$ initial ratio of approximately 0.7045 ± 1 but they did not speculate any further on the nature of this endmember.

Holden (1987) and Holden *et al.* (1987, 1988) presented the results of a study of the numerous mafic enclaves which occur at the margins of the granodiorite and within the granite. They recognised several populations of inclusions, some of which were clearly derived from the surrounding country rocks, but also a number of mafic enclaves which have distinctive trace element and isotope characteristics. In particular many of these mafic inclusions have ϵNd isotope values which are more radiogenic than any of the surrounding country rocks and have high LREE abundances. Holden *et al.* (1987, 1988) argued that these “microdioritic” enclaves were the remnants of disrupted syn-plutonic dykes of a mafic, mantle-derived magma and suggested that such a magma may well be parental to the Criffell granitic magmas.

5.3) Evidence for lamprophyre involvement in the petrogenesis of the Criffell–Dalbeattie granitoid

The potential importance of the lamprophyres for the petrogenesis of the Criffell pluton was recognised by Macdonald *et al.* (1986) in their investigation of the nearby Newmains lamprophyre dyke. Their combined geochemical and Sr isotopic study demonstrated that contamination of the felsic differentiates with local sedimentary crust produced trends similar to those observed in the Criffell pluton. This study also showed that fluids derived from the crystallising lamprophyric magma had infiltrated the nearby country rocks and, together with the heat from the cooling lamprophyre, had metasomatised the Lower Palaeozoic and promoted localised partial melting along their contact with the intrusion. It was concluded that these processes were important for the genesis of many of the late Caledonian granitoids and that lamprophyric magmas were directly involved in the genesis of the Criffell–Dalbeattie pluton.

Sheared and disrupted lamprophyres are reported to cut the inner granite of the Criffell pluton (Phillips, 1956b) however in the present study this was not confirmed. Although numerous intermediate and acid dykes were found to cut the granodiorites and granites in some localities no lamprophyres were found within the pluton. Similarly, a study of the calc–alkaline lamprophyres associated with the Hercynian granites of SW England has revealed that very few lamprophyres are found intruding the granites (Leat *et al.* 1987). These authors suggested that although the two magmas were contemporaneous the large volume of granitic magma acted as a density filter through which the dense, mafic lamprophyres could not be intruded without being disrupted and dispersed. Many of the mafic inclusions found within the Criffell–Dalbeattie pluton are thought to be the remnants of disrupted, syn–plutonic dykes of a mantle–derived magma which was directly involved in the petrogenesis of the granitoid pluton (Holden *et al.* 1987). These authors demonstrated that, although the Sr isotopic composition of the inclusions reflected partial re–equilibration with the host magmas, the Nd isotope composition of the enclaves was unaltered and includes a component which is more radiogenic than the granites. Similarly, thermodynamic modelling of the

diffusion of elements between the enclaves and granitic magmas, demonstrates that although some element exchange, particularly of LILE, may have taken place, the REE and HFS element content of the mafic inclusions has been little changed by interaction with the host magmas (Holden *et al.* in press; Stephens *et al.* in press).

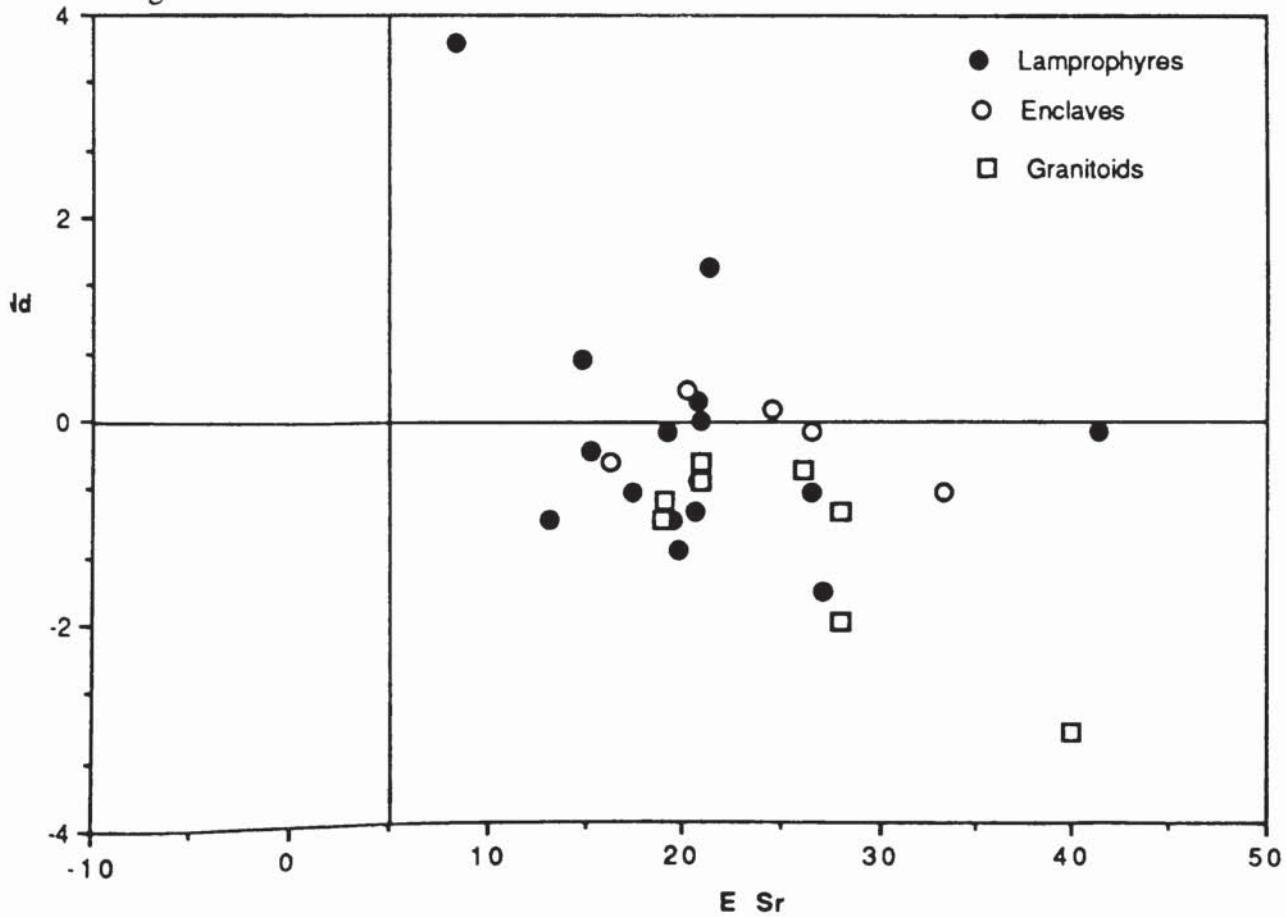
Primordial–mantle normalised spidergrams (Fig. 5.2a–b) show the fields for the Criffell mafic inclusions together with the fields for the Criffell hornblende (Fig. 5.2a) and mica lamprophyres (Fig 5.2b) superimposed for comparison. The field for the mafic inclusions overlaps with the fields for the lamprophyres and has a very similar pattern to those for the lamprophyres, with high LILE and LREE abundances together with low Nb, Ti and Y contents. A plot of ϵNd versus ϵSr data (Fig. 5.2) for the lamprophyres, mafic inclusions and Criffell–Dalbeattie granitoids shows that the field for the mafic inclusions overlaps extensively with the field for the Criffell lamprophyres and partially with the field for the Criffell granitoids in terms of their ϵSr values. Significantly, however, the inclusions have more radiogenic ϵNd compositions than the granitoids, which precludes their origin as cognate inclusions derived from the pluton itself, and the local lower Palaeozoic sediments. The mineralogy of the mafic inclusions, characterised by abundant acicular amphibole set in a feldspathic groundmass with accessory apatite, was described by Holden (1987) who classified them as “microdiorites”. These mafic inclusions have similar mineralogies to many of the hornblende lamprophyres from the Criffell swarm (Chapter 2). The chemical, isotopic and petrographic similarity between these mafic inclusions and the hornblende lamprophyres suggests that the two may have a petrogenetic association. It is concluded that at least some of the mafic inclusions found in the Criffell–Dalbeattie pluton are lamprophyric in nature and represent the disrupted remnants of syn–plutonic hornblende lamprophyre dykes injected into the partially consolidated Criffell–Dalbeattie granitoid magmas.

The presence of lamprophyric inclusions within acid magmas has also been described by Van Bergen *et al.* (1983), who described inclusions of minette within dacites and rhyolites from the Mt Amiata complex in Italy, and by Leat *et al.* (1988)

Fig. 5.2



Fig. 5.3



who described minette inclusions found in trachytes from the Elkhead Mountain region of Colorado. In both cases the lamprophyric inclusions are petrogenetically associated with the evolved magmas. Although the occurrence of these lamprophyric inclusions within the Criffell–Dalbeattie pluton is not direct evidence for the involvement of lamprophyres in the petrogenesis of the pluton they do show that mantle–derived magmas were present during the evolution of the granitoid magmas and thus a heat source was available to facilitate crustal melting.

5.4) Petrogenetic modelling of the Criffell–Dalbeattie granitoid–lamprophyre association

This section presents the results of petrogenetic modelling of the relationship between the granitoid magmas and the lamprophyres, specifically the relative importance of fractional crystallisation and combined assimilation and fractional crystallisation (AFC).

5.4.1) Fractional crystallisation

Miocene trachytes from the Elkhead Mountain region of Colorado are considered to be produced by fractionation of a mafic minette parent, represented by mafic inclusions within the trachytes (Leat *et al.* 1988). The trachytes are peralkaline, characterised by high K/Na ratios and, significantly, have similar isotopic compositions to the minettes, which is taken to indicate that interaction with the crust was minimal during their evolution. Many of the felsic segregations and veinlets described from lamprophyres in S.W Scotland are characterised by high K/Na ratios, are broadly syenitic in composition and may represent residual liquids from late stage, in–situ, fractionation of the host lamprophyric magma (Barnes *et al.* 1986; Macdonald *et al.* 1986). Similarly many of the Caledonian syenitic intrusions found in Northern Scotland, eg: Glen Dessary, are considered by Thompson & Fowler (1986) to result from fractionation of a mafic, shoshonitic precursor, similar in composition to the late Caledonian minettes from the same area. These authors suggested that generation of oversaturated granitic

compositions requires the lamprophyric liquids to be contaminated with crustal material.

Although it is possible to generate silicic compositions by fractional crystallisation of a lamprophyric parent it is considered unlikely that this on its own has played a significant role in the evolution of the Criffell–Dalbeattie pluton for several reasons. Although the fields for the Criffell–Dalbeattie granitoid and the lamprophyres partially overlap (Fig. 5.3), the granitoids generally have more evolved isotopic compositions than the lamprophyres, with more radiogenic Sr and unradiogenic Nd values. These changes in isotopic composition from lamprophyre to granitoids cannot be explained by fractional crystallisation alone because this will not alter isotopic ratios unless accompanied by contamination with material of a different isotopic composition. Similarly, the Criffell–Dalbeattie pluton has a range in isotopic values, with the inner granites characterised by radiogenic Sr and unradiogenic Nd compositions compared to the outer granodiorites which cannot be explained by fractional crystallisation processes (Halliday *et al.* 1980; Stephens *et al.* 1985). The large volume of the Criffell–Dalbeattie pluton would require a very large body of lamprophyric magma to produce the granitoid magmas by crystal fractionation and a large body of cumulates would also form. It is most unlikely that such a large body of LILE– and LREE–enriched magmas could be produced in the mantle given that low degrees of partial melting are required to explain the composition of the lamprophyres and there is no petrological or geophysical evidence for the existence of large volumes of mafic cumulates.

5.4.2) Crustal contamination–binary mixing and AFC

Halliday *et al.* (1980) argued that the isotopic zonation observed in the Criffell–Dalbeattie pluton could only be explained by the progressive incorporation of metasedimentary crust into a primitive parental magma. On the basis of simple mixing calculations, they argued that the parental magma, with an $^{87}\text{Sr}/^{86}\text{Sr}$ initial ratio of around 0.7045 and Sr content up to 2000ppm, underwent progressive contamination and that the inner granites contain the greatest proportion of the crustal endmember. A

simple mixing model can explain the gross isotopic features of the Criffell–Dalbeattie pluton (Stephens *et al.* 1985) however it cannot explain the combined trace element and isotope data. An AFC model for the evolution of the Criffell granitoids was developed by Stephens *et al.* (*op. cit.*) in which a clinopyroxene-hornblende bearing granodiorite is contaminated with a partial melt of the local crustal rocks while undergoing simultaneous fractional crystallisation. In this a ratio of 0.3 for the rate of assimilation to crystallisation was assumed and a fractionating assemblage of 66% plagioclase, 33% amphibole with the remainder consisting of sphene, apatite and zircon was used. This AFC model successfully duplicates the HFS element, LREE and Sr isotope variations observed in the pluton. A granodioritic composition was used as the magmatic endmember because this was the least evolved composition found within the pluton. This granodiorite, however, is not representative of the most primitive compositions associated with the pluton and in the present work an AFC model has been constructed representing the interaction of a primitive hornblende lamprophyre melt with a crustal contaminant. This model is based on endmembers described earlier (Chapter 4) and assumes a ratio of rate of assimilation to the rate of crystallisation (r) of 0.4. Curves were calculated for D values representing a range of fractionating assemblages comprised of varying proportions of plagioclase, amphibole, biotite, K-feldspar and accessory phases.

The results of this AFC model for several LILE, LREE and HFS elements, represented by curves, are plotted with data for the Criffell–Dalbeattie pluton (Stephens *et al.* 1985) in figures 5.4(a-d). There is a narrow linear trend of decreasing Ce and Y abundances in the pluton with evolution (Fig. 5.4a). The model curves have similar trends, with the majority of the least evolved (high Ce & Y) granodiorites lying on or close to these curves except for one granite, with very low Ce and Y. The latter can be explained by an increase in the bulk distribution coefficient (D) for Y in the most evolved liquids where there are more HFS element bearing accessory phases in the fractionating assemblage (Stephens *et al.* 1985). Ba and Sr abundances decrease and K increases in the more evolved magmas (Figs 5.4b & c). The datapoints representing the

Fig. 5.4a

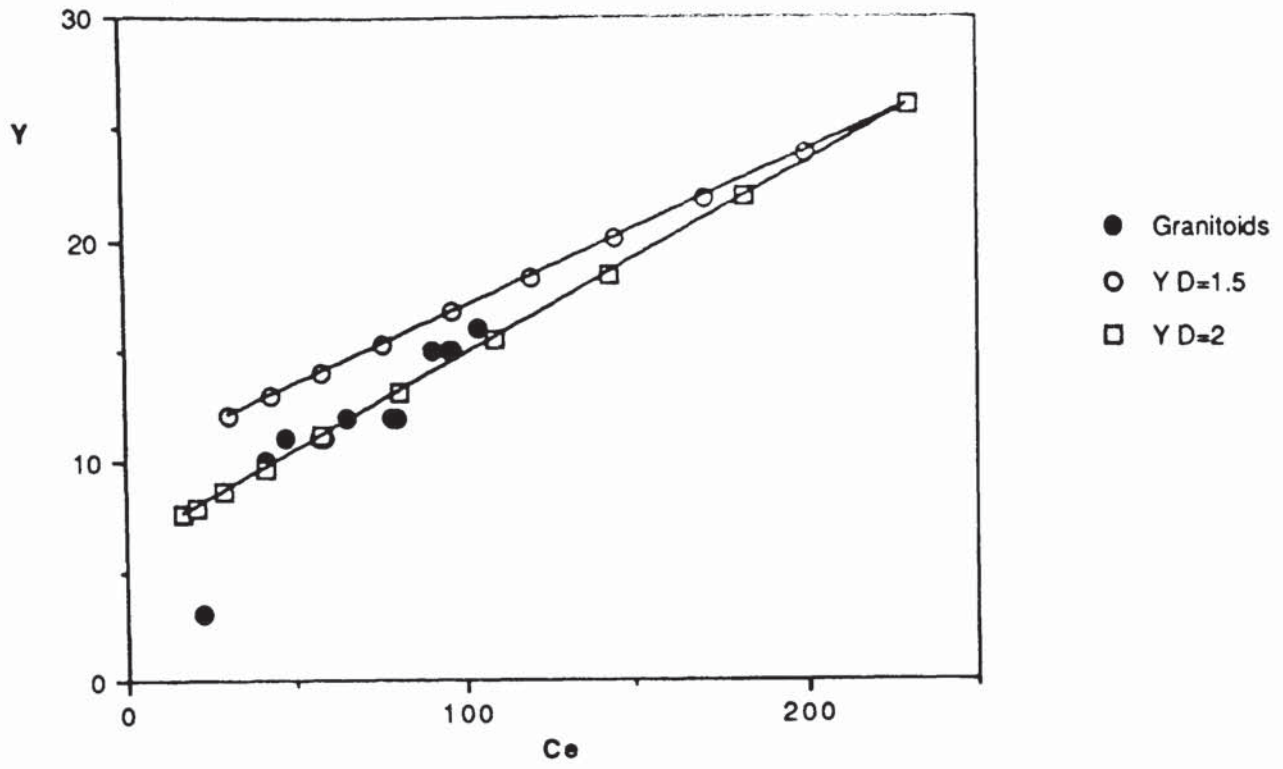


Fig. 5.4b

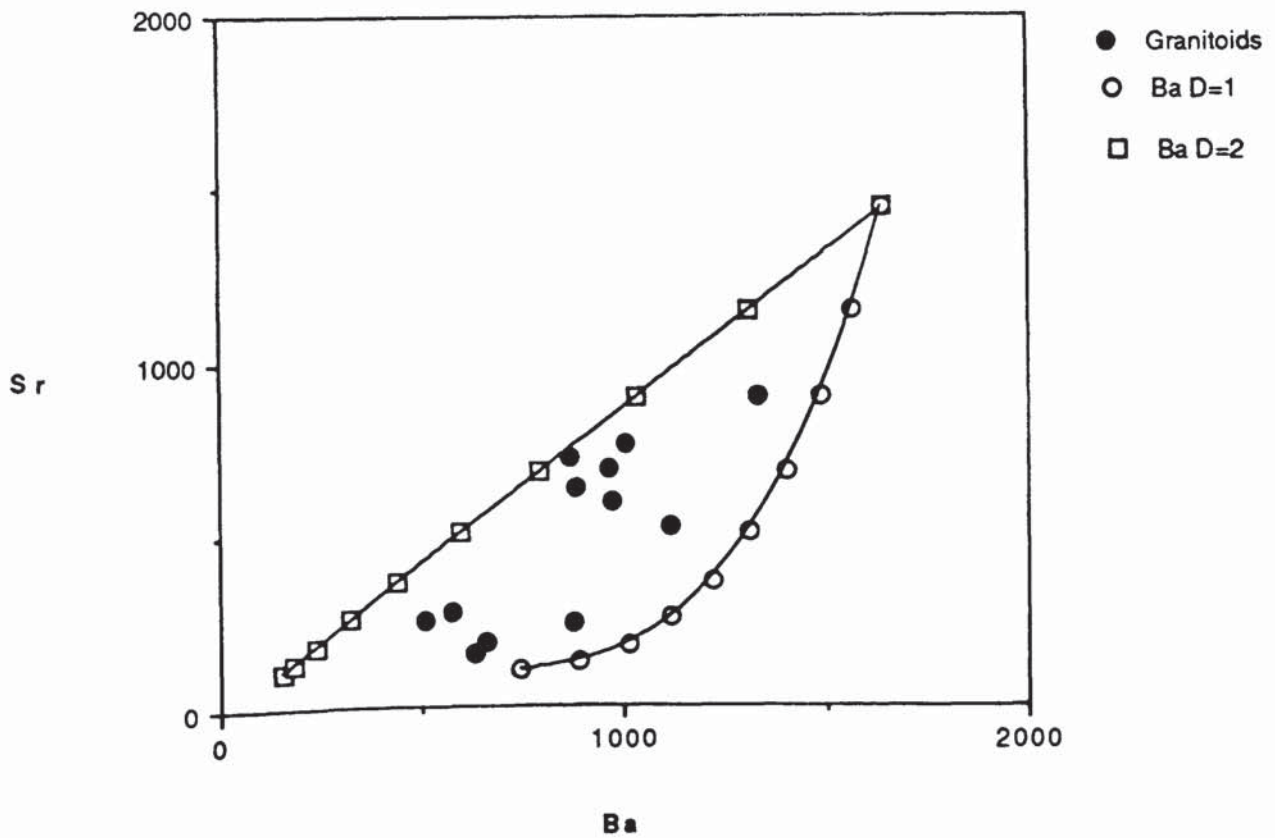


Fig. 5.4c

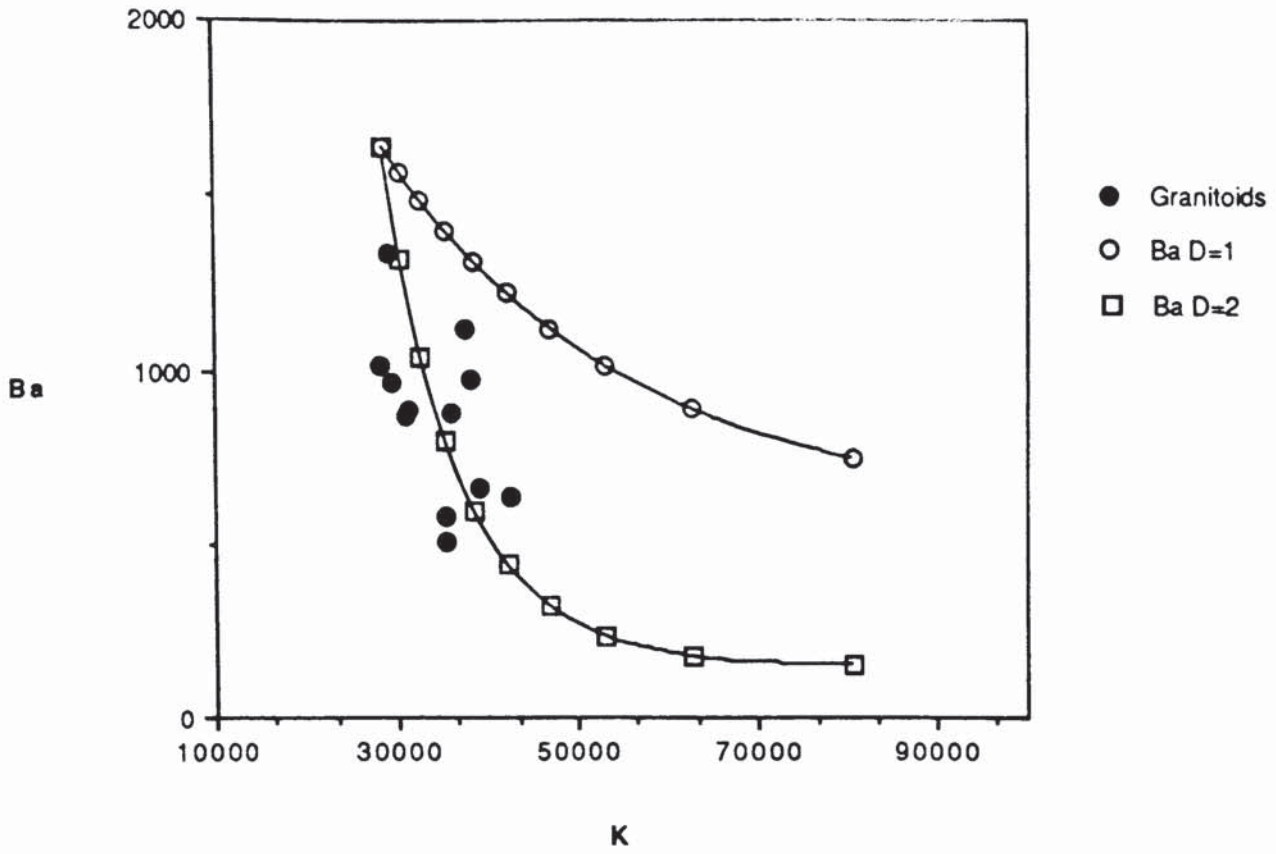
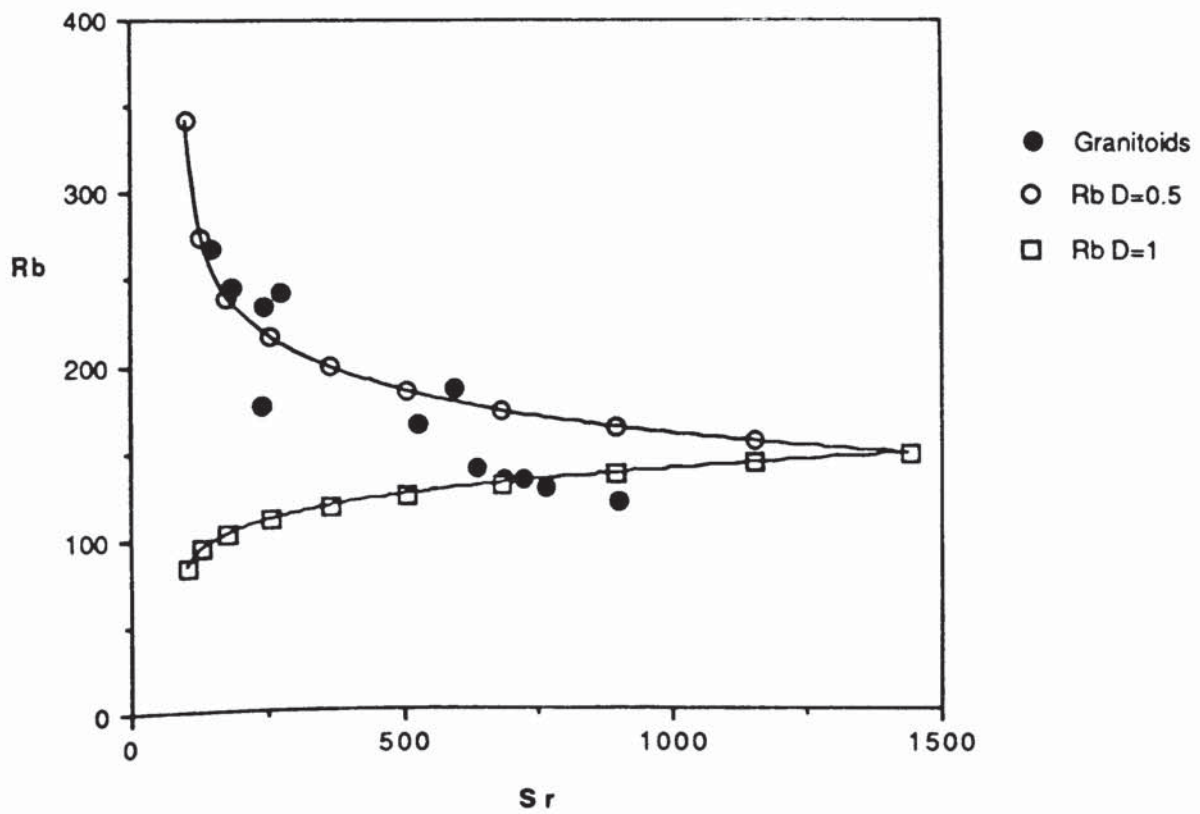


Fig. 5.4d



Criffell–Dalbeattie granitoids lie between the two model curves for Sr and Ba which is considered to indicate that they both behave compatibly during AFC and have bulk distribution coefficients between 1 and 2. Ba and K data for the granitoids are more scattered about the model curves, which represent an assemblage with a D of 2 for Ba and 0.5 for K. This compatible behaviour of Ba in the magmas can only be explained if biotite, which has a high distribution coefficient (K_d) for Ba, is part of the fractionating assemblage.

A more complex pattern is produced by Rb and Sr (Fig 5.4d) where the least evolved granodiorites straddle the curve representing an assemblage in which Rb has a D of 1, while the more evolved granites sit on the curve representing an assemblage in which Rb is incompatible ($D=0.5$). This may be explained by changes in the composition of the fractionating assemblage during the evolution of the magmas with the proportion of K–feldspar increasing at the expense of biotite. K–feldspar has a low K_d for Rb (<0.5) while biotite has a high K_d for Rb (> 3.5) so that variation in the proportions of biotite and K–feldspar in the fractionating assemblage will cause changes in the D of the assemblage for Rb. These changes should cause no change in the D for Ba because both phases have K_d values >1 for this element thus it would continue to behave compatibly in the evolving magma.

The Sr and Nd isotope composition of the lamprophyres, granitoids and the lower Palaeozoic country rocks show considerable overlaps (Fig. 5.5). The field for Sulp sediments is the most extensive and overlaps with the fields for both the Criffell–Dalbeattie granitoids and the lamprophyres. This suggests that the isotopic composition of the granitoids does not conflict with a model invoking contamination of a lamprophyric magma with lower Palaeozoic sediments.

This has been tested in an AFC model using Sr isotope data. Data for the Criffell–Dalbeattie pluton (Stephens *et al.* 1985) mostly fall along or within AFC model curves for Ce– Sr_i , Y– Sr_i and Sr– Sr_i (Figs. 5.6 a–c), however for Ba– Sr_i the more evolved granites fall outside these curves (Fig. 5.6 d). This discrepancy is most probably due to changes in the composition of the fractionating assemblage or changes

Fig. 5.5

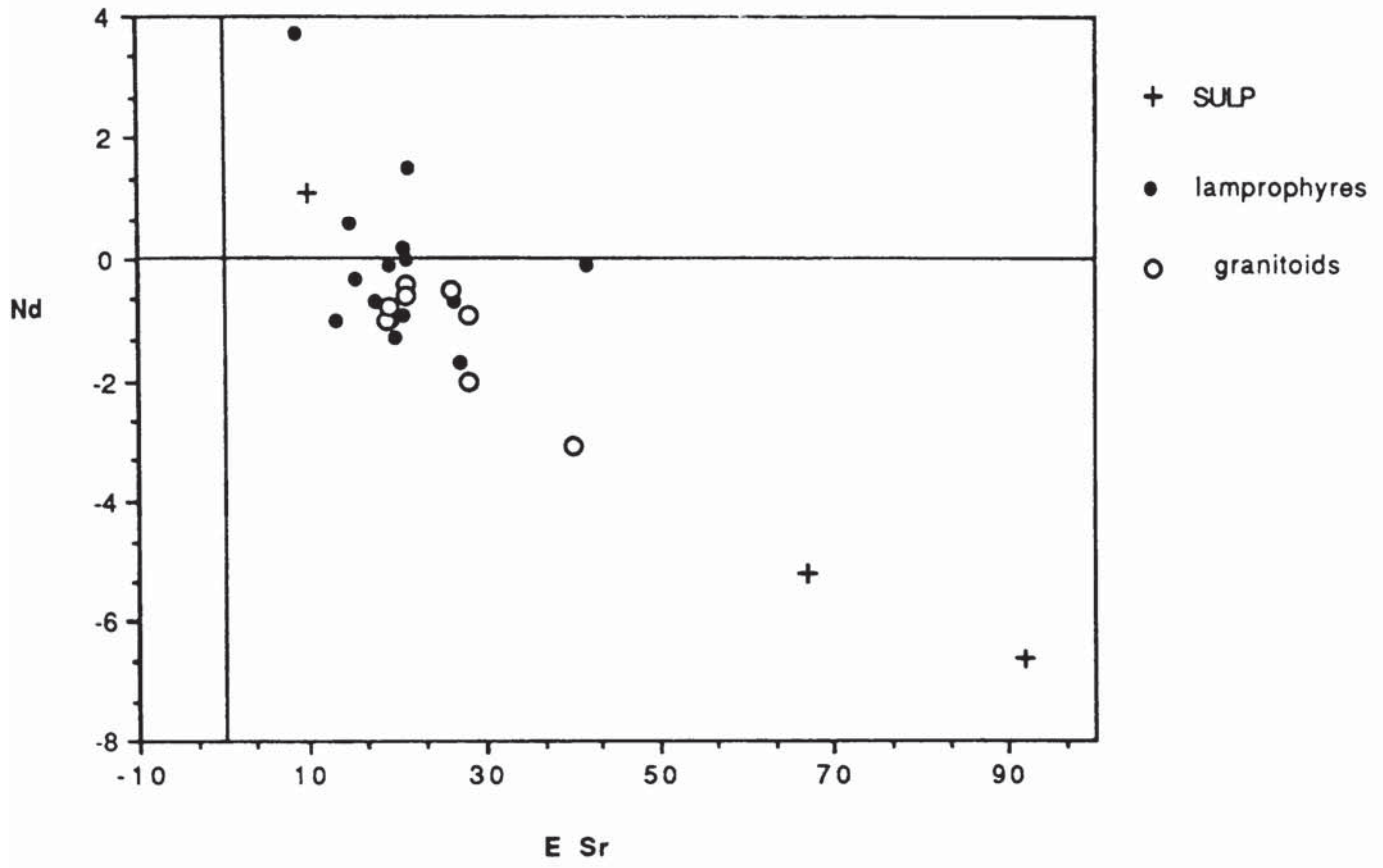


Fig. 5.6a

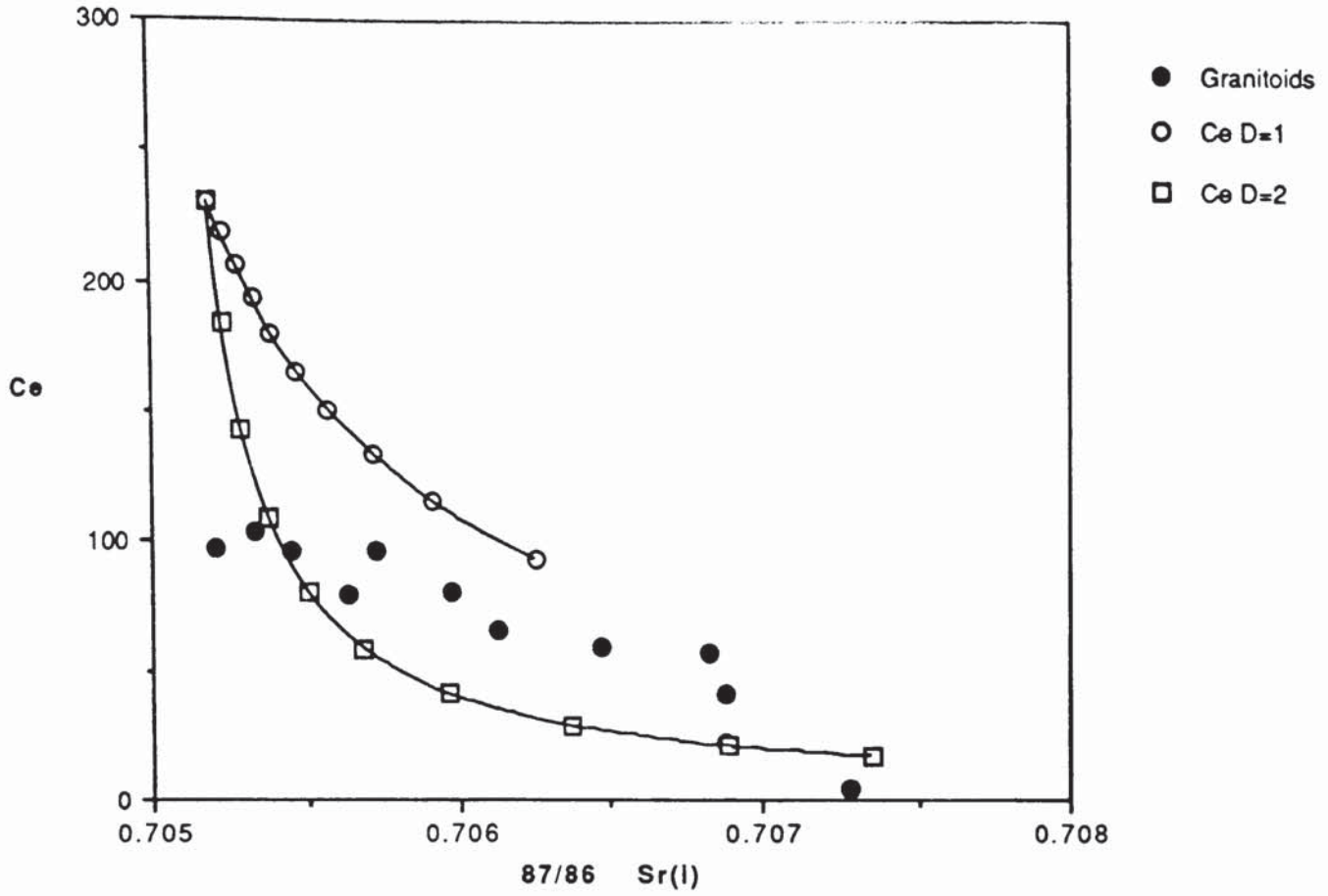


Fig. 5.6b

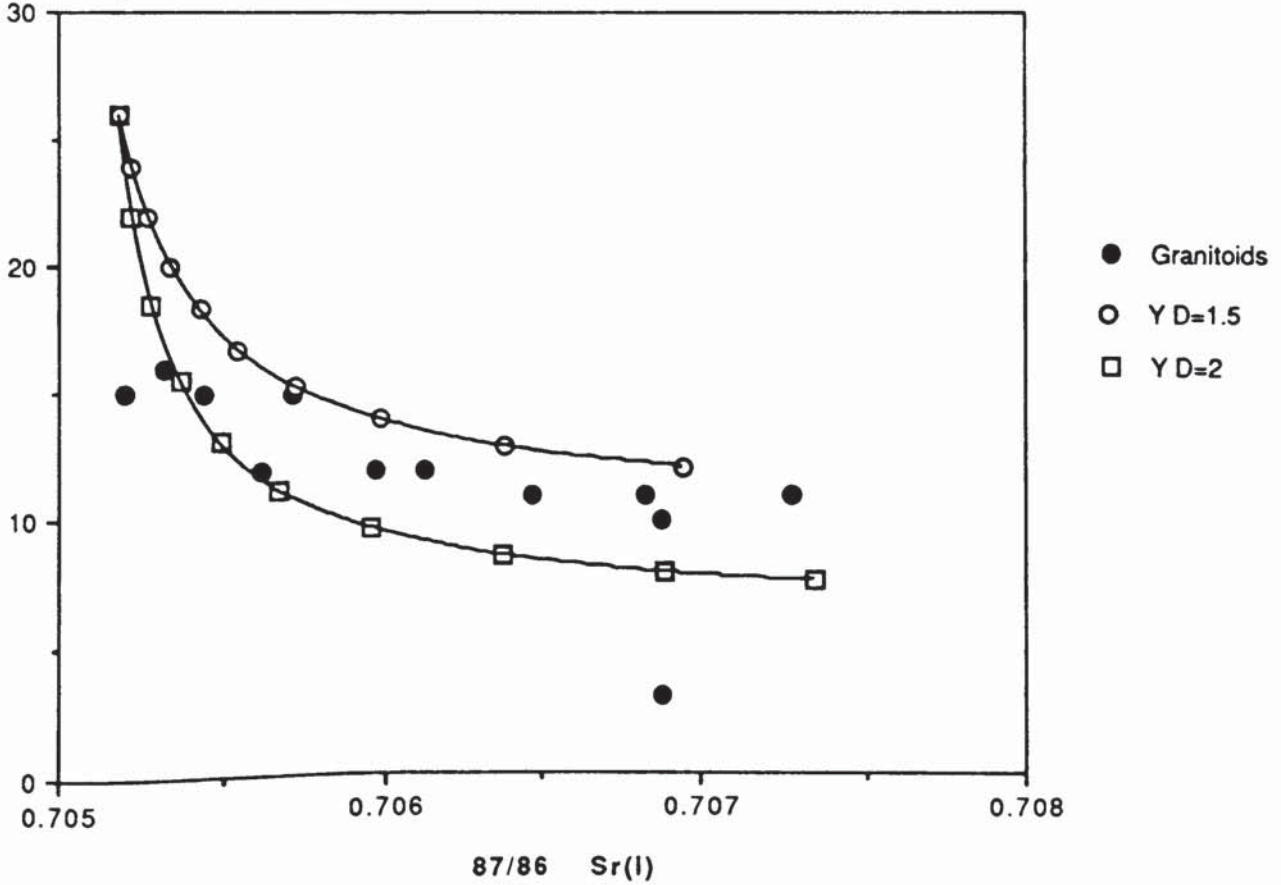


Fig. 5.6c

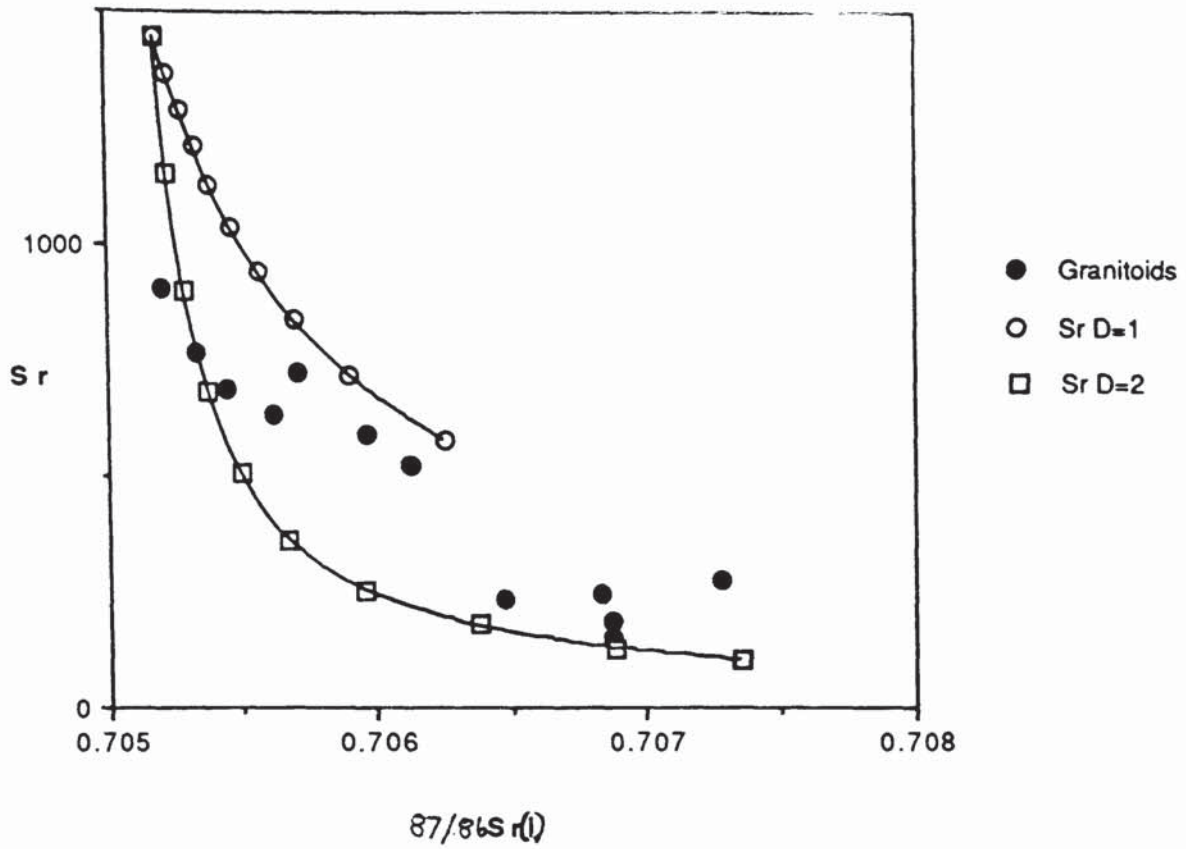
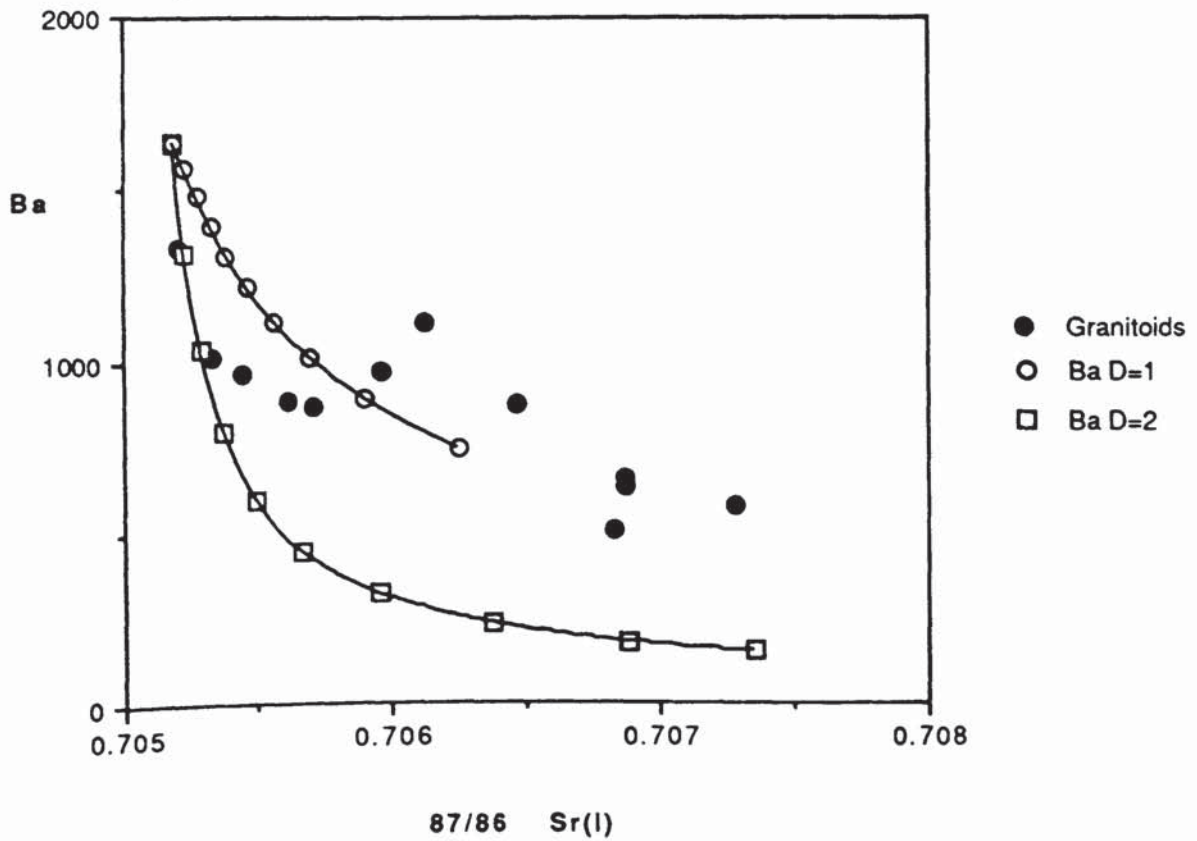


Fig. 5.6d



in the value of r as the magmas evolve. Changes in the value of r will be most noticeable in the Sr isotope composition of the magmas because the isotope systematics are strongly influenced by the amount of crustal contamination but are unaffected by fractional crystallisation (DePaolo, 1981). The inner granites of the Criffell–Dalbeattie pluton are thought to include a larger component of a metasedimentary melt derived from the local country rocks than the outer granodiorites as a result of the rise in the local crustal geotherms produced by the intrusion of the earlier granodiorites (Halliday, 1983). The discrepancy between the AFC model and the real data is most pronounced in the more evolved granites with the high $^{87}\text{Sr}/^{86}\text{Sr}_i$ samples falling off the curves on which the less evolved granodiorites (low $^{87}\text{Sr}/^{86}\text{Sr}_i$) sit. The general agreement between the model AFC trends and the trends for the Criffell–Dalbeattie data, particularly the granodiorites, strongly suggests that the granitoids are the product of the interaction of a high Sr, Ba mantle–derived magma with local crustal rocks.

5.4.3) CAL contribution to granitoid petrogenesis: Thermal triggers and/or magmatic component?

Although the results of AFC modelling suggest that CAL magmas have contributed materially to the granitoid magmas, is this realistic considering the volumetric and thermal requirements of granitoid magmatism? This is particularly pertinent given the small volume of CAL magma observed at the present day surface and that they most probably represent very low degrees of partial melting (McKenzie, 1985). Huppert & Sparks (1988) argued that 500m thick basalt sill at 1200°C could produce a 1km thick layer of convecting silicic magma, assuming a crustal melting point of 850°C. Further injections of basaltic magma would promote further crustal melting, resulting eventually in a partially molten source region through which further basic magma could not penetrate. Experimental work carried out on CAL by Esperanca & Holloway (1987) demonstrated that these magmas are characterised by liquidus temperatures c.1000–1200°C, certainly high enough to cause crustal melting. However, some question remains as to whether a sufficient volume of CAL melt would be available at any one

time given the minimum size of c.5-10m required for magma bodies to initiate crustal melting by Huppert & Sparks (1988a). Luhr et al. (1989) suggested that in the Colima Graben (MVB) much of the lamprophyric magma was unable to reach the surface due to its high density relative to the crust and because of volatile degassing during ascent which promoted rapid freezing of the melts within the crust. Esperanca & Holloway (1987) also implied that for CAL melts to be found at high levels within the crust they must be emplaced quickly or they would undergo rapid volatile loss and freeze during ascent. This suggests that the volume of CAL magma found at the surface may not reflect the true amount of melt produced in the mantle. As Huppert & Sparks (1988a) suggested, episodic basalt emplacement into the lower crust should promote and maintain a zone of partial melting. A similar model may be applicable for CAL magmas, discrete pulses of which may aggregate over a short period of time to promote crustal melting. Certainly field evidence suggest that CAL magmatism preceded and overlapped with the emplacement of the Criffell–Dalbeattie granitoid complex implying that a thermal input was continuing from the mantle during granitoid genesis. This is supported by evidence from mafic enclaves within the granitoid intrusion which have been interpreted as the disrupted remnants of synplutonic, mantle-derived, basic dykes injected into the still mobile granitoid magmas (Holden et al, 1987; Holden et al. in press; Stephens et al. in press). In addition, the relatively high H₂O content of CAL magmas (Esperanca & Holloway, 1987) could be expected to be released during cooling and crystallisation of these melts. As Huppert & Sparks (1988a, b, c) demonstrated, the presence of volatiles, in particular aqueous fluids derived from the crust and/or the basic magma, would promote partial melting of the crust. Thus the release of volatile from aggregated CAL magmas may in fact enhance the degree of crustal melting or at least compensate for any volumetric imbalance relative to models based on basaltic magmas. As demonstrated by the AFC modelling and isotopic data, the Criffell CAL magmas satisfy the necessary compositional and isotopic criteria to be considered as parental magmas to the less evolved components of the Criffell–Dalbeattie granitoid complex with high Sr and Ba contents (Stephens et al. 1985,

Stephens & Halliday, 1984). The exact mechanism of interaction is unclear although it is likely that volatile–phase transfer plays an important role. Therefore it is suggested that CAL magmas can act both as the thermal trigger for initiating crustal melting and as a component of the least evolved granitoid magmas.

5.5) Petrogenetic model for the Criffell–Dalbeattie granitoid

Lamprophyric magmas were probably produced by low degrees of partial melting in the lithospheric mantle underlying the Southern Uplands during the final stages of the Caledonian orogeny. Small amounts of these melts were then able to escape to high levels in the crust along deep seated faults and fractures active during a transpressional regime dominated by strike–slip faulting (Watson, 1984; Stone *et al.* 1987). However, it is likely that much of the lamprophyric magma was unable to escape to high crustal levels because of its greater density relative to the overlying crust and the volatile–rich nature of the magmatism, as is thought to be the case in the Colima graben (Luhr *et al.* 1989). Thus lamprophyric magmas may have ponded at the crust–mantle boundary or have been trapped as dykes and sills within the lower crust, under similar conditions to those modelled for the intrusion of basaltic magmas into the crust (Huppert & Sparks, 1988a, b, c).

Cooling of the trapped lamprophyric magmas by conductive heat transfer into the surrounding or overlying crust would promote crystallisation and also partial melting of the crustal rocks. Magmas saturated with hydrous fluids are thought to be more effective in promoting partial melting than anhydrous ones because the volatiles would lower the melting point of the crustal rocks (Huppert and Sparks, *op. cit.*). Lamprophyric magmatism as a whole is characterised by high volatile contents (Rock, 1987) and the Criffell lamprophyres, as with other CAL, require high H₂O contents to stabilise their high modal amphibole and phlogopite contents (Esperanca & Holloway, 1987). The volatile content of the lamprophyric magmas will be released with cooling and crystallisation, thus enhancing partial melting in the enclosing crustal rocks. It is also possible that these volatiles will transfer some of the magmatic LILE into the zone

of melting where they may contaminate partial melts (Macdonald et al. 1986). The loss of volatiles has also implications for the mineralogy of the fractionating assemblages and of the hybrid magmas. In the AFC model, plagioclase is an essential phase, forming at least 50% of the fractionating assemblage in order to deplete the evolving magmas in Sr (Stephens et al. 1985). However, the high H₂O content of the lamprophyres will suppress the stability field of plagioclase, making it an unlikely phenocryst phase in lamprophyric melts and reducing its significance as a fractionating phase during AFC (Gill, 1981). For the AFC model to be applicable, a lamprophyric magma must lose most of its magmatic volatiles before plagioclase can begin to fractionate from the magma. In addition to stabilising plagioclase, lower H₂O contents will also stabilise clinopyroxene which is a common phase in the granodiorites of the Criffell–Dalbeattie pluton.

Evidence from enclaves suggests that lamprophyric magmas were available throughout the evolution of the pluton and field data and radiometric age dating indicate that intrusion of lamprophyres precedes and overlaps with the emplacement of the Criffell–Dalbeattie pluton. Partial melting therefore probably continues in the mantle during the development of the pluton with fresh pulses of lamprophyric magma providing thermal energy and volatiles to promote further crustal melting. It is also likely that the fresh lamprophyric magma interacted with crustal melts undergoing AFC style modification to produce more evolved hybrid magmas (Henney et al. 1989). As a zone of melting develops, and the volume of partial melt increases, then these lower density melts will begin to coalesce into buoyant, coherent magma bodies which will start to rise from their source area into the upper crust (Huppert & Sparks, 1988a, b, c). Such magma bodies will transfer heat into the upper crust and are thought to be responsible for the genesis of the more evolved granitic magmas (Halliday et al. 1980; Halliday, 1983).

5.6) Summary

Calc-alkaline lamprophyres have a close spatial and temporal association with the late Caledonian Criffell-Dalbeattie granitoid in SW Scotland and are the only contemporaneous basic rocks associated with the intrusion. Existing models for the petrogenesis of this compositionally-zoned pluton propose that the granitoid magmas result from the combined contamination and fractionation of a basic or intermediate magma derived from the mantle or lower crust. The results of AFC modelling show that combined fractionation and contamination of a lamprophyric melt with local crustal rocks can explain many of the isotopic and trace element characteristics of the Criffell-Dalbeattie granitoids. It is proposed that mantle-derived lamprophyric melts are trapped at the crust-mantle boundary and within the lower crust as a result of their greater density, relative to the surrounding crust, and by rapid freezing due to a loss of magmatic volatiles during magma ascent. Under these conditions the trapped lamprophyric magmas may act as melting triggers to promote partial melting of the overlying or surrounding crust, aided by the volatiles released from the lamprophyric magma. Fresh pulses of magma injected into the zone of melting may interact with the crustal melts and undergo AFC style modification. Intermediate hybrid magmas produced by this process, represented by the Criffell granodiorites, ascend to higher crustal levels transferring heat which promotes further crustal melting. This will produce more evolved granitic magmas and further dilute the contribution derived from the lamprophyric magmas. It is therefore suggested that the close spatial and temporal association between the lamprophyres and the Criffell-Dalbeattie granitoid is not accidental but is the result of a direct petrogenetic link with the lamprophyres acting both as a heat source promoting crustal melting, and contributing directly to the composition of the granitoid magmas.

Chapter 6

The Porphyrite–Porphyry series: Intermediate and acid dykes associated with the Criffell–Dalbeattie pluton

6.1) Introduction

The majority of the minor intrusions associated with the late Caledonian Criffell–Dalbeattie granitoids are intermediate to acid microdiorites, microgranodiorites and microgranites. They are commonly porphyritic, with phenocrysts of plagioclase, amphibole, biotite and quartz, set in a feldspathic groundmass and are known collectively as the porphyrite–porphyry series (Hatch et al. 1972; King, 1927; Macgregor, 1937; Phillips, 1956b). The compositions represented by the porphyrite–porphyry series have most commonly been interpreted as the hypabyssal equivalents of the granitoid magmas of the Criffell–Dalbeattie pluton (Phillips, 1956b; Phillips et al. 1981). Emplacement of this group of dykes overlapped with the intrusion of the Criffell–Dalbeattie pluton. The D1 porphyrites of the Black Stockarton Moor complex are cut by the outer Criffell granodiorites whereas the porphyrites and porphyries of the D2 and D3 phases intrude both the granodiorites and granites (Leake & Cooper, 1983).

For this study, approximately 100 samples of the porphyrite–porphyry series of minor intrusions were collected from around and within the Criffell–Dalbeattie pluton. They were analysed by XRF for major and trace elements including La, Ce and Nd. This was done in order to characterise the chemistry of the porphyrite–porphyry series and to examine the suggestion that the dykes were derived from the same magmas as the granodiorites and granites forming the pluton.

6.2) Field relations and petrography

The field relations and petrography of the dykes of porphyrite–porphyry series associated with the Criffell–Dalbeattie pluton have been described in detail by previous workers (King, 1927; Macgregor, 1937; Leeder, 1971; Phillips, 1956b). These studies highlight some of the difficulties in classifying the members of the porphyrite–porphyry

series because of hydrothermal alteration, weathering, heteromorphism and their dominantly porphyritic texture. A 3-fold classification of the porphyrite–porphyry series, based on mineralogy and geochemistry has been described from the late Caledonian dyke swarm present in the Wigtown Peninsula (Barnes *et al.* 1986).

The series is divided into porphyrites, with phenocrysts of plagioclase (\pm clinopyroxene \pm amphibole \pm biotite) set in a feldspathic matrix with minor K-feldspar and quartz and; acid porphyrites with a similar mineralogy but with little or no amphibole and more K-feldspar and quartz in the matrix. A third group, the porphyries, is characterised by phenocrysts of quartz and K-feldspar and has biotite as the principal mafic phase. This classification is the basis of the nomenclature used in this study but has been slightly modified by “merging” the acid porphyrites with the porphyrite group. This has been done for the Criffell porphyrites because the use of the relative proportions of quartz and K-feldspar present in the groundmass to differentiate the porphyrites is not a robust discriminator where the effects of alteration and weathering can obscure the texture and mineralogy of the groundmass.

In the field porphyrite–porphyry series rocks most commonly occur as dykes, 1-3 metre wide, characterised by a pink-red coloration. These commonly contain abundant pale phenocrysts of feldspar which are commonly flow-aligned parallel to the dyke margins. In the lower Palaeozoic sediments the dykes generally strike NE–SW, parallel to the bedding, though some of the D2 phase dykes in the Black Stockarton Moor complex cut NW-SE across the strike (Leake & Cooper, 1983). Dykes intruding the granodiorites and granites of the Criffell–Dalbeattie pluton most commonly strike NW–SE. In the southern part of the study area, in the sediments close to the southern margin of the pluton, the porphyrite–porphyry dykes are associated with breccia pipes and localised pyrite and chalcopyrite bearing mineralisation.

6.2.1) Porphyrites

These are the most abundant and widespread component of the porphyrite–porphyry series associated with the Criffell–Dalbeattie pluton, and make up approximately 70%

of the samples collected. They are intruded into both the lower Palaeozoic sediments and the granodiorites and granites of the pluton. In thin section the porphyrites range from clinopyroxene–phyric (\pm amphibole) compositions, with sparse plagioclase, through plagioclase–phyric (\pm amphibole, \pm biotite) types, with up to 70% feldspar phenocrysts, to varieties with abundant interstitial “pools” of quartz and K-feldspar. Many show the effects of hydrothermal alteration with sericitisation of the feldspars, chloritisation of the mafic phases (both the phenocrysts and groundmass), and silicification of the groundmass. As a result no subdivision of the porphyrites on the basis of the petrography was made.

Clinopyroxene is present in a few of the more melanocratic, D2 phase porphyrites of the BSM complex. It occurs most commonly as colourless, anhedral phenocrysts which are commonly corroded and, in some specimens, as small grains in the groundmass. Hornblende is a more common phase, occurring as subhedral to euhedral phenocrysts, and as prismatic grains and acicular needles in the groundmass. It is commonly zoned with dark green cores and paler rims. The phenocrysts are commonly altered with actinolite and chlorite, together with Ti-Fe oxides and minor amounts of sphene, rimming and replacing the primary hornblende. Biotite is more abundant in the leucocratic porphyrites and occurs both as sparse phenocrysts and, more commonly, as small flakes in the groundmass. Alteration is common with the development of chlorite and Fe-Ti oxides along cleavages and many phenocrysts are bleached and are partially replaced by chlorite.

Plagioclase is the most abundant feldspar in the porphyrites and occurs both as euhedral phenocrysts and as interlocking laths in the groundmass. Both phenocrysts and groundmass crystals are commonly zoned, some showing complex patterns, particularly at the edges of the crystals. Many of the phenocrysts have a later thin rim of unzoned, clear feldspar, thought to be albite. In most of the sections studied the plagioclases are altered with some being completely replaced by “clays”, sericite, epidote and carbonate, and others having altered cores but relatively fresh margins. K-feldspar and quartz occur together and are restricted to the groundmass in porphyrites in

interstitial “pools” or graphic intergrowths. Accessory phases include apatite in the more mafic rocks, and epidote, chlorite, carbonate and Fe-Ti oxides associated with alteration. A few grains of subhedral to euhedral zircon, associated with biotite, also occur in the more felsic porphyrites.

6.2.2) Porphyries

The porphyries are distinguished from the porphyrites by the presence of phenocrysts of quartz and, less commonly, K-feldspar. They range from biotite-bearing microgranodiorites to quartz- and K-feldspar-rich microgranites and aplites. Some porphyries intrude the lower Palaeozoic country rocks but more commonly intrude the granodiorite and granite phases of the Criffell–Dalbeattie pluton. Hydrothermal alteration occurs mainly in those bodies which cut the sediments rather than those intruded into the plutonic rocks. A dark brown biotite is the most abundant mafic mineral and occurs both as euhedral phenocrysts and as flakes in the groundmass. In some instances it is accompanied by minor quantities of green hornblende.

Biotite phenocrysts exhibit “bleaching” with the development of chlorite and Fe-Ti oxides along the cleavage while groundmass biotite is replaced by fibrous “mats” of chlorite. Biotites are least altered in the porphyries intruded into the inner granite of the pluton. Plagioclase has a similar habit to that exhibited in the porphyrites and, although phenocrysts are generally less abundant in the porphyries, they have similar patterns of complex zoning and development of albitic rims. K-feldspar is most common in the groundmass, as anhedral “plates” and in graphic intergrowths with quartz, and in sparse, euhedral, phenocrysts in the more leucocratic samples. Quartz forms anhedral, interstitial “pools” and subhedral to euhedral phenocrysts set in a quartzo-feldspathic matrix. Accessory minerals include apatite and sphene both of which occur associated with biotite, epidote and carbonate from the alteration of plagioclase. Small round grains of zircon are present in biotites surrounded by well developed pleochroic halos. In some of the more felsic samples, small, colourless flakes of muscovite occur associated with K-feldspar and quartz.

The porphyrites and porphyries are a series of porphyritic microdiorites, microgranodiorites and microgranites with similar mineralogies to those of the plutonic rocks (Phillips, 1956a, 1956b). The porphyrite–porphyry series however show a greater textural variation, complicated by the effects of widespread hydrothermal alteration which restricts the effectiveness of classifications based on petrographical data.

6.3.1) Alteration of the porphyrite-porphyry series

As reported for the Criffell CAL in Chapter 3, samples of the porphyrite-porphyry series were screened petrographically and significantly altered samples removed from the dataset or not submitted for analysis. The data for the porphyrite-porphyry series have been tested for the effects of alteration using the criteria discussed in section 3. of Chapter 3. Samples from the Black Stockarton Moor (BSM) complex (Leake & Cooper, 1983) consistently show the greatest petrographic evidence for alteration (Appendix E) and plots of mobile vs immobile element behaviour (Figures 6.1 (a-b) show the geochemical consequences of this alteration. Many of the BSM samples show a great deal of scatter with regard to Ba, with both losses and gains relative to the field for less altered samples. However, Rb shows much less evidence for mobilisation, with the bulk of the BSM samples falling along the trend defined by the less altered samples. Therefore it would appear that although alteration has clearly modified the Ba abundance of the BSM samples, there has not been systematic alteration of all 'mobile' elements e.g. Rb. All the BSM samples have been excluded from plots and chemical discussions in this chapter although the analysis are presented in Appendix C. HFSE-HFSE and LILE-LILE behaviour in the less altered porphyrite-porphyry series are illustrated in figures 6.2 (a-b) with linear correlations evident between Y and TiO_2 and between Rb and K_2O , suggesting that post-magmatic alteration appears to have had little significant effect on the distribution of these elements. Similarly, linear trends (figures 6.3 (c-d) between Rb and TiO_2 and between Ba and TiO_2 argue against systematic alteration of the LILE in these samples. However, some of the samples,

Fig. 6.1a

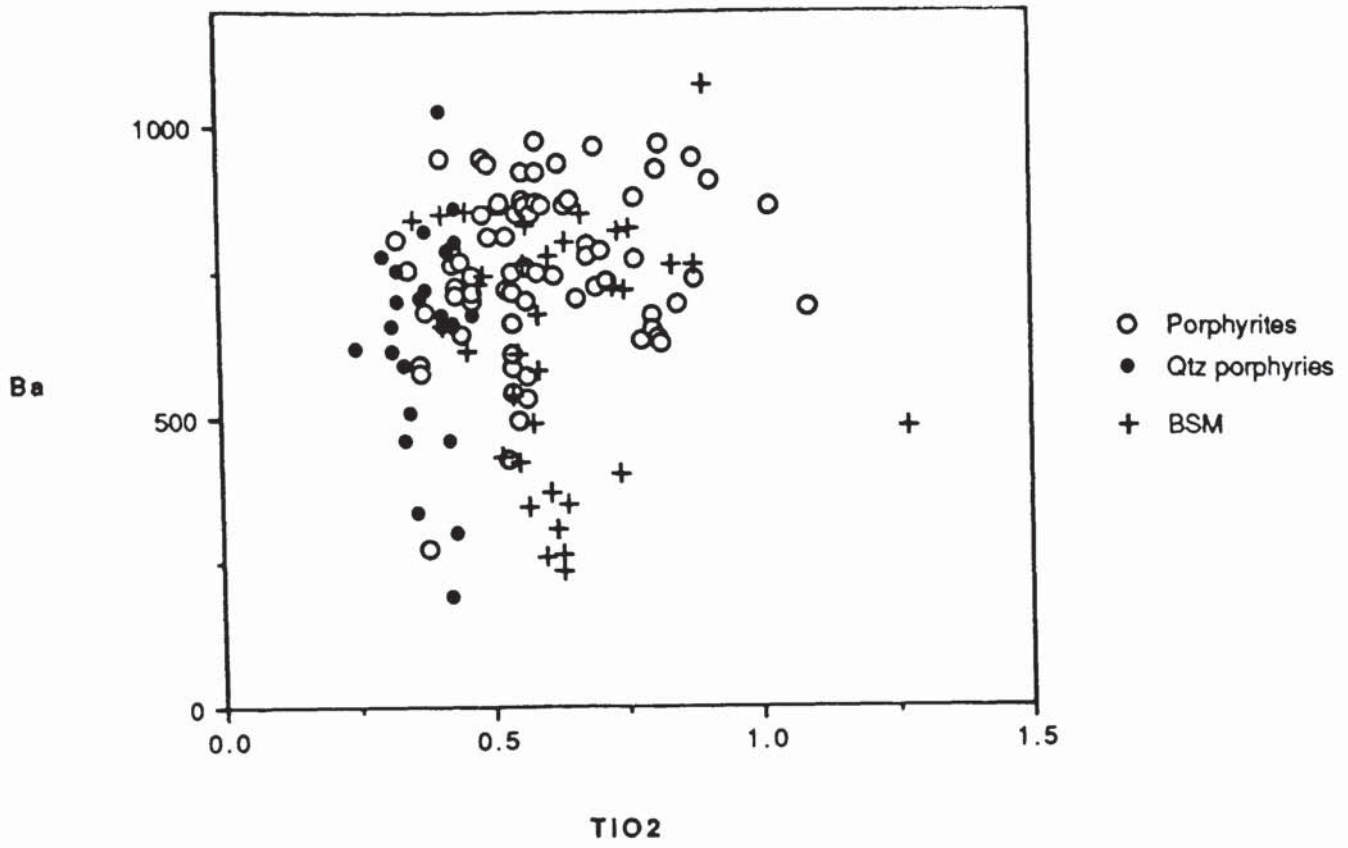


Fig. 6.1b

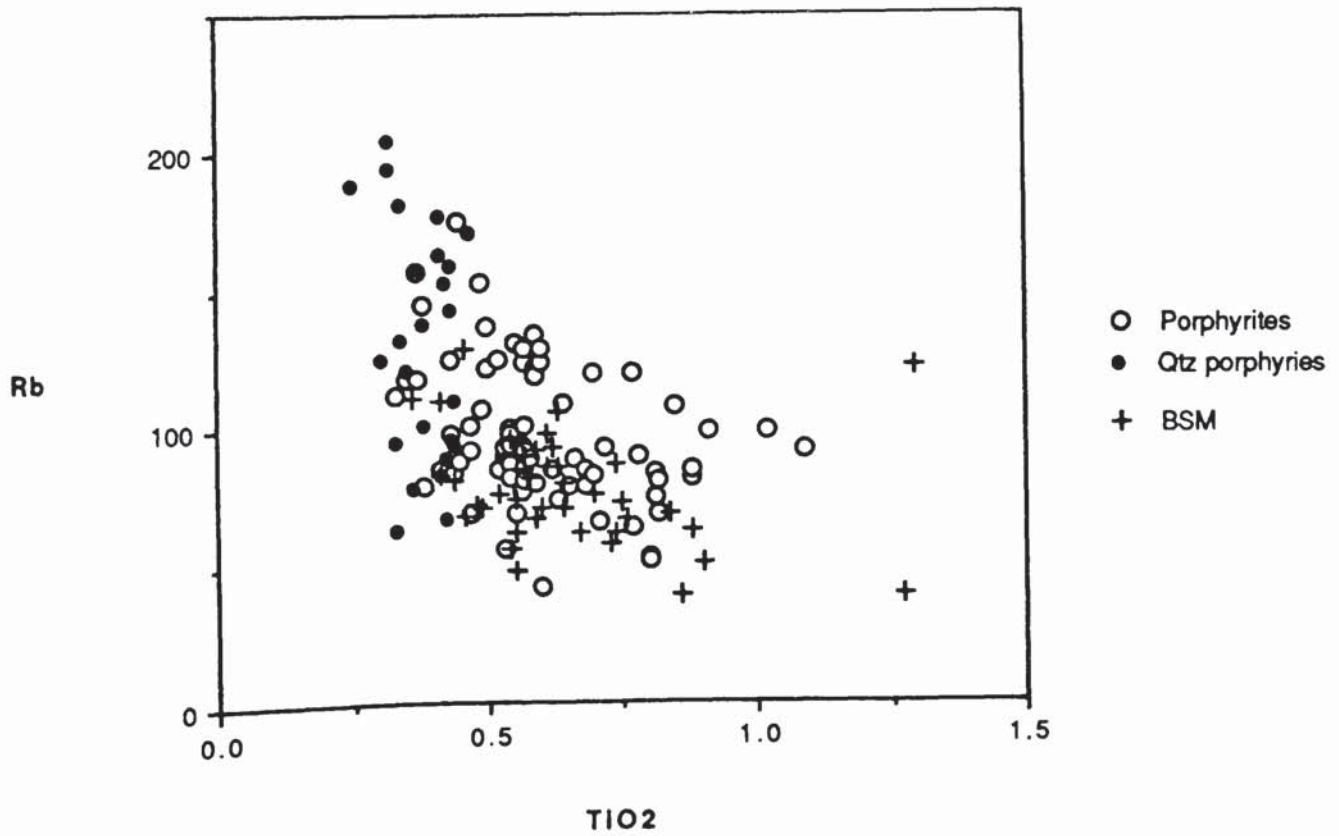


Fig. 6.2a

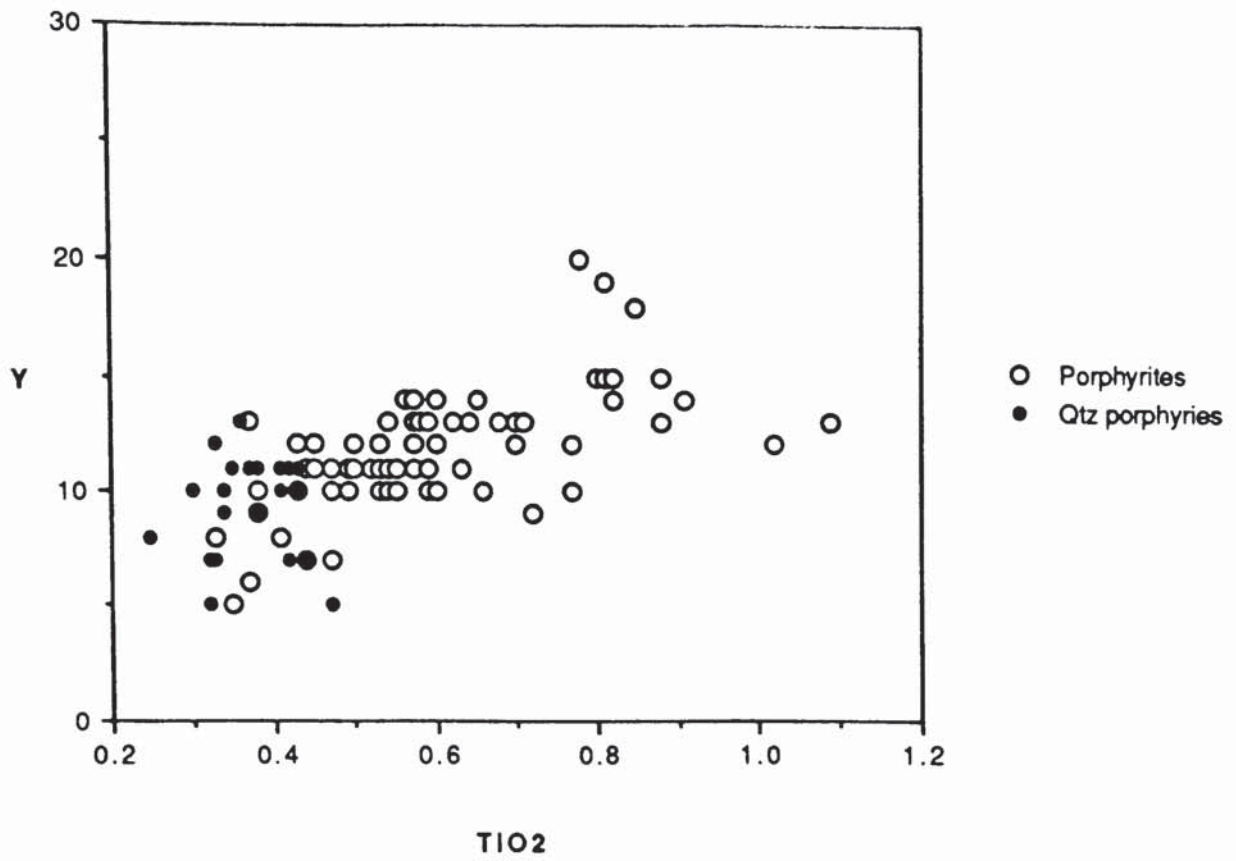
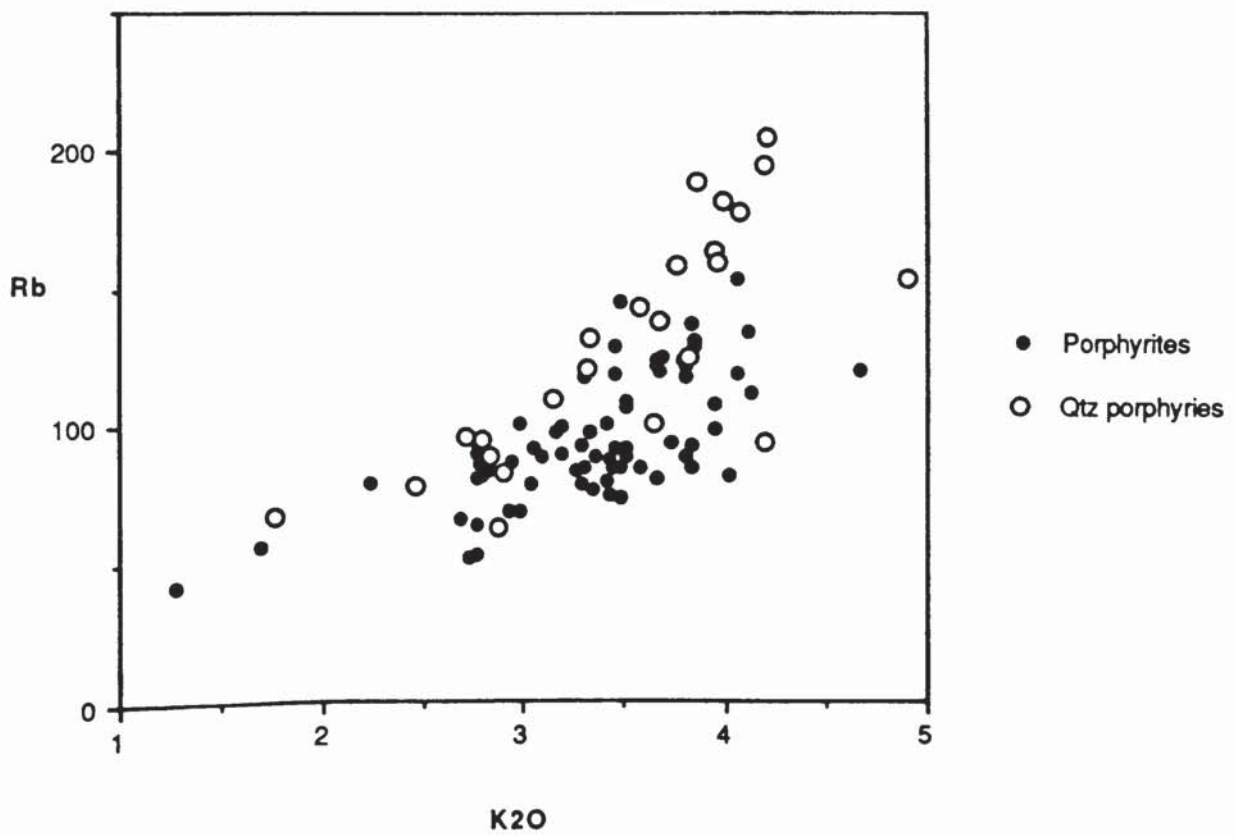


Fig. 6.2b



K2O

174

Fig. 6.3a

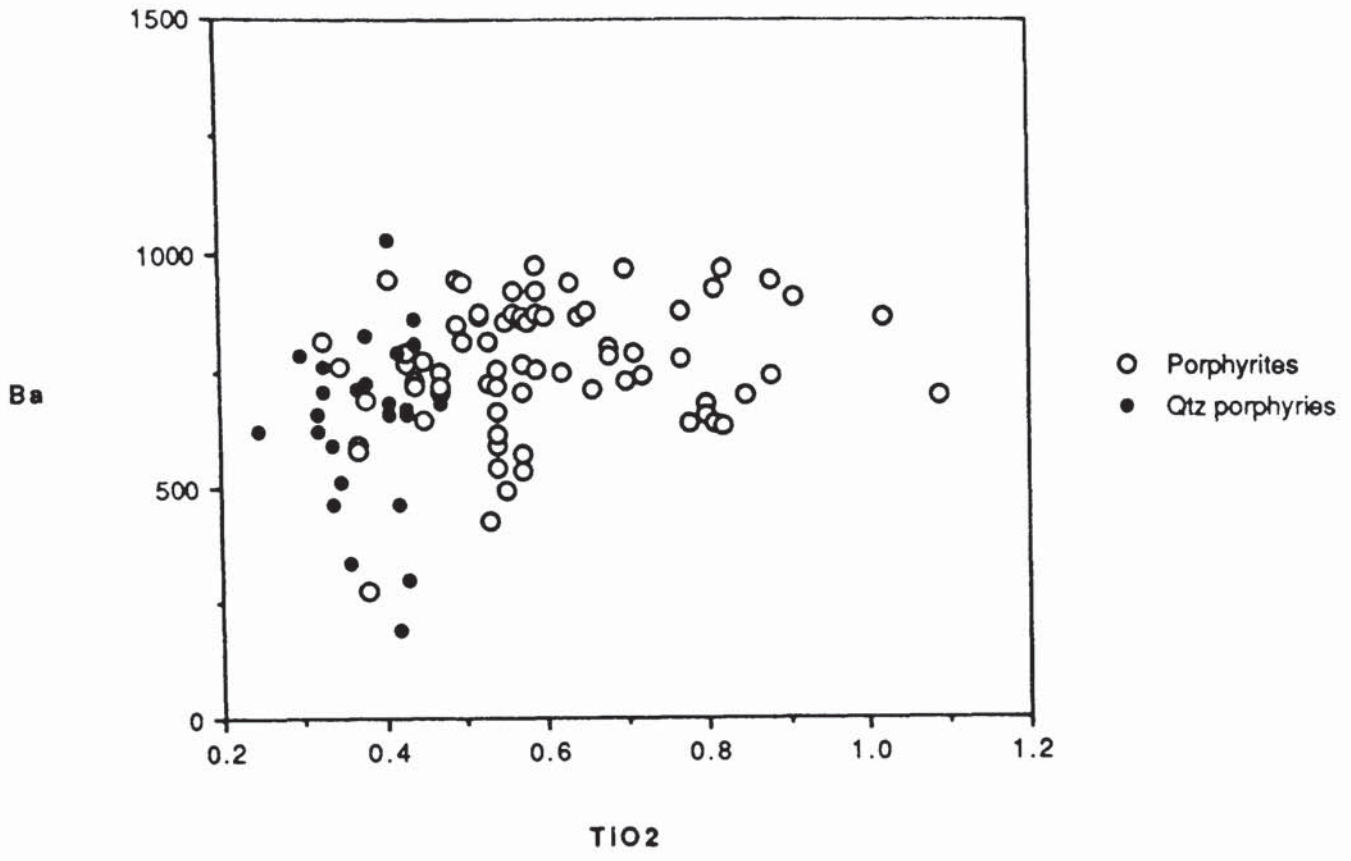
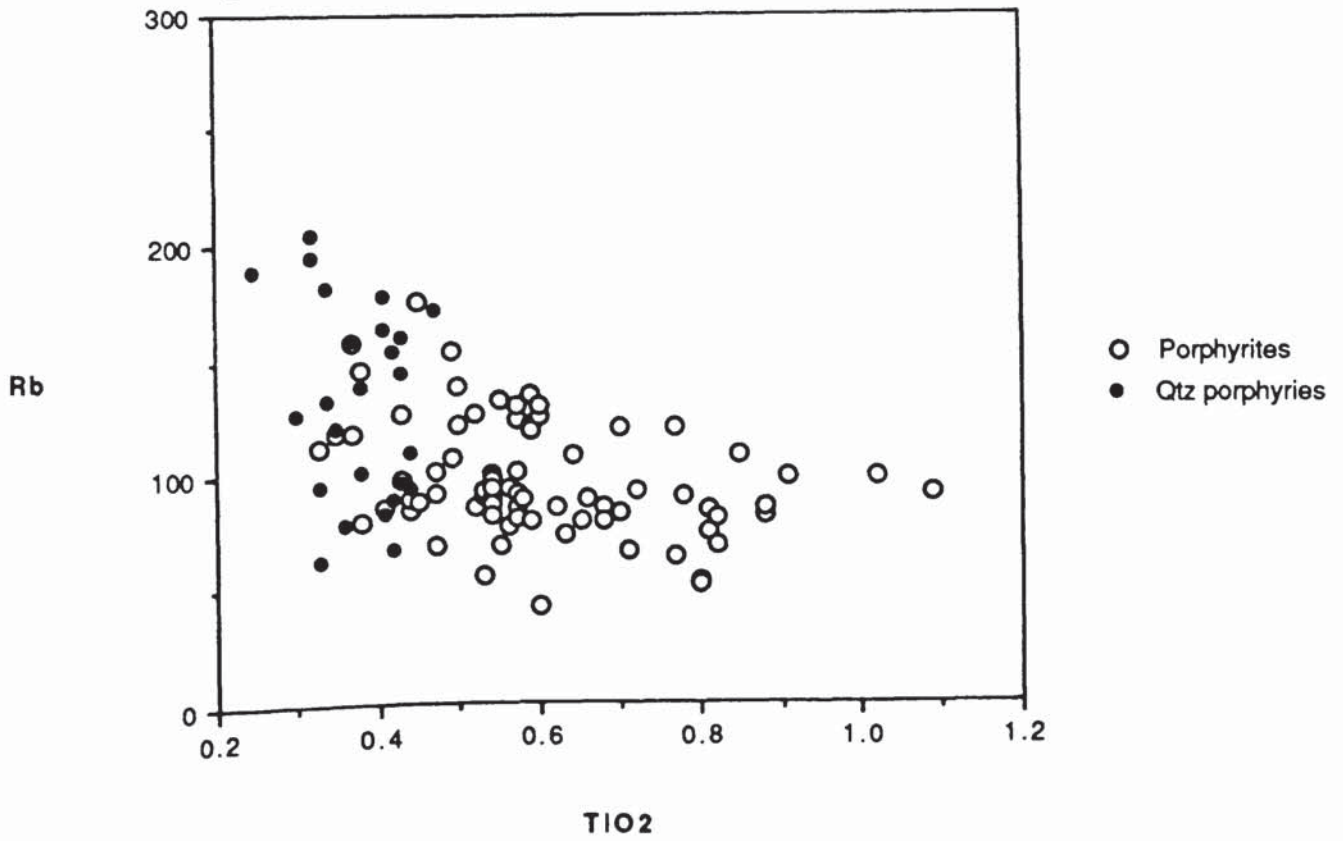


Fig. 6.3b



TiO₂

particularly of the quartz porphyry series, show low Ba and localised alteration cannot be excluded in light of the petrographic evidence for sericitisation (c.f BSM samples).

6.3.2) Chemistry of the porphyrite–porphyry series

As described from the Wigtown Peninsula porphyrites are the least evolved of porphyrite–porphyry series rocks with SiO₂ contents ≤ 60%.and the more evolved acid porphyrites and porphyries form a continuous series with SiO₂ 64-71% (Barnes *et al.* 1986). The existence of the silica gap between the two groups led Barnes *et al.* (op.cit) to argue that they could not be directly related and must have derived from two separate parent magmas. Phillips (1956b) and Leeder (1971) presented some analyses of the Criffell–Dalbeattie porphyrite-porphyry series dykes and observed that the porphyries were more evolved than the porphyrites with lower MgO, CaO, TiO₂ and P₂O₅ but greater K₂O, Na₂O and SiO₂ contents. Both authors noted the compositional similarity of the porphyrite–porphyry series and the Criffell–Dalbeattie granitoids. In this study, all major element data has been recalculated on a volatile–free basis, with total iron quoted as Fe₂O₃, and full analyses are listed in Appendix C.

The porphyrites have a wide range in SiO₂ contents (56.4-71.6%), which correlates negatively with MgO (0.5–5%), CaO (0.4–5.5%), TiO₂ (0.3–1.6%) and P₂O₅ (0.12–0.6%) (Figs 6.4a–d) and positively with K₂O (1.3–7.2%) and Na₂O (2.3–5.9%). They all have high Ba (<2000ppm) and Sr (<890ppm) abundances, typical of many late Caledonian granitoids, with moderate Ni (<100ppm) and Cr (<215ppm) contents. All are quartz (<29%) and corundum (<3.9%) normative and also have normative hypersthene (<12.9%) and diopside (<3.1%) (Table 6.1).

The porphyries extend to slightly higher SiO₂ (68.5–73.1%) than the porphyrites but there is a considerable overlap. MgO (0.5–2.1%), CaO (0.6–2.9%), TiO₂ (0.25–0.5%) and P₂O₅ (0.11–0.25%) all have negative correlations with SiO₂ while K₂O (1.8–5.7%) and Na₂O (3.0–5.6%) have positive correlations. Ba (<1030ppm) and Sr (<715ppm) abundances are not as great as those in the porphyrites and those of Ni (<49ppm) and Cr (<48ppm) are considerably lower. The porphyries

Table 6.1 Representative analyses of the Porphyrite–Porphyry series from the Criffell dyke swarm

Sample	Porphyrite TQ04	Porphyrite BHD01	Porphyrite 1357	Qtz Porphyry 1342	Qtz Porphyry CF02	Qtz Porphyry 1344
SiO ₂	62.37	65.94	70.34	70.43	71.71	73.04
TiO ₂	0.77	0.61	0.45	0.38	0.32	0.25
Al ₂ O ₃	16.19	16.23	16.11	15.94	15.19	15.65
Fe ₂ O ₃	4.77	3.64	2.56	2.38	1.99	1.77
MgO	5.66	2.29	1.36	1.00	0.82	0.58
CaO	3.02	3.66	1.06	1.58	1.74	0.59
Na ₂ O	4.30	4.02	4.46	4.35	3.85	4.05
K ₂ O	2.57	3.36	3.43	3.68	4.21	3.86
P ₂ O ₅	0.29	0.21	0.18	0.20	0.14	0.18
MnO	0.07	0.05	0.05	0.04	0.04	0.03
LOI	3.16	0.58	2.81	2.87	0.62	1.69
DX	63.71	72.01	84.81	84.63	85.54	89.63
MG#0.3	77.05	63.97	60.16	54.37	53.77	48.10
Qz	12.02	18.11	26.76	26.02	28.11	32.56
Ab	36.47	34.03	37.76	36.84	32.55	34.27
Or	15.22	19.87	20.29	21.77	24.88	22.80
An	13.09	16.39	4.06	6.53	7.69	1.76
Di	0.00	0.33	0.00	0.00	0.00	0.00
Hy	17.35	7.96	5.08	4.13	3.39	2.71
Ol	0.00	0.00	0.00	0.00	0.00	0.00
Mt	2.08	1.59	1.11	1.04	0.87	0.77
Il	1.46	1.16	0.85	0.71	0.61	0.48
Ap	0.67	0.49	0.42	0.47	0.33	0.42
Cm	1.56	0.00	3.59	2.43	1.50	4.18
Ne	0.00	0.00	0.00	0.00	0.00	0.00
Ni	117	47	32	39	30	17
V	110	73	41	41	33	28
Cr	193	58	14	15	22	11
Rb	56	121	88	139	205	189
Sr	1109	601	290	371	320	212
Ba	1563	718	646	723	618	620
U	2	3	4	6	6	5
Th	11	14	13	12	14	13
Zn	63	48	55	48	34	41
Cu	40	20	1	10	9	11
Pb	12	25	9	25	34	11
Zr	183	165	224	182	142	142
Nb	11	11	9	11	10	10
Y	13	12	11	11	7	8
La	35	33	42	34	35	28
Ce	70	65	88	66	68	57
Nd	32	25	33	24	28	25

have high normative quartz (<32.5%) and corundum (<4.24%) contents with correspondingly low normative hypersthene (<7.2%) and no normative diopside (Table 6.1).

In both groups La and Ba show a slight decrease with increasing silica (Figs. 6.4e–f) although the trend for La is not as pronounced as that for Ba (see section 6.3.1). The Rb/Sr ratio of the porphyrites has a slight increase with increasing silica but there is a marked increase generally in the porphyries (Fig. 6.1g) and the K/Rb has a general steady decrease (Fig. 6.4h). Mantle-normalised “spidergram” patterns show both groups to have pronounced negative Nb anomalies, low Ti abundances and high abundances of LILE and LREE (Fig 6.5), patterns which are characteristic of arc-related magmas (Pearce, 1983). Patterns for the two groups have a large overlap though the porphyrites extend to higher levels for La, Ce, Sr, Nd, P, Zr, Ti and Y and are very similar for Rb, Th, U and K. Both groups have a slight negative Sr anomaly relative to the LREE and the porphyries exhibit a slight depletion in Ba relative to Rb and Th. These depletions may reflect the progressive removal of Sr in plagioclase and Ba in biotite, both of which are important phenocryst phases in the majority of rocks. The more restricted range of LREE abundances in the porphyries most probably reflects removal of LREE bearing accessory phases, such as apatite, and this is supported by the lower P content of this group.

6.4) Comparative chemistry of the Criffell pluton and porphyrite–porphyry series

Porphyrite–porphyry series rocks have similar major element and normative compositions to those of the Criffell–Dalbeattie pluton (Phillips, 1956a, 1956b). He suggested that the dyke rocks represent magmas released from the granite magma chamber as it evolved. A similar model was proposed for the origin of porphyries on the southern margin of the pluton (Leeder, 1971). The porphyrites show almost complete overlap with the fields for the granodiorites (unpublished data from W E Stephens; data comparison in Appendix A) of the Criffell–Dalbeattie pluton (Figs. 6.6a–b) but have lower La and Ce abundances. The field for the porphyries overlaps

Fig. 6.4a

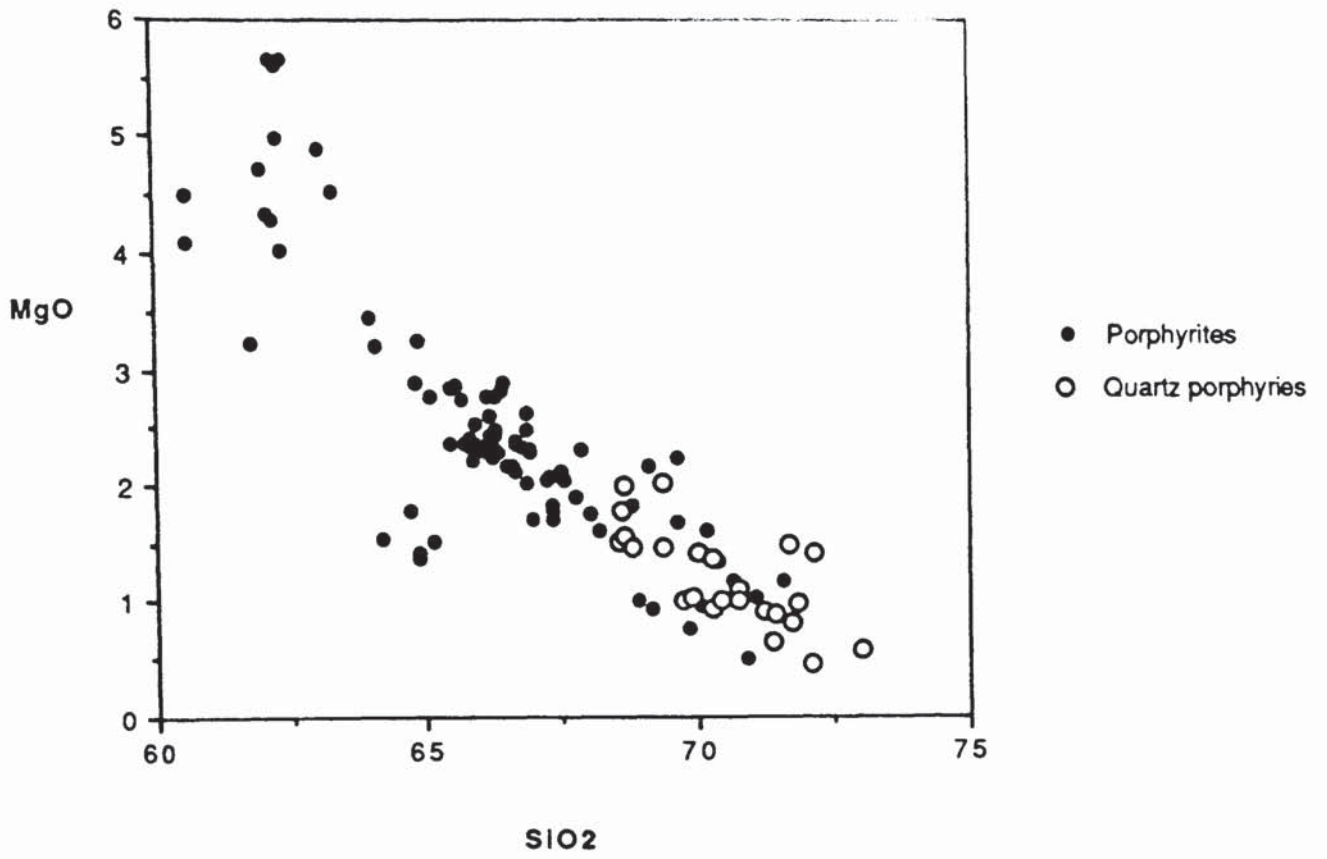


Fig. 6.4b

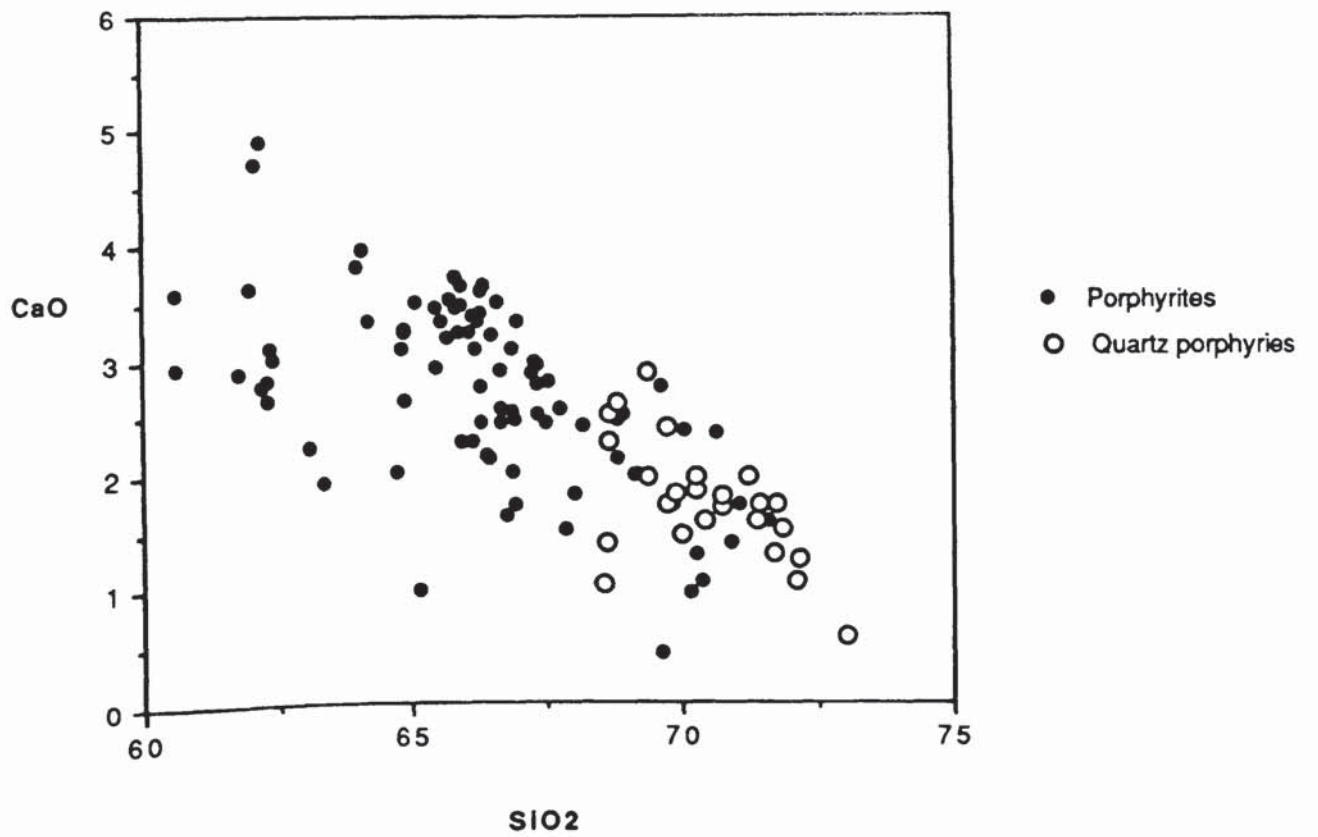


Fig. 6.4c

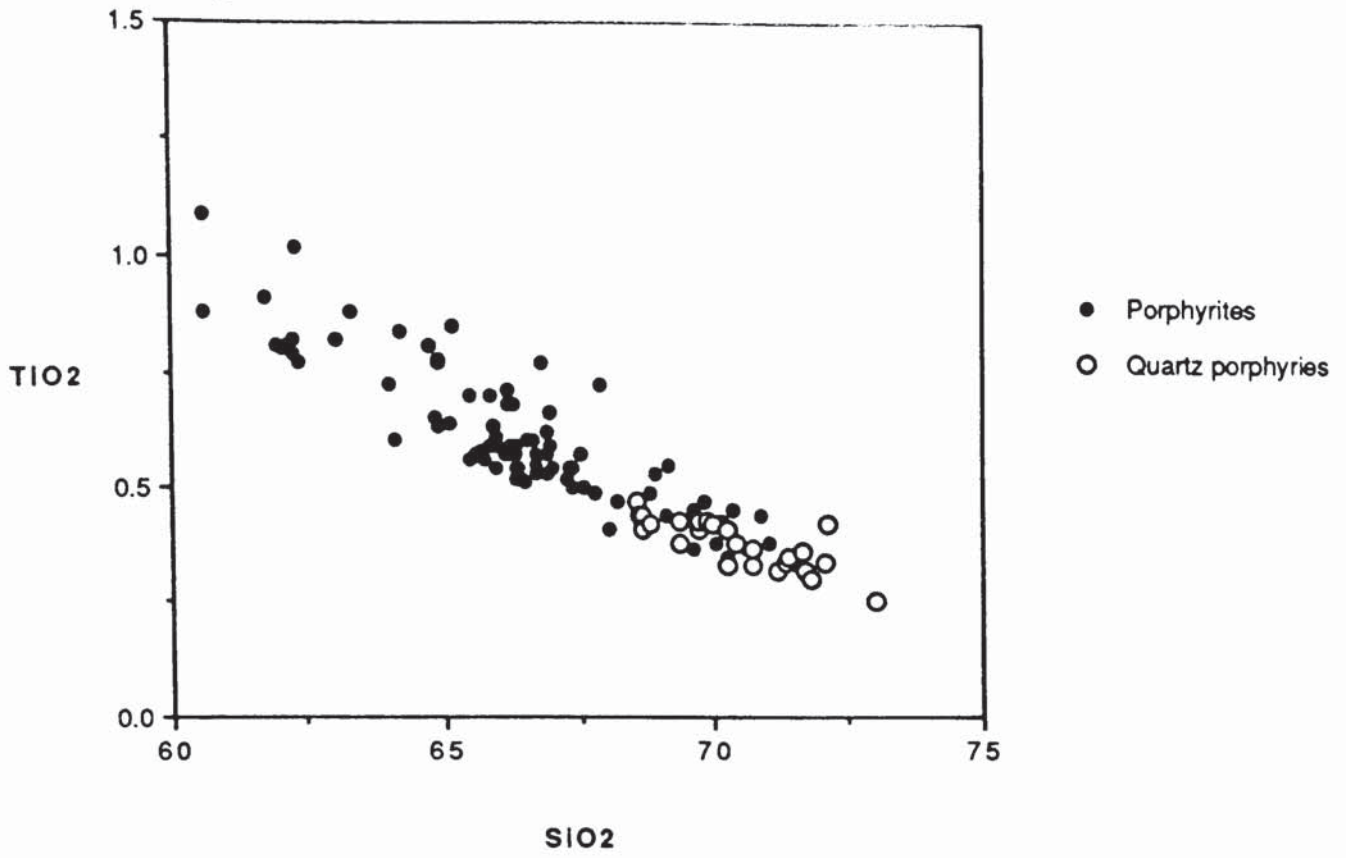


Fig. 6.4d

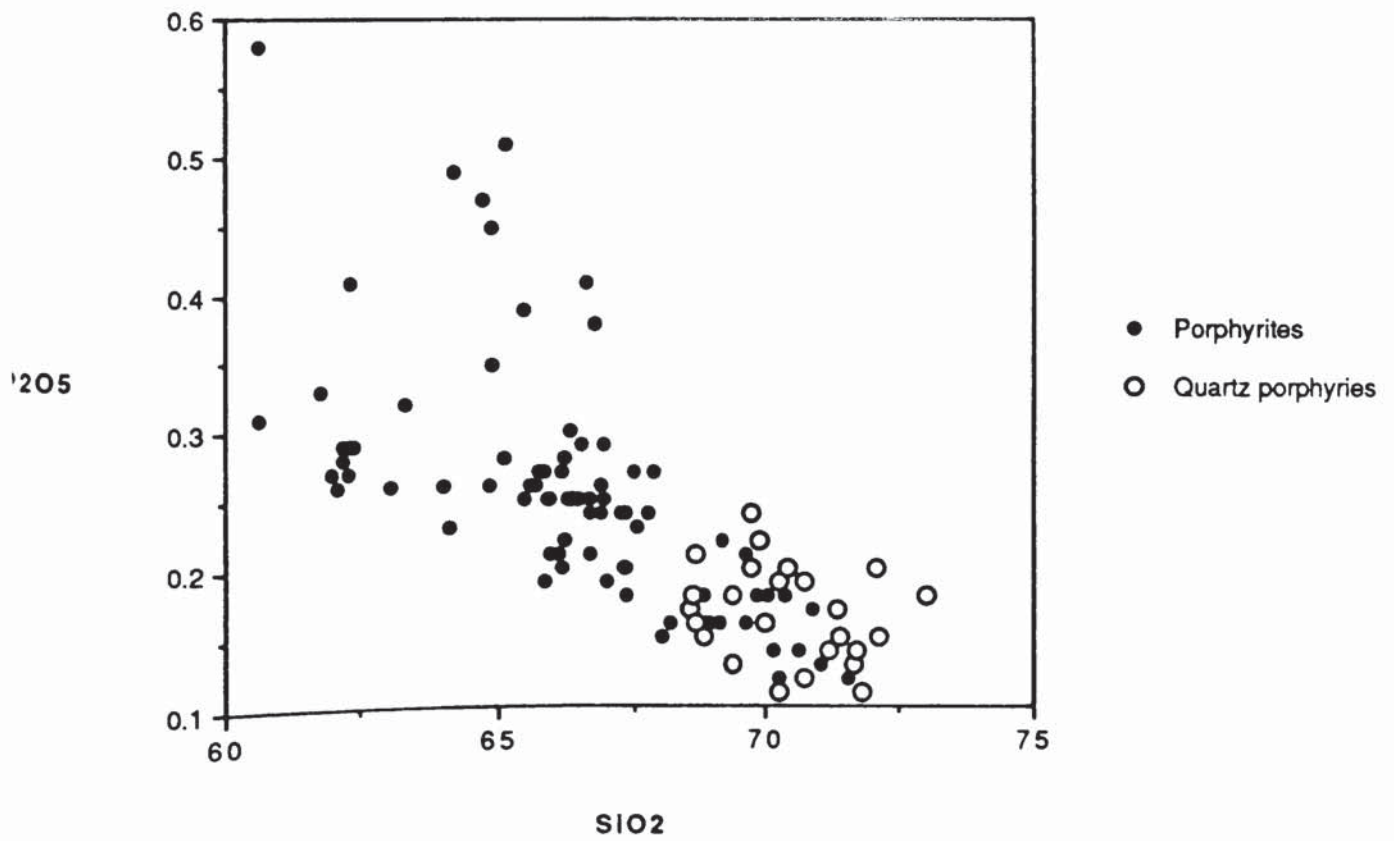


Fig. 6.4e

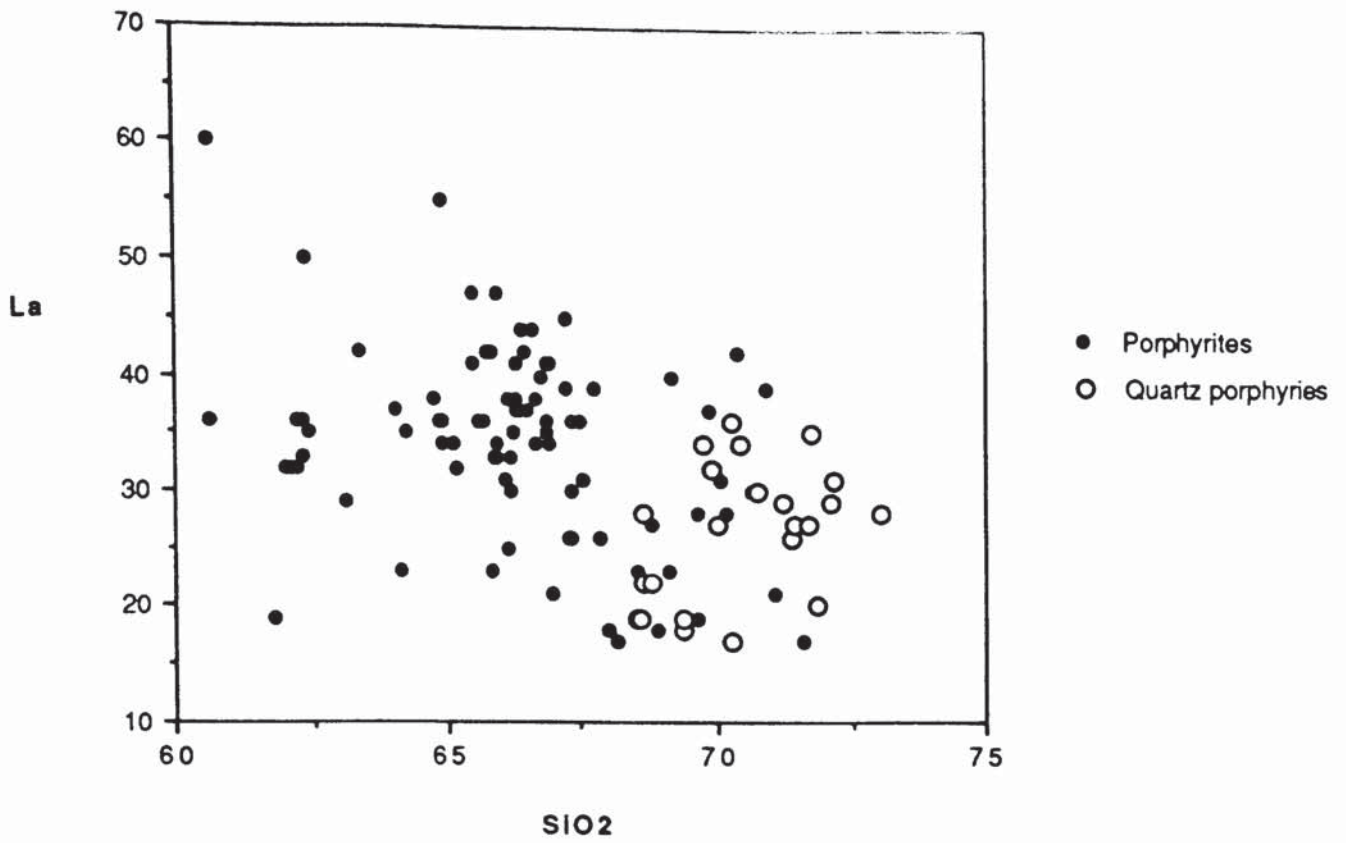


Fig. 6.4f

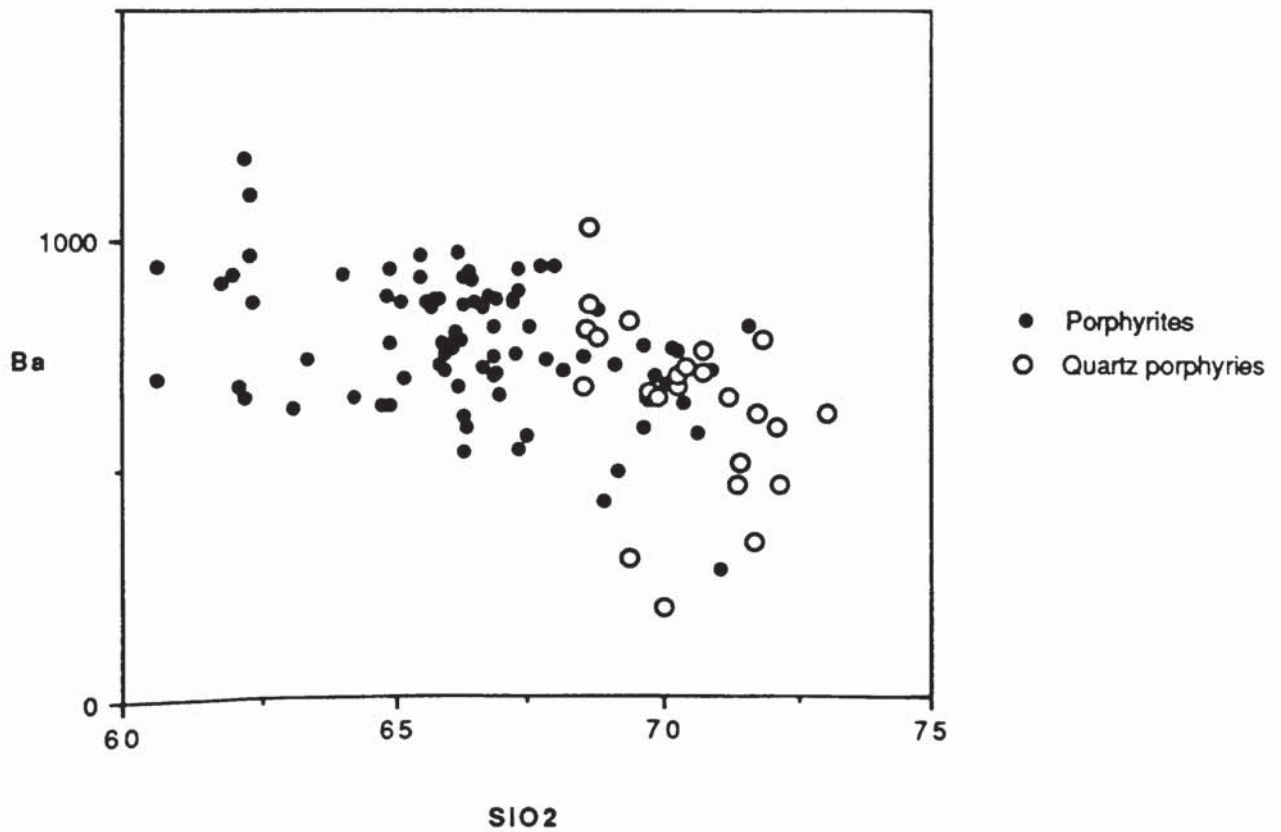


Fig. 6.4g

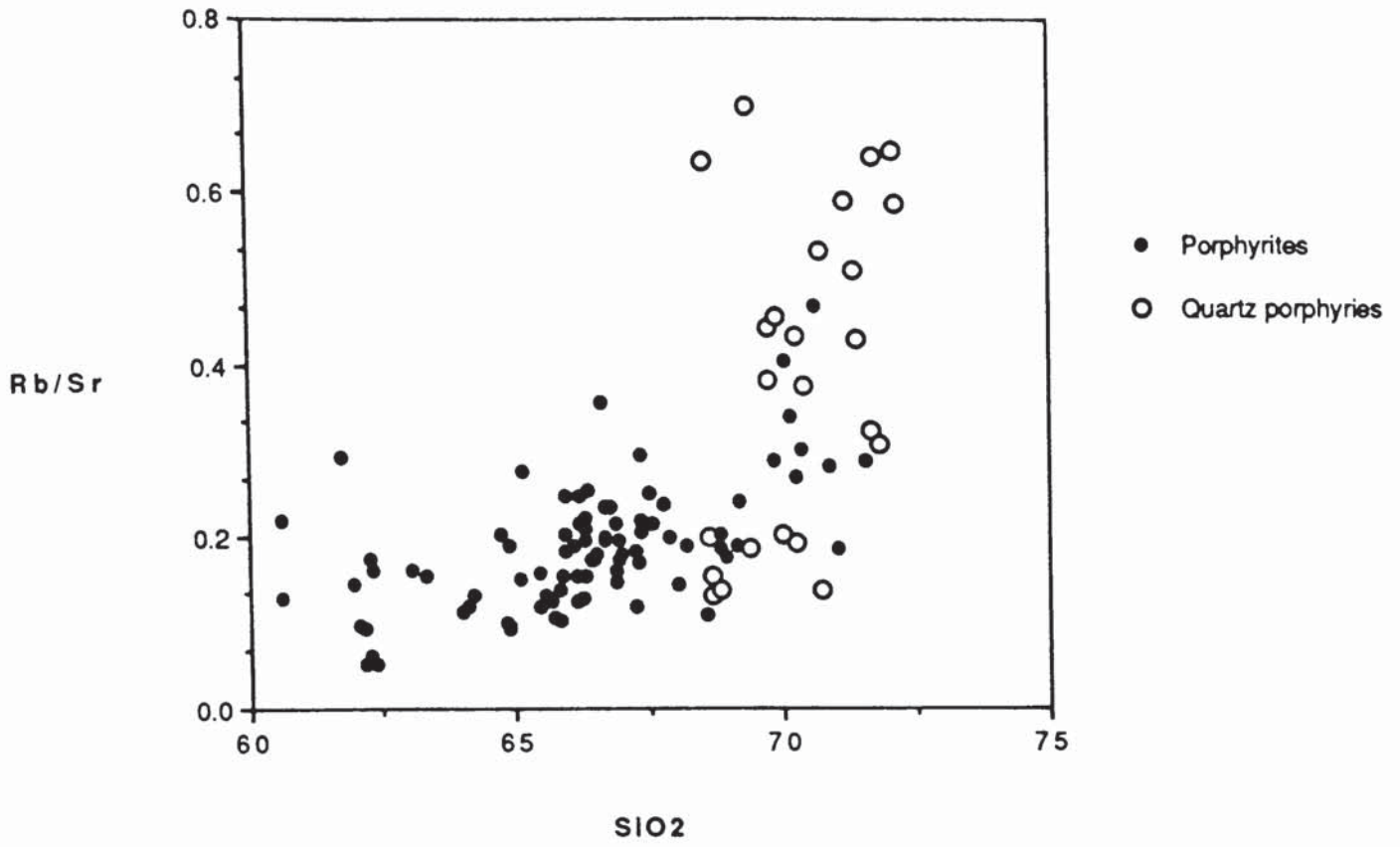


Fig. 6.4h

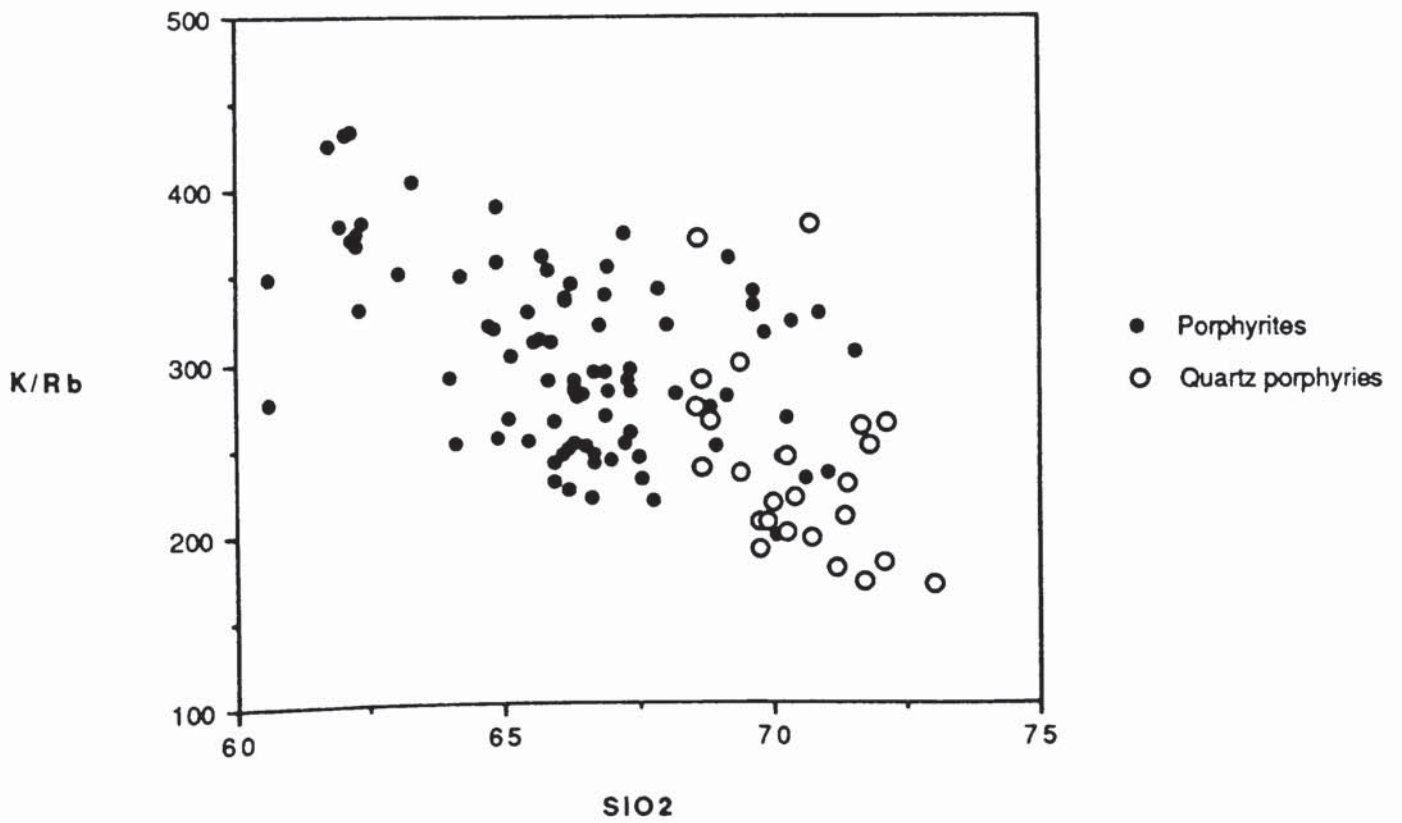


Fig. 6.5

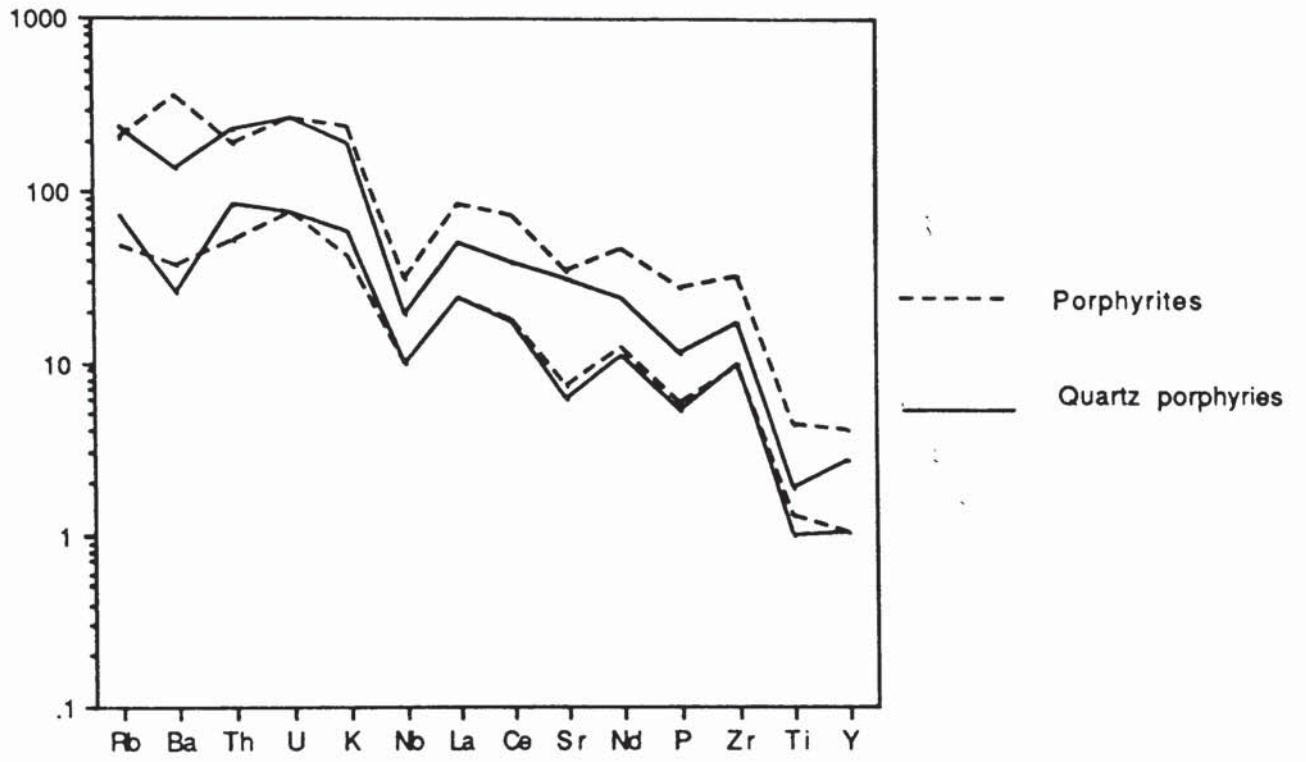


Fig. 6.6a

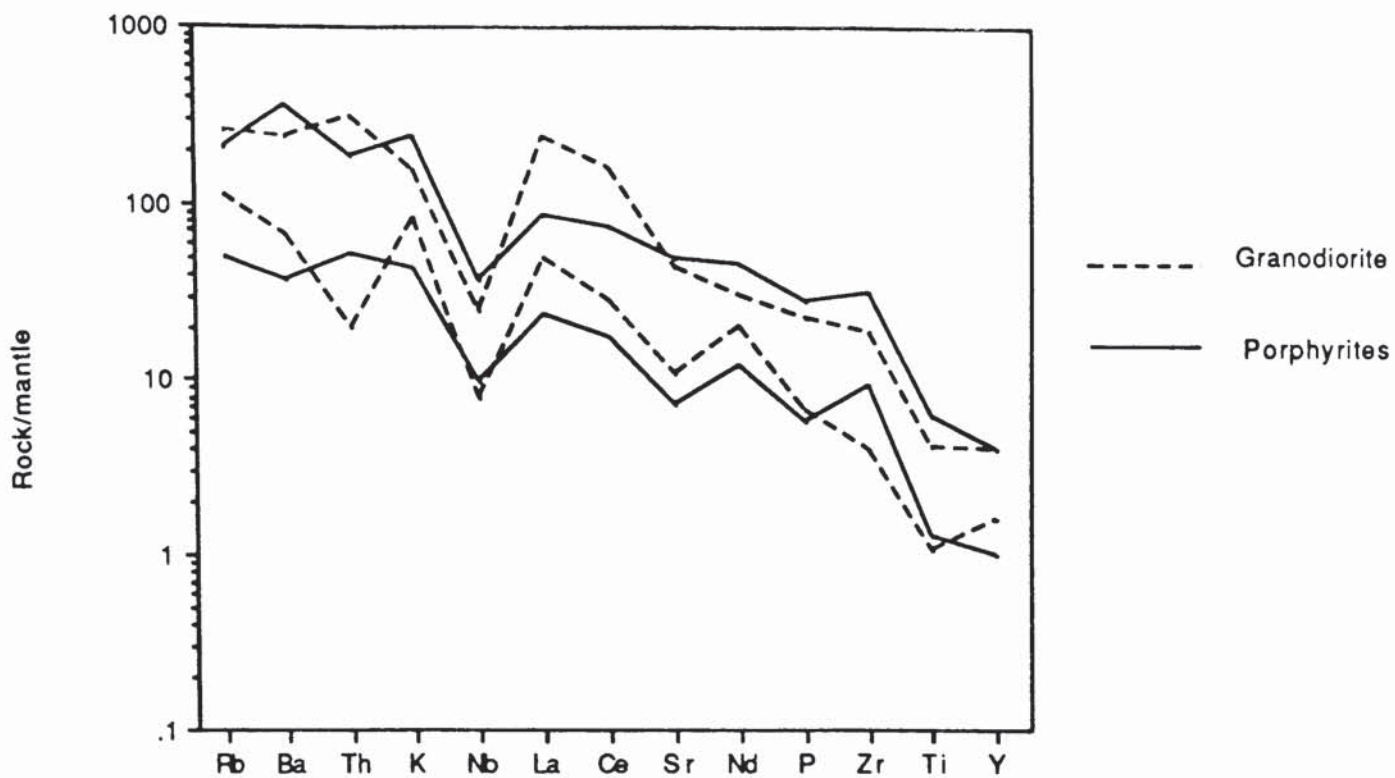
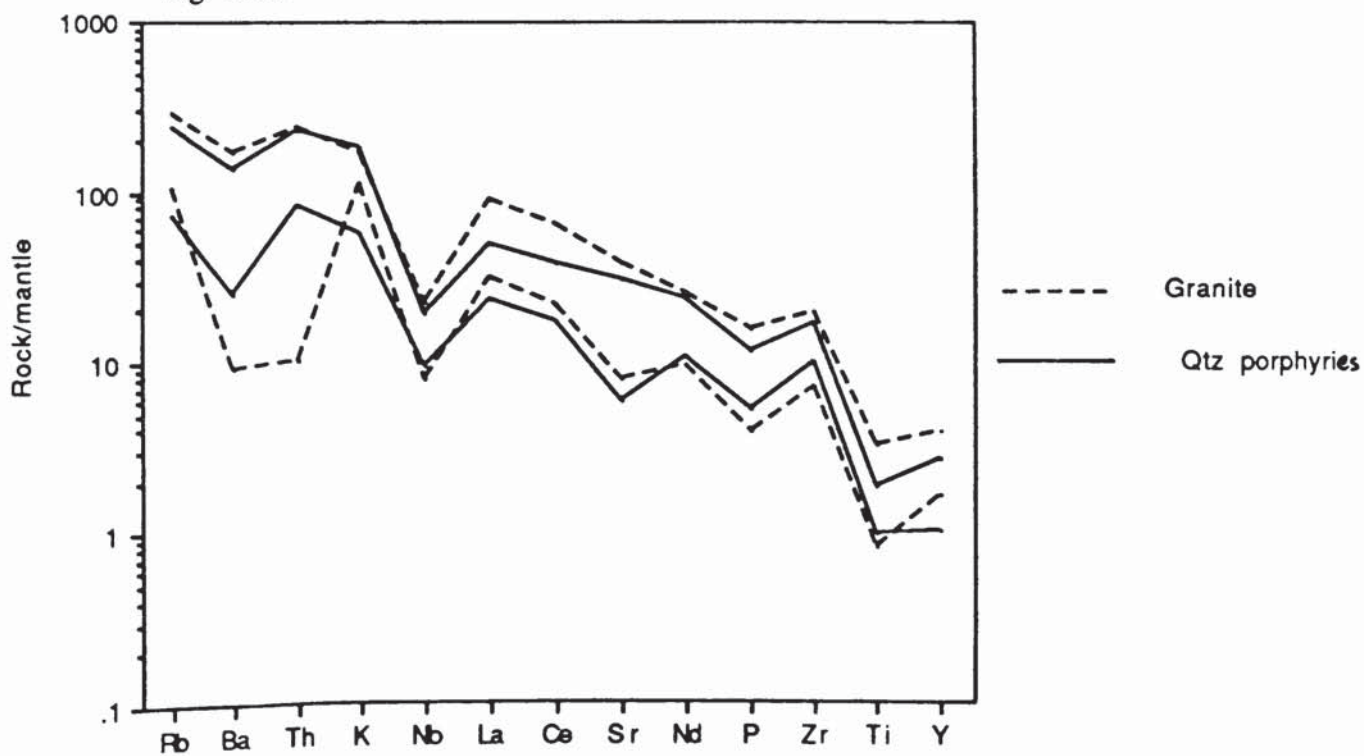


Fig. 6.6b



with that of the granites, which have slightly greater LREE abundances but very similar Rb and K values. Both granites and porphyries have slight negative Ba anomalies but Ba and Th abundances in the granites fall to much lower values than in the porphyries. The spidergram patterns show that the porphyrites–porphyry series rocks have very similar compositions to the plutonic rocks and suggest that the dykes may represent magmas derived from a similar source to that of the pluton.

This point is reinforced by Figures 6.7(a–h) in which the data for the Criffell–Dalbeattie granitoid are compared with those for the porphyrite–porphyry series. Trends for SiO₂ versus MgO, CaO, TiO₂ and P₂O₅ (figures 6.7a–d) in the plutonic rocks are very similar to those of the porphyrite–porphyry series and almost completely overlap with the fields for the dyke rocks except for a few porphyrites which have higher MgO and P₂O₅ contents. A more complex pattern occurs for La and Ba where, although the direction and slope of the trends for the plutonic rocks are similar to those of the dykes, the less siliceous granitoids have higher La and Ba abundances than their equivalents in the porphyrite–porphyry series (Figs. 6.7e–f). These differences are also reflected by K/Rb and Rb/Sr where the plutons again have similar trends to the dykes, with increasing Rb/Sr and decreasing K/Rb, although the plutons have systematically higher K/Rb than the dykes (6.7g–h).

6.4.1) Liquid-crystal separation & crystal mushes: Differences in composition between dykes and plutons.

The overall similarities in composition between the porphyrite–porphyry series and the Criffell–Dalbeattie granitoids suggests that the two groups are related petrogenetically. The fact that slight differences between dykes and pluton are more apparent in the trace elements than the major elements may indicate that partitioning of trace elements between minerals and liquid has been slightly different in the two suites or that crystal–liquid separation has been more efficient in the dyke rocks. The greater degree of alteration in the dyke rocks cannot explain the differences because the La and Rb contents of both altered and “fresh” porphyrites and porphyries are similar (section

Fig. 6.7a

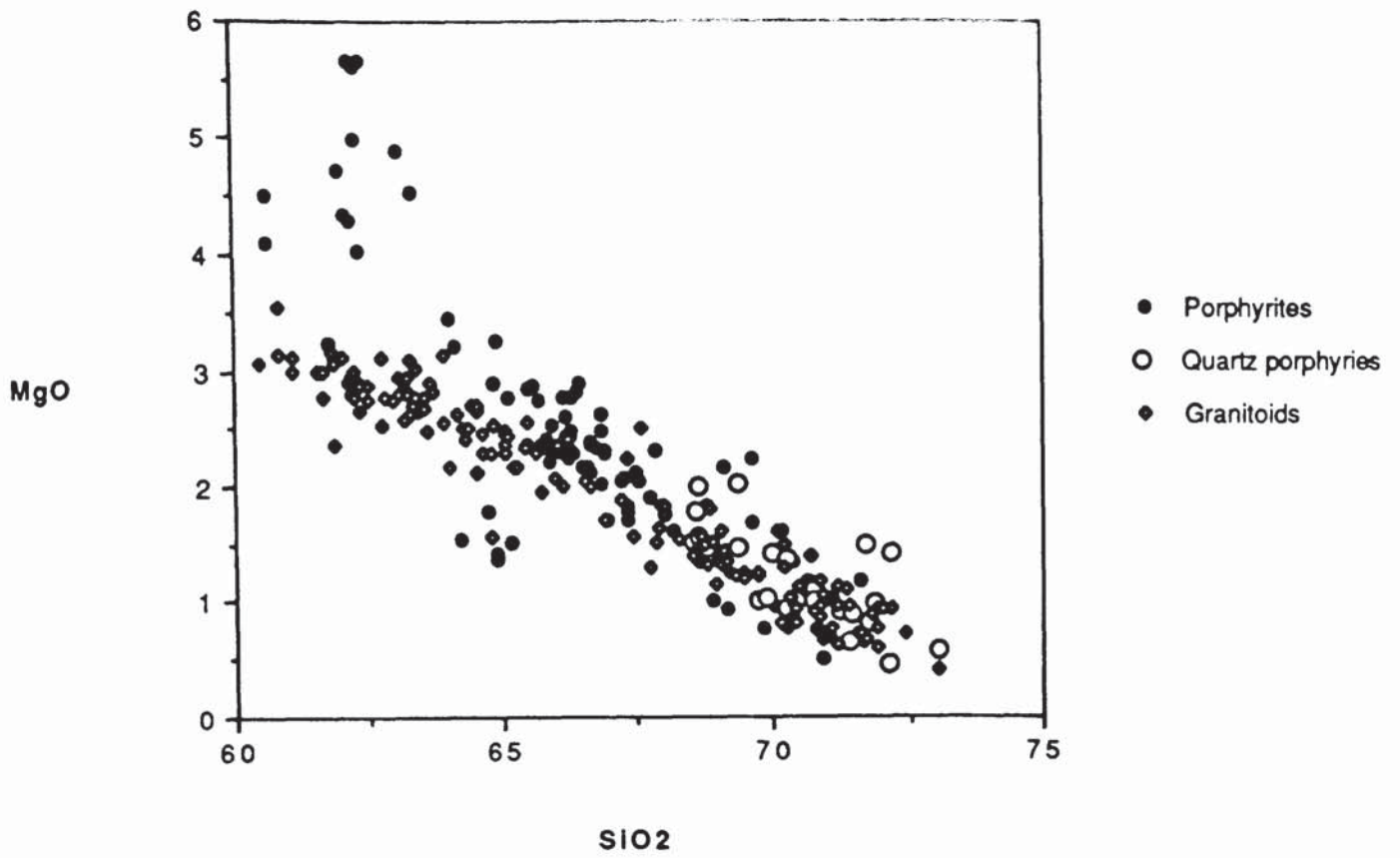


Fig. 6.7b

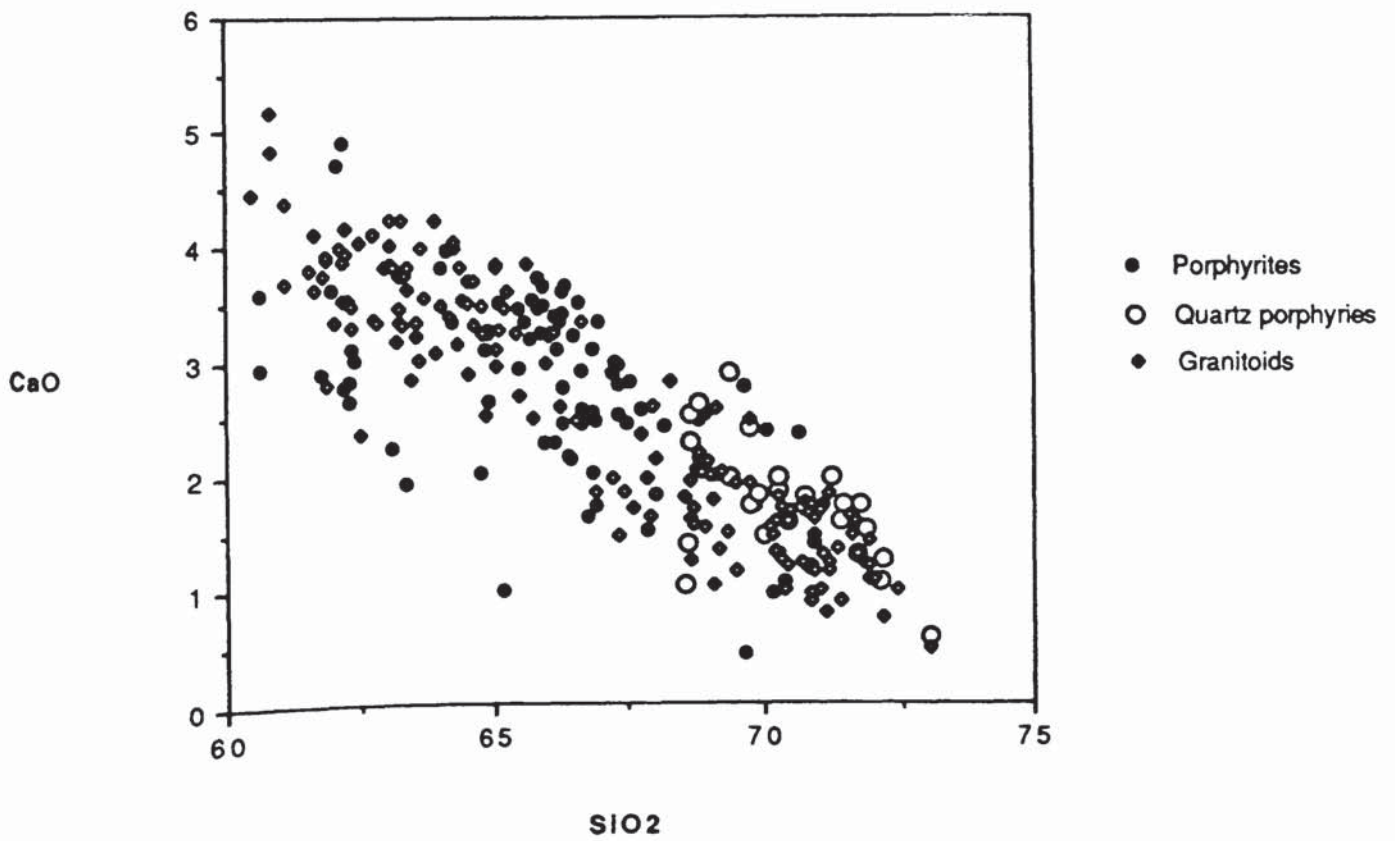


Fig. 6.7c

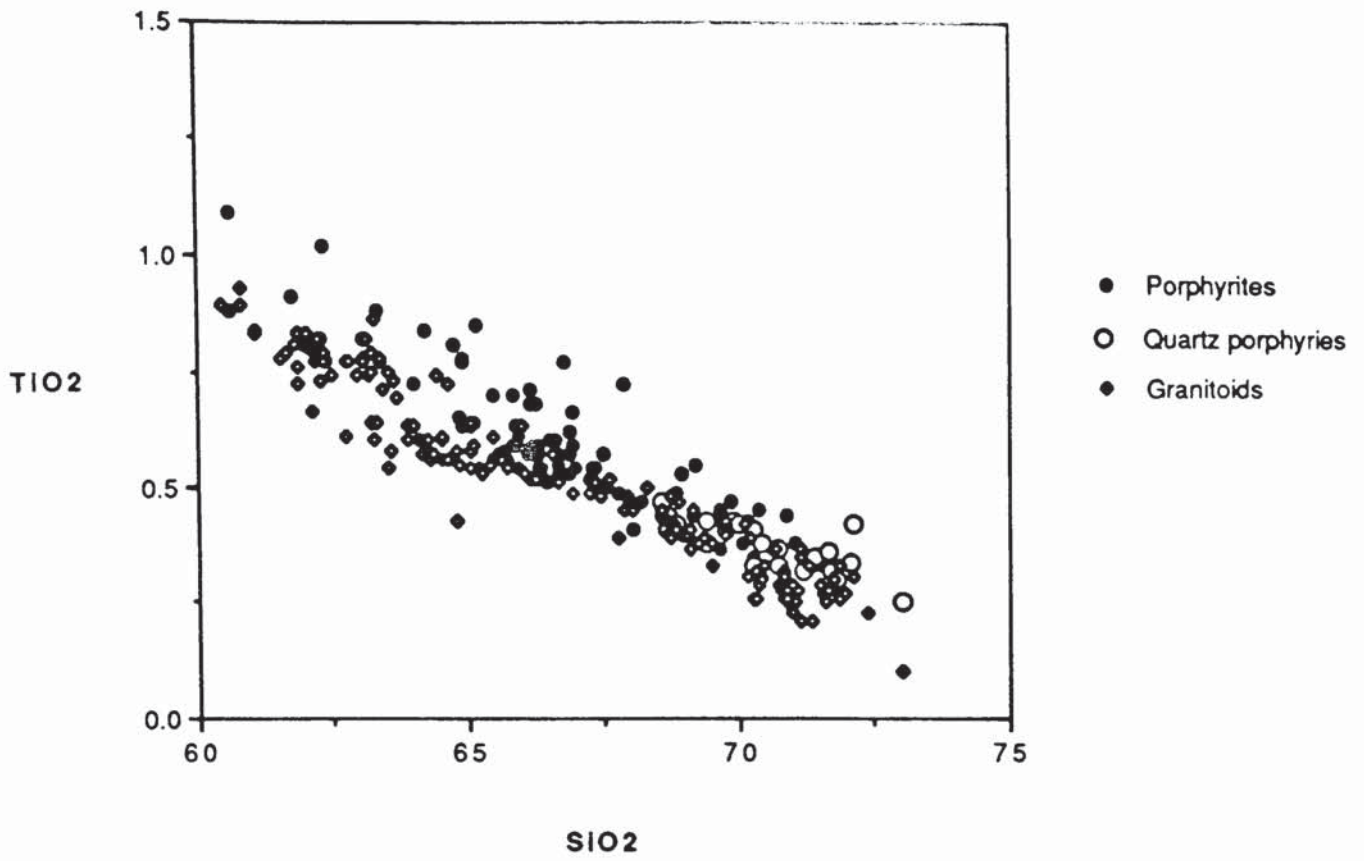


Fig. 6.7d

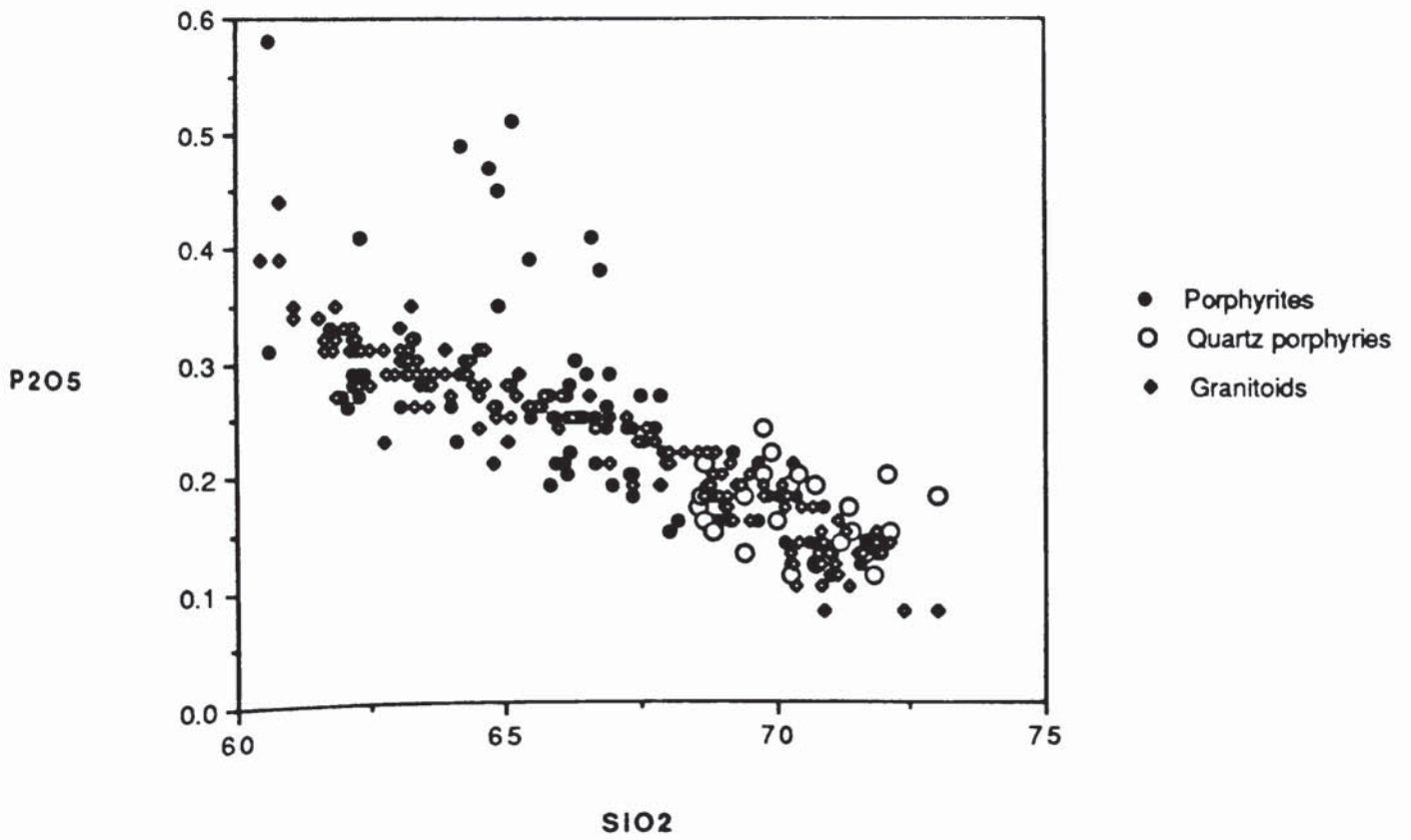


Fig. 6.7e

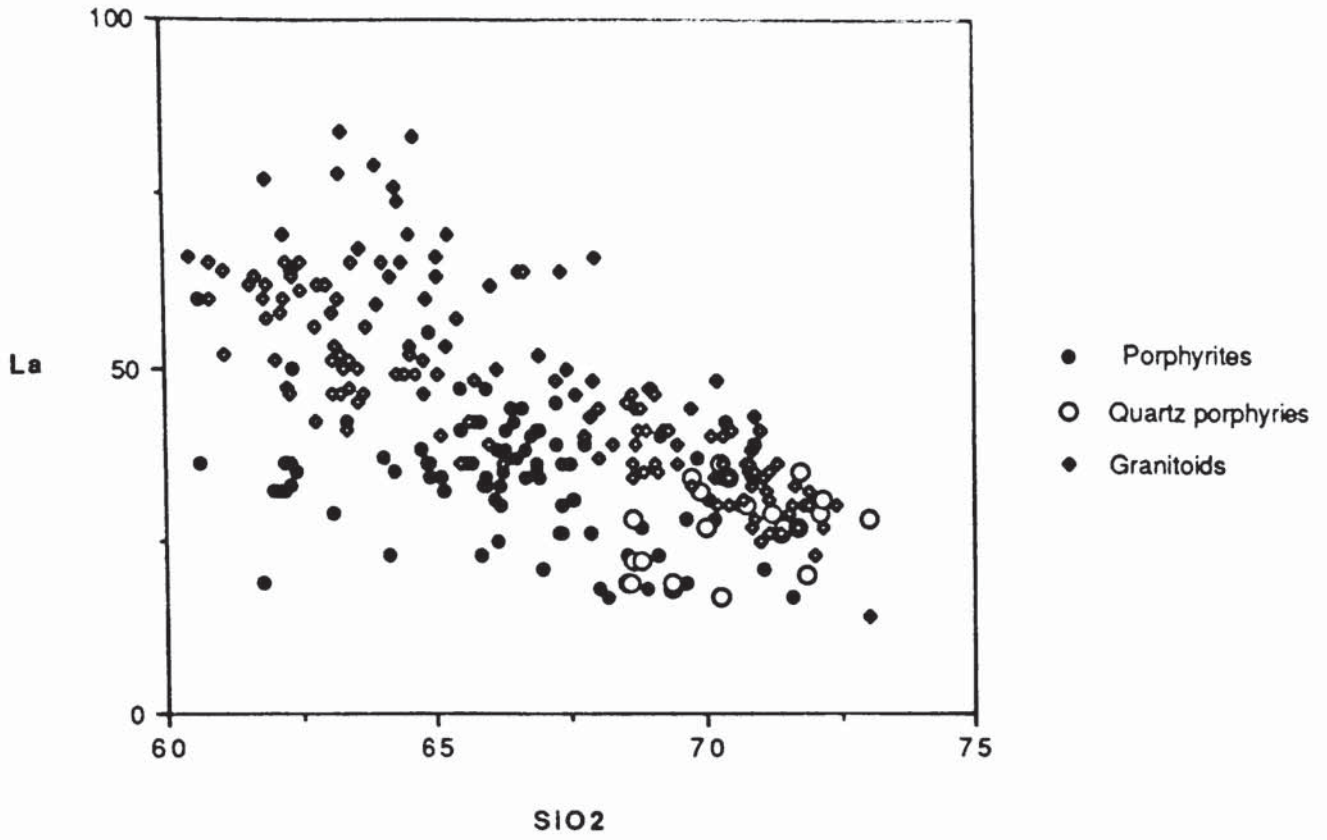


Fig. 6.7f

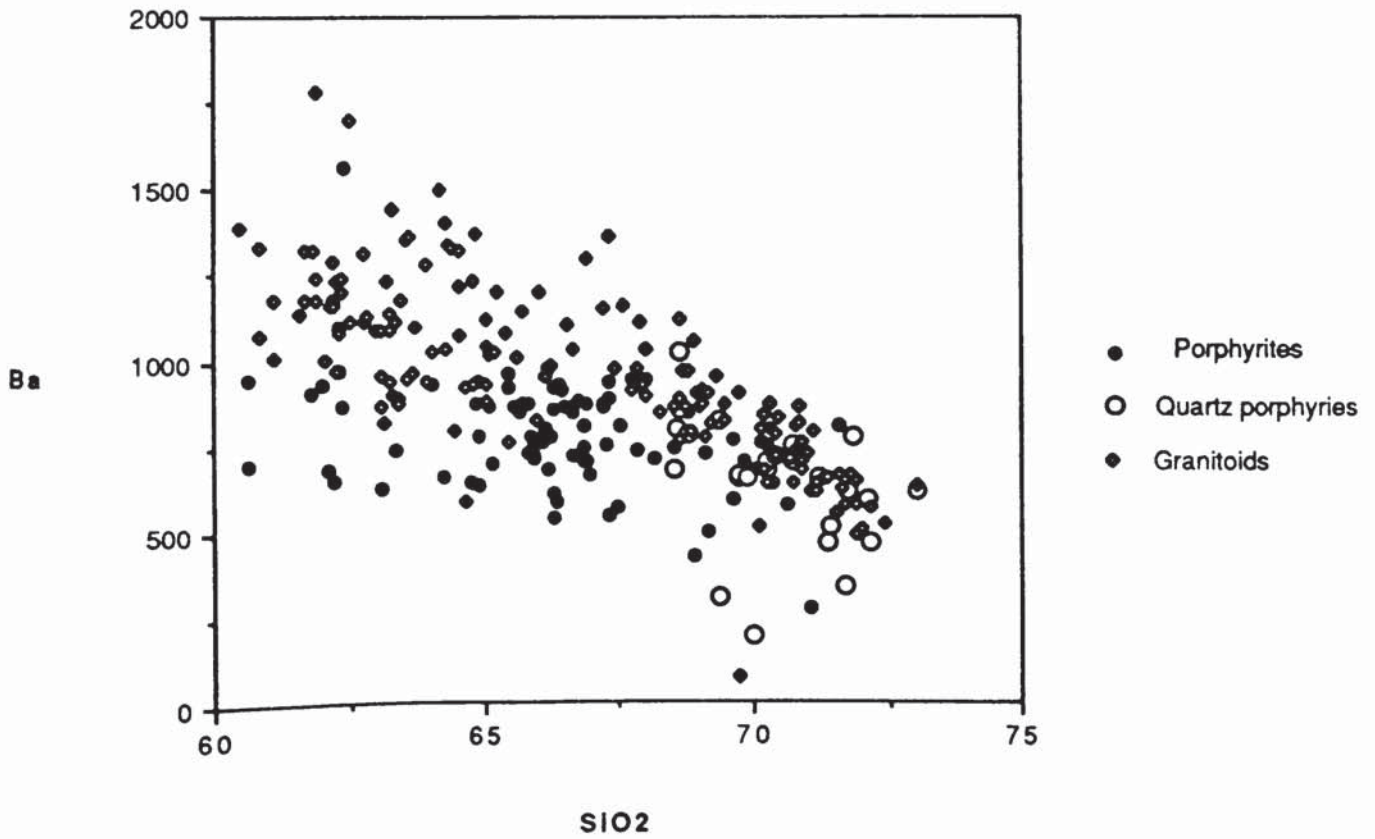


Fig. 6.7g

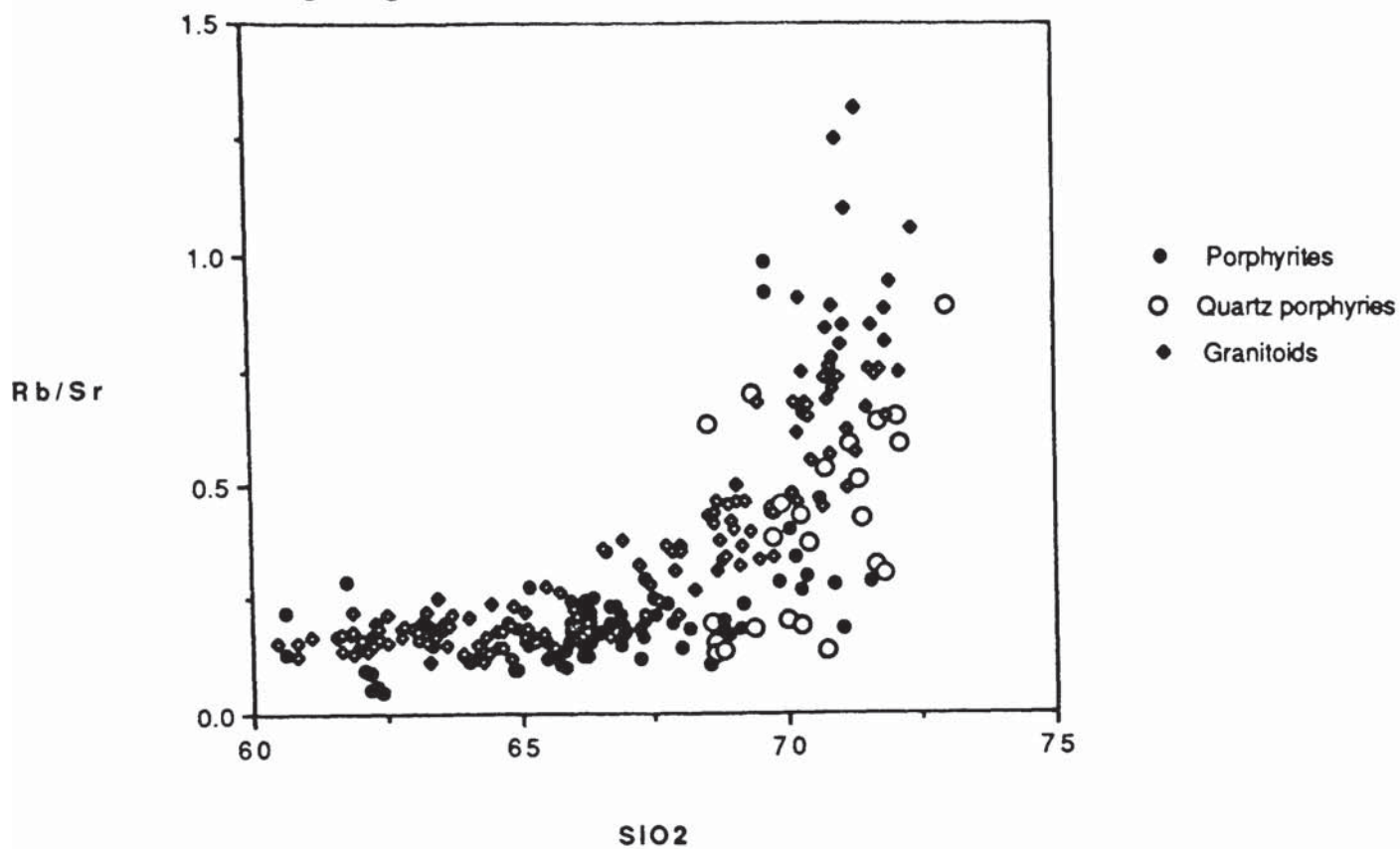
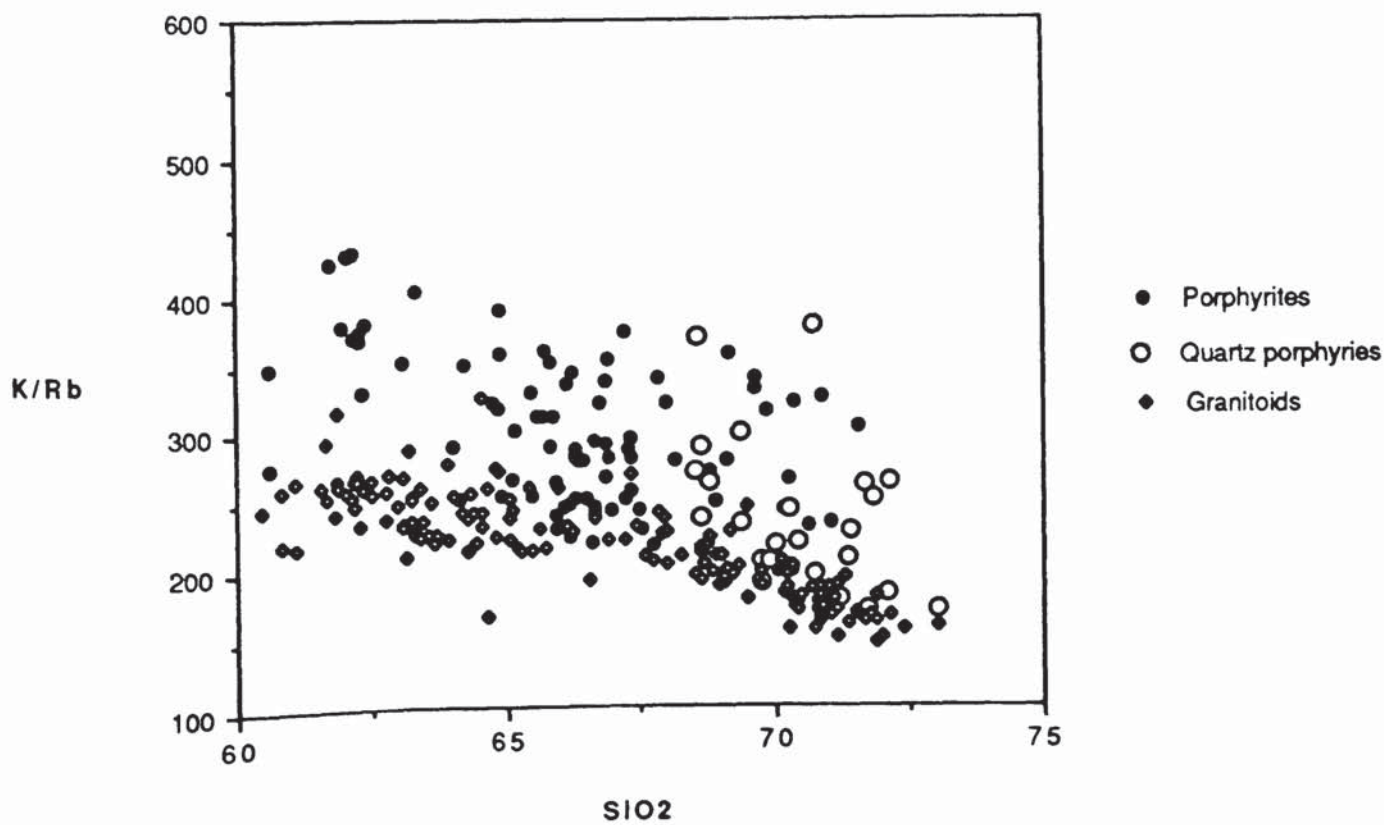


Fig. 6.7h



6.3.1). Phases crystallising from siliceous, granitic magmas are unlikely to separate completely from the parent magma because of the high viscosity of the host melts (McCarthy & Hasty, 1976). Many granitoid magmas represent mixtures of “residual” liquid and “cumulate” crystals, thus varying the proportions of the two would produce scatter in variation diagrams purporting to show evolutionary trends. Trace elements are likely to be the most sensitive indicators of such processes because they are preferentially incorporated into different phases depending on their relative distribution coefficients. It is therefore possible that displacement of the trends for the Criffell–Dalbeattie pluton from those of the dyke rocks is due, at least in part, to the differing degrees of separation of crystals and liquids in the granitoids and dykes, ie: the granitoids retain the fractionating minerals with the residual liquids. The dykes, although as siliceous as the plutonic rocks and retaining many of their “cumulate” minerals as phenocrysts, may undergo more efficient crystal–liquid separation, by processes such as filter–pressing and flowage differentiation, during their transport from the magma chamber (Brouxel, 1991; Cox *et al.* 1979). One possible explanation for the higher MgO and P₂O₅ in some of the porphyrites relative to the granitoids is that they represent some of the first, phenocryst–rich melts produced during the initial stages of crustal melting, compositions not preserved, or else grossly modified, during the ascent of the granitoid plutons (Huppert & Sparks, 1988a). The geochemical effects of these processes will vary depending upon a number of factors including the temperature of the melt, its silica and volatile contents (influencing viscosity) as well as the composition of the phenocryst minerals, the rate of magma ascent and the composition and mineralogy of the melt+crystal mixture in the magma chamber (Komar, 1972a, b; Richardson, 1979; Ross, 1983, 1986), many of which are very difficult to constrain.

6.5) Petrogenesis of the porphyrite–porphyry series

The overall chemical similarity between the porphyrite–porphyry series and the Criffell–Dalbeattie granitoids, and the similar orientations of variation trends for the two

groups indicate that petrogenesis of the porphyrite–porphyry series is closely related to that of the pluton. One model suggests that the Criffell–Dalbeattie granitoids evolved by an AFC–style process involving the simultaneous fractionation and contamination of a primitive granodiorite (Stephens *et al.* 1985). An AFC model was tested in this study for the porphyrite–porphyry series using fractionation and contamination of one of the least altered, less evolved, sparsely porphyritic, porphyrites from Tongland Quarry and a partial melt of local lower Palaeozoic sedimentary country rocks (Appendix D).

Several fractionating assemblages, comprising various proportions of plagioclase, amphibole, biotite, K–feldspar, quartz and accessory phases (zircon, apatite), were modelled using a range of bulk distribution coefficients (D) (Gill, 1981; Henderson, 1982) and an r (mass assimilated/mass crystallised) value of 0.4. Rb and K are both modelled as incompatible elements, with Rb considerably more incompatible than K because of the different K_d values for Rb in K–feldspar. The model curves run through the data for the porphyrites and porphyries suggesting that the AFC model can largely explain the Rb and K distribution in these rocks (Fig 6.8a). However, some porphyrites and porphyries lie above the curve representing D for Rb of 0.1, thus Rb has a lower D than that used in the model. This is likely, particularly in more evolved rocks where biotite is replaced by K–feldspar in the fractionating assemblage. A similar situation is also produced on a plot of Rb against Sr (Fig. 6.8b) with some porphyrites and porphyries sitting above the model curves and again this may result from an increase in the proportion of K–feldspar, at the expense of biotite, in the fractionating assemblage. It is possible that the high–Sr porphyrites have been derived from an endmember, slightly more enriched in Rb than that used in this model, because biotite is likely to be a more important fractionating phase than K–feldspar in these less–evolved compositions. This does not invalidate the AFC model used here because the trend towards low Sr and high Rb, as expressed by the majority of the porphyrite–porphyry series, is satisfactorily explained by the model. AFC would therefore still operate despite small changes in the composition of the parent endmember. It is likely that both Y and Zr are compatible due to the presence of apatite and zircon in the

Fig. 6.8a

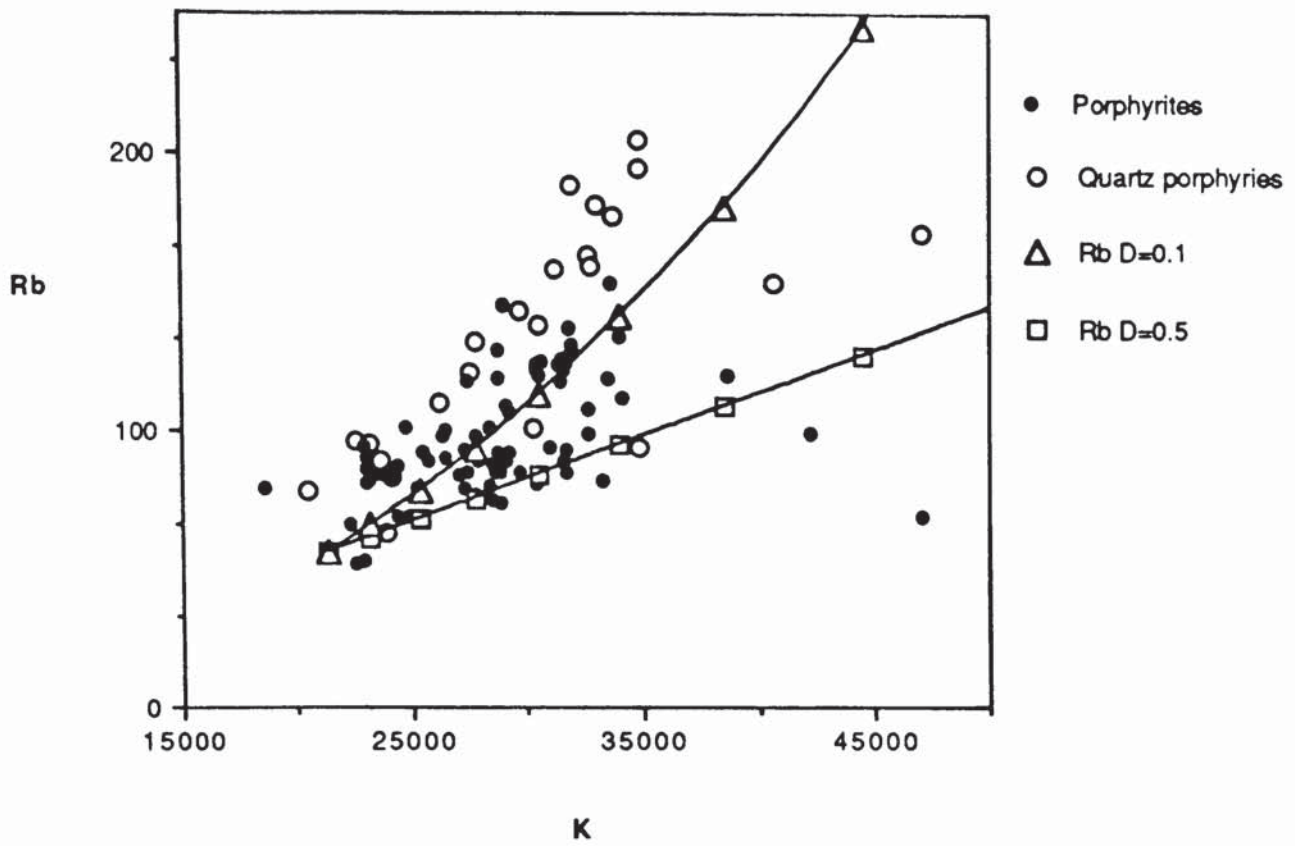
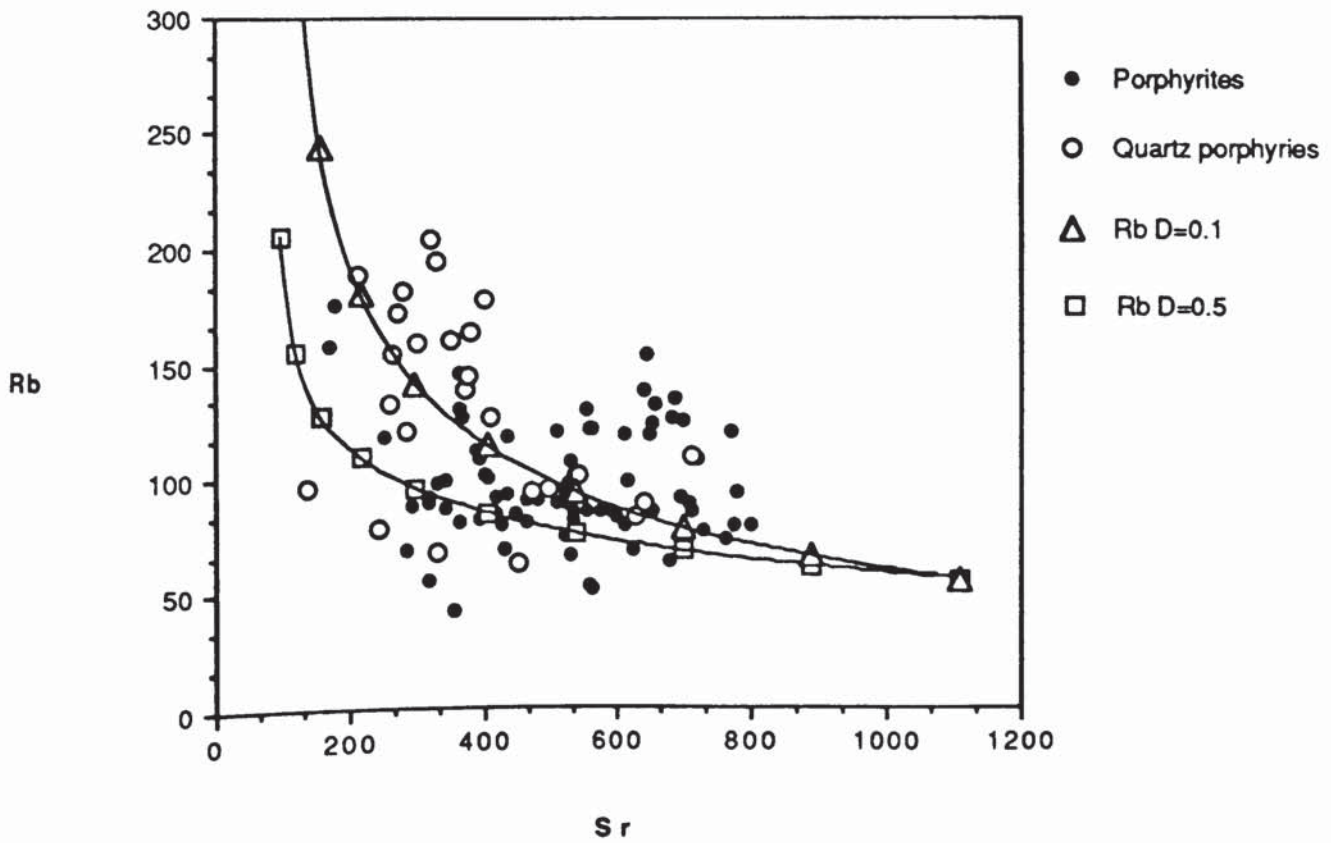


Fig. 6.8b



fractionating assemblage, with the abundances of Cr and Sr largely controlled by the proportion of mafics and plagioclase respectively. In the case of Y–Cr (Fig. 6.8c), the model trends are relatively flat at first, with little change in Y abundances but as the proportion of residual liquid decreases, representing more contaminated and fractionated compositions, the Y content of the liquids drops rapidly. This corresponds to the change from the porphyrites to the porphyries and is similar to the decrease in Y reported by Stephens *et al.* (1985) in the transition from the outer granodiorites to the inner granites in the Criffell–Dalbeattie pluton. The data for Zr–Sr (Fig. 6.8d) are more scattered but the model curves, representing D's of 1–2 for Zr, largely encompass the data for the porphyrite–porphyry series.

To summarise, an AFC model based on the combined fractionation and contamination of a mafic porphyrite composition can satisfactorily explain much of the LILE, HFS and compatible element variation in dykes of the porphyrite–porphyry series associated with the Criffell–Dalbeattie pluton. However isotope data for the porphyrites and porphyries would be required to fully constrain this model.

6.6) Summary

The porphyrite–porphyry suite of hypabyssal intrusions associated with the Criffell–Dalbeattie granite represents a series of porphyritic microdiorites, microgranodiorites and microgranites similar in mineralogy and chemistry to the granodiorites and granites forming the pluton. The dykes are texturally diverse and are characterised by varying degrees of hydrothermal alteration and weathering which often obscures primary igneous textures, rendering classification based on petrography difficult. The Criffell dykes form a chemical continuum from porphyrite to porphyry which is similar to that for the granodiorite–granites of Criffell–Dalbeattie pluton. Mantle normalised spidergram patterns have considerable compositional overlap between the dykes and the various phases of the pluton. Some differences in trace element abundances may result from a number of different processes including varying degrees crystal–liquid separation during transport and emplacement of the porphyrites and porphyries. The

Fig. 6.8c

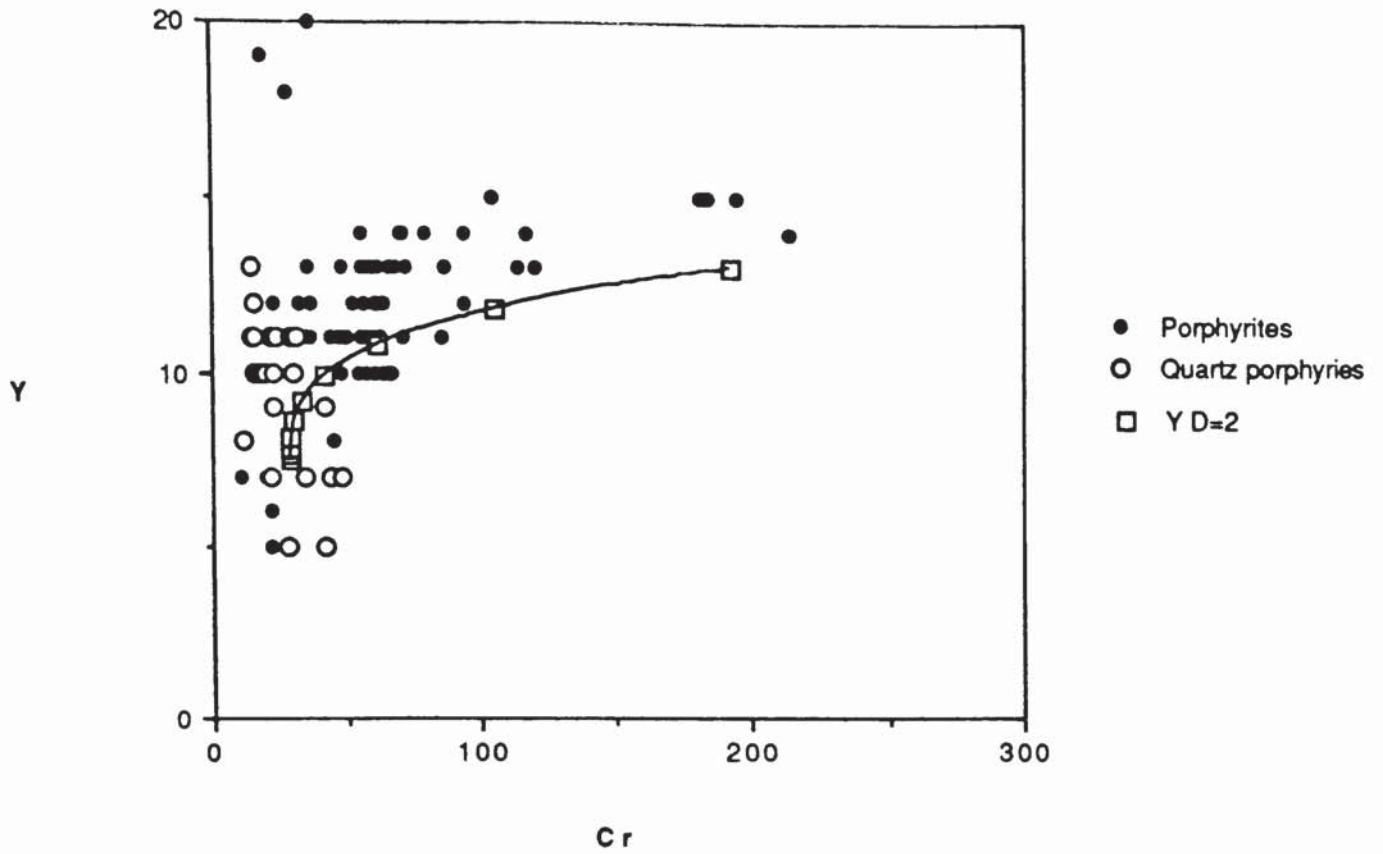
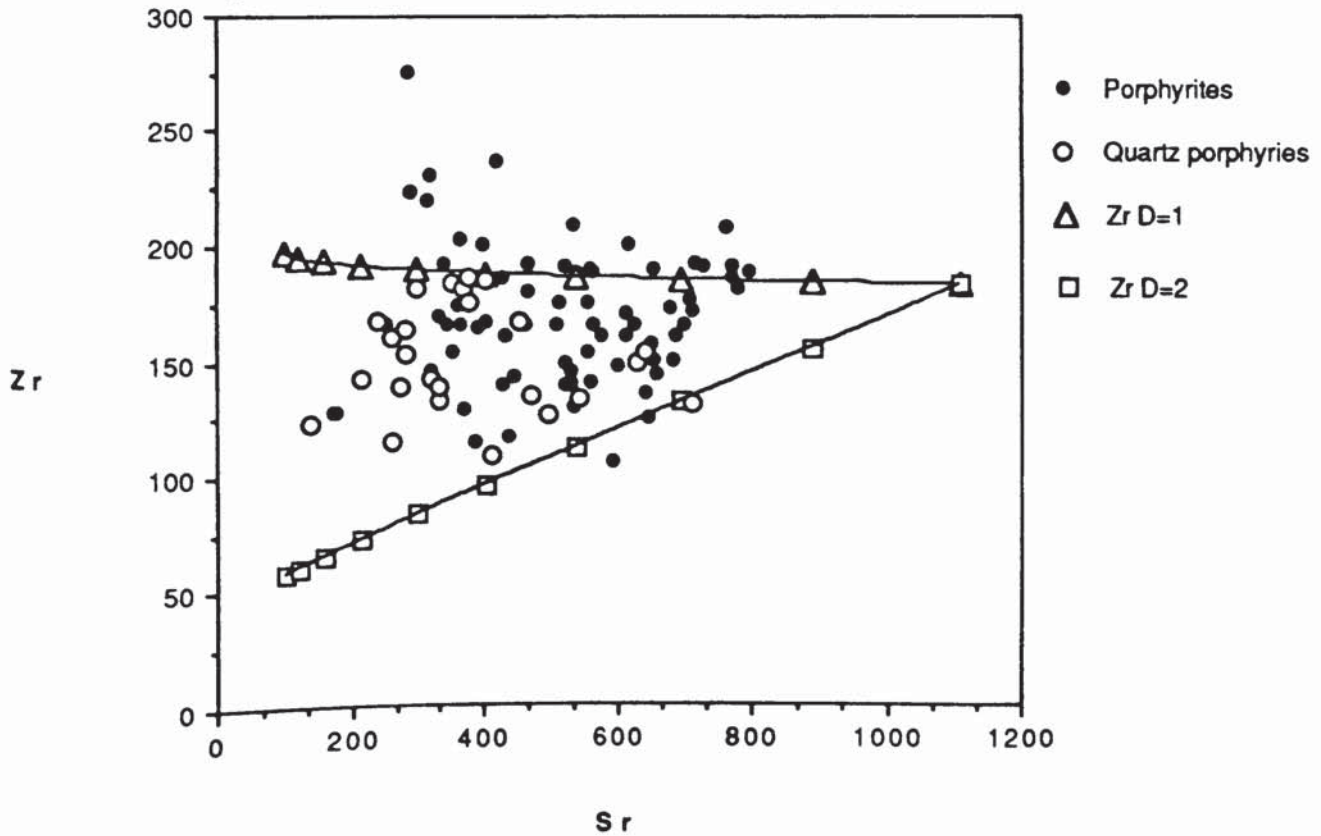


Fig. 6.8d



compositional similarity between the dykes and pluton indicates that the two are petrogenetically linked and this is supported by AFC modelling of the evolution of the porphyrite–porphyry series. It is suggested that the porphyrite–porphyry dykes represent magmas periodically tapped from the granitoid magma chamber as it evolves.

Chapter 7

Conclusions and recommendations for future work

7.1) Conclusions

1) The minor intrusive suite associated with the late Caledonian Criffell–Dalbeattie granitoid pluton in SW Scotland is dominantly composed of a series of dykes comprising a suite of compositions ranging from siliceous porphyritic microgranites (quartz porphyries) through porphyritic microgranodiorites and diorites (porphyrites), together with a group of basic and potassic calc-alkaline hornblende and mica lamprophyres. Compositions in the porphyry–porphyrite suite are the most abundant, and like the lamprophyres, overlap with the intrusion of the zoned Criffell-Dalbeattie pluton. In the Black Stockarton Moor complex, dykes of these compositions are associated with minor granodiorite stocks, intrusion breccias, and small volcanic vents.

2) The calc-alkaline lamprophyres (CAL) of this suite of minor intrusions are characterised by high MgO, Ni, Cr and V contents together with elevated LILE and LREE abundances. They are compositionally similar to CAL described from elsewhere in the Caledonian belt and to Recent CAL from the Mexican Volcanic Belt and late Palaeozoic CAL from SW England and Central Europe. LILE/HFSE abundances are characteristic of subduction related magmas and, in common with other CAL, it is thought that they have been derived from a mantle source modified by subduction. Chemically, they overlap with the late Silurian LORS basalts found elsewhere in the Caledonian, particularly those described from the SW Highlands, although some of the lamprophyres have greater LILE and LREE abundances. However they have a distinctive isotopic composition, compared to the basalts, but which overlaps with values reported from Tertiary CAL in the USA and Hercynian CAL from SW England and Central Europe. Isotopic compositions also overlap with those reported from lithospheric mantle xenoliths recovered from several localities across Scotland, particularly those from Streap Comlaidh.

3) Modelling of the Criffell CAL major, trace element, Sr and Nd isotope and mineral chemistry data suggests that systematic fractional crystallisation and crustal contamination have not significantly altered the chemical or isotopic composition of the Criffell CAL although it is not possible to constrain the effects of minor amounts of fractionation and/or contamination on individual intrusions. Therefore it is thought that the LILE, LREE and isotopic composition of the lamprophyres largely reflects the composition of their mantle source and the partial melting processes responsible for them. It is suggested that this source acquired many of its compositional characteristics during a recent, most probably Lower Palaeozoic, subduction event. Consideration of the Sr and Nd isotope data suggest that the mantle source of the lamprophyres may reflect mixing between a slightly heterogeneous mantle with bulk ϵNd c. 0 and subducted Lower Palaeozoic sediment (SLPS). However, characterisation of LILE and LREE abundances in the source and their origin is difficult to constrain given that the volatile-rich Criffell CAL may represent very low degree partial melts (< c.0.1%) which have altered their LILE and LREE abundances by remobilisation of these elements by the migrating melt from the mantle wallrocks during its ascent. It is unlikely that the mantle source of the lamprophyres resided within a convecting, depleted, asthenospheric mantle and some indication of the depth of the mantle source may be obtained from the stability field of phlogopite and hornblende and available experimental data (c. 20kbars). Consideration of CAL magmatism within existing tectonic models of the Southern Uplands suggest that the subduction event responsible for modifying their mantle source cannot be equated with that responsible for LORS basaltic magmatism to the north. It is tentatively suggested that the source of the Criffell CAL may well be underthrust "Lake District" lithosphere.

4) The close spatial and temporal association observed between CAL and granitoid magmatism suggests that the two may be petrogenetically related. Consideration of Sr and Nd isotope data as well as the results of AFC modelling suggest that the Criffell CAL may well represent the mantle endmember invoked in petrogenetic models for the

pluton. The suitability of CAL magmas in this role on the basis of thermal and volumetric considerations was evaluated and it was concluded that a CAL magma could well be parental to the less evolved components of the Criffell-Dalbeattie granitoid pluton.

5) The geochemistry of porphyrite-porphyry series dykes was characterised and compared with that of the Criffell–Dalbeattie granitoid and it is thought that dyke rocks represent magmas periodically tapped from the evolving granitoid magma. The presence of dykes with higher MgO and P₂O₅ than observed within the pluton suggest that the dykes may well preserve some of the more primitive granitoid magmas which are not represented within the pluton. It is also thought that some of the geochemical differences between dyke and pluton compositions may be due to a number of intrusion processes, which are difficult to constrain, which may have altered the composition of the dyke magmas, including flow differentiation, and filter pressing.

7.2) Recommendations for future work

1) The provision of Pb and O isotope data for the Criffell CAL in order to try and constrain:

- a) the nature of the SLPS component
- b) the role of contamination within the crust
- c) contribution of CAL to the granitoid magmas

2) Sr isotope studies on separated phlogopite, hornblende and clinopyroxene phenocrysts to constrain possible modification of whole rock Sr isotope values by alteration and/or contamination.

3) Sr-Pb-Nd isotope and INAA study of the porphyrite-porphyry series to constrain trace element AFC models.

4) EMPA of phenocryst phases in the porphyrite-porphyry series and comparison of the same with the mineral chemistry of the Criffell–Dalbeattie granitoids in order to constrain fractionating phase compositions.

References

- Alibert, C., Michard, A. and Albarede, F. 1986. Isotope and trace element geochemistry of the Colorado Plateau volcanics. *Geochim.Cosmochim.Acta* 50, 2735-2750
- Allen, J. F. and Carmichael, I.S.E. 1984. Lamprophyric lavas in the Colima graben, SW Mexico. *Contrib. Mineral. Petrol.* 88, 203-216.
- Arima, M. and Edgar, A.D. 1983. High pressure experimental studies on a katungite and their bearing on the genesis of some potassium-rich magmas of the west branch of the African Rift. *J.Petrol.* 24, 166-187
- Arth, J.G. 1976. Behaviour of trace elements during magmatic processes—a summary of theoretical models and their applications. *J. Res. US Geol. Surv.* 4, 41–47
- Bachinski, S.W. and Scott, R.B. 1979. Rare-earth and other trace element contents and the origin of minettes (mica–lamprophyres). *Geochim. Cosmochim. Acta.* 43, 93-100.
- Bachinski, S.W. and Simpson, E.L. 1984. Ti-phlogopites of the Shaws Cove minette: a comparison with micas of other lamprophyres, potassic rocks, kimberlites, and mantle xenoliths. *Am. Mineral.* 69, 41-56.
- Bailey, E.B. 1960. *Geology of Ben Nevis and Glencoe*. Mem. Geol. Surv. U.K (2nd Ed).
- Barnes, R.P., Rock, N.M.S. and Gaskarth, J.W. 1986. Late Caledonian dyke-swarms of Southern Scotland: new field, petrological and geochemical data for the Wigtown peninsula, Galloway. *Geol. J.* 21, 101-125
- Barton, M. and Hamilton, D.L. 1979. The melting relationships of a madupite from the Leucite Hills, Wyoming to 30kb. *Contrib.Mineral.Petrol.* 69, 133-42.
- Barton, M. and Hamilton, D.L. 1982. Water-undersaturated melting experiments bearing upon the origin of potassium-rich magmas. *Mineral.Mag.* 45, 267-278.
- Bergman, S.C. 1987. Lamproites and other potassium-rich igneous rocks: a review of their occurrence, mineralogy and geochemistry. In: Fitton J.G. and Upton, B.G.J. (eds). *Alkaline igneous rocks*. Spec.Publ.Geol.Soc.London. 30, 103–190
- Beswick, A.E. 1976. K and Rb relations in basalts and other mantle derived materials: Is phlogopite the key? *Geochim.Cosmochim.Acta.* 40, 1167-1183

Bowen, N.L. 1928. The Evolution of the Igneous rocks. Princeton University Press, New Jersey.

Bowes, D.R. and McArthur, A.C. 1976. Nature and genesis of the appinite suite. *Kristalinikum* 12, 31-46.

Bowes, D.R. and Wright, A.E. 1961. An explosion-breccia complex at Back Settlement, near. Kentallen, Argyll. *Tr. Edinb. Geol.Soc.* 18, 293-314.

Bowes, D.R., Kinloch, E.D. and Wright, A.E. 1964. Rhythmic amphibole overgrowths in appinites associated with explosion breccias in Argyll. *Mineral.Mag.* 33, 963-73.

Brouxel, M. 1991. Geochemical consequences of flow differentiation in a multiple injection dyke (Trinity ophiolite, N. California) *Lithos*, 26, 245-252.

Brown, G.C., Cassidy, J., Tindle, A.G. and Hughes, D.J. 1979. The Loch Doon granite: an example of granite petrogenesis in the British Caledonides. *J.Geol.Soc.Lond.* 136, 745-753

Cawthorn, R.G. and O'Hara, M.J. 1976. Amphibole fractionation in calc-alkaline magma genesis. *Am.J.Sci.* 276, 309-329

Clayburn, J.A.P. 1988. The crustal evolution of Central Scotland and the nature of the lower crust: Pb, Nd and Sr isotope evidence from Caledonian granites. *Earth Planet.Sci.Lett.* 90, 41-51

Cooper, A.F. 1979. Petrology of ocellar lamprophyres from western Otago, New Zealand. *J. Petrol.* 20, 139-64.

Cox, K.G., Bell, J. D. and Pankhurst, R.J. 1979. The interpretation of igneous rocks. George Allen and Unwin, London.

Currie, K.L. and Ferguson, J. 1970. The mechanism of intrusion of lamprophyre dikes as indicated by "offsetting" of dikes. *Tectonophysics* 9, 525-35.

Dal Piaz, G.V., Venturelli, G. and Scolari, A. 1979. Calc-alkaline to ultrapotassic post collisional volcanic activity in the internal northwestern Alps. *Mem. Ist. Geol. Mineral. Univ. Padova* 9, 1-32.

Dawson J.B. 1987. The kimberlite clan: relationship to olivine- and leucite- lamproites, and inferences for upper-mantle metasomatism. In: Fitton J.G. and Upton, B.G.J. (eds). Alkaline igneous rocks. Spec.Publ.Geol.Soc.London. 30, 95–102

Dawson, J.B. 1980. Kimberlites and their xenoliths. Springer-Verlag, Berlin.

Deer, W.A., Howie, R.A. and Zussman, J. 1963. Rock-forming minerals. Longmans

Delaney, P.T. and Pollard, D.D. 1981. Deformation of host rocks and flow of magma during growth of minette dykes and breccia-bearing intrusions near Ship Rock, New Mexico. Prof.Pap. U.S. Geol.Surv. 1202.

DePaolo, D.J. 1981. Trace element and isotopic effects of combined wallrock assimilation and fractional crystallisation. Earth.Planet.Sci.Lett. 53, 189-202

DePaolo, D.J. 1988. Neodymium isotope geochemistry: an introduction. Springer-Verlag, Heidelberg.

Eby, G.N. 1980. Minor and trace element partitioning between immiscible ocelli-matrix pairs from lamprophyre dykes and sills, Monteregean Hills petrographic province, Quebec. Contrib.Mineral.Petrol. 75, 269-78.

Edgar, A.D. 1987. The genesis of alkaline magmas with emphasis on their source regions: inferences from experimental studies. In: In: Fitton J.G. and Upton, B.G.J. (eds). Alkaline igneous rocks. Spec.Publ.Geol.Soc.London. 30, 29–52

Edgar, A.D. and Arima, M. 1983. Conditions of phlogopite crystallisation in ultrapotassic volcanic rocks. Mineral.Mag. 47, 11-19

Ehrenberg, S.N. 1979. Garnetiferous ultramafic inclusions in minette from the Navajo volcanic field. In: Boyd, F.R. and Meyer, H.A.O. (eds.). The mantle sample; Inclusions in kimberlites and other volcanics. Am.Geophys.Union., Washington, 330–344

Ehrenberg, S.N. 1982. Rare earth element geochemistry of garnet lherzolite and megacrystalline nodules from minette of the Colorado plateau province. Earth Planet.Sci.Lett. 57, 191-210.

Esperanca, S. and Holloway, J.R. 1986. The origin of the high-K latites from Camp Creek, Arizona: constraints from experiments with variable fO₂ and aH₂O. Contrib.Mineral.Petrol. 93, 504–512

- Esperanca, S. and Holloway, J.R. 1987. On the origin of some mica-lamprophyres: experimental evidence from a mafic minette. *Contrib.Mineral.Petrol.* 95, 207-216
- Faure, G. 1986. *Principles of Isotope geology*. John Wiley and Sons, New York.
- Fitton, J. G. and Hughes, D. J. 1970. Volcanism and plate tectonics in the British Ordovician. *Earth Planet.Sci.Lett.* 8, 223-228
- Foley, S.F. 1984. Liquid immiscibility and melt segregation in alkaline lamprophyres from Labrador. *Lithos* 17, 127-38.
- Fowler, M.B. 1988. Ach'uaine hybrid appinite pipes: evidence for mantle-derived shoshonitic parent magmas in Caledonian granite genesis. *Geology.* 16, 1026-1030
- Fraser, K.J., Hawkesworth, C.J., Erlank, A.J., Mitchell, R.H. and Scott-Smith, B.H. 1986. Sr, Nd and Pb isotope and minor element geochemistry of lamproites and kimberlites. *Earth Planet. Sci.Lett.* 76, 57-70.
- Frost, C.D. and O'Nions, R.K. 1985. Caledonian magma genesis and crustal recycling. *J.Petrol.* 26, 515-544
- Furnes, H. and Stillman, C.J. 1987. The petrology and geochemistry of an alkaline lamprophyre sheet intrusion complex on Maio, Cape Verde Republic. *J.Geol.Soc.Lond.* 144, 227-241
- Gast, P.W. 1968. Trace element fractionation and the origin of tholeiite and alkaline magma types. *Geochim.Cosmochim.Acta.* 32, 1057-1086
- Gill, J.B. 1981. *Orogenic andesites and plate tectonics*. Springer-Verlag, Berlin.
- Green, T.H. and Pearson, N.J. 1986. Ti-rich accessory phase saturation in hydrous mafic-felsic compositions at high pressure and temperature. *Chem.Geol.* 54, 185-201
- Greig, D. C. 1971. *British Regional Geology: South of Scotland (3d Ed.)*: HMSO, London.
- Halliday, A.N. 1983. Crustal melting and the genesis of isotopically and chemically zoned plutons in the Southern Uplands of Scotland In: Atherton, M.P. and Gribble, C.D. (eds.) *Migmatites, melting and metamorphism*: Shiva, Orpington, 54-61
- Halliday, A.N. 1984. Coupled Sm-Nd and U-Pb systematics in late Caledonian granites and the basement under Northern Britain. *Nature* 307, 229-233

- Halliday, A.N., Stephens, W.E. and Harmon, R.S. 1980. Rb-Sr and O isotopic relationship in 3 zoned Caledonian granitic plutons, Southern Uplands: evidence for varied sources and hybridisation of magmas. *J.Geol.Soc.Lond.* 137, 329-348
- Halliday, A.N., Stephens, W.E., Hunter, R.H. and 3 others. 1985. Isotopic and chemical constraints on the building of the deep Scottish lithosphere. *Scott.J.Geol.* 21, 465-491
- Harmon, R. S., Halliday, A. N., Clayburn, J. A. P. and Stephens, W. E. 1984. Chemical and isotopic systematics of the Caledonian intrusions of Scotland and northern England: a guide to magma source regions and magma-crust interaction: *Philos. Trans. R. Soc. Lond.* A310, 709-742
- Harris, P.G. 1957. Zone refining and the origin of potassic basalts. *Geochim.Cosmochim.Acta* 12, 195-208
- Harris, P.G. and Middlemost, E.A.K. 1970. The evolution of kimberlites. *Lithos.* 3, 77-88
- Haskin, L. A. 1983. Petrogenetic modelling—rare earth elements. In: Henderson, P. (ed.) *Rare earth element geochemistry*. Elsevier, Amsterdam, 115-152.
- Hatch, F.H., Wells, A.K. and Wells, M.K. 1972. *Petrology of the igneous rocks*. 13th Ed. Murby, London.
- Hawkesworth, C.J., Van Calsteren, P., Rogers, N.W. and Menzies, M.A. 1987. Isotope variations in Recent Volcanics: A Trace Element Perspective. In: Menzies, M.A. and Hawkesworth, C.J. (eds). *Mantle Metasomatism*. Academic Press Inc. (London) Limited, 365-388
- Henderson, P. 1982. *Inorganic geochemistry*. Pergamon Press, Oxford.
- Henney, P.J., Evans, J.A, Holden, P. and Rock, N.M.S. 1989. Granite–lamprophyre associations in the Scottish Caledonides: trace element and isotopic evidence for mantle involvement in Caledonian granite genesis. *Terra Abstracts.* 1, 285-286
- Holden, P. 1987. Source and equilibration studies of Scottish Caledonian xenolith suites. Unpublished Ph.D. Thesis, Univ. St. Andrews, Scotland.

- Holden, P., Halliday, A.N. and Stephens, W.E. 1987. Neodymium and strontium isotope content of microdioritic enclaves points to mantle input to granitoid production. *Nature*. 330, 53-56
- Holden, P., Halliday, A.N., Stephens, W.E and Henney, P.J. 1991. Mass transfer between mafic enclaves and silicic magmas with particular reference to mobile versus immobile elements. *Chem. Geol* (In Press)
- Huppert, H.E. and Sparks, R.S.J. 1988a. The generation of granitic magmas by intrusion of basalt into continental crust. *J.Petrol.* 29, 599-624
- Huppert, H.E. and Sparks, R.S.J. 1988b. Melting of the roof of a chamber containing hot, turbulently convecting fluid. *J Fluid.Mech.* 188, 107-131
- Huppert, H.E. and Sparks, R.S.J. 1988c. The fluid dynamics of crustal melting by injection of basaltic sills. *Trans.R.Soc. Edinburgh: EarthSci.* 79, 237-244
- Irvine, T.N. 1974. Petrology of the Duke Island Ultramafic complex, southeastern Alaska. *Geol. Soc. Am. Mem.* 138, 240pp
- Kennedy, W.Q. and Read, H.H. 1936. The differentiated dyke at Newmains, Dumfries-shire and its contact and contamination phenomena. *Q. J. Geol. Soc. Lond.* 92, 116-144.
- King, B.C. 1937. The minor intrusions of Kirkcudbrightshire. *Proc. Geol. Assoc.* 48, 282-306.
- Komer, P.D. 1972a. Mechanical interactions of phenocrysts and flow differentiation of igneous dikes and sills. *Geol. Soc. Am. Bull.* 83, 973-988
- Komer, P.D. 1972b. Flow differentiation in igneous dikes and sills: profiles of velocity and phenocryst concentration. *Geol. Soc. Am. Bull.* 83, 3443-3448
- Kushiro, I., Syono, Y. and Akimoto, S. 1967. Stability of phlogopite at high pressures and possible presence of phlogopite in the earth's upper mantle. *Earth Planet.Sci.Lett.* 3, 197-203
- Leake, B.E. 1978. Nomenclature of amphiboles. *Can. Mineral.* 16, 501-520.
- Leake, R.C and Cooper, C. 1983. The Black Stockarton Moor sub-volcanic complex, Galloway. *J.Geol.Soc.Lond.* 140, 665-676

- Leake, R.C. and Brown, M.J. 1979. Porphyry-style mineralisation at Black Stockarton Moor, southwest Scotland. *Trans.Inst.Min.Metall.* B 88, 177-181
- Leat, P.T., Thompson, R.N., Morrison, M.A. Hendry, G.L and Trayhorn, S.C. 1987. Geodynamic significance of post-Variscan intrusive and extrusive potassic magmatism in S.W England. *Trans.R.Soc. Edinburgh: EarthSci.* 77, 349-360
- Leat, P.T., Thompson, R.N., Morrison, M.A., Hendry, G.L. and Dickin, A.P. 1988. Silicic magmas derived by fractional crystallisation from Miocene minette, Elkhead Mountains, Colorado. *Mineral.Mag.* 52, 577-585
- Leeder, M. 1971. Aspects of the geology of the south-eastern part of the Criffell intrusion and its associated dykes. *Trans.Dumfries.Galloway.Nat.Hist.Antiq.Soc.* 48, 1-11
- Lees, G.J. 1974. Petrochemistry of the mica lamprophyres (minettes) of Jersey. *Proc. Ussher Soc.* 3, 149-55.
- Leggett, J.K., McKerrow, W.S. and Casey, D.M. 1982. The anatomy of a Lower Palaeozoic accretionary fore-arc: the Southern Uplands of Scotland. In: Leggett, J.K. (ed.) *Trench-Forearc geology. Spec.Publ.Geol.Soc.London.* 10, 495-520.
- Leggett, J.K., McKerrow, W.S. and Eales, M.H. 1979. The Southern Uplands of Scotland; a Lower Palaeozoic accretionary prism. *J.Geol.Soc.Lond.* 136, 755-770
- Leggett, J.K., McKerrow, W.S. and Soper, N.J. 1983. A model for the evolution of Southern Scotland. *Tectonics.* 2, 187-210
- Luhr, J.F. and Carmichael, I.S.E. 1981. The Colima volcanic complex, Mexico. Part II. Late Quaternary cinder cones. *Contrib.Mineral.Petrol.* 76, 127-47.
- Luhr, J.F., Allan, J.F., Carmichael, I.S.E., Nelson, S.A. and Hasenaka, T. 1989. Primitive calc-alkaline and alkaline rock types from the Western Mexican volcanic belt. *J.Geophys.Res.* 94, 4515-4530
- Maaloe, S. 1985. *Principles of Igneous Petrology.* Springer-Verlag, Berlin. 375pp.
- Macdonald, R., Rock, N.M.S., Rundle, C.C. and Russell, O.J. 1986. Relationships between late Caledonian lamprophyric, syenitic and granitic magmas in a differentiated dyke, southern Scotland. *Mineral.Mag.* 50, 547-557

- Macdonald, R., Thorpe, R.S., Gaskarth, W and Grindrod, A.R. 1985. Multi-component origin of Caledonian lamprophyres of northern England. *Mineral.Mag.* 49, 485-494
- Macgregor, M. 1937. The western part of the Criffell-Dalbeattie igneous complex. *Q.J. Geol. Soc. Lond.* 93, 457-86.
- Mauger, R.L. 1988. Geochemical evidence for sediment recycling from North Carolina (U.S.A) minettes. *Can.Mineral.* 26, 133-141
- McCarthy, T.S. and Hasty, R.A. 1976. Trace element distribution patterns and their relationship to the crystallisation of granitic melts. *Geochim.Cosmochim.Acta.* 40, 1351-1358
- McKenzie, D. 1985. The extraction of magma from the crust and mantle. *Earth.Planet. Sci. Letters.* 74, 81-91
- Menzies, M.A. and Halliday, A.N. 1988. Lithospheric domains beneath the Scottish Highlands. In: Menzies, M.A. and Cox, K.G. (eds.) *Oceanic and continental lithosphere: Similarities and differences. J.Petrol. special volume (1988)*, 275-302
- Menzies, M.A., Halliday, A.N., Palacz, Z., Hunter, R.H., Upton, B.G.J., Aspen, P. and Hawkesworth, C.J. 1987. Evidence from mantle xenoliths for an enriched lithospheric keel under the Outer Hebrides. *Nature.* 325, 44-47
- Mitchell, R.H. 1986. *Kimberlites: Mineralogy, Geochemistry and Petrology.* Plenum Press, New York.
- Murray, C.G. 1972. Zoned ultramafic complexes of the Alaskan type: Feeder pipes of andesitic volcanoes. *Geol. Soc. Am. Mem.* 132, 313-335
- Mykura, W. 1976. *British regional Geology: Orkney and Shetland:* HMSO, London.
- Nakamura, N. 1974. Determination of REE, Ba, Fe, Mg, Na and K in carbonaceous and ordinary chondrites. *Geochim.Cosmochim.Acta* 38, 757-75.
- Nixon, P.H., Mitchell, R.H. and Rogers, N.W. 1980. Petrogenesis of alnoitic rocks from Malaita, Solomon Is. *Mineral.Mag.* 43, 587-96.
- Nockolds, S.R. 1941. The Garabal Hill-Glen Fyne igneous complex. *Q.J.Geol.Soc.Lond.* 96, 451-510.

- Patchett, P.J. 1980. Thermal effects of basalt on continental crust and crustal contamination of magmas. *Nature*. 283, 559-561
- Pearce, J.A. 1982. Trace element characteristics of lavas from destructive plate boundaries. In: Thorpe, R.S. (ed.) *Andesites*. Wiley, New York, 525-48.
- Pearce, J.A. 1983. Role of the sub-continental lithosphere in magma genesis at active continental margins. In: Hawkesworth, C.J. and Norry, M.J. (eds.) *Continental Basalts and mantle xenoliths*. Shiva, Nantwich, 230-249.
- Pearce, J.A. and Norry, M.J. 1979. Petrogenetic implications of Ti, Zr, Y and Nb variations in volcanic rocks. *Contrib.Mineral.Petrol.* 69, 33-47
- Peccerillo, A. and Manetti, P. 1985. The potassium alkaline volcanism of central-southern Italy: a review of the data relevant to petrogenesis and geodynamic significance. *Trans.Geol.Soc.S.Afr.* 88, 379-394
- Peccerillo, A., Poli, G. and Serri, G. 1988. Petrogenesis of orenditic and kamafugitic rocks from central Italy. *Can.Mineral.* 26, 45-65
- Phillips, W.J. 1956a. The Criffell-Dalbeattie granodiorite complex. *Q.J.Geol.Soc.Lond.* 112, 221-239
- Phillips, W.J. 1956b. Minor intrusive suite associated with the Criffell-Dalbeattie granodiorite complex. *Proc.Geol.Assoc.* 67, 103-21.
- Phillips, W.J., Fuge, R. and Phillips, N. 1981. Convection and crystallisation in the Criffell-Dalbeattie pluton. *J.Geol.Soc.Lond.* 138, 351-366
- Pitcher, W.S. and Berger, A.R. 1972. *Geology of Donegal*, Wiley, New York.
- Read, H.H. 1961. Aspects of Caledonian magmatism in Britain. *Lpool. Manchr. Geol. J.* 2, 653-683.
- Richey, J.E. 1939. The dykes of Scotland. *Tr.Edinb.Geol.Soc.* 13, 393-435.
- Richardson, S.H. 1979. Chemical variation induced by flow differentiation in an extensive Karroo dolerite sheet, southern Namibia. *Geochimica.Cosmochimica. Acta* 43, 1433-1441.
- Rock, N. M. S. and Rundle, C. C. 1986. Lower Old Red Sandstone age for the "Great (Basal) Conglomerate", Scottish Borders. *Scott J. Geol.* 22, 285-288

Rock, N.M.S. 1977. The nature and origin of lamprophyres: some definitions, derivations and distinctions. *Earth Sci rev.* 13, 123-69.

Rock, N.M.S. 1984. Nature and origin of calc-alkaline lamprophyres: minettes, vogesites, kersantites and spessartites. *Trans.R.Soc. Edinburgh: EarthSci.* 74, 193-227.

Rock, N.M.S. 1987. The nature and origin of lamprophyres: an overview. In: Fitton J.G. and Upton, B.G.J. (eds). *Alkaline igneous rocks. Spec.Publ.Geol.Soc.London.* 30, 191-226

Rock, N.M.S. 1991. *Lamporphyres.* Blackie & Son Ltd, Glasgow, 285pp.

Rock, N.M.S. and Hunter, R.H. 1987. Late Caledonian dyke-swarms of northern Britain: Spatial and temporal intimacy between lamprophyric and granitic magmatism around the Ross of Mull pluton, Inner Hebrides. *Geol. Rund.* 76, 805-826

Rock, N.M.S., Cooper, C. and Gaskarth, J.W. 1986b. Late Caledonian subvolcanic vents and associated dykes in the Kirkcudbright area, Galloway, SW Scotland. *Proc.Yorks.Geol.Soc.* 46, 29-37

Rock, N.M.S. and Leake, B.E. 1984. The International Mineralogical Association amphibole nomenclature scheme: computerization and its consequences. *Mineral. Mag.* 48, 211-227

Rock, N.M.S., Gaskarth, J.W. and Rundle, C.C. 1986a. Late Caledonian dyke-swarms of Southern Scotland: a regional zone of primitive K-rich lamprophyres and associated vents. *J. Geol.* 94, 505-522 .

Rock, N.M.S., Gaskarth, J.W., Henney, P.J. and Shand, P. 1988. Late Caledonian dyke swarms of northern Britain: some preliminary petrogenetic and tectonic implications of their distribution and chemical variations. *Can.Mineral.* 26, 3-22

Roden, M.F. 1981. Origin of coexisting minette and ultramafic breccia, Navajo volcanic field. *Contrib.Mineral.Petrol.* 77, 195-206.

Roden, M.F. and Smith, D. 1979. Field geology, chemistry and petrology of Buell Park minette diatreme, Apache county, Arizona. In: Boyd, F.R. and Meyer, H.O.A. (Eds.) *Kimberlites, diatremes and diamonds.* Am.Geophys.Union, Washington, 364-81

- Rogers, N.W., Bachinski, S.W., Henderson, P. and Parry, S.J. 1982. Origin of potash-rich basic lamprophyres: trace element data from Arizona minettes. *Earth Planet Sci.Lett.* 57, 305-312.
- Rogers, N.W., Hawkesworth, C.J. Parker, R.J. and Marsh, J.S. 1985. The geochemistry of potassic lavas from Vulcini, central Italy and implications for mantle enrichment processes beneath the Roman region. *Contrib.Mineral.Petrol.* 90, 244-257
- Ross, M.E. 1983. Chemical and mineralogic variations within four dikes of the Columbia River Basalt Group, south-eastern Columbia Plateau. *Geol. Soc. Am. Bull.* 94, 1117-1126.
- Ross, M.E. 1986. Flow differentiation, phenocryst alignment, and compositional trends within a dolerite dyke at Rockport, Massachusetts. *Geol. Soc.Am. Bull.* 97, 232-240.
- Ryerson, F.J. and Watson, E.B. 1987. Rutile saturation in magmas: implications for Ti-Nb-Ta depletion in island arc basalts. *Earth Planet.Sci.Lett.* 86, 225-239
- Sabine, P.A. 1953. The petrography and geological significance of the post-Cambrian minor intrusions of Assynt and the adjoining districts of north-west Scotland. *Q.J.Geol.Soc.Lond.* 109, 137-171.
- Schulze, D.J., Smith, J.V. & Nemeč, D. 1985. Mica chemistry of lamprophyres from the Bohemian Massif, Czechoslovakia. *Neues Jahrbuch Miner. Abh.* 152, 321-334.
- Smedley, P.L. 1986. The relationship between calc-alkaline volcanism and within-plate continental rift volcanism: evidence from Scottish Palaeozoic lavas. *Earth Planet.Sci.Lett.* 77, 113-128
- Stephens, W. E., and Halliday, A. N. 1984. Geochemical contrasts between Late Caledonian granitoid plutons of northern, central and southern Scotland. *Trans.R.Soc. Edinburgh: EarthSci.* 75, 259-73.
- Stephens, W.E. and Halliday, A.N. 1979. Compositional variations in the Galloway plutons. In: Atherton, M.P and Tarney, J. (eds). 1979. *Origin of granite batholiths-geochemical evidence*. Shiva, Nantwich., 9-17
- Stephens, W.E. and Halliday, A.N. 1980. Discontinuities in the composition surface of a zoned pluton, Criffell, Scotland. *Geol. Soc. Am. Bull.* 91, 165-170

Stephens, W.E., Holden, P. & Henney, P.J. 1991. The origin of mafic xenoliths in the Strontian and Criffell granites. In: Didier, J & Barbarin, B. (eds) *Granites & their enclaves* (2nd Ed), Elsevier. (In Press).

Stephens, W.E., Whitley, J.E., Thirlwall, M.F. and Halliday, A.N. 1985. The Criffell zoned pluton: correlated behaviour of rare earth element abundances with isotopic systems. *Contrib.Mineral.Petrol.* 89, 226–238

Stone, P., Floyd, J.D., Barnes, R.P. and Lintern, B.C. 1987. A sequential back–arc and foreland basin thrust duplex model for the Southern Uplands of Scotland. *J.Geol.Soc.Lond.* 144, 753-764

Tatsumi, Y. 1989. Migration of fluid phases and genesis of basaltic magmas in subduction zones. *J.Geophys.Res.* 94, 4697-4707

Tatsumi, Y., Hamilton, D.L. and Nesbitt, R.W. 1986. Chemical characteristics of fluid phase released from a subducted lithosphere and origin of arc magmas: evidence from high–pressure experiments and natural rocks. *J.Volcanol.Geotherm.Res.* 29, 293–309

Tatsumi, Y., Sakuyama, M., Fukuyama, H. and Kushiro, I. 1983. Generation of arc basalt magmas and thermal structure of the mantle wedge in subduction zones. *J.Geophys.Res.* 88, 5815–5825

Taylor, H.P. 1967. The zoned ultramafic complexes of Southeastern Alaska. In: Wyllie, P.J. (ed.) *Ultramafic and Related rocks*. John Wiley and Sons, New York. 97–121

Thirlwall, M. F. 1979. The petrochemistry of the British Old Red sandstone volcanic province. PhD. Thesis, University of Edinburgh.

Thirlwall, M. F. 1981. Implications for Caledonian plate tectonic models of chemical data for volcanic rocks of the British Old Red Sandstone: *Jour. Geol. Soc. Lond.* 138, 123-38

Thirlwall, M. F. 1982. Systematic variation in chemistry and Nd-Sr isotopes across a Caledonian calc-alkaline volcanic arc: implications for source materials: *Earth Planet.Sci.Lett.* 58, 27-50

Thirlwall, M. F. 1983. Isotope geochemistry and origin of calc-alkaline lavas from a Caledonian continental margin volcanic arc. In: Aramaki, S., and Kushiro, I. (eds.) *Arc Volcanism*. Elsevier *Developments in Volcanology* 2, 589-623

Thirlwall, M.F. 1986. Lead isotope evidence for the nature of the mantle beneath Caledonian Scotland. *Earth Planet.Sci.Lett.* 80, 55-70

Thirlwall, M.F. 1988. Geochronology of late Caledonian magmatism in Northern Britain. *J.Geol.Soc.Lond.* 145, 951-967

Thirlwall, M.F. and Burnard, P. 1990. Pb-Sr-Nd isotope evidence and chemical study of the origin of undersaturated and oversaturated shoshonitic magmas from the Borralan pluton, Assynt, NW Scotland. *J. Geol. Soc. Lond.* 147, 259-269.

Thirlwall, M.F. and Jones, N.W. 1983. Isotope geochemistry and contamination mechanics of Tertiary lavas from Skye, Northwest Scotland. In: Hawkesworth, C.J. & Norry, M. J. *Continental basalts and mantle xenoliths*. Shiva, Nantwich. 273pp.

Thirlwall, M.F., Maynard, J., Stephens, W.E. and Shand, P. 1989. Calc-alkaline magmagenesis in the Scottish Southern Uplands forearc: a Pb-Sr-Nd isotope study. *Terra Abstracts.* 1, 178

Thompson, R.N. and Fowler, M.B. 1986. Subduction-related shoshonitic and ultrapotassic magmatism: a study of Siluro-Ordovician syenites from the Scottish Caledonides. *Contrib.Mineral.Petrol.* 94, 507-522

Thompson, R.N., Morrison, M.A., Hendry, G.L. and Parry, S.J. 1984. An assessment of the relative roles of crust and mantle in magma genesis: an elemental approach. *Phil.Tr.R.Soc.Lond.* A310, 549-90.

Thorpe, R.S. 1987. Permian K-rich volcanic rocks of Devon: petrogenesis, tectonic setting and geological significance. *Trans.R.Soc. Edinburgh: EarthSci.* 77, 361-366

Thorpe, R.S., Cosgrove, M.E. and van Calsteren, P.W.C. 1986. Rare earth element, Sr and Nd isotope evidence for petrogenesis of Permian basaltic and K-rich volcanic rocks from S.W. England. *Mineral.Mag.* 50, 481-490

Turpin, L., Velde, D. and Pinte, G. 1988. Geochemical comparison between minettes and kersantites from the Western European Hercynian orogen: trace element and Pb-Sr-Nd isotope constraints on their origin. *Earth Planet.Sci.Lett.* 87, 73-86

Upton, B.G.J., Aspen, P. and Chapman, N.A. 1983. The upper mantle and deep crust beneath the British Isles: evidence from inclusions in volcanic rocks. *J.Geol.Soc.Lond.* 140, 105-21.

- Van Bergen, M.J., Ghezzo, C. and Ricci, C.A. 1983. Minette inclusions in the rhyodacitic lavas of Mt. Amiata (central Italy): mineralogical and geochemical evidence of mixing between Tuscan and Roman-type magmas. *J. Volcanol. Geotherm. Res.* 19, 1-35.
- Venturelli, G., Capedri, S., Battistini, G. Di, Crawford, A., Kogarko, L.N. and Celestini, S. 1984. The ultrapotassic rocks from southeastern Spain. *Lithos.* 17, 37-54.
- Wallace, P. and Carmichael, I.S.E. 1989. Minette lavas and associated leucitites from the Western Front of the Mexican Volcanic Belt: petrology, chemistry, and origin. *Contrib. Mineral. Petrol.* 103, 470-492.
- Waters, F.G. 1987. A suggested origin of MARID xenoliths in kimberlites by high pressure crystallisation of an ultrapotassic rock such as lamproite. *Contrib. Mineral. Petrol.* 95, 523-533
- Watson, J. 1984. The ending of the Caledonian orogeny in Scotland. *J. geol. Soc. Lond.* 141, 193-214.
- White, A.J.R. and Chappell, B.W. 1988. Some supracrustal (S-type) granites of the Lachlan Fold Belt. *Trans. R. Soc. Edinburgh: Earth Sci.* 79, 169-182
- Wilson, M. 1989. *Igneous Petrogenesis: a global tectonic approach*. Unwin Hyman, London, 466pp.
- Wimmenauer, W. and Muller, H. 1985. Intermediate and acid dyke rocks of lamprophyric affinity. *Geol. Soc. Can. Ann. Meeting, Fredericton NB, Progr. Abstr.* A69.
- Wood, D.A., Joron, J.L., Treuil, M., Norry, M. and Tarney, J. (1979). Elemental and Sr isotope variations in basic lavas from Iceland and the surrounding ocean floor. *Contrib. Mineral. Petrol.* 70, 319-339
- Wright, A.E. and Bowes, D.R. 1979. Geochemistry of the appinite suite. In: Harris, A.L. *et al.* (eds.) *The Caledonides of the British Isles—reviewed*. *Spec. Pub. Geol. Soc. Lond.* 8, 699-704
- Wyllie, P.J. and Sekine, T. 1982. The formation of mantle phlogopite in subduction zone hybridization. *Contrib. Mineral. Petrol.* 79, 375-380

Wyman, D. and Kerrich, R. 1988. Alkaline magmatism, major structures and gold deposits: Implications for greenstone belt gold metallogeny. *Econ.Geol.* 83, 454-461

Yagi, K. and Takeshita, H. 1987. Impact of hornblende crystallisation for the genesis of calc-alkalic andesites. In: Mysen, B. O. (ed.) *Magmatic Processes: Physiochemical Principles*. Spec.Pub. Geochem.Soc. 1, 183-190

Yoder, H.S. and Kushiro, I. 1969. Melting of a hydrous phase: phlogopite. *Am.J. Sci.*, Schairer Vol. 267-A, 558-582

**PAGE
MISSING
IN
ORIGINAL**

Appendix A

Analytical methods

A1.1) Introduction

Data collection involved using of several analytical techniques for determination of elemental and isotopic abundances. 250 samples were collected for analysis. They were split free of weathered surfaces using a hydraulic splitter and a hand specimen retained for thin section and probe slide preparation. The remainder was crushed to gravel using a steel plate jaw crusher, down to 5-10mm gravel. This was homogenised and a 100g aliquot separated and ground to <150 mesh powder by using a Tema mill fitted with tungsten carbide components. All major element analysis were recalculated to 100% free of volatiles following the recommendations of Rock (1984, 1987, 1991) for lamprophyric rocks.

A1.2) X-Ray Fluorescence Analysis

XRF was the principal analytical method used for whole rock major and trace element determinations, because it is able to determine a wide range of elements, to high degrees of accuracy and precision in a wide range of geological materials. Elements determined for this study were Si, Mg, Fe, Ca, K, Na, P, Ti, Mn, Al, Ni, Cr, U, Th, V, Rb, Ba, Sr, La, Ce, Nd, Sm, Nb, Zr, Y, Pb, Zn and Cu. Samples were prepared for XRF analyses using techniques similar to those developed at University of Edinburgh after Norrish & Hutton (1969).

Trace elements were determined on pressed powder pellets made from homogeneous mixing of rock powder with 15% Bakelite as a binding agent. The mixture was pressed at 20 tonnes in a die then extruded and cured at 110°C. The resultant pellets are uniform and durable and can be subjected to repeated analysis with minimal degradation of the analytical surface or loss of material into the sample chamber. Major elements were determined on glass discs produced by fusion of sample powder with a La oxide doped flux (Spectroflux 105) to reduce matrix effects and

ensure a homogeneous sample. Samples were fused "wet" with the weight loss made up with the addition of more flux and a separate LOI figure determined by heating 4 gm of sample at 1000°C for an hour and calculating percentage weight loss.

The equipment used for analysis at Aston University was a Philips PW1400 automated wavelength dispersive XRF fitted with a 3kW Rh tube. The use of a Rh tube together with 5 different crystals enabled the determination of a wide range of majors and traces without the need to change tubes in exchange for a small decrease in excitation potential for some elements. Counting was done using a CH₄-Ar fed flow counter for light elements and a NaI(Tl) scintillation counter for the heavier elements. The best analytical conditions for any element require matching the ideal power settings (kV and mA) with the optimum crystal, collimator and background positions to achieve the optimal peak to background ratio and count rate. Analytical conditions were based on those recommended by Kikkert (1981) with the more intense K alpha and beta lines being used as much as possible to give optimum count rates and peak to background ratios. L lines were used for elements which have an unavoidable K line interferences (eg: Ba, U & Th) or with K line absorption edges too short for efficient excitation by the tube (LREE). Several significant line overlap corrections were required for analysis of some elements. These include Rb K-beta on the Y K-alpha line and the Sr K-beta on Zr K-alpha line. The Compton-scattered Rh tube line was used for calculating the bulk matrix absorption correction for most elements. V and Cr are exceptions and required the use of calculated "alpha" factors to compensate for the effect of the intense Fe K alpha line. Full details of the analytical conditions for each element are listed in Table A.1 with figures for analytical precision and accuracy listed in Tables A.2 and A.3. The regression lines for both major and trace elements were calculated using the De Jongh equation, supported in the Phillips X14D software:

$$C_i = (D_i + E_i \cdot R_i) (1 + \sum a_{ij} \cdot C_j / 100)$$

where C_i is concentration in the sample, D_i and E_i are constants whose values is dependent on the particular spectrometer settings for that element, R_i is the countrate or countrate ratio in the sample, a_{ij} are the matrix correction coefficients (alphas) for

Table A.1
Analytical conditions for XRF determinations

Element	Line	Collim.	Detector	Crystal	U. Wind.	L. Wind.	kV	mA	Angle	Off.(+)	Off.(-)
Cr	KA	Fine	Flow	1	64	14	50	55	107.115	1.64	1.64
V	KA	Fine	Flow	1	62	10	50	55	123.2	3.54	2.22
Sr	KA	Fine	Scint.	1	72	26	70	40	35.825	0.5	0.5
Ba	KA	Fine	Scint.	1	60	30	70	40	15.525	0	0.18
Pb	LB	Fine	Scint.	2	70	28	70	40	28.24	0.3	0.3
Th	LA	Fine	Scint.	1	68	20	70	40	39.215	0.26	0.26
U	LA	Fine	Scint.	1	64	22	70	40	37.3	0.22	0.22
Nb	KA	Fine	Scint.	1	66	28	70	40	30.39	0.5	0
Zr	KA	Fine	Scint.	1	70	28	70	40	32.035	0.4	0.4
Rb	KA	Fine	Scint.	1	72	28	70	40	37.93	0.4	0.4
Ni	KA	Fine	Flow/Scint.	2	64	22	60	45	48.63	0	0.4
La	LA	Fine	Flow	2	62	10	50	55	82.92	1.32	0.8
La(k)	KA	Fine	Scint.	1	54	22	95	30	14.94	0	0.18
Ce	LB	Fine	Flow	1	58	38	50	55	111.75	2.4	1
Ce(k)	KA	Fine	Scint.	1	52	22	95	30	14.385	0	0.18
Nd	LA	Fine	Flow	1	60	38	50	55	112.74	1.38	2
SiO2	KA	Coarse	Flow	4	72	32	50	55	109.165	2	2
TiO2	KA	Fine	Flow	2	68	10	50	55	86.125	1.1	1.1
Al2O3	KA	Coarse	Flow	4	74	32	50	55	145.01	1.5	1.5
Fe2O3	KA	Fine	Flow	2	64	18	50	55	57.485	1.5	1.5
MgO	KA	Coarse	Flow	5	68	62	40	70	45.235	1.7	1.7
CaO	KA	Coarse	Flow	2	66	36	50	55	113.205	2	2
Na2O	KA	Coarse	Flow	5	74	25	40	70	55.18	2.5	2.5
K2O	KA	Coarse	Flow	2	66	34	50	55	136.78	3.5	0
P2O5	KA	Coarse	Flow	3	66	34	40	70	141.115	2.2	0
MnO	KA	Flow	Flow	1	64	18	50	55	95.18	0.6	0.6

Crystals: 1 LIF 220
 Phillips 2 LIF200
 PW 140C 3 Ge
 4 PE
 5 TIAP

Table A.2

Reproducibility of major
element data on multiple XRF runs (N=4).

	BP 11 Mean (%)	± Std Dev.	PH1A Mean (%)	± Std Dev.
SiO ₂	45.05	0.091	64.73	0.122
TiO ₂	1.29	0.005	0.57	0.008
Al ₂ O ₃	11.69	0.063	15.63	0.050
Fe ₂ O ₃	8.87	0.023	3.18	0.015
MgO	12.75	0.015	2.21	0.015
CaO	9.83	0.008	2.39	0.005
Na ₂ O	1.70	0.032	3.74	0.090
K ₂ O	2.50	0.005	3.92	0.008
P ₂ O ₅	1.20	0.005	0.28	0.000
MnO	0.14	0.007	0.06	0.004
LOI	3.16	0.005	1.81	0.007

Reproducibility of trace elements
element data on multiple XRF runs(N=8).

	BSM 01 Mean (ppm)	± Std Dev.	BP 23 Mean (ppm)	± Std Dev.
Ni	193.40	1.600	55.25	0.760
V	178.80	3.450	97.13	4.050
Cr	280.00	5.230	83.00	3.020
Rb	59.30	0.710	79.38	0.920
Sr	921.30	1.040	799.75	2.760
Ba	1139.60	6.460	886.00	8.090
Zn	82.50	1.770	42.50	0.760
Cu	28.10	0.350	11.25	0.460
Zr	348.00	1.070	183.00	1.200
Nb	26.00	0.530	10.38	0.520
Y	27.75	1.160	14.50	0.760
	1301C Mean (ppm)	± Std Dev.		
La	54.80	1.640		
Ce	126.00	2.730		
Nd	60.00	1.220		
	1245 Mean (ppm)	± Std Dev.		
Pb	17.00	0.930		
U	3.38	1.190		
Th	8.38	0.740		

Table A.3
Accuracy

Standard	AGV-1		BCR-1	
	A-V	C-V	A-V	C-V
SiO ₂	59.25	58.83	54.35	54.14
TiO ₂	1.06	1.04	2.22	2.26
Al ₂ O ₃	17.15	16.62	13.63	13.35
Fe ₂ O ₃	6.76t	6.72	13.45t	13.26
MgO	1.53	1.543	3.45	3.47
CaO	4.94	4.89	6.95	6.98
Na ₂ O	4.25	4.05	3.27	3.15
K ₂ O	2.9	2.94	1.69	1.73
P ₂ O ₅	0.48	0.5	0.37	0.36
MnO	0.096	0.1	0.182	0.187
Ni	15, 17	15.6	10, 13	10.7
V	125, 123	124.8	404	403.7
Cr	10, 12	10.7	15, 16	13.7
Rb	67	67.9	47	49.1
Sr	660	669	330	338
Ba	1200, 1220	1167	680, 678	645
Zn	86, 88	84	125, 129	122.4
Cu	59, 60	56.9	16, 18	12.8
Zr	230, 225	228.8	185, 191	187.6
Nb	16, 15	14.2	19, 14	12.8
Y	19, 21	20.1	40, 39	37.9
Pb	33, 36	34.8	14, 13.6	17.8
U	1.95, 1.89	2.7	1.7, 1.72	2.3
Th	6.4, 6.5	8.3	6.1, 6.04	6.2
La	38	40.9	25	25.4
Ce	66	66.4	54	49
Nd	34	30.4	29	23.6

Accepted values from compilations in Geostandards Newsletter.
C-V Aston data

element j on i and C_j is the concentration of the interfering element j . In most instances the Compton-scattered tube line was used to calculate mass absorption except for V, Cr and the L-line LREE for which alphas were calculated.

Full details of the various XRF regression techniques are given in Kikkert (1981) and in Jenkins *et al.* (1981).

A1.2.1) Rare earth element determinations

In an attempt to provide some LREE data for the samples, attempts were made to analyse La, Ce, Nd and Sm on the PW1400. Two methods were tried, one using the short wavelength, high energy K-alpha lines and the other using the longer wavelength L-alpha and L-beta lines of these elements. Analytical conditions for these two methods are listed in Table A.1 and in both cases the De Jongh equations were used for calculating the regression line. The K-alpha technique was successful in determining La values (AGV-1: reference concentration La – 36/37 ppm, calculated concentration La – 35.75 ± 1.71 (n=4)). However it was not possible to get accurate or precise determinations of Ce, Nd or Sm due to poor peak to background count ratios as the K line absorption edges for these elements were at the limit of the excitation potential of the 3kW Rh tube. One of the advantages of using the K lines was that counting times relative to the L lines were appreciably shorter, however the tube is required to run close to its full 3kW capacity and its life is significantly reduced. The determinations of the LREE on the L lines was generally more successful, except for Sm for which it was again difficult to obtain an acceptable peak to background count ratio, despite extended counting times. Accuracy and precision for the L-line technique are listed in Tables A.2 and A.3.

A1.2.2) Comparison of XRF trace element data with other sites and techniques.

In order to test the compatibility of the XRF determined dataset provided by Dr W E Stephens for the Criffell–Dalbeattie intrusion with the data produced on the Aston PW1400, a comparison was made with XRF data obtained from the Egham (RHBNC)

XRF, the calibration conditions of which were similar to that of the equipment used by Dr Stephens (Dr M Thirlwall, pers.comm). Trace element data obtained from a set of samples run on the Egham XRF were compared with the results obtained for the same samples run on the Aston XRF (Dr P Shand, pers.comm). These data are plotted in figures A.1(a-m) together with simple regression lines and correlation coefficients. For most elements, there is satisfactory agreement between the Aston and Egham data and reduced scatter about the regression line (e.g: Ni, Sr), although some elements do show greater discrepancies (Th, Pb, Zn, V & Cr). Some differences are expected considering possible variations in machine conditions, mass absorption corrections (V & Cr), sample preparation methods, line overlap corrections and calibrations between the two sites. An additional check on Rb and Sr determinations was made by comparing the values of these elements obtained by the BGS isotope facility in London with those from Aston (Figures A.2a-b). The results of this comparison are satisfactory given the difference in calibration procedure between the BGS and Aston equipment as well as a number other factors listed above.

LREE data in this study was obtained using XRF, INAA and Isotope Dilution (ID) techniques and the results of these three different methods are compared in figures A.3(a-f). Comparison of INAA and XRF LREE data (figures A.3a-c) reveal that the scatter around the regression line increases at higher LREE abundances, which is not unexpected given the bias of the XRF calibration towards lower values (controlled by the number of standards with high LREE contents available at Aston). There is also a significant bias in the Ce values as revealed by the large intercept value on the Y axis, the origins of which are unclear. Nd values determined by XRF and ID methods are compared in figure A.3(d) and the regression line shows a small intercept value. INAA and ID Sm and Nd abundances are compared in figures A.3(e-f) with a low intercept value on the Nd regression but a significantly greater one on the Sm line, suggesting some analytical bias of unknown origin.

Fig. A.1a

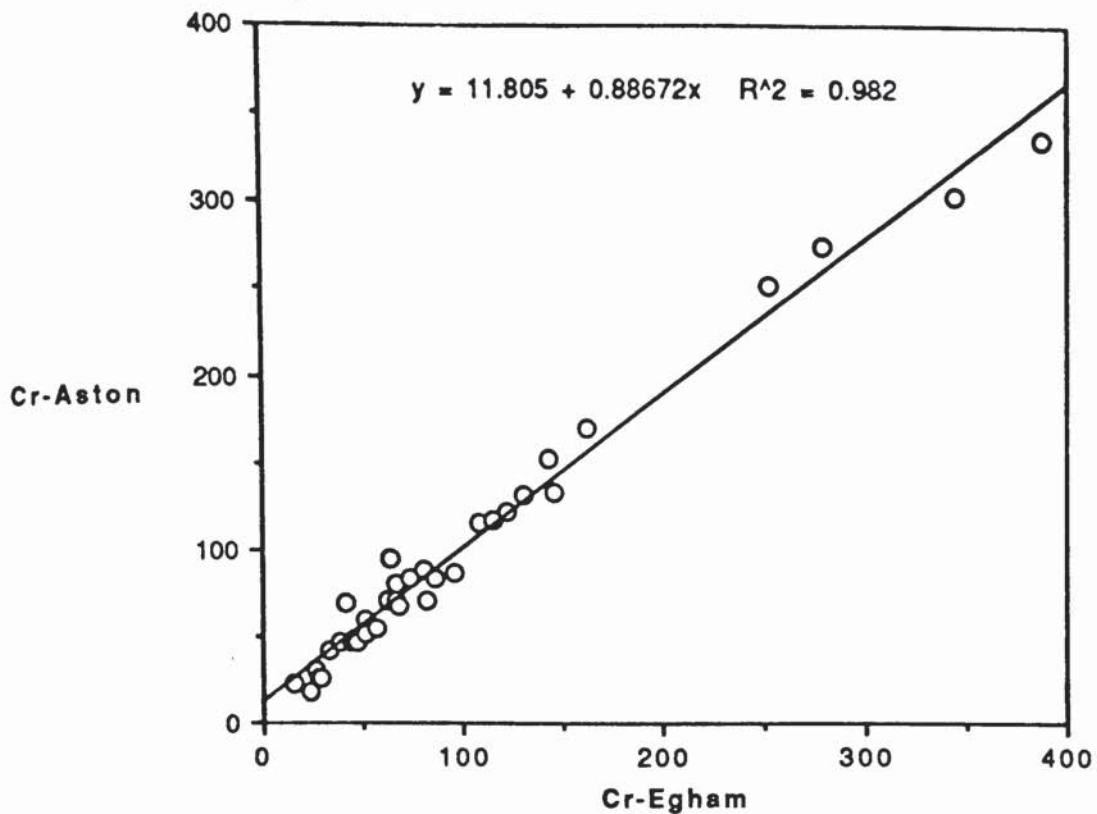


Fig. A.1b

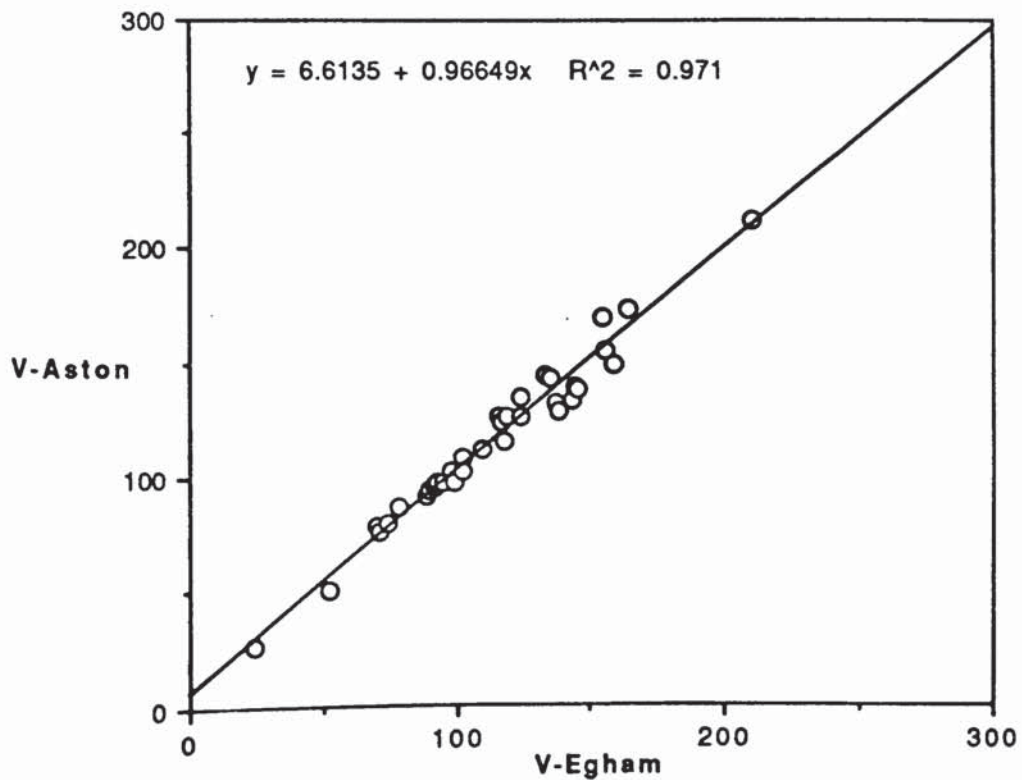


Fig. A.1c

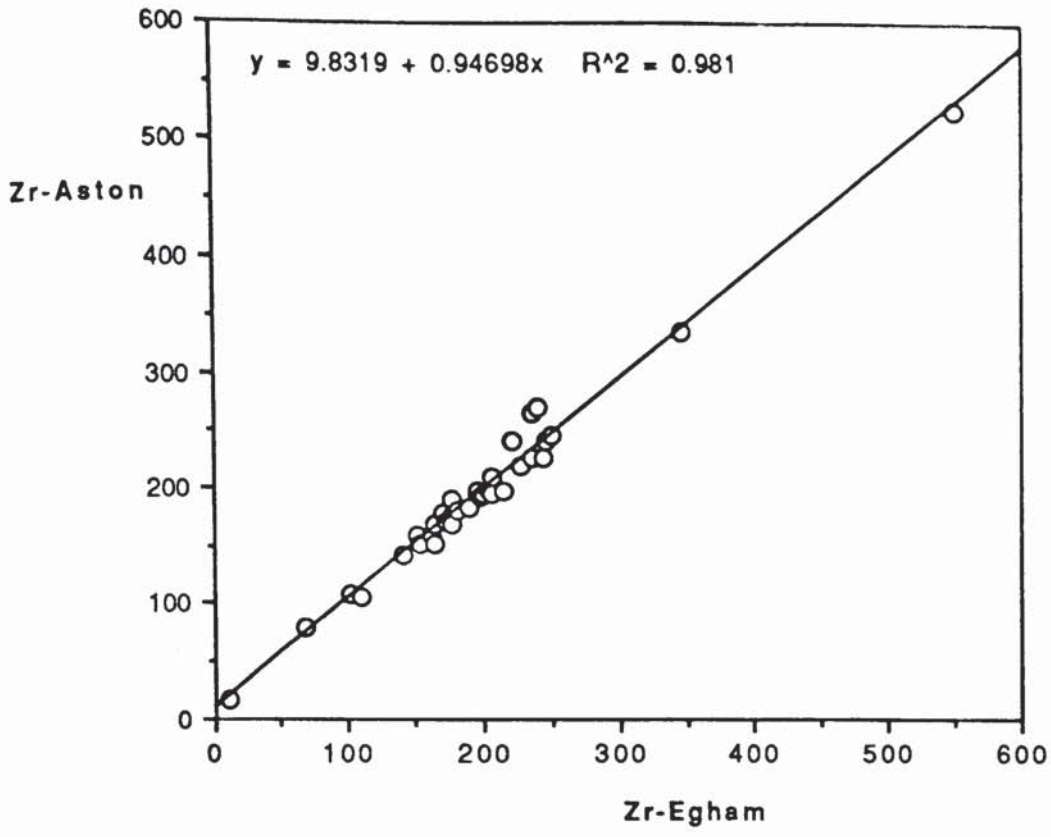


Fig. A.1d

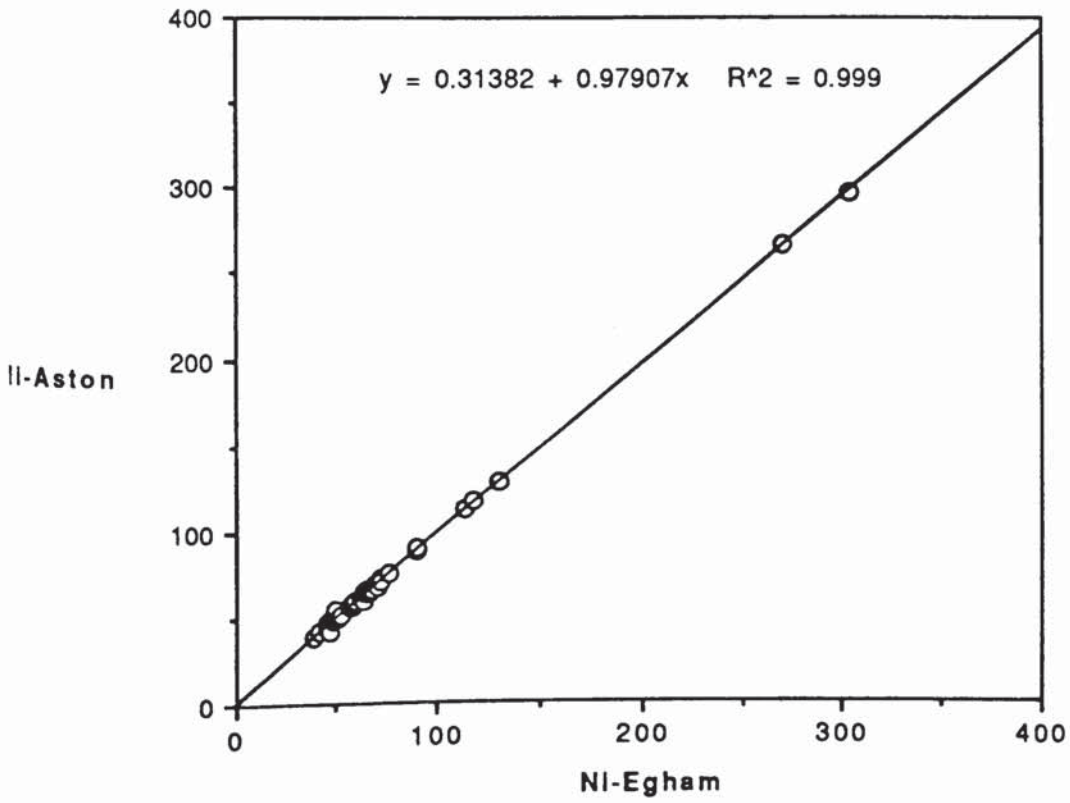


Fig. A.1e

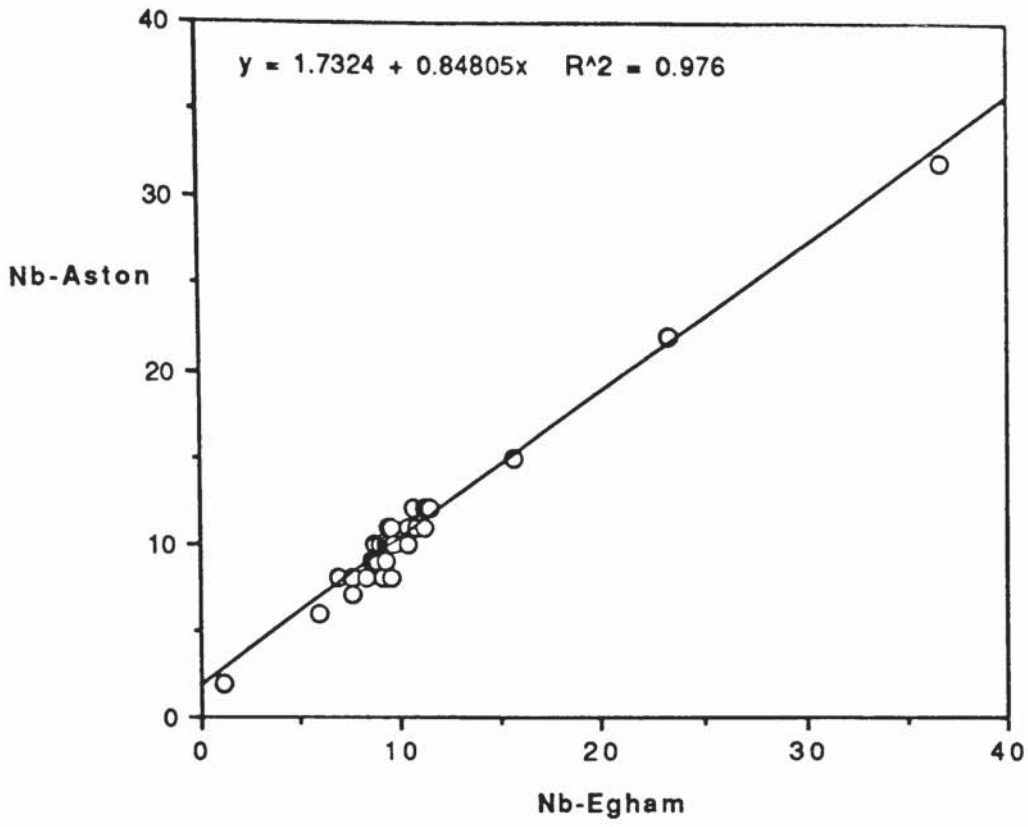


Fig. A.1f

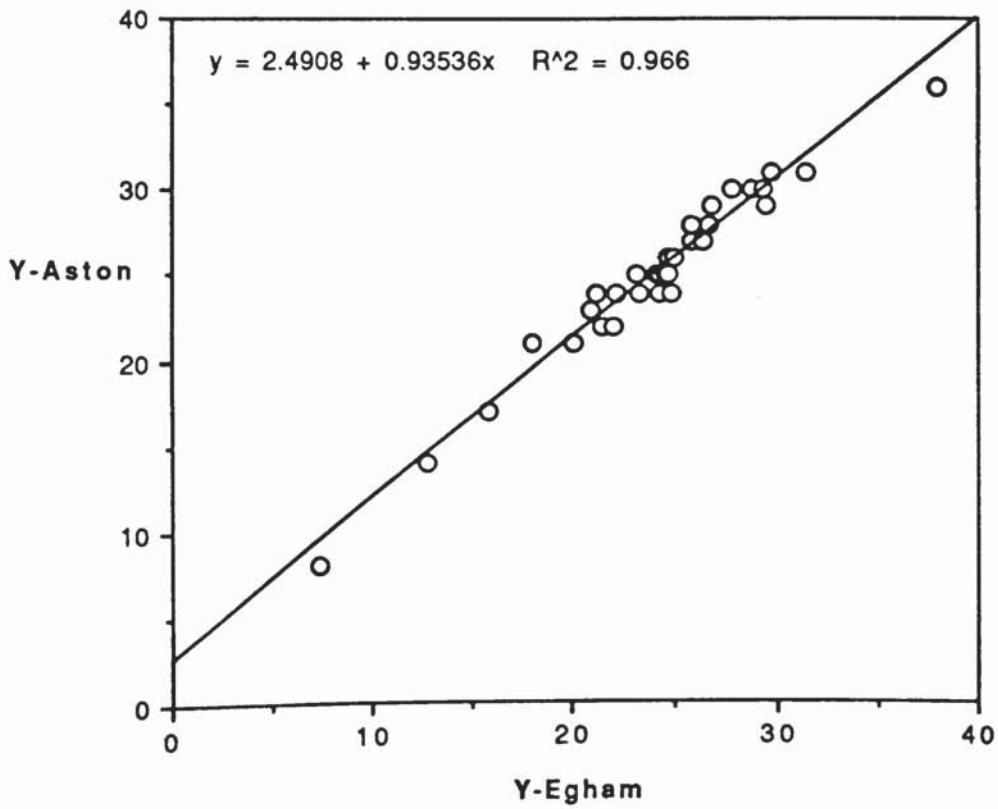


Fig. A.1g

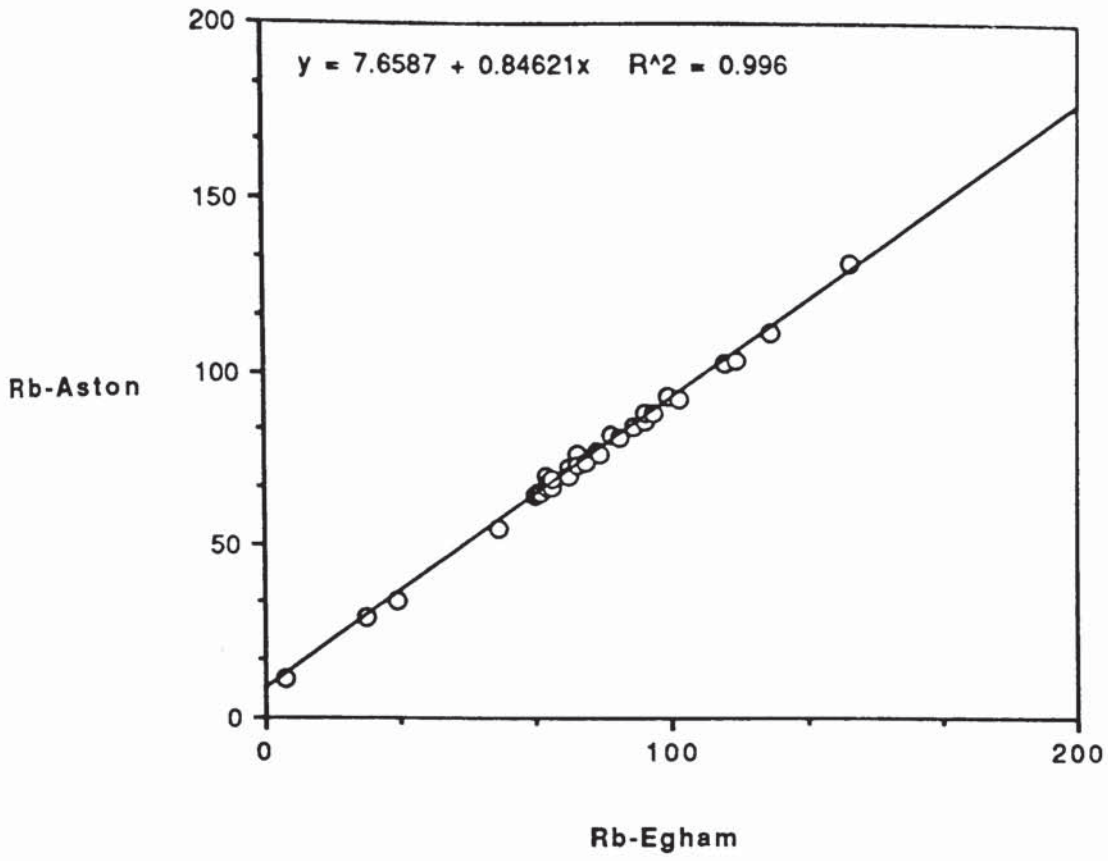


Fig. A.1h

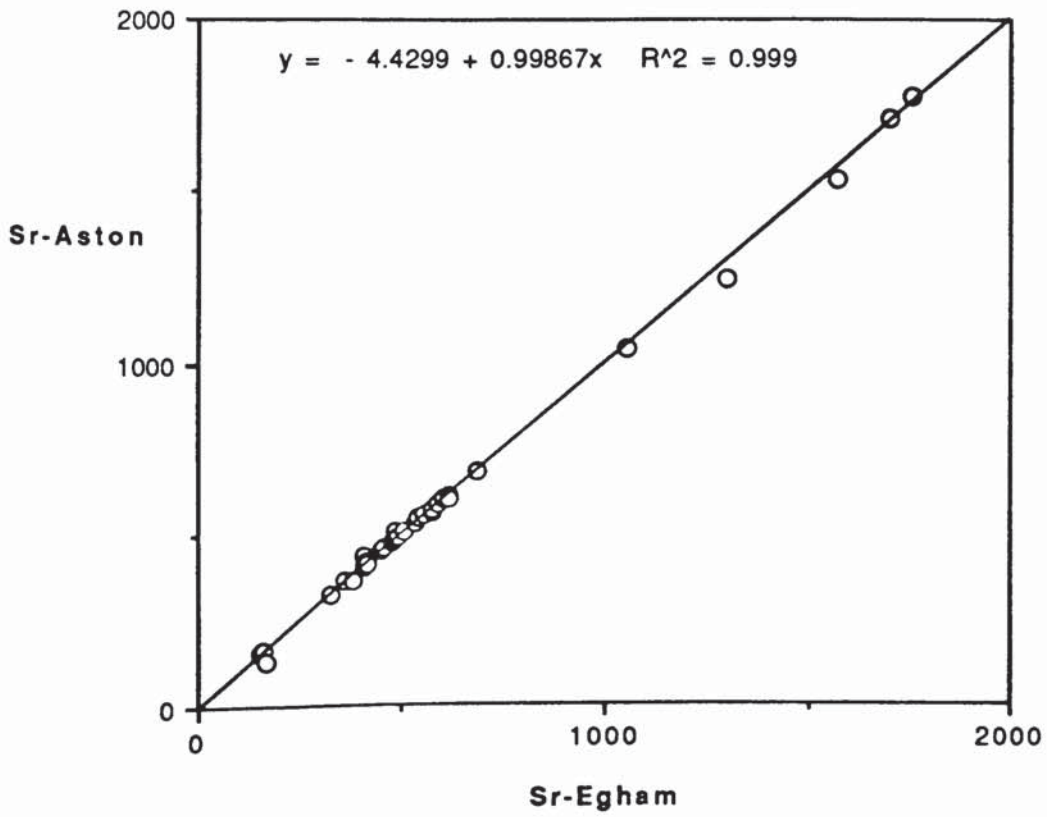


Fig. A.1i

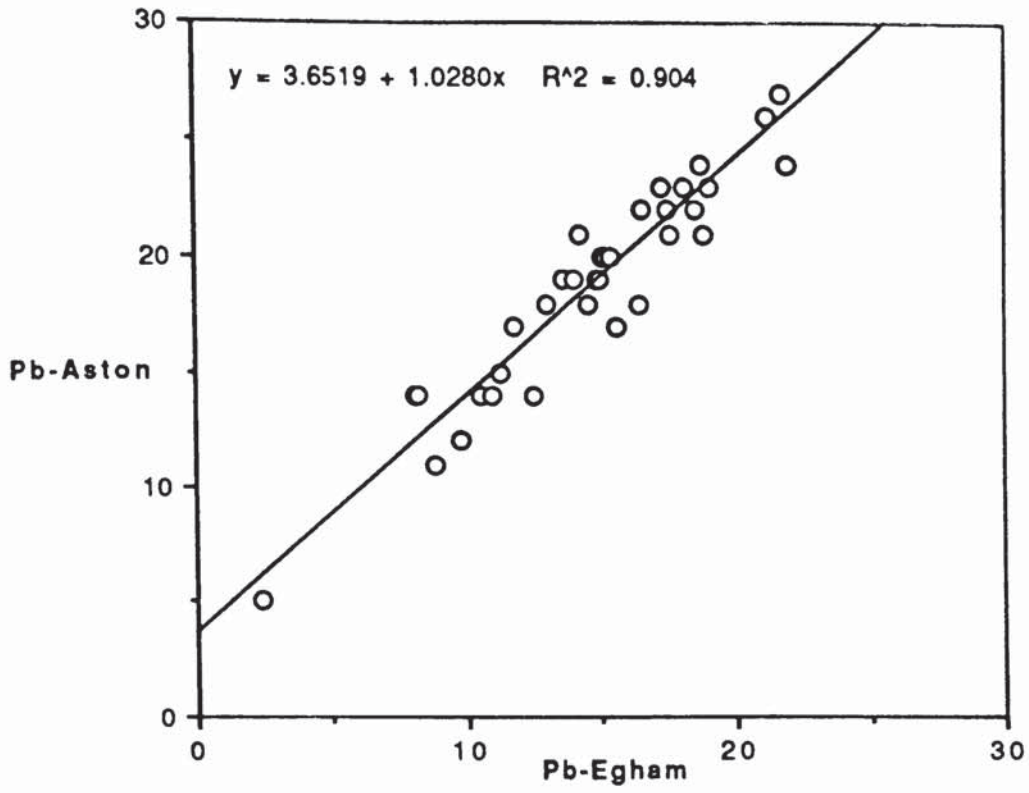


Fig. A.1j

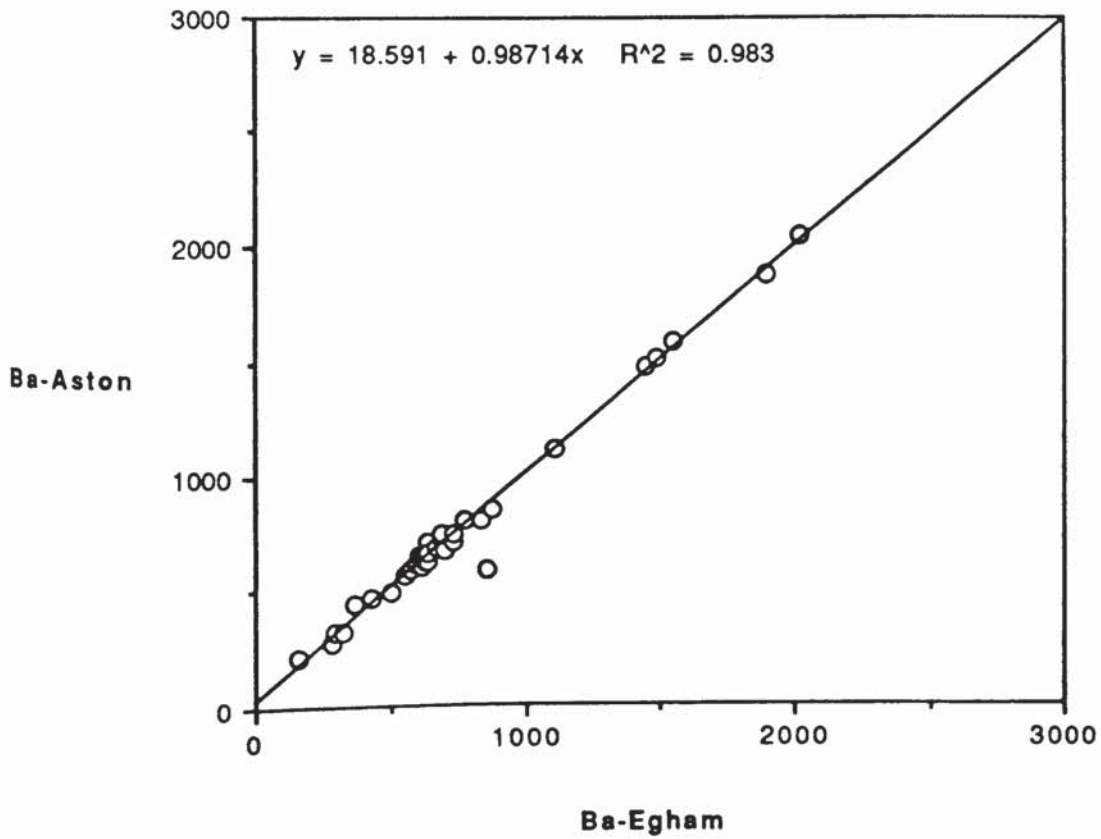


Fig. A.1k

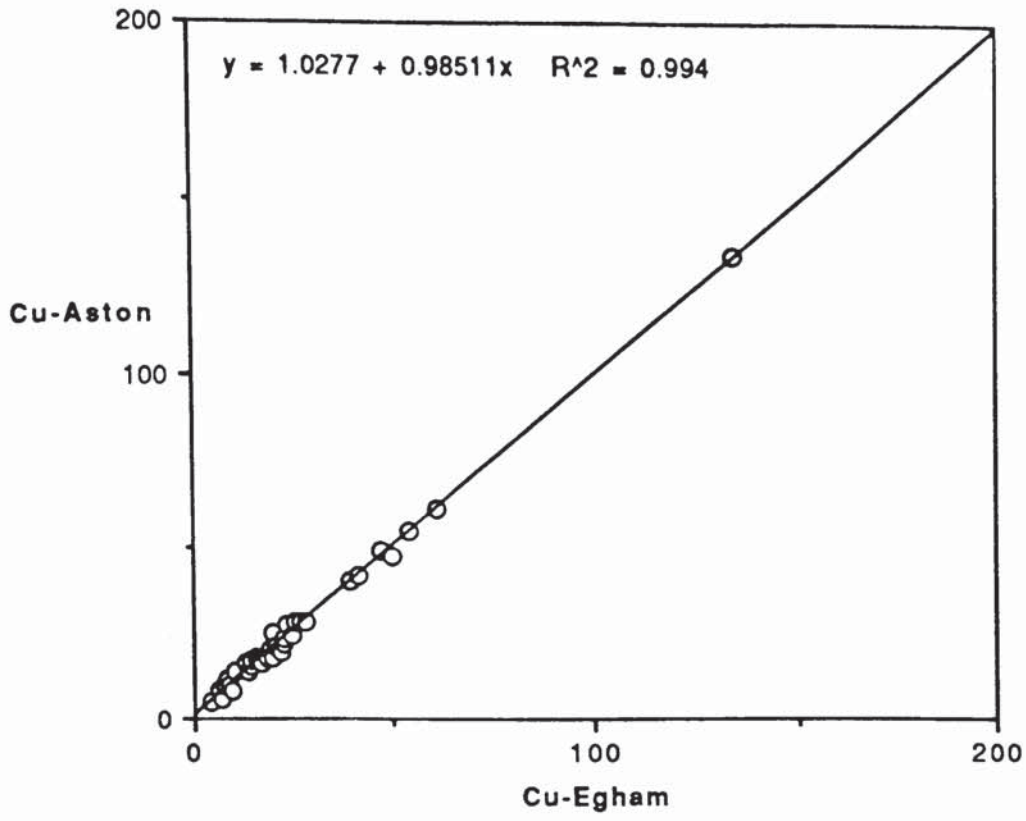


Fig. A.1l

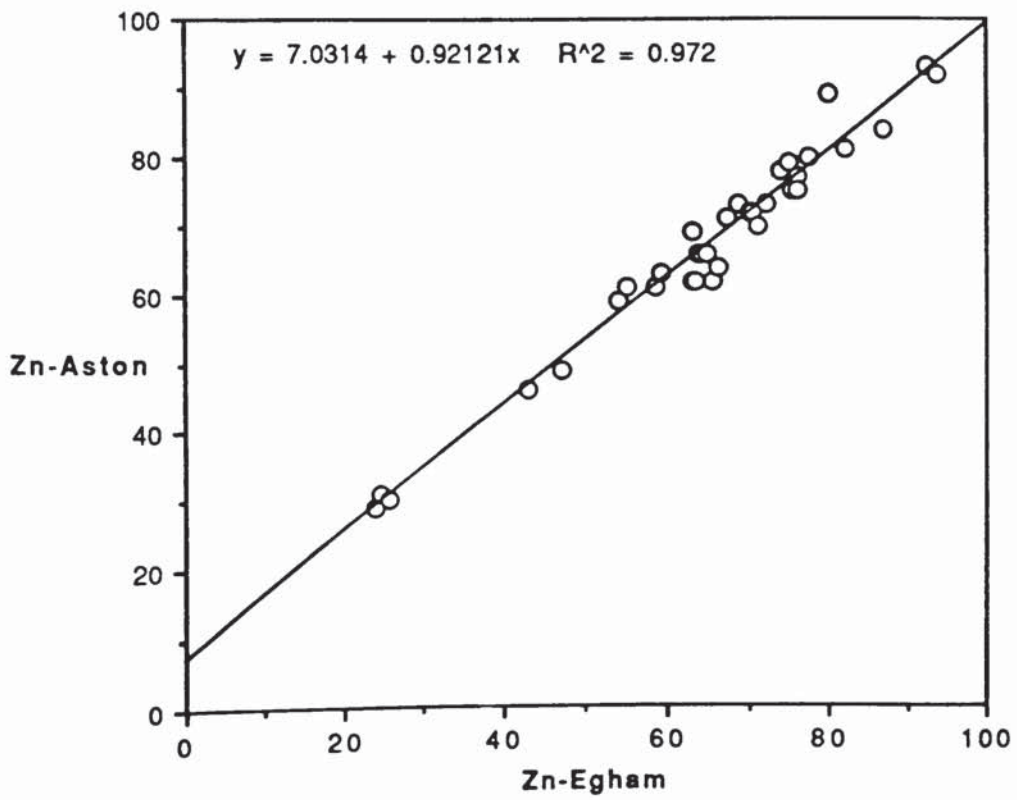


Fig. A.1m

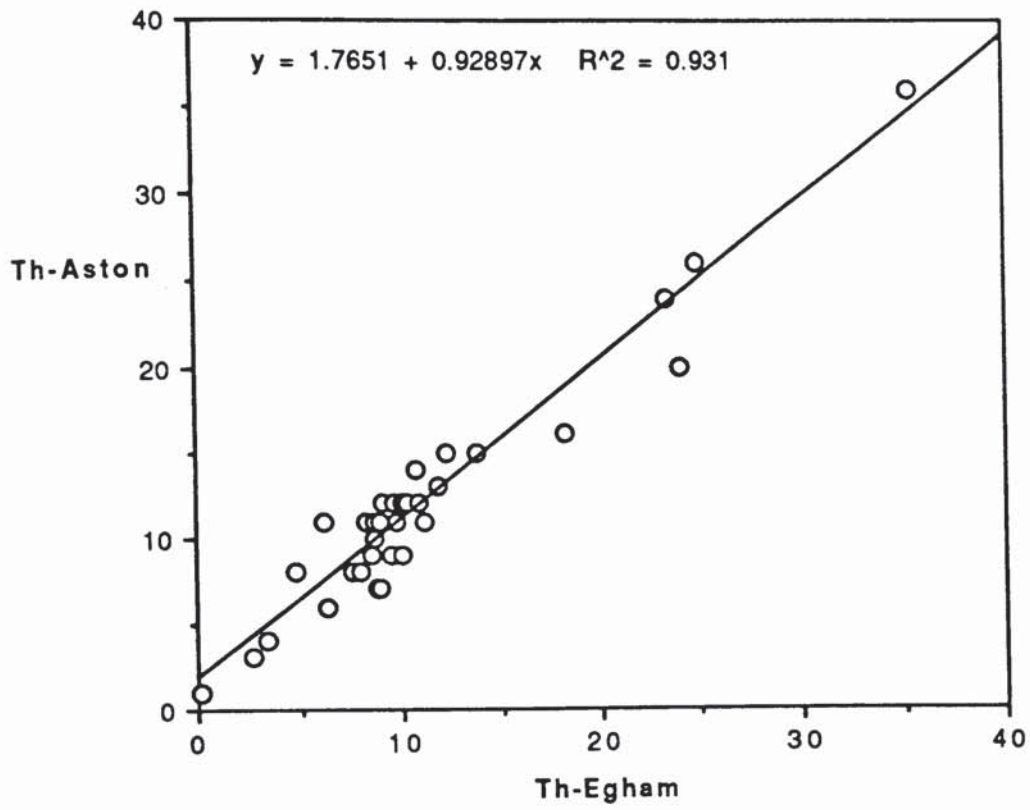


Fig. A.2a

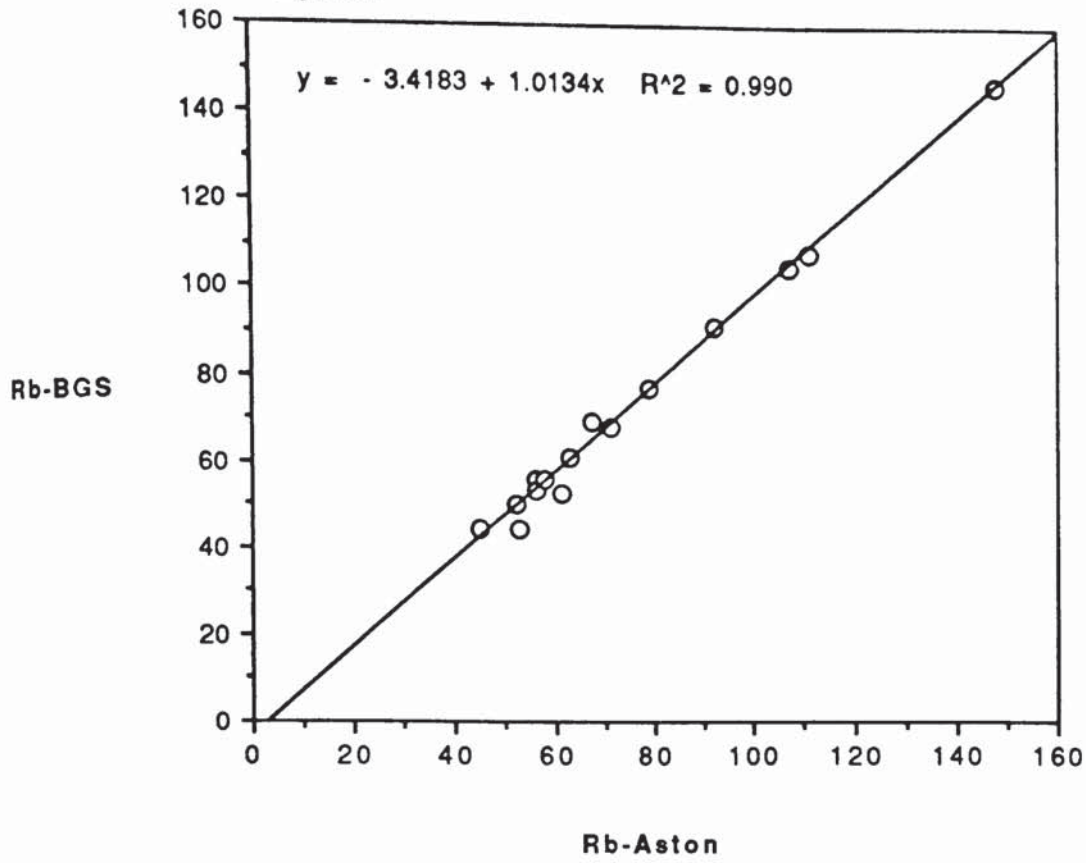


Fig. A.2b

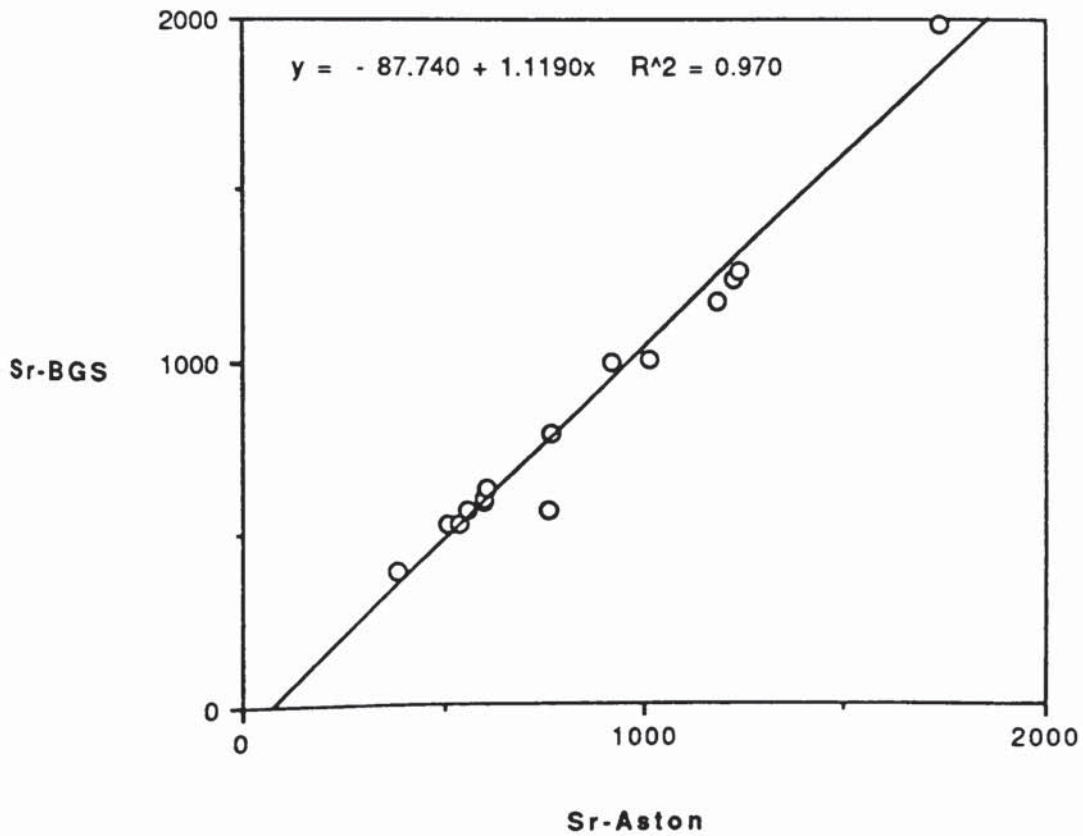


Fig. A.3a

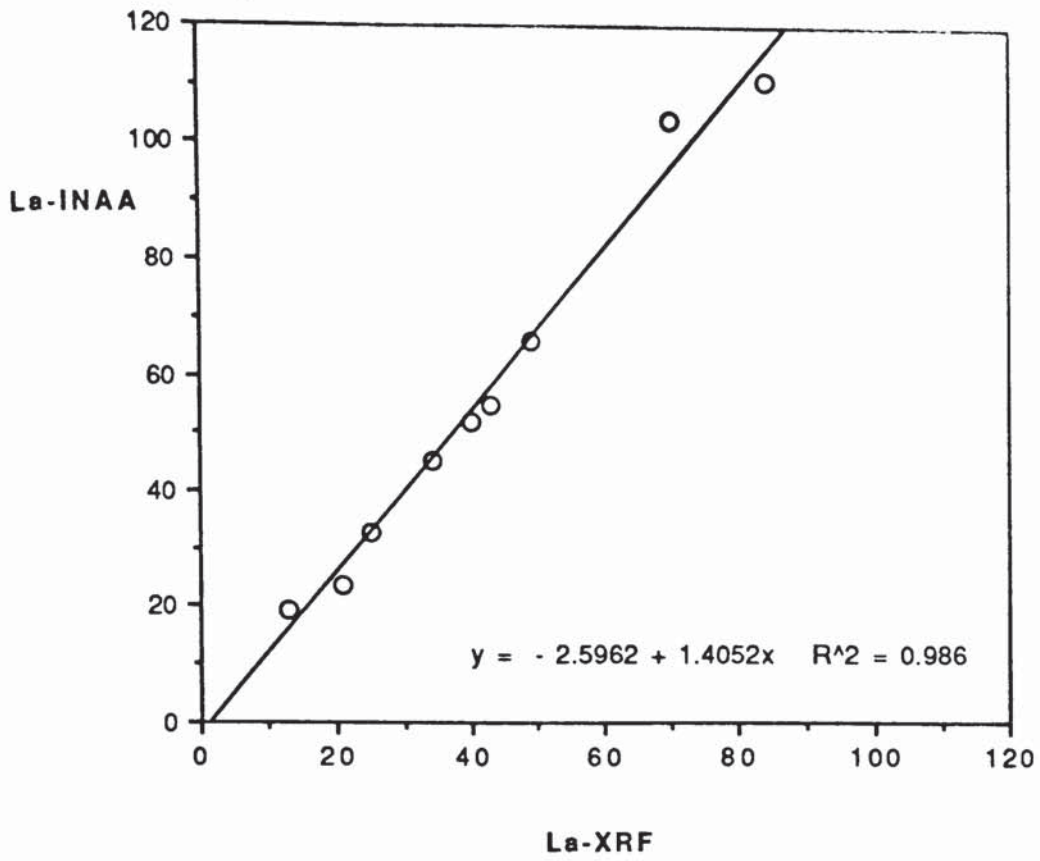


Fig. A.3b

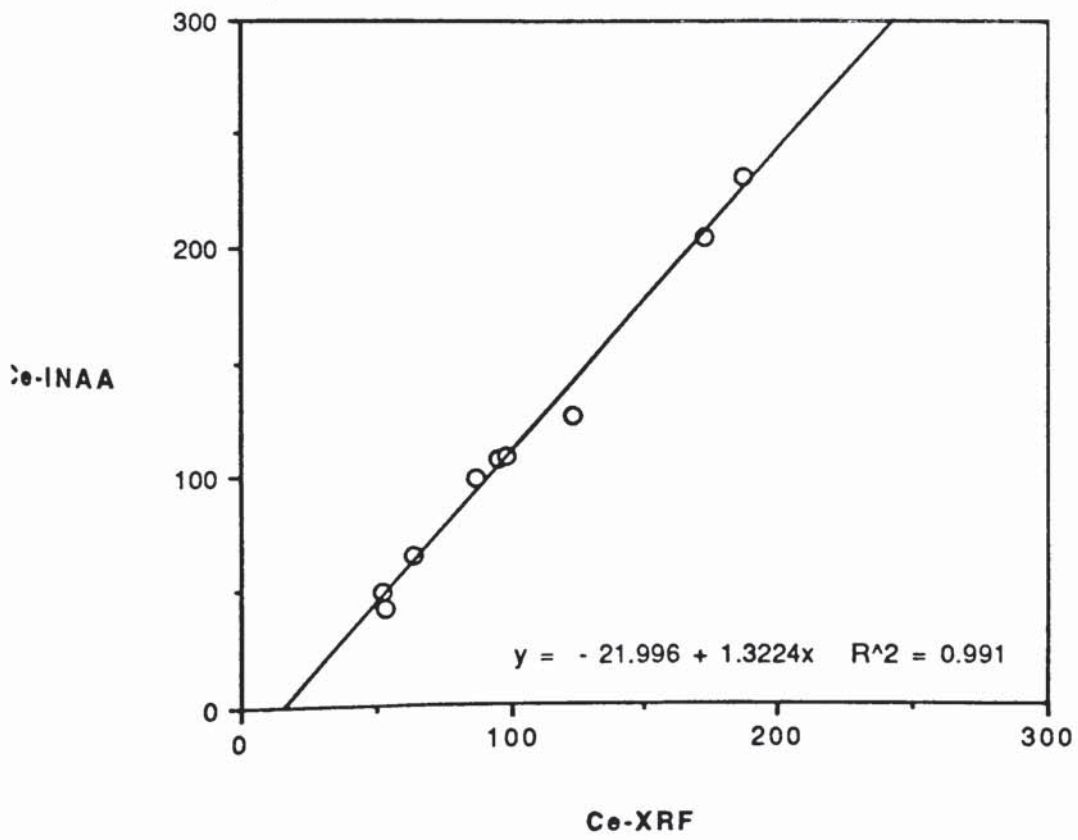


Fig. A.3c

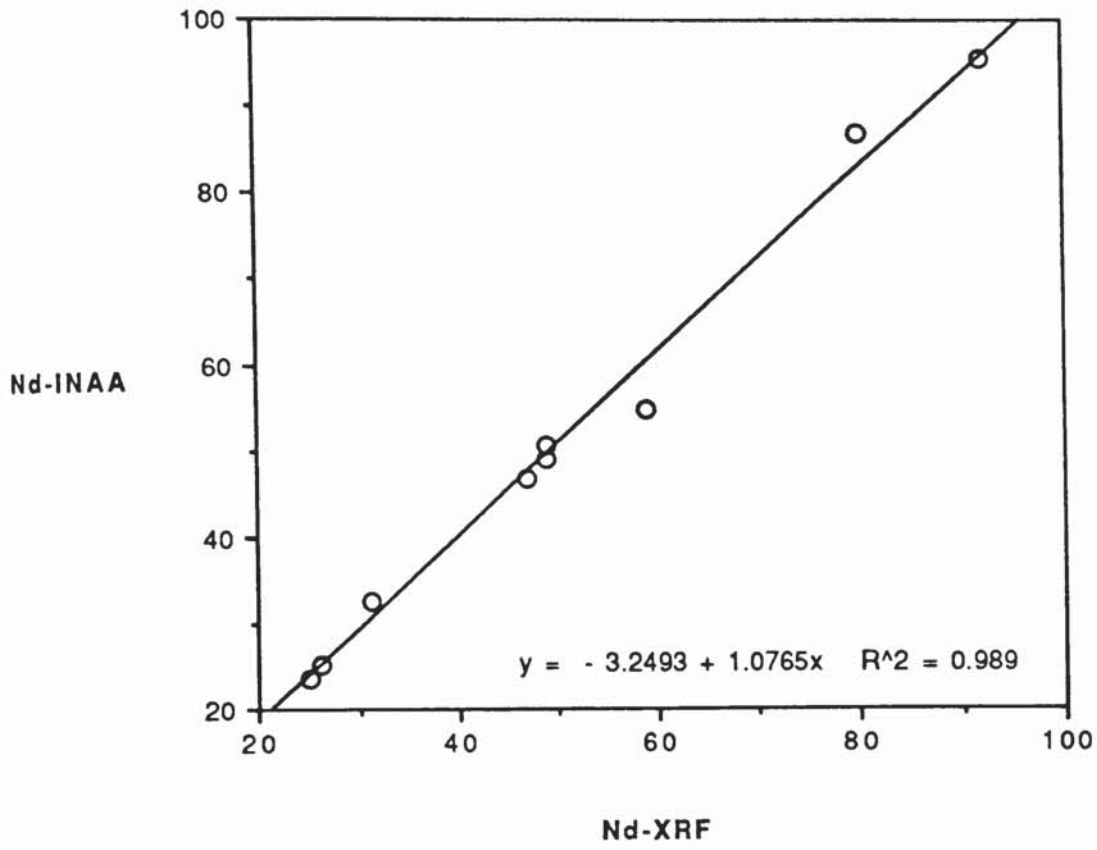


Fig. A.3d

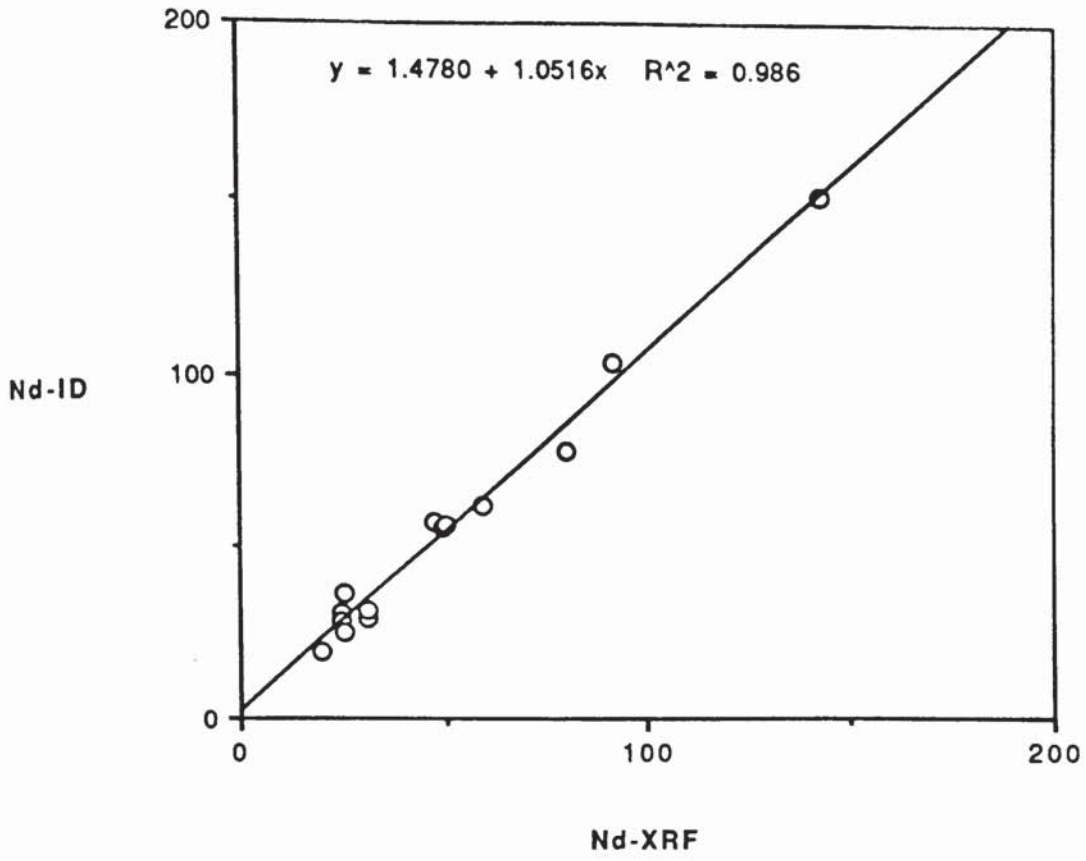


Fig. A.3e

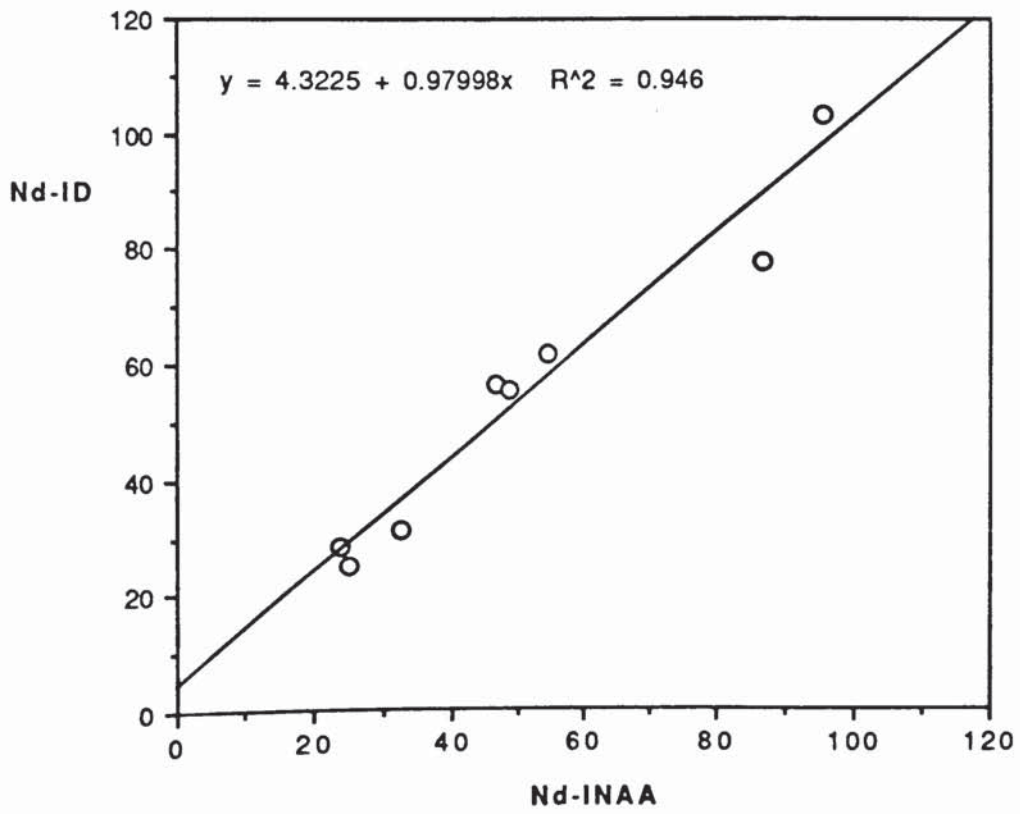
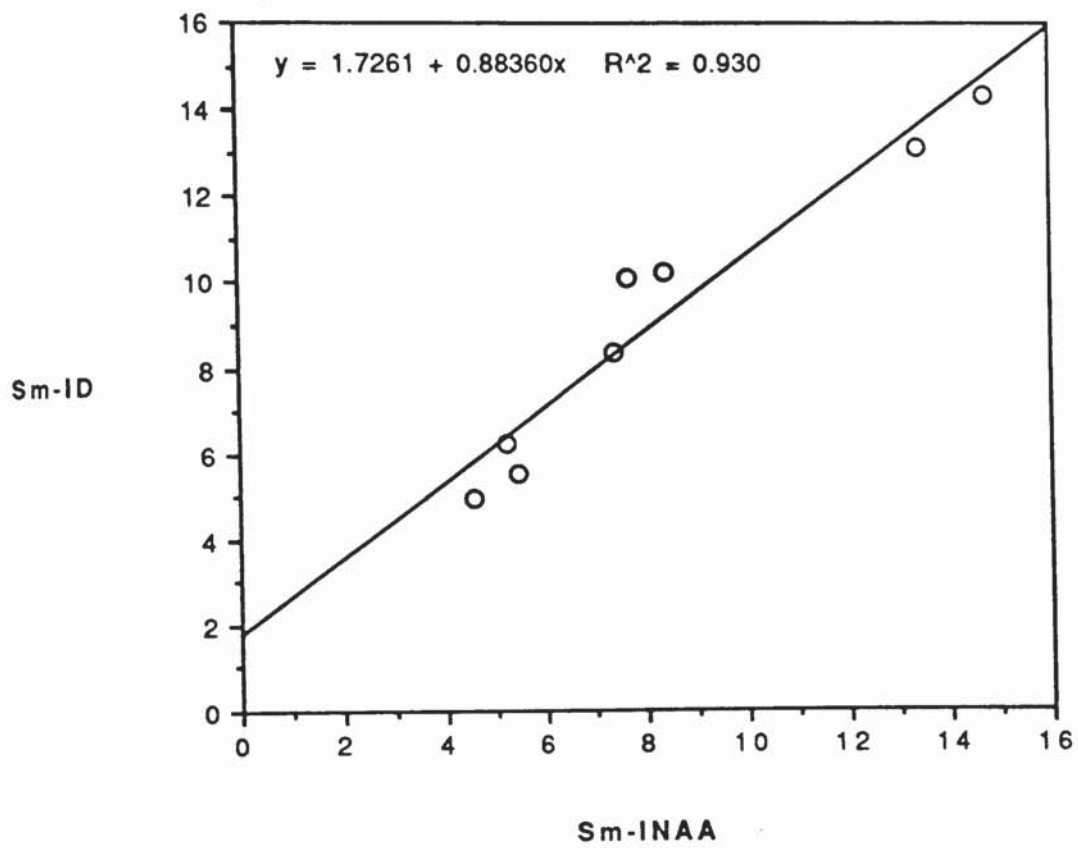


Fig. A.3f



A1.3) Rb-Sr and Sm-Nd isotopes

Sr isotopic determinations were carried out by the author in conjunction with Ms Jane Evans of BGS Isotope Unit. Sm-Nd determinations were carried out by Ms Jane Evans. All isotopic ratios were measured using a V.G 354 mass spectrometer. During the period of the analysis this instrument produced the following values for international standards; NBS 987 $0.710233 \pm 28\text{ppm}$; La Jolla = $0.511833 \pm 19\text{ppm}$. Sm and Nd concentrations were determined by isotope dilution using ^{149}Sm and ^{150}Nd enriched isotopic tracers.

The Rb/Sr ratios, used for initial ratio calculations, were determined at BGS using a Philips automated 1450 XRF spectrometer. The ratios used are averages of analyses of both sides of a powder pellet and are accurate to $\pm 0.5\%$ (1-sigma).

Initial ratios and ϵ values were calculated using the following values:

CHUR	=	0.512640
D _{mur}	=	0.5131
λ ^{147}Sm	=	$6.54 \times 10^{-12}\text{a}^{-1}$
λ ^{87}Rb	=	$1.42 \times 10^{-11}\text{a}^{-1}$
$^{147}\text{Sm}/^{144}\text{Nd}_{\text{chur}}$	=	0.1967
$^{147}\text{Sm}/^{144}\text{Nd}_{\text{dmur}}$	=	0.225
$^{87}\text{Rb}/^{86}\text{Sr}_{\text{bulk}}$	=	0.0839
$^{87}\text{Sr}/^{86}\text{Sr}_{\text{bulk}}$	=	0.7045

A1.4) Instrumental neutron activation analysis

A selected subset of samples were analysed by INAA at the Open University for rare earth elements. This was done for me by Dr N.W. Rogers using the techniques outlined in Paul *et al.* (1975).

A1.5) Electron Microprobe analysis

All analyses were carried out on a Cameca Camebax WDS electron microprobe at the University of Edinburgh by Dr D. Rae. The beam (faraday) current was 25nA at 20 kV with time on peak of 20 seconds with 10 seconds on background. All analyses were taken with a fully focussed beam except for some micas which were taken with a rastering beam to avoid beam damage to the sample.

A full range of synthetic and natural standards were used and full ZAF corrections applied. Analyses were computer-processed with micas recalculated to 22 oxygens, amphiboles recalculated to 23 oxygens and pyroxenes recalculated to 6 oxygens. The oxygen equivalent of fluorine was calculated based on: $O=F = \text{wt}\%F(\text{at.wt.O}/2*\text{at.wt.F})$.

The detection limits were of the order of 100-200 ppm.

A1.6) References for analytical methods:

Jenkins, R. ; Gould, R.W & Gedcke, D. 1981. Quantitative x-ray spectrometry. Marcel Decker Inc. New York.

Kikkert, J.N. 1981. Accurate geochemical analysis of samples of unknown composition. Proceedings of the 31st. Annual Denver X-ray conference.

Norrish, K. and Hutton, J.T. 1969. An accurate X-ray spectrographic method for the analysis of a wide range of geological samples. *Geochim.Cosmochim.Acta.* 33, 431–453

Paul, D. K., Potts, P.J., Gibson, I.L and Hains, P. G. 1975. Rare-earth abundances in Indian kimberlite. *Earth Planet.Sci.Lett.* 25, 151–158

Appendix B

Hornblende lamprophyres of the Criffell dyke swarm

Samples	1295	1302	1305	1306	1308	1313	1314
SiO ₂	60.77	55.87	56.47	56.92	56.75	47.19	58.31
TiO ₂	0.91	1.20	1.25	1.18	1.20	2.11	0.90
Al ₂ O ₃	16.68	15.65	15.47	15.68	15.59	14.58	14.90
Fe ₂ O ₃	5.26	7.32	7.36	7.41	7.31	10.37	6.88
MgO	5.22	7.54	8.02	7.55	7.70	9.02	7.77
CaO	2.71	5.61	4.71	4.85	4.91	9.52	5.29
Na ₂ O	4.74	3.56	3.44	3.40	3.54	2.57	3.38
K ₂ O	3.32	2.68	2.70	2.45	2.45	2.80	2.19
P ₂ O ₅	0.31	0.46	0.46	0.46	0.45	1.73	0.26
MnO	0.08	0.11	0.11	0.10	0.10	0.11	0.12
LOI	2.89	3.05	3.60	6.47	3.95	2.47	3.71
DX	66.12	48.16	48.78	48.81	48.88	38.11	48.71
MG#	73.73	74.43	75.50	74.24	74.88	71.11	76.16
Qz	6.22	2.02	3.49	5.32	4.29	0.00	7.06
Ab	40.22	30.23	29.26	28.93	30.08	21.03	28.69
Or	19.69	15.90	16.03	14.57	14.51	16.63	12.96
An	11.46	18.92	18.88	20.37	19.53	20.16	19.15
Di	0.00	4.81	1.24	0.60	1.57	12.76	4.37
Hy	16.49	21.49	24.37	23.59	23.42	0.00	22.37
Ol	0.00	0.00	0.00	0.00	0.00	16.29	0.00
Mt	2.30	3.20	3.22	3.24	3.20	4.54	3.01
Il	1.74	2.29	2.38	2.26	2.29	4.04	1.72
Ap	0.72	1.07	1.08	1.07	1.06	4.04	0.61
Cm	1.11	0.00	0.00	0.00	0.00	0.00	0.00
Ne	0.00	0.00	0.00	0.00	0.00	0.45	0.00
Ni	76	209	216	216	212	15	225
V	147	150	152	167	160	292	144
Cr	106	343	398	406	403	7	417
Rb	82	55	56	61	47	71	63
Sr	671	903	762	776	796	579	381
Ba	1021	908	786	1406	1077	1201	613
U	3	5	2	3	3	2	2
Th	9	12	14	10	13	4	8
Zn	58	65	77	68	70	70	68
Cu	21	22	16	20	52	65	36
Pb	8	19	15	21	16	17	9
Zr	159	211	213	203	211	142	138
Nb	8	14	14	13	14	9	8
Y	17	20	20	21	20	29	19
La	27	50	49	51	49	14	14
Ce	70	114	123	119	115	50	35
Nd	36	57	59	57	54	31	20

Samples	1315	1317	1318	1320	1323	1325	1326
SiO2	58.85	58.27	58.33	56.91	53.50	54.07	55.27
TiO2	0.89	0.90	0.89	0.80	1.00	0.96	1.11
Al2O3	15.19	15.31	15.28	15.47	13.52	14.70	14.53
Fe2O3	6.54	6.50	6.28	6.39	8.57	8.56	7.30
MgO	7.33	7.32	7.17	8.68	8.79	10.46	8.40
CaO	4.83	4.84	5.06	4.97	8.79	5.75	7.32
Na2O	3.53	3.78	4.18	3.02	2.94	3.54	3.25
K2O	2.48	2.67	2.37	3.39	2.34	1.62	2.14
P2O5	0.26	0.32	0.32	0.27	0.44	0.21	0.53
MnO	0.11	0.11	0.11	0.10	0.13	0.14	0.13
LOI	4.61	4.73	4.85	5.00	6.09	4.13	2.36
DX	51.71	52.59	53.39	48.08	38.85	39.68	42.53
MG#	76.03	76.09	76.35	79.33	74.35	77.56	76.49
Qz	7.07	4.69	3.79	2.32	0.00	0.00	2.18
Ab	29.95	32.09	35.52	25.64	24.96	30.09	27.63
Or	14.70	15.82	14.07	20.12	13.89	9.60	12.72
An	18.39	17.02	15.98	18.72	16.91	19.60	18.83
Di	3.12	3.97	5.69	3.41	19.21	6.11	11.30
Hy	21.54	21.05	19.69	24.78	15.83	25.22	20.75
Ol	0.00	0.00	0.00	0.00	2.46	3.26	0.00
Mt	2.86	2.84	2.75	2.79	3.75	3.74	3.19
Il	1.70	1.72	1.70	1.53	1.91	1.84	2.12
Ap	0.62	0.74	0.74	0.62	1.01	0.49	1.23
Cm	0.00	0.00	0.00	0.00	0.00	0.00	0.00
Ne	0.00	0.00	0.00	0.00	0.00	0.00	0.00
Ni	204	232	212	250	100	309	231
V	142	129	127	184	227	180	150
Cr	381	391	383	445	403	593	394
Rb	79	69	50	67	72	35	51
Sr	315	383	334	742	479	515	647
Ba	1299	734	596	1875	1387	645	714
U	2	2	2	3	4	3	3
Th	5	8	5	5	5	5	10
Zn	68	65	60	71	77	71	77
Cu	23	4	9	136	21	68	35
Pb	32	8	7	20	13	16	29
Zr	139	159	157	153	123	109	193
Nb	9	10	9	8	8	7	14
Y	19	19	18	16	21	18	23
La	12	16	16	27	14	19	56
Ce	42	42	39	56	33	48	128
Nd	18	23	21	33	21	24	68

Samples	1327	1329	1332	1333	1334	1335	1337
SiO2	53.09	52.70	61.64	59.35	59.91	59.84	53.34
TiO2	1.05	1.08	0.67	0.96	0.84	0.84	1.00
Al2O3	13.75	13.70	15.05	16.65	16.33	15.69	13.79
Fe2O3	8.91	9.09	5.60	6.88	6.04	5.80	8.50
MgO	8.75	9.08	7.13	5.08	6.53	7.55	8.40
CaO	7.43	8.10	2.43	4.09	3.70	4.00	7.72
Na2O	3.44	2.95	3.83	4.39	3.72	3.81	3.17
K2O	2.98	2.70	3.28	2.25	2.57	2.11	3.49
P2O5	0.47	0.47	0.28	0.26	0.29	0.26	0.47
MnO	0.15	0.13	0.10	0.09	0.08	0.10	0.13
LOI	2.41	2.12	3.41	5.92	4.29	3.03	3.25
DX	46.94	41.14	61.84	58.04	56.50	53.53	47.70
MG#	73.54	73.86	78.26	67.65	75.34	78.66	73.64
Qz	0.00	0.00	9.86	7.47	9.71	8.70	0.00
Ab	29.27	25.09	32.53	37.26	31.55	32.32	26.99
Or	17.67	16.05	19.44	13.32	15.24	12.52	20.71
An	13.37	16.29	10.27	18.64	16.50	18.18	13.18
Di	16.51	16.86	0.00	0.00	0.00	0.00	17.77
Hy	4.46	11.06	22.01	17.59	20.60	22.98	3.59
Ol	11.66	7.47	0.00	0.00	0.00	0.00	10.98
Mt	3.90	3.98	2.44	3.01	2.64	2.53	3.72
Il	2.00	2.06	1.27	1.83	1.60	1.61	1.92
Ap	1.09	1.08	0.64	0.61	0.67	0.60	1.09
Cm	0.00	0.00	1.45	0.21	1.43	0.51	0.00
Ne	0.00	0.00	0.00	0.00	0.00	0.00	0.00
Ni	98	98	188	118	175	193	92
V	222	221	115	149	122	120	225
Cr	364	382	326	232	274	344	355
Rb	81	58	89	82	75	57	94
Sr	501	560	297	447	466	537	481
Ba	998	913	732	525	856	435	1448
U	3	2	3	2	4	3	4
Th	4	8	8	6	8	7	5
Zn	75	73	85	68	67	65	69
Cu	78	113	1	2	16	20	26
Pb	11	11	7	9	9	8	9
Zr	132	131	143	154	152	153	135
Nb	8	8	7	9	9	9	8
Y	24	25	15	18	16	17	22
La	17	16	16	19	21	19	17
Ce	42	41	34	49	52	46	43
Nd	24	25	20	22	21	24	22

Samples	1346	1355	1360	1363	1365	1367	1380
SiO2	58.77	52.43	61.55	56.08	55.34	52.60	51.17
TiO2	0.82	1.28	0.78	1.11	1.26	1.80	1.76
Al2O3	14.57	16.23	15.66	15.17	16.17	14.34	16.54
Fe2O3	6.28	8.36	5.60	7.39	7.33	8.49	9.42
MgO	6.96	8.50	4.72	7.86	7.09	10.33	9.66
CaO	5.98	5.73	4.09	5.69	5.63	6.72	6.20
Na2O	3.36	2.75	4.07	3.27	3.85	2.81	3.12
K2O	2.89	4.16	3.19	2.97	2.83	2.43	1.65
P2O5	0.27	0.45	0.24	0.36	0.39	0.34	0.37
MnO	0.11	0.12	0.10	0.10	0.13	0.13	0.12
LOI	4.83	4.70	2.50	2.96	3.27	3.40	3.94
DX	51.88	48.05	63.00	47.58	49.48	38.32	36.32
MG#	75.82	74.19	70.44	75.06	73.23	77.49	74.37
Qz	6.23	0.00	9.52	2.22	0.00	0.00	0.00
Ab	28.53	23.37	34.56	27.76	32.72	23.89	26.51
Or	17.12	24.67	18.92	17.61	16.76	14.43	9.82
An	16.22	19.79	15.10	18.07	18.60	19.47	26.44
Di	9.36	4.65	2.97	6.30	5.52	9.39	1.65
Hy	17.53	8.88	14.38	21.78	19.53	20.75	21.76
Ol	0.00	11.42	0.00	0.00	0.30	4.07	5.43
Mt	2.74	3.66	2.44	3.23	3.20	3.72	4.13
Il	1.56	2.45	1.48	2.13	2.40	3.44	3.36
Ap	0.63	1.04	0.55	0.84	0.90	0.78	0.86
Cm	0.00	0.00	0.00	0.00	0.00	0.00	0.00
Ne	0.00	0.00	0.00	0.00	0.00	0.00	0.00
Ni	209	195	95	192	161	259	181
V	125	183	134	152	147	257	166
Cr	378	302	152	347	302	493	370
Rb	70	110	79	57	58	53	45
Sr	557	562	535	594	599	757	554
Ba	933	1006	684	574	812	864	376
U	3	3	4	4	2	2	3
Th	8	8	7	7	4	4	4
Zn	56	69	62	67	59	66	78
Cu	38	85	21	34	33	38	43
Pb	7	8	13	13	10	8	7
Zr	139	189	160	168	194	140	226
Nb	9	13	10	9	12	10	10
Y	19	22	18	20	19	24	28
La	27	23	17	16	15	12	13
Ce	55	65	42	39	44	38	53
Nd	29	31	22	16	26	25	25

Samples	1381	1296C	1296M	1301N	1379A	1379B	BP11
SiO2	55.18	57.32	59.12	55.50	56.50	59.63	47.47
TiO2	0.95	0.99	1.24	1.26	1.11	0.93	1.36
Al2O3	15.73	15.55	15.18	15.02	15.49	15.74	12.29
Fe2O3	7.43	7.10	6.05	7.54	7.15	6.39	9.30
MgO	8.86	7.46	5.80	7.96	7.71	6.16	13.43
CaO	5.10	4.82	4.10	6.34	6.28	4.82	10.33
Na2O	3.55	4.20	3.77	3.32	3.37	3.39	1.77
K2O	2.69	2.17	3.98	2.45	1.99	2.54	2.63
P2O5	0.39	0.28	0.67	0.51	0.26	0.27	1.26
MnO	0.12	0.11	0.08	0.11	0.14	0.13	0.15
LOI	3.42	3.46	3.19	3.88	3.38	3.92	3.16
DX	46.14	51.24	61.08	45.28	45.06	53.67	30.44
MG#	77.11	74.83	73.07	74.89	75.32	73.16	80.33
Qz	0.00	2.72	5.47	2.54	4.58	9.84	0.00
Ab	30.20	35.64	32.03	28.23	28.66	28.75	14.53
Or	15.94	12.88	23.59	14.51	11.81	15.07	15.63
An	19.16	17.27	12.79	18.97	21.36	20.35	17.96
Di	2.96	3.90	2.58	7.39	6.53	1.48	20.08
Hy	24.49	21.87	16.92	21.42	21.14	19.24	0.00
Ol	1.21	0.00	0.00	0.00	0.00	0.00	21.87
Mt	3.25	3.10	2.64	3.30	3.13	2.79	4.07
Il	1.82	1.89	2.36	2.40	2.12	1.77	2.60
Ap	0.90	0.65	1.56	1.18	0.61	0.64	2.94
Cm	0.00	0.00	0.00	0.00	0.00	0.00	0.00
Ne	0.00	0.00	0.00	0.00	0.00	0.00	0.28
Ni	228	182	90	210	146	123	328
V	160	127	242	144	178	142	209
Cr	435	320	187	360	420	337	525
Rb	67	52	81	44	45	64	71
Sr	601	596	1206	758	579	496	1738
Ba	762	483	1751	662	771	830	2114
U	4	2	4	3	2	3	4
Th	7	4	16	12	5	8	27
Zn	146	65	70	63	70	69	133
Cu	33	43	140	16	19	40	111
Pb	14	7	18	13	15	25	45
Zr	163	157	188	220	156	170	192
Nb	10	8	11	15	9	9	16
Y	20	18	15	21	20	20	25
La	25	21	54	55	19	20	142
Ce	64	52	124	127	41	51	313
Nd	31	26	58	59	23	20	143

Samples	BP19	BP21	BSM01	BSMPD01	CC18	CC20	CC20B
SiO2	57.15	55.06	49.71	55.92	55.40	53.90	54.40
TiO2	1.15	1.26	1.72	0.86	1.49	1.44	1.45
Al2O3	14.88	15.16	15.42	16.61	17.87	15.21	15.50
Fe2O3	6.30	7.25	8.72	7.94	6.55	8.14	7.95
MgO	6.66	8.42	8.74	5.60	6.28	9.11	9.17
CaO	5.49	5.59	8.26	6.47	3.37	6.23	5.10
Na2O	2.98	2.96	3.46	4.20	5.83	3.13	3.30
K2O	4.74	3.63	2.92	2.00	2.29	2.30	2.61
P2O5	0.54	0.57	0.90	0.24	0.82	0.43	0.41
MnO	0.10	0.09	0.14	0.15	0.10	0.11	0.10
LOI	1.67	2.22	3.50	3.24	4.88	2.43	2.62
DX	55.35	47.00	44.13	49.26	63.07	40.62	43.63
MG#	74.94	76.67	73.93	66.60	73.07	76.01	76.53
Qz	1.93	0.32	0.00	1.69	0.00	0.41	0.10
Ab	25.30	25.15	23.65	35.72	49.48	26.58	28.02
Or	28.12	21.53	17.36	11.85	13.59	13.63	15.51
An	13.29	17.47	18.05	20.70	11.39	20.82	19.91
Di	8.37	5.31	13.72	8.05	0.00	5.94	2.22
Hy	16.72	23.25	0.00	16.25	8.15	25.26	26.96
Ol	0.00	0.00	14.82	0.00	2.86	0.00	0.00
Mt	2.75	3.17	3.82	3.48	2.84	3.56	3.48
Il	2.20	2.41	3.30	1.65	1.92	2.76	2.77
Ap	1.25	1.31	2.10	0.56	1.66	0.99	0.96
Cm	0.00	0.00	0.00	0.00	5.92	0.00	0.00
Ne	0.00	0.00	3.13	0.00	0.00	0.00	0.00
Ni	188	230	199	57	52	222	208
V	218	235	177	176	215	165	182
Cr	305	408	282	166	79	420	417
Rb	107	92	61	39	37	51	51
Sr	1189	1011	918	759	674	615	659
Ba	1992	1592	1138	1801	469	630	698
U	4	4	4	3	4	4	3
Th	10	10	15	4	20	5	9
Zn	76	83	83	76	46	66	69
Cu	110	53	30	37	30	30	36
Pb	12	12	9	14	10	9	7
Zr	213	203	359	139	312	206	212
Nb	12	14	26	7	22	17	18
Y	16	20	26	23	25	22	23
La	42	40	70	16	65	31	33
Ce	89	95	173	40	153	73	79
Nd	50	47	80	20	69	40	37

Samples	PFT02B	1366
SiO2	48.05	59.04
TiO2	1.47	1.18
Al2O3	14.34	15.53
Fe2O3	10.12	6.88
MgO	11.45	6.65
CaO	8.62	4.37
Na2O	1.57	3.61
K2O	3.42	2.27
P2O5	0.80	0.37
MnO	0.15	0.09
LOI	2.01	3.68
DX	33.69	53.24
MG#	76.19	73.23
Qz	0.00	9.13
Ab	13.34	30.66
Or	20.35	13.46
An	22.16	19.34
Di	12.42	0.00
Hy	4.08	21.15
Ol	18.47	0.00
Mt	4.43	3.01
Il	2.82	2.24
Ap	1.87	0.86
Cm	0.00	0.09
Ne	0.00	0.00
Ni	264	144
V	221	154
Cr	306	307
Rb	148	56
Sr	1445	508
Ba	1641	608
U	5	3
Th	20	7
Zn	131	71
Cu	67	42
Pb	12	5
Zr	200	187
Nb	18	14
Y	26	21
La	105	23
Ce	230	60
Nd	98	31

Mica lamprophyres from the Criffell dyke swarm

Samples	1271	1285	1368	1371	BP22	PFT03	1270
SiO2	51.59	53.89	54.26	50.06	56.08	55.78	52.19
TiO2	0.87	1.36	1.84	0.92	1.25	1.12	0.88
Al2O3	12.64	15.9	16.02	12.33	15.29	14.06	12.65
MgO	12.07	8.61	7.39	14.01	6.99	7.5	9.28
CaO	8.3	3.73	3.46	9.16	5.68	5.97	9.26
Fe2O3	9.94	8.74	8.99	9.27	6.7	6.44	8.52
K2O	3.13	5.36	3.52	1.74	4.48	5.88	4.51
Na2O	0.82	1.55	3.7	1.72	2.83	2.33	1.4
P2O5	0.53	0.75	0.7	0.64	0.59	0.81	1.2
MnO	0.85	0.75	0.13	0.15	0.1	0.1	0.2
LOI	10.6	7.66	4.01	10.91	1.79	1.95	6.89
Mg#0.3	77.45	73.59	69.94	81.04	74.69	76.71	75.47
DX	26.06	47.99	52.73	24.98	52.07	54.61	38.63
Qz	0.47	3	0.32	0	1.45	0	0
Ab	6.99	13.18	31.49	14.63	24.03	19.75	11.87
Or	18.6	31.82	20.92	10.35	26.59	34.86	26.76
An	21.72	13.66	12.68	20.93	15.88	10.63	15.03
Di	12.93	0	0	16.33	6.79	10.97	18.55
Hy	32	27.51	23.94	19.95	18.51	14.63	15.91
Ol	0	3.83	0	10.45	0	2.24	3.6
Mt	4.35	2.61	3.93	4.06	2.93	2.81	3.73
Il	1.66	1.75	3.51	1.76	2.38	2.14	1.69
Ap	1.23	2.59	1.62	1.48	1.38	1.88	2.8
Cm	0	7.66	1.52	0	0	0	0
Ne	0	0	0	0	0	0	0
Ni	371	73	114	381	197	209	295
Cr	771	96	177	866	320	289	682
V	204	226	165	209	230	205	208
Rb	53	124	77	38	111	148	156
Sr	151	232	913	665	1245	1230	575
Ba	1028	1475	2754	2578	2021	2638	4186
U	2	4	3	3	4	7	4
Th	6	8	10	11	13	21	9
Zn	70	80	102	70	70	91	66
Cu	38	31	22	177	114	158	56
Pb	7	13	18	13	12	17	12
Zr	88	169	275	294	214	288	133
Nb	6	9	21	13	14	14	8
Y	17	24	25	21	18	16	20
La	11	21	45	34	43	84	11
Ce	25	63	107	86	98	187	37
Nd	17	33	56	49	49	92	16
Sm	1	4	5	5	4	7	1

Samples	1279C	1279I	1279M	1280	1370
SiO2	52.75	53.96	49.37	54.44	50.44
TiO2	0.95	0.94	1.02	0.97	1.4
Al2O3	14.3	13.89	13.37	12.9	12.89
MgO	8.83	8.63	6.76	11.45	10.41
CaO	5.48	5.42	11.7	5.2	8.37
Fe2O3	10.04	9.48	9.48	8.98	8.84
K2O	4.09	4.24	4.94	3.85	2.55
Na2O	2.33	2.3	2.05	1.01	3.07
P2O5	1.06	0.97	1.11	1.11	1.86
MnO	0.09	0.07	0.07	0.04	0.1
LOI	6.28	5.92	8.77	9.04	9.93
Mg#0.3	71.33	72.04	66.85	78.29	76.9
DX	44.14	45.18	40.77	37.17	41.32
Qz	0	0.45	0	5.7	0
Ab	19.85	19.56	4.3	8.59	26.09
Or	24.29	25.17	29.34	22.88	15.14
An	16.62	15.19	12.77	18.66	13.98
Di	3.02	4.38	30.92	0	12.37
Hy	24.52	26.97	0	35.48	9.47
Ol	2.95	0	6.79	0	12.02
Mt	4.4	4.15	4.15	3.93	3.87
Il	1.82	1.8	1.95	1.85	2.67
Ap	2.47	2.27	2.58	2.58	4.33
Cm	0	0	0	0.28	0
Ne	0	0	7.13	0	0
Ni	87	88	88	227	219
Cr	391	399	405	845	324
V	240	235	241	248	182
Rb	147	154	233	86	55
Sr	433	407	616	186	842
Ba	1227	1336	1970	640	6659
U	2	5	4	6	5
Th	10	10	6	9	25
Zn	69	77	72	64	83
Cu	88	121	107	10	30
Pb	11	15	15	6	13
Zr	118	114	114	123	341
Nb	10	10	8	9	21
Y	24	22	24	21	31
La	16	17	13	12	149
Ce	46	46	38	27	332
Nd	21	31	21	24	205
Sm	6	4	3	3	19

INAA results for Hornblende and Mica lamprophyres from the Criffell dyke swarm

Sample	Hornblende 1296C	Hornblende 1381.00	Hornblende BSM01	Hornblende BP21	Hornblende 1305.00	Hornblende 1380.00	Mica BP22	Mica PFT03	Mica 1371.00
La	23.80	32.60	104.00	52.10	66.10	19.40	55.10	111.00	45.10
Ce	49.00	65.20	205.00	107.00	127.00	42.60	108.00	231.00	98.40
Nd	25.10	32.40	86.70	46.60	54.70	23.60	48.80	95.40	50.50
Sm	4.75	5.47	13.40	7.65	8.38	5.20	7.38	14.70	8.89
Eu	1.34	1.54	3.56	1.93	2.31	1.75	1.88	3.15	2.10
Tb	0.68	0.69	1.23	0.70	0.82	0.81	0.78	1.10	0.81
Yb	1.66	1.64	2.04	1.48	1.68	2.38	1.39	1.25	1.41
Lu	0.25	0.25	0.22	0.20	0.27	0.33	0.23	0.19	0.19
Th	5.15	7.33	14.90	9.68	11.30	3.01	10.70	22.70	9.82
U	1.81	2.80	3.38	2.75	2.28	1.40	3.03	5.20	3.02
Ta	0.60	0.65	1.54	0.73	0.95	0.68	0.75	0.81	0.74
Hf	3.67	4.03	7.82	4.98	4.56	4.67	5.45	7.19	7.60
Rb	53.00	67.00	65.00	102.00	58.00	46.00	110.00	143.00	45.00
Cs	2.78	1.06	0.52	2.38	1.18	1.59	2.55	7.26	1.96
Sc	17.40	18.00	19.60	17.60	18.00	23.40	15.60	14.90	27.00
Co	29.50	34.70	37.20	31.40	32.10	47.50	28.20	30.90	47.90
Cr	312.00	402.00	277.00	391.00	386.00	344.00	310.00	321.00	940.00

Appendix C

Porphyrites from the Criffell dyke swarm

Sample	1252	1254	1255	1258	1261	1263	1272
SiO ₂	67.34	65.46	65.72	66.22	65.47	67.53	68.00
TiO ₂	0.54	0.56	0.56	0.59	0.70	0.50	0.41
Al ₂ O ₃	16.07	16.40	16.66	16.15	16.18	15.85	16.26
Fe ₂ O ₃	3.35	3.78	3.26	3.65	3.88	3.27	2.83
MgO	1.83	2.84	2.35	2.44	2.35	2.05	1.75
CaO	2.97	2.94	3.55	3.10	3.47	2.81	1.82
Na ₂ O	3.74	3.95	4.24	3.92	3.80	3.85	5.44
K ₂ O	3.89	3.74	3.35	3.66	3.68	3.84	3.30
P ₂ O ₅	0.20	0.25	0.27	0.22	0.39	0.23	0.15
MnO	0.06	0.07	0.04	0.05	0.07	0.06	0.04
LOI	3.82	1.71	2.60	1.75	0.95	0.94	1.74
DX	75.90	72.77	72.70	73.54	72.34	76.37	82.37
MG#0.3	60.75	67.98	67.16	65.47	63.17	63.91	63.62
Qz	21.19	17.18	16.94	18.66	18.35	21.03	16.80
Ab	31.72	33.45	35.94	33.24	32.22	32.62	46.06
Or	22.99	22.15	19.82	21.64	21.77	22.72	19.52
An	13.43	13.01	15.86	14.00	14.68	12.43	8.03
Di	0.00	0.00	0.00	0.00	0.00	0.00	0.00
Hy	6.84	9.74	8.00	8.55	8.39	7.38	6.33
Ol							
Mt	1.46	1.65	1.42	1.59	1.69	1.43	1.23
Il	1.03	1.07	1.07	1.12	1.34	0.95	0.78
Ap	0.47	0.57	0.63	0.50	0.90	0.54	0.36
Cm	0.81	1.12	0.26	0.64	0.59	0.82	0.82
Ne							
Ni	36	51	43	49	40	40	36
V	63	87	89	80	74	65	70
Cr	45	71	55	68	61	47	45
Rb	109	94	77	122	120	138	85
Sr	530	781	728	564	771	640	591
Ba	894	923	875	977	967	815	947
U	6	5	4	5	5	5	4
Th	12	13	14	12	12	13	6
Zn	44	42	35	68	60	45	33
Cu	47	16	18	10	28	31	5
Pb	20	14	16	29	26	38	11
Zr	161	182	192	166	192	136	106
Nb	11	12	12	12	12	11	6
Y	12	14	14	13	12	11	8
La	30	41	42	30	47	31	18
Ce	59	90	86	57	92	70	37
Nd	26	37	35	26	39	30	17

Sample	1293	1338	1339	1343	1350	1352	1353
SiO2	64.12	66.22	66.85	66.60	71.04	68.53	67.49
TiO2	0.60	0.57	0.57	0.60	0.38	0.47	0.57
Al2O3	16.39	15.84	16.12	15.82	15.87	16.58	15.95
Fe2O3	4.60	3.82	4.06	3.60	2.50	2.97	3.79
MgO	3.20	2.61	2.03	2.16	1.04	1.52	2.11
CaO	3.97	3.10	3.11	3.51	1.73	1.03	2.46
Na2O	5.53	4.28	4.16	3.76	5.03	3.01	4.29
K2O	1.28	3.20	2.78	3.46	2.24	5.67	2.98
P2O5	0.23	0.28	0.26	0.41	0.13	0.17	0.27
MnO	0.09	0.07	0.07	0.06	0.05	0.03	0.08
LOI	5.61	1.45	1.25	5.64	3.13	1.58	2.18
DX	67.86	73.37	75.53	73.21	83.41	75.40	76.33
MG#0.3	66.30	65.96	58.64	62.92	53.98	60.62	61.19
Qz	13.38	18.16	21.83	20.87	27.59	21.83	22.31
Ab	46.90	36.24	35.23	31.89	42.60	40.33	36.36
Or	7.58	18.97	16.46	20.45	13.22	13.23	17.66
An	16.19	13.59	13.71	14.73	7.71	14.34	10.43
Di	1.68	0.00	0.00	0.00	0.00	0.00	0.00
Hy	10.53	9.19	7.97	7.80	4.34	6.47	7.95
Ol							
Mt	2.01	1.66	1.77	1.57	1.09	1.36	1.66
Il	1.15	1.09	1.08	1.15	0.72	0.88	1.08
Ap	0.52	0.65	0.61	0.96	0.31	0.43	0.63
Cm	0.00	0.38	1.27	0.51	2.36	1.06	1.86
Ne							
Ni	49	65	44	30	31	28	60
V	92	69	76	70	49	60	63
Cr	94	67	55	44	18	28	60
Rb	42	118	86	130	79	69	101
Sr	354	476	532	364	427	625	400
Ba	2681	679	703	2456	277	747	574
U	3	3	4	3	5	3	4
Th	9	11	12	12	7	9	10
Zn	53	63	61	58	46	61	63
Cu	20	19	20	24	1	40	15
Pb	11	16	13	7	19	29	19
Zr	154	217	210	204	140	166	201
Nb	9	11	11	11	6	8	11
Y	14	13	13	10	10	11	12
La	23	33	35	44	21	23	36
Ce	42	70	69	95	41	45	75
Nd	21	29	28	38	22	19	32

Sample	1357	1358	1359	1362	1364	1242*	1351
SiO2	70.34	69.86	70.91	69.15	70.60	68.79	68.90
TiO2	0.45	0.47	0.44	0.55	0.37	0.49	0.53
Al2O3	16.11	16.30	15.97	16.66	15.82	16.30	16.48
Fe2O3	2.56	2.39	2.41	2.74	2.18	3.02	3.05
MgO	1.36	0.78	0.50	0.95	1.18	1.84	1.01
CaO	1.06	1.74	1.40	2.01	2.35	2.14	2.54
Na2O	4.46	4.72	4.62	4.68	3.98	3.67	5.61
K2O	3.43	3.52	3.51	2.99	3.30	3.52	1.69
P2O5	0.18	0.18	0.17	0.22	0.14	0.18	0.16
MnO	0.05	0.04	0.06	0.04	0.07	0.05	0.04
LOI	2.81	3.05	2.60	3.18	4.34	1.30	3.74
DX	84.81	84.68	86.52	81.96	81.00	78.18	79.95
MG#0.3	60.16	47.86	36.72	49.64	60.45	63.23	48.44
Qz	26.76	23.91	26.64	24.66	27.79	26.30	22.46
Ab	37.76	39.98	39.14	39.63	33.70	31.05	47.49
Or	20.29	20.79	20.74	17.67	19.51	20.84	10.00
An	4.06	7.48	5.89	8.57	10.73	9.45	11.57
Di	0.00	0.00	0.00	0.00	0.00	0.00	0.00
Hy	5.08	3.41	2.81	4.04	4.43	6.62	4.50
Ol							
Mt	1.11	1.04	1.05	1.19	0.95	1.32	1.33
Il	0.85	0.90	0.84	1.05	0.71	0.93	1.01
Ap	0.42	0.41	0.38	0.50	0.33	0.43	0.36
Cm	3.59	2.00	2.43	2.61	1.78	3.01	1.20
Ne							
Ni	32	19	18	13	24	32	18
V	41	47	35	47	43	68	63
Cr	14	20	10	18	22	34	23
Rb	88	92	89	69	118	107	56
Sr	290	318	315	285	251	530	317
Ba	646	705	715	496	579	851	427
U	4	3	3	2	4	5	3
Th	13	13	11	11	15	11	7
Zn	55	34	57	72	20	47	51
Cu	1	36	25	10	20	281	45
Pb	9	9	21	16	7	43	11
Zr	224	231	221	276	166	140	146
Nb	9	8	8	10	7	9	6
Y	11	7	7	10	6	11	12
La	42	37	39	40	30	22	18
Ce	88	74	82	86	70	48	42
Nd	33	28	29	36	25	20	20

Sample	AD01	AD02	AD03	AD05	AD06	AD12	AD13
SiO2	64.00	67.33	71.55	65.84	66.15	68.80	66.97
TiO2	0.72	0.50	0.33	0.70	0.71	0.43	0.54
Al2O3	16.24	16.39	15.27	16.43	16.57	16.19	16.49
Fe2O3	4.38	3.31	2.16	3.82	3.77	2.86	3.47
MgO	3.45	1.79	1.19	2.34	2.30	1.44	1.72
CaO	3.83	2.80	1.58	3.47	3.39	2.49	3.34
Na2O	3.92	3.84	3.64	4.24	4.16	4.38	2.26
K2O	3.15	3.81	4.12	2.90	2.68	3.17	2.76
P2O5	0.26	0.18	0.12	0.19	0.20	0.16	0.19
MnO	0.06	0.06	0.04	0.05	0.07	0.06	0.06
LOI	1.25	1.35	1.44	1.37	2.07	0.90	0.88
DX	67.09	76.34	84.31	71.71	71.65	79.16	74.37
MG#0.3	69.06	60.44	60.84	63.46	63.34	58.75	58.36
Qz	15.26	21.28	29.15	18.65	20.52	23.26	20.28
Ab	33.20	32.52	30.78	35.92	35.25	37.12	37.77
Or	18.63	22.53	24.38	17.15	15.88	18.77	16.32
An	17.38	12.69	7.07	15.97	15.54	11.31	15.32
Di	0.00	0.00	0.00	0.00	0.00	0.00	0.00
Hy	11.55	6.76	4.47	8.32	8.14	5.60	6.68
Ol							
Mt	1.91	1.44	0.94	1.67	1.64	1.25	1.51
Il	1.37	0.95	0.62	1.33	1.36	0.82	1.03
Ap	0.59	0.43	0.28	0.45	0.45	0.37	0.45
Cm	0.05	1.32	2.25	0.49	1.15	1.42	0.58
Ne							
Ni	70	33	32	35	34	36	34
V	103	67	39	88	89	52	67
Cr	116	52	45	35	57	36	36
Rb	90	122	112	83	66	98	94
Sr	793	557	387	601	530	527	519
Ba	928	942	811	728	788	791	664
U	5	2	5	4	5	4	4
Th	10	8	7	9	8	10	9
Zn	55	49	60	55	51	50	57
Cu	42	7	29	4	12	17	14
Pb	67	24	56	21	17	29	20
Zr	190	141	114	148	146	141	140
Nb	11	9	10	9	10	9	9
Y	14	12	8	13	13	12	11
La	37	26	17	23	25	27	21
Ce	76	55	36	55	51	50	46
Nd	35	27	16	21	22	26	16

Sample	BGN01	BGN03	BGN04	BGN05	BGN06	BHD01	BHD02
SiO2	68.17	65.86	65.67	67.23	65.56	65.94	66.65
TiO2	0.47	0.63	0.58	0.52	0.57	0.61	0.57
Al2O3	16.23	16.29	16.29	15.86	16.19	16.23	16.53
Fe2O3	3.03	3.73	3.66	3.37	3.69	3.64	3.37
MgO	1.62	2.21	2.74	2.05	2.86	2.29	2.35
CaO	2.43	3.25	3.21	2.89	3.35	3.66	2.45
Na2O	4.39	4.13	4.18	3.95	3.98	4.02	3.97
K2O	3.42	3.57	3.36	3.83	3.46	3.36	3.85
P2O5	0.16	0.25	0.26	0.24	0.26	0.21	0.21
MnO	0.06	0.07	0.05	0.06	0.06	0.05	0.04
LOI	1.74	1.27	2.34	2.43	2.32	0.58	1.58
DX	78.89	73.65	72.49	73.13	71.57	72.01	76.14
MG#0.3	60.23	62.60	67.92	68.29	68.68	63.97	66.41
Qz	21.43	17.51	17.17	17.81	17.31	18.11	19.73
Ab	37.22	35.01	35.42	35.49	33.75	34.03	33.64
Or	20.25	21.12	19.90	19.83	20.50	19.87	22.77
An	11.01	14.55	14.24	14.38	14.95	16.39	10.74
Di	0.00	0.00	0.00	0.00	0.00	0.33	0.00
Hy	6.16	8.00	9.32	8.82	9.69	7.96	8.07
Ol							
Mt	1.32	1.63	1.60	1.49	1.61	1.59	1.47
Il	0.89	1.21	1.10	1.06	1.09	1.16	1.09
Ap	0.38	0.57	0.60	0.62	0.60	0.49	0.50
Cm	1.28	0.32	0.57	0.42	0.43	0.00	1.92
Ne							
Ni	30	44	49	43	49	47	40
V	60	72	84	77	85	73	70
Cr	24	49	61	60	70	58	50
Rb	101	95	89	85	92	121	130
Sr	533	618	709	713	696	601	554
Ba	718	777	854	874	869	718	864
U	4	6	4	5	6	3	5
Th	9	13	14	14	13	14	12
Zn	53	79	51	52	55	48	68
Cu	19	15	29	10	15	20	12
Pb	29	44	19	17	19	25	25
Zr	130	163	177	172	183	165	154
Nb	6	13	11	12	12	11	11
Y	10	13	13	11	14	12	11
La	17	33	36	45	36	33	34
Ce	37	74	87	90	72	65	74
Nd	19	30	35	40	30	25	29

Sample	BHD03	BHD04	BHD05	BHD06	BHD07	BHD08	BHD09
SiO2	67.76	66.65	67.23	66.50	66.29	66.09	65.94
TiO2	0.49	0.55	0.52	0.60	0.59	0.57	0.59
Al2O3	15.91	16.08	15.86	15.88	16.06	16.35	16.26
Fe2O3	3.14	3.49	3.37	3.49	3.52	3.55	3.64
MgO	1.91	2.12	2.05	2.18	2.31	2.33	2.35
CaO	2.58	2.91	2.89	3.22	2.78	3.25	3.49
Na2O	3.86	4.03	3.95	3.98	3.97	3.91	3.99
K2O	4.06	3.85	3.83	3.79	4.11	3.67	3.46
P2O5	0.24	0.25	0.24	0.29	0.30	0.21	0.21
MnO	0.06	0.07	0.06	0.06	0.06	0.06	0.06
LOI	0.82	0.95	0.94	0.87	1.12	0.95	0.84
DX	77.85	75.67	76.15	74.69	75.84	73.28	72.33
MG#0.3	63.25	63.17	63.20	63.83	64.98	64.95	64.67
Qz	21.17	18.76	20.04	18.50	17.84	18.41	18.01
Ab	32.66	34.15	33.46	33.76	33.76	33.13	33.83
Or	24.01	22.76	22.65	22.44	24.35	21.75	20.49
An	11.21	12.80	12.76	14.08	11.88	14.72	15.96
Di	0.00	0.00	0.00	0.00	0.00	0.00	0.00
Hy	6.93	7.69	7.43	7.73	8.12	8.22	8.32
Ol							
Mt	1.37	1.52	1.47	1.52	1.54	1.55	1.59
Il	0.93	1.05	0.99	1.14	1.13	1.09	1.13
Ap	0.56	0.59	0.57	0.68	0.68	0.50	0.50
Cm	1.09	0.62	0.56	0.08	0.74	0.57	0.11
Ne							
Ni	39	44	38	51	50	49	57
V	67	71	68	68	68	70	74
Cr	42	44	49	56	54	55	67
Rb	154	132	126	125	135	124	119
Sr	645	659	684	699	689	654	649
Ba	948	854	866	869	923	763	752
U	5	5	4	6	4	4	4
Th	13	14	12	14	10	14	12
Zn	46	53	44	36	35	50	46
Cu	11	15	7	28	26	19	24
Pb	30	24	23	23	24	24	23
Zr	125	145	151	166	161	151	158
Nb	11	11	10	12	12	10	11
Y	10	11	11	12	10	11	10
La	39	38	39	37	37	31	34
Ce	72	72	73	81	75	64	67
Nd	35	28	34	30	35	25	27

Sample	BP01	BP04	BP06	BP10	BP14	BP15	BP16
SiO2	61.79	60.64	69.61	64.92	64.92	65.82	65.12
TiO2	0.91	0.88	0.37	0.77	0.63	0.59	0.64
Al2O3	17.58	17.16	14.14	16.69	16.71	16.54	16.40
Fe2O3	4.29	5.58	1.84	4.61	3.85	3.25	3.81
MgO	3.24	4.51	2.23	1.38	3.26	2.40	2.78
CaO	2.89	3.60	2.77	3.28	2.65	3.73	3.53
Na2O	3.79	3.67	2.47	5.06	4.10	3.93	3.82
K2O	5.08	3.58	6.35	2.77	3.48	3.41	3.51
P2O5	0.33	0.31	0.16	0.45	0.35	0.27	0.28
MnO	0.11	0.06	0.07	0.07	0.04	0.06	0.06
LOI	4.96	3.94	4.44	1.56	2.77	2.16	1.39
DX	71.27	62.74	80.89	75.03	72.43	71.65	70.62
MG#0.3	68.11	69.57	77.39	45.85	70.55	67.59	67.41
Qz	9.08	10.39	22.47	15.71	17.09	18.17	17.50
Ab	32.11	31.15	20.87	42.92	34.75	33.28	32.35
Or	30.09	21.20	37.55	16.41	20.59	20.20	20.77
An	12.19	15.84	8.78	13.37	10.87	16.79	15.73
Di	0.00	0.00	3.13	0.00	0.00	0.00	0.00
Hy	10.68	15.03	5.27	6.52	10.69	8.09	9.47
Ol							
Mt	1.87	2.44	0.80	2.01	1.68	1.42	1.66
Il	1.74	1.68	0.70	1.46	1.20	1.12	1.23
Ap	0.76	0.73	0.36	1.04	0.82	0.62	0.64
Cm	1.41	1.48	0.00	0.49	2.24	0.25	0.58
Ne							
Ni	71	74	30	30	56	44	55
V	139	134	38	75	98	84	90
Cr	117	104	35	32	85	66	86
Rb	99	85	158	64	74	80	109
Sr	340	654	171	680	764	773	719
Ba	909	948	592	776	942	874	869
U	3	4	3	3	5	4	5
Th	10	9	9	14	13	14	12
Zn	36	54	13	34	34	40	52
Cu	0	11	3	6	14	5	40
Pb	10	10	10	9	11	18	20
Zr	193	190	128	174	209	187	193
Nb	11	11	8	9	14	12	12
Y	14	15	13	12	11	13	13
La	19	36	19	34	55	42	34
Ce	46	75	36	74	115	87	76
Nd	23	36	21	30	47	38	36

Sample	BP23	BSM 26	BSM03	BSM05*	BSM06	BSM08	BSM11
SiO2	64.82	59.28	63.61	66.04	65.87	68.53	64.41
TiO2	0.65	0.90	0.74	0.56	0.57	0.41	0.73
Al2O3	16.53	16.58	17.19	16.27	16.27	16.06	17.04
Fe2O3	3.87	5.92	4.39	3.54	3.61	2.84	4.39
MgO	2.89	5.63	2.28	2.37	2.50	1.54	2.30
CaO	3.12	4.22	4.18	3.06	3.16	2.32	3.83
Na2O	4.77	4.77	4.76	4.56	4.39	4.62	4.51
K2O	3.04	2.28	2.50	3.29	3.31	3.48	2.47
P2O5	0.26	0.33	0.26	0.25	0.25	0.15	0.25
MnO	0.05	0.09	0.08	0.06	0.07	0.04	0.06
LOI	2.24	5.33	4.05	1.92	2.82	2.22	3.29
DX	72.46	58.81	68.79	74.58	73.55	80.33	69.40
MG#0.3	67.87	72.90	59.49	65.44	66.20	60.59	59.71
Qz	14.07	4.85	13.60	16.48	16.81	20.67	16.52
Ab	40.43	40.46	40.37	38.61	37.17	39.10	38.27
Or	17.97	13.49	14.81	19.49	19.58	20.55	14.61
An	13.81	17.21	18.21	13.58	14.09	10.53	17.40
Di	0.00	1.31	0.70	0.00	0.00	0.00	0.00
Hy	9.77	17.54	8.30	8.33	8.72	5.83	8.64
Ol		0.00	0.00	0.00	0.00	0.00	0.00
Mt	1.69	2.59	1.92	1.54	1.57	1.24	1.91
Il	1.24	1.71	1.40	1.08	1.09	0.78	1.40
Ap	0.60	0.77	0.61	0.57	0.58	0.36	0.58
Cm	0.36	0.00	0.00	0.25	0.33	0.86	0.59
Ne		0	0	0	0	0	0
Ni	56	135	29	51	43	26	29
V	93	137	99	82	80	57	103
Cr	79	222	30	64	76	36	31
Rb	79	51	62	95	90	110	58
Sr	798	601	650	835	752	554	669
Ba	879	1074	822	768	835	852	728
U	3	3	3	3	5	5	3
Th	12	6	7	13	13	10	10
Zn	40	67	58	45	56	56	37
Cu	11	32	15	9	9	24	10
Pb	19	10	12	17	17	27	10
Zr	189	153	166	186	181	146	168
Nb	10	9	9	12	12	7	9
Y	14	16	16	12	13	10	15
La	36	29	23	37	37	24	27
Ce	81	70	55	82	81	48	63
Nd	36	36	22	35	34	20	27

Sample	BSM13	BSM14N	BSM15	BSM17N*	BSM18N*	BSM19	BSM21A
SiO2	63.62	65.73	67.31	63.33	60.85	60.23	66.10
TiO2	0.75	0.54	0.49	0.70	0.84	0.88	0.59
Al2O3	17.18	16.71	16.69	16.47	16.05	16.15	16.59
Fe2O3	4.42	3.62	3.30	4.41	5.30	5.47	3.62
MgO	2.34	2.29	1.82	3.58	4.57	5.48	2.51
CaO	4.20	3.77	2.66	3.25	5.09	4.71	3.02
Na2O	4.54	4.72	4.58	4.71	4.07	4.10	4.55
K2O	2.59	2.33	2.91	3.19	2.81	2.55	2.75
P2O5	0.26	0.22	0.19	0.29	0.33	0.33	0.21
MnO	0.08	0.07	0.06	0.06	0.09	0.09	0.06
LOI	4.80	3.34	2.52	2.37	2.58	2.87	3.88
DX	68.13	71.15	76.65	69.74	60.46	58.18	73.23
MG#0.3	59.96	64.08	60.87	69.66	70.90	73.92	66.21
Qz	14.30	17.39	20.62	10.92	9.27	8.32	18.44
Ab	38.48	39.99	38.82	39.96	34.54	34.77	38.52
Or	15.35	13.78	17.22	18.87	16.65	15.10	16.28
An	18.93	17.29	12.01	14.25	17.30	18.24	13.65
Di	0.21	0.00	0.00	0.00	4.71	2.41	0.00
Hy	8.69	8.26	6.85	11.93	12.79	16.26	8.71
Ol	0.00	0.00	0.00	0.00	0.00	0.00	0.00
Mt	1.93	1.58	1.44	1.93	2.31	2.39	1.58
Il	1.43	1.02	0.92	1.33	1.60	1.69	1.12
Ap	0.61	0.51	0.43	0.67	0.77	0.77	0.49
Cm	0.00	0.11	1.62	0.07	0.00	0.00	1.15
Ne	0	0	0	0	0	0	0
Ni	29	39	26	66	97	102	38
V	103	88	73	101	111	119	90
Cr	36	56	32	108	154	176	70
Rb	73	56	71	76	69	63	67
Sr	637	740	555	650	804	840	481
Ba	723	1323	749	1502	768	767	679
U	4	4	4	4	4	3	4
Th	9	7	11	12	12	9	8
Zn	68	49	51	58	62	62	46
Cu	10	8	6	24	32	30	12
Pb	13	22	14	20	20	10	16
Zr	164	133	152	208	192	192	161
Nb	10	8	8	12	12	11	9
Y	15	11	11	14	16	18	11
La	23	26	28	41	38	36	27
Ce	49	56	60	86	82	76	61
Nd	23	25	26	38	35	39	29

Sample	BSM22N	BSM23N	BSM24N	BSM25	BSM2N	BSMPD02*	CC02
SiO2	66.64	64.67	66.26	65.53	65.42	62.16	67.31
TiO2	0.55	0.64	0.52	0.55	0.67	0.76	0.54
Al2O3	16.60	16.36	16.59	16.59	16.77	16.30	16.55
Fe2O3	3.87	4.16	3.48	3.86	4.09	4.79	3.13
MgO	2.11	2.85	2.33	2.55	2.16	4.72	2.07
CaO	3.33	4.24	3.65	3.58	3.35	3.78	3.00
Na2O	4.80	4.30	4.40	4.50	4.52	4.34	4.05
K2O	1.84	2.50	2.51	2.57	2.72	2.79	3.10
P2O5	0.19	0.21	0.19	0.21	0.23	0.29	0.20
MnO	0.07	0.07	0.06	0.06	0.06	0.07	0.05
LOI	4.66	5.15	4.83	4.89	2.34	2.62	1.59
DX	72.28	67.69	71.39	70.78	72.19	63.82	74.68
MG#0.3	60.66	65.97	65.38	65.09	59.94	73.58	65.23
Qz	20.77	16.48	19.22	17.49	17.79	10.50	22.10
Ab	40.65	36.42	37.29	38.11	38.28	36.77	34.26
Or	10.86	14.79	14.87	15.19	16.13	16.55	18.31
An	15.31	18.04	16.91	16.42	15.14	16.84	13.58
Di	0.00	1.34	0.00	0.00	0.00	0.04	0.00
Hy	8.03	9.35	8.23	9.08	8.14	15.03	7.22
Ol	0.00	0.00	0.00	0.00	0.00	0.00	
Mt	1.69	1.81	1.52	1.68	1.79	2.09	1.36
Il	1.05	1.22	0.99	1.05	1.28	1.44	1.03
Ap	0.44	0.49	0.44	0.49	0.53	0.67	0.47
Cm	1.14	0.00	0.46	0.42	0.87	0.00	1.59
Ne	0	0	0	0	0	0	
Ni	44	48	42	42	32	101	37
V	84	84	86	86	83	114	69
Cr	61	88	78	72	41	157	44
Rb	48	71	76	62	62	67	89
Sr	476	518	416	474	665	623	522
Ba	612	804	434	1212	853	827	752
U	2	4	2	3	3	3	3
Th	8	8	8	10	9	7	9
Zn	48	46	46	45	49	63	46
Cu	1	8	14	17	4	25	16
Pb	15	14	11	15	11	13	20
Zr	134	148	127	136	160	182	150
Nb	8	8	7	7	9	10	9
Y	12	12	11	13	14	13	11
La	26	24	24	24	23	35	26
Ce	60	48	54	54	52	81	56
Nd	24	22	22	28	24	36	26

Sample	CC03A	CC03B	CC04	CC07	CC08	CC12	CC14
SiO2	62.36	70.26	66.24	66.12	67.85	69.12	66.87
TiO2	1.02	0.35	0.68	0.68	0.72	0.44	0.62
Al2O3	16.98	16.15	16.36	16.45	16.67	16.11	16.42
Fe2O3	4.54	2.33	3.60	3.81	2.86	3.13	3.37
MgO	4.03	1.39	2.23	2.77	2.31	2.17	2.49
CaO	3.10	1.31	3.34	2.29	1.52	2.00	2.56
Na2O	3.55	4.25	3.97	4.09	3.92	3.99	3.89
K2O	3.95	3.80	3.29	3.45	3.83	2.84	3.48
P2O5	0.41	0.12	0.25	0.27	0.27	0.16	0.24
MnO	0.06	0.03	0.05	0.06	0.04	0.04	0.06
LOI	3.59	1.57	2.00	2.44	2.35	1.75	1.96
DX	67.47	84.28	72.91	74.86	79.67	77.63	74.99
MG#0.3	71.50	62.79	63.64	67.26	69.50	66.28	67.60
Qz	14.01	25.75	19.80	19.77	23.78	27.05	21.48
Ab	30.06	36.00	33.64	34.67	33.24	33.78	32.95
Or	23.41	22.48	19.47	20.42	22.66	16.80	20.57
An	12.72	5.69	14.98	9.64	5.82	8.86	11.18
Di	0.00	0.00	0.00	0.00	0.00	0.00	0.00
Hy	12.62	5.07	7.81	9.38	7.25	7.62	8.38
Ol							
Mt	1.98	1.02	1.57	1.66	1.25	1.36	1.47
Il	1.95	0.66	1.30	1.30	1.37	0.84	1.18
Ap	0.95	0.28	0.57	0.62	0.62	0.38	0.55
Cm	2.24	2.97	0.80	2.47	3.95	3.25	2.18
Ne							
Ni	63	34	48	36	38	36	32
V	133	49	84	83	85	65	81
Cr	94	22	59	60	42	55	48
Rb	99	118	79	85	93	84	85
Sr	615	435	611	555	466	445	576
Ba	869	758	783	801	739	728	747
U	4	3	4	5	7	4	5
Th	16	8	14	13	13	7	14
Zn	54	36	37	50	44	38	51
Cu	6	4	5	9	51	16	9
Pb	14	18	15	15	13	15	22
Zr	201	117	162	176	181	143	161
Nb	15	6	12	14	14	7	13
Y	12	5	13	13	9	11	13
La	50	17	35	38	26	23	36
Ce	108	34	72	76	64	50	74
Nd	44	16	35	31	26	24	29

Sample	CC16	CC21*	CC22	CCO5N(A)	CF05	PH10N	PH1A
SiO2	63.09	63.32	66.94	66.78	70.03	69.66	66.91
TiO2	0.82	0.88	0.66	0.77	0.38	0.45	0.59
Al2O3	17.03	16.54	16.34	16.35	15.79	15.15	16.21
Fe2O3	4.52	4.86	4.04	3.51	2.56	2.81	3.25
MgO	4.88	4.54	2.32	2.33	0.97	1.69	2.30
CaO	2.23	1.92	1.73	1.65	2.39	0.44	2.48
Na2O	4.19	3.54	3.87	3.51	4.16	2.33	3.86
K2O	2.93	4.01	3.81	4.66	3.49	7.22	4.05
P2O5	0.26	0.32	0.25	0.38	0.18	0.21	0.29
MnO	0.05	0.07	0.04	0.05	0.04	0.04	0.06
LOI	4.04	3.53	2.08	1.98	0.82	1.77	1.81
DX	67.79	69.81	77.58	79.06	81.52	87.23	76.78
MG#0.3	75.32	72.53	61.93	65.18	51.57	62.98	66.69
Qz	14.97	16.07	22.24	21.69	25.64	24.82	20.13
Ab	35.49	30.00	32.76	29.78	35.26	19.74	32.71
Or	17.33	23.73	22.57	27.59	20.63	42.67	23.94
An	9.39	7.43	6.97	5.72	10.70	0.78	10.42
Di	0.00	0.00	0.00	0.00	0.00	0.00	0.00
Hy	15.05	14.47	8.47	7.83	4.19	6.11	7.85
Ol							
Mt	1.97	2.12	1.76	1.53	1.12	1.22	1.42
Il	1.56	1.67	1.25	1.46	0.73	0.85	1.12
Ap	0.61	0.75	0.57	0.88	0.41	0.50	0.67
Cm	3.56	3.69	3.33	3.45	1.26	3.24	1.68
Ne							
Ni	96	66	47	46	27	42	45
V	133	117	83	87	42	58	74
Cr	214	120	66	64	24	36	57
Rb	69	82	89	120	146	176	119
Sr	428	535	508	510	361	178	611
Ba	630	742	709	882	684	771	874
U	3	4	5	4	5	4	5
Th	9	15	13	14	14	12	13
Zn	47	62	52	48	55	49	42
Cu	41	6	3	12	16	1	8
Pb	9	11	15	18	23	4	18
Zr	187	189	166	176	175	128	171
Nb	11	13	12	13	10	10	12
Y	14	13	10	10	9	12	11
La	29	42	34	40	31	28	41
Ce	66	91	76	90	61	58	81
Nd	31	39	30	38	24	24	37

Sample	PH5N	PH9	RF01	RF03	RF04	RF04B	TQ01A
SiO2	70.16	56.42	64.75	64.87	65.14	64.24	67.36
TiO2	0.43	1.59	0.81	0.78	0.85	0.84	0.54
Al2O3	16.13	17.84	16.77	16.61	16.77	16.78	16.30
Fe2O3	2.49	6.90	4.71	4.62	5.10	4.86	2.74
MgO	1.61	3.95	1.79	1.43	1.53	1.54	1.70
CaO	0.97	5.48	2.02	3.26	0.99	3.35	2.53
Na2O	4.32	4.09	5.37	5.13	5.09	5.19	5.18
K2O	3.70	3.06	3.26	2.77	3.95	2.62	3.34
P2O5	0.14	0.55	0.47	0.45	0.51	0.49	0.24
MnO	0.05	0.12	0.05	0.07	0.06	0.08	0.06
LOI	1.55	1.11	1.99	1.32	1.78	1.16	2.10
DX	84.53	56.47	78.87	75.15	82.59	74.06	77.40
MG#0.3	64.67	61.79	51.85	46.70	45.89	47.34	63.62
Qz	26.13	3.57	14.08	15.21	16.00	14.51	15.54
Ab	36.54	34.74	45.51	43.53	43.18	44.05	41.81
Or	21.86	18.15	19.28	16.41	23.41	15.50	20.05
An	3.87	21.39	6.94	13.27	1.54	13.46	9.17
Di	0.00	1.87	0.00	0.00	0.00	0.00	0.00
Hy	5.66	12.88	7.52	6.64	7.18	7.05	9.35
Ol							
Mt	1.08	3.02	2.05	2.02	2.23	2.12	1.47
Il	0.83	3.03	1.55	1.48	1.62	1.60	0.99
Ap	0.33	1.27	1.10	1.04	1.19	1.14	0.57
Cm	3.63	0.00	1.90	0.32	3.58	0.49	0.98
Ne							
Ni	34	25	22	17	27	24	34
V	57	160	67	59	72	66	72
Cr	48	27	19	36	28	25	60
Rb	126	113	84	90	108	62	98
Sr	368	889	418	479	393	469	331
Ba	766	952	640	637	698	659	544
U	5	5	2	4	3	3	4
Th	8	9	7	7	5	8	12
Zn	30	83	87	81	87	83	19
Cu	44	50	39	12	3	15	0
Pb	17	20	9	26	13	15	16
Zr	129	235	350	347	342	354	170
Nb	8	23	19	19	19	19	10
Y	10	20	19	20	18	20	10
La	28	39	38	36	32	35	36
Ce	59	93	92	79	90	83	79
Nd	30	43	41	36	40	40	31

Sample	TQ01B	TQ02B	TQ03	TQ04	TQA-1	TQA-2	TQB-1
SiO2	60.63	65.93	66.28	62.37	66.39	66.46	66.68
TiO2	1.09	0.54	0.52	0.77	0.52	0.51	0.53
Al2O3	17.13	15.98	16.12	16.19	16.11	16.18	16.13
Fe2O3	5.41	3.39	3.31	4.77	3.37	3.28	3.43
MgO	4.10	2.53	2.76	5.66	2.82	2.88	2.38
CaO	2.94	2.28	2.45	3.02	2.17	2.15	2.57
Na2O	4.99	5.88	4.90	4.30	4.93	4.89	4.80
K2O	3.06	3.19	3.35	2.57	3.39	3.32	3.19
P2O5	0.58	0.25	0.25	0.29	0.25	0.25	0.24
MnO	0.09	0.04	0.06	0.07	0.06	0.07	0.05
LOI	5.16	2.67	2.52	3.16	2.10	2.24	3.73
DX	68.08	79.66	76.62	63.71	77.40	77.19	76.70
MG#0.3	68.19	67.85	70.25	77.05	70.27	71.29	66.22
Qz	7.68	10.96	15.27	12.02	15.54	16.10	17.18
Ab	42.29	49.83	41.54	36.47	41.81	41.44	40.64
Or	18.11	18.87	19.81	15.22	20.05	19.65	18.88
An	10.86	7.82	10.56	13.09	9.17	9.05	11.17
Di	0.00	1.50	0.00	0.00	0.00	0.00	0.00
Hy	13.55	7.86	9.17	17.35	9.35	9.47	8.28
Ol							
Mt	2.36	1.48	1.44	2.08	1.47	1.43	1.50
Il	2.07	1.03	0.98	1.46	0.99	0.97	1.01
Ap	1.34	0.58	0.57	0.67	0.57	0.58	0.56
Cm	1.67	0.00	0.58	1.56	0.98	1.25	0.71
Ne							
Ni	81	42	46	117	46	46	50
V	147	89	78	110	80	78	73
Cr	114	72	69	193	61	68	57
Rb	92	100	96	56	100	98	90
Sr	418	403	625	1109	574	566	462
Ba	696	719	859	1563	933	913	723
U	3	5	4	2	4	5	3
Th	18	14	14	11	13	14	14
Zn	68	44	50	63	54	57	46
Cu	11	12	16	40	12	12	2
Pb	14	16	12	12	20	20	14
Zr	237	167	164	183	168	172	166
Nb	17	12	11	11	11	12	11
Y	13	13	12	13	12	12	10
La	60	47	41	35	44	42	38
Ce	140	92	91	70	87	88	79
Nd	60	41	38	32	37	37	33

Sample	TQC-1	TQC-2	TQD-1	TQE-1	TQE-2	TQF-1	TQG-1
SiO2	61.97	62.28	66.28	66.32	66.36	66.86	62.19
TiO2	0.81	0.82	0.57	0.54	0.54	0.53	0.81
Al2O3	16.46	16.49	16.23	16.10	16.07	16.18	16.24
Fe2O3	5.07	5.19	3.39	3.29	3.33	3.29	4.96
MgO	4.73	4.98	2.43	2.47	2.28	2.62	5.66
CaO	3.63	2.66	3.62	3.43	3.66	2.02	2.76
Na2O	3.56	3.60	4.40	4.75	4.51	4.92	4.27
K2O	3.43	3.66	2.77	2.79	2.94	3.29	2.73
P2O5	0.27	0.27	0.25	0.25	0.25	0.24	0.29
MnO	0.06	0.05	0.05	0.06	0.05	0.05	0.08
LOI	4.64	4.39	4.88	4.52	4.74	3.30	3.17
DX	63.09	65.70	72.11	73.67	73.32	78.27	64.30
MG#0.3	72.53	73.07	66.96	67.99	65.94	69.20	76.34
Qz	12.58	13.43	18.43	16.92	17.68	17.13	11.91
Ab	30.22	30.55	37.31	40.27	38.21	41.66	36.23
Or	20.29	21.71	16.37	16.49	17.42	19.48	16.17
An	16.24	11.43	16.34	14.42	14.95	8.47	11.82
Di	0.00	0.00	0.00	0.77	1.27	0.00	0.00
Hy	15.23	15.92	8.31	8.03	7.33	8.75	17.47
Ol							
Mt	2.21	2.27	1.48	1.44	1.45	1.44	2.16
Il	1.55	1.56	1.09	1.02	1.02	1.01	1.55
Ap	0.64	0.63	0.59	0.59	0.59	0.56	0.68
Cm	0.98	2.44	0.03	0.00	0.00	1.44	1.96
Ne							
Ni	80	81	47	42	42	48	116
V	113	119	77	74	72	77	109
Cr	184	195	64	62	57	71	192
Rb	75	81	81	82	87	93	61
Sr	521	464	364	392	342	432	1144
Ba	928	972	537	613	588	813	1183
U	4	3	4	4	4	5	3
Th	9	10	13	12	11	14	11
Zn	62	62	46	46	42	45	60
Cu	6	5	14	5	5	11	29
Pb	14	14	11	13	21	11	13
Zr	191	193	166	165	166	162	182
Nb	10	11	12	12	11	12	11
Y	15	15	12	11	11	11	14
La	32	33	37	38	37	41	36
Ce	69	77	85	82	82	85	80
Nd	31	32	37	35	35	38	33

Sample	TQG-2	TQH-1	TQH-2
SiO2	62.28	62.20	62.08
TiO2	0.79	0.80	0.80
Al2O3	16.02	16.27	16.30
Fe2O3	4.92	4.97	5.03
MgO	5.62	4.28	4.33
CaO	2.82	4.91	4.73
Na2O	4.43	3.51	3.64
K2O	2.75	2.72	2.76
P2O5	0.29	0.28	0.26
MnO	0.08	0.06	0.06
LOI	3.13	4.81	4.79
DX	64.77	60.07	60.58
MG#0.3	76.35	70.90	70.90
Qz	10.92	14.21	13.40
Ab	37.54	29.73	30.84
Or	16.31	16.12	16.34
An	12.10	20.70	20.09
Di	0.00	1.55	1.38
Hy	17.39	13.27	13.55
Ol			
Mt	2.15	2.17	2.20
Il	1.51	1.53	1.53
Ap	0.68	0.64	0.61
Cm	1.35	0.00	0.00
Ne			
Ni	112	77	80
V	110	120	121
Cr	183	181	182
Rb	62	52	53
Sr	1042	562	560
Ba	1104	654	681
U	4	3	4
Th	8	9	8
Zn	60	53	55
Cu	30	41	39
Pb	11	11	13
Zr	185	189	190
Nb	11	11	11
Y	15	15	15
La	36	32	32
Ce	74	72	76
Nd	35	31	30

Quartz porphyries from the Criffell dyke swarm

Samples	BP18	BP25	PH4N	1248	1253	1281	1299
SiO2	68.62	68.66	72.14	69.36	68.53	70.02	69.39
TiO2	0.44	0.41	0.42	0.38	0.47	0.42	0.43
Al2O3	16.68	16.31	14.36	16.20	16.58	16.28	15.45
Fe2O3	2.43	2.96	2.19	2.62	2.97	2.84	2.96
MgO	2.01	1.57	1.42	1.48	1.52	1.41	2.02
CaO	2.29	2.54	1.26	1.97	1.03	1.47	2.88
Na2O	4.14	4.45	3.13	4.13	3.01	5.60	3.91
K2O	3.15	2.90	4.90	3.65	5.67	1.76	2.71
P2O5	0.21	0.16	0.15	0.13	0.17	0.16	0.18
MnO	0.03	0.05	0.03	0.07	0.03	0.04	0.08
LOI	1.22	1.16	1.30	1.64	2.29	2.84	5.66
DX	78.18	78.26	85.69	81.05	83.53	82.88	75.81
MG#0.3	70.07	59.98	64.70	61.57	59.07	58.31	65.89
Qz	24.56	23.46	30.21	24.47	24.46	25.09	26.70
Ab	35.02	37.66	26.52	34.98	25.50	47.39	33.09
Or	18.60	17.14	28.95	21.59	33.56	10.40	16.02
An	9.96	11.57	5.25	8.93	4.00	6.28	13.12
Di	0.00	0.00	0.00	0.00	0.00	0.00	0.00
Hy	6.56	6.04	4.90	5.59	5.77	5.48	7.19
Ol	0.00	0.00	0.00	0.00	0.00	0.00	0.00
Mt	1.06	1.29	0.95	1.14	1.30	1.24	1.29
Il	0.84	0.77	0.79	0.72	0.90	0.81	0.81
Ap	0.50	0.36	0.35	0.31	0.40	0.36	0.41
Cm	2.84	1.64	1.99	2.20	4.04	2.89	1.30
Ne	0.00	0.00	0.00	0.00	0.00	0.00	0.00
Ni	49	34	40	32	37	24	38
V	58	60	48	57	62	51	43
Cr	44	30	34	42	42	24	22
Rb	110	83	154	101	172	67	96
Sr	714	630	262	542	271	330	137
Ba	861	1030	462	825	680	192	302
U	3	3	5	4	3	3	2
Th	8	9	22	8	12	10	10
Zn	30	38	25	45	29	48	20
Cu	1	15	12	21	2	9	3
Pb	12	18	20	15	17	10	14
Zr	131	150	114	134	138	138	123
Nb	7	7	10	7	9	8	10
Y	7	10	7	9	5	11	11
La	28	22	31	18	19	27	19
Ce	58	50	55	33	37	65	44
Nd	19	20	20	16	14	25	18
Sm	4	3	4	3	3	3	4

Samples	1303	1307	1341	1342	1344	1345	1374
SiO2	71.39	71.37	70.72	70.43	73.04	72.08	70.72
TiO2	0.35	0.34	0.37	0.38	0.25	0.34	0.33
Al2O3	15.60	15.92	15.53	15.94	15.65	15.56	15.73
Fe2O3	2.15	2.44	2.49	2.38	1.77	2.34	2.59
MgO	0.89	0.64	1.02	1.00	0.58	0.46	1.11
CaO	1.73	1.60	1.80	1.58	0.59	1.07	1.70
Na2O	4.37	4.13	4.03	4.35	4.05	3.92	4.76
K2O	3.32	3.34	3.77	3.68	3.86	3.99	2.88
P2O5	0.15	0.17	0.19	0.20	0.18	0.20	0.12
MnO	0.04	0.05	0.06	0.04	0.03	0.04	0.05
LOI	2.48	3.04	2.57	2.87	1.69	2.36	2.04
DX	84.69	84.64	83.67	84.63	89.63	87.69	83.58
MG#0.3	53.79	42.69	53.73	54.37	48.10	35.52	54.80
Qz	28.01	29.92	27.25	26.02	32.56	30.91	26.21
Ab	37.03	34.94	34.14	36.84	34.27	33.22	40.32
Or	19.65	19.77	22.28	21.77	22.80	23.56	17.05
An	7.57	6.81	7.69	6.53	1.76	4.00	7.65
Di	0.00	0.00	0.00	0.00	0.00	0.00	0.00
Hy	3.66	3.35	4.31	4.13	2.71	2.77	4.67
Ol	0.00	0.00	0.00	0.00	0.00	0.00	0.00
Mt	0.94	1.06	1.09	1.04	0.77	1.02	1.13
Il	0.67	0.65	0.71	0.71	0.48	0.65	0.63
Ap	0.36	0.40	0.45	0.47	0.42	0.47	0.29
Cm	2.05	3.03	2.02	2.43	4.18	3.34	1.99
Ne	0.00	0.00	0.00	0.00	0.00	0.00	0.00
Ni	17	32	26	39	17	31	23
V	40	41	43	41	28	44	46
Cr	29	23	15	15	11	16	16
Rb	121	133	159	139	189	182	63
Sr	282	260	298	371	212	281	452
Ba	513	464	709	723	620	591	759
U	6	5	5	6	5	5	3
Th	12	11	11	12	13	12	10
Zn	44	37	73	48	41	32	51
Cu	16	32	11	10	11	6	0
Pb	19	13	24	25	11	17	16
Zr	164	160	182	182	142	153	168
Nb	10	9	11	11	10	11	10
Y	11	9	11	11	8	10	12
La	27	26	30	34	28	29	30
Ce	57	54	64	66	57	56	55
Nd	24	23	26	24	25	28	24
Sm	5	4	5	6	5	6	6

Samples	1376	AD04	BP07	BP24	BP26	CF01	CF02
SiO2	71.66	71.81	68.60	68.82	70.25	69.75	71.71
TiO2	0.36	0.30	0.44	0.42	0.33	0.41	0.32
Al2O3	15.83	15.17	16.40	16.19	16.03	15.83	15.19
Fe2O3	2.51	2.05	3.12	2.91	2.41	2.64	1.99
MgO	1.50	0.99	1.79	1.46	1.38	1.01	0.82
CaO	1.31	1.53	1.39	2.63	1.98	1.73	1.74
Na2O	4.17	4.17	3.84	4.53	4.65	4.26	3.85
K2O	2.46	3.82	4.20	2.84	2.79	4.07	4.21
P2O5	0.13	0.11	0.18	0.15	0.11	0.24	0.14
MnO	0.06	0.05	0.03	0.04	0.06	0.05	0.04
LOI	3.52	1.29	1.80	1.05	1.17	0.93	0.62
DX	82.38	85.75	81.49	78.51	81.64	84.20	85.54
MG#0.3	62.83	57.72	61.89	58.66	61.78	52.10	53.77
Qz	32.54	27.85	24.06	23.36	25.80	24.07	28.11
Ab	35.30	35.30	32.56	38.35	39.33	36.07	32.55
Or	14.54	22.60	24.87	16.81	16.52	24.05	24.88
An	5.70	6.86	5.76	12.04	9.12	7.02	7.69
Di	0.00	0.00	0.00	0.00	0.00	0.00	0.00
Hy	5.54	3.94	6.64	5.68	5.19	4.36	3.39
Ol	0.00	0.00	0.00	0.00	0.00	0.00	0.00
Mt	1.09	0.89	1.36	1.27	1.05	1.15	0.87
Il	0.69	0.56	0.84	0.80	0.64	0.77	0.61
Ap	0.29	0.26	0.41	0.36	0.26	0.56	0.33
Cm	4.24	1.67	3.43	1.27	2.04	1.87	1.50
Ne	0.00	0.00	0.00	0.00	0.00	0.00	0.00
Ni	22	33	42	36	30	40	30
V	45	38	60	54	53	42	33
Cr	15	18	48	31	34	16	22
Rb	78	126	94	89	95	178	205
Sr	240	410	471	640	494	401	320
Ba	339	781	807	791	703	659	618
U	4	4	4	5	4	5	6
Th	12	12	8	8	9	12	14
Zn	49	42	24	36	52	60	34
Cu	0	7	1	20	9	12	9
Pb	11	38	10	18	15	36	34
Zr	168	108	135	154	126	186	142
Nb	10	9	9	8	6	11	10
Y	13	10	7	11	7	11	7
La	27	20	19	22	17	34	35
Ce	54	40	41	45	40	72	68
Nd	23	17	24	21	14	31	28
Sm	4	4	5	3	4	5	5

Samples	CF03	CF04	CFO6N	PH8	BSM4	BSM9	BSM16N
SiO2	70.24	71.21	69.76	69.90	68.81	69.31	67.21
TiO2	0.41	0.32	0.43	0.43	0.41	0.36	0.48
Al2O3	15.69	15.27	15.68	15.74	16.31	16.40	16.93
Fe2O3	2.45	2.06	2.69	2.65	2.80	2.41	3.15
MgO	0.94	0.91	1.02	1.03	1.69	1.29	1.81
CaO	1.86	1.98	2.40	1.84	2.43	2.35	2.59
Na2O	4.20	3.85	4.16	4.18	4.67	4.70	4.96
K2O	3.95	4.20	3.58	3.96	2.70	3.01	2.64
P2O5	0.19	0.14	0.20	0.22	0.14	0.13	0.19
MnO	0.06	0.06	0.07	0.05	0.05	0.04	0.05
LOI	0.72	0.48	0.52	1.64	2.24	2.90	2.69
DX	84.05	84.34	81.36	83.63	78.67	80.76	77.23
MG#0.3	52.08	55.39	51.60	52.45	63.04	60.19	61.96
Qz	25.14	26.89	24.95	24.83	23.17	23.16	19.62
Ab	35.53	32.60	35.25	35.37	39.51	39.80	42.00
Or	23.38	24.85	21.17	23.43	15.99	17.80	15.61
An	7.98	8.91	10.62	7.66	11.10	10.76	11.62
Di	0.00	0.00	0.00	0.00	0.00	0.00	0.00
Hy	4.00	3.71	4.40	4.37	6.17	4.88	6.69
Ol	0.00	0.00	0.00	0.00	0.00	0.00	0.00
Mt	1.07	0.90	1.17	1.15	1.22	1.05	1.37
Il	0.79	0.61	0.82	0.82	0.78	0.69	0.91
Ap	0.45	0.33	0.47	0.52	0.33	0.31	0.44
Cm	1.60	1.13	1.09	1.79	1.66	1.48	1.68
Ne	0.00	0.00	0.00	0.00	0.00	0.00	0.00
Ni	33	30	32	30	30	20	24
V	40	31	42	46	59	54	67
Cr	15	28	20	23	45	24	42
Rb	164	195	144	160	83	111	72
Sr	379	330	376	352	502	569	564
Ba	681	659	666	659	659	845	733
U	4	7	6	7	3	4	4
Th	14	14	14	11	8	10	11
Zn	54	40	46	45	50	42	46
Cu	10	9	12	5	11	11	26
Pb	31	31	26	25	18	13	15
Zr	176	132	187	184	133	116	160
Nb	10	10	10	12	7	6	9
Y	11	5	10	10	9	6	12
La	36	29	34	32	22	20	30
Ce	63	65	70	62	48	47	61
Nd	29	25	30	26	20	20	25
Sm	3	5	5	6	2	3	4

Samples	BSM7B
SiO2	67.39
TiO2	0.46
Al2O3	16.22
Fe2O3	3.11
MgO	2.12
CaO	2.21
Na2O	4.10
K2O	4.15
P2O5	0.19
MnO	0.05
LOI	2.25
DX	78.60
MG#0.3	65.86
Qz	19.37
Ab	34.70
Or	24.54
An	9.78
Di	0.00
Hy	7.45
Ol	0.00
Mt	1.36
Il	0.88
Ap	0.43
Cm	1.43
Ne	0.00
Ni	41
V	70
Cr	70
Rb	130
Sr	752
Ba	859
U	3
Th	11
Zn	52
Cu	18
Pb	18
Zr	144
Nb	10
Y	11
La	32
Ce	61
Nd	26
Sm	6

Appendix D

Endmembers used in geochemical modelling

Sample	TQ04	PFT02B	1371	SULP
SiO ₂	62.37	48.05	50.06	
TiO ₂	0.77	1.47	0.92	
Al ₂ O ₃	16.19	14.34	12.33	
Fe ₂ O ₃	4.77	10.12	14.01	
MgO	5.66	11.45	9.16	
CaO	3.02	8.62	9.27	
Na ₂ O	4.3	1.57	1.74	
K ₂ O	2.57	3.42	1.72	
P ₂ O ₅	0.29	0.8	0.64	
MnO	0.07	0.15	0.15	
Ni	117	264	381	117.54
V	110	221	866	178
Cr	193	306	209	323.81
Rb	56	148	38	66.46
Sr	1109	1445	665	338.63
Ba	1563	1641	2578	500.18
U	2	5	3	
Th	11	20	11	
Zn	63	131	70	
Cu	4	67	177	
Pb	12	12	13	
Zr	183	200	294	202
Nb	11	18	13	10.72
Y	13	26	21	26.2
La	35	105	34	25.5
Ce	70	230	86	55.1
Nd	32	98	49	
Sm	5	9	5	
K(ppm)				20754
ε Nd	-0.7			-6.1
⁸⁷ Sr/ ⁸⁶ Sr _I	0.70525			0.7075

Equations used in modelling

Assimilation and fractional crystallisation (AFC)

(after Wilson, 1989)

$$C_L = C_L^0 f + \frac{r}{r-1+D} \cdot C^* (1-f)$$

C_L^0 = concentration of element in initial magma

C_L = concentration of element in contaminated magma

C^* = concentration of element in contaminant

r = ratio of rate of assimilation to the rate of fractional crystallisation

$f = F^{-(r-1+D)/(r-1)}$, where F = fraction of magma remaining

D = Bulk distribution coefficient for the fractionating assemblage

$$\epsilon_L = \epsilon_L^0 + (\epsilon^* - \epsilon_L^0) \left(\frac{1 - C_L}{C_L} f \right)$$

ϵ_L^0 = isotopic composition of initial magma

ϵ_L = isotopic composition of contaminated magma

ϵ^* = isotopic composition of contaminant

Rayleigh Fractionation

$$C_L = C_L^0 F^{(D-1)}$$

subscripts as above

Appendix E

Sample list and summary of phenocryst mineralogy

Codes used in tables

P:	Phenocryst	A:	Acicular (lamprophyre amphibole)
MP:	Microphenocryst	PN:	Panidiomorphic (lamprophyre groundmass)
A:	Acicular	*	Pseudomorph

Alteration Codes

- 1 Minor sericite or chlorite alteration of primary phases.
- 2 Patches of sericite in feldspar, ores+chlorite patches associated with mafics.
- 3 Sericite common, chlorite+ores associated with mafics. Some pseudomorphing of mafics.
- 4 Samples shows extensive alteration, feldspar showing extensive replacement, pseudomorphing of mafics, recrystallisation of groundmass, silicification. Epidote & carbonate formation.
- 4* Samples from boreholes-all heavily altered, no detailed description

Notes

NA:	Not analysed
IS:	Insufficient sample (collected for TS only)
BGS:	Stored at BGS Edinburgh or Keyworth
CC-BGS:	Sample from by C. Cooper, Rio Finex (from BGS Borehole)
CDIC:	Criffell-Dalbeattie Intrusive complex
BSMC:	Black Stockarton Moor Intrusive complex
Probe:	Probe slide prepared
TSNA:	Thin section not available

Sample designation

CC:	Colvend Coast section
AD:	Almorness Point section
BHD:	Bainloch Hill section
BGN:	Bengairn Hill section
CF:	Criffell section
BP:	Balcary Point section
RF:	Round Fell section
PFT:	Potterland Forest section
TQ:	Tongland Quarry

Sample	Grid ref/locality	Lithology	Alt. code	Cpx	Amph	Bte	Plag	K-fspar	Quartz	Notes
BP 01	(824 487)	Porphyrite	4	-	-	P	P			
BP 04	(827 489)	Porphyrite	3	-	-	P	P			
BP 06	(827 489)	Porphyrite	3-4	-	-	P	P, MP			
BP 07	(827 489)	Quartz Porphyry	3	-	-	P	P		P	
BP 10	(829 493)	Porphyrite	2-3	-	-	MP	P			
BP 11	(828 493)	Lamprophyre	3	?p*	A					PN
BP 14	(827 494)	Porphyrite	2-3	-	-	P	P			
BP 15	(827 494)	Porphyrite	2	-	-	P	P, MP			
BP 16	(826 495)	Porphyrite	2	-	-	MP	P			
BP 18	(826 496)	Quartz Porphyry	2	-	-	P, MP	P			
BP 19	(826 493)	Lamprophyre	3	?MP*	MP	MP				
BP 21	(828 492)	Lamprophyre	2-3	-	A	MP				PN
BP 22	(814 485)	Lamprophyre	3	-	A	0				PN
BP 23	(814 485)	Porphyrite	3	-	?p*	P	P			
BP 24	(821 498)	Quartz Porphyry	2	-	MP	P, MP	P			
BP 25	(821 498)	Quartz Porphyry	2-3	-	P*	P, MP	P			
BP 26	(819 501)	Quartz Porphyry	2	-	-	P	P		P	
BSM 01	(738 561)	Lamprophyre	2-3	?p*	A	-				PN, BSMIC
BSM 02	(737 562)	Porphyrite	3	-	-	P	P			BSMIC
BSM 03	(740 554)	Porphyrite	3-4	-	P	P	P			BSMIC
BSM 04	(739 553)	Quartz Porphyry	3-4	-	-	P*	P		P	BSMIC
BSM 05	(738 553)	Porphyrite	3-4	-	P	P*	P			BSMIC
BSM 06	(738 553)	Porphyrite	3-4	-	-	P*	P			BSMIC
BSM 07	(738 552)	Quartz Porphyry	3-4	-	-	P*	P		P, MP	BSMIC
BSM 08	(738 551)	Porphyrite	4	-	-	P*	P		P, MP	BSMIC
BSM 09	(736 550)	Quartz Porphyry	4	-	-	P*	P			BSMIC
BSM 11	(737 563)	Porphyrite	3	-	-	P	P			BSMIC
BSM 13	(744 555)	Porphyrite	3	-	P	P	P			BSMIC
BSM 14	(744 557)	Porphyrite	2-3	-	-	P	P			BSMIC
BSM 15	(743 556)	Porphyrite	4	-	P*	P*	P			BSMIC
BSM 16	(743 555)	Quartz Porphyry	3-4	-	-	P*	P		P	BSMIC
BSM 17	(735 547)	Porphyrite	3-4	MP, P	P*	P*	P			BSMIC
BSM 18	(734 545)	Porphyrite	3-4	P	-	MP*	P			BSMIC
BSM 19	(734 546)	Porphyrite	3-4	P	-	MP	P			BSMIC
BSM 21	(708 535)	Porphyrite	3-4	-	-	P*	P			BSMIC
BSM 22	(705 533)	Porphyrite	3-4	-	-	P	P			BSMIC
BSM 23	(706 531)	Porphyrite	3-4	-	P*	P*	P		P	BSMIC
BSM 24	(708 532)	Porphyrite	3-4	-	-	P	P			BSMIC
BSM 25	(710 532)	Porphyrite	3-4	-	-	P	P, MP			BSMIC
BSM 26	(712 532)	Porphyrite	3-4	-	MP, P	P	P			BSMIC

Sample	Grid ref/locality	Lithology	Alt. code	Cpx	Amph	Btc	Plag	K-fspar	Quartz	Notes
BSPMD1	(745 575)	Lamprophyre	3-4	-	A					PN, BSMIC
BSPMD2	Black Stockarton	Porphyrite	3-4	-	MP*	MP*	P			BSMIC
BGN 01	(772 545)	Porphyrite	3-4	-	-	P*	P			
BGN 03	(784 552)	Porphyrite	2-3	-	MP, P	P	P			
BGN 04	(756 540)	Porphyrite	3	-	P*	P	P			
BGN 05	(756 539)	Porphyrite	3	-	P*	P	P			
BGN 06	(757 535)	Porphyrite	3	-	P*	MP	P			
AD 01	(841 517)	Porphyrite	3	-	-	MP	P			
AD 02	(841 517)	Porphyrite	3	-	-	MP	P			
AD 03	(841 516)	Porphyrite	3	-	-	MP	P			
AD 04	(841 516)	Quartz Porphyry	2	-	-	P, MP	P	P		
AD 05	(841 516)	Porphyrite	3	-	-	MP	P			
AD 06	(839 515)	Porphyrite	3	-	-	MP	P			
AD 12	(811 572)	Porphyrite	2	-	-	P, MP	P			
AD 13	(813 569)	Porphyrite	2-3	-	-	P, MP	P			
CC 02	(845 531)	Porphyrite	3-4	-	-	P	P			
CC 03A	(894 548)	Porphyrite	3	-	-	P	P			
CC 03B	(894 548)	Porphyrite	2	-	-	MP	P			
CC 04	(893 542)	Porphyrite	3	-	-	P	P			
CC 05	(892 546)	Porphyrite	2-3	-	-	P, MP	P			
CC 07	(885 542)	Porphyrite	3	-	-	P	P			
CC 08	(885 542)	Porphyrite	2-3	-	-	P	P			
CC 12	(886 544)	Porphyrite	3	-	P	MP	P			
CC 14	(886 544)	Porphyrite	2-3	-	-	P	P			
CC 16	(888 544)	Porphyrite	3	-	-	P	P			
CC 18	(888 545)	Lamprophyre	3-4	-	A	MP*				PN
CC 20B	(889 546)	Lamprophyre	2-3	-	P	-				PN
CC 20	(889 546)	Lamprophyre	3	-	P	-				PN
CC 21	(892 547)	Porphyrite	3-4	-	-	P	P		MP	
CC 22	(892 547)	Porphyrite	3-4	-	-	P	P			
BHD 01	(895 565)	Porphyrite	2	P	P*	MP	P			
BHD 02	(893 566)	Porphyrite	3	-	P*	P*	P			
BHD 03	(893 566)	Porphyrite	2	-	MP	P	P			
BHD 04	(897 568)	Porphyrite	2	-	MP	P	P			
BHD 05	(897 568)	Porphyrite	2	-	MP	P, MP	P, MP			
BHD 06	(889 561)	Porphyrite	2	-	P	P	P			
BHD 07	(889 561)	Porphyrite	2-3	-	MP	P	P			
BHD 08	(893 564)	Porphyrite	2	P*	P*	P	P			
BHD 09	(895 563)	Porphyrite	2	P*	P*	P	P			
TQ 01	(698 544)	Porphyrite	3-4	-	P	P	P			BSMIC

Sample	Grid ref/locality	Lithology	Alt. code	Cpx	Amph	Bic	Plag	K-fspar	Quartz	Notes
TQ 02	Tongland Quarry	Porphyritic	3-4	-	-	P	P			BSMIC
TQ 03	Tongland Quarry	Porphyritic	3-4	-	P	MP	P			BSMIC
TQ 04	Tongland Quarry	Porphyritic	3-4	P	P*	P*	P			BSMIC
TQ-A	Tongland Quarry	Porphyritic	3-4	-	P, MP	P*, MP*	P			BSMIC
TQ-B	Tongland Quarry	Porphyritic	3-4	-	-	P*	P			BSMIC
TQ-C	Tongland Quarry	Porphyritic	3-4	-	P*	P*	P			BSMIC
TQ-D	Tongland Quarry	Porphyritic	3-4	-	P*	P*	P			BSMIC
TQ-E	Tongland Quarry	Porphyritic	3-4	-	-	P*	P			BSMIC
TQ-F	Tongland Quarry	Porphyritic	3-4	-	P*	P*	P			BSMIC
TQ-G	Tongland Quarry	Porphyritic	3-4	P	P*	P*	P			BSMIC
TQ-H	Tongland Quarry	Porphyritic	3-4	-	P*	P*	P			BSMIC
PFT 02	(793 557)	Lamprophyre	2-3	?MP*	A	-				PN
PFT 03	(792 558)	Lamprophyre	3-4	-	-	P				PN
RF 01	(895 613)	Porphyritic	3-4	-	MP*	MP*	P			PN
RF 03	Round Fell	Porphyritic	2-3	-	-	MP, P	P			
RF 04	Round Fell	Porphyritic	3-4	-	-	P*	P			
RF 04B	Round Fell	Porphyritic	2-3	-	MP, P	MP	P			
CF 01	(965 603)	Quartz Porphyry	2	-	-	P, MP	P	P		
CF 02	Criffell	Quartz Porphyry	1-2	-	-	P	P	MP		
CF 03	Criffell	Quartz Porphyry	1	-	-		P	P		
CF 04	Criffell	Quartz Porphyry	1-2	-	-	MP, P	P	MP		
CF 05	Criffell	Porphyritic	1-2	-	-	P	P			
CF 06	Criffell	Quartz Porphyry	1-2	-	-	MP, P	P, MP	MP		
1242	(8958 5538)	Porphyritic	3	-	-	MP	P	MP		
1248	(8525 5281)	Quartz Porphyry	2-3	-	-	MP	P	P		
1252	(7815 5634)	Porphyritic	2-3	-	-	MP	P			
1253	(8244 4884)	Quartz Porphyry	2-3	-	P, MP	MP, P	P			
1254	(8287 4917)	Porphyritic	2-3	-	-	P	P	P		
1255	(8281 4939)	Porphyritic	2-3	-	-	P	P			
1258	(8055 5969)	Porphyritic	3	-	-	P	P			
1261	(8546 6580)	Porphyritic	2-3	-	MP	P	P			
1263	(8271 6277)	Porphyritic	2	-	-	P	P			
1270	(6325 5350)	Lamprophyre	3	-	-	P, MP	P			PN, BGS
1271	(6946 4943)	Lamprophyre	3-4	P*	-	MP				PN
1272	(6955 4929)	Porphyritic	3	-	P	P	P			
1279 M	(6725 4851)	Lamprophyre	3	-	-	P				PN, BGS
1279 I	(6725 4851)	Lamprophyre	3	-	-	P, MP				PN, BGS
1279 C	(6725 4851)	Lamprophyre	3	-	-	P, MP				PN, BGS
1280	(7322 5165)	Lamprophyre	3	MP*	-	P, MP				PN, BGS
1281	(7328 5153)	Quartz Porphyry	3-4	-	-	P	P	P		

Sample	Grid ref/locality	Lithology	Alt. code	Cpx	Amph	Btc	Plag	K-fspar	Quartz	Notes
1285	(7314 5121)	Lamprophyre	3-4	P*	-	P*	-	-	-	PN
1293	(6347 4811)	Porphyrite	4	-	-	P*	P	-	-	PN
1295	(0272 7895)	Lamprophyre	3-4	-	P	-	-	-	-	PN
1296 C	(0465 7907)	Lamprophyre	3	-	P	-	-	-	-	PN
1296 M	(0465 7907)	Lamprophyre	3	-	P, A	-	P	MP	-	PN
1299	(0841 7384)	Quartz Porphyry	4	-	-	P	-	-	-	PN
1301	(8812 7349)	Lamprophyre	3	P*	A	-	-	-	-	PN
1302	Slacks Farm	Lamprophyre	2-3	-	A	-	-	-	-	PN
1303	Slacks Farm	Quartz Porphyry	3-4	-	-	P	P	P	-	PN
1305	Slacks Farm	Lamprophyre	3	-	A	-	-	-	-	PN
1306	(8805 7344)	Lamprophyre	3-4	-	A*	-	-	-	-	PN
1307	Slacks Farm	Quartz Porphyry	4	-	-	P	P	P	-	PN
1308	Slacks Farm	Lamprophyre	3	-	A	-	-	-	-	PN
1313	(3892 9327)	Lamprophyre	2	-	P	-	-	-	-	PN
1314	(9022 7644)	Lamprophyre	2-3	-	P, A	-	-	-	-	PN, BGS
1315	(9057 7666)	Lamprophyre	3	MP*	P, A	-	-	-	-	PN, BGS
1317	(8986 7765)	Lamprophyre	3	MP	A	-	-	-	-	PN, BGS
1320	(8982 7802)	Lamprophyre	3	-	A	-	-	-	-	PN, BGS
1323	(9031 7800)	Lamprophyre	2-3	-	P, A	-	-	-	-	PN, BGS
1325	(9011 7784)	Lamprophyre	3	MP	P, A	-	-	-	-	PN, BGS
1326	(9020 7774)	Lamprophyre	3	-	P, A	-	-	-	-	PN, BGS
1327	(9018 7770)	Lamprophyre	2-3	-	P, A	-	-	-	-	PN, BGS
1329	(8850 7691)	Lamprophyre	3	MP	P, MP	-	-	-	-	PN, BGS
1332	(1770 8290)	Lamprophyre	2-3	-	P	-	-	-	-	PN
1333	(2418 9070)	Lamprophyre	3	-	MP	MP	-	-	-	PN
1334	(9135 9663)	Lamprophyre	2-3	-	P	-	-	-	-	PN
1338	(9243 7110)	Porphyrite	2-3	-	MP	P	P	-	-	PN
1339	(9247 7109)	Porphyrite	3	-	-	MP	P	-	-	PN
1341	(9047 7403)	Quartz Porphyry	3-4	-	-	P*	P	MP	-	PN
1342	(9107 7460)	Quartz Porphyry	3-4	-	-	P*	P	MP	-	PN
1343	(9116 7441)	Porphyrite	4	-	-	MP*	P	-	-	PN
1344	(8771 7284)	Quartz Porphyry	3-4	-	-	P*	P	P	-	PN
1345	(8742 7265)	Quartz Porphyry	3-4	-	-	MP	P	P	-	PN
1346	(8601 7043)	Lamprophyre	3	-	-	P, A	-	-	-	PN
1350	(8225 7142)	Porphyrite	3-4	-	-	P	P	MP	-	PN
1351	(8529 7357)	Porphyrite	3	-	-	MP	P	-	-	PN
1352	(9595 7043)	Porphyrite	3	-	-	MP	P	-	-	PN
1353	(9547 7039)	Porphyrite	1-2	-	-	MP	P	-	-	PN
1355	(8254 8713)	Lamprophyre	2-3	?P*	A	-	-	-	-	PN
1357	(7990 8826)	Porphyrite	3	-	-	P	P	-	-	PN

Sample	Grid ref/locality	Lithology	Alt. code	Cpx	Amph	Bte	Plag	K-fspar	Quartz	Notes
1358	(7932 8423)	Porphyrite	3-4	-	-	P	P			
1359	(7920 8363)	Porphyrite	3-4	-	-	P	P			
1360	(7653 7962)	Lamprophyre	3	-	A					PN
1362	(7515 7669)	Porphyrite	3-4	-	-	MP	P			
1363	(7621 7721)	Lamprophyre	3	P*	A	-	P			PN
1364	(7580 7760)	Porphyrite	3	-	-	P				PN
1365	(7572 7767)	Lamprophyre	3	-	A					PN
1367	(6665 7267)	Lamprophyre	3	-	P	-				PN
1368	(7047 7168)	Lamprophyre	3	-	-	P, MP				PN
1370	(6798 8310)	Lamprophyre	3	-	-	P				PN
1371	(6027 8125)	Lamprophyre	3	-	-	P, MP				PN
1374	(6046 8607)	Quartz Porphyry	3-4	-	-	P	P	P		
1376	(6008 8771)	Quartz Porphyry	3-4	-	-	MP	P		MP	
1379A	(6833 7746)	Lamprophyre	1-2	-	P	MP				PN
1379B	(6833 7746)	Lamprophyre	3	-	P	P				PN
1380	(852 532)	Lamprophyre	1-2	-	P	-				PN
1381		Lamprophyre	2-3	P*	A	-				PN
PH1A	(898 553)	Porphyrite	2	-	-	P	P			
PH4	(915 562)	Quartz Porphyry	2	-	-	P	P		MP	
PH5	(915 562)	Porphyrite	3	-	-	MP	P			
PH8	(956 591)	Quartz Porphyry	3	-	-	MP	P		MP	
PH9		Porphyritic	2-3	-	P*	MP, P	P			
PH10	(966 586)	Porphyrite	4	-	-	P*	P			

Samples not included in the thesis but collected for the project

BP1A	Auchencairn	Granodiorite	2	-	MP	P	P			CDIC
BP4A	Auchencairn	Granodiorite	2	-	MP	P	P			CDIC
BP3A	Auchencairn	Granodiorite	1-2	-	MP, P	MP, P	P			CDIC
BP2A	Auchencairn	Granodiorite	1-2	-	MP, P	P	P			CDIC
AD09	(829 544)	Qtz Diorite	1-2	MP*	-	P	P			CDIC
AD10	(831 552)	Qtz Diorite	1-2	MP*	-	P	P			CDIC
BP28	(817 504)	Granodiorite	2	-	-	P	P			CDIC
BP33	(821 498)	Granodiorite	1-2	-	P	P	P			CDIC
BP37	(816 505)	Granodiorite	1-2	-	-	P	P			CDIC
BP35	(819 501)	Granodiorite	2	-	-	P	P			CDIC
BGN02	(772 547)	Qtz Diorite	1-2	-	P	MP, P	P			CDIC
PH6	SandyHills Bay	Granite	2	-	-	P	P			CDIC
AD07	(835 516)	Qtz Diorite	2-3	-	-	MP	P			CDIC
AD11	(834 548)	Qtz Diorite	1-2	MP*	-	P	P			CDIC

Sample	Grid ref/locality	Lithology	Alt. code	Cpx	Amph	Bte	Plag	K-fspar	Quartz	Notes
BP27	(817 505)	Granodiorite	2	-	-	P	P			CDIC
BP36	(819 502)	Granodiorite	2	-	-	P	P			CDIC
BP38	(814 507)	Granodiorite	2	-	-	MP	P			CDIC
BP32	(821 498)	Granodiorite	1-2	-	-	P	P			CDIC
BP34	(821 497)	Granodiorite	2	-	-	MP, P	P			CDIC
BP29	(818 504)	Granodiorite	2-3	-	-	MP, P	P			CDIC
BP30B	(818 503)	Granodiorite	2	-	-	MP, P	P			CDIC
BP5N(A)	Auchencairn	Granodiorite	1-2	-	-	P	P			CDIC
AD08	(831 542)	Qtz Diorite	1-2	MP*	-	P	P			CDIC
BP30	(818 504)	Granodiorite	2	-	-	P	P			CDIC
BP31	(819 503)	Granodiorite	2	-	-	P	P			CDIC
BP40	(823 518)	Qtz Diorite	2-3	-	-	MP, P	P			CDIC
BP39	(816 517)	Granodiorite	2	-	-	P	P			CDIC
GDT559	Black Stockarton	Granodiorite	4*	-	-					TSNA, BSMIC
GDT561	Black Stockarton	Granodiorite	4*	-	-					TSNA, BSMIC
GDT560	Black Stockarton	Granodiorite	4*	-	-					TSNA, BSMIC
GDT505	Black Stockarton	Granodiorite	4*	-	-					TSNA, BSMIC
GDT504	Black Stockarton	Granodiorite	4*	-	-					TSNA, BSMIC
GDT564	Black Stockarton	Granodiorite	4*	-	-					TSNA, BSMIC
GDT565	Black Stockarton	Granodiorite	4*	-	-					TSNA, BSMIC
GDT567	Black Stockarton	Granodiorite	4*	-	-					TSNA, BSMIC
GDT562	Black Stockarton	Granodiorite	4*	-	-					TSNA, BSMIC
GDT563	Black Stockarton	Granodiorite	4*	-	-					TSNA, BSMIC
GDT558	Black Stockarton	Granodiorite	4*	-	-					TSNA, BSMIC
GDT566	Black Stockarton	Granodiorite	4*	-	-					TSNA, BSMIC
GDT568	Black Stockarton	Granodiorite	4*	-	-					TSNA, BSMIC
GDT557	Black Stockarton	Granodiorite	4*	-	-					TSNA, BSMIC
GDT550	Black Stockarton	Granodiorite	4*	-	-					TSNA, BSMIC
1241	(8153 6697)	Lamprophyre	2	-	P	-				PN, NA, IS
1246	(8552 5265)	Porphyrite	4	-	-	P*	P			NA
1259	(8155 6063)	Porphyrite	3-Feb	-	-	P	P			NA, IS
1260	(8134 6190)	Porphyrite	4	-	-	MP*, P*	P			NA, IS
1264	(8264 6266)	Porphyrite	3	-	-	P	P			NA
1269	(5888 5748)	Porphyrite	4	-	-	-	-			Schistose, NA
1287	(6893 5725)	Porphyrite	4	-	-	P	P			NA
1290	(7238 5315)	Porphyrite	4	-	-	-	P			NA
1347	(8569 7073)	Lamprophyre	4	-	-	-	P			PN, NA
1369	(6939 7296)	Porphyrite	4	-	A	-	-			NA
1373	(5915 8278)	Sediment	4	-	-	-	P			NA
1375	(6059 5633)	Sediment		-	-	-	-			NA

Sample	Grid ref/locality	Lithology	Alt. code	Cpx	Amph	Bte	Plag	K-fspar	Quartz	Notes
1378	(6390 9423)	Lamprophyre	4	P*	P*	-				PN, NA
PH1B	(898 553)	Porphyrite	4	-	MP	P				NA
PH3	(897 552)	Sediment								NA
PH-BCA	(899 553)	Brccia								NA
BP 20	(828 492)	Microdiorite	3	-	MP	MP	P			PN
1291	(6195 4657)	?altd basic	4	-	MP	MP				
1377	(6002 8779)	Porphyrite	4	P	-	-	P			
1245	(8962 5537)	Porphyrite	4	-	-	-	P			Schistose
BGN07	(757 534)	Porphyrite	3	MP	?MP*	P*	P			
1366	(6582 7439)	Porphyrite	3	-	P*	MP	P			
1382	(852 532)	Porphyrite	3-4	-	-	P	P			
1262	(8276 6255)	Porphyrite	4	-	P*	P*	P			
1294N	(0277 7809)	?altd basic	4	P*	-	-				
1244N	(8961 5537)	Porphyrite	4	-	-	MP, P				Schistose
CC01	(845 532)	Porphyrite	3-4	-	-	P	P			
CC19	(889 546)	?altd basic	4	-	P*	P*				
CC11	886 545)	Porphyrite	4	-	P*	-	MP			PN
CC13	(886 544)	Porphyrite	4	-	-	MP				NA
BP13	(828 494)	Porphyrite	4	-	P	MP	P			
CC10	(886 545)	Porphyrite	4	-	-	P	P, MP			
BSM12	(724 545)	?altd basic	4	?MP*	-	-				
1240	(8288 6899)	Lamprophyre	2	P	A, P	-				PN, Probe
BP02	(824 487)	Porphyrite	3	-	-	P	P			NA
BP08W	(824 487)	Porphyrite	4	-	-	P	P			NA
BP12A	(828 493)	Lamprophyre	3	-	P, A	MP				PN, NA
BP12B	(828 493)	Quartz Porphyry	4	-	-	MP		P		NA
BP17	(826 496)	Porphyrite	4	-	-	P	P			NA
CC-AGB	(892 546)	Agglomerate								NA
CC06	(892 546)	Porphyrite	4	-	-	P	P			NA
CC 09	(885 542)	Agglomerate								NA
CC15	(888 544)	Porphyrite	4	-	-	-	P			NA
CC17	(888 545)	?altd basic	4	-	P*	-				PN, NA
CC23	(892 547)	Porphyrite	4	-	-	P*	P			NA
CC24	(892 547)	Porphyrite	4	-	-	P	P			NA
TQ-X	(698 544)	Porphyrite	4	-	-	P*	P			NA
PFT01	(795 555)	Porphyrite	4	-	-	P	P			NA
RF02	(895 613)	Porphyrite	4	-	MP, P	P	P			NA
1247	(8527 5272)	?altd basic	4	-	MP*	-				NA
1249	(8531 5299)	Brccia								BGS, TSNA
1250	(8523 5310)	Microdiorite								BGS, TSNA

Sample	Grid ref/locality	Lithology	Alt. code	Cpx	Amph	Btc	Plag	K-fspar	Quartz	Notes
1251	(8521 5324)	Porphyrite								BGS, IS, TSNA
1256	(8280 4940)	Breccia								BGS, TSNA
1257	(8266 4958)	Porphyrite								BGS, IS, TSNA
1277	(7246 4978)	Agglomerate								BGS, TSNA
1282	(7322 5144)	Agglomerate								BGS, TSNA
1283	(7317 5143)	Agglomerate								BGS, TSNA
1284	(7317 5143)	Agglomerate								BGS, TSNA
1288	(6873 5649)	Lamprophyre								BGS, IS, TSNA
1289	(7108 5813)	Lamprophyre								BGS, IS, TSNA
1292	(6217 4670)	Lamprophyre								BGS, IS, TSNA
1297	(0465 7907)	Lamprophyre								BGS, IS, TSNA
1300	(8812 7349)	Sediment								BGS, TSNA
1304	(8811 7346)	Porphyrite								BGS, IS, TSNA
1309	(9022 7639)	Lamprophyre								BGS, IS, TSNA
1312	(8982 7662)	Lamprophyre	1-2	P*						PN, BGS, Probe
1316	(8979 7749)	Lamprophyre								BGS, IS, TSNA
1318	(8984 7769)	Lamprophyre								BGS, IS, TSNA
1319	(8989 7779)	Lamprophyre								BGS, IS, TSNA
1321	(8992 7816)	Lamprophyre								BGS, IS, TSNA
1322	(8973 7825)	Lamprophyre								BGS, IS, TSNA
1324	(9027 7794)	Lamprophyre								BGS, IS, TSNA
1328	(8871 7720)	Lamprophyre								BGS, IS, TSNA
1329	(8850 7691)	Lamprophyre								BGS, IS, TSNA
1331	(2925 9141)	Lamprophyre								BGS, IS, TSNA
1336	(9058 7780)	Lamprophyre								BGS, IS, TSNA
1340	(9240 7077)	Porphyrite								BGS, IS, TSNA
1348	(8568 7061)	Microdiorite								BGS, IS, TSNA
1349	(8567 7059)	Microdiorite								BGS, IS, TSNA
1354	(8767 8922)	Sediment								BGS, IS, TSNA
1356	(8433 8815)	Lamprophyre								BGS, IS, TSNA
1372	(5942 8257)	Porphyritic								BGS, IS, TSNA
CDD 372	BSMIC	Sediment	4*							CC-BGS
CDD 363	BSMIC	Breccia	4*							CC-BGS
2748	BSMIC	Sed/phyt contact	4*							CC-BGS
CDD 365	BSMIC	Sediment	4*							CC-BGS
CDD 363	BSMIC	Sediment	4*							CC-BGS
CDD 358	BSMIC	Breccia	4*							CC-BGS
BH8 23.7	BSMIC	Porphyrite	4*							CC-BGS
BH8 39.56	BSMIC	Porphyrite	4*							CC-BGS

Sample	Grid ref/locality	Lithology	Alt. code	Cpx	Amph	Bte	Plag	K-fspar	Quartz	Notes
BH8 17.37	BSMIC	Porphyrite	4*							CC-BGS
BH8 23.63	BSMIC	Sed/phyt contact	4*							CC-BGS
BH8 21.43	BSMIC	Granodiorite	4*							CC-BGS
BH8 14.78	BSMIC	Granodiorite	4*							CC-BGS
BH8 130.07	BSMIC	?contact rock	4*							CC-BGS
BH8 145.82	BSMIC	Porphyrite	4*							CC-BGS
BH8 183.2	BSMIC	Porphyrite	4*							CC-BGS
BH8 179.35	BSMIC	Sediment	4*							CC-BGS
BH8 207.1	BSMIC	Granodiorite	4*							CC-BGS
BH8 143.74	BSMIC	Sediment	4*							CC-BGS
BH8 64.4	BSMIC	Granodiorite	4*							CC-BGS
BH8 128.8	BSMIC	?carb-sectie-qtz	4*							CC-BGS
BH8 71.63	BSMIC	?Sediment	4*							CC-BGS
BH8 76.2	BSMIC	Contact rock	4*							CC-BGS
BH8 129.13	BSMIC	Qtz-rich sed.	4*							CC-BGS
BH8 125.47	BSMIC	Qtz-carb rock	4*							CC-BGS
BH8 203.2	BSMIC	Sediment	4*							CC-BGS
BH8 205.27	BSMIC	Sediment	4*							CC-BGS
BH8 196.33	BSMIC	Breccia	4*							CC-BGS
BH8 174.96	BSMIC	Granodiorite	4*							CC-BGS
BH8 193.25	BSMIC	?Contact rock	4*							CC-BGS
CDD 374	BSMIC	Sediment	4*							CC-BGS
CDD 368	BSMIC	Sediment	4*							CC-BGS
CDD1000	BSMIC	Sediment	4*							CC-BGS
BH8 160	BSMIC	Granodiorite	4*							CC-BGS
BH8 177.7	BSMIC	Sediment	4*							CC-BGS
BH8 143.12	BSMIC	Sediment	4*							CC-BGS
BH8 206.53	BSMIC	Granodiorite	4*							CC-BGS
BH8 163.35	BSMIC	Granodiorite	4*							CC-BGS
CDD 1029	BSMIC	Granodiorite	4*							CC-BGS
CDD 394	BSMIC	Sediment	4*							CC-BGS
CDD 410	BSMIC	?Carb-qtz rock	4*							CC-BGS
CDD 408	BSMIC	Granodiorite	4*							CC-BGS
BH8 25.75	BSMIC	Granodiorite	4*							CC-BGS
CDD 421	BSMIC	Granodiorite	4*							CC-BGS
CDD 415	BSMIC	Granodiorite	4*							CC-BGS
BH8 57.9	BSMIC	Granodiorite	4*							CC-BGS
BH8 133.84	BSMIC	Granodiorite	4*							CC-BGS
BH8 49.31	BSMIC	Granodiorite	4*							CC-BGS
CDD 1042	BSMIC	Granodiorite	4*							CC-BGS

Sample	Grid ref/locality	Lithology	Alt. code	Cpx	Amph	Btc	Plag	K-fspar	Quartz	Notes
CDD(372)	BSMIC	Porphyrite	4*							CC-BGS
BH8 130.24	BSMIC	Granodiorite	4*							CC-BGS
CDD(357.1)	BSMIC	Granodiorite	4*							CC-BGS
CDD(380)	BSMIC	Granodiorite	4*							CC-BGS
CDD 1039	BSMIC	Granodiorite	4*							CC-BGS
CDD 1013	BSMIC	?Qtz-carb rock	4*							CC-BGS
CDD 376	BSMIC	?Adamellite	4*							CC-BGS
CDD 1025	BSMIC	?Diorite	4*							CC-BGS
CDD 10001	BSMIC	Sediment	4*							CC-BGS
CDD 341	BSMIC	Sediment	4*							CC-BGS
CDD 303	BSMIC	Sediment	4*							CC-BGS
CDD 44	BSMIC	Sediment	4*							CC-BGS
CDD 1048	BSMIC	?Contact rock	4*							CC-BGS
CDD(390.6)	BSMIC	?Carb-qtz rock	4*							CC-BGS
CDD 355	BSMIC	Pelitic sediment	4*							CC-BGS
CDD 348	BSMIC	Sediment	4*							CC-BGS
CDD 402	BSMIC	?sediment	4*							CC-BGS

Appendix F

Mica compositions from the Criffell CAL

	1370MC1	1370MRA1	1370MRB1	1370MC2	1370MR2	1370MC3LF	1370MR3LF
SiO ₂	38.56	35.06	36.54	38.99	36.02	38.89	35.11
Al ₂ O ₃	14.76	15.30	14.75	14.75	14.65	14.44	15.42
K ₂ O	9.52	7.65	8.47	9.26	8.32	9.69	8.11
MnO	0.07	0.27	0.12	0.04	0.18	0.02	0.16
Na ₂ O	0.34	0.57	0.46	0.40	0.54	0.24	0.62
CaO	0.00	0.02	0.02	0.02	0.00	0.03	0.02
FeO	5.56	14.74	10.83	5.28	11.12	4.75	13.13
MgO	20.99	15.68	18.42	21.22	18.00	21.45	16.59
P ₂ O ₅	0.00	0.00	0.02	0.01	0.00	0.00	0.01
TiO ₂	3.36	3.89	3.97	3.25	3.83	3.15	4.26
NiO	0.17	0.02	0.05	0.27	0.03	0.31	0.02
CR ₂ O ₅	0.13	0.02	0.02	0.97	0.00	1.00	0.02
F	1.52	1.06	1.11	1.28	1.29	1.03	0.94
TOTAL	94.98	94.29	94.78	95.73	93.98	94.98	94.42
Fc	0.7001	0.5089	0.5231	0.5817	0.6173	0.4716	0.4496
AL ₃₊	2.5349	2.7463	2.5886	2.5035	2.6038	2.4648	2.7458
K ₊	1.7697	1.4866	1.609	1.7014	1.6	1.7898	1.5639
Mn ₂₊	0.0084	0.0346	0.0148	0.0043	0.023	0.0025	0.0212
Na ₂₊	0.0948	0.1683	0.1334	0.1108	0.1576	0.067	0.1812
Si ₄₊	5.6197	5.3397	5.4422	5.6161	5.4333	5.6333	5.3045
Ca ₂₊	0	0.0027	0.0028	0.003	0	0.0051	0.0029
Fe _{2+(t)}	0.6779	1.8774	1.349	0.6367	1.4024	0.575	1.6597
Mg ₂₊	4.5591	3.56	4.0883	4.5559	4.0479	4.6309	3.7359
P ₅₊	0	0	0.0027	0.0017	0	0	0.0017
Ti ₄₊	0.368	0.4456	0.4442	0.352	0.4349	0.3428	0.4835
Ni ₂₊	0.0203	0.0024	0.006	0.0313	0.0039	0.0365	0.003
Cr ₃₊	0.0152	0.0023	0.0025	0.1103	0	0.114	0.003
CA total	16.3682	16.175	16.2068	16.2088	16.3242	16.1332	16.1558
Mg#	0.871	0.655	0.752	0.877	0.743	0.89	0.692
Mg/Fe	6.725	1.896	3.031	7.155	2.886	8.054	2.251
Ti+Al+Si	8.523	8.532	8.475	8.472	8.472	8.441	8.534
%Al	32.616	33.558	32.253	32.529	32.329	32.133	33.726
%Fe	8.722	22.941	16.808	8.273	17.412	7.496	20.386
%Mg	58.661	43.501	50.939	59.198	50.259	60.371	45.888

Recalculation details in Appendix A
Mg# and %Al, Fe, Mg after Rock, 1984; Bachinski & Simpson, 1984

1370MC4LF 1370MR4T1 1370MR4T2 1370MR4T3 1370MR4T4 1370MR4T5 1370MC5

SiO2	38.63	37.89	38.23	36.99	36.78	34.90	38.40
Al2O3	14.37	14.88	14.74	14.76	14.78	14.82	15.04
K2O	9.01	8.90	8.87	8.64	8.40	7.21	9.16
MnO	0.06	0.05	0.08	0.08	0.14	0.25	0.04
Na2O	0.41	0.40	0.42	0.53	0.54	0.45	0.43
CaO	0.01	0.03	0.01	0.01	0.02	0.02	0.02
FeO	6.63	6.97	7.59	9.12	10.70	14.81	6.11
MgO	20.40	20.78	20.55	19.37	18.84	16.37	21.52
P2O5	0.01	0.02	0.02	0.02	0.01	0.01	0.02
TiO2	3.27	3.29	3.20	3.98	3.92	4.30	3.27
NiO	0.13	0.11	0.07	0.05	0.09	0.04	0.16
CR2O5	0.03	0.03	0.02	0.02	0.00	0.01	0.07
F	1.36	1.16	0.98	0.90	1.11	1.04	1.18
TOTAL	94.85	94.51	94.77	94.49	95.34	94.20	95.40
Fc	0.6257	0.5371	0.4523	0.4213	0.5188	0.4981	0.5399
AL3+	2.4717	2.5703	2.538	2.5721	2.576	2.6576	2.5638
K+	1.6772	1.6625	1.6528	1.6295	1.5851	1.3992	1.6902
Mn2+	0.0073	0.0064	0.0101	0.0105	0.0175	0.0319	0.0051
Na2+	0.117	0.1127	0.1178	0.1522	0.156	0.1317	0.12
Si4+	5.6393	5.5518	5.5851	5.4694	5.4401	5.3108	5.5561
Ca2+	0.0022	0.0044	0.0017	0.0015	0.0031	0.0034	0.0036
Fe2+(t)	0.8095	0.8537	0.9275	1.1281	1.3234	1.8843	0.7392
Mg2+	4.5565	4.5384	4.4762	4.2687	4.1525	3.7124	4.6405
P5+	0.0006	0.0026	0.0025	0.0025	0.0016	0.0013	0.0025
Ti4+	0.359	0.3621	0.3517	0.4431	0.4364	0.4918	0.3557
Ni2+	0.0153	0.0133	0.008	0.0055	0.0105	0.0051	0.0184
Cr3+	0.0033	0.0035	0.002	0.0028	0	0.0009	0.0076
CA total	16.2847	16.2187	16.1256	16.1071	16.2211	16.1283	16.2424
Mg#	0.849	0.842	0.828	0.791	0.758	0.663	0.863
Mg/Fe	5.629	5.316	4.826	3.784	3.138	1.97	6.278
Ti+Al+Si	8.47	8.484	8.475	8.485	8.453	8.46	8.476
%Al	31.536	32.28	31.958	32.277	31.992	32.197	32.275
%Fe	10.328	10.722	11.679	14.156	16.436	22.828	9.306
%Mg	58.136	56.998	56.363	53.567	51.572	44.975	58.419

1370MR5T1 1370MR5T2 1370MR5T3

SiO2	38.22	36.47	35.73
Al2O3	14.64	14.50	15.04
K2O	9.04	8.57	8.47
MnO	0.03	0.16	0.29
Na2O	0.47	0.56	0.58
CaO	0.02	0.03	0.02
FeO	7.18	10.45	14.06
MgO	21.25	18.51	15.75
P2O5	0.01	0.02	0.01
TiO2	3.26	3.82	4.11
NiO	0.10	0.06	0.04
CR2O5	0.03	0.04	0.01
F	1.36	1.21	1.01
TOTAL	95.61	94.41	95.11
Fc	0.6238	0.5746	0.4813
AL3+	2.5089	2.5572	2.6752
K+	1.6762	1.6362	1.6307
Mn2+	0.0034	0.0207	0.0368
Na2+	0.1333	0.1624	0.1683
Si4+	5.5565	5.4594	5.3933
Ca2+	0.0027	0.0047	0.0037
Fe2+(t)	0.8734	1.3081	1.7745
Mg2+	4.6045	4.1294	3.5425
P5+	0.0017	0.0028	0.0007
Ti4+	0.3563	0.4303	0.4668
Ni2+	0.0119	0.0073	0.0047
Cr3+	0.0032	0.0047	0.0014
CA total	16.3558	16.2977	16.18
Mg#	0.841	0.759	0.666
Mg/Fe	5.272	3.157	1.996
Ti+Al+Si	8.422	8.447	8.535
%Al	31.413	31.986	33.473
%Fe	10.936	16.362	22.203
%Mg	57.651	51.652	44.324

Clinopyroxene compositions from Criffell CAL

	1240PC1	1240PR1	1240PC2	1240PR2	1240PC3	1240PR3	1240PC4
SiO2	52.12	50.23	53.50	52.47	52.91	51.70	51.32
Al2O3	1.86	2.85	1.10	2.06	1.84	2.40	2.77
K2O	0.01	0.01	0.00	0.00	0.01	0.04	0.00
MnO	0.20	0.17	0.15	0.15	0.11	0.22	0.20
Na2O	0.40	0.52	0.31	0.40	0.36	0.41	0.53
CaO	21.93	21.69	19.91	21.14	21.33	20.94	21.66
FeO	5.57	6.76	4.17	4.38	4.76	7.60	6.49
MgO	15.88	14.14	18.76	17.44	17.55	15.42	15.36
P2O5	0.34	0.31	0.33	0.31	0.27	0.31	0.30
TiO2	0.28	0.39	0.18	0.33	0.26	0.34	0.34
NiO	0.01	0.00	0.03	0.02	0.02	0.01	0.05
Cr2O3	0.47	0.14	0.81	0.75	0.34	0.03	0.27
TOTAL	99.06	97.33	99.42	99.50	99.75	99.44	99.30
AL3+	0.081	0.128	0.048	0.089	0.079	0.105	0.121
K+	0.000	0.000	0.000	0.000	0.000	0.002	0.000
MN2+	0.006	0.005	0.005	0.005	0.003	0.007	0.006
NA+	0.029	0.038	0.022	0.028	0.026	0.030	0.038
SI4+	1.935	1.913	1.956	1.926	1.937	1.924	1.909
CA2+	0.872	0.885	0.780	0.831	0.837	0.835	0.864
FE2+	0.173	0.215	0.127	0.134	0.146	0.236	0.202
MG2+	0.879	0.803	1.022	0.954	0.958	0.855	0.852
P5+	0.011	0.010	0.010	0.010	0.008	0.010	0.009
TI4+	0.008	0.011	0.005	0.009	0.007	0.010	0.010
NI2+	0.000	0.000	0.001	0.001	0.001	0.000	0.002
CR3+	0.014	0.004	0.024	0.022	0.010	0.001	0.008
CATOTAL	4.008	4.027	4.017	4.017	4.012	4.015	4.021
F	0.000	0.120	0.160	0.070	0.000	0.000	0.000
Fc	0.000	0.014	0.018	0.009	0.000	0.000	0.000
Mg#	0.84	0.79	0.89	0.88	0.87	0.78	0.81
%Ca	45.34	46.50	40.42	43.31	43.12	43.33	45.05
%Fe	8.99	11.32	6.60	7.00	7.52	12.27	10.54
%Mg	45.68	42.18	52.98	49.70	49.36	44.39	44.42

	1240PR4	1240PC5	1240PR5	1240PC6	1240PR6	1240PC7	1240PR7
SiO2	50.26	52.14	52.19	52.21	53.46	52.38	52.80
Al2O3	3.62	2.71	2.90	2.44	1.13	2.95	1.91
K2O	0.02	0.01	0.02	0.01	0.00	0.02	0.01
MnO	0.16	0.14	0.19	0.16	0.10	0.17	0.17
Na2O	0.54	0.43	0.48	0.44	0.30	0.46	0.36
CaO	21.28	20.92	20.49	20.99	20.90	20.88	20.99
FeO	7.22	5.10	6.56	4.88	4.08	5.15	4.76
MgO	14.70	17.23	16.52	17.24	18.72	17.35	17.96
P2O5	0.31	0.30	0.30	0.32	0.29	0.33	0.30
TiO2	0.50	0.45	0.43	0.39	0.21	0.50	0.31
NiO	0.01	0.01	0.00	0.02	0.06	0.03	0.05
Cr2O3	0.26	0.30	0.06	0.38	0.43	0.31	0.28
TOTAL	98.99	99.79	100.13	99.47	99.73	100.65	100.10
AL3+	0.160	0.117	0.125	0.106	0.048	0.126	0.082
K+	0.001	0.001	0.001	0.000	0.000	0.001	0.000
MN2+	0.005	0.004	0.006	0.005	0.003	0.005	0.005
NA+	0.039	0.031	0.034	0.031	0.021	0.032	0.025
SI4+	1.884	1.912	1.915	1.918	1.950	1.905	1.930
CA2+	0.855	0.822	0.805	0.826	0.817	0.814	0.822
FE2+	0.226	0.156	0.201	0.150	0.124	0.157	0.145
MG2+	0.821	0.942	0.903	0.944	1.018	0.941	0.978
P5+	0.010	0.009	0.009	0.010	0.009	0.010	0.009
TI4+	0.014	0.012	0.012	0.011	0.006	0.014	0.009
NI2+	0.000	0.000	0.000	0.001	0.002	0.001	0.002
CR3+	0.008	0.009	0.002	0.011	0.012	0.009	0.008
CATOTAL	4.036	4.021	4.013	4.013	4.018	4.028	4.039
F	0.110	0.060	0.000	0.000	0.070	0.120	0.200
Fc	0.013	0.007	0.000	0.000	0.008	0.014	0.024
Mg#	0.78	0.86	0.82	0.86	0.89	0.86	0.87
%Ca	44.93	42.82	42.17	43.02	41.69	42.58	42.25
%Fe	11.90	8.14	10.54	7.81	6.35	8.20	7.47
%Mg	43.17	49.04	47.29	49.17	51.96	49.23	50.28

	1329PC1	1329PR1	1329PC2	1329PR2	1329PC3	1329PR3	1329PC4
SiO2	52.78	52.11	52.01	52.32	52.95	53.23	52.43
Al2O3	0.65	2.58	2.71	2.51	1.60	1.66	2.19
K2O	0.00	0.02	0.00	0.02	0.00	0.00	0.00
MnO	0.21	0.13	0.15	0.15	0.14	0.14	0.14
Na2O	0.45	0.38	0.41	0.38	0.39	0.38	0.40
CaO	21.71	21.41	20.89	21.91	22.02	21.98	21.32
FeO	8.72	5.43	5.25	5.72	4.31	4.29	3.94
MgO	14.63	16.89	16.91	16.51	17.56	17.35	17.53
P2O5	0.33	0.32	0.35	0.31	0.31	0.30	0.31
TiO2	0.23	0.44	0.43	0.42	0.28	0.25	0.33
NiO	0.02	0.04	0.06	0.02	0.02	0.03	0.03
Cr2O3	0.03	0.19	0.25	0.06	0.46	0.43	1.13
TOTAL	99.78	100.00	99.41	99.97	100.17	100.22	99.88
AL3+	0.029	0.112	0.118	0.109	0.069	0.071	0.094
K+	0.000	0.001	0.000	0.001	0.000	0.000	0.000
MN2+	0.007	0.004	0.005	0.005	0.004	0.004	0.004
NA+	0.033	0.027	0.029	0.027	0.028	0.027	0.029
SI4+	1.969	1.912	1.914	1.922	1.934	1.942	1.918
CA2+	0.868	0.842	0.824	0.863	0.862	0.859	0.836
FE2+	0.272	0.167	0.162	0.176	0.132	0.131	0.120
MG2+	0.814	0.924	0.928	0.885	0.956	0.944	0.956
P5+	0.011	0.010	0.011	0.010	0.010	0.009	0.010
TI4+	0.007	0.012	0.012	0.012	0.008	0.007	0.009
NI2+	0.001	0.001	0.002	0.001	0.001	0.001	0.001
CR3+	0.001	0.006	0.007	0.002	0.013	0.013	0.033
CATOTAL	4.011	4.022	4.010	4.010	4.030	4.030	4.027
F	0.020	0.050	0.000	0.000	0.120	0.190	0.160
Fc	0.002	0.006	0.000	0.000	0.014	0.022	0.018
Mg#	0.75	0.85	0.85	0.83	0.88	0.88	0.89
%Ca	44.42	43.56	43.06	44.86	44.20	44.43	43.71
%Fe	13.93	8.63	8.44	9.14	6.76	6.76	6.30
%Mg	41.65	47.81	48.50	46.00	49.05	48.80	50.00

	1329PR4	1329PC5	1329PR5	1329PC6	1329PR6	1312PC1	1312PR1
SiO2	52.65	49.75	51.18	51.87	52.05	52.75	53.09
Al2O3	1.87	4.34	3.18	2.48	2.50	1.86	1.98
K2O	0.02	0.01	0.01	0.00	0.00	0.00	0.00
MnO	0.13	0.16	0.21	0.17	0.11	0.16	0.15
Na2O	0.42	0.51	0.49	0.39	0.36	0.42	0.43
CaO	21.84	21.39	21.79	21.93	21.31	19.38	19.91
FeO	3.81	7.89	6.90	5.53	5.33	0.49	4.74
MgO	17.35	14.17	14.83	16.40	16.97	18.47	18.26
P2O5	0.31	0.30	0.30	0.27	0.29	0.28	0.28
TiO2	0.28	0.74	0.53	0.42	0.43	0.33	0.35
NiO	0.01	0.03	0.01	0.03	0.06	0.01	0.02
Cr2O3	0.93	0.05	0.04	0.16	0.15	0.35	0.36
TOTAL	99.64	99.34	99.54	99.69	99.69	99.00	99.77
AL3+	0.081	0.191	0.139	0.108	0.109	0.081	0.085
K+	0.001	0.001	0.000	0.000	0.000	0.000	0.000
MN2+	0.004	0.005	0.007	0.005	0.004	0.005	0.005
NA+	0.030	0.037	0.036	0.028	0.026	0.030	0.031
SI4+	1.929	1.863	1.903	1.914	1.916	1.938	1.939
CA2+	0.857	0.858	0.868	0.867	0.840	0.763	0.779
FE2+	0.117	0.247	0.215	0.171	0.164	0.152	0.145
MG2+	0.947	0.791	0.822	0.902	0.931	1.011	0.994
P5+	0.010	0.010	0.010	0.008	0.009	0.009	0.009
TI4+	0.078	0.021	0.015	0.012	0.012	0.009	0.010
NI2+	0.000	0.001	0.000	0.001	0.002	0.000	0.000
CR3+	0.027	0.001	0.001	0.005	0.004	0.010	0.011
CATOTAL	4.010	4.026	4.023	4.024	4.032	4.013	4.029
F	0.000	0.010	0.060	0.040	0.150	0.040	0.200
Fc	0.000	0.001	0.008	0.005	0.017	0.005	0.023
Mg#	0.89	0.76	0.79	0.84	0.85	0.87	0.87
%Ca	44.62	45.27	45.58	44.70	43.42	39.61	40.62
%Fe	6.08	13.03	11.27	8.80	8.48	7.88	7.56
%Mg	49.31	41.71	43.15	46.50	48.10	52.51	51.82

	1312PC2	1312PR2	1312PC3	1312PR3	1312PC4	1312PR4	1312PC5
SiO2	51.83	51.45	52.05	50.07	51.32	52.28	51.75
Al2O3	2.91	3.45	2.45	4.72	3.66	2.76	3.08
K2O	0.00	0.01	0.00	0.00	0.00	0.02	0.00
MnO	0.11	0.21	0.19	0.20	0.14	0.13	0.15
Na2O	0.54	0.56	0.48	0.67	0.50	0.51	0.54
CaO	20.34	19.46	19.46	20.21	20.30	20.45	20.29
FeO	4.36	5.99	6.76	7.04	5.24	4.70	5.21
MgO	17.20	16.95	16.78	15.16	16.46	17.12	16.98
P2O5	0.30	0.28	0.26	0.27	0.30	0.30	0.27
TiO2	0.44	0.56	0.45	0.82	0.60	0.42	0.51
NiO	0.05	0.03	0.00	0.02	0.03	0.03	0.00
Cr2O3	1.21	0.29	0.05	0.03	0.32	0.54	0.32
TOTAL	99.29	99.25	99.04	99.20	98.94	99.25	99.16
AL3+	0.126	0.150	0.107	0.207	0.160	0.119	0.134
K+	0.000	0.001	0.000	0.000	0.000	0.001	0.000
MN2+	0.004	0.007	0.006	0.006	0.005	0.004	0.005
NA+	0.039	0.040	0.035	0.048	0.036	0.036	0.038
SI4+	1.905	1.898	1.929	1.863	1.897	1.920	1.908
CA2+	0.801	0.769	0.773	0.806	0.804	0.805	0.802
FE2+	0.134	0.185	0.210	0.219	0.162	0.144	0.161
MG2+	0.942	0.932	0.927	0.841	0.907	0.937	0.933
P5+	0.009	0.009	0.008	0.009	0.009	0.009	0.008
TI4+	0.012	0.016	0.013	0.023	0.017	0.012	0.014
NI2+	0.001	0.001	0.000	0.001	0.001	0.001	0.000
CR3+	0.035	0.008	0.002	0.001	0.009	0.016	0.009
CATOTAL	4.008	4.016	4.020	4.022	4.013	4.005	4.020
F	0.000	0.020	0.100	0.000	0.060	0.000	0.060
Fc	0.000	0.002	0.011	0.000	0.007	0.000	0.008
Mg#	0.88	0.84	0.82	0.79	0.85	0.87	0.85
%Ca	42.67	40.78	40.48	43.20	42.93	42.66	42.30
%Fe	7.13	9.80	10.98	11.74	8.66	7.65	8.47
%Mg	50.20	49.42	48.54	45.07	48.41	49.69	49.23

	1312PR5	1312PC6	1312PR6
SiO2	51.53	52.24	52.78
Al2O3	1.64	2.83	2.29
K2O	0.02	0.00	0.01
MnO	0.76	0.15	0.19
Na2O	0.57	0.56	0.47
CaO	22.04	19.05	20.02
FeO	8.73	4.93	4.64
MgO	12.97	17.54	17.23
P2O5	0.34	0.29	0.27
TiO2	0.27	0.44	0.38
NiO	0.00	0.00	0.03
Cr2O3	0.12	0.82	0.55
TOTAL	99.00	98.95	98.86
AL3+	0.073	0.123	0.099
K+	0.001	0.000	0.001
MN2+	0.024	0.005	0.006
NA+	0.042	0.040	0.033
SI4+	1.948	1.922	1.942
CA2+	0.893	0.751	0.789
FE2+	0.276	0.152	0.143
MG2+	0.731	0.962	0.945
P5+	0.011	0.009	0.009
TI4+	0.008	0.012	0.010
NI2+	0.000	0.000	0.001
CR3+	0.004	0.024	0.016
CATOTAL	4.011	4.010	3.994
F	0.000	0.100	0.000
Fc	0.000	0.011	0.000
Mg#	0.73	0.86	0.87
%Ca	46.99	40.28	42.04
%Fe	14.53	8.14	7.61
%Mg	38.48	51.58	50.35

Code	Amphibole compositions from the Criffell CAL					
	1 1312MC1	1 1312MR1	1 1312C2	1 1312R2	1 1312C3	1 1312R3
SiO2	41.42	41.37	40.87	41.19	41.29	41.71
Al2O3	12.85	13.14	13.66	13.18	13.32	11.86
Fe2O3	0.00	0.00	0.00	0.00	0.00	0.00
FeO	11.05	10.48	10.50	10.70	10.45	11.00
MgO	14.12	14.21	14.04	13.97	14.16	14.18
CaO	10.98	11.04	10.96	11.28	11.01	11.25
Na2O	2.40	2.22	2.23	2.24	2.09	2.15
K2O	1.38	1.46	1.57	1.36	1.67	1.19
TiO2	2.79	2.81	3.03	2.86	3.14	3.01
MnO	0.17	0.18	0.29	0.19	0.25	0.23
Total	97.16	96.91	97.15	96.97	97.38	96.58
Si	6.04	6.04	5.95	6.03	6	6.13
Al	2.21	2.26	2.35	2.27	2.28	2.05
Fe3+	0.72	0.7	0.73	0.61	0.7	0.65
Fe2+	0.62	0.58	0.54	0.7	0.57	0.7
Mg	3.07	3.09	3.05	3.05	3.07	3.11
Ca	1.72	1.73	1.71	1.77	1.72	1.77
Na	0.68	0.63	0.63	0.64	0.59	0.61
K	0.26	0.27	0.29	0.25	0.31	0.22
Ti	0.31	0.31	0.33	0.31	0.34	0.33
Mn	0.02	0.02	0.04	0.02	0.03	0.03
NaB	0.284	0.274	0.289	0.231	0.285	0.23
NaKA	0.652	0.626	0.633	0.658	0.613	0.606
Al(vi)	0.254	0.299	0.303	0.304	0.286	0.182
Mg#	0.831	0.842	0.849	0.814	0.843	0.816
Al(iv)	1.956	1.961	2.047	1.966	1.994	1.868
Fe3+/Fe2+	1.161	1.207	1.352	0.871	1.228	0.929
P2O5	0.25	0.22	0.2	0.24	0.18	0.19
NiO	0.02	0	0.03	0.04	0.02	0.02
Cr2O3	0.02	0.04	0.08	0.05	0.08	0.07
F	0.23	0.08	0.36	0.31	0.12	0.36

Fe reallocated on basis of 13.0 cations (Rock & Leake, 1984)
Analyses calculated on the basis of 23 Oxygens (Rock & Leake, 1984)

	C-Phenocryst core		MC-Microphenocryst/groundmass core
	R-Phenocryst rim		MR-Microphenocryst/groundmass rim
Classification codes:		1	Titanian Potassian Magnesio-Hastingsite
(Rock & Leake, 1984)		2	Titanian Magnesio-Hastingsite
		3	Potassian Magnesio-Hastingsite
		4	Potassian Ferroan Pargasite

Code	1 1312MC4	2 1312MR4	1 11312MC5	2 1312MR5	1 1312MC6	1 1312MR6	1 1312C7
SiO2	41.07	41.58	40.51	41.33	39.89	41.16	42.48
Al2O3	13.54	12.01	13.84	12.16	14.51	13.49	12.23
Fe2O3	0.00	0.00	0.00	0.00	0.00	0.00	0.00
FeO	12.05	11.12	13.14	10.60	12.22	10.90	9.52
MgO	12.58	14.12	12.10	14.23	12.57	13.81	15.15
CaO	10.98	11.16	10.85	11.42	11.01	10.83	11.36
Na2O	2.17	2.23	2.36	2.10	2.33	2.27	2.29
K2O	1.50	1.12	1.43	1.18	1.50	1.42	1.42
TiO2	3.01	2.84	2.92	3.57	2.66	2.89	2.79
MnO	0.16	0.22	0.21	0.18	0.17	0.19	0.13
Total	97.06	96.40	97.36	96.77	96.86	96.96	97.37
Si	6.05	6.11	5.97	6.06	5.88	6	6.16
Al	2.35	2.08	2.41	2.11	2.52	2.32	2.09
Fe3+	0.52	0.7	0.64	0.57	0.68	0.74	0.55
Fe2+	0.96	0.66	0.97	0.73	0.82	0.58	0.61
Mg	2.76	3.1	2.66	3.11	2.77	3	3.28
Ca	1.73	1.76	1.71	1.8	1.74	1.69	1.76
Na	0.62	0.64	0.67	0.6	0.67	0.64	0.64
K	0.28	0.21	0.27	0.22	0.28	0.26	0.26
Ti	0.33	0.31	0.32	0.39	0.29	0.32	0.3
Mn	0.02	0.03	0.03	0.02	0.02	0.02	0.02
NaB	0.268	0.242	0.287	0.205	0.26	0.307	0.236
NaKA	0.634	0.604	0.655	0.614	0.689	0.599	0.671
Al(vi)	0.4	0.196	0.373	0.169	0.411	0.326	0.25
Mg#	0.741	0.823	0.732	0.81	0.771	0.837	0.844
Al(iv)	1.95	1.884	2.037	1.941	2.109	1.994	1.84
Fe3+/Fe2+	0.542	1.061	0.66	0.781	0.829	1.276	0.902
P2O5	0.18	0.22	0.23	0.24	0.22	0.21	0.19
NIO	0	0.02	0.02	0.01	0.02	0.02	0.03
CR2O3	0.03	0.06	0	0.07	0.01	0.09	0.04
F	0.02	0.14	0	0.21	0.29	0.32	0.43
		5					
		6					
		7					
		8					
		9					
		10					
		11					

Magnesio-Hornblende
 Magnesio-Hastingsitic Hornblende
 Magnesio-Hastingsite
 Ferri-Subcalcic Tschermakitic Hornblende

 Ferri-Magnesio Hornblende
 Ferri-Tremolitic-Hornblende
 Kaersutite

Code	2 1312R7	1 1312C8	2 1312R8	3 1240C1	1 1240R1	1 1240MC2	2 1240MR2
SiO2	41.63	40.64	41.71	41.05	41.23	41.74	40.99
Al2O3	12.08	13.27	12.63	12.53	12.25	12.28	12.36
Fe2O3	0.00	0.00	0.00	0.00	0.00	0.00	0.00
FeO	10.86	12.50	10.04	11.88	11.28	13.26	11.87
MgO	14.14	12.46	14.64	13.51	13.84	12.46	13.54
CaO	11.27	10.95	11.16	11.45	11.83	11.24	11.86
Na2O	2.26	2.28	2.34	2.13	2.15	2.01	2.17
K2O	1.17	1.52	1.34	1.71	1.36	1.50	1.32
TiO2	3.30	2.62	2.83	1.85	2.30	2.34	2.45
MnO	0.19	0.30	0.20	0.16	0.16	0.17	0.17
Total	96.90	96.54	96.89	96.27	96.40	97.00	96.73
Si	6.1	6.03	6.08	6.1	6.12	6.18	6.08
Al	2.09	2.32	2.17	2.2	2.14	2.14	2.16
Fe3+	0.58	0.59	0.64	0.6	0.47	0.55	0.49
Fe2+	0.75	0.96	0.58	0.88	0.93	1.09	0.98
Mg	3.09	2.76	3.18	3	3.06	2.75	2.99
Ca	1.77	1.74	1.74	1.82	1.88	1.78	1.88
Na	0.64	0.66	0.66	0.61	0.62	0.58	0.62
K	0.22	0.29	0.25	0.32	0.26	0.28	0.25
Ti	0.36	0.29	0.31	0.21	0.26	0.26	0.27
Mn	0.02	0.04	0.03	0.02	0.02	0.02	0.02
NaB	0.23	0.258	0.256	0.176	0.12	0.217	0.116
NaKA	0.631	0.686	0.655	0.762	0.756	0.643	0.758
Al(vi)	0.191	0.359	0.256	0.301	0.262	0.325	0.24
Mg#	0.804	0.742	0.845	0.773	0.767	0.715	0.754
Al(iv)	1.899	1.961	1.914	1.899	1.878	1.815	1.92
Fe3+/Fe2+	0.773	0.615	1.103	0.682	0.505	0.505	0.5
P2O5	0.19	0.22	0.18	0.2	0.23	0.22	0.2
NIO	0	0.02	0.03	0	0	0	0.02
CR2O3	0.03	0.02	0.1	0.05	0.05	0.03	0.01
F	0.3	0.07	0.27	0	0.27	0.26	0.26

Code	3 1240C3	3 1240R3Z1	1 1240R3Z2	3 1240C4	1 1240R4	3 1240MC5	1 1240MR5
SiO2	39.47	40.69	41.51	41.64	41.24	39.77	41.93
Al2O3	13.06	12.41	11.92	12.40	11.81	13.52	11.50
Fe2O3	0.00	0.00	0.00	0.00	0.00	0.00	0.00
FeO	15.56	13.84	11.23	11.99	11.68	14.45	11.03
MgO	11.06	11.97	14.16	13.62	13.75	11.29	14.25
CaO	11.32	11.38	11.85	11.50	11.84	11.57	11.90
Na2O	2.13	2.07	2.13	2.10	2.10	1.98	1.96
K2O	1.66	1.68	1.41	1.72	1.40	1.92	1.39
TiO2	2.12	2.10	2.47	1.91	2.46	1.88	2.35
MnO	0.18	0.18	0.17	0.18	0.22	0.21	0.14
Total	96.56	96.32	96.85	97.06	96.50	96.59	96.45
Si	5.96	6.12	6.13	6.14	6.13	6	6.2
Al	2.33	2.2	2.08	2.16	2.07	2.4	2.01
Fe3+	0.67	0.5	0.5	0.59	0.48	0.49	0.46
Fe2+	1.29	1.24	0.89	0.89	0.97	1.33	0.9
Mg	2.49	2.68	3.12	2.99	3.05	2.54	3.14
Ca	1.83	1.83	1.87	1.82	1.89	1.87	1.89
Na	0.62	0.6	0.61	0.6	0.6	0.58	0.56
K	0.32	0.32	0.27	0.32	0.26	0.37	0.26
Ti	0.24	0.24	0.27	0.21	0.28	0.21	0.26
Mn	0.02	0.02	0.02	0.02	0.03	0.03	0.02
NaB	0.169	0.167	0.126	0.184	0.115	0.131	0.114
NaKA	0.774	0.758	0.749	0.74	0.756	0.817	0.711
Al(vi)	0.283	0.317	0.202	0.294	0.199	0.4	0.212
Mg#	0.659	0.684	0.779	0.771	0.759	0.656	0.777
Al(iv)	2.047	1.883	1.878	1.866	1.871	2	1.798
Fe3+/Fe2+	0.519	0.403	0.562	0.663	0.495	0.368	0.511
P2O5	0.21	0.21	0.22	0.19	0.2	0.17	0.32
NiO	0.01	0.07	0.05	0	0.01	0.02	0.03
CR2O3	0.02	0.02	0.02	0.04	0.04	0.08	0.02
F	0.13	0.12	0.25	0.27	0.3	0.24	0.2

Code	3 1240MC6	1 1240MR6	3 1240C7	3 1240R7	4 1240MC8	3 1240MR8	5 1329MC1
SiO2	39.70	41.51	40.21	40.70	39.01	42.32	46.64
Al2O3	13.41	11.65	13.05	12.63	14.24	11.71	8.10
Fe2O3	0.00	0.00	0.00	0.00	0.00	0.00	0.00
FeO	15.77	11.41	14.17	13.33	15.98	12.09	11.74
MgO	10.49	13.95	11.70	12.24	10.04	13.86	14.51
CaO	11.55	11.77	11.52	11.46	11.58	11.71	12.05
Na2O	2.16	2.10	2.13	1.95	2.04	2.14	1.18
K2O	1.74	1.38	1.76	1.69	1.98	1.50	0.97
TiO2	1.89	2.34	1.95	2.10	2.07	1.98	1.86
MnO	0.30	0.18	0.22	0.19	0.22	0.13	0.24
Total	97.01	96.29	96.71	96.29	97.16	97.44	97.29
Si	6	6.17	6.04	6.1	5.91	6.22	6.79
Al	2.39	2.04	2.31	2.23	2.54	2.03	1.39
Fe3+	0.47	0.49	0.5	0.52	0.44	0.53	0.34
Fe2+	1.52	0.93	1.28	1.15	1.58	0.96	1.09
Mg	2.36	3.09	2.62	2.74	2.27	3.04	3.15
Ca	1.87	1.87	1.85	1.84	1.88	1.84	1.88
Na	0.63	0.6	0.62	0.57	0.6	0.61	0.33
K	0.34	0.26	0.34	0.32	0.38	0.28	0.18
Ti	0.21	0.26	0.22	0.24	0.24	0.22	0.2
Mn	0.04	0.02	0.03	0.02	0.03	0.02	0.03
NaB	0.13	0.127	0.146	0.16	0.122	0.157	0.12
NaKA	0.838	0.74	0.811	0.73	0.859	0.733	0.394
Al(vi)	0.39	0.208	0.352	0.333	0.448	0.245	0.185
Mg#	0.609	0.769	0.673	0.705	0.589	0.76	0.743
Al(iv)	2	1.832	1.958	1.897	2.092	1.785	1.205
Fe3+/Fe2+	0.309	0.527	0.391	0.452	0.278	0.552	0.312
P2O5	0.2	0.2	0.22	0.22	0.2	0.2	0.17
NiO	0.05	0.01	0.03	0.04	0.02	0.08	0.02
CR2O3	0.04	0.02	0.02	0.04	0.01	0.06	0.02
F	0.17	0.17	0.35	0.08	0.02	0.33	0.2

Code	6 1329MR1	3 1329C2	7 1329R2	3 1329MC3	7 1329MR3	3 1329C4	2 1329R4
SiO2	43.29	41.72	41.96	41.08	40.95	41.51	41.07
Al2O3	10.72	12.38	12.26	12.18	12.75	12.38	12.56
Fe2O3	0.00	0.00	0.00	0.00	0.00	0.00	0.00
FeO	11.85	12.78	11.78	13.81	11.51	12.25	10.71
MgO	14.35	13.27	13.83	12.85	13.67	13.75	14.44
CaO	11.72	11.54	11.63	11.41	11.61	11.43	11.92
Na2O	2.05	2.09	2.07	2.10	2.04	2.22	2.35
K2O	1.01	1.56	1.24	1.51	1.27	1.56	1.14
TiO2	1.95	1.96	2.09	2.18	2.21	2.14	2.78
MnO	0.19	0.16	0.19	0.19	0.20	0.16	0.16
Total	97.13	97.46	97.05	97.31	96.21	97.40	97.13
Si	6.33	6.13	6.16	6.07	6.06	6.09	6.03
Al	1.85	2.15	2.12	2.12	2.23	2.14	2.17
Fe3+	0.61	0.62	0.63	0.75	0.65	0.69	0.53
Fe2+	0.84	0.95	0.81	0.96	0.77	0.82	0.78
Mg	3.13	2.91	3.02	2.83	3.02	3.01	3.16
Ca	1.84	1.82	1.83	1.81	1.84	1.8	1.87
Na	0.58	0.6	0.59	0.6	0.58	0.63	0.67
K	0.19	0.29	0.23	0.28	0.24	0.29	0.21
Ti	0.21	0.22	0.23	0.24	0.25	0.24	0.31
Mn	0.02	0.02	0.02	0.02	0.03	0.02	0.02
NaB	0.163	0.182	0.172	0.193	0.159	0.203	0.126
NaKA	0.607	0.707	0.648	0.693	0.666	0.72	0.756
Al(vi)	0.182	0.282	0.276	0.195	0.287	0.233	0.2
Mg#	0.789	0.755	0.788	0.747	0.796	0.787	0.801
Al(iv)	1.668	1.868	1.844	1.925	1.943	1.907	1.97
Fe3+/Fe2+	0.726	0.653	0.778	0.781	0.844	0.841	0.679
P2O5	0.2	0.21	0.2	0.2	0.21	0.2	0.39
NiO	0.05	0	0.01	0.03	0.03	0.04	0.03
CR2O3	0.03	0.03	0.02	0	0.04	0.03	0.04
F	0.08	0.27	0.05	0.18	0.2	0.3	0.19

Code	3 1329MC5	8 1329MR5	3 1329C6	7 1329R6	2 1329MC7	2 1329MR7	3 1329C8
SiO2	42.25	44.49	42.22	41.32	40.87	41.26	41.66
Al2O3	11.86	9.82	11.69	12.86	12.44	11.74	12.25
Fe2O3	0.00	0.00	0.00	0.00	0.00	0.00	0.00
FeO	10.46	14.95	11.50	11.61	10.66	11.30	12.06
MgO	15.10	13.01	14.22	14.02	14.72	13.76	13.89
CaO	11.35	9.53	11.65	11.65	11.72	11.91	11.38
Na2O	2.22	2.73	2.01	2.18	2.31	2.03	2.24
K2O	1.42	0.88	1.65	1.26	1.21	1.17	1.45
TiO2	2.22	1.56	2.02	2.14	2.92	2.89	2.09
MnO	0.11	0.36	0.16	0.20	0.14	0.20	0.16
Total	96.99	97.33	97.12	97.24	96.99	96.26	97.18
Si	6.15	6.47	6.2	6.04	5.99	6.14	6.11
Al	2.04	1.68	2.03	2.22	2.15	2.06	2.12
Fe3+	0.74	1.14	0.57	0.72	0.67	0.42	0.71
Fe2+	0.53	0.67	0.84	0.7	0.64	0.98	0.77
Mg	3.28	2.82	3.12	3.06	3.22	3.05	3.04
Ca	1.77	1.48	1.83	1.83	1.84	1.9	1.79
Na	0.63	0.77	0.57	0.62	0.66	0.58	0.64
K	0.26	0.16	0.31	0.23	0.23	0.22	0.27
Ti	0.24	0.17	0.22	0.23	0.32	0.32	0.23
Mn	0.01	0.04	0.02	0.03	0.02	0.03	0.02
NaB	0.229	0.516	0.166	0.175	0.16	0.103	0.211
NaKA	0.662	0.416	0.716	0.679	0.722	0.705	0.697
Al(vi)	0.19	0.149	0.229	0.262	0.139	0.195	0.232
Mg#	0.86	0.807	0.788	0.814	0.834	0.756	0.798
Al(iv)	1.85	1.531	1.801	1.958	2.011	1.865	1.888
Fe3+/Fe2+	1.396	1.701	0.679	1.029	1.047	0.429	0.922
P2O5	0.19	0.17	0.2	0.2	0.21	0.21	0.23
NiO	0.05	0	0.05	0.04	0.03	0.02	0.02
CR2O3	0.08	0.03	0.03	0.03	0.03	0.01	0.02
F	0.13	0.14	0.34	0.12	0.19	0.06	0.19

Code	7 1329R8	2 1326C1	9 1326R1	6 1326C2	10 1326R2	11 1326C3	9 1326R3
SiO2	40.94	42.45	47.38	42.92	52.86	41.02	46.41
Al2O3	12.84	11.52	7.62	11.34	2.77	12.13	8.57
Fe2O3	0.00	0.00	0.00	0.00	0.00	0.00	0.00
FeO	11.32	10.18	11.12	10.64	9.77	9.27	10.89
MgO	13.95	15.06	16.50	15.00	18.20	14.60	16.12
CaO	11.82	11.31	10.93	11.16	10.70	11.43	11.00
Na2O	2.19	2.59	2.04	2.61	0.96	2.64	2.15
K2O	1.30	0.85	0.54	0.79	0.18	0.94	0.58
TiO2	2.19	2.58	0.53	1.98	0.08	4.77	0.85
MnO	0.16	0.16	0.43	0.17	0.59	0.11	0.31
Total	96.71	96.70	97.09	96.61	96.11	96.91	96.88
Si	6.04	6.19	6.77	6.26	7.47	6.02	6.66
Al	2.23	1.98	1.28	1.95	0.46	2.1	1.45
Fe3+	0.6	0.63	1.06	0.73	1.05	0.28	0.95
Fe2+	0.8	0.61	0.26	0.56	0.11	0.86	0.35
Mg	3.07	3.28	3.51	3.26	3.83	3.2	3.45
Ca	1.87	1.77	1.67	1.74	1.62	1.8	1.69
Na	0.63	0.73	0.56	0.74	0.26	0.75	0.6
K	0.25	0.16	0.1	0.15	0.03	0.18	0.11
Ti	0.24	0.28	0.06	0.22	0.01	0.53	0.09
Mn	0.02	0.02	0.05	0.02	0.07	0.01	0.04
NaB	0.132	0.232	0.328	0.257	0.263	0.202	0.308
NaKA	0.739	0.659	0.335	0.627	0.032	0.726	0.396
Al(vi)	0.273	0.178	0.05	0.205	0	0.124	0.113
Mg#	0.793	0.844	0.93	0.853	0.973	0.787	0.907
Al(iv)	1.957	1.802	1.23	1.745	0.46	1.976	1.337
Fe3+/Fe2+	0.75	1.033	4.077	1.304	9.545	0.326	2.714
P2O5	0.22	0.18	0.17	0.21	0.17	0.18	0.2
NiO	0.01	0.03	0.04	0.04	0.05	0.05	0
CR2O3	0.01	0.19	0.02	0.18	0.15	0.08	0.02
F	0.17	0.35	0.11	0.16	0	0.18	0.08

Code	2 1326C4	9 1326R4	2 1326C5	10 1326R5	2 1326C6	9 1326R6	7 1326C7
SiO2	41.97	50.97	42.13	51.96	42.76	50.71	42.74
Al2O3	11.62	5.00	11.48	3.52	11.30	4.73	11.40
Fe2O3	0.00	0.00	0.00	0.00	0.00	0.00	0.00
FeO	9.47	10.32	9.28	10.40	10.28	10.23	10.57
MgO	14.83	17.94	15.18	17.65	15.28	17.63	15.00
CaO	11.26	10.58	11.28	11.02	11.16	10.82	11.08
Na2O	2.56	1.45	2.59	0.99	2.68	1.41	2.66
K2O	0.83	0.30	0.86	0.24	0.78	0.32	0.78
TiO2	4.06	0.18	4.24	0.25	2.42	0.25	2.27
MnO	0.12	0.53	0.11	0.58	0.16	0.51	0.12
Total	96.72	97.27	97.15	96.61	96.82	96.61	96.62
Si	6.14	7.14	6.13	7.36	6.22	7.19	6.23
Al	2	0.83	1.97	0.59	1.94	0.79	1.96
Fe3+	0.41	1.21	0.43	0.98	0.72	1.06	0.73
Fe2+	0.75	0	0.69	0.25	0.52	0.15	0.56
Mg	3.23	3.75	3.29	3.73	3.31	3.73	3.26
Ca	1.77	1.59	1.76	1.67	1.74	1.64	1.73
Na	0.73	0.39	0.73	0.27	0.75	0.39	0.75
K	0.15	0.05	0.16	0.04	0.14	0.06	0.14
Ti	0.45	0.02	0.46	0.03	0.26	0.03	0.25
Mn	0.02	0.06	0.01	0.07	0.02	0.06	0.02
NaB	0.235	0.394	0.242	0.272	0.262	0.358	0.27
NaKA	0.646	0.054	0.648	0.043	0.638	0.088	0.627
Al(vi)	0.145	0	0.1	0	0.154	0	0.189
Mg#	0.812	1	0.826	0.938	0.863	0.96	0.854
Al(iv)	1.855	0.83	1.87	0.59	1.786	0.79	1.771
Fe3+/Fe2+	0.547		0.623	3.92	1.385	7.067	1.304
P2O5	0.19	0.19	0.21	0.16	0.2	0.18	0.23
NiO	0.02	0.03	0.05	0.05	0.06	0.04	0.04
CR2O3	0.16	0.01	0.14	0.03	0.04	0.02	0.09
F	0.05	0.12	0.17	0.14	0.38	0	0.24

Code	9 1326R7	1 1313C1	1 1313R1	1 1313C2	2 1313R2A	1 1313R2B	1 1313C3
SiO2	51.46	40.91	40.81	40.42	39.58	41.22	40.19
Al2O3	4.49	13.40	13.31	13.71	13.41	11.51	13.70
Fe2O3	0.00	0.00	0.00	0.00	0.00	0.00	0.00
FeO	10.12	10.67	11.29	11.66	12.11	12.22	11.60
MgO	17.94	13.95	13.50	13.17	12.64	13.12	13.36
CaO	10.56	11.35	11.43	11.14	11.76	11.46	11.23
Na2O	1.32	2.41	2.35	2.46	2.49	2.45	2.38
K2O	0.28	1.61	1.58	1.58	1.18	1.44	1.65
TiO2	0.18	3.03	3.04	3.02	3.43	3.06	3.14
MnO	0.57	0.12	0.14	0.15	0.18	0.42	0.10
Total	96.92	97.45	97.45	97.31	96.78	96.90	97.35
Si	7.22	5.99	6	5.95	5.91	6.14	5.91
Al	0.74	2.31	2.31	2.38	2.36	2.02	2.38
Fe3+	1.18	0.5	0.47	0.55	0.35	0.36	0.58
Fe2+	0.01	0.8	0.92	0.88	1.16	1.16	0.84
Mg	3.76	3.05	2.96	2.89	2.81	2.92	2.93
Ca	1.59	1.78	1.8	1.76	1.88	1.83	1.77
Na	0.36	0.68	0.67	0.7	0.72	0.71	0.68
K	0.05	0.3	0.3	0.3	0.22	0.27	0.31
Ti	0.02	0.33	0.34	0.33	0.38	0.34	0.35
Mn	0.07	0.02	0.02	0.02	0.02	0.05	0.01
NaB	0.359	0.22	0.201	0.244	0.12	1.17	0.231
NaKA	0.05	0.764	0.765	0.754	0.826	0.811	0.757
Al(vi)	0	0.301	0.302	0.324	0.268	0.166	0.285
Mg#	0.998	0.791	0.763	0.766	0.708	0.716	0.777
Al(iv)	0.74	2.009	2.008	2.056	2.092	1.854	2.095
Fe3+/Fe2+	118	0.625	0.511	0.625	0.302	0.31	0.69
P2O5	0.18	0.2	0.19	0.2	0.22	0.17	0.2
NiO	0.03	0.03	0.01	0	0	0.01	0.04
CR2O3	0.04	0.03	0.02	0.01	0.02	0.03	0.02
F	0.08	0.24	0.14	0.16	0.18	0.24	0.18

Code	2 1313R3	1 1313C4	2 1313R4	1 1313C5	4 1313R6	1 1313C6	1 1313R6
SiO2	41.36	40.75	40.70	40.78	39.99	40.55	40.54
Al2O3	11.73	13.33	12.29	13.46	13.42	13.49	12.05
Fe2O3	0.00	0.00	0.00	0.00	0.00	0.00	0.00
FeO	12.25	10.93	12.02	10.72	11.97	11.66	12.58
MgO	13.33	13.66	12.97	13.88	12.42	13.34	12.81
CaO	11.53	11.25	11.74	11.24	11.79	11.27	11.52
Na2O	2.45	2.46	2.23	2.55	2.46	2.39	2.47
K2O	1.25	1.59	1.10	1.63	1.16	1.61	1.45
TiO2	3.22	3.04	3.34	2.99	3.26	3.10	3.09
MnO	0.29	0.10	0.18	0.14	0.18	0.12	0.40
Total	97.41	97.11	96.57	97.39	96.65	97.53	96.91
Si	6.11	6	6.06	5.98	5.98	5.95	6.05
Al	2.04	2.31	2.16	2.33	2.37	2.34	2.12
Fe3+	0.43	0.47	0.36	0.5	0.23	0.54	0.39
Fe2+	1.08	0.87	1.13	0.82	1.26	0.89	1.18
Mg	2.94	3	2.88	3.03	2.77	2.92	2.85
Ca	1.83	1.77	1.87	1.77	1.89	1.77	1.84
Na	0.7	0.7	0.64	0.72	0.71	0.68	0.71
K	0.24	0.3	0.21	0.3	0.22	0.3	0.28
Ti	0.36	0.34	0.37	0.33	0.37	0.34	0.35
Mn	0.04	0.01	0.02	0.02	0.02	0.02	0.05
NaB	0.175	0.227	0.126	0.235	0.112	0.227	0.157
NaKA	0.763	0.774	0.727	0.795	0.823	0.755	0.835
Al(vi)	0.156	0.309	0.224	0.305	0.345	0.291	0.178
Mg#	0.731	0.775	0.717	0.788	0.687	0.767	0.708
Al(iv)	1.884	2.001	1.936	2.025	2.025	2.049	1.942
Fe3+/Fe2+	0.398	0.54	0.319	0.61	0.183	0.607	0.331
P2O5	0.18	0.21	0.19	0.19	0.19	0.19	0.14
NiO	0.01	0.02	0.01	0.01	0.04	0.02	0.02
CR2O3	0.01	0.02	0.02	0.03	0.04	0.03	0
F	0.28	0.05	0.03	0.17	0.23	0.13	0.25

Code	1 1313C7	1 1313R7	1 1313C8	12 1313R8	1 1313C9	1 1313R9
SiO2	40.53	41.34	40.49	39.94	39.83	40.23
Al2O3	13.48	11.29	13.43	13.67	13.81	13.30
Fe2O3	0.00	0.00	0.00	0.00	0.00	0.00
FeO	10.93	13.68	10.74	12.60	12.11	12.04
MgO	13.64	12.12	14.02	12.45	12.78	13.12
CaO	11.30	11.41	11.25	11.75	11.23	11.56
Na2O	2.38	2.30	2.43	2.46	2.46	2.50
K2O	1.63	1.58	1.60	1.23	1.67	1.41
TiO2	3.09	3.06	3.04	3.05	3.12	2.83
MnO	0.09	0.48	0.13	0.22	0.15	0.33
Total	97.07	97.26	97.13	97.37	97.16	97.32
Si	5.97	6.19	5.94	5.92	5.9	5.95
Al	2.34	1.99	2.32	2.39	2.41	2.32
Fe3+	0.49	0.32	0.6	0.41	0.51	0.52
Fe2+	0.85	1.39	0.72	1.16	0.99	0.97
Mg	2.99	2.7	3.07	2.75	2.82	2.89
Ca	1.78	1.83	1.77	1.87	1.78	1.83
Na	0.68	0.67	0.69	0.71	0.71	0.72
K	0.31	0.3	0.3	0.23	0.32	0.27
Ti	0.34	0.34	0.33	0.34	0.35	0.31
Mn	0.01	0.06	0.02	0.03	0.02	0.04
NaB	0.218	0.171	0.232	0.133	0.218	0.17
NaKA	0.768	0.798	0.759	0.807	0.804	0.813
Al(vi)	0.307	0.179	0.264	0.316	0.312	0.265
Mg#	0.778	0.66	0.81	0.704	0.74	0.749
Al(iv)	2.033	1.811	2.056	2.074	2.098	2.055
Fe3+/Fe2+	0.576	0.23	0.833	0.353	0.515	0.536
P2O5	0.2	0.18	0.23	0.16	0.21	0.19
NIO	0.02	0.02	0.03	0.01	0.04	0
CR2O3	0.01	0	0.03	0.01	0.03	0
F	0.04	0.26	0.39	0.04	0.3	0.26